ADVANCEMENTS IN THE UNDERSTANDING OF ANTHROPOGENIC IMPACTS ON THE MICROBIAL ECOLOGY AND FUNCTION OF AQUATIC ENVIRONMENTS

EDITED BY: Rodrigo Gouvea Taketani, Sara Beier, Francisco Dini-Andreote and Camila Fernandez

PUBLISHED IN: Frontiers in Microbiology and Frontiers in Marine Science

frontiers Research Topics

frontiers

ISSN 1664-8714
ISBN 978-2-88974-519-7
DOI 10.3389/978-2-88974-519-7

About Frontiers

Frontiers is more than just an open-access publisher of scholarly articles: it is a pioneering approach to the world of academia, radically improving the way scholarly research is managed. The grand vision of Frontiers is a world where all people have an equal opportunity to seek, share and generate knowledge. Frontiers provides immediate and permanent online open access to all its publications, but this alone is not enough to realize our grand goals.

Frontiers Journal Series

The Frontiers Journal Series is a multi-tier and interdisciplinary set of open-access, online journals, promising a paradigm shift from the current review, selection and dissemination processes in academic publishing. All Frontiers journals are driven by researchers for researchers; therefore, they constitute a service to the scholarly community. At the same time, the Frontiers Journal Series operates on a revolutionary invention, the tiered publishing system, initially addressing specific communities of scholars, and gradually climbing up to broader public understanding, thus serving the interests of the lay society, too.

Dedication to Quality

Each Frontiers article is a landmark of the highest quality, thanks to genuinely collaborative interactions between authors and review editors, who include some of the world's best academicians. Research must be certified by peers before entering a stream of knowledge that may eventually reach the public - and shape society; therefore, Frontiers only applies the most rigorous and unbiased reviews.
Frontiers revolutionizes research publishing by freely delivering the most outstanding research, evaluated with no bias from both the academic and social point of view. By applying the most advanced information technologies, Frontiers is catapulting scholarly publishing into a new generation.

What are Frontiers Research Topics?

Frontiers Research Topics are very popular trademarks of the Frontiers Journals Series: they are collections of at least ten articles, all centered on a particular subject. With their unique mix of varied contributions from Original Research to Review Articles, Frontiers Research Topics unify the most influential researchers, the latest key findings and historical advances in a hot research area! Find out more on how to host your own Frontiers Research Topic or contribute to one as an author by contacting the Frontiers Editorial Office: frontiersin.org/about/contact

ADVANCEMENTS IN THE UNDERSTANDING OF ANTHROPOGENIC IMPACTS ON THE MICROBIAL ECOLOGY AND FUNCTION OF AQUATIC ENVIRONMENTS

Topic Editors:
Rodrigo Gouvea Taketani, Rothamsted Research, United Kingdom
Sara Beier, Leibniz Institute for Baltic Sea Research (LG), Germany
Francisco Dini-Andreote, The Pennsylvania State University (PSU), United States
Camila Fernandez, UMR7621 Laboratoire d'océanographie microbienne (LOMIC), France

Citation: Taketani, R. G., Beier, S., Dini-Andreote, F., Fernandez, C., eds. (2022). Advancements in the Understanding of Anthropogenic Impacts on the Microbial Ecology and Function of Aquatic Environments. Lausanne: Frontiers Media SA. doi: 10.3389/978-2-88974-519-7

Table of Contents

frontiers in Microbiology

EDITORIAL
published: 24 January 2022
doi: 10.3389/fmicb.2021.820697

Editorial: Advancements in the Understanding of Anthropogenic Impacts on the Microbial Ecology and Function of Aquatic Environments

Rodrigo G. Taketani[1]*, *Francisco Dini-Andreote*[2], *Sara Beier*[3] and *Camila Fernandez*[4,5,6]

[1] Sustainable Agriculture Sciences. Rothamsted Research, Harpenden, United Kingdom, [2] Department of Plant Science & Huck Institutes of the Life Sciences, The Pennsylvania State University, University Park, PA, United States, [3] Department of Biological Oceanography, Leibniz Institute for Baltic Sea Research, Warnemünde, Germany, [4] LOMIC UMR7621 CNRS Observatoire Oceanologique de Banyuls sur Mer, Languedoc-Roussillon, France, [5] COPAS SUR AUSTRAL, COPAS COASTAL, INCAR Center, Universidad de Concepcion, Concepción, Chile, [6] IDEAL Center, Universidad Austral, Valdivia, Chile

Keywords: microbial diversity, anthropogenic impact, bioremediation, biodiversity, global climate change

Editorial on the Research Topic

Advancements in the Understanding of Anthropogenic Impacts on the Microbial Ecology and Function of Aquatic Environments

OPEN ACCESS

Edited and reviewed by:
Lasse Riemann,
University of Copenhagen, Denmark

***Correspondence:**
Rodrigo G. Taketani
rgtaketani@gmail.com

Specialty section:
This article was submitted to Aquatic Microbiology, a section of the journal Frontiers in Microbiology

Received: *23 November 2021*
Accepted: *15 December 2021*
Published: *24 January 2022*

Citation:
Taketani RG, Dini-Andreote F, Beier S and Fernandez C (2022) Editorial: Advancements in the Understanding of Anthropogenic Impacts on the Microbial Ecology and Function of Aquatic Environments. Front. Microbiol. 12:820697. doi: 10.3389/fmicb.2021.820697

Aquatic environments are important ecosystems providing multiple services to humankind and directly affecting economic income worldwide. These ecosystems have increasingly been threatened by changes in global climate and diverse anthropogenic activities—from agriculture to industry (Häder et al., 2020). In general, the continuous exploitation of aquatic ecosystems has caused severe impacts on biological diversity despite some efforts to control habitat exploitation via local legislation (Popper et al., 2020). For instance, the leaching of pollutants and chemical hazards, the eutrophisation caused by extensive use of chemicals in agriculture and aquaculture, changes in land use, and the disposal of urban wastes; are the major factors responsible for most of the anthropogenic impacts on these ecosystems worldwide (Cotta et al., 2019). As such, properly monitoring the effects of these human activities is critical to aid the early detection of potential chemicals and activities with large impacts in aquatic ecosystems. Besides, advances in ecological research can provide the basis for developing new strategies of remediation and recovery of impacted systems (Taketani et al., 2010).

Microbial organisms are highly abundant, ubiquitous, and main drivers of all biochemical cycles (Falkowski et al., 2008), which makes them important players of ecosystem services in all systems, including aquatic environments (Cavicchioli et al., 2019). Due to the sensitivity of microbial community dynamics to any kind of environmental change (Shade et al., 2012), microbes may further serve as indicator species for detecting anthropogenic activities in natural environments (Parmar et al., 2016).

The goal of this research topic was to collect studies that helped to understand the impacts of human presence and activities on the microbial ecology of aquatic ecosystems, and to harness microbial metabolisms to remediate impacted areas. This topic contains a series of 12 articles that cover a wide range of aquatic systems, including lakes, corals, estuaries, and marine waters. We were fortunate to receive research articles in systems across the globe, from North and South America,

Africa, Oceania, Asia, and Europe, covering also variation in biogeography and climate conditions.

Out of the 12 articles published in this topic, three manuscripts focused on different aspects of the coral holobiont. Wambua et al. showed the effect of different levels of anthropogenic impacts on Kenyan corals using metagenome analysis. The results indicate that corals from sites under relatively higher anthropogenic activities were enriched in genes associated with a reduction in intracellular levels of environmental contaminants and DNA repair. Moreover, Ezzat et al. evaluated the effect of elevated water temperature and sturgenfish fecal pellet on the microbiome of the coral *Porites lobata*. This study revealed an increase in the abundance of some coral pathogenic taxa and linked the presence of feces with the inability of corals to recover from wounds. Thus, it suggests that the interaction between higher temperatures and feces are detrimental to coral health. Last, Assis et al. studied the use of rotifers as a delivery system of Beneficial Microorganisms for Corals (BMCs) to improve coral health. This research article nicely illustrates that corals are capable of uptaking the rotifer carrying BMC probiotic, as visualized by electron microscopy. Together, these articles cover various important aspects on the issue of anthropogenic impacts in coral systems that range from detecting the nature and magnitude of the impact toward understanding the ecological effect, and proposing methods for remediation.

Chen et al. assessed how different environmental factors influence surface water *Vibrio* populations from seven seasonally sampled sites located in the Maowei Sea, China. These authors showed that factors related to eutrophication (e.g., total dissolved N and total dissolved P) are key determinants for the selection of different *Vibrio* taxa. Of critical importance, this was argued to have a direct impact on the health of the surrounding human population. In another article, Abioye et al. assessed the prevalence of a set of medically important *Vibrio* species in South African water sources. Most interestingly, this study revealed the presence of Vibrio spp. in a higher number of tested samples, and this fact was later associated with the pollution level of these sources. Both articles highlight the importance of monitoring the presence of pathogenic organisms in water systems, and link their presence with levels and types of chemical pollution.

This research topic also includes three articles focusing on aquaculture. Valdés-Castro and Fernandez studied the effect of aquaculture pesticides on the natural microbial community in the coast of Chile. The authors showed the response of microbial communities to the addition of pesticides to be variable; i.e., either stimulating or inhibiting microbial activity, but with a potentially important and consistent impact on nitrogen budget in the system. Wang et al. studied the effect of different management practices in crayfish production. This study illustrates how different practices exert intense impacts on microbial communities in the system, and discuss strategies for the development of better practices. Fieler et al. investigated seasonal variation in coastal waters off Norway in kelp production through the seasons assessing the kelp matter balance. The obtained results indicate that the time of harvest was a key factor influencing carbon fixation in the system and balance in kelp production. Together, these articles show the importance of informed management practices and their idiosyncrasies across different aquaculture systems.

Two research papers also investigated the impact of xenobiotics on aquatic microbial communities. Kamalanathan et al. used mesocosms to investigate the short- and long-term effects of oil exposure following the Macondo oil spill on microbial diversity and function. In brief, this study describes a disruption of the co-occurrence pattern in microbial taxa due to oil exposure. This was suggested to have a direct impact on community composition, the ecology of biological interactions between taxa, and the functions they perform in the system. Janßen et al. developed a method using Machine Learning to analyse microbial signatures in community composition, and to detect 2,4,6-trinitrotoluene (TNT) in southwestern Baltic Sea sediments via microbial community fingerprints. The use of this method nicely predicted the presence of TNT with 81.5% balanced accuracy, even though the presence of this compound was not *per se* a significant driver of community divergences.

Li et al. studied differences in microbial communities in freshwater lakes occurring at different elevations. This study shows a higher prevalence of genes related to environmental stresses in microbial communities inhabiting lakes at higher elevations. Liu et al. investigated the influence of environmental factors on the community assembly among subalpine lakes. They observed that the community was influenced by carbon content and spatial distance.

Taken together, the studies presented in this research topic cover a wide variety of issues related to anthropogenic activity from aquaculture to global climate change including the presence of xenobiotics and other disturbances. These articles highlight the greater importance of microorganisms as pivotal biotic factors directly impacted by these practices and the most important agents to be properly exploited for ecosystem remediation in affected areas. In summary, articles in this Frontiers research topic shed light on the continuous negative and potentially deleterious effects of human action on aquatic ecosystems. We hope that this collection of papers will be a valuable resource for researchers and stakeholders and will enhance the role of microbial ecology as a foundational basis toward improving research and public policy. We ultimately hope to contribute to promoting advances in sustainability and monitoring anthropogenic impacts on aquatic ecosystems.

AUTHOR CONTRIBUTIONS

All authors of this editorial article have contributed in the conceptualization, writing, reviewing, revising, and have approved it for publication.

ACKNOWLEDGMENTS

The Editors generously thank all authors who have contributed to this Research Topic. Editors are also grateful to the expert reviewers for their critical assessment and precious time spent in helping to improve the quality of the texts presented in the research articles submitted to this Research Topic.

REFERENCES

Cavicchioli, R., Ripple, W. J., Timmis, K. N., Azam, F., Bakken, L. R., Baylis, M., et al. (2019). Scientists' warning to humanity: microorganisms and climate change. *Nat. Rev. Microbiol.* 17, 569–586. doi: 10.1038/s41579-019-0222-5

Cotta, S. R., Cadete, L. L., van Elsas, J. D., Andreote, F. D., and Dias, A. C. F. (2019). Exploring bacterial functionality in mangrove sediments and its capability to overcome anthropogenic activity. *Mar. Pollut. Bull.* 141, 586–594. doi: 10.1016/j.marpolbul.2019.03.001

Falkowski, P. G., Fenchel, T., and Delong, E. F. (2008). The microbial engines that drive Earth's biogeochemical cycles. *Science* 320, 1034–1039. doi: 10.1126/science.1153213

Häder, D.-P., Banaszak, A. T., Villafañe, V. E., Narvarte, M. A., González, R. A., and Helbling, E. W. (2020). Anthropogenic pollution of aquatic ecosystems: emerging problems with global implications. *Sci. Total Environ.* 713:136586. doi: 10.1016/j.scitotenv.2020.136586

Parmar, T. K., Rawtani, D., and Agrawal, Y. K. (2016). Bioindicators: the natural indicator of environmental pollution. *Front. Life Sci.* 9, 110–118. doi: 10.1080/21553769.2016.1162753

Popper, A. N., Hawkins, A. D., and Thomsen, F. (2020). Taking the animals' perspective regarding anthropogenic underwater sound. *Trends Ecol. Evol.* 35, 787–794. doi: 10.1016/j.tree.2020.05.002

Shade, A., Peter, H., Allison, S. D., Baho, D. L., Berga, M., Bürgmann, H., et al. (2012). Fundamentals of microbial community resistance and resilience. *Front. Microbio.* 3:417. doi: 10.3389/fmicb.2012.00417

Taketani, R. G., Franco, N. O., Rosado, A. S., van Elsas, J. D., and Elsas, J. D. (2010). Microbial community response to a simulated hydrocarbon spill in mangrove sediments. *J. Microbiol.* 48, 7–15. doi: 10.1007/s12275-009-0147-1

Conflict of Interest: The authors declare that the research was conducted in the absence of any commercial or financial relationships that could be construed as a potential conflict of interest.

Publisher's Note: All claims expressed in this article are solely those of the authors and do not necessarily represent those of their affiliated organizations, or those of the publisher, the editors and the reviewers. Any product that may be evaluated in this article, or claim that may be made by its manufacturer, is not guaranteed or endorsed by the publisher.

frontiers in Microbiology

ORIGINAL RESEARCH
published: 14 December 2020
doi: 10.3389/fmicb.2020.610974

Responses of Free-Living *Vibrio* Community to Seasonal Environmental Variation in a Subtropical Inland Bay

*Xing Chen[1,2], Huaxian Zhao[1], Gonglingxia Jiang[1], Jinli Tang[1], Qiangsheng Xu[1], Lengjinghua Huang[1], Si Chen[2], Shuqi Zou[3], Ke Dong[3] and Nan Li[1]**

[1] Key Laboratory of Environment Change and Resources Use in Beibu Gulf, Ministry of Education, Nanning Normal University, Nanning, China, [2] State Key Laboratory for Conservation and Utilization of Subtropical Agro-Bioresources, Guangxi Microorganism and Enzyme Research Center of Engineering Technology, College of Life Science and Technology, Guangxi University, Nanning, China, [3] Department of Biological Sciences, Kyonggi University, Suwon-si, South Korea

OPEN ACCESS

Edited by:
Sara Beier,
Leibniz Institute for Baltic Sea Research (LG), Germany

Reviewed by:
Peng Luo,
South China Sea Institute of Oceanology (CAS), China
Man Kit Cheung,
The Chinese University of Hong Kong, China

***Correspondence:**
Nan Li
nli0417@163.com

Specialty section:
This article was submitted to Aquatic Microbiology, a section of the journal Frontiers in Microbiology

Received: 28 September 2020
Accepted: 11 November 2020
Published: 14 December 2020

Citation:
Chen X, Zhao H, Jiang G, Tang J, Xu Q, Huang L, Chen S, Zou S, Dong K and Li N (2020) Responses of Free-Living Vibrio Community to Seasonal Environmental Variation in a Subtropical Inland Bay. Front. Microbiol. 11:610974. doi: 10.3389/fmicb.2020.610974

Vibrio are widely distributed in aquatic environments and strongly associated with eutrophic environments and human health through the consumption of contaminated seafood. However, the response of the *Vibrio* community to seasonal variation in eutrophic environments is poorly understood. In this study, we used a *Vibrio*-specific 16S rRNA sequencing approach to reveal the seasonal distribution pattern and diversity of the *Vibrio* community in the Maowei Sea, Beibu Gulf of China. The Shannon diversity of the *Vibrio* community was highest in the summer, while β-diversity analysis showed that *Vibrio* community structures were significantly different between seasons. Distance-based redundancy analysis (dbRDA) and Mantel test analysis suggested that total dissolved nitrogen (TDN), total dissolved phosphorus (TDP), dissolved inorganic nitrogen (DIN), salinity, and temperature were the key environmental factors shaping the *Vibrio* community structure, indicating a strong filtering effect of trophic condition on *Vibrio* communities. Furthermore, through random forest analysis, *V. fluvialis*, *V. alginolyticus*, *V. proteolyticus*, *V. splendidus*, and the other eight *Vibrio* species were more sensitive to eutrophic changes. This study revealed seasonal changes in *Vibrio* communities and the influence of environmental variation on *Vibrio* community composition, contributing to a better understanding of their potential ecological roles in a subtropical inland bay.

Keywords: 16S rRNA, *Vibrio* diversity, seasonal variation, eutrophication, Beibu Gulf

INTRODUCTION

The genus *Vibrio* consists of heterotrophic bacteria that are common in marine ecosystems, especially in coastal areas (Westrich, 2015; Shelford and Suttle, 2018; Zhang et al., 2019). Due to their remarkable capability for decomposition of a range of nutrient resources, including chitin and alginate, *Vibrio* may exert large impacts on biogeochemical cycling in coastal habitats (Kopprio et al., 2017; Zhang et al., 2018). Furthermore, the genus *Vibrio* encompasses many facultatively symbiotic and potential pathogenic strains, such as *Vibrio cholerae*, *Vibrio parahaemolyticus*, and *Vibrio vulnificus*, which are all capable of infecting humans through the consumption of

contaminated seafood (Guin et al., 2019; hun Yoon and Waters, 2019; King et al., 2019). Since they drive major biogeochemical cycles and support food webs globally, *Vibrio* communities are a vital component of the marine ecosystem. Furthermore, the diversity and dynamics of the *Vibrio* community have attracted growing interest worldwide, including in the Northern Chinese marginal seas, coastal North Atlantic, and Gulf Coast of Mexico (López-Hernández et al., 2015; Vezzulli et al., 2016; Wang et al., 2019). Understanding when and where pathogenic *Vibrio* will break out is important for aquaculture and marine health. A range of studies (Hartwick et al., 2019; Lamon et al., 2019; Baddam et al., 2020) have indicated that the *Vibrio* community undergoes substantial temporal variation. However, the response of the *Vibrio* community to seasonal variation in eutrophic environments is still poorly understood.

Vibrio communities are highly diverse and complex and vary between habitats due to changing environmental conditions. This increases the necessity of studying the ecology of *Vibrio*. Previous studies have demonstrated that the dynamics of *Vibrio* populations are linked to multiple factors, including seasonal changes, biological parameters, and physicochemical properties such as temperature, salinity, pH, and dissolved oxygen (DO), as well as associations with nutrients (Urquhart et al., 2016; Greenfield et al., 2017; Froelich et al., 2019). For example, Siboni et al. (2016) revealed that shifts in the composition of the *Vibrio* community between seasons were primarily driven by changes in temperature, salinity, and NO_2^-. Takemura et al. (2014) found temperature-associated increases in the abundance of pathogenic *Vibrio* species observed in Australian coastal areas. Considering that the occurrence of specific vibrios has frequently been linked to the temperature, salinity, and nutrients, we hypothesized that seasonal variability in the coastal ecosystem could characterize the level of *Vibrio* community differentiation under ongoing environmental forcing.

Moreover, *Vibrio* disease events and community structure appear to be inextricably linked to anthropogenic disturbance of the aquatic environment. An influx of anthropogenically derived pollutants and nutrients into aquatic systems significantly disrupts the *Vibrio* community structure, contributing to changes in diversity and an increase in potentially pathogenic *Vibrio* species (Shore-Maggio et al., 2018). For example, the dense human population and low-lying geography of an estuarine environment were hypothesized to have allowed the enrichment of *V. cholerae*, which causes fatal damage to the human gut (Boucher et al., 2015). Besides, *Vibrio* are strongly associated with high nutrient environments, which are considered a potential indicator for environmental changes and eutrophication (Gregoracci et al., 2012; Takemura et al., 2014). Consequently, gaining deeper insight into the diversity of marine *Vibrio* and the role of environmental factors as filters of *Vibrio* community composition will help people evaluate their ecological role and public health effect in the marine coastal ecosystem.

To better understand the associations between the free-living *Vibrio* community and eutrophic perturbation, we collected surface water samples from the Maowei Sea, which is an estuarine-bay ecosystem that suffers from anthropogenic activities and receives large inputs of terrestrial nutrients from the QinJiang and Maoling rivers, existing serious eutrophication in the area (Zhu et al., 2019). Therefore, this research presented here focuses on the associations between *Vibrio* community composition and seasonal patterns under broadly eutrophic condition. Our aims were to (a) fill the gap in knowledge of the seasonal composition and variation in the *Vibrio* community in the Maowei Sea, (b) determine the gradients of the key controlling environmental factors driving the dynamics of the *Vibrio* community, (c) and identify the potential indicative *Vibrio* species for eutrophic conditions in the local ecosystem.

MATERIALS AND METHODS

Sampling Sites and Environmental Parameters

We collected a total of 140 surface seawater samples (0.5 m deep) seasonally from seven sites of the Maowei Sea from June 2017 through March 2018 (**Figure 1**). Two liters of seawater was collected from four corners and the middle of a 5 m × 5 m square area in each site by a five-point sampling method. Thereafter, all seawater samples were stored at 4°C on board and transferred to the laboratory before filtration. A vacuum pump was used to sequentially filter 1 L of seawater per sample through 3-μm filters (Port Washington, NY, United States) to remove debris and larger organisms, and the resulting samples were collected on 0.22-μm-pore-size polycarbonate membranes (Millipore Corporation, Billerica, MA, United States) for subsequent analysis. During sampling, seawater temperature, pH, and salinity in each sample were measured using a portable meter (556 MPS; YSI, United States). Other nutrients in each sample were measured by standard methods previously described by Yao et al. (2014). For example, dissolved inorganic nutrients (NO_2^-, NO_3^-, and NH_4^+) were measured using spectrophotometric and colorimetric methods (Han et al., 2012). Dissolved inorganic nitrogen (DIN) was composed of NO_2^-, NO_3^-, and NH_4^+, and dissolved inorganic phosphorus (DIP) represented the concentration of PO_4-P (Lai et al., 2014). Chl *a* was measured using a fluorescence spectrophotometer (Holm-Hansen and Riemann, 1978). The total organic carbon (TOC) and the chemical oxygen demand (COD) were measured using the standard method (Visco et al., 2005). The total dissolved nitrogen (TDN) and the total dissolved phosphorus (TDP) were determined using the Cu–Cd column reduction and the spectrophotometric phosphomolybdate blue method, respectively (Sah, 1994; Cai and Guo, 2009). The eutrophication index (EI) was indicated as a Chinese eutrophication status index, which was calculated as the following formula: $EI = DIN \times DIP \times COD \times 10^6/4500$ (Lai et al., 2014; Chen et al., 2016). According to the degree of eutrophication, we found that the samples could be classified into three eutrophication statues: low eutrophication ($1 < EI < 3$), medium eutrophication ($3 < EI < 9$), and high eutrophication ($EI > 9$) (**Supplementary Table 1**). Samples nearby the ocean area showed the lower eutrophication, whereas samples located next to the river mouth presented higher eutrophication.

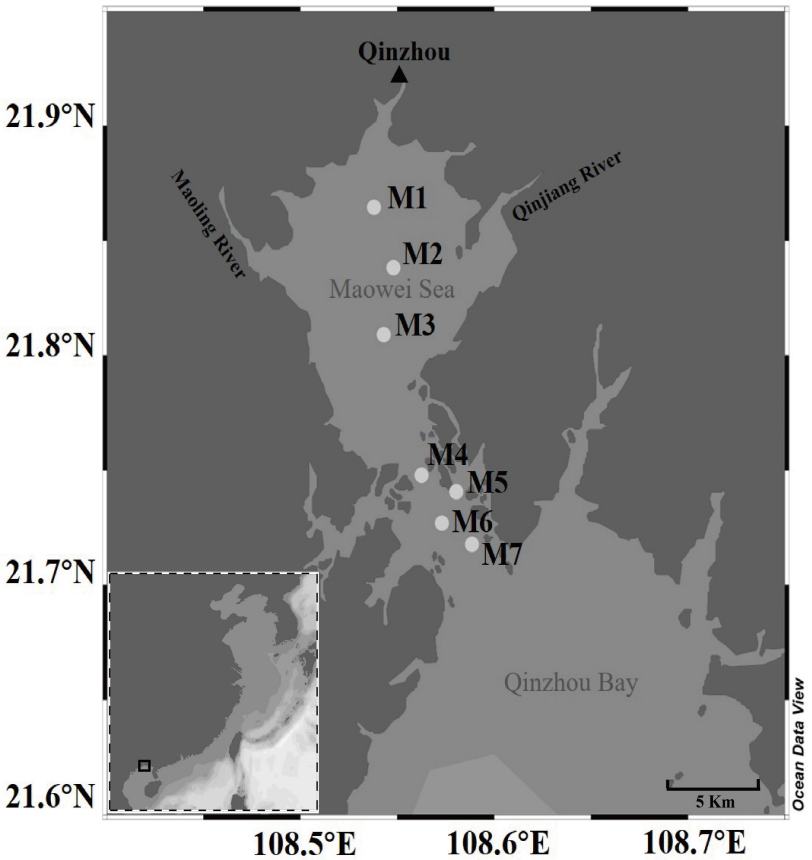

FIGURE 1 | Map of the seven sampling sites along the Maowei Sea in the Beibu Gulf of China.

DNA Extraction and PCR Amplification

Genomic DNA extraction was performed by a DNeasy PowerWater Kit (QIAGEN, United States) using 0.22-μm-pore-size polycarbonate membranes according to the manufacturer's protocols. DNA yield and purity were evaluated using a Nanodrop-2000 Spectrophotometer (Thermo Scientific, United States). The DNA sample was preserved at −80°C. The extracted DNA was tested by PCR using the *Vibrio*-specific 16S rRNA primers 169F (5′-GGCGTAAAGCGCATGCAGGT-3′) and 680R (5′-GAAATTCTACCCCCCTCTACAG-3′) (Thompson et al., 2004). A total reaction volume of 20 μL PCR mixture containing 2 μL DNA template, 6 μL ddH_2O, 10 μL 2 × Taq PCR Mastermix (TIANGEN, China), and 2 μL forward and reverse primers were conducted on a Bio-Rad thermocycler (Hercules, CA). The amplification process was as follows: an initial activation step at 94°C for 1 min, followed by 35 cycles of 30 s denaturation at 95°C, annealing at 56°C for 30 s, extension at 72°C for 30 s, and a final elongation step at 72°C for 10 min. Ultrapure water was used instead of a sample solution as a negative control, which ruled out the possibility of false-positive PCR results. The PCR products were verified by 2% agarose gel electrophoresis and visualized with a UV light and gel image system.

High-Throughput Sequencing Processing

Sequencing was performed on the Illumina MiSeq platform of Lianchuan Bio-Technology Company (China) after preparing DNA libraries. Sequences with low-quality reads (quality scores <30) were removed using Trimmomatics (Bolger et al., 2014). Adapter and barcode sequences were eliminated by Cutadapt (Martin, 2011). The paired-end demultiplexed sequencing reads were processed in a QIIME2 environment (Bolyen et al., 2019). Using a VSEARCH plugin (Rognes et al., 2016), the paired-end reads were joined followed by dereplicating, chimeras filtering, and operational taxonomic units (OTUs) clustering (*de novo*) at a 97% sequence similarity level. Taxonomic classification of OTUs was assigned by a local Blastn (cutoff E-value 1e-10) against a Ribosomal Database Project (RDP) database (Release 11) (Cole et al., 2014).

Statistical Analysis

Seasonal differences in environmental parameters were evaluated using a one-way analysis of variance (ANOVA) followed by Tukey's HSD test in SPSS Statistics v24.0 (Subtype and Sloan, 2018). The α-diversity indices between different groups of samples, including Shannon, Simpson, Chao1, and observed

number of OTUs were calculated using the vegan package in R (Dixon, 2003). The β-diversity was performed with Bray-Curtis dissimilarity, principal coordinate analysis (PCoA), ANOSIM, and PERMANOVA for comparison between the seasonal *Vibrio* communities. Random forest analysis was used to examine the important indicator taxa. Spearman correlation, Mantel test analysis, redundancy analysis (RDA), variation partitioning analysis (VPA), and linear regression were also run in R to reveal correlations between the *Vibrio* community and environmental factors. The R software packages used in this study are mainly the "vegan," "random forest," and "psych" packages (R Core Team, 2013). Analysis of the quantitative and evolutionary relationships of *Vibrio* species in different seasons was performed using TBtool (Chen C. et al., 2018).

RESULTS

Variation in Environmental Parameters

The environmental parameters of seawater samples collected from the Maowei Sea in the Beibu Gulf were measured during the seasonal cruises (**Supplementary Table 1**). The environmental parameters of the seawater samples all varied significantly between seasons as per ANOVA (Tukey's HSD test, $p < 0.001$) (**Table 1**). The temperature (24.58 ± 6.25°C), Chl *a* (2.23 ± 1.10 μg/L), TOC (1.20 ± 0.29 mg/L), and COD (2.82 ± 0.69 mg/L) were significantly higher in summer and autumn than in spring and winter. In contrast, the value for salinity (18.19 ± 5.13), DO (7.64 ± 1.37 mg/L), and TDP (0.06 ± 0.01 mg/L) showed higher in spring and winter. In TDN, there were differences between fall and winter, with the lowest value (0.57 ± 0.07) in winter and the highest value (0.79 ± 0.180) in fall. Moreover, NO_2^-, NO_3^-, and NH_4^+ concentrations all showed lower values in winter. According to EI indicators, the eutrophication level was significantly lowest in winter and highest in fall. Also, within each season, the eutrophication showed a decreasing spatial trend from the river mouth site M1 to the open sea site M7 (**Supplementary Table 1**). Overall, environmental parameters varied between all the sites, and the eutrophication conditions showed significant seasonal changes ($p < 0.001$; **Table 1**).

Correlation of α-Diversity With Environmental Factors

A total of 12,589 ± 5,735 sequences were generated from the samples after quality control and clustered into 85 ± 18 OTUs at a 97% similarity level (**Supplementary Table 2**). Good's coverage values were greater than 99%, indicating that the current sequences reflected the actual situation of the majority of the *Vibrio* community. The α-diversity of the *Vibrio* community including Shannon, Simpson, Chao1, and the observed number of OTU indices varied and differed significantly across seasons (ANOVA, $p < 0.001$) (**Figure 2**). The summer group showed the highest α-diversity, including Shannon, Simpson, and Chao1 indices, indicating that evenness and richness were significantly higher than in other seasons (**Figure 2**). However, the Shannon and Simpson diversities of the *Vibrio* community were lowest in the spring samples and significantly different from summer and winter. According to Spearman's correlation analysis, the α-diversity of the *Vibrio* community was negatively ($p < 0.01$) correlated to NO_2^-, NO_3^-, NH_4^+, TDN, DIN, DIP, and COD but only positively correlated to salinity ($p < 0.001$) (**Supplementary Table 3**). Since the EI is a synthetic index of the multiple nutrients of DIN (NO_2^-, NO_3^-, and NH_4^+), DIP, and COD, we determined that the occurrence of eutrophication, especially in summer and fall, was accompanied by a decrease

TABLE 1 | One-way ANOVA test on variation of each water chemical parameter in year-round.

Variables	*P*-values	All		Spring		Summer		Fall		Winter	
		Mean	Std. Dev.	Mean	Std. Dev.	Mean	Std. Dev.	Mean	Std. Dev.	Mean	Std. Dev.
Temp	<0.001	24.588	6.245	24.119	0.692	27.820	0.842	31.524	0.854	14.890	0.471
pH	<0.001	7.629	0.285	7.784	0.214	7.776	0.249	7.474	0.258	7.483	0.252
Salinity	<0.001	18.193	5.130	21.222	1.862	18.398	4.231	12.281	5.443	20.871	1.932
DO	<0.001	7.641	1.367	8.992	0.318	6.430	0.480	6.232	0.393	8.910	0.266
NO_2^-	<0.001	0.024	0.025	0.015	0.005	0.010	0.004	0.062	0.022	0.006	0.002
NO_3^-	<0.001	0.340	0.157	0.376	0.045	0.519	0.123	0.314	0.102	0.149	0.036
NH_4^+	<0.001	0.111	0.047	0.143	0.027	0.115	0.034	0.122	0.059	0.064	0.009
Chl *a*	<0.001	2.227	1.106	1.607	0.417	2.809	1.299	3.100	0.861	1.390	0.385
TDN	<0.001	0.690	0.144	0.765	0.060	0.636	0.105	0.790	0.180	0.569	0.067
DIN	<0.001	0.474	0.181	0.535	0.074	0.644	0.102	0.498	0.125	0.219	0.044
DIP	<0.001	0.029	0.014	0.044	0.011	0.015	0.004	0.038	0.006	0.018	0.005
TDP	<0.001	0.061	0.019	0.084	0.004	0.039	0.010	0.058	0.011	0.064	0.011
e	<0.001	1.197	0.285	0.938	0.149	1.317	0.183	1.470	0.277	1.065	0.144
COD	<0.001	2.818	0.691	2.508	0.424	3.330	0.554	3.218	0.566	2.255	0.513
EI	<0.001	9.385	6.877	13.632	6.203	7.125	2.108	14.543	6.650	2.242	1.577

Temp, temperature; DO, dissolved oxygen; Chl a, chlorophyll A; TDN, total dissolved nitrogen; DIN, dissolved inorganic nitrogen; DIP, dissolved inorganic phosphorus; TDP, total dissolved phosphorus; TOC, total organic carbon; COD, chemical oxygen demand; EI, eutrophication index.

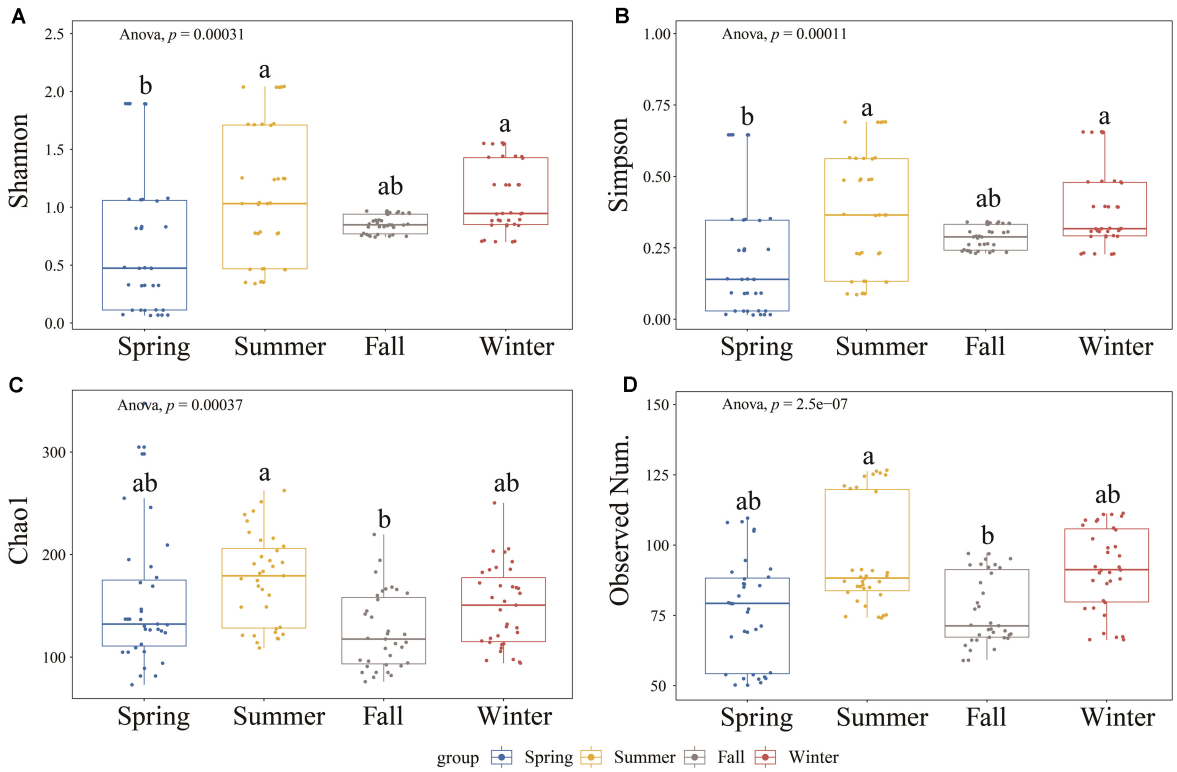

FIGURE 2 | The α-diversity indices (**A–D**: Shannon, Simpson, Chao 1, and Observed Number of OTUs) among the four seasons by boxplot. The differences between any two groups were tested by Tukey's HSD test, presented by lowercase letters on the plots.

in the α-diversity of the *Vibrio* community. In addition, TDN, DIN, NO_2^-, and salinity were the most influential ($|r| > 0.28$, $p < 0.001$) among these factors.

Seasonal Changes in *Vibrio* Community Composition

The representative sequences of each OTU were analyzed to determine the taxonomic status and calculate the relative abundance (**Supplementary Figure 1**). The results showed that the total sequences were affiliated with 36 known *Vibrio* species. *V. fluvialis*, *V. gigantis*, *V. natriegens*, *V. aestuarianus*, *V. plantisponsor*, *V. proteolyticus*, and *V. parahaemolyticus* were predominant in all seasonal samples. *V. fluvialis* was the most abundant species occupying a large proportion (>50%) of each sample. The variation in community composition was largely attributable to the presence of *V. fluvialis* that dominated the *Vibrio* community. Meanwhile, a considerable proportion (∼10%) of the sequence was assigned to an unclassified group, which might represent novel *Vibrio* species. To better understand the seasonal differences of the *Vibrio* species, a heat map was generated to reflect the relative abundance among the four seasonal groups (**Figure 3**). A total of 21 *Vibrio* species were detected in all four seasonal groups, whereas 15 *Vibrio* species were found to be seasonally dependent. For example, *V. azureus*, *V. brasiliensis*, *V. cidicii*, and *V. porteresiae* existed only in summer, while *V. anguillarum*, *V. renipiscarius*, and *V. splendidus* were only found in winter and *Vibrio nereis and V. mytili* were only found in spring. In addition, *V. cyclitrophicus* and *V. diazotrophicus* existed widely in all groups except the summer group. The cluster cladogram analysis in the heat map illustrated that the fall and winter samples grouped together, while groups of spring and summer were clustered separately. Moreover, the main abundant *Vibrio* species were significantly correlated with the seasonal changes via ANOVA (**Figure 3**). The above results suggested that the *Vibrio* community composition was significantly different seasonally and followed a seasonal distribution pattern in the Beibu Gulf.

Effects of Environmental Variables on the β-Diversity

Principal coordinate analysis (PCoA) based on the OTU level was performed to investigate the β-diversity of the *Vibrio* community in different seasonal groups (**Figure 4A**). The first two PCoA axes explained 22.76 and 11.61% of the total variation, respectively. The results demonstrated that summer samples were clearly separated from the others, indicating that the *Vibrio* community composition differed strongly between the summer and the other groups, whereas the *Vibrio* community of fall and winter groups was similar, which was consistent with the cluster cladogram (**Figure 3**). Both ANOSIM ($r = 0.33$, $p = 0.001$) and PERMANOVA ($r^2 = 0.29$, $p = 0.001$) tests further confirmed that the differences in *Vibrio* community structures

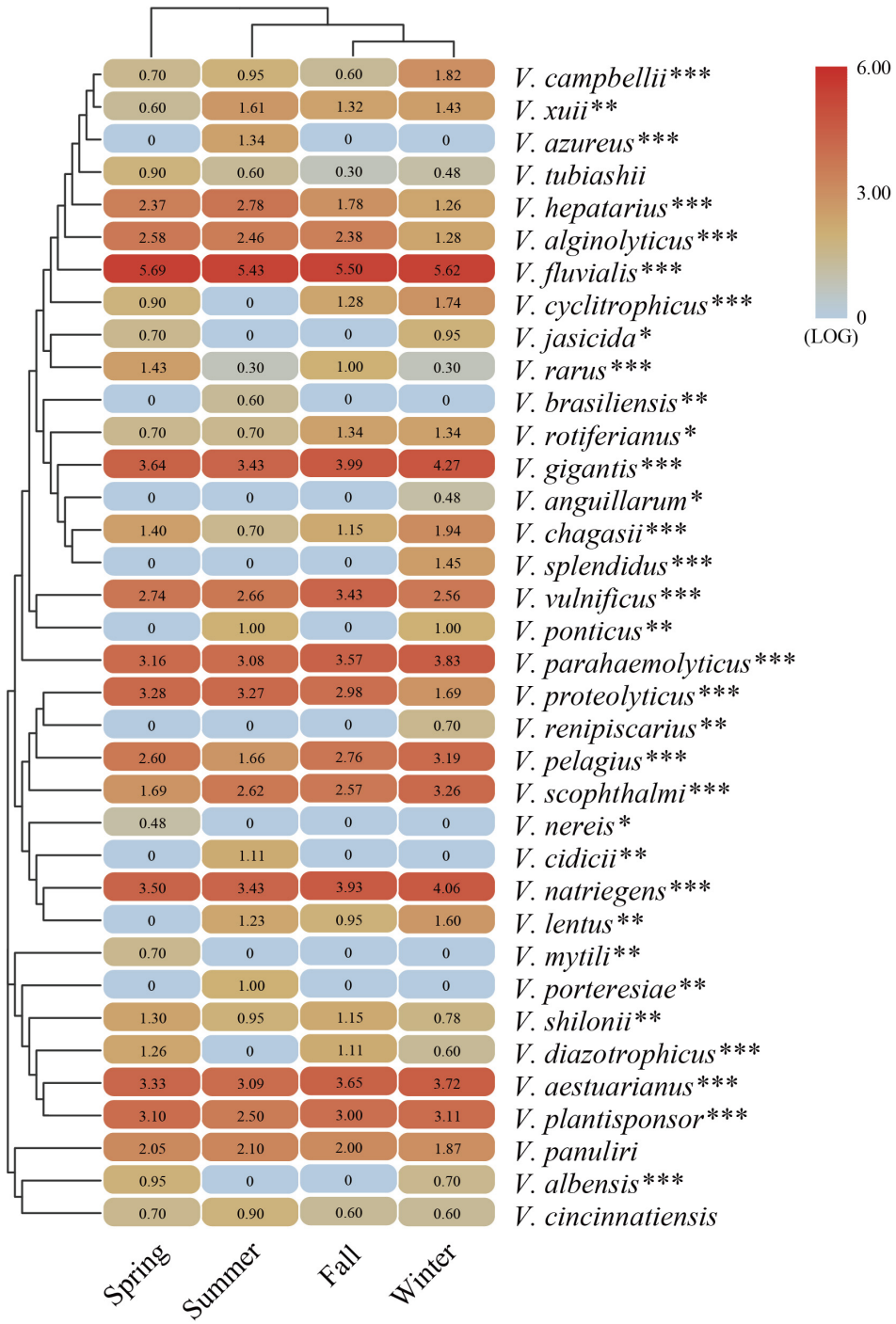

FIGURE 3 | The heat map generated from the major abundant *Vibrio* species with representative sequences in four seasons. The color code represents the difference in relative abundance, ranging from blue to red. The top tree shows the cluster relationship of sampling groups. The significant differences between seasonal changes and distribution of *Vibrio* species are presented by one-way ANOVA test (*$p < 0.05$; **$p < 0.01$; ***$p < 0.001$).

between the four seasons were significant. Furthermore, the Bray-Curtis dissimilarity showed that the dissimilarity of the *Vibrio* community structure among the different samples was highest in spring and lowest in fall (**Supplementary Figure 2**). The significant differences in the Bray-Curtis dissimilarity between seasons also further reflected the seasonal difference of the *Vibrio* community structure in the Maowei sea. To further determine the relationship between the *Vibrio* community dissimilarity and the eutrophic changes, linear regressions were performed based on Bray-Curtis dissimilarity and showed significantly

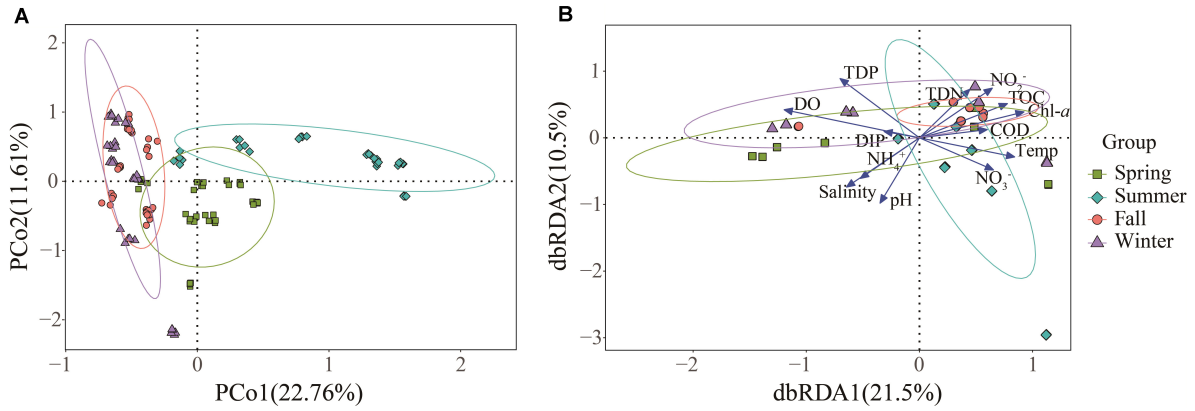

FIGURE 4 | The β-diversity of the *Vibrio* community and its relationship with environmental factors in four seasons. **(A)** The PCoA of different samples based on Bray-Curtis dissimilarity of *Vibrio* communities. **(B)** The dbRDA plot shows the relationship between samples and environmental factors.

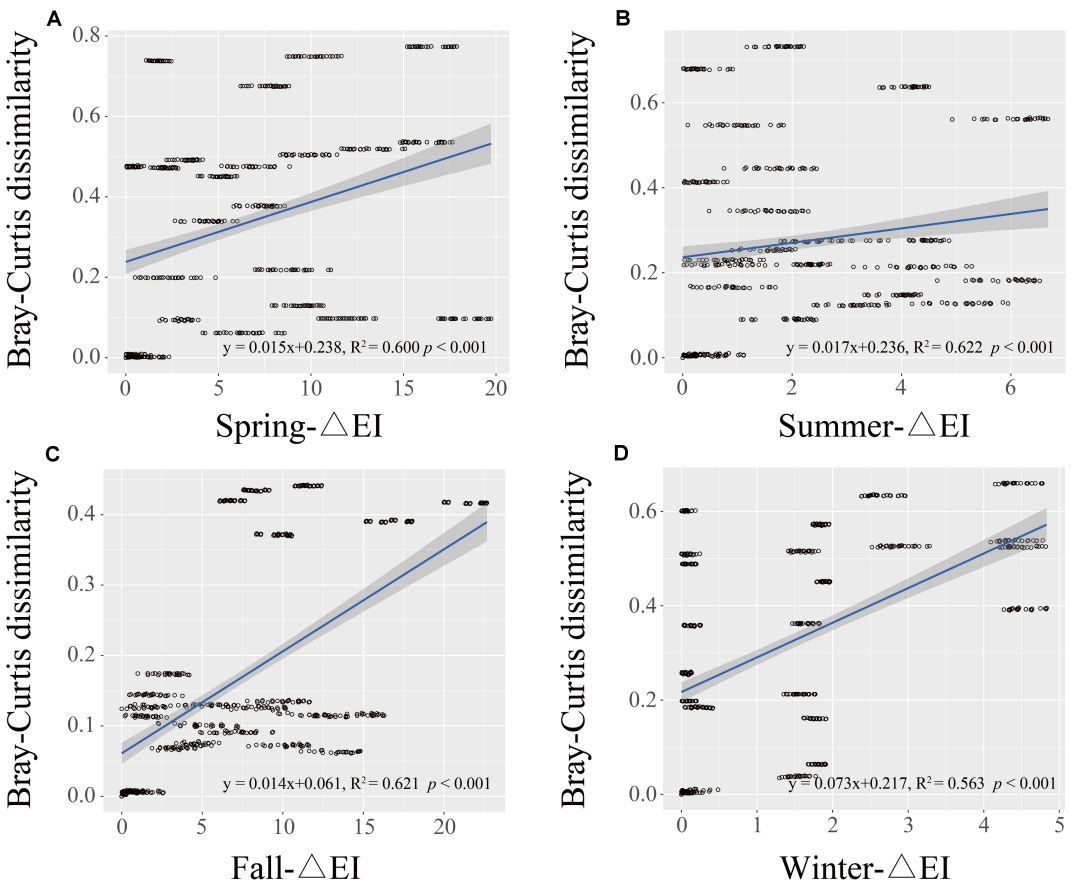

FIGURE 5 | The regression between Bray-Curtis dissimilarity and variation of Delta EI in four seasons (**A–D** represents spring to winter). The black line represents the linear regression, and *P*-values were calculated to indicate significant differences.

increasing β-diversity correlated with the eutrophic variations in seasons (**Figure 5**).

Variation partitioning analysis (VPA) was used to analyze the effects of nutrient variables (NO_2^-, NO_3^-, NH_4^+, TDN, TDP, TOC, DIN, and DIP) and water properties (temperature, pH, salinity, DO, Chl *a*, and COD) on seasonal *Vibrio* community heterogeneity. The results showed that the pure effect of nutrient variables (20%) was higher than that of water properties (12%), and the combined effects explained 38% of the total community variation (**Figure 6**). In seasons,

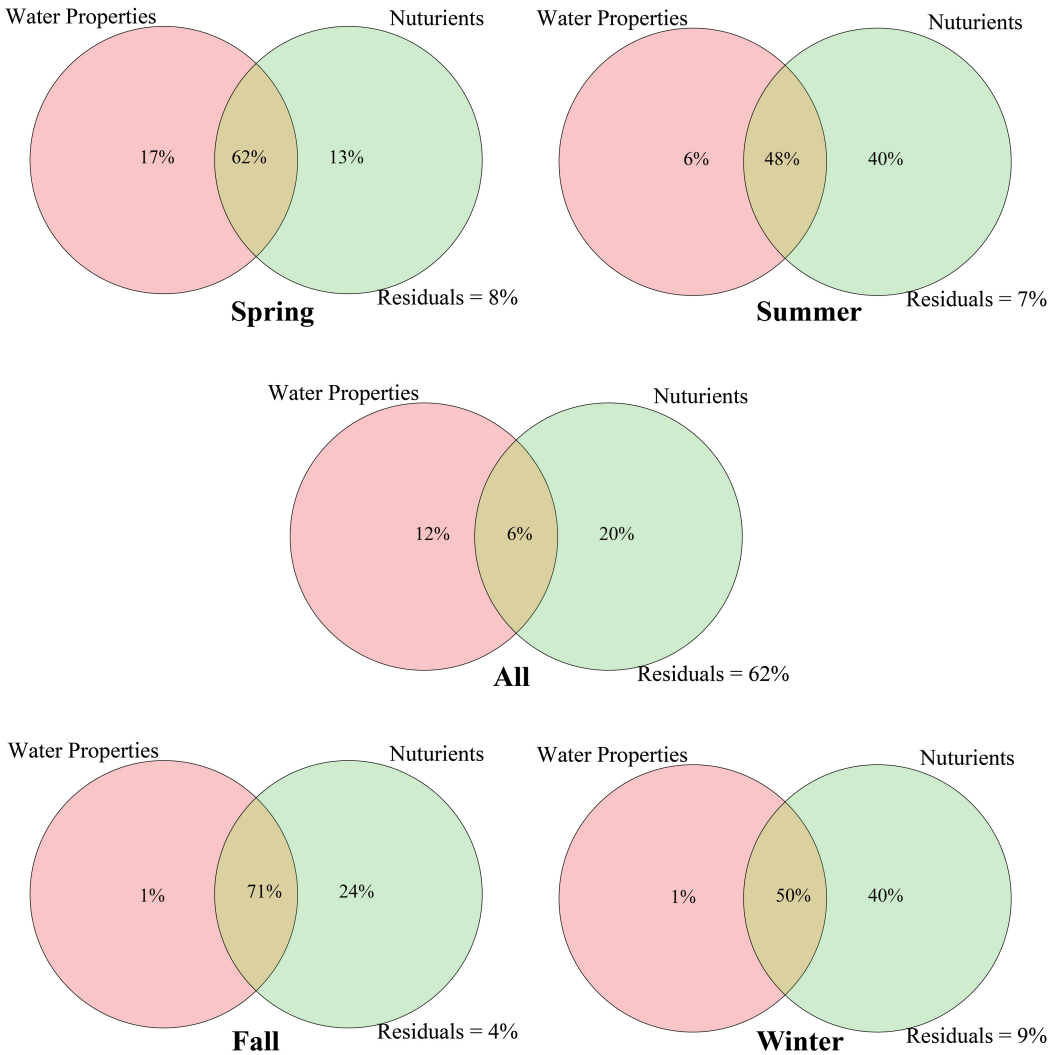

FIGURE 6 | Variation partitioning analysis shows the effects of water properties (temperature, pH, salinity, DO, Chl *a*, and COD) and nutrients (NO_2^-, NO_3^-, NH_4^+, TDN, TDP, TOC, DIN, and DIP) on the *Vibrio* community.

the pure effects of nutrient variables were almost all higher than those of water properties, except spring. For example, in winter samples, the pure effect of nutrient variables was 40%, and the combined effects explained of the total community variation was 91%. The dbRDA was performed to determine the specific environmental factors that governed the *Vibrio* community structure in different seasons. The dbRDA suggested that almost all environmental factors were strongly correlated with *Vibrio* community structures (**Figure 4B**), and shifts in the *Vibrio* community structure may be due to main environmental factors, such as TDN, TDP, DO, temperature, and salinity (**Supplementary Table 4**). Furthermore, the Mantel test calculated the correlation between environmental factors and the β-diversity of the *Vibrio* community (**Table 2**). The partial Mantel results showed that the *Vibrio* community composition along environmental gradients was significantly correlated with TDN, TDP, temperature, and DO, with shifts in community composition being better correlated with changes in TDP than TDN.

Indicator Species of *Vibrio* for Eutrophication

The random forest method was utilized to analyze the most important *Vibrio* species for classifying the seasonal samples, indicating that *V. scophthalmi*, *V. natriegens*, *V. proteolyticus*, *V. hepatarius*, and *V. vulnificus* were the most important species with relatively high abundances (**Figure 7**). Furthermore, linear regression analysis was used to explore the trend of sensitive *Vibrio* species with EI (**Supplementary Figure 3**). The results revealed that 12 of the top 20 important *Vibrio* species were significantly correlated with the EI values. For example, *V. splendidus* was negatively correlated with EI changes ($R^2 = 0.535$, $p < 0.001$), while *V. fluvialis* ($R^2 = 0.662$, $p < 0.001$),

V. alginolyticus (R^2 = 0.576, $p < 0.001$), and *V. proteolyticus* (R^2 = 0.386, $p < 0.001$) were positively correlated with the degree of eutrophication. These *Vibrio* species from the region with trophic gradients may be more sensitive to the eutrophication, which can assess whether nutrient contents had posed an important selective constraint on the communities.

DISCUSSION

This study investigated the seasonal variation in *Vibrio* diversity in a subtropical coastal sea system. Analysis of *Vibrio*-specific 16S rRNA sequences showed that *V. fluvialis* was present year-round and occupied the largest proportion of the *Vibrio* community, followed by *V. gigantis*, *V. natriegens*, and *V. parahaemolyticus* (**Figure 3**). *V. fluvialis* is known as an emerging foodborne pathogen, which was isolated from marine and estuarine environments and humans exhibiting severe diarrheal disease indicating its considerable adaptability (Ramamurthy et al., 2014). In Toulon harbor, France, detections of *V. fluvialis* have increased considerably (29.3%) in seawater during the process of filter feeding in marine mollusks (Martin and Bonnefont, 1990). Similarly, *V. fluvialis* was predominantly detected (>50%) in all samples, indicating the higher possibility and risk of causing gastroenteritis in humans year-round in the studied area. The second most abundant group was *V. gigantis*, which has been reported to originate from the hemolymph of diseased cultured oysters (Le Roux et al., 2005). The Maowei sea is a natural ecosystem rich in wild oyster populations, providing an opportunity for the bloom of pathogenic *Vibrio* species such as *V. fluvialis*, *V. gigantis*, *V. parahaemolyticus*, and *V. vulnificus*, which infect humans through oyster consumption (Chen X. et al., 2018). These may also lead to frequent outbreak of diseases in aquatic organisms and thereby impair aquaculture economy. Moreover, the relative abundance of the different *Vibrio* species varied between the different seasons, and several *Vibrio* species detected in this study showed season-specific prevalence, including *V. brasiliensis* and *V. splendidus*, which were detected only in summer and winter, respectively (**Figure 3**). These results indicated that *Vibrio* communities from the four seasons exhibited contrasting community compositions and were sensitive to seasonal environmental changes.

Regarding α-diversity, we elucidated the temporal changes in *Vibrio* diversity in the Beibu Gulf. The α-diversity of *Vibrio* was highest in summer, which is consistent with previous research in which the diversity of *Vibrio* was found to be greater in summer than in winter (Siboni et al., 2016). Meanwhile, the results of β-diversity revealed distinct seasonal changes in the *Vibrio* community composition of the Maowei Sea and the summer group showing a significant difference from the others on the PCoA (**Figure 4A**). From spring to summer, Shannon and Simpson diversities increased significantly, and the *Vibrio* community structure in summer was significantly different from those in other seasons. This could be partly due to the arrival of the wet season and an increase in runoff. Conversely, it could be that summer is the fastest growing season for shellfish, increasing their filter-feeding rate, and a large number of metabolites were excreted as the water temperature rose (Zheng et al., 2012). Moreover, one possible explanation for the seasonal fluctuation pattern of Bray-Curtis dissimilarity (high in spring and winter and low in summer and autumn) is that the river inflows and seawater temperature increase in summer can stimulate the rapid growth of the motile, chemotactic species of *Vibrio* making them the dominant species (**Figure 5**). This may be the cause of the higher similarity of the *Vibrio* community in summer and fall. When exposed to cold seawater in winter, *Vibrio* enter into a viable but non-culturable state, leading to the persistence of various *Vibrio* species (Oliver, 2016). In

TABLE 2 | The mantel and partial mantel tests (Pearson) show the correlations between Bray-Curtis dissimilarity of the *Vibrio* community and the environmental factors (*$p < 0.05$; **$p < 0.01$; ***$p < 0.001$).

Environmental factors	Whole		Spring		Summer		Fall		Winter	
	Mantel	Partial mantel	Mantel	Partial mantel	Mantel	Partial mantel	Mantel	Partial mantel	Mantel	Partial mantel
Temp	0.120***	0.114***	−0.061	−0.120	0.003	−0.021	−0.066	−0.064	0.051	0.056
pH	0.064*	0.055	−0.009	−0.023	0.258**	0.081	0.001	0.014	−0.016	0.010
Salinity	−0.024	−0.076	0.294**	0.357***	0.763***	0.686***	0.493***	0.441***	0.181**	−0.064
DO	0.225***	0.207***	0.594***	0.564***	0.264**	0.126	−0.077	−0.105	0.092	0.085
NO_2^-	−0.104	−0.156	0.330***	0.294***	0.673***	0.566***	0.456***	0.376***	0.485***	0.271***
NO_3^-	0.074*	0.049	0.661***	0.753***	0.861***	0.789***	0.150*	0.050	0.537***	0.402***
NH_4^+	0.009	−0.043	0.006	−0.378	0.021	−0.404	0.284***	0.124*	0.179**	−0.035
Chl *a*	−0.011	−0.049	0.090	−0.289	0.135*	−0.202	0.578***	0.562***	0.280***	0.206**
TDN	0.124**	0.085*	0.780***	0.783***	0.700***	0.383***	−0.061	−0.079	0.407***	0.296***
DIN	0.110***	0.073*	0.764***	0.786***	0.657***	0.178**	0.219**	0.075	0.482***	0.322***
DIP	0.103**	0.073*	0.615***	0.591***	0.906***	0.853***	0.024	−0.250	0.394***	0.062
TDP	0.200***	0.200***	0.334***	0.278***	−0.039	−0.086	0.135*	0.068	0.419***	0.334***
TOC	0.077*	0.036	0.493***	0.481***	0.794***	0.607***	0.509***	0.444***	0.269***	−0.075
COD	0.032	−0.014	0.570***	0.625***	0.210**	−0.606	0.470***	0.398***	0.324***	−0.012
EI	0.045	0.005	0.067	−0.182	0.528***	−0.288	0.244**	−0.022	0.472***	0.426***

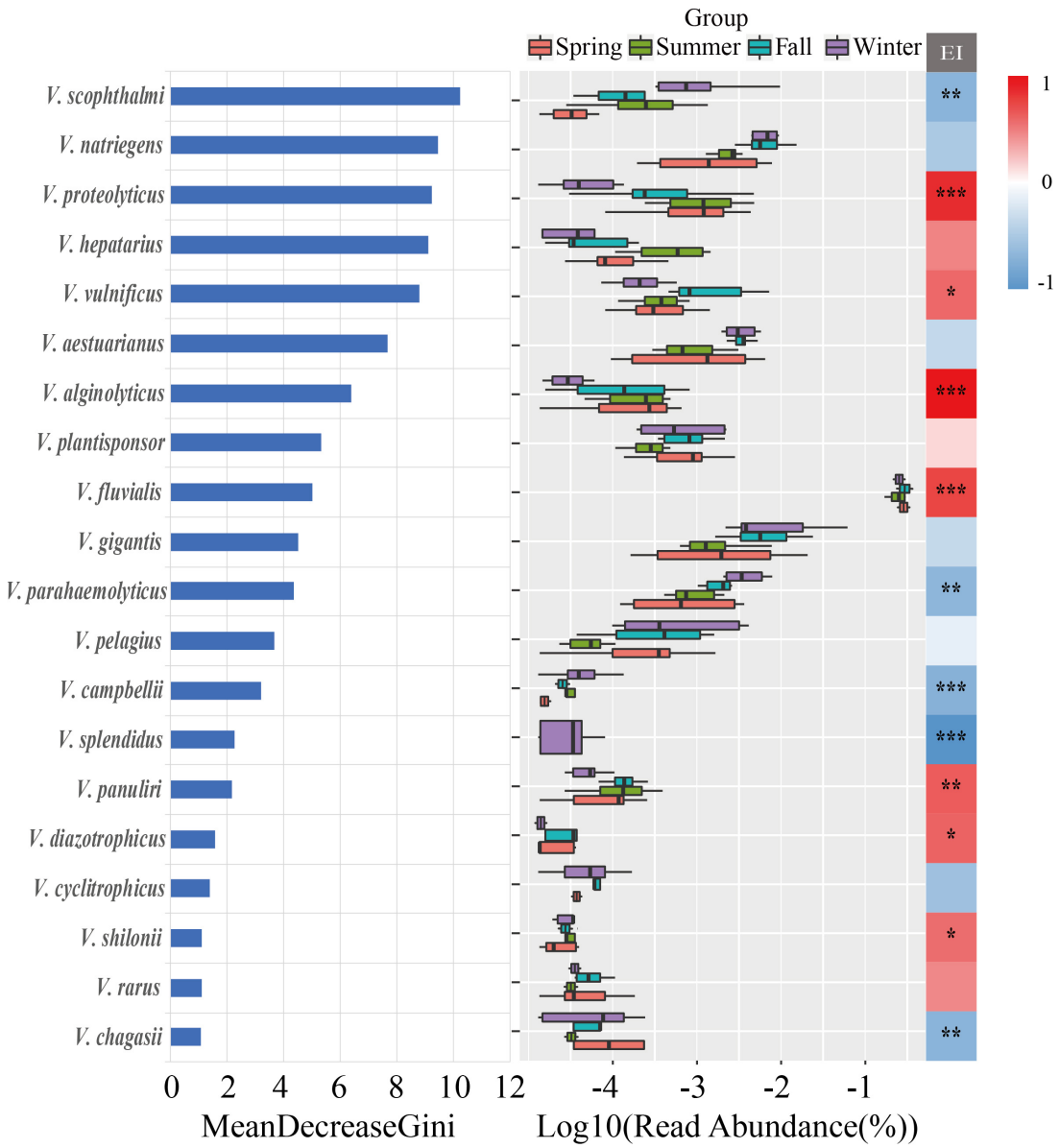

FIGURE 7 | The random forest analysis of the top 20 important *Vibrio* species, ranked by Gini index. Middle: ranked by the richness of the top 20 *Vibrio* species with boxplot. Right: the correlations between the abundances of top 20 *Vibrio* species and EI variable by Spearman correlation analysis. $^{*}p < 0.05$; $^{**}p < 0.01$; $^{***}p < 0.001$.

addition, previous studies have suggested that marine bacterial diversity increased with the input of human-derived pollution and nutrients, such as N, P, and C, which could contribute to the creation of favorable conditions for the proliferation of different microorganisms (Nogales et al., 2011; Numberger et al., 2019). Therefore, our results were consistent with these studies, indicating that nutrient variations may lead to the increase in *Vibrio* diversity in the Beibu Gulf.

We observed that the changes in the *Vibrio* community composition and diversity in relation to seasons were more likely to be a result of a direct influence of temperature, salinity, TDN, DIN, and TDP. Our findings confirmed that salinity was the most important environmental determinant of α-diversity in the *Vibrio* community as described in previous studies (Siboni et al., 2016; Wang et al., 2019), and observed a similar positive correlation (Spearman, $p < 0.001$). The Bray-Curtis dissimilarity of the *Vibrio* community was also significantly correlated with temperature in the Maowei sea (**Table 2** Mantel test, $p < 0.001$) providing further evidence that warmer seawater increased the dissimilarity of the *Vibrio* community (Liang et al., 2019). Except for the temperature and salinity, RDA and Mantel test analysis indicated that the roles of TDN and TDP were significantly positively correlated with the seasonal variation in the *Vibrio* community

(**Figure 4** and **Table 2**). Moreover, the regression analysis showed that *Vibrio* community dissimilarity was significantly increased with the variation in main environmental factors (TDN, TDP, salinity, and DO) (**Supplementary Figure 4**). The positive correlation between DO and *Vibrio* community dissimilarity demonstrated that the relative accumulation of dissolved oxygen in seawater enhanced the heterogeneity of the *Vibrio* community, which was consistent with previous studies (Liang et al., 2019; Wang et al., 2019). With these environmental factors becoming the main factors constraining the community composition, the pool of *Vibrio* species that would have been capable of surviving these high trophic conditions and able to outcompete and replace less adapted ones may have decreased. In this study, the VPA result also revealed that the effects of nutrients were stronger than those of water properties, indicating that the variations of nitrogen and phosphorus availably shaped and filtered the observed variations in the *Vibrio* community.

High concentrations of TDN, TDP, and DIN were closely related to the occurrence of eutrophication (Ko et al., 2019). Recently, the eutrophication in the Maowei sea could be attributed to land-based runoff and pollution produced by aquaculture in the area due to a lack of water exchange and large quantities of oyster excreta (Yang et al., 2019). Particularly in summer, the discharge from the Qinjiang River and Maoling River into the Maowei sea led to a high concentration of nutrients (Lai et al., 2014). Consequently, the input of the nutrients led to the *Vibrio* community showing the highest diversity in summer and significant seasonal variation. Besides, previous studies found that the *Vibrio* diversity was increased with nutritional levels, suggesting that *Vibrio* species could be considered as indicators of trophic conditions (Gregoracci et al., 2012; Mansergh and Zehr, 2014). In this study, we identified 12 *Vibrio* species such as *V. fluvialis*, *V. proteolyticus*, *V. alginolyticus*, and *V. splendidus* that had significant positive or negative relationships with the eutrophication (**Figure 7** and **Supplementary Figure 3**). For example, *V. fluvialis* has the capacity to utilize a wide range of organic and inorganic nutrients containing C, N, and P (such as L-arginine, L-arabinose, D-glucose, chitin, malonate, phosphate, and citrate) (Brenner et al., 1983). This strong capacity for nutrient utilization may cause increased population levels in these species with increased pollution levels. By contrast, *V. splendidus* is a pathogen associated with oysters (Vezzulli et al., 2015). The degradation and destruction of the host due to overfishing and eutrophication in the nearshore region may cause the loss of associated microbiomes. In summary, discovery of these indicative species may facilitate the assessment of a trophic shift and its subsequent ecological effects.

CONCLUSION

This study demonstrated that highly diverse *Vibrio* communities were present in the Maowei Sea with great temporal resolution. Additionally, our study observed that the variation in *Vibrio* diversity and community composition was mainly affected by changes of salinity, temperature, nitrogen, and phosphorus (TDN, TDP, and DIN). Several important *Vibrio* species, such as *V. splendidus*, *V. proteolyticus*, *V. fluvialis*, and *V. alginolyticus* were significantly correlated with trophic changes, which may be more sensitive to eutrophic status in coastal ecosystems. This investigation enhanced our understanding of the *Vibrio* seasonal distribution in response to environmental factors under eutrophication pressure and their ecological effects and public health in a subtropical inland bay.

DATA AVAILABILITY STATEMENT

The datasets presented in this study can be found in online repositories. The names of the repository/repositories and accession number(s) can be found below: https://www.ncbi.nlm.nih.gov/, PRJNA607420.

AUTHOR CONTRIBUTIONS

NL and HZ conceived and designed the experiments. XC performed the experiments and analyzed the data. XC, GJ, JT, QX, LH, SC, SZ, and KD wrote and helped increase the quality of this manuscript. All authors contributed to the article and approved the submitted version.

FUNDING

This study was financially supported by the following funding sources: Guangxi Natural Science Foundation (Nos. 2018GXNSFDA281006 and 2017GXNSFAA198081), the National Natural Science Foundation of China (No. 41966005), the National Research Foundation of Korea (No. 2018R1C1B6007755100), and the "One Hundred Talents" Project of Guangxi (No. 6020303891251).

SUPPLEMENTARY MATERIAL

The Supplementary Material for this article can be found online at: https://www.frontiersin.org/articles/10.3389/fmicb.2020.610974/full#supplementary-material

REFERENCES

Baddam, R., Sarker, N., Ahmed, D., Mazumder, R., Abdullah, A., Morshed, R., et al. (2020). Genome dynamics of *Vibrio cholerae* isolates linked to seasonal outbreaks of cholera in Dhaka, Bangladesh. *mBio* 11:e3339-19. doi: 10.1128/mBio.03339-19

Bolger, A. M., Lohse, M., and Usadel, B. (2014). Trimmomatic: a flexible trimmer for illumina sequence data. *Bioinformatics* 30, 2114–2120. doi: 10.1093/bioinformatics/btu170

Bolyen, E., Rideout, J. R., Dillon, M. R., Bokulich, N. A., Abnet, C. C., Al-Ghalith, G. A., et al. (2019). Reproducible, interactive, scalable and extensible microbiome data science using QIIME 2. *Nat. Biotechnol.* 37, 852–857. doi: 10.1038/s41587-019-0209-9

Boucher, Y., Orata, F. D., and Alam, M. (2015). The out-of-the-delta hypothesis: dense human populations in low-lying river deltas served as agents for the evolution of a deadly pathogen. *Front. Microbiol.* 6:1120. doi: 10.3389/fmicb.2015.01120

Brenner, D. J., Hickmanbrenner, F. W., Lee, J. V., Steigerwalt, A. G., Fanning, G. R., Hollis, D. G., et al. (1983). *Vibrio furnissii* (formerly aerogenic biogroup of *Vibrio fluvialis*), a new species isolated from human feces and the environment. *J. Clin. Microbiol.* 18, 816–824. doi: 10.1128/jcm.18.4.816-824.1983

Cai, Y., and Guo, L. (2009). Abundance and variation of colloidal organic phosphorus in riverine, estuarine, and coastal waters in the northern Gulf of Mexico. *Limnol. Oceanogr.* 54, 1393–1402. doi: 10.4319/lo.2009.54.4.1393

Chen, C., Chen, H., He, Y., and Xia, R. (2018). TBtools, a Toolkit for Biologists integrating various biological data handling tools with a user-friendly interface. *bioRxiv [Preprint]* doi: 10.1101/289660

Chen, X., Lao, Y., Wang, J., Du, J., Liang, M., and Yang, B. (2018). Submarine groundwater-borne nutrients in a tropical bay (Maowei Sea, China) and their impacts on the oyster aquaculture. *Geochem. Geophys. Geosyst.* 19, 932–951. doi: 10.1002/2017GC007330

Chen, C. W., Ju, Y.-R., Chen, C.-F., and Dong, C.-D. (2016). Evaluation of organic pollution and eutrophication status of Kaohsiung Harbor, Taiwan. *Int. Biodeterior. Biodegradation* 113, 318–324. doi: 10.1016/j.ibiod.2016.03.024

Cole, J. R., Wang, Q., Fish, J. A., Chai, B., McGarrell, D. M., Sun, Y., et al. (2014). Ribosomal database project: data and tools for high throughput rRNA analysis. *Nucleic Acids Res.* 42, D633–D642. doi: 10.1093/nar/gkt1244

Dixon, P. (2003). VEGAN, a package of R functions for community ecology. *J. Veg. Sci.* 14, 927–930. doi: 10.1111/j.1654-1103.2003.tb02228.x

Froelich, B., Gonzalez, R., Blackwood, D., Lauer, K., and Noble, R. (2019). Decadal monitoring reveals an increase in *Vibrio* spp. concentrations in the Neuse River Estuary, North Carolina, USA. *PLoS One* 14:e0215254. doi: 10.1371/journal.pone.0215254

Greenfield, D., Gooch Moore, J., Stewart, J., Hilborn, E., George, B., Li, Q., et al. (2017). Temporal and environmental factors driving *Vibrio vulnificus* and *V. parahaemolyticus* populations and their associations with harmful algal blooms in South Carolina detention ponds and receiving tidal creeks. *GeoHealth* 1, 306–317. doi: 10.1002/2017GH000094

Gregoracci, G. B., Nascimento, J. R., Cabral, A. S., Paranhos, R., Valentin, J. L., Thompson, C. C., et al. (2012). Structuring of bacterioplankton diversity in a large tropical bay. *PLoS One* 7:e31408. doi: 10.1371/journal.pone.0031408

Guin, S., Saravanan, M., Chowdhury, G., Pazhani, G. P., Ramamurthy, T., and Das, S. C. (2019). Pathogenic *Vibrio parahaemolyticus* indiarrhoeal patients, fish and aquatic environments and their potential for inter-source transmission. *Heliyon* 5:e01743. doi: 10.1016/j.heliyon.2019.e01743

Han, A., Dai, M., Kao, S.-J., Gan, J., Li, Q., Wang, L., et al. (2012). Nutrient dynamics and biological consumption in a large continental shelf system under the influence of both a river plume and coastal upwelling. *Limnol. Oceanogr.* 57, 486–502. doi: 10.4319/lo.2012.57.2.0486

Hartwick, M. A., Urquhart, E. A., Whistler, C. A., Cooper, V. S., Naumova, E. N., and Jones, S. H. (2019). Forecasting seasonal *Vibrio parahaemolyticus* concentrations in New England shellfish. *Int. J. Env. Res. Public Health* 16:4341. doi: 10.3390/ijerph16224341

Holm-Hansen, O., and Riemann, B. (1978). Chlorophyll a determination: improvements in methodology. *Oikos* 30, 438–447. doi: 10.2307/3543338

hun Yoon, S., and Waters, C. M. (2019). Vibrio cholerae. *Trends Microbiol.* 27, 806–807.

King, M., Rose, L., Fraimow, H., Nagori, M., Danish, M., and Doktor, K. (2019). *Vibrio vulnificus* infections from a previously Nonendemic Area. *Ann. Intern. Med.* 171, 520–521. doi: 10.7326/L19-0133

Ko, S.-R., Srivastava, A., Lee, N., Jin, L., Oh, H.-M., and Ahn, C.-Y. (2019). Bioremediation of eutrophic water and control of cyanobacterial bloom by attached periphyton. *Int. J. Environ. Sci. Technol.* 16, 4173–4180. doi: 10.1007/s13762-019-02320-8

Kopprio, G. A., Streitenberger, M. E., Okuno, K., Baldini, M., Biancalana, F., Fricke, A., et al. (2017). Biogeochemical and hydrological drivers of the dynamics of *Vibrio* species in two Patagonian estuaries. *Sci. Total Environ.* 579, 646–656.

Lai, J., Jiang, F., Ke, K., Xu, M., Lei, F., and Chen, B. (2014). Nutrients distribution and trophic status assessment in the northern Beibu Gulf, China. *Chin. J. Oceanol. Limnol.* 32, 1128–1144. doi: 10.1007/s00343-015-4289-1

Lamon, S., Consolati, S. G., Fois, F., Cambula, M. G., Pes, M., Porcheddu, G., et al. (2019). Occurrence, seasonal distribution, and molecular characterization of *Vibrio vulnificus*, *Vibrio cholerae*, and *Vibrio parahaemolyticus* in Shellfish (Mytilus galloprovincialis and ruditapes decussatus) collected in Sardinia (Italy). *J. Food Prot.* 82, 1851–1856. doi: 10.4315/0362-028x.jfp-19-021

Le Roux, F., Goubet, A., Thompson, F., Faury, N., Gay, M., Swings, J., et al. (2005). *Vibrio gigantis* sp. nov., isolated from the haemolymph of cultured oysters (*Crassostrea gigas*). *Int. J. Syst. Evol. Microbiol.* 55, 2251–2255. doi: 10.1099/ijs.0.63666-0

Liang, J., Liu, J., Wang, X., Lin, H., Liu, J., Zhou, S., et al. (2019). Spatiotemporal dynamics of free-living and particle-associated *Vibrio* communities in the northern Chinese marginal seas. *Appl. Environ. Microbiol.* 85, e00217–e00219.

López-Hernández, K. M., Pardío-Sedas, V. T., Lizárraga-Partida, L., Williams, J. D. J., Martínez-Herrera, D., Flores-Primo, A., et al. (2015). Environmental parameters influence on the dynamics of total and pathogenic *Vibrio parahaemolyticus* densities in *Crassostrea virginica* harvested from Mexico's Gulf coast. *Mar. Pollut. Bull.* 91, 317–329.

Mansergh, S., and Zehr, J. (2014). *Vibrio* diversity and dynamics in the monterey bay upwelling region. *Front. Microbiol.* 5:48. doi: 10.3389/fmicb.2014.00048

Martin, M. (2011). Cutadapt removes adapter sequences from high-throughput sequencing reads. *EMBnet J.* 17, 10–12. doi: https://doi.org/10.14806/ej.17.1.200

Martin, Y., and Bonnefont, J. (1990). Annual variations and identification of Vibrios growing at 37 degrees C in urban sewage, in mussels and in seawater at Toulon harbour (Mediterranean, France). *Can. J. Microbiol.* 36, 47–52. doi: 10.1139/m90-008

Nogales, B., Lanfranconi, M. P., Piña-Villalonga, J. M., and Bosch, R. (2011). Anthropogenic perturbations in marine microbial communities. *FEMS Microbiol. Rev.* 35, 275–298. doi: 10.1111/j.1574-6976.2010.00248.x

Numberger, D., Ganzert, L., Zoccarato, L., Mühldorfer, K., Sauer, S., Grossart, H.-P., et al. (2019). Characterization of bacterial communities in wastewater with enhanced taxonomic resolution by full-length 16S rRNA sequencing. *Sci. Rep.* 9:9673. doi: 10.1038/s41598-019-46015-z

Oliver, J. D. (2016). The viable but nonculturable state for bacteria: status update. *Microbe* 11, 159–164. doi: 10.1128/microbe.11.159.1

R Core Team (2013). *R: A Language and Environment for Statistical Computing*. Vienna: R Core Team.

Ramamurthy, T., Chowdhury, G., Pazhani, G. P., and Shinoda, S. (2014). *Vibrio fluvialis*: an emerging human pathogen. *Front. Microbiol.* 5:91. doi: 10.3389/fmicb.2014.00091

Rognes, T., Flouri, T., Nichols, B., Quince, C., and Mahé, F. (2016). VSEARCH: a versatile open source tool for metagenomics. *PeerJ* 4;e2584. doi: 10.7717/peerj.2584

Sah, R. (1994). Nitrate-nitrogen determination—a critical review. *Commun. Soil Sci. Plant Anal.* 25, 2841–2869. doi: 10.1080/00103629409369230

Shelford, E. J., and Suttle, C. A. (2018). Virus-mediated transfer of nitrogen from heterotrophic bacteria to phytoplankton. *Biogeosciences* 15, 809–819. doi: 10.5194/bg-15-809-2018

Shore-Maggio, A., Aeby, G., and Callahan, S. (2018). Influence of salinity and sedimentation on *Vibrio* infection of the Hawaiian coral Montipora capitata. *Dis. Aquat. Org.* 128, 63–71. doi: 10.3354/dao03213

Siboni, N., Balaraju, V., Carney, R., Labbate, M., and Seymour, J. R. (2016). Spatiotemporal dynamics of *Vibrio* spp. within the Sydney Harbour estuary. *Front. Microbiol.* 7:460. doi: 10.3389/fmicb.2016.00460

Subtype, H.-G. H., and Sloan, M. (2018). *Lesions were Morphologically Different or had Differing Gene Mutation Status were Considered Separate Histologies (7). Data were Compared using the Pearson chi-Squared test with SPSS Statistics v24. 0*. Endicott, NY: IBM Corporation.

Takemura, A. F., Chien, D. M., and Polz, M. F. (2014). Associations and dynamics of *Vibrionaceae* in the environment, from the genus to the population level. *Front. Microbiol.* 5:38. doi: 10.3389/fmicb.2014.00038

Thompson, J. R., Randa, M. A., Marcelino, L. A., Tomita-Mitchell, A., Lim, E., and Polz, M. F. (2004). Diversity and dynamics of a North Atlantic coastal *Vibrio* community. *Appl. Environ. Microbiol.* 70, 4103–4110. doi: 10.1128/AEM.70.7.4103-4110.2004

Vezzulli, L., Grande, C., Reid, P. C., Hélaouët, P., Edwards, M., Höfle, M. G., et al. (2016). Climate influence on *Vibrio* and associated human diseases during the past half-century in the coastal North Atlantic. *Proc. Natl. Acad. Sci. U.S.A.* 113, E5062–E5071. doi: 10.1073/pnas.1609157113

Urquhart, E. A., Jones, S. H., Jong, W. Y., Schuster, B. M., Marcinkiewicz, A. L., Whistler, C. A., et al. (2016). Environmental conditions associated with elevated Vibrio parahaemolyticus concentrations in Great Bay Estuary, New Hampshire. *PloS one* 11:e0155018. doi: 10.1371/journal.pone.0155018

Vezzulli, L., Pezzati, E., Stauder, M., Stagnaro, L., Venier, P., and Pruzzo, C. (2015). Aquatic ecology of the oyster pathogens *Vibrio splendidus* and *Vibrio aestuarianus*. *Environ. Microbiol.* 17, 1065–1080. doi: 10.1111/1462-2920.12484

Visco, G., Campanella, L., and Nobili, V. (2005). Organic carbons and TOC in waters: an overview of the international norm for its measurements. *Microchem. J.* 79, 185–191. doi: 10.1016/j.microc.2004.10.018

Wang, X., Liu, J., Li, B., Liang, J., Sun, H., Zhou, S., et al. (2019). Spatial heterogeneity of *Vibrio spp*. in sediments of Chinese marginal seas. *Appl. Environ. Microbiol.* 85:e3064-18. doi: 10.1128/aem.03064-18

Westrich, J. R. (2015). *Consilience of iron in the ecology of Vibrio bacteria*. Athens, GA: UGA.

Yang, B., Zhou, J.-B., Lu, D.-L., Dan, S. F., Zhang, D., Lan, W.-L., et al. (2019). Phosphorus chemical speciation and seasonal variations in surface sediments of the Maowei Sea, northern Beibu Gulf. *Mar. Pollut. Bull.* 141, 61–69. doi: 10.1016/j.marpolbul.2019.02.023

Yao, P., Zhao, B., Bianchi, T. S., Guo, Z., Zhao, M., Li, D., et al. (2014). Remineralization of sedimentary organic carbon in mud deposits of the Changjiang Estuary and adjacent shelf: implications for carbon preservation and authigenic mineral formation. *Cont. Shelf Res.* 91, 1–11. doi: 10.1016/j.csr.2014.08.010

Zhang, R., Kelly, R. L., Kauffman, K. M., Reid, A. K., Lauderdale, J. M., Follows, M. J., et al. (2019). Growth of marine *Vibrio* in oligotrophic environments is not stimulated by the addition of inorganic iron. *Earth Planet. Sci. Lett.* 516, 148–155. doi: 10.1016/j.epsl.2019.04.002

Zhang, X., Lin, H., Wang, X., and Austin, B. (2018). Significance of *Vibrio* species in the marine organic carbon cycle—A review. *Sci. China Earth Sci.* 61, 1357–1368. doi: 10.1007/s11430-017-9229-x

Zheng, Q., Zhang, R., Wang, Y., Pan, X., Tang, J., and Zhang, G. (2012). Occurrence and distribution of antibiotics in the Beibu Gulf, China: impacts of river discharge and aquaculture activities. *Mar. Environ. Res.* 78, 26–33.

Zhu, J., Zhang, Q., Li, Y., Tan, S., Kang, Z., Yu, X., et al. (2019). Microplastic pollution in the Maowei Sea, a typical mariculture bay of China. *Sci. Total Environ.* 658, 62–68. doi: 10.1016/j.scitotenv.2018.12.192

Conflict of Interest: The authors declare that the research was conducted in the absence of any commercial or financial relationships that could be construed as a potential conflict of interest.

frontiers in Microbiology

ORIGINAL RESEARCH
published: 15 December 2020
doi: 10.3389/fmicb.2020.608506

Delivering Beneficial Microorganisms for Corals: Rotifers as Carriers of Probiotic Bacteria

Juliana M. Assis[1], Fernanda Abreu[2], Helena M. D. Villela[1], Adam Barno[1], Rafael F. Valle[3], Rayssa Vieira[3], Igor Taveira[2], Gustavo Duarte[1,3], David G. Bourne[4,5], Lone Høj[4] and Raquel S. Peixoto[1,3]**

[1] Laboratory of Molecular Microbial Ecology, Institute of Microbiology Paulo de Góes, Universidade Federal do Rio de Janeiro, Rio de Janeiro, Brazil, [2] Laboratory of Cellular Biology and Magnetotaxis, Institute of Microbiology Paulo de Góes, Universidade Federal do Rio de Janeiro, Rio de Janeiro, Brazil, [3] IMAM-AquaRio – Rio de Janeiro Aquarium Research Center, Rio de Janeiro, Brazil, [4] Australian Institute of Marine Science, Townsville, WA, Australia, [5] College of Science and Engineering, James Cook University, Townsville, QLD, Australia

OPEN ACCESS

Edited by:
Rodrigo Taketani,
Centro de Tecnologia Mineral, Brazil

Reviewed by:
Gabriel Vinderola,
Facultad de Ingeniería Química,
Universidad Nacional del Litoral
(FIQ-UNL), Argentina
Danilo Tosta Souza,
University of São Paulo, Brazil

***Correspondence:**
Raquel S. Peixoto
raquelpeixoto@micro.ufrj.br
Fernanda Abreu
fernandaabreu@micro.ufrj.br

Specialty section:
This article was submitted to
Aquatic Microbiology,
a section of the journal
Frontiers in Microbiology

Received: 21 September 2020
Accepted: 25 November 2020
Published: 15 December 2020

Citation:
Assis JM, Abreu F, Villela HMD,
Barno A, Valle RF, Vieira R, Taveira I,
Duarte G, Bourne DG, Høj L and
Peixoto RS (2020) Delivering
Beneficial Microorganisms for Corals:
Rotifers as Carriers of Probiotic
Bacteria. Front. Microbiol. 11:608506.
doi: 10.3389/fmicb.2020.608506

The use of Beneficial Microorganisms for Corals (BMCs) to increase the resistance of corals to environmental stress has proven to be effective in laboratory trials. Because direct inoculation of BMCs in larger tanks or in the field can be challenging, a delivery mechanism is needed for efficient transmission of the BMC consortium. Packaged delivery mechanisms have been successfully used to transmit probiotics to other organisms, including humans, lobsters, and fish. Here, we tested a method for utilizing rotifers of the species *Brachionus plicatilis* for delivery of BMCs to corals of the species *Pocillopora damicornis*. Epifluorescence microscopy combined with a live/dead cell staining assay was used to evaluate the viability of the BMCs and monitor their *in vivo* uptake by the rotifers. The rotifers efficiently ingested BMCs, which accumulated in the digestive system and on the body surface after 10 min of interaction. Scanning electron microscopy confirmed the adherence of BMCs to the rotifer surfaces. BMC-enriched rotifers were actively ingested by *P. damicornis* corals, indicating that this is a promising technique for administering coral probiotics *in situ*. Studies to track the delivery of probiotics through carriers such as *B. plicatilis,* and the provision or establishment of beneficial traits in corals are the next proof-of-concept research priorities.

Keywords: Beneficial Microorganisms for Corals (BMCs), rotifers, marine probiotics, *Brachionus plicatilis*, *Pocillopora damicornis*, delivery, coral reefs, microscopy

INTRODUCTION

Coral reefs are increasingly impacted by global climate change, which raises the mean sea surface temperature (SST) and the incidence of marine heatwaves (Hughes et al., 2018). Due to increases in the duration and intensity of these thermal stress events, higher rates of coral mortality have been reported globally (Pandolfi et al., 2011; Duarte et al., 2020). Efforts to mitigate the negative effects of global changes on coral reefs have led to the implementation of different strategies in conservation studies. A report published by the United States National Academies of Sciences, Engineering, and Medicine listed several methods of intervention that are currently being

studied and developed to increase coral resistance and resilience (National Academies of Sciences and Medicine, 2019). One promising approach is the manipulation of different coral-associated microbes to increase host resistance and resilience to stressors (Peixoto et al., 2017; National Academies of Sciences and Medicine, 2019). This strategy relies on key host–microbiome symbiotic relationships that can be exploited to increase the fitness of the coral holobiont (Peixoto et al., 2017; Pita et al., 2018; Wilkins et al., 2019). Coral-associated bacteria have been shown to fix nitrogen, degrade polysaccharides, and produce antimicrobial compounds that can inhibit pathogen growth (reviewed by Peixoto et al., 2017). Although the ecological relationships, taxonomic composition, and metabolic pathways of microbial communities associated with corals have been determined (Rohwer et al., 2001; Bourne and Munn, 2005; Sánchez-Quinto and Falcón, 2019), the selection and use of specific microorganisms as probiotics for corals on an ecologically relevant scale is a relatively new field of research (Teplitski and Ritchie, 2009; Santos et al., 2015; Peixoto et al., 2017; Damjanovic et al., 2019; Rosado et al., 2019).

Selection and manipulation of specific members of the resident coral microbiome to mitigate the effects ofthermal stress on the animal health was proposed by Peixoto et al. (2017). The coral-associated bacteria are chosen as beneficial microorganisms involved in the protection, health maintenance, and growth of corals (Rosado et al., 2019). Administering Beneficial Microorganisms for Corals (BMCs) has helped to increase coral resistance against different threats, such as oil contamination, disease, and thermal stress (Santos et al., 2015; Rosado et al., 2019). In these proof-of-concept experiments, a consortium containing BMCs was concentrated and applied directly to corals and the surrounding water, without a biological carrier system (Rosado et al., 2019). Although possible delivery systems have been proposed for closed- and open-water systems (see Peixoto et al., 2017), there is still a lack of studies on potential effective strategies for BMC delivery to corals in aquarium or field settings.

In humans, probiotic foods and beverages are common ways to deliver *Lactobacillus* species (Roobab et al., 2020) and other beneficial bacteria to improve health (Dunne et al., 1999; Casas and Dobrogosz, 2000; Stolzenbach et al., 2020). Likewise, small organisms such as brine shrimp (*Artemia*), rotifers, and copepods can be used as vectors for transmitting probiotic bacteria to larger animals in aquaculture, such as fish (Planas et al., 2005, 2006; Sun et al., 2013; Hai, 2015), prawns (Hai et al., 2010), and lobsters (Daniels et al., 2013). Here, we evaluated the potential of the rotifer *Brachionus plicatilis* (**Figure 1** and **Supplementary Figure 1**) as a vector for delivering BMCs into corals by feeding the rotifers with a previously validated BMC consortium assembled by Rosado et al. (2019), and tracking the uptake of rotifers by the coral *Pocillopora damicornis*.

MATERIALS AND METHODS

The steps described in the next topics are summarized in the flowchart shown in **Figure 1**.

Rotifer and Coral Cultures

Brachionus plicatilis rotifers and *P. damicornis* nubbins were cultured at the Rio de Janeiro Marine Aquarium Research Center (AquaRio). Rotifers were cultured in natural seawater, at a temperature of 25°C, salinity of 3.2%, in the dark. Water circulation and oxygenation were produced by bubbling air with an air pump. Using standard culture conditions, rotifers were fed daily with 100 mL of a culture of the alga *Tetraselmis gracilis* containing 10^6 cells mL^{-1}. Conversely, before starting the experiment, rotifers were transferred to 1 L containers with oxygenation produced by bubbling air with an air pump. The container was kept in the dark to avoid the growth of photosynthetic organisms. Rotifers were kept under starvation by culturing them in 0.22-μm daily filtered seawater, for a 7-day period.

Corals were kept in tanks containing 100L of seawater at 25°C, salinity of 3.2%, light intensity of 200 μmol m^{-2} s^{-1}, and water recirculation by circulation pumps. Twenty percent of the water in the coral tank system was exchanged every 7 days. Corals were fed daily with 100 mL of a culture containing 200 rotifers mL^{-1} under standard culture conditions (i.e., not starved).

BMC Uptake by Rotifers

The seven strains of bacteria used in the experiment were isolated by Rosado et al. (2019) and stored in the microbial collection of the Microbial Molecular Ecology Lab (MMEL), UFRJ, Rio de Janeiro, Brazil. This consortium was composed of five strains of *Pseudoalteromonas* spp., isolated from *P. damicornis*; plus one strain of *Cobetia marina* and one strain of *Halomonas taeanensis*, isolated from the artificial seawater surrounding *P. damicornis*. The accession numbers of each isolate and their classifications according to their 16S rRNA gene sequences are provided in **Supplementary Table 1**.

Localization of the BMC Consortium Associated With Rotifers

To prepare the BMC consortium assembled by Rosado et al. (2019), individual BMC strains were first grown in Marine Agar (MA) medium to evaluate purity. Sterile inoculation loops were used to pick single bacterial colonies of each strain from the MA plates, and the cells were inoculated into 5 mL of Marine Broth (MB) medium. Cultures were grown overnight at 26°C, and 1% (v/v) of each strain was individually inoculated into 100 mL of MB medium in a 250-mL culture flask and incubated at 26°C with agitation of 100 rpm until each culture reached 10^7 cells mL^{-1}. The cells were collected by centrifugation at 12,000 × *g* for 5 min at 4°C and washed twice under the same conditions with sterile saline (2.5% w/v NaCl) to remove the culture medium. All cells from each culture were homogenized together, resuspended in a final volume of 40 mL of saline solution (2.5% w/v NaCl), and stored at 4°C until used in the experiment, which occurred on the same day of the preparation of the cells.

Fluorescence and differential interference contrast (DIC) images were obtained with a Zeiss Axio Imager D2 microscope (Zeiss, Germany). Fluorescence filters used were: (i) Filter set 10 (excitation: BP 332 450–490 nm; beam splitter: FT 510 nm;

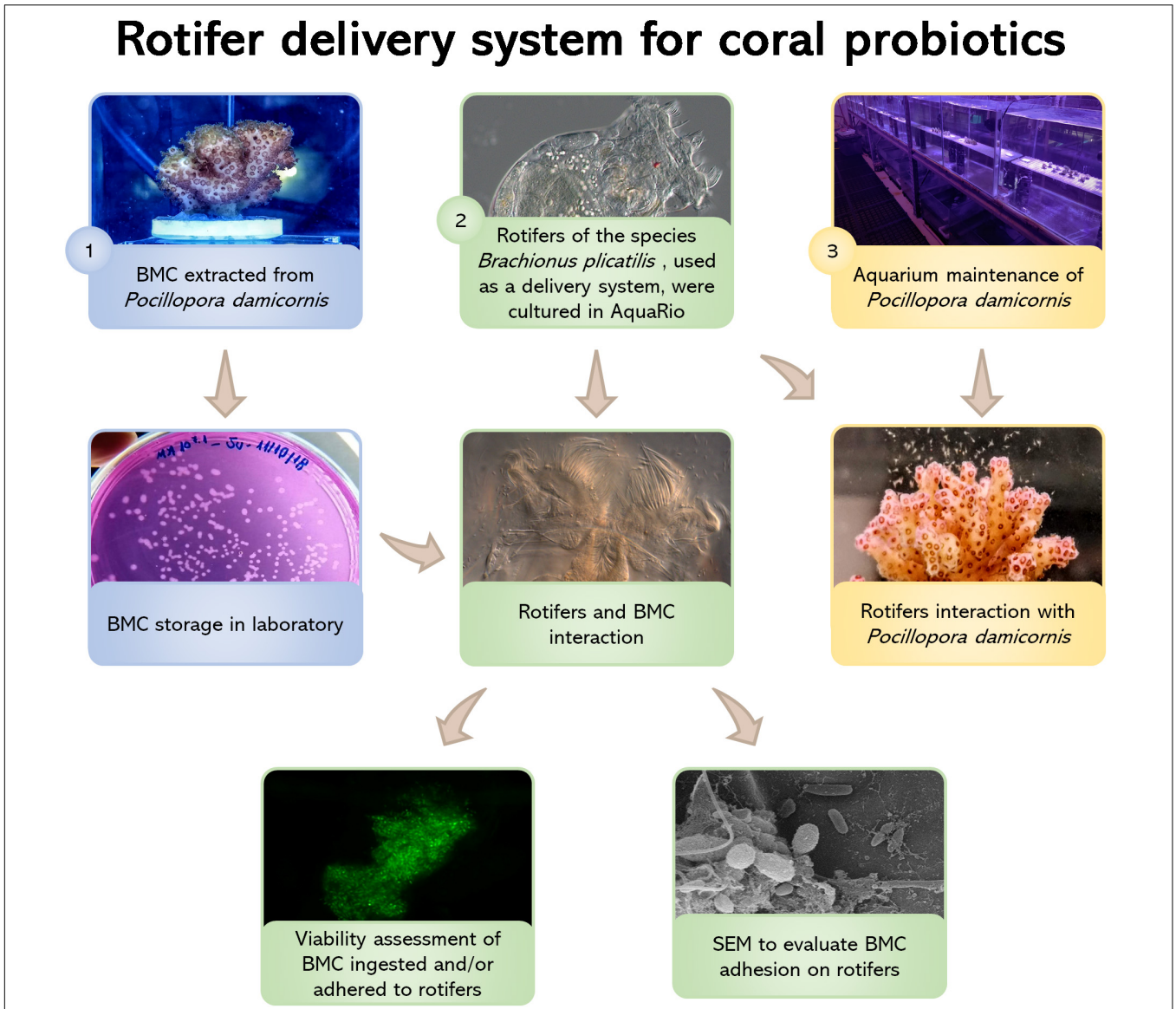

FIGURE 1 | Flowchart showing all treatment steps: (1) BMC strains were isolated from the coral *Pocillopora damicornis* by Rosado et al. (2019) and deposited in the microbial collection of the Microbial Molecular Ecology Laboratory (MMEL), UFRJ, Rio de Janeiro, Brazil; (2) Rotifers *Brachionus plicatilis* were cultured at the Rio de Janeiro Marine Aquarium Research Center (AquaRio) and incubated with the BMCs from the MMEL collection. Two different methods were used to assess rotifer-BMC interactions: fluorescence microscopy (using the LIVE/DEAD *Bac*Light™ Bacterial Viability Kit) and scanning electron microscopy (SEM); (3) Nubbins of *P. damicornis* were cultured at AquaRio and transferred to aquarium for the interaction experiment with rotifers *B. plicatilis*. Video and still images of the polyps capturing the rotifers show that the corals were able to take up the rotifers.

emission: LP 515 nm); and (ii) Filter set 00 (excitation: BP 546/12; beam splitter: FT 560; emission: BP 575–640 nm).

Based on initial trials, rotifers were starved for 7 days before use in experiments, to limit their autofluorescence by food ingestion. The viability of the rotifers after 7 days of starvation was determined by observing their mobility and cilia beating, using DIC microscopy. The LIVE/DEAD™ Bacterial Viability Kit (Thermo-Fisher Scientific, United States) was used to stain BMCs, following the manufacturer's protocol. BMCs were washed in sterile seawater to remove excess stain prior to delivery to the rotifers. For BMC-rotifer interactions, the stained BMC homogenized consortium (100 μL of a suspension containing approximately 10^7cells) was inoculated into a 2-mL polypropylene tube containing 900 μL of seawater and a concentration of 70 rotifers mL^{-1}. Promptly after inoculation (around 10 min), a 20-μL aliquot of BMC-rotifer suspension was mounted on a glass slide, alongside a control with unstained bacteria, and both preparations were observed by means of fluorescence microscopy.

The interactions between rotifers and BMCs were also observed using scanning electron microscopy (SEM). Images were produced from two periods: 4 and 16 h following incubation

of the BMC consortium and the rotifer cultures. Starved rotifers without BMC inoculation were used as a control treatment, and performed in parallel with the rotifer-BMC interaction treatments. BEEM-modified capsules (pre-shaped polyethylene molds with hinged lids) with a 100-μm polyester mesh filter were used to initiate the sample treatment procedure for SEM. The rotifers were fixed in 2.5% glutaraldehyde and 0.1 M sodium cacodylate buffer for 1 h and then washed three times with 0.1 M sodium cacodylate buffer solution and sterile seawater. Samples were post-fixed using 1% osmium tetroxide for 1 h at room temperature and washed three times with 0.1 M sodium cacodylate buffer solution and sterile seawater. A series of dehydration washes were performed in ethanol (30, 50, 70, 90, and 100% concentration) for 10 min each, with the final 100% ethanol step repeated three times. Samples were CO_2 critical-point dried, metallized with gold, and observed in an EVO MA10 scanning electron microscope (Zeiss, Germany) with a voltage between 1 and 30 kV.

Coral Uptake of BMC-Enriched Rotifers

To monitor uptake of rotifers by corals, one nubbin of *P. damicornis* was transferred to a 1-L aquarium containing 0.22 μm filtered natural seawater at 25°C, salinity of 3.2%, and a magnetic stirrer to circulate the water. To normalize the concentration of rotifers/mL, the culture was filtered using 100 μM, and reinoculated in 50mL of 0.22 μm filtered natural seawater. The concentration of rotifers was calculated by counting the number of rotifers in 3 × 1 mL replicates of water samples from the previously concentrated samples, using a stereomicroscope (Digilab Zoom binocular stereomicroscope, Brazil). Appropriate dilutions were performed to achieve the desired final concentration of 200 rotifers mL^{-1}. Before added to the coral aquarium, 100 mL of the culture, containing ∼20,000 rotifers, was washed twice in 0.22-μm filtered seawater to clean the maximum of autofluorescence particles that could interfere with the results. Also, the 10-cm coral nubbin acclimatized in the aquarium for 20 min before the rotifers were inoculated. Video and still images to search for *in vivo* evidence of rotifer uptake by the corals were taken with a USB digital microscope (Digital USB Microscope, Alloet, China).

RESULTS

Brachionus plicatilis rotifers cultured under standard conditions (natural unfiltered seawater, at 25°C, salinity of 3.2%) and fed the alga *Tetraselmis gracilis* displayed autofluorescence signals due to uptake of the algae, which contain photosynthetic pigments that are naturally fluorescent (**Figures 2A–C**). After 7 days of starvation in 0.22-μm filtered seawater, the rotifers displayed no signs of autofluorescence as confirmed by epifluorescence microscopy (**Figures 2D–F**).

The LIVE/DEAD bacterial assay was used to demonstrate that the members of the BMC consortium, containing five strains of *Pseudoalteromonas* spp., one of *C. marina*, and one of *H. taeanensis* (**Supplementary Table 1**), were viable prior to addition to the rotifer cultures (**Figure 3**). Using the same staining assay, the uptake of fluorescently stained BMCs by

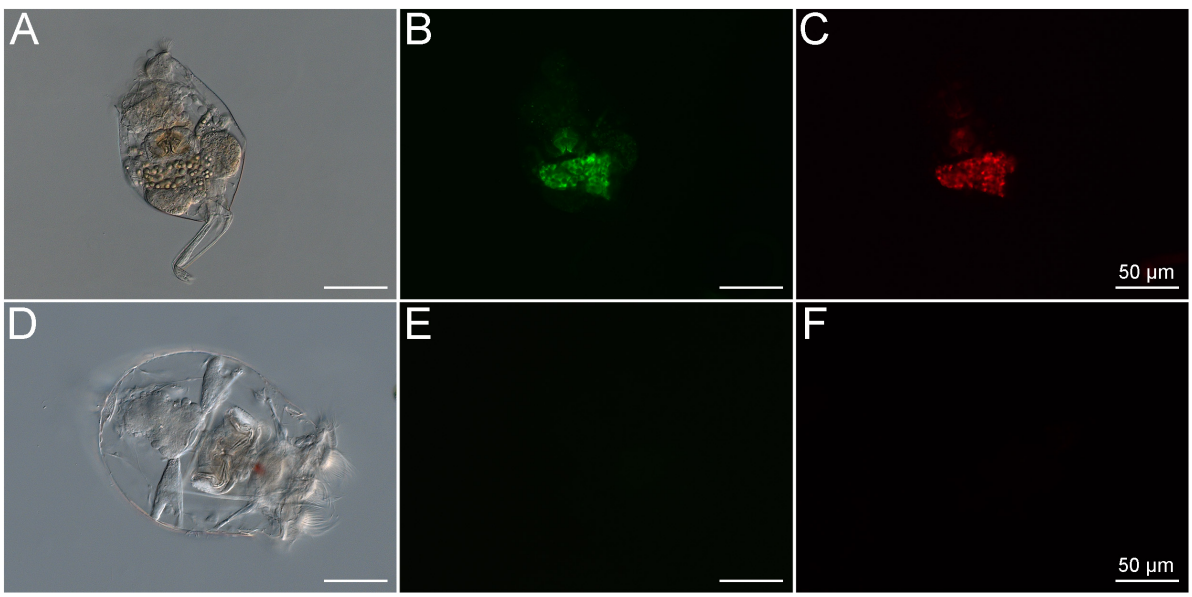

FIGURE 2 | *Brachionus plicatilis* in standard culture conditions observed in differential interference contrast (DIC) **(A)** and fluorescence microscopy, using the Filter set 10 (Zeiss, Germany) **(B)** and the Filter set 00 (Zeiss, Germany) **(C)**. Note that the internal structures of the rotifer show high autofluorescence signals at the same wavelength as both stains used in the LIVE/DEAD™ BacLight™ Bacterial Viability Kit. This shows that the rotifers take up microbes containing pigments with autofluorescence, probably photosynthetic microorganisms. *B. plicatilis* cultured after fasting, observed in differential interference contrast (DIC) **(D)** and fluorescence microscopy using the GFP filter **(E)** and the Rhodamine filter **(F)**. Note the absence of autofluorescence after starvation. This shows that the starvation period was crucial for the success of the experiment.

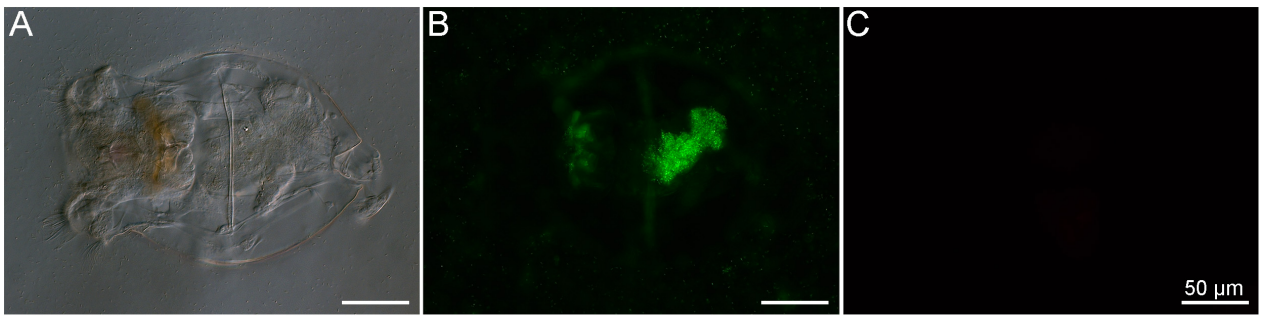

FIGURE 3 | *Brachionus plicatilis* after incubation with the BMC consortium previously stained with the LIVE/DEAD™ BacLight™ Bacterial Viability Kit observed in differential interference contrast (DIC) **(A)** and fluorescence microscopy, using the Filter set 10 (Zeiss, Germany) **(B)** and the Filter set 00 (Zeiss, Germany) **(C)**. Using this kit, viable bacteria cells stain in green while dead cells stain in red. Note that the rotifer ingested a large number of viable bacterial cells (stained in green), resulting in accumulation of stained cells in the stomach and intestine. Bacterial cells also accumulated on the surface of the rotifer, suggesting another possible means of transport of BMC cells.

starved rotifers was observed, using fluorescence microscopy. Large numbers of bacterial cells were ingested within a few minutes after the BMC consortium was inoculated into the rotifer culture (**Supplementary Video 1**). In parallel, we were able to follow the pathway of BMCs into the rotifer digestive system *in vivo*, by observing the accumulation of fluorescence in their digestive tract. In addition, we observed strong fluorescence on the external surface of the rotifer body, likely due to the presence of stained BMCs on these surfaces (**Figure 3**).

Controls (starved, non-BMC-inoculated rotifers) can be visualized with under SEM and show no bacteria interacting with rotifers (**Figures 4A,B**). Contrarily, SEM revealed the presence of bacteria attached to the corona cilia and rotifer surface after 4 h of interaction (**Figures 4C,D**); after 16 h, bacteria were also observed on the body surface (**Figure 4E**) and corona cilia (**Figure 4F**).

Finally, rotifers fed with BMCs were added to an aquarium containing nubbins of *P. damicornis*. Using the digital microscope, polyps were seen capturing and ingesting the rotifers containing BMCs (**Figure 5** and **Supplementary Video 2**).

DISCUSSION

Rotifers are commonly used in aquaculture settings to feed fish and shrimp larvae because they are easy to grow, and, through diet supplementation, they can deliver essential nutrients (Lubzens et al., 1989). *Brachionus plicatilis* has been widely used for these purposes because of its indiscriminate feeding behavior (Watanabe et al., 1983; Costa et al., 2016) and tolerance to a wide range of salinity levels, making it an ideal organism for transitioning between culture settings and field applications (Lowe et al., 2005).

In this study, we aimed to alter the internal microbiome of *B. plicatilis* to use this species of rotifer as a possible vector for delivery of specific beneficial bacteria to corals. Previous studies have shown that rotifers are hosts to several symbiotic bacteria, but gnotobiotic rotifers are relatively easy to obtain by changing the composition of their diet (Tinh et al., 2006; Qi et al., 2009). Additionally, it has been shown that *Lactobacillus* probiotic treatment, delivered by rotifers, positively affected growth, survival, and resistance of western white shrimp in aquaculture (Najmi et al., 2018). Here, we show that the BMC strains isolated from corals seemed to accumulate inside and outside the rotifers body in a stable way, suggesting that rotifers are also a promising vector to deliver probiotics for corals. However, further studies need to be performed to elucidate the viability of the bacteria delivered by the rotifers in the coral body. By optimizing this rotifers-based delivery system and selecting BMC strains with potential to face specific threats, we hope to be able to increase coral resistance against adverse stress conditions, such as ocean warming, diseases, and toxic compounds.

A high proportion of the inoculated BMC consortium likely remained viable throughout the duration of the experiments. The BMC consortium was live/dead-stained prior to inoculation into the rotifer culture, to avoid staining non-BMC bacteria associated with the native rotifers. This confirmed the viability of the BMC bacteria prior to inoculation, although we were unable to determine the viability of BMCs within the rotifers after the uptake. The ingestion rate of the rotifers is indirectly related to digestion and nutrient assimilation rates (Salt, 1987). The 7-day starvation period followed by the high availability of BMC cells potentially increased the rate of bacterial ingestion by the rotifers, and, in parallel, decreased the digestion and assimilation rates (Salt, 1987), thereby prolonging the survival of ingested BMCs.

The bacteria selected to be part of the BMC consortium consisted of five strains of *Pseudoalteromonas* spp., one of *C. marina*, and one of *H. taeanensis*, that, as a consortium, have been used to mitigate the harmful effects of the coral pathogen *Vibrio coralliilyticus* in a high-temperature stress scenario (Rosado et al., 2019). Strains of *Pseudoalteromonas* species have been commonly observed adhering to the surfaces of eukaryotic cells (Holmström and Kjelleberg, 1999; Thomas et al., 2008; Goulden et al., 2013). For example, a probiotic strain of *Pseudoalteromonas* selectively attached to external surfaces of both the vector organism *Artemia* and lobster larvae, when introduced as part of a probiotic mixture (Goulden et al., 2013). Here, a strong fluorescent signal consistent with stained bacteria was observed

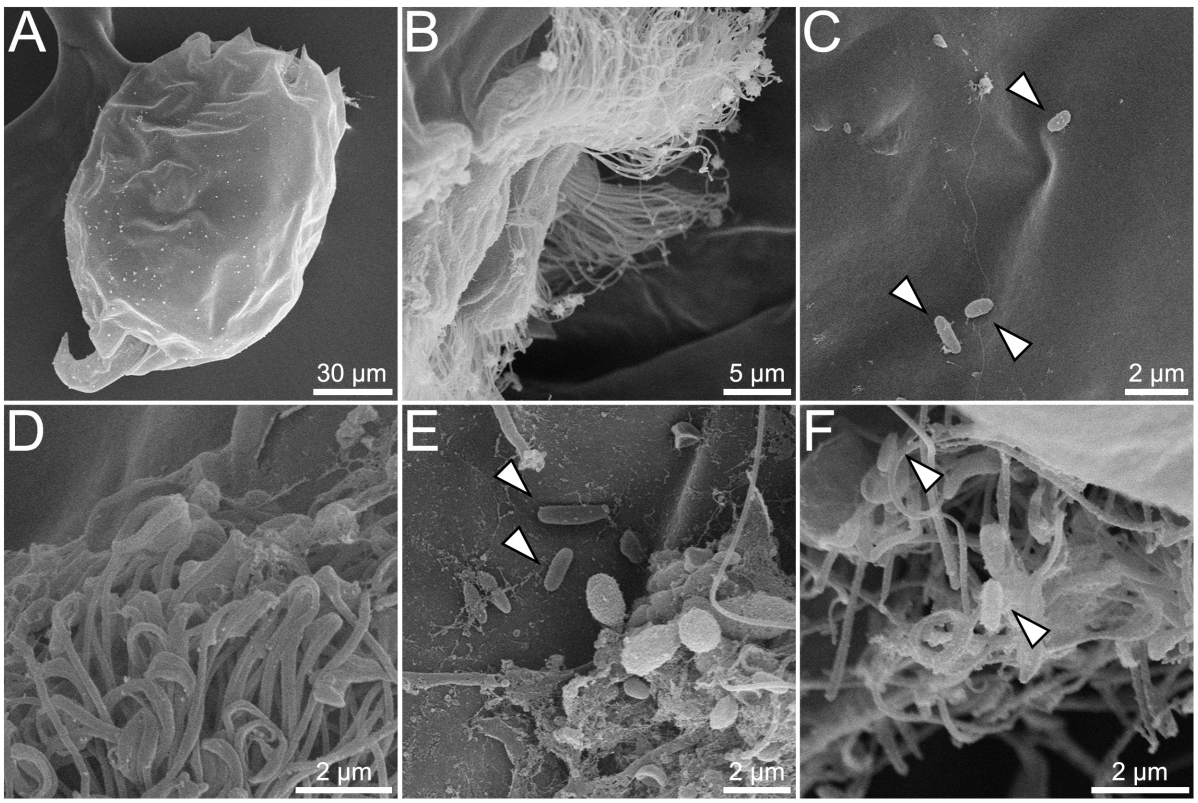

FIGURE 4 | SEM showing interaction between rotifer *Brachionus plicatilis* and BMCs. Control, with no bacteria visible on the surface of *B. plicatilis* **(A)**. Higher magnification of control rotifer, showing no bacteria adhered to the corona cilia **(B)**. Rotifer interaction with BMCs after 4 h **(C,D)**. Higher magnification shows BMCs with rod-shaped bacteria adhered to the rotifer surface **(C)** (white arrowheads). Corona cilia, showing no BMCs adhered to the rotifer corona cilia **(D)**. Rotifer interaction with BMCs after 16 h, showing rod-shaped bacteria adhered to the rotifer surface **(E)** and corona cilia **(F)** (white arrowheads).

on the external surfaces of the rotifers, and these were potentially some of the *Pseudoalteromonas* spp. strains present in the BMC consortium (**Figure 3**). Many *Pseudoalteromonas* strains produce antifouling compounds that can prevent the growth or adhesion of other microorganisms (Holmström and Kjelleberg, 1999; Holmström et al., 2002), including a class of bacteriostatic and amphiphilic anti-*Vibrio* molecules (Aranda et al., 2012). The *Pseudoalteromonas* spp. strains included in the BMC consortium may therefore be able to suppress unwanted surface attachment to BMC-enriched rotifers by other opportunistic bacteria before the rotifers are ingested by corals. *Pseudoalteromonas* spp. strains also protect the gastric region in corals by killing *Vibrio* pathogens at high temperatures (Tang et al., 2019). All BMC strains used in this study also possess high catalase activity, which can reduce damage from reactive oxygen species (ROS) that are produced in response to stress on the coral (Peixoto et al., 2017; Rosado et al., 2019). Six of the strains (five *Pseudoalteromonas* spp. and one *Halomonas taeanensis*) contain enzymes involved in nitrogen fixation or sulfur cycling (Rosado et al., 2019), metabolic processes that may underpin nutrient cycling within the coral holobiont (Raina et al., 2009; Rädecker et al., 2015).

Beneficial Microorganisms for Coral studies are targeted toward delivering microbial communities with traits that promote coral health. Delivery of these BMCs through prey items such as rotifers has proven to be possible, with *P. damicornis* corals readily ingesting the rotifers, representing a promising directed-delivery system for bacteria that provide putative beneficial functions for corals. The rotifer itself also provides a nutritional benefit to stressed corals. For example, *Acropora cervicornis* increased its feeding rate of the rotifer *B. plicatilis* under high CO_2 conditions, and this raised the coral's total lipid content, which can be a proxy for coral health (Towle et al., 2015). The next steps in establishing this proof of concept consist of determining whether the BMCs delivered through prey items such as rotifers can establish a symbiosis with the coral and provide benefits to the host, and the duration of these associations and benefits.

In summary, this study demonstrated that BMC-enriched rotifers can serve as direct vectors for delivering BMCs to the coral *P. damicornis*. The rotifers freely ingested the BMC consortium, which accumulated in the digestive tract and on the surface. The rotifers were also captured and ingested by the coral polyps, demonstrating the efficacy of using rotifers as a BMC delivery system. These observations represent a step forward in the administration of coral probiotics, which has the potential to increase the persistence and resistance of corals. These findings are also important for probiotic delivery to a wide range of aquaculture species for which rotifers are used as live feed.

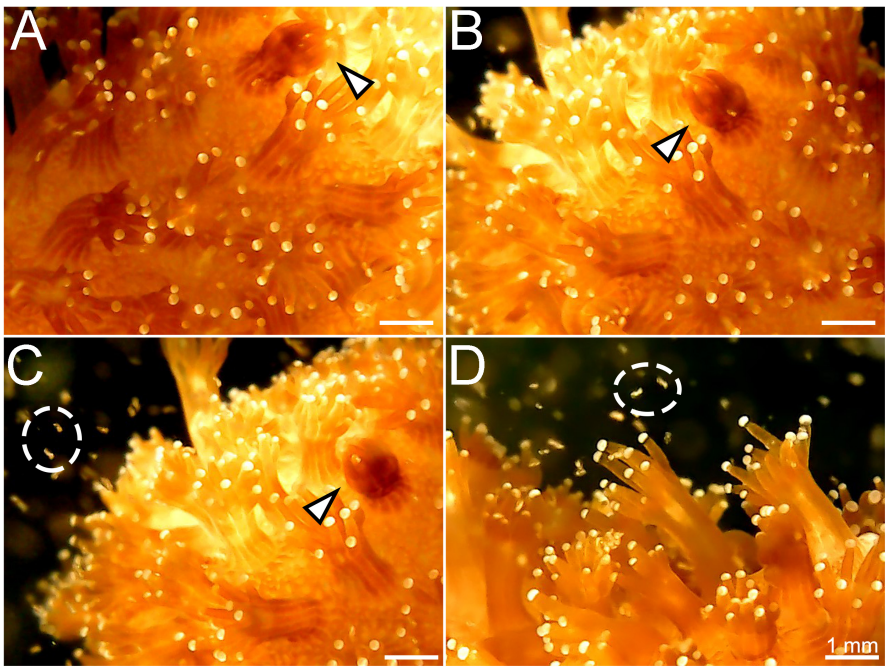

FIGURE 5 | Stages of capture of the rotifer *Brachionus plicatilis* by the coral *Pocillopora damicornis*. **(A)** Coral polyp starting to contract after capturing the rotifer (white arrowhead); **(B)** Polyp totally contracted, engulfing the rotifer; **(C)** The contracted polyp (white arrowhead) and rotifers swimming around the colony (white circle); **(D)** Coral polyps widely extended to capture the rotifers (white circle).

Further studies to test this approach in the field and to determine whether BMCs delivered via rotifers are able to establish within the coral microbiome will advance our knowledge of the proper administration of beneficial microorganisms *in situ*.

DATA AVAILABILITY STATEMENT

The original contributions presented in the study are included in the article/**Supplementary Material**, further inquiries can be directed to the corresponding author/s.

AUTHOR CONTRIBUTIONS

RP, DB, LH, FA, and JMA conceived and designed the study. JMA, RFV, GD, and RV maintained the coral and rotifer cultures. JMA, IT, and FA performed the microscopy experiments. RP, JMA, FA, HV, and AB drafted the manuscript. RP provided financial support. All authors were involved in critical revision.

FUNDING

This manuscript is part of the research project that won the Great Barrier Reef Foundation's Out of the Blue Box Reef Innovation Challenge People's Choice Award, supported by The Tiffany & Co. Foundation. It also received support from the Graduate Programs of Science (Microbiology) and Plant Biotechnology and Bioprocess Engineering (PBV)/Federal University of Rio de Janeiro, the National Council for Scientific and Technological Development (CNPq), the Rio de Janeiro Marine Aquarium Research Center, the Carlos Chagas Filho Foundation for Research Support of Rio de Janeiro State (FAPERJ), and the Coordenação de Aperfeiçoamento de Pessoal de Nível Superior – Brazil (CAPES).

ACKNOWLEDGMENTS

We thank the Great Barrier Reef Foundation, the Tiffany & Co. Foundation, IMAM-AquaRio, CNPq, FAPERJ, the Graduate Programs of Science (Microbiology) and Plant Biotechnology and Bioprocess Engineering (PBV)/Federal University of Rio de Janeiro for sponsoring this work. IMAM-AquaRio for providing infrastructure, corals, and rotifers. We also thank UniMicro for the support with the fluorescence microscopy experiments. Finally, we thank the National Center for Structural Biology and Bioimaging for the support with the SEM analyses.

SUPPLEMENTARY MATERIAL

The Supplementary Material for this article can be found online at: https://www.frontiersin.org/articles/10.3389/fmicb.2020.608506/full#supplementary-material

Supplementary Figure 1 | Differential interference contrast (DIC) of the rotifer Brachionus plicatilis. The image was taken with a Zeiss Axio Imager D2 microscope (Carl Zeiss, Oberkochen, Germany). Visible morphological features include the corona cilia (purple arrowhead), mouth (blue arrowhead), eye (red

arrowhead), mastax (yellow arrowhead), intestine (green arrowhead) and anus (orange arrowhead).

Supplementary Table 1 | BMC strains isolated by Rosado et al. (2019) used in this experiment and their respective accession numbers.

Supplementary Video 1 | *In vivo* fluorescence microscopy showing the fluorescently stained BMCs being ingested by the starved rotifer within 10 minutes of the interaction. The video was recorded with a Zeiss Axio Imager D2 microscope (Carl Zeiss, Oberkochen, Germany) fitted with a GFP filter. (GFP filter details: Zeiss filter set 09 - Excitation: BP 332 450–490 nm; Beam splitter: FT 510 nm; Emission: LP 515 nm).

Supplementary Video 2 | Pocillopora damicornis polyps capturing *Brachionus plicatilis* rotifers. The video was recorded with a digital USB microscope (Alloet, China).

REFERENCES

Aranda, C. P., Valenzuela, C., Barrientos, J., Paredes, J., Leal, P., Maldonado, M., et al. (2012). Bacteriostatic anti-*Vibrio Parahaemolyticus* activity of *Pseudoalteromonas* sp. strains DIT09, DIT44 and DIT46 isolated from Southern Chilean intertidal *Perumytilus purpuratus*. *World J. Microbiol. Biotechnol.* 28, 2365–2374. doi: 10.1007/s11274-012-1044-z

Bourne, D. G., and Munn, C. B. (2005). Diversity of bacteria associated with the coral *Pocillopora damicornis* from the Great Barrier Reef. *Environ. Microbiol.* 7, 1162–1174. doi: 10.1111/j.1462-2920.2005.00793.x

Casas, I. A., and Dobrogosz, W. J. (2000). Validation of the probiotic concept: *Lactobacillus reuteri* confers broad-spectrum protection against disease in humans and animals. *Microb. Ecol. Health Dis.* 12, 247–285. doi: 10.1080/08910600050216246-1

Costa, A. P. L., Calado, R., Marques, B., Lillebø, A. I., Serôdio, J., Soares, A. M. V. M., et al. (2016). The effect of mixotrophy in the ex situ culture of the soft coral *Sarcophyton* cf. glaucum. *Aquaculture* 452, 151–159. doi: 10.1016/j.aquaculture.2015.10.032

Damjanovic, K., van Oppen, M. J. H., Menéndez, P., and Blackall, L. L. (2019). Experimental inoculation of coral recruits with marine bacteria indicates scope for microbiome manipulation in *Acropora tenuis* and *Platygyra daedalea*. *Front. Microbiol.* 10:1702. doi: 10.3389/fmicb.2019.01702

Daniels, C. L., Merrifield, D. L., Ringø, E., and Davies, S. J. (2013). Probiotic, prebiotic and synbiotic applications for the improvement of larval European lobster (*Homarus gammarus*) culture. *Aquaculture* 416, 396–406. doi: 10.1016/j.aquaculture.2013.08.001

Duarte, G. A. S., Villela, H. D. M., Deocleciano, M., Silva, D., Barno, A., Cardoso, P. M., et al. (2020). Heat waves are a major threat to turbid coral reefs in Brazil. *Front. Mar. Sci.* 7:179. doi: 10.3389/fmars.2020.00179

Dunne, C., Murphy, L., Flynn, S., O'Mahony, L., O'Halloran, S., Feeney, M., et al. (1999). Probiotics: from myth to reality. Demonstration of functionality in animal models of disease and in human clinical trials. Antonie van Leeuwenhoek. *Int. J. Gen. Mol. Microbiol.* 76, 279–292. doi: 10.1007/978-94-017-2027-4_14

Goulden, E. F., Hall, M. R., Pereg, L. L., Baillie, B. K., and Høj, L. (2013). Probiont niche specialization contributes to additive protection against *Vibrio owensii* spiny lobster larvae. *Environ. Microbiol. Rep.* 5, 39–48. doi: 10.1111/1758-2229.12007

Hai, N. V. (2015). The use of probiotics in aquaculture. *J. Appl. Microbiol.* 119, 917–935.

Hai, N. V., Buller, N., and Fotedar, R. (2010). Encapsulation capacity of *Artemia* nauplii with customized probiotics for use in the cultivation of western king prawns (*Penaeus latisulcatus* Kishinouye, 1896). *Aquac. Res.* 41, 893–903. doi: 10.1111/j.1365-2109.2009.02370.x

Holmström, C., and Kjelleberg, S. (1999). Marine *Pseudoalteromonas* species are associated with higher organisms and produce biologically active extracellular agents. *FEMS Microbiol. Ecol.* 30, 285–293. doi: 10.1016/s0168-6496(99)00063-x

Holmström, C., Egan, S., Franks, A., McCloy, S., and Kjelleberg, S. (2002). Antifouling activities expressed by marine surface associated *Pseudoalteromonas* species. *FEMS Microbiol. Ecol.* 41, 47–58. doi: 10.1016/s0168-6496(02)00239-8

Hughes, T. P., Anderson, K. D., Connolly, S. R., Heron, S. F., Kerry, J. T., Lough, J. M., et al. (2018). Spatial and temporal patterns of mass bleaching of corals in the Anthropocene. *Science* 359, 80–83. doi: 10.1126/science.aan8048

Lowe, C. D., Kemp, S. J., Bates, A. D., and Montagnes, D. J. S. (2005). Evidence that the rotifer *Brachionus plicatilis* is not an osmoconformer. *Mar. Biol.* 146, 923–929. doi: 10.1007/s00227-004-1501-9

Lubzens, E., Tandler, A., and Minkoff, G. (1989). Rotifers as food in aquaculture. *Hydrobiologia* 18, 387–400. doi: 10.1007/bf00048937

Najmi, N., Yahyavi, M., and Haghshena, A. (2018). Effect of enriched rotifer (*Brachionus plicstilis*) with probiotic lactobacilli on growth, survival and resistance indicators of western white shrimp (*Litopenaeus vannamei*) larvae. *Iran. J. Fish. Sci.* 17, 11–20.

National Academies of Sciences and Medicine (2019). *A Research Review of Interventions to Increase the Persistence and Resilience of Coral Reefs. Consensus Study Report*. Washington, DC: The National Academies Press, doi: 10.17226/25279

Pandolfi, J. M., Connolly, S. R., Marshall, D. J., and Cohen, A. L. (2011). Projecting coral reef futures under global warming and ocean acidification. *Science* 333, 418–422. doi: 10.1126/science.1204794

Peixoto, R., Rosado, P. M., Leite, D. C., de, A., Rosado, A. S., and Bourne, D. G. (2017). Beneficial microorganisms for corals (BMC): proposed mechanisms for coral health and resilience. *Front. Microbiol.* 8:341. doi: 10.3389/fmicb.2017.00341

Pita, L., Rix, L., Slaby, B. M., Franke, A., and Hentschel, U. (2018). The sponge holobiont in a changing ocean: from microbes to ecosystems. *Microbiome* 6:46.

Planas, M., Pérez-Lorenzo, M., Hjelm, M., Gram, L., Fiksdal, I. U., Bergh, Ø, et al. (2006). Probiotic effect in vivo of *Roseobacter* strain 27-4 against *Vibrio* (*Listonella*) *anguillarum* infections in turbot (*Scophthalmus maximus* L.) larvae. *Aquaculture* 255, 323–333. doi: 10.1016/j.aquaculture.2005.11.039

Planas, M., Pérez-Lorenzo, M., Vázquez, J. A., and Pintado, J. (2005). A model for experimental infections with *Vibrio* (*Listonella*) *anguillarum* in first feeding turbot (*Scophthalmus maximus* L.) larvae under hatchery conditions. *Aquaculture* 250, 232–243. doi: 10.1016/j.aquaculture.2005.04.050

Qi, Z., Dierckens, K., Defoirdt, T., Sorgeloos, P., Boon, N., Bao, Z., et al. (2009). Effects of feeding regime and probionts on the diverting microbial communities in rotifer *Brachionus* culture. *Aquac. Int.* 17, 303–315. doi: 10.1007/s10499-008-9202-x

Rädecker, N., Pogoreutz, C., Voolstra, C. R., Wiedenmann, J., and Wild, C. (2015). Nitrogen cycling in corals: the key to understanding holobiont functioning? *Trends Microbiol.* 23, 490–497. doi: 10.1016/j.tim.2015.03.008

Raina, J.-B., Tapiolas, D., Willis, B. L., and Bourne, D. G. (2009). Coral-associated bacteria and their role in the biogeochemical cycling of sulfur. *Appl. Environ. Microbiol.* 75, 3492–3501. doi: 10.1128/aem.02567-08

Rohwer, F., Breitbart, M., Jara, J., Azam, F., and Knowlton, N. (2001). Diversity of bacteria associated with the Caribbean coral *Montastraea franksi*. *Coral Reefs* 20, 85–91. doi: 10.1007/s003380100138

Roobab, U., Batool, Z., Manzoor, M. F., Shabbir, M. A., Khan, M. R., and Aadil, R. M. (2020). Sources, formulations, advanced delivery and health benefits of probiotics. *Curr. Opin. Food Sci.* 32, 17–28. doi: 10.1016/j.cofs.2020.01.003

Rosado, P., Leite, D. C. A., Duarte, G. A. S., Chaloub, R. M., Jospin, G., Nunes da Rocha, U., et al. (2019). Marine probiotics: increasing coral resistance to bleaching through microbiome manipulation. *ISME J.* 13, 921–936. doi: 10.1038/s41396-018-0323-6

Salt, G. W. (1987). The components of feeding behavior in rotifers. *Hydrobiologia* 147, 271–281. doi: 10.1007/bf00025754

Sánchez-Quinto, A., Falcón, L. I. (2019). Metagenome of *Acropora palmata* coral rubble: potential metabolic pathways and diversity in the reef ecosystem. *PLoS One* 14:e0220117. doi: 10.1371/journal.pone.0220117

Santos, H. F. A., Duarte, G. A. S., Rachid, C. T., Chaloub, R. M., Calderon, E. N., Marangoni, L. F., et al. (2015). Impact of oil spills on coral reefs can be reduced by bioremediation using probiotic microbiota. *Sci. Rep.* 5:18268.

Stolzenbach, S., Myhill, L. J., Andersen, L. O., Krych, L., Mejer, H., Williams, A. R., et al. (2020). Dietary inulin and *Trichuris suis* infection promote beneficial

bacteria throughout the porcine gut. *Front. Microbiol.* 11:312. doi: 10.3389/fmicb.2020.00312

Sun, Y-Z., Yang, H-L., Huang, K-P., Ye, J-D., Zhang, C-X. (2013). Application of autochthonous Bacillus bioencapsulated in copepod to grouper *Epinephelus coioides* larvae. *Aquaculture* 392:44–50. doi: 10.1016/j.aquaculture.2013.01.037

Tang, K., Zhan, W., Zhou, Y., Xu, T., Chen, X., Wang, W., et al. (2019). Antagonism between coral pathogen *Vibrio coralliilyticus* and other bacteria in the gastric cavity of scleractinian coral *Galaxea fascicularis*. *Sci. China Earth Sci.* 63, 157–166. doi: 10.1007/s11430-019-9388-3

Teplitski, M., and Ritchie, K. (2009). How feasible is the biological control of coral diseases? *Trends Ecol. Evol.* 24, 378–385. doi: 10.1016/j.tree.2009.02.008

Thomas, T., Evans, F. F., Schleheck, D., Mai-Prochnow, A., Burke, C., Penesyan, A., et al. (2008). Analysis of the Pseudoalteromonas tunicata genome reveals properties of a surface-associated life style in the marine environment. *PLoS One* 3:e3252. doi: 10.1371/journal.pone.0003252

Tinh, N. T. N., Phuoc, N. N., Dierckens, K., Sorgeloos, P., and Bossier, P. (2006). Gnotobiotically grown rotifer *Brachionus plicatilis* sensu strictu as a tool for evaluation of microbial functions and nutritional value of different food types. *Aquaculture* 253, 421–432. doi: 10.1016/j.aquaculture.2005.09.006

Towle, E. K., Enochs, I. C., and Langdon, C. (2015). Threatened Caribbean coral is able to mitigate the adverse effects of ocean acidification on calcification by increasing feeding rate. *PLoS One* 10:e0123394. doi: 10.1371/journal.pone.0123394

Watanabe, T., Kitajima, C., and Fujita, S. (1983). Nutritional values of live organisms used in Japan for mass propagation of fish: a review. *Aquaculture* 34, 115–143. doi: 10.1016/0044-8486(83)90296-x

Wilkins, L. G. E., Leray, M., O'Dea, A., Yuen, B., Peixoto, R. S., Pereira, T. J., et al. (2019). Host-associated microbiomes drive structure and function of marine ecosystems. *PLoS Biol.* 17:e3000533. doi: 10.1371/journal.pbio.3000533

Conflict of Interest: The authors declare that the research was conducted in the absence of any commercial or financial relationships that could be construed as a potential conflict of interest.

frontiers in Microbiology

ORIGINAL RESEARCH
published: 13 January 2021
doi: 10.3389/fmicb.2020.595967

Enhanced Metabolic Potentials and Functional Gene Interactions of Microbial Stress Responses to a 4,100-m Elevational Increase in Freshwater Lakes

Huabing Li[1], Jin Zeng[1], Lijuan Ren[2], Qingyun Yan[3] and Qinglong L. Wu[1,4]**

[1] State Key Laboratory of Lake Science and Environment, Nanjing Institute of Geography and Limnology, Chinese Academy of Sciences, Nanjing, China, [2] Department of Ecology and Institute of Hydrobiology, Jinan University, Guangzhou, China, [3] Environmental Microbiomics Research Center, School of Environmental Science and Engineering, Southern Marine Science and Engineering Guangdong Laboratory (Zhuhai), Sun Yat-sen University, Guangzhou, China, [4] Sino-Danish Centre for Education and Research, University of Chinese Academy of Sciences, Beijing, China

OPEN ACCESS

Edited by:
Camila Fernandez, UMR7621 Laboratoire d'Océanographie Microbienne (LOMIC), France

Reviewed by:
Weidong Kong, Institute of Tibetan Plateau Research (CAS), China
Kai Xue, University of Chinese Academy of Sciences, China

***Correspondence:**
Jin Zeng
jzeng@niglas.ac.cn
Qinglong L. Wu
qlwu@niglas.ac.cn

Specialty section:
This article was submitted to Aquatic Microbiology, a section of the journal Frontiers in Microbiology

Received: *18 August 2020*
Accepted: *30 November 2020*
Published: *13 January 2021*

Citation:
Li H, Zeng J, Ren L, Yan Q and Wu QL (2021) Enhanced Metabolic Potentials and Functional Gene Interactions of Microbial Stress Responses to a 4,100-m Elevational Increase in Freshwater Lakes. Front. Microbiol. 11:595967. doi: 10.3389/fmicb.2020.595967

Elevation has a strong influence on microbial community composition, but its influence on microbial functional genes remains unclear in the aquatic ecosystem. In this study, the functional gene structure of microbes in two lakes at low elevation (ca. 530 m) and two lakes at high elevation (ca. 4,600 m) was examined using a comprehensive functional gene array GeoChip 5.0. Microbial functional composition, but not functional gene richness, was significantly different between the low- and high-elevation lakes. The greatest difference was that microbial communities from high-elevation lakes were enriched in functional genes of stress responses, including cold shock, oxygen limitation, osmotic stress, nitrogen limitation, phosphate limitation, glucose limitation, radiation stress, heat shock, protein stress, and sigma factor genes compared with microbial communities from the low-elevation lakes. Higher metabolic potentials were also observed in the degradation of aromatic compounds, chitin, cellulose, and hemicellulose at higher elevations. Only one phytate degradation gene and one nitrate reduction gene were enriched in the high-elevation lakes. Furthermore, the enhanced interactions and complexity among the co-occurring functional genes in microbial communities of lakes at high elevations were revealed in terms of network size, links, connectivity, and clustering coefficients, and there were more functional genes of stress responses mediating the module hub of this network. The findings of this study highlight the well-developed functional strategies utilized by aquatic microbial communities to withstand the harsh conditions at high elevations.

Keywords: elevation, freshwater lakes, microbial functional genes, stress response, metabolic potentials

INTRODUCTION

Elevational patterns of biodiversity have attracted interest in the scientific fields of microbial ecology and biogeography because of the importance of these patterns in facilitating a comprehensive understanding of the influences of climate change on ecosystems. Numerous studies concerning elevational gradients have focused on terrestrial organisms and revealed that species richness generally exhibits decreasing or unimodal patterns with increases in elevation

(e.g., Rahbek, 2005; Grytnes and Mccain, 2007). Studies on elevational species richness of a few freshwater taxa including aquatic plants (Jones et al., 2003), phytoplankton (Jankowski and Weyhenmeyer, 2006), rotifers (Obertegger et al., 2010), crustaceans (Hessen et al., 2007), stream macro-invertebrates (Jacobsen, 2004), and molluscs (Sturm, 2007) reported a linear decreasing pattern in species richness with elevation. In contrast, studies on chironomids (Nyman et al., 2005) and stream fish (Bhatt et al., 2012) showed a hump-shaped pattern in species richness with elevation. However, studies focusing on microbial diversity across elevation gradients in freshwater lakes are limited (Hayden and Beman, 2016; Li et al., 2017), even though microbial communities are the most important groups driving biogeochemical cycles and sustaining the whole ecosystem in lakes (Cole et al., 2000).

Microbial communities play central roles in biogeochemical processes such as carbon, nitrogen, and phosphorus cycling (Whitman et al., 1998; Cole et al., 2000). The development of microbial molecular biology technologies has led to considerable attention being directed at the phylogenetic and functional diversity patterns of microbial communities along elevations (Wang et al., 2011; Hayden and Beman, 2016; Li et al., 2017). However, most of these studies focused on taxonomy. The limited number of studies on microbial communities inhabiting soils (Bryant et al., 2008; Fierer et al., 2011; Singh et al., 2012), stones in streams (Wang et al., 2011), leaf surfaces (Fierer et al., 2011), and lake waters (Hayden and Beman, 2016; Li et al., 2017) indicated that the elevational patterns of microbial species richness varied with elevational ranges or habitat types. Microbial functional metabolic potentials are influenced by the changes in microbial species richness and environmental conditions (Kuang et al., 2016). However, little is known about the elevational patterns of microbial functional traits. Elucidating these patterns could improve our understanding of the influences of climate change on microbial-related ecological processes.

Many of the environmental factors that vary with elevation might affect the functional gene structure of microbial communities. Studies on microbial functional gene diversity along elevation gradients are very limited (Yang et al., 2014; Qi et al., 2017; Picazo et al., 2020). Yang et al. (2014) and Qi et al. (2017) reported that soil microbial functional gene structure (MFS) changed significantly with an increase in elevation from 3,200 to 3,800 m, and these changes were predominantly caused by decreases in temperature and concentrations of nutrients. A similar pattern was observed in biofilm microbes along three elevational gradients lower than 4,000 m (Picazo et al., 2020). The shifts in these environmental variables in lakes can be greater than twofold between elevations of approximately 530 to 4,600 m (Li et al., 2017). Furthermore, in contrast to data obtained from elevational studies of grassland, the high-elevation lakes (HELs), especially those with elevations above 4,000 m, are characterized by harsher conditions, including high UV, low primary production, and more recalcitrant dissolved organic carbon (DOC), than those of the low-elevation lakes (LELs; Li et al., 2017; Zhou et al., 2018). The harsh conditions in HELs are hypothesized to result in distinct patterns of microbial metabolic potentials compared to those in LELs, but this has not yet been investigated. It has been confirmed that microbial recruitment to exposed rocky surface habitats is based strongly on the selection of stress tolerance traits (Chan et al., 2013). It is thus very likely that microbial communities of HELs might have higher functional capacities in stress responses such as cold shock and radiation stress, and higher metabolic potentials in the degradation of recalcitrant DOC.

In an ecosystem, microorganisms interact with other organisms and their environment to form a complicated network (Zengler and Zaramela, 2018). Understanding this complex network over time and space is a key issue in ecology (Montoya et al., 2006; Zengler and Zaramela, 2018). Network analysis has been proven as a powerful method for examining complex interactions among microbes and identifying keystone species in different ecosystems, such as the human gut (Greenblum et al., 2012), river (Hu et al., 2017), marine environment (Gilbert et al., 2012), soils (Zhou et al., 2011; Barberán et al., 2012), and rhizosphere (Shi et al., 2016). Furthermore, this method has been applied to investigate changes in microbial metabolic potentials in elevated atmospheric CO_2 and oil-contaminated soils (Zhou et al., 2010; Liang et al., 2011) and an acidic mining lake (Ren et al., 2018). These studies provide perspectives on microbial assemblages that cannot easily be found by simple alpha- and beta-diversity analyses (Shi et al., 2016). The network complexity of different microbial functional genes under elevated atmospheric CO_2 or more stress conditions (e.g., low pH, limited carbon, nitrogen, and phosphorus sources) increased in terms of network size, connectivity, and clustering coefficients (Zhou et al., 2010; Ren et al., 2018). However, the patterns of microbial functional gene interactions have not yet been investigated in lakes with contrasting patterns of environmental variables at different elevations.

In this study, it was hypothesized that (1) the MFS differs significantly among lakes under different elevations; (2) the microbial functional potentials of stress responses increase with harsher environments at high elevations; (3) the harsh conditions of HELs alter the microbial functional molecular ecological network. These hypotheses were tested by focusing on four shallow freshwater lakes, including two HELs (at 4,652 and 4,608 m) and two LELs (at 530 and 525 m), at Mount Siguniang in Sichuan province, China. A comprehensive functional gene array (GeoChip 5.0) was utilized to analyze the functional gene diversity and metabolic potentials of the microbial communities in the four lakes. Random matrix theory (RMT)-based network analysis was performed to compare the interaction patterns of the co-occurring functional genes between the HELs and LELs. Overall, the contrasting patterns of freshwater microbial metabolic potentials and functional gene interactions between the HELs and LELs were demonstrated.

MATERIALS AND METHODS

Field Sampling and Measurement of Environmental Parameters

The sampling sites were two HELs and two LELs at Mount Siguniang, a mountain system located in the eastern region of

the Tibetan Plateau in China. Mount Siguniang, often referred to as the "Alps of Asia," comprises a number of peaks, the highest of which has an elevation of 6,250 m. The upper slopes of the high mountains are mostly covered by snow throughout the year, which offers a desirable elevation gradient as well as a relatively geologically uniform environmental gradient within a small spatial scale (Li et al., 2017). The elevations of the two LELs were 525 and 530 m above sea level, whereas those of the two HELs were 4,652 and 4,608 m above sea level (Li et al., 2017). The two LELs (Maojiakou and Baigongyan; **Supplementary Table 1** and **Supplementary Figure 1**) had much higher water temperature and concentrations of DOC, Chl *a*, and nutrients compared with the two HELs (Heihaizi and Baihaizi; **Supplementary Table 1** and **Supplementary Figure 1**). Morphometric variables (elevation, latitude, longitude, surface area, and maximum depth) of each lake were measured and six uniformly distributed sites were selected in each lake for sampling. At each sampling point, approximately 1 and 9 L of surface water (top 50 cm) were collected for analysis of microbial functional structure and chemical variables, respectively. The methods used for sampling and determination of environmental characteristics were as described by Li et al. (2017).

DNA Extraction and GeoChip Analysis

Total microbial nucleic acids were extracted and purified as described previously (Li et al., 2017). GeoChip 5.0, which includes more than 57,000 oligonucleotide probes and covers over 144,000 gene sequences from 393 functional gene families involved in cycling of carbon, nitrogen, phosphorus, and sulfur, stress response, etc. (Wang et al., 2014), was used to analyze the obtained DNA samples. For each sample, the DNA (500 ng) was labeled with Cy-3 fluorescent dye (GE Healthcare, CA, United States) by random priming as described previously (He et al., 2010) and then the labeled DNA was purified using a QIAquick purification kit (Qiagen, CA, United States) and dried in a SpeedVac (Thermo Savant, NY, United States). Dried DNA was resuspended in 42 μl of hybridization solution containing 1 × Hi-RPM hybridization buffer, 1 × CGH blocking agent, 0.05 μg μl^{-1} Cot-1 DNA, 10 pM universal standard, and 10% formamide (final concentrations). After mixing completely, the mixture was denatured at 95°C for 3 min and then kept at 37°C until hybridization. The hybridization was conducted at 67°C in an Agilent hybridization station (Agilent Technologies Inc., Santa Clara, CA, United States). Hybridized GeoChips were scanned by a NimbleGen MS200 scanner (Roche NimbleGen, Inc., Madison, WI, United States) and the image data were extracted using Agilent Feature Extraction 11.5 software (Agilent Technologies).

Data Preprocessing

Raw data were uploaded to the microarray analysis pipeline[1] and analyzed as previously described (Yang et al., 2014; Yan et al., 2015). Briefly, the following steps were performed: (i) good quality spots were selected, which were defined as having a signal-to-noise ratio (SNR) > 2; (ii) probes that appeared in more than approximately 30% of samples in one lake (two of the six samples from each lake) were selected for subsequent analysis; (iii) for each sample, the signal intensity of each probe was ln (x+1)-transformed and then normalized by dividing the initial signal intensity of each probe by the mean intensity of positive probes in each sample (Chan et al., 2013). The obtained microarray data matrix (normalized signal intensity) was considered as "species" abundance for microbial functional gene richness and composition analysis (Zhou et al., 2010); and (iv) the normalized signal intensities of all spots of each sample were transferred into relative signal intensities by dividing the normalized signal intensity of a probe by the total normalized signal intensity of a sample. These relative signal intensities were used for further evaluation of the microbial metabolic potentials (Ren et al., 2018). Finally, (v) the difference in normalized signal intensity (or the difference in relative signal intensity) of a specific gene family was calculated as: (S_{HELs}/S_{LELs}) - 1, where the S_{HELs} and S_{LELs} are the total normalized signal intensity of a specific gene family in the HELs and LELs, respectively.

Network Construction

To reduce the complexity of the datasets, this study specifically focused on the commonly detected functional genes involved in key biogeochemical and ecological processes in lakes along elevation gradients, including carbon, nitrogen, and phosphorus cycling, and stress responses. These genes in the LELs and HELs were selected for the construction of the functional molecular ecological networks (fMENs), which were based on a RMT approach using a publicly available Molecular Ecological Network Analysis Pipeline (MENAP; http://ieg2.ou.edu/MENA/, Zhou et al., 2010; Deng et al., 2012). Briefly, the fMEN was constructed based on the Pearson correlation matrix calculated by the correlation coefficient (r value) between each of the two detected genes (Deng et al., 2012). A series of thresholds was then applied to the matrix and the similarity threshold (st) was kept or matrix eigenvalues were calculated using an RMT-based approach (Deng et al., 2016). During these calculations, the most suitable st was selected to obtain the Poisson distribution of the calculated eigenvalues, which indicates the non-random properties of a complex system (Deng et al., 2016). Each network was then separated into modules by fast greedy modularity optimization. For each network, 100 corresponding random networks were then generated with the same network size and an average number of links. Differences in the indices between the constructed and random networks were determined by statistical Z test.

Cytoscape 3.6.1 software (Shannon et al., 2003) and Gephi 0.9.2-beta (Bastian et al., 2009) were applied to visualize the network of the nodes.

Identification of Node Roles

Topological roles of each functional gene were assessed by the within-module connectivity (Zi) and among-module connectivity (Pi; Guimerà and Amaral, 2005). Nodes in a network were organized into the following four categories: network hubs (Zi > 2.5 and Pi > 0.62), connectors (Pi > 0.62), module hubs (Zi > 2.5), and peripherals (Zi < 2.5 and Pi < 0.62); the former two have important roles in network topology (Zhou et al., 2010).

[1] http://ieg.ou.edu/microarray/

Statistical Analyses

Using the microarray analysis pipeline (see text footnote 1), Student's *t* tests were performed to determine the differences in functional gene diversity and relative signal intensity of each functional gene category and certain subcategories or phylogenetic groups between the HELs and LELs. Three non-parametric multivariate statistical tests, including a permutational multivariate analysis of variance using distance matrices (ADONIS, "Adonis" function), an analysis of similarity (ANOSIM, "anosim" function), and a multiple response permutation procedure (MRPP, "mrpp" function), and detrended correspondence analysis (DCA) were performed to determine the differences in MFS. These four analyses were conducted using the vegan package (version 2.3-0; Oksanen et al., 2013) in the R statistical computing environment.

Canonical correspondence analysis (CCA) was performed to detect the relationships between MFS and environmental parameters because the length of the first DCA axis run on the species data was >2. Forward selection was carried out to determine the significant factors in the CCA model by 999 simulated permutations ($p < 0.05$). All environmental variables were log (x+1)-transformed except for the values of water temperature and pH. In addition, variation partitioning analysis (VPA) was performed to identify individual and interactive contributions of productivity (Chl *a* and DOC), space (elevation and lake area), and the rest of the tested environmental heterogeneity to MFS (Li et al., 2017). CCA and VPA were performed using the vegan package in R.

Correlation coefficients between modules and environmental factors were tested on MENAP. The module eigengene E (the first principal component of modules; de Menezes et al., 2015) of the top modules for both the HELs and LELs networks were calculated, and their relationships with environmental variables were then estimated using Spearman's rank correlation test.

RESULTS

Microbial Functional Gene Richness

In total, 17,238 functional genes were detected in the 24 samples, of which 14,912 genes were derived from bacteria, 631 genes were from archaea, 1603 genes were from fungi, and the remaining genes were from bacteriophages. There were no significant differences in overall gene richness between the studied lakes at low and high elevations ($p > 0.05$, **Figure 1A**). Within all of the detected gene categories (carbon, nitrogen, phosphorus, and sulfur cycling; organic remediation; metal homeostasis; secondary metabolism; stress response; and virulence), only the richness of stress response genes was significantly higher in the HELs than in the LELs ($p < 0.05$ in all cases, **Figure 1A**), and no significant differences in richness were observed for the other detected gene categories ($p > 0.05$, **Figure 1A**).

Microbial functional gene overlap between elevations was calculated and revealed that 75.58–87.32% of the genes were shared between the HELs and LELs (**Figure 1B** and **Supplementary Table 2**). In the LELs, 7% of the genes were unique, and most of the total genes (81%) and the genes detected in each gene category (73–82%) could be found in the HELs (**Figure 1B** and **Supplementary Table 2**), while the HELs had 12% unique genes, most of which were associated with stress resistance (**Figure 1B**).

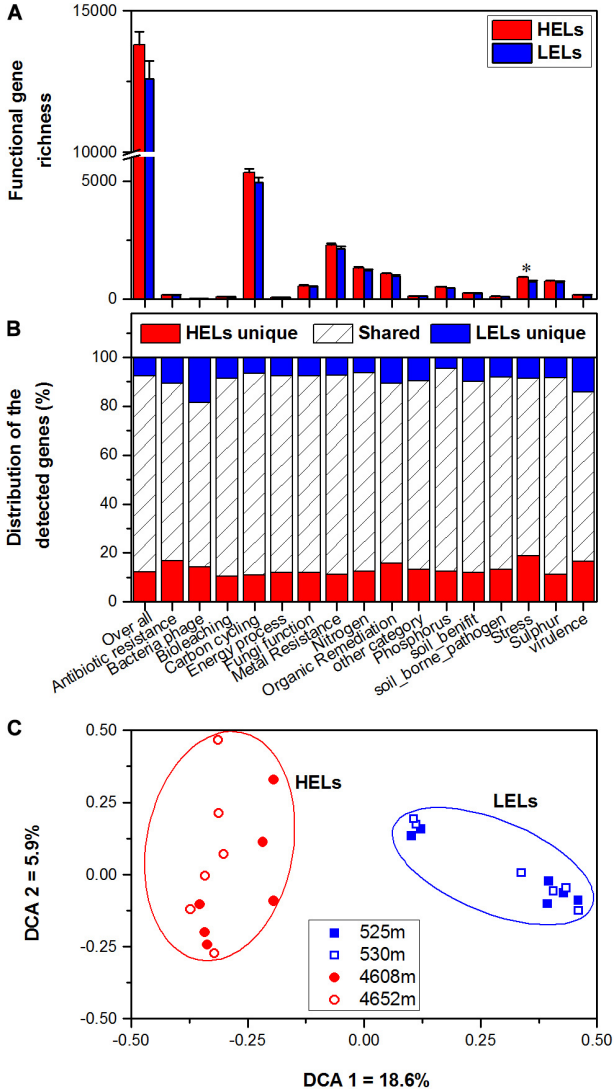

FIGURE 1 | Microbial functional gene richness **(A)**, distribution (shared or unique) of the detected genes **(B)**, and DCA **(C)** of the microbial functional community structure in the two HELs and two LELs involved in certain biogeochemical cycling processes. All data in panels a and b are presented as the mean ± s.e. calculated from 12 biological replicates. Asterisks (*) above the bars indicate significant ($p < 0.05$) differences. The values on axes 1 and 2 in panel **(C)** are percentages of total variations that can be attributed to the corresponding axis.

Microbial Functional Gene Structure

The MFS differed markedly between the LELs and HELs. DCA of GeoChip data indicated that the MFSs in the two LELs and those in the two HELs were separated by elevation along DCA axis 1 (**Figure 1C**). Consistently, three different non-parametric multivariate statistical tests also demonstrated that MFS differed

significantly between the HELs and LELs (ADONIS, ANOSIM, and MRPP; $p < 0.01$ in all cases, **Table 1**) but not within the two HELs or the two LELs ($p > 0.21$ in all cases, **Table 1**).

Functional Genes Involved in Stress Response

Among all evaluated functional pathways, stress response genes were the most variable, and most of these genes (30 out of 41) had significantly higher normalized signal intensities in the HELs than in the LELs ($p < 0.05$, **Figure 2**). These functional genes with higher normalized signal intensities in the HELs represented all of the detected stress gene categories including pathway-specific genes for responses to nutrient and oxygen stress, radiation, cold shock, heat shock, and sigma factors. This suggested that the stress response potential in the HELs was greater than that in the LELs. For example, the normalized signal intensities of the functional genes related to glucose limitation (*bglP*), oxygen limitation (*cydA* and *ahpF*), and osmotic stress (*proW*) increased by more than 50% in the HELs compared with those in the LELs ($p < 0.05$ in all cases, **Figure 2**). In addition, normalized signal intensities of the functional genes related to radiation stress, heat shock, nitrogen limitation, phosphate limitation, sigma factors, and protein stress, such as *obgE*, *grpE*, *glnR*, *pstA*, sigma_32, and *clpC*, increased by more than 20% in the HELs compared with those in the LELs ($p < 0.05$ in all cases, **Figure 2**).

Taxa–function relationships revealed that most of the differences in the glucose limitation between the HELs and LELs were exclusively derived from *Firmicutes*, which was not found in the LELs ($p < 0.05$, **Supplementary Figure 2A**). Differences in oxygen limitation between the HELs and LELs were mostly related to *Firmicutes*, *Betaproteobacteria*, *Deltaproteobacteria*, *Gammaproteobacteria*, and fungi (**Supplementary Figure 2B**). Variations in the pathways related to osmotic stress and nitrogen limitation were largely attributed to a greater abundance of *Gammaproteobacteria* in the HELs (**Supplementary Figures 2C**, **1E**). Differences in heat shock were mostly related to *Actinobacteria* and *Firmicutes* (**Supplementary Figure 2D**, $p < 0.05$ in both cases). Similarly, cold shock genes derived from *Actinobacteria* had higher normalized signal intensities in the HELs than those in the LELs (**Supplementary Figure 2A**, $p < 0.05$). Genes indicative of pathways that respond to phosphate limitation were relatively widespread, but particularly abundant among the *Gammaproteobacteria*, *Cyanobacteria*, and *Betaproteobacteria* (**Supplementary Figure 2F**). Differences in sigma factors were mostly attributed to *Actinobacteria*, *Alphaproteobacteria*, *Cyanobacteria*, *Deinococcus-Thermus* (primarily *Deinococcus deserti* and *Deinococcus geothermalis*), and *Gammaproteobacteria* (**Supplementary Figure 2G**). Differences in protein stress were mostly attributed to *Firmicutes* (primarily *Exiguobacterium* sp., some strains of which can grow within a wide range of pH and tolerate high levels of UV radiation) and *Verrucomicrobia*, which were only detected in

TABLE 1 | Significance tests of the microbial functional gene structure in lakes at low and high elevations.

		MRPP		ANOSIM		Adonis	
		δ	*p*	*R*	*p*	*F*	*p*
525 m vs 4,652 m	Euclidean	56.03	**0.002**	0.64	**0.002**	6.51	**0.001**
	Horn	0.12	**0.003**	0.53	**0.002**	7.56	**0.002**
	Bray	0.14	**0.003**	0.58	**0.001**	7.13	**0.002**
525 m vs 4,608 m	Euclidean	56.26	**0.003**	0.56	**0.002**	0.30	**0.004**
	Horn	0.13	**0.002**	0.45	**0.004**	0.31	**0.005**
	Bray	0.14	**0.006**	0.44	**0.004**	0.30	**0.002**
530 m vs 4,652 m	Euclidean	55.8	**0.002**	0.71	**0.001**	0.39	**0.001**
	Horn	0.12	**0.004**	0.59	**0.005**	0.42	**0.001**
	Bray	0.14	**0.003**	0.58	**0.004**	0.40	**0.002**
530 m vs 4,608 m	Euclidean	56.49	**0.005**	0.58	**0.003**	0.35	**0.003**
	Horn	0.13	**0.006**	0.48	**0.002**	0.38	**0.001**
	Bray	0.14	**0.003**	0.48	**0.001**	0.37	**0.002**
Low vs high	Euclidean	56.32	**0.001**	0.59	**0.001**	11.85	**0.001**
	Horn	0.13	**0.001**	0.48	**0.001**	11.76	**0.001**
	Bray	0.14	**0.001**	0.48	**0.001**	11.13	**0.001**
525 m vs 530 m	Euclidean	57.98	0.304	0.03	0.293	0.04	0.773
	Horn	0.14	0.304	0.02	0.290	0.03	0.755
	Bray	0.15	0.281	0.03	0.279	0.03	0.750
4,608 m vs 4,652 m	Euclidean	54.3	0.233	0.06	0.219	0.05	0.778
	Horn	0.11	0.219	0.04	0.279	0.04	0.739
	Bray	0.13	0.238	0.02	0.317	0.04	0.753

Three different permutation tests were performed, including multiple response permutation procedure (MRPP), analysis of similarity (ANOSIM), and permutational multivariate analysis of variance (Adonis), based on Euclidean, Horn, or Bray distance. Bold values indicate test results with p < 0.05.

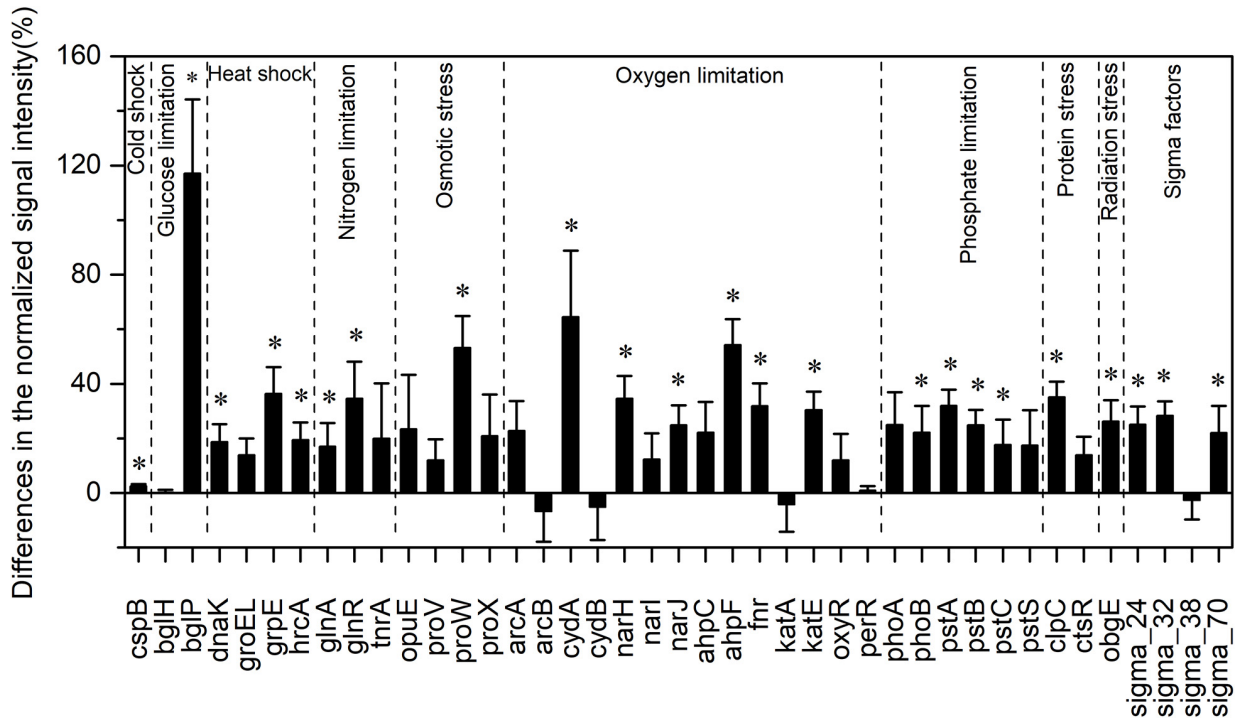

FIGURE 2 | Differences in the normalized intensities of the stress response gene categories between the two LELs and two HELs. All data are presented as mean ± s.e. calculated from biological 12 replicates. Asterisks (*) above the bars indicated significant ($p < 0.05$) differences.

HELs (**Supplementary Figure 2H**). Differences in radiation stress were related to the most diverse range of taxa, including *Chlorobi*, *Cyanobacteria*, *Deltaproteobacteria*, *Deinococcus-Thermus*, *Firmicutes*, *Gammaproteobacteria*, and *Thermotogae* (**Supplementary Figure 2I**).

Functional Genes Involved in Carbon Cycling

For autotrophic carbon fixation genes, although ATP citrate lyase (*aclB*), carbon-monoxide dehydrogenase (*CODH*), ribulose-1,5-bisphosphate carboxylase/oxygenase (*rubisco*), and acetyl-CoA carboxylase biotin carboxylase subunit (*pcc*) gene groups were observed in both HELs and LELs, the normalized signal intensities of all of them were not significantly different (**Figure 3A**, $p > 0.20$ in all cases). Similarly, the metabolic potential of acetogenesis [i.e., formyltetrahydrofolate synthetase (*FTHFS*)] in the Wood–Ljungdahl pathway was also not significantly changed with the increase of elevation (**Figure 3A**, $p = 0.43$). The same pattern was observed in methane oxidation genes of *mmoX* and *pmoA* (**Figure 3A**, $p > 0.22$ in both cases). However, the normalized signal intensity of a methanogenesis gene, *hdrB* (methyl-coenzyme M reductase), was nearly twofold higher in the HELs compared with the LELs (**Figure 3A**, $p < 0.05$).

Taxa–function relationships revealed that most of these differences in carbon fixation genes were derived from *Euryarchaeota* and *Crenarchaeota* and that these *Euryarchaeota* (primarily *Archaeoglobus fulgidus* and *Methanolinea tarda*) and *Crenarchaeota* (*Metallosphaera yellowstonensis*) were not detected in the LELs (**Supplementary Figure 3A**).

In contrast to the carbon-fixing genes, eight genes involved in carbon degradation, especially the metabolic potentials of recalcitrant carbon such as chitin, and aromatic compounds, had significantly different normalized signal intensities between the HELs and the LELs (**Figure 3B**). Compared with the LELs, the most significantly enhanced carbon degradation genes in the HELs were related to aromatic metabolism (*camDCAB*, increased 48%), followed by another aromatic metabolizing gene [vanillin dehydrogenase (*vdh*), increased 25%], three genes involved in chitin metabolism (*hyaluronidase*, *acetylglucosaminidase*, and *chitinase*, increased 26, 20, and 15%, respectively), and one involved in cellulose metabolism (*cellobiase*, increased 20%). Other markedly increased normalized signal intensities in the HELs were detected in a starch degradation gene [cyclomaltodextrinase (*cda*), increased 8%] and a hemicellulose degradation gene (*mannanase*, increased 14%; $p < 0.05$ in all cases). These differences were ascribed to some common carbon degradation microorganisms, including *Firmicutes*, *Actinobacteria*, *Gammaproteobacteria*, *Alphaproteobacteria*, and *Betaproteobacteria* (**Supplementary Figures 3B–I**).

Functional Genes Involved in Phosphorus and Nitrogen Metabolism

Among the three phosphorus cycling genes, only the functional potential of *phytase* for phytate degradation was significantly higher in HELs than in LELs ($p < 0.05$, **Figure 3C**). This was in

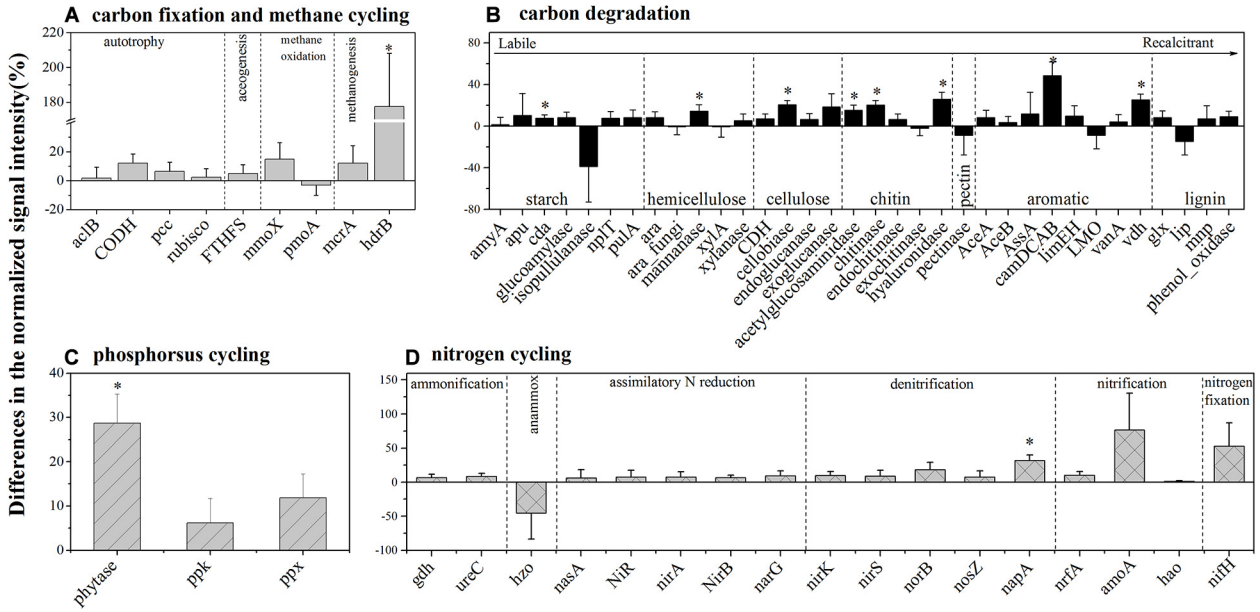

FIGURE 3 | Differences in the normalized intensities of certain biogeochemical cycling processes between the two LELs and two HELs. **(A)** Each subcategory of the carbon fixation and methane cycling; **(B)** each subcategory of carbon degradation; **(C)** each subcategory of phosphorus cycling; and **(D)** each subcategory of nitrogen cycling. All data are presented as mean ± s.e. calculated from biological 12 replicates. Asterisks (*) above the bars indicated significant ($p < 0.05$) differences.

accordance with the higher relative abundance of polyphosphate-degrading microorganisms from *Gammaproteobacteria*, *Firmicutes*, *Alphaproteobacteria*, *Betaproteobacteria*, and *Bacteroidetes* in the HELs ($p < 0.05$, **Supplementary Figure 3K**). Regarding the 17 nitrogen cycling gene groups, only one nitrate reduction gene (*napA*) had a significantly higher normalized signal intensity in the HELs compared with those in the LELs ($p < 0.05$, **Figure 3D**). Taxa–function relationship analysis revealed that this marked difference in normalized signal intensity for nitrate reduction between HELs and LELs was observed primarily in *Actinobacteria* and *Deltaproteobacteria* ($p < 0.05$, **Supplementary Figure 3J**).

Microbial Functional Gene Network Analysis

The two networks generated in this study produced 1873 nodes and 7550 links (47% negative and 53% positive) for the HELs and 1355 nodes and 4548 links (45% negative and 55% positive) for the LELs, respectively (**Figure 4**). Typical correlation values of the two constructed fMENs were both 0.98 (**Table 2**), indicating that connectivity of the two fMENs fitted the power law model. The indexes including modularity, clustering coefficients, and harmonic geodesic distance were significantly different from those of the corresponding random networks for the lakes at both elevations (**Table 2**). This indicated that the fMENs in both lakes were non-random ($p < 0.001$ in all cases, **Table 2**). Compared with the network of the LELs, the fMEN in the HELs generally had higher connectivity, shorter geodesic distances, higher clustering efficiencies, and more modules (**Table 2**).

More interactions and module hubs in relation to stress response and carbon cycling functional genes were found in the network of the HELs than in that of the LELs (**Supplementary Table 3**). Hub nodes in the LELs network predominantly belonged to carbon cycling genes (i.e., carbon degradation subcategory; **Supplementary Table 3**). In contrast, most hub nodes in the HELs network belonged to stress response genes (i.e., oxygen stress, oxygen limitation, sigma factors, and phosphate limitation), and some belonged to carbon cycling genes (**Supplementary Table 3**). No connectors were detected in the LELs network, but two were present in the HELs network, one of which was a stress response gene (**Supplementary Table 3**). The top-ranked functional genes, whose connectivity (links between genes) ranked in the top five of each network, in the HELs network were distinct from those in the LELs (**Supplementary Figure 4**). The top five genes in the HELs network belonged to stress response genes (*katE*, *fnr*, and *sigma_24*) and carbon cycling genes (*cellobiose* and *hyaluronidase*), while those in the network from the LELs belonged to carbon cycling genes (*chitinase* and *hyaluronidase*), a nitrogen reduction gene (*napA*), and a stress response gene (*sigma_70*). Moreover, the interactions of the top five genes in the HELs network (**Supplementary Figure 4A**) were much more complex in terms of network size and connectivity than those in the LELs network (**Supplementary Figure 4B**).

Linkages Between MFS and Lake Environmental Parameters

Canonical correspondence analysis indicated that four factors—temperature, PO_4-P, DOC, and turbidity—played key roles in

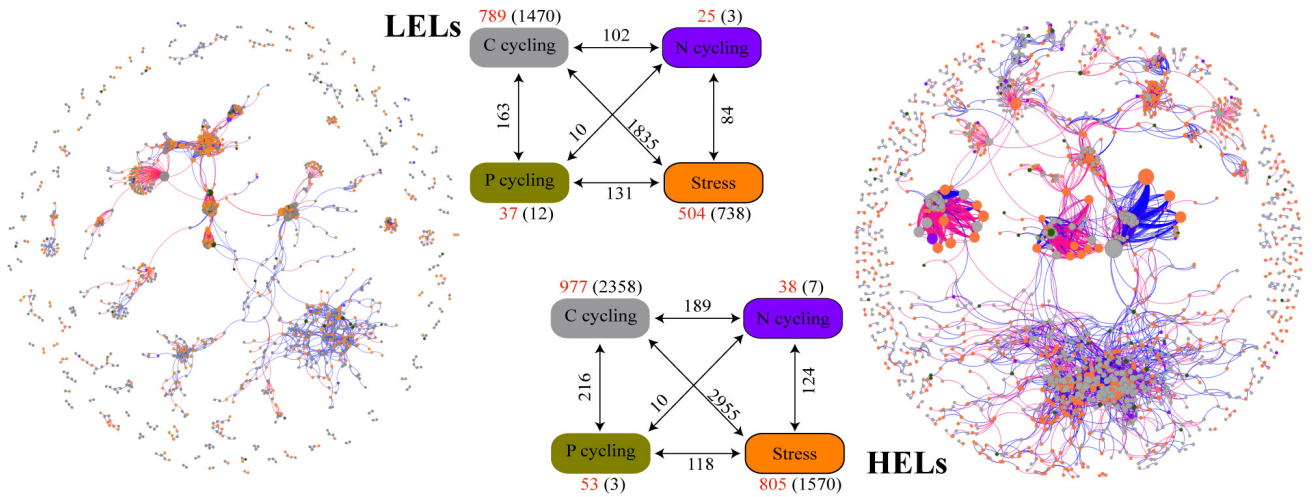

FIGURE 4 | Differences in network interactions of these genes between the two LELs and two HELs. Network analysis showing the associations within each gene category and associations between different gene categories. A connection indicates a strong (Spearman's $r > 0.8$ or $r < -0.8$) and significant ($p < 0.01$) correlation. A blue line indicates a positive interaction between two nodes, and a red line indicates a negative interaction. The size of each node is proportional to the number of connections (i.e., degree). Colors of the nodes indicate different functional gene categories: orange, stress response; gray, carbon cycling; dark violet, nitrogen cycling; dark goldenrod, and phosphorus cycling. Numbers outside and inside parentheses represent the node numbers and inner connections belonging to the corresponding gene category (i.e., there were 504 nodes and 738 inner connections for stress response genes in LELs); the numbers adjacent to edge connections represent cross-gene-category interactions.

shaping the variance of the differences in MFS in the four lakes (for all canonical axes, $p < 0.05$, **Figure 5A**). The first two axes explained 19.8% of the observed variation in the composition of the MFS, and 37.6% was explained by all four canonical axes. All four selected factors showed high canonical correlations with the first axis.

Variation partitioning analysis indicated that environmental heterogeneity was most important in explaining the variance of the differences in MFS in the four lakes (**Figure 5B**). The three categories of variables—environmental heterogeneity, productivity, and space (elevation and lake area)—explained 37.7, 4.6, and 5.4% of the total variance, respectively. Interactions among the three groups contributed 30.3% of the total variance. A smaller portion (22%) of the MFS variations could not be explained by the tested variables.

The five top-ranking modules detected in the HELs and LELs networks demonstrated different relationships with the environmental variables (**Supplementary Figure 5**). In the network of the HELs, modules 1 and 5 were positively correlated with turbidity; modules 3 and 4 were negatively correlated with water temperature, but the concentrations of Chl *a* and DOC were positively correlated with pH; and module 2 was negatively correlated with oxidation reduction potential. In contrast, in the network of the LELs, the largest module, module 1, showed positive and negative correlations with water temperature and total phosphorus, respectively. Modules 3 and 4, which were negatively correlated with DOC, showed positive correlations with DO, while module 2 did not correlate with any of the investigated environmental variables.

DISCUSSION

Enhanced Potentials of Stress Response in the HELs

In this study, two LELs were used as a reference to investigate the responses of microbial functional traits to elevational increase. Microbial metabolic potentials were significantly different between the HELs and the LELs. The biggest difference was that the normalized signal intensities of microbial stress genes were higher in the HELs than in the LELs (**Figure 1**). Soil microbial communities at higher elevations were previously shown to maintain high normalized signal intensities in stress response genes including those involved in cold shock, oxygen limitation, and osmotic stress (Yang et al., 2014). In addition to these genes, another seven subcategories of stress response genes with higher normalized signal intensities in the HELs were identified in the present study; these were nitrogen limitation, phosphate limitation, glucose limitation, radiation stress, heat shock, protein stress, and sigma factors (**Figure 2**). Previous studies using different versions of GeoChip to this study detected all the probes related to these seven subcategories of stress response genes (Tu et al., 2014; Picazo et al., 2020); these studies used GeoChip 4.0, the same as that used by Yang et al. (2014). Detection of more stress response genes with higher normalized signal intensities in the HELs in the present study may be due to more significant changes in environmental factors of the water within a broader elevation gradient and to the characteristics of the lakes themselves. With the increase in elevation from approximately 530 m to more than 4,600 m, the water temperature dropped significantly from 27 to 3°C; Chl *a* concentration decreased more than 20-fold; the concentrations of nutrients such as phosphate,

TABLE 2 | Major topological properties of the empirical fMENs and their associated random networks in the LELs and HELs.

Elevation of Lakes (m)	No. of original genes[a]	Empirical networks								Random networks[c]		
		Similarity threshold (St)	Network size (*n*)[b]	Links	R^2 of power law	Average connectivity (avgK)	Harmonic geodesic distance (HD)	Average clustering coefficient (avgCC)	Modularity (no. of modules)	Transitivity (Trans)	Harmonic geodesic distance (HD ± SD)	Average clustering coefficient (avgCC ± SD)	Average modularity (M ± SD)
LELs	1,808	0.98	1,355	4,548	0.881	6.713	6.668[d]	0.350[d]	0.790[d](133)	0.333	3.408 ± 0.014	0.029 ± 0.003	0.333 ± 0.003
HELs	2,397	0.98	1,873	7,550	0.877	8.062	6.269[d]	0.366[d]	0.865[d](156)	0.340	3.379 ± 0.009	0.023 ± 0.002	0.340 ± 0.002

[a] The number of genes used for network construction. [b] The number of nodes in a network in a functional molecular ecological network. [c] The parameters were generated from 100 times of random rewired networks. [d] Significant difference between the empirical network and the random network ($p < 0.001$, Z test).

nitrate, and ammonium were negligible; and DO decreased by 50% (**Supplementary Table 1**). These environmental conditions in the HELs could cause higher microbial metabolic potentials of nitrogen limitation, phosphate limitation, glucose limitation, and protein stress genes.

The normalized signal intensities of microbial radiation stress genes were also significantly higher in the HELs compared with those in the LELs. This was in contrast to data from grass soil in which radiation stress genes were more abundant at the lower elevation (Yang et al., 2014). This difference might be attributed to the fact that UV radiation is more intensive in surface water than in grass soil where aboveground vegetation prevents UV penetration (Yang et al., 2014). The discovery of more functional genes with high normalized signal intensities in diverse subcategories of the stress response pathways in the HELs than in grass soil confirms that recruitment of microbes to exposed habitats is strongly based on selection of stress tolerance traits. Furthermore, this finding indicates that these microbial communities have more diverse abilities with which to tolerate harsh environmental conditions than more sheltered habitats (Chan et al., 2013).

Higher normalized signal intensities in the microbial functional genes related to heat shock and sigma factors were observed in the HELs compared with the LELs. Similar results were also found on Antarctica rock surface (Chan et al., 2013), in Tibetan mountainous grass soil (Yang et al., 2014; Qi et al., 2017), and on stones in streams (Picazo et al., 2020). Mounting evidence suggests that besides protecting microbial cells from environmental insults of sudden temperature increases, the transcriptional activities of heat shock genes are maintained at a steady-state level that is frequently greater than the initial basal level for the purpose of facilitating microbial growth under non-optimal environmental conditions (Macario et al., 1999; Roncarati and Scarlato, 2017). Moreover, some heat shock proteins are also required and are abundant during normal growth conditions. For example, the genes *GroEL* and *dnaK* are instrumental in protein folding even during non-stressed growth conditions, although their activities become more important during stress (Macario et al., 1999; Roncarati and Scarlato, 2017). In addition to temperature variations, several other stress conditions, such as osmotic changes, desiccation, antibiotics, solvents, and heavy metals, can elicit heat shock responses (Roncarati and Scarlato, 2017). In the present study, HELs are frozen for most of the year. However, there are diurnal temperature variations in the summer, which are likely to cause an increase in heat shock genes. Alternative sigma factors are the positive transcriptional regulators of heat shock genes (Roncarati and Scarlato, 2017), and these were also increased in the HELs in the present study.

Enhanced Potentials of Carbon Degradation in the HELs

There were no significant changes in the normalized signal intensities of the functional gene categories of carbon, phosphorus, and nitrogen metabolisms in the HELs (**Figure 1A**). However, there were a few marked increases in the normalized

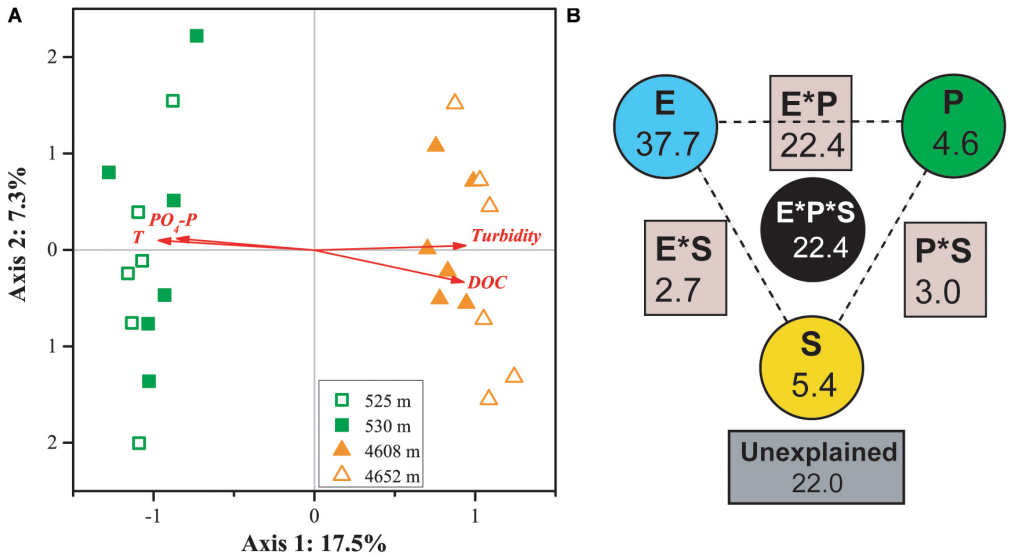

FIGURE 5 | CCA **(A)** and VPA **(B)** of relationships between the microbial functional community structure and the environmental variables. P: productivity: Chl *a*, DOC; S: space: elevation and area; and E: the rest of the tested environmental variables. Numbers on the CCA axis and in the VPA diagram show the percentages of explained variations in the microbial functional gene profile. In the VPA diagram, the edges of the triangle presented the variation explained by each factor alone, while the sides of the triangles presented interactions of any two factors and the middle of the triangles represented interactions of all three factors.

signal intensities of carbon degradation genes at the single functional gene level (**Figure 3B**). Differences in the composition of DOC may be a principal factor causing changes in microbial taxonomic structure in aquatic ecosystems (Teeling et al., 2012; Sarmento et al., 2013), and this may subsequently influence the microbial functional metabolic potentials (Kuang et al., 2016). Generally, there are two main carbon sources in lake ecosystems: terrestrial (allochthonous) inputs of carbon received from the landscape around lakes and autochthonous carbon provided by in-lake primary production (Rose et al., 2015). The relative contribution of allochthonous carbon inputs increases with increasing elevation whereas their lability decreases with increasing elevation (Zhou et al., 2018). Zhou et al. (2019) reported that dissolved organic matter aromaticity and the relative abundance of lignin compounds in glacial-fed streams and rivers on the Tibetan Plateau all increased during water flows downstream from the glacial terminus, and the same may apply in the HELs in the present study. The DOC-to-Chl *a* ratio is an allochthony indicator (Carpenter et al., 2005; Bade et al., 2007; Pace et al., 2007). In the present study, the DOC-t- Chl *a* ratios in the two HELs were on average 12-fold greater than those in the two LELs (**Supplementary Table 1**). The more allochthonous DOC in the HELs may promote the microbial functional potentials of carbon degradation, such as *camDCA*, *chitinaseb*, *hyaluronidase*, *cellobiase*, *cda*, and *mannanase* (**Figure 3B**).

Enhanced Interactions Among the Co-occurring Functional Genes in the HELs

Comparison of network properties, such as links, network size, connectivity, and clustering coefficients, in the lakes at the two elevations identified reinforced complexity in the HELs network. Soil microbial networks detected in northern China were previously reported to be more complex than those found in southern China, suggesting that temperature affects the complexity of microbial networks at a continental scale (Ma et al., 2016; Zhang et al., 2018). Network analyses in the current study indicated that, with the increase in elevation from approximately 530 to 4,600 m, the functional gene network increased in network size and became much more connected and clustered (**Table 2** and **Figure 4**). Temperature and DOC were two of the most important environmental causes of these changes in network properties (**Supplementary Figure 5**). This finding was consistent with that of acidic mining lakes, in which harsh conditions such as low pH, high concentrations of sulfate and metals, and limited carbon, nitrogen, and phosphorus sources resulted in more complex microbial functional gene networks (Ren et al., 2018). These discoveries may be attributed to the fact that to survive in harsh environments, microorganisms cooperate by participating in diverse metabolic pathways of the microbial food chain, such as degrading (complex) organics or metabolizing carbon, nitrogen, and phosphorus (Dong et al., 2020). Similarly, to adapt to the high elevation and its related factors, some microorganisms in the HELs enhanced their potentials of recalcitrant carbon degradation genes (such as *cellobiase_bact_arch*, *chitinaseb*, and *hyaluronidase*; **Figure 3B**) to provide carbon sources for other microorganisms. In return, other microbes increased their potentials of stress response genes (e.g., *katE*, *fnr*, and sigma_24 and sigma_70 genes; **Figure 2**) to help other microorganisms survive under conditions of low oxygen, low temperature and large variation of temperature, and high UV radiation. These results were confirmed by the HELs network having more interactions and also containing

more module hubs and two connectors in relation to stress response and carbon cycling functional genes, compared with the LELs network (**Supplementary Table 3** and **Supplementary Figure 4**). A previous report confirmed that one member of nodes that had high connections in the bacterial co-occurrence network could facilitate one member of the peripheral vertexes by providing the latter with several low-molecular-weight organic substrates (Xian et al., 2020). However, the mechanisms of our findings in the present study require further investigation using a combination of culture-dependent and culture-independent techniques, such as metatranscriptomics, metaproteomics, and metabolomics approaches.

No Differences in Overall Functional Gene Richness Between the HELs and LELs

The overall functional gene diversity was not significantly different between the HELs and LELs. This is in contrast to data from grass soil where the number of detected microbial genes at the 3,200-m site was approximately half of those at the three higher elevations (3,400, 3,600, and 3,800 m; Yang et al., 2014). These differences may predominantly be due to covariance of elevation and regional characteristics in terrestrial ecosystems, whereas lakes are more homogeneous (Li et al., 2017). For example, the pH in soil changed more within the elevational range of 600 m (Yang et al., 2014) than in lake water within the elevational range of 4,100 m (this study), and pH is known to have an adverse effect on microbial gene diversity (Yang et al., 2014; Ren et al., 2018). Furthermore, large numbers of introduced rare bacterial taxa, which enter lakes from surrounding catchments or sediments, can increase the overall bacterial diversity in small lakes with large catchment areas at high elevations (e.g., Lindström and Bergström, 2004; Crump et al., 2012; Li et al., 2017) and are also likely to influence microbial functional gene diversity. Thus, in comparison to the LELs, the microbial gene richness in the two HELs did not decrease but increased slightly.

CONCLUSION

This study demonstrated that the elevation increase of approximately 4,100 m, which relates to changes in different environmental variables, has a strong influence on the profile of microbial functional potentials in lake water columns. Harsh conditions (e.g., nutrient limitation, low temperature and large variation of temperature, high UV radiation, and more recalcitrant DOC) at high elevations may significantly promote the microbial metabolic potentials among functional genes involved in stress responses and recalcitrant carbon degradation in freshwater lakes. Microbes exposed to higher elevation stressors had increased signal intensities of stress response functional genes, increased numbers of module hubs of these genes, and enhanced complexity of gene interactions. This study highlights that the limnetic microbial communities develop functional strategies to cope with the harsh conditions at high elevations.

DATA AVAILABILITY STATEMENT

The datasets presented in this study can be found in online repositories. The names of the repository/repositories and accession number(s) can be found below: www.ncbi.nlm.nih.gov/geo/query/acc.cgi?acc=GSE156784.

AUTHOR CONTRIBUTIONS

HL, JZ, and QW conceived and initiated the study and led the writing of the manuscript. LR collected the samples. QY analyzed the data. All the authors contributed substantially to the study.

FUNDING

This work was supported by the Chinese Academy of Sciences (QYZDJ-SSW-DQC030), the National Science Foundation of China (31971471, 91951000, and 41621002), and the Second Tibetan Plateau Scientific Expedition and Research Program (2019QZKK0503).

ACKNOWLEDGMENTS

We thank Joe Zhou and Ruizhu Huang for their support on GeoChip and data analysis of the samples. This manuscript has been released as a pre-print at bioRxiv (Li et al., 2020).

SUPPLEMENTARY MATERIAL

The Supplementary Material for this article can be found online at: https://www.frontiersin.org/articles/10.3389/fmicb.2020.595967/full#supplementary-material

REFERENCES

Bade, D. L., Carpenter, S. R., Cole, J. J., Pace, M. L., Kritzberg, E., Van De Bogert, M. C., et al. (2007). Sources and fates of dissolved organic carbon in lakes as determined by whole–lake carbon isotope additions. *Biogeochemistry* 84, 115–129. doi: 10.1007/s10533-006-9013-y

Barberán, A., Bates, S. T., Casamayor, E. O., and Fierer, N. (2012). Using network analysis to explore co-occurrence patterns in soil microbial communities. *ISME J.* 6, 343–351. doi: 10.1038/ismej.2011.119

Bastian, M., Heymann, S., and Jacomy, M. (2009). "Gephi: An Open Source Software for Exploring and Manipulating Networks," in *International AAAI Conference on Weblogs and Social Media*. (New York: BibSonomy).

Bhatt, J. P., Manish, K., and Pandit, M. K. (2012). Elevational gradients in fish diversity in the Himalaya: water discharge is the key driver of distribution patterns. *PLoS One* 7:e46237. doi: 10.1371/journal.pone.0046237

Bryant, J. A., Lamanna, C., Morlon, H., Kerkhoff, A. J., Enquist, B. J., and Green, J. L. (2008). Microbes on mountainsides: contrasting elevational patterns of

bacterial and plant diversity. *Proc. Natl. Acad. Sci. U S A.* 105, 11505–11511. doi: 10.1073/pnas.0801920105

Carpenter, S. R., Cole, J. J., Pace, M. L., Van de Bogert, M., Bade, D. L., Bastviken, D., et al. (2005). Ecosystem subsidies: terrestrial support of aquatic food webs from ^{13}C addition to contrasting lakes. *Ecology* 86, 2737–2750. doi: 10.1890/04-1282

Chan, Y., Van Nostrand, J. D., Zhou, J., Pointing, S. B., and Farrell, R. L. (2013). Functional ecology of an Antarctic Dry Valley. *Proc. Natl. Acad. Sci. U S A.* 110, 8990–8995. doi: 10.1073/pnas.1300643110

Cole, J. J., Pace, M. L., Carpenter, S. R., and Kitchell, J. F. (2000). Persistence of net heterotrophy in lakes during nutrient addition and food web manipulations. *Limnol. Oceanogr.* 45, 1718–1730. doi: 10.4319/lo.2000.45.8.1718

Crump, B. C., Amaral-Zettler, L. A., and King, G. W. (2012). Microbial diversity in arctic freshwaters is structured by inoculation of microbes from soils. *ISME J.* 6, 1629–1639. doi: 10.1038/ismej.2012.9

de Menezes, A. B., Prendergast-Miller, M. T., Richardson, A. E., Toscas, P., Farrell, M., Macdonald, L. M., et al. (2015). Network analysis reveals that bacteria and fungi form modules that correlate independently with soil parameters. *Environ. Microbiol.* 17, 2677–2689. doi: 10.1111/1462-2920.12559

Deng, Y., Jiang, Y., Yang, Y., He, Z., Luo, F., and Zhou, J. (2012). Molecular ecological network analyses. *BMC Bioinform.* 13:113. doi: 10.1186/1471-2105-13-113

Deng, Y., Zhang, P., Qin, Y., Tu, Q., Yang, Y., He, Z., et al. (2016). Network succession reveals the importance of competition in response to emulsified vegetable oil amendment for uranium bioremediation. *Environ. Microbiol.* 18, 205–218. doi: 10.1111/1462-2920.12981

Dong, Y., Gao, J., Wu, Q., Ai, Y., Huang, Y., Wei, W., et al. (2020). Co-occurrence pattern and function prediction of bacterial community in Karst cave. *BMC Microbiol.* 20:137. doi: 10.1186/s12866-020-01806-7

Fierer, N., Mccain, C. M., Meir, P., Zimmermann, M., Rapp, J. M., Silman, M. R., et al. (2011). Microbes do not follow the elevational diversity patterns of plants and animals. *Ecology* 92, 797–804. doi: 10.1890/10-1170.1

Gilbert, J. A., Steele, J. A., Caporaso, J. G., Steinbruck, L., Reeder, J., Temperton, B., et al. (2012). Defining seasonal marine microbial community dynamics. *ISME J.* 6, 298–308. doi: 10.1038/ismej.2011.107

Greenblum, S., Turnbaugh, P. J., and Borenstein, E. (2012). Metagenomic systems biology of the human gut microbiome reveals topological shifts associated with obesity and inflammatory bowel disease. *Proc. Natl. Acad. Sci. U S A.* 109, 594–599. doi: 10.1073/pnas.1116053109

Grytnes, J. A., and Mccain, C. M. (2007). "Elevational trends in biodiversity," in *Encyclopedia of biodiversity*, ed. S. A. Levin (Netherland: Elsevier Inc), 1–8. doi: 10.1016/b978-012226865-6/00503-1

Guimerà, R., and Amaral, L. A. N. (2005). Functional cartography of complex metabolic networks. *Nature* 433, 895–900. doi: 10.1038/nature03288

Hayden, C. J., and Beman, J. M. (2016). Microbial diversity and community structure along a lake elevation gradient in Yosemite National Park. *Calif. USA. Environ. Microbiol.* 18, 1782–1791. doi: 10.1111/1462-2920.12938

He, Z., Deng, Y., Van Nostrand, J. D., Tu, Q., Xu, M., Hemme, C. L., et al. (2010). GeoChip 3.0 as a high-throughput tool for analyzing microbial community composition, structure and functional activity. *ISME J.* 4, 1167–1179. doi: 10.1038/ismej.2010.46

Hessen, D. O., Bakkestuen, V., and Walseng, B. (2007). Energy input and zooplankton species richness. *Ecography* 30, 749–758. doi: 10.1111/j.2007.0906-7590.05259.x

Hu, A., Ju, F., Hou, L., Li, J., Yang, X., Wang, H., et al. (2017). Strong impact of anthropogenic contamination on the co-occurrence patterns of a riverine microbial community. *Environ. Microbiol.* 19, 4993–5009. doi: 10.1111/1462-2920.13942

Jacobsen, D. (2004). Contrasting patterns in local and zonal family richness of stream invertebrates along an Andean altitudinal gradient. *Freshwater Biol.* 49, 1293–1305. doi: 10.1111/j.1365-2427.2004.01274.x

Jankowski, T., and Weyhenmeyer, G. A. (2006). The role of spatial scale and area in determining richness–altitude gradients in Swedish lake phytoplankton communities. *Oikos* 115, 433–442. doi: 10.1111/j.2006.0030-1299.15295.x

Jones, J. I., Li, W., and Maberly, S. C. (2003). Area, altitude and aquatic plant diversity. *Ecography* 26, 411–420. doi: 10.1034/j.1600-0587.2003.03554.x

Kuang, J., Huang, L., He, Z., Chen, L., Hua, Z., Jia, P., et al. (2016). Predicting taxonomic and functional structure of microbial communities in acid mine drainage. *ISME J.* 10, 1527–1539. doi: 10.1038/ismej.2015.201

Li, H., Zeng, J., Ren, L., Wang, J., Xing, P., and Wu, Q. L. (2017). Contrasting patterns of diversity of abundant and rare bacterioplankton in freshwater lakes along an elevation gradient. *Limnol. Oceanogr.* 62, 1570–1585. doi: 10.1002/lno.10518

Li, H., Zeng, J., Ren, L., Yan, Q., and Wu, Q. L. (2020). Enhanced metabolic potentials and functional gene interactions of microbial stress response towards high elevation in freshwater lakes. *bioRxiv* doi: 10.1101/2020.07.10.198234

Liang, Y., Van Nostrand, J. D., Deng, Y., He, Z., Wu, L., Zhang, X., et al. (2011). Functional gene diversity of soil microbial communities from five oil contaminated fields in China. *ISME J.* 5, 403–413. doi: 10.1038/ismej.2010.142

Lindström, E. S., and Bergström, A. (2004). Influence of inlet bacteria on bacterioplankton assemblage composition in lakes of different hydraulic retention time. *Limnol. Oceanogr.* 49, 125–136. doi: 10.4319/lo.2004.49.1.0125

Ma, B., Wang, H., Dsouza, M., Lou, J., He, Y., Dai, Z., et al. (2016). Geographic patterns of co-occurrence network topological features for soil microbiota at continental scale in eastern China. *ISME J.* 10, 1891–1901. doi: 10.1038/ismej.2015.261

Macario, A. J. L., Lange, M., Ahring, B. K., and De Macario, E. C. (1999). Stress Genes and Proteins in the Archaea. *Microbiol. Mole. Biol. Rev.* 63, 923–967. doi: 10.1128/MMBR.63.4.923-967.1999

Montoya, J. M., Pimm, S. L., and Sole, R. V. (2006). Ecological networks and their fragility. *Nature* 442, 259–264. doi: 10.1038/nature04927

Nyman, M., Korhola, A., and Brooks, S. J. (2005). The distribution and diversity of Chironomidae (Insecta: Diptera) in western Finnish Lapland, with special emphasis on shallow lakes. *Globl. Ecol. Biogeogr.* 14, 137–153. doi: 10.1111/j.1466-822X.2005.00148.x

Obertegger, U., Thaler, B., and Flaim, G. (2010). Rotifer species richness along an altitudinal gradient in the Alps. *Glob. Ecol. Biogeogr.* 19, 895–904. doi: 10.1111/j.1466-8238.2010.00556.x

Oksanen, J., Blanchet, F. G., Kindt, R., Legendre, P., Minchin, P. R., O'Hara, R. B., et al. (2013). *vegan: Community ecology package*. URL: https://cran.r--project.org/web/packages/vegan/index.html

Pace, M. L., Carpenter, S. R., Cole, J. J., Coloso, J. J., Kitchell, J. F., Hodgson, J. R., et al. (2007). Does terrestrial organic carbon subsidize the planktonic food web in a Clear-water lake? *Limnol. Oceanogr.* 52, 2177–2189. doi: 10.4319/lo.2007.52.5.2177

Picazo, F., Vilmi, A., Aalto, J., Soininen, J., Casamayor, E. O., Liu, Q., et al. (2020). Climate mediates continental scale patterns of stream microbial functional diversity. *Microbiome* 8:92. doi: 10.1186/s40168-020-00873-2

Qi, Q., Zhao, M., Wang, S., Ma, X., Wang, Y., Gao, Y., et al. (2017). The Biogeographic Pattern of Microbial Functional Genes along an Altitudinal Gradient of the Tibetan Pasture. *Front. Microbiol.* 8:976. doi: 10.3389/fmicb.2017.00976

Rahbek, C. (2005). The role of spatial scale and the perception of large–scale species–richness patterns. *Ecol. Lett.* 8, 224–239. doi: 10.1111/j.1461-0248.2004.00701.x

Ren, L., Song, X., Jeppesen, E., Xing, P., Liboriussen, L., Xu, X., et al. (2018). Contrasting patterns of freshwater microbial metabolic potentials and functional gene interactions between an acidic mining lake and a weakly alkaline lake. *Limnol. Oceanogr.* 63, S354–S366. doi: 10.1002/lno.10744

Roncarati, D., and Scarlato, V. (2017). Regulation of heat-shock genes in bacteria: from signal sensing to gene expression output. *FEMS Microbiol. Rev.* 41, 549–574. doi: 10.1093/femsre/fux015

Rose, K. C., Williamson, C. E., Kissman, C. E. H., and Saros, J. E. (2015). Does allochthony in lakes change across an elevation gradient? *Ecology* 96, 3281–3291. doi: 10.1890/14-1558.1

Sarmento, H., Romera-Castillo, C., Lindh, M. V., Pinhassi, J., Sala, M. M., Gasol, J. M., et al. (2013). Phytoplankton species-specific release of dissolved free amino acids and their selective consumption by bacteria. *Limnol. Oceanogr.* 58, 1123–1135. doi: 10.4319/lo.2013.58.3.1123

Shannon, P., Markiel, A., Ozier, O., Baliga, N. S., Wang, J., Ramage, D., et al. (2003). Cytoscape: A Software Environment for Integrated Models of Biomolecular Interaction Networks. *Genome Res.* 13, 2498–2504. doi: 10.1101/gr.1239303

Shi, S., Nuccio, E. E., Shi, Z. J., He, Z., Zhou, J., and Firestone, M. K. (2016). The interconnected rhizosphere: high network complexity dominates rhizosphere assemblages. *Ecol. Lett.* 19, 926–936. doi: 10.1111/ele.12630

Singh, D., Takahashi, K., Kim, M., Chun, J., and Adams, J. M. (2012). A hump–backed trend in bacterial diversity with elevation on Mount Fuji. *Japan. Microbial. Ecol.* 63, 429–437. doi: 10.1007/s00248-011-9900-1

Sturm, R. (2007). Freshwater molluscs in mountain lakes of the Eastern Alps (Austria): relationship between environmental variables and lake colonization. *J. Limnol.* 66, 160–169. doi: 10.4081/jlimnol.2007.160

Teeling, H., Fuchs, B. M., Becher, D., Klockow, C., Gardebrecht, A., Bennke, C. M., et al. (2012). Substrate controlled succession of marine bacterioplankton populations induced by a phytoplankton bloom. *Science* 336, 608–611. doi: 10.1126/science.1218344

Tu, Q., Yu, H., He, Z., Deng, Y., Wu, L., Van Nostrand, J. D., et al. (2014). GeoChip 4: a functional gene-array-based high-throughput environmental technology for microbial community analysis. *Mole. Ecol. Resour.* 14, 914–928. doi: 10.1111/1755-0998.12239

Wang, C., Wang, X., Liu, D., Wu, H., Lu, X., Fang, Y., et al. (2014). Aridity threshold in controlling ecosystem nitrogen cycling in arid and semi–arid grasslands. *Nat. Commun.* 5:4799. doi: 10.1038/ncomms5799

Wang, J., Soininen, J., Zhang, Y., Wang, B., Yang, X., and Shen, J. (2011). Contrasting patterns in elevational diversity between microorganisms and macroorganisms. *J. Biogeogr.* 38, 595–603. doi: 10.1111/j.1365-2699.2010.02423.x

Whitman, W. B., Coleman, D. C., and Wiebe, W. J. (1998). Prokaryotes: the unseen majority. *Proc. Natl. Acad. Sci. U S A.* 95, 6578–6583. doi: 10.1073/pnas.95.12.6578

Xian, W., Salam, N., Li, M., Zhou, E., Yin, Y., and Liu, Z. (2020). Network-directed efficient isolation of previously uncultivated *Chloroflexi* and related bacteria in hot spring microbial mats. *NPJ Biofil. Microbiom.* 6:20. doi: 10.1038/s41522-020-0131-4

Yan, Q., Bi, Y., Deng, Y., He, Z., Wu, L., Van Nostrand, J. D., et al. (2015). Impacts of the Three Gorges Dam on microbial structure and potential function. *Scient. Rep.* 5:8605. doi: 10.1038/srep08605

Yang, Y., Gao, Y., Wang, S., Xu, D., Yu, H., Wu, L., et al. (2014). The microbial gene diversity along an elevation gradient of the Tibetan grassland. *ISME J.* 8, 430–440. doi: 10.1038/ismej.2013.146

Zengler, K., and Zaramela, L. S. (2018). The social network of microorganisms – how auxotrophies shape complex communities. *Nat. Rev. Microbiol.* 16, 383–390. doi: 10.1038/s41579-018-0004-5

Zhang, B., Zhang, J., Liu, Y., Shi, P., and Wei, G. (2018). Co–occurrence patterns of soybean rhizosphere microbiome at a continental scale. *Soil Biol. Biochem.* 118, 178–186. doi: 10.1016/j.soilbio.2017.12.011

Zhou, J., Deng, Y., Luo, F., He, Z., and Yang, Y. (2011). Phylogenetic molecular ecological network of soil microbial communities in response to elevated CO_2. *Mbio* 2, 122–111.e. doi: 10.1128/mBio.00122-11

Zhou, J., Deng, Y., Luo, F., He, Z., Tu, Q., and Zhi, X. (2010). Functional molecular ecological networks. *Mbio* 1, 169–110 e. doi: 10.1128/mBio.00169-10

Zhou, Y., Davidsond, T. A., Yao, X., Zhang, Y., Jeppesen, E., de Souza, J. G., et al. (2018). How autochthonous dissolved organic matter responds to eutrophication and climate warming: Evidence from a cross-continental data analysis and experiments. *Earth Sci. Rev.* 185, 928–937. doi: 10.1016/j.earscirev.2018.08.013

Zhou, Y., Zhou, L., He, X., Jang, K., Yao, X., Hu, Y., et al. (2019). Variability in Dissolved Organic Matter Composition and Biolability across Gradients of Glacial Coverage and Distance from Glacial Terminus on the Tibetan Plateau. *Environ. Sci. Technol.* 53, 12207–12217. doi: 10.1021/acs.est.9b03348

Conflict of Interest: The authors declare that the research was conducted in the absence of any commercial or financial relationships that could be construed as a potential conflict of interest.

The reviewer KX declared a shared affiliation with one of the authors QW to the handling editor at the time of review.

frontiers in Marine Science

ORIGINAL RESEARCH
published: 25 January 2021
doi: 10.3389/fmars.2020.602002

Effect of Three Pesticides Used in Salmon Farming on Ammonium Uptake in Central-Southern and Northern Patagonia, Chile

Valentina Valdés-Castro[1] *and Camila Fernandez*[1,2,3,4]*

[1] *Centro de Investigación Oceanográfica COPAS Sur-Austral, Universidad de Concepción, Concepción, Chile,* [2] *Interdisciplinary Center for Aquaculture Research (INCAR), Universidad de Concepción, Concepción, Chile,* [3] *Sorbonne Universités, UPMC Univ Paris 06, CNRS, Laboratoire d'Océanographie Microbienne (LOMIC), Observatoire Océanologique, Banyuls-sur-Mer, France,* [4] *Centro FONDAP de Investigación en Dinámica de Ecosistemas Marinos de Altas Latitudes (IDEAL), Valdivia, Chile*

Chile is the second largest global producer of farmed salmon. The growth of salmon production has not been free of environmental challenges, such as the increasing use of pesticides to control the parasitic load of the sea lice *Caligus rogercresseyi.* The lack of the specificity of pesticides can potentially affect non-target organisms, as well as the structure and functioning of aquatic ecosystems. The aim of this study, was to understand the effect of pesticides on natural microbial communities to the addition of the anti-lice pesticide azamethiphos, deltamethrin and emamectin benzoate, and their potential impact in ammonium uptake rates in the coast off central-southern Chile and Northern Patagonia. The addition of pesticides on natural microbial communities resulted in a rapid response in ammonium uptake, which was significant for the single use of pesticide, azamethiphos and emamectin benzoate, as well as the combination, azamethiphos, deltamethrin and emamectin benzoate. In northern Patagonia, azamethiphos addition produced a 53% decrease in photoautotrophic uptake. However, an increase, although variable, was observed in chemoautotrophic uptake. Emamectin benzoate produced a 36 to 77% decrease in chemo and photoautotrophic ammonium uptake, respectively. The combined use of pesticides, also produced up to 42% decrease in both photo and chemoautotrophic assimilation. We conclude that the use of pesticides in salmon farming produces diverse responses at the microbial level, stimulating and/or inhibiting microbial communities with subsequent impact on nitrogen budgets. Further studies are necessary to understand the impact of pesticides in the ecology of central-southern and northern Patagonia, Chile.

Keywords: ammonium uptake, salmon farming, azamethiphos, deltamethrin, emamectin benzoate, Chile

OPEN ACCESS

Edited by:
Jose Luis Iriarte,
Austral University of Chile, Chile

Reviewed by:
Lasse Mork Olsen,
University of Bergen, Norway
Alexander Godfrey Murray,
Marine Scotland, United Kingdom

***Correspondence:**
Camila Fernandez
fernandez@obs-banyuls.fr

Specialty section:
This article was submitted to Marine Fisheries, Aquaculture and Living Resources, a section of the journal Frontiers in Marine Science

Received: *09 October 2020*
Accepted: *30 December 2020*
Published: *25 January 2021*

Citation:
Valdés-Castro V and Fernandez C (2021) Effect of Three Pesticides Used in Salmon Farming on Ammonium Uptake in Central-Southern and Northern Patagonia, Chile. Front. Mar. Sci. 7:602002. doi: 10.3389/fmars.2020.602002

INTRODUCTION

Chile is the second largest global producer of farmed salmon, with an annual production of over 700 thousand tons (Avendaño-Herrera, 2018). The growth of Chilean salmon production has not been free of sanitary and environmental difficulties, such as benthic accumulation of organic matter, eutrophication, massive escapes of farmed salmon, input of chemicals such as antibiotic and

pesticides into the ecosystem, fish diseases, and social issues (Burridge et al., 2010; Hargrave, 2010; Baskett et al., 2013; Dresdner et al., 2019; Quiñones et al., 2019).

The intensive use of pesticides to control sea lice infections of *Caligus rogercresseyi* has become a key environmental concern for Chilean aquaculture (Millanao et al., 2011; Núñez-Acuña et al., 2015; Avendaño-Herrera, 2018). Infestations result in severe skin erosion and epidermal hemorrhage, leading to chronic stress, reduced growth (González and Carvajal, 2003; Rozas and Asencio, 2007; González et al., 2015) and increasing the vulnerability of fish to other diseases (Bravo, 2003; Johnson et al., 2004; Dresdner et al., 2019).

Since the earliest reported infections, sea lice in Chile have been controlled using chemicals originally used in agriculture (Reyes and Bravo, 1983). Feed additives such as emamectin benzoate have been used since the 1990s (Bravo, 2003; Bravo et al., 2008) and later complemented by pyrethroids such as deltamethrin in 2007 due to the appearance of resistance of *C. rogercresseyi* to emamectin benzoate. In 2009, the Chilean authorities allowed the use of another pyrethroid, cypermethrin. Diflubenzuron was used between 2008 and 2012 and finally the organophosphate azamethiphos was introduced in Chile in 2013 (Helgesen et al., 2014).

Currently, the most commonly used products in Chile are the organophosphate azamethiphos and the pyrethroid deltamethrin. They are applied *in situ* by bath solution and are subsequently discharged into the surrounding environment in large volumes (Nash, 2003; Burridge et al., 2010; Gebauer et al., 2017). Helgesen et al. (2014) reported that 677 kg of active compound cypermethrin and 197 kg of deltamethrin were discarded in 2012.

The anti-lice treatments lack specificity and therefore may affect indigenous organisms with the potential to affect sensitive non-target species (Johnson et al., 2004). However, until now the studies available describing the impacts of pesticides in non-target organism are scarce and are mainly focus in invertebrates (Burridge et al., 2004; Knapp et al., 2005; Gebauer et al., 2017). Studies focusing on microorganism are even more scarce, and recently was reported that the use of pesticides in marine waters can produce changes in microbial photo and chemoautotrophic carbon uptake (Rain-Franco et al., 2018).

Microorganism are important habitants of aquatic ecosystems, playing a pivotal role in primary productivity and nutrient recycling. In the traditional view of the marine nitrogen (N) cycle, phytoplankton use dissolved inorganic N as nitrate (NO_3^-) or ammonium (NH_4^+) to create biomass while heterotrophic bacterioplankton remineralize dissolved organic N into the inorganic forms hence supporting primary production. By being in contact with pesticides, microbial community structure and metabolic fluxes can be modified, an effect that varies according to their chemical form and characteristics while interacting with the nutrient pool of the water column (Rain-Franco et al., 2018). This can result in an alteration of biogeochemical fluxes and local primary production.

To understand the impact of pesticides on non-target organisms and biogeochemistry, we investigated the potential effect of three pesticides used against *C. rogercresseyi* (azamethiphos, deltamethrin, and emamectin benzoate) on photo and chemoautotrophic ammonium uptake in two key regions of the Chilean coast that hold high levels of biological productivity but contrasting levels of influence from salmon farming.

MATERIALS AND METHODS

Study Area and Sampling Strategy

The study was conducted in two sites in central-southern and norther Patagonia, Chile: Llico Bay and Caucahue Channel, respectively. Llico Bay is a close bay located south of Gulf of Arauco in central Chile (37.1°S 73.5°W; **Figure 1A**) in an area untouched by salmon farming while, Caucahue Channel was located in the inland sea of Chiloe island, Northern Patagonia (42.1°S 73.4°W; **Figure 1B**) and is intensely influenced by salmon farming. Llico Bay was visited 4 times on board of R/V Kay Kay II (Universidad de Concepción) between July 2015 and April 2016 (**Table 1**). Caucahue Channel was visited twice on board the L/M "Don José" in June 2014 and January 2015 (**Table 1**).

During the sampling, we first assessed physical parameters such as temperature and salinity (CTD Minus; AML Oceanographic, Canada) at the three stations in Llico (**Figure 1** and **Table 1**). During Caucahue Channel sampling, we used a CTDO data sensor (SAIV A/S, Norway; **Figure 1** and **Table 1**). Chemical and biological samples were collected with Niskin bottles at all sampling stations (**Table 1**). Ammonium samples were taken in duplicate using 50 mL glass bottles (Duran Schott) and analyzed by the fluorometric method described by Holmes et al. (1999), using a Turner Designs fluorometer. Samples for nitrate (NO_3^-), nitrite (NO_2^-) and phosphate (PO_4^{3-}) were stored in high-density polyethylene (HDPE) plastic bottles (11 mL in duplicate) at −20°C until analyses by standard colorimetric techniques (Aminot and Kérouel, 2007). Bacterioplankton abundance was analyzed by flow cytometry (Marie et al., 1997) at Laboratory for oceanographic Processes and Climate (PROFC; Universidad de Concepción, Chile) with a FACSCalibur flow cytometer (Becton Dickinson). Total chlorophyll-a (Chl-a) were estimated using a Turner design fluorometer according (Holm-Hansen et al., 1965).

Isotopic Analysis and *in situ* Ammonium Uptake Experiments

Rates of ammonium uptake (ρNH_4^+) were determined using the $^{13}C/^{15}NH_4^+$ stable isotope technique (Fernández et al., 2009; Fernandez and Farías, 2012). Results of Carbon-13 tracer were published previously by Rain-Franco et al. (2018), which describes carbon fluxes for the same experiments. For ammonium uptake experiments, seawater samples taken from depths described in **Table 1** were incubated in 600 mL polycarbonate bottles using $^{15}NH_4Cl$ (ICON isotopes IN 5037; 99% at 0.5 μmol mL^{-1}). ^{15}N-ammonium tracer additions were generally kept close to 10% of ambient ammonium concentration.

Incubations were done using an *in situ* mooring line deployed at sunrise and recovered at sunset (∼7 h later). Once recovered,

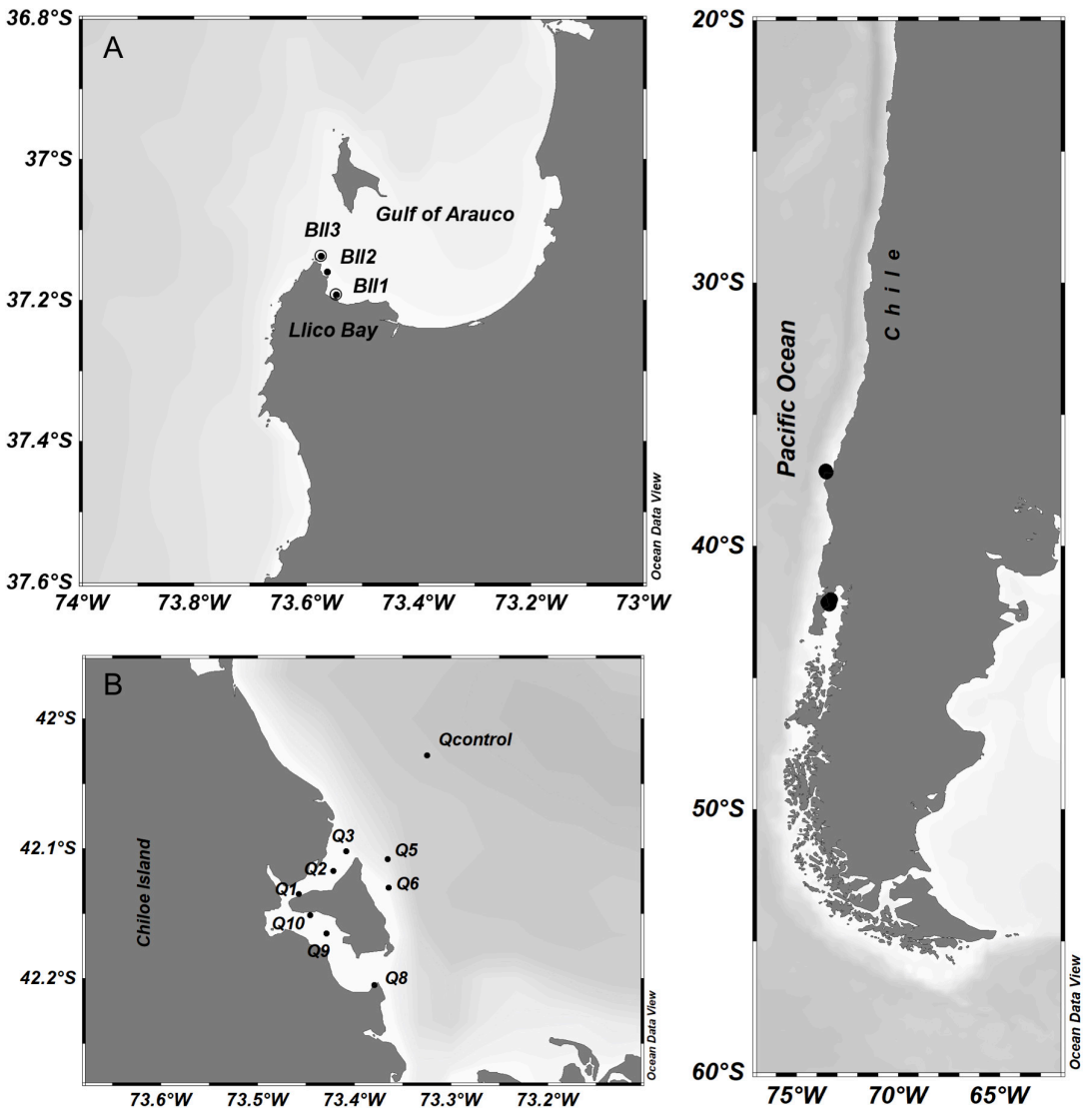

FIGURE 1 | Study area in central-southern and Norther Patagonia Chile showing the sampling location in **(A)** Llico Bay in Gulf of Arauco and **(B)** Caucahue channel in the inner sea of Chiloé. Circles indicate sampling stations.

TABLE 1 | Geographical location and seawater sampling depths for hydrographic characterization at Llico Bay and Caucahue channel stations.

Location	Station	Latitude (°S)	Longitude (°W)	Sampling depth
Llico	Bll1	37.192	73.547	2*, 4*, 6
	Bll2	37.159	73.563	2*, 10*, 15
	Bll3	37.137	73.574	2*, 10*, 20
Caucahue	Q2	42.177	73.422	2*, 10*, 20, 30*, 40
	Q3	42.102	73.409	2*, 10*, 20, 30*, 50
	Q5	42.108	73.366	2*, 10*, 20, 30*, 50, 60
	Q6	42.130	73.365	2*, 10*, 20, 30*
	Q9	42.165	73.429	2*, 10*, 20, 30*, 50
	Qc	42.028	73.325	2*, 10*, 20, 30*, 50, 65, 80

Incubations and seawater sampling used for in situ ammonium uptake experiments are in asterisk (*).

the bottles were filtered through 0.7 μm GF/F filters (Whatman; pre-combusted at 540°C, 4 h) using a vacuum pump. Filters were stored at −20°C until analysis by isotope mass spectrometry at the Laboratory of Biogeochemistry and Applied Stable Isotopes (LABASI) of Pontificia Universidad Católica de Chile using a Thermo Delta V Advantage IRMS coupled with Flash2000 Elemental Analyzer.

Deltamethrin and azamethiphos were added to primary production incubations at dosses determined according to the concentrations used in sea lice treatments: 3 μg L^{-1} for deltamethrin (Siwicki et al., 2010) and 200 μg L^{-1} for azamethiphos (Davies, 2001; Canty et al., 2007; Burridge et al., 2010). Stock solutions of azamethiphos (Dr. Ehrenstorfer GmbH, 98.5% purity) and deltamethrin (Dr. Ehrenstorfer GmbH, 99.5% purity) were prepared by dissolving the reagents in dimethylsulphoxide (DMSO, MERCK, 99.9% analytical grade). The concentration of the pesticide solution added was 1.2 and 3 μmol L^{-1} for azamethiphos and deltamethrin, respectively, as described in the **Table 2**. Bottles without pesticides were incubated as controls ($^{15}NH_4$; **Table 2**).

Seawater sampling and incubation depths at the sampling points were set between surface and the compensation depth (which in this case coincided with app ∼2.7 times the depth of view of the Secchi disk). At this level the light availability allows phytoplankton growth and the oxygen produced is equal to the consumed by respiration. Incubation and sampling depths for Llico Bay were at 2 and 4 m (Bll1) and 2 and 10 m depth (Bll2 and Bll3). At Caucahue Channel the depths sampling and for incubation were 2, 10 and 30 m depth (**Table 1**). More details of treatments and controls for *in situ* ammonium uptake experiments were described in **Table 2**.

On-Deck Ammonium Uptake Experiments

To study ammonium photo and chemoautotrophic uptake, four on-deck experiments were performed using dual stable isotopes techniques ($^{13}C/^{15}NH_4$). Results of Carbon-13 tracer were published in Rain-Franco et al. (2018). On-deck experiments were developed at Llico Bay (Bll2 station) with surface waters (2 m), during winter and spring 2015, and summer and autumn 2016.

In order to simulate solar radiation, we performed atmospheric measurements of incident Photosynthetically Active Radiation (PAR) using a portable radiometer (RM-21 Dr. Gröbel, Germany) and these results are available in Rain-Franco et al. (2018). Photoautotrophic samples were incubated under a combination of two cut off filters to simulate the irradiance at the sampling depths: 0.3 Neutral density 209 (47% of average transmittance between 400 and 700 nm, Lee filters) and Steel Blue 117 (Lee filters). Dark treatments to obtain chemoautotrophic ammonium uptake were put in a closed incubator. Incubations were done in Duran Schott bottles (580 mL) and amended with a $^{15}NH_4$ solution (ICON isotopes IN 5037; 99% at 0.5 μmol mL^{-1}; final concentration in the sample in the 83 nmol L^{-1}) and pesticide solution as described in **Table 3**. The pesticide treatments used were azamethiphos ($^{15}NH_4$ + Az), deltamethrin ($^{15}NH_4$ + Dm) and emamectin benzoate ($^{15}NH_4$ + Em). The dose of emamectin benzoate (0.66 mmol L^{-1}, Dr. Ehrenstorfer GmbH) was estimated in order to obtain the highest possible experimental concentration by dividing the standard into two equal parts. Also, combined treatments were evaluated, azamethiphos-deltamethrin ($^{15}NH_4$ + Az + Dm) and azamethiphos-deltamethrin-emamectin benzoate ($^{15}NH_4$ + Az + Dm + Em). All the incubations (light and dark) were done in duplicate for 6 h, with a subsample at 2 h. Bottles were incubated in 3 large aquariums of 50 L each, which were interconnected and received surface seawater with a continuous flow to maintain *in situ* temperature conditions (ca. 13°C). More details of treatments and controls of on-deck incubation are available at **Table 3**.

Data Analysis

Ammonium uptake rates were estimated as described in previous studies (Fernández et al., 2009; Fernandez and Farías, 2012) following Eq. (1):

$$\rho DI^{15}N = \left[\%R_{PON} - 0.36912)^{*}(PON^{*}\frac{1000}{14}{}^{*}V_f))/\%R_{DIN}\right]^{*} 14/1000 \quad (1)$$

where V_f is the filtrated volume, PON represents the amount of particulate N obtained by mass spectrometry (μg) and$\%R_{PON}$ is the enrichment in $^{15}NH_4$ in the GF/F filter after the incubation. $\%R_{DIN}$ is the excess of enrichment of ^{15}N after the inoculation (T_0) computed according to Eq. (2):

$$\%R_{DIN} = (({}^{15}N^{*}{}^{15}DIN/V_b + \left(DIN_i^{*}0.0036912\right))/$$

$$DIN_i - ({}^{15}N^{*}{}^{15}DIN/V_b) \quad (2)$$

where ^{15}N is the volume of isotopic solution ($^{15}NH_4$), ^{15}DIN represents the concentration of the ^{15}N added inoculums. The term 0.0036912 represents the natural abundance (average) of ^{15}N. DIN_i represents the concentration of DIN in the sample before the addition of tracer. Vb represent the incubation bottle volume. For *in situ* incubations, hourly rates were multiplied by 12 in order to obtain daily ammonium fixation values. Initial ammonium concentrations were taken from a nutrient profile prior to incubation and subsamples for final ammonium concentrations were taken directly from the incubation bottle before filtration.

For Llico Bay and Caucahue Channel *in situ* incubations a paired *t*-test was done to compare treatments with their respective control conditions. For on-deck incubations (Llico Bay), a two-way ANOVA was computed to evaluate significant variations among treatments and between incubation times after checking for normality assumptions (Kolmogorov-Smirnov test) and homoscedasticity (Levene's test). Whenever data did not pass the test, a log transformation was implemented. Pairwise multiple comparison was performed using a Tukey test as *a posteriori* analysis. All the statistical analyses were performed using the statistical software R[1].

[1]https://www.r-project.org/

TABLE 2 | Summary of *in situ* ammonium assimilation experiment setup during Llico and Caucahue campaigns.

Location	Dates	Season	Station	Isotopes and pesticide solution concentration
Caucahue	18-30/06/2014	Winter	Qc, Q2, Q5, Q6, Q9	$^{15}NH_4$ (0.083 μmol L^{-1})
				$^{15}NH_4$ (0.083 μmol L^{-1}) + Az (1.2 μmol L^{-1})
				$^{15}NH_4$ (0.083 μmol L^{-1}) + Dm (3 μmol L^{-1})
				$^{15}NH_4$ (0.083 μmol L^{-1}) + Az (1.2 μmol L^{-1}) + Dm (3 μmol L^{-1})
Caucahue	20-30/01/2015	Summer	Qc, Q2, Q3, Q5, Q9	$^{15}NH_4$ (0.083 μmol L^{-1})
				$^{15}NH_4$ (0.083 μmol L^{-1}) + Az (1.2 μmol L^{-1})
Llico	21-25/07/2015	Winter	BLL1, BLL2, BLL3	$^{15}NH_4$ (0.083 μmol L^{-1})
				$^{15}NH_4$ (0.083 μmol L^{-1}) + Az (1.2 μmol L^{-1})
				$^{15}NH_4$ (0.083 μmol L^{-1}) + Dm (3 μmol L^{-1})
				$^{15}NH_4$ (0.083 μmol L^{-1}) + Az (1.2 μmol L^{-1}) + Dm (3 μmol L^{-1})
Llico	21-25/10/2015	Spring	BLL1, BLL2, BLL3	$^{15}NH_4$ (0.083 μmol L^{-1})
Llico	05-01/01/2016	Summer	BLL1, BLL2, BLL3	$^{15}NH_4$ (0.083 μmol L^{-1})
Llico	21-29/04/2016	Autumn	BLL1, BLL2, BLL3	$^{15}NH_4$ (0.083 μmol L^{-1})
				$^{15}NH_4$ (0.083 μmol L^{-1}) + Az (1.2 μmol L^{-1})
				$^{15}NH_4$ (0.083 μmol L^{-1}) + Dm (3 μmol L^{-1})
				$^{15}NH_4$ (0.083 μmol L^{-1}) + Az (1.2 μmol L^{-1}) + Dm (3 μmol L^{-1})

Az, Azamethiphos and Dm, Deltamethrin.

TABLE 3 | Summary of on-deck ammonium uptake incubations in Llico campaigns.

Location	Dates	Season	Station	Isotopes and pesticide solution concentration
Llico	21-25/07/2015	Winter	BLL2	$^{15}NH_4$ (0.083 μmol L^{-1})
				$^{15}NH_4$ (0.083 μmol L^{-1}) + Az (1.2 μmol L^{-1})
				$^{15}NH_4$ (0.083 μmol L^{-1}) + Dm (3 μmol L^{-1})
				$^{15}NH_4$ (0.083 μmol L^{-1}) + Em (600 μmol L^{-1})
Llico	21-25/10/2015	Spring	BLL2	$^{15}NH_4$ (0.083 μmol L^{-1})
				$^{15}NH_4$ (0.083 μmol L^{-1}) + Az (1.2 μmol L^{-1})
				$^{15}NH_4$ (0.083 μmol L^{-1}) + Dm (3 μmol L^{-1})
				$^{15}NH_4$ (0.083 μmol L^{-1}) + Em (600 μmol L^{-1})
				$^{15}NH_4$ (0.083 μmol L^{-1}) + Az (1.2 μmol L^{-1}) + Dm (3 μmol L^{-1})
				$^{15}NH_4$ (0.083 μmol L^{-1}) + Az (1.2 μmol L^{-1}) + Dm (3 μmol L^{-1}) + Em (600 μmol L^{-1})
Llico	05-01/01/2016	Summer	BLL2	$^{15}NH_4$ (0.083 μmol L^{-1})
				$^{15}NH_4$ (0.083 μmol L^{-1}) + Az (1.2 μmol L^{-1})
				$^{15}NH_4$ (0.083 μmol L^{-1}) + Dm (3 μmol L^{-1})
				$^{15}NH_4$ (0.083 μmol L^{-1}) + Em (600 μmol L^{-1})
				$^{15}NH_4$ (0.083 μmol L^{-1}) + Az (1.2 μmol L^{-1}) + Dm (3 μmol L^{-1})
				$^{15}NH_4$ (0.083 μmol L^{-1}) + Az (1.2 μmol L^{-1}) + Dm (3 μmol L^{-1}) + Em (600 μmol L^{-1})
Llico	21-29/04/2016	Autumn	BLL2	$^{15}NH_4$ (0.083 μmol L^{-1})
				$^{15}NH_4$ (0.083 μmol L^{-1}) + Az (1.2 μmol L^{-1})
				$^{15}NH_4$ (0.083 μmol L^{-1}) + Dm (3 μmol L^{-1})
				$^{15}NH_4$ (0.083 μmol L^{-1}) + Em (600 μmol L^{-1})
				$^{15}NH_4$ (0.083 μmol L^{-1}) + Az (1.2 μmol L^{-1}) + Dm (3 μmol L^{-1})
				$^{15}NH_4$ (0.083 μmol L^{-1}) + Az (1.2 μmol L^{-1}) + Dm (3 μmol L^{-1}) + Em (600 μmol L^{-1})

Az, Azamethiphos, Dm, Deltamethrin and Em, emamectin benzoate.

RESULTS

Chemical and Biological Seasonal Variability in Llico Bay and Caucahue Channel

Temperature and salinity in Llico Bay varied between seasons, showed a marked thermal stratification during spring 2015 and summer 2016 in Bll1 and Bll2 stations, the maximum surface values was nearly 17°C at Bll1 station in summer 2016 and the maximum salinity values was ∼ 35 in summer 2016 for the three stations (**Supplementary Figure 1**). Whereas in winter and autumn lower temperature values was observed (∼ 12°C in winter) and as well lower salinity values (∼ 32°C in winter 2015). Ammonium showed higher concentrations in autumn 2016 and spring 2015 compared with winter 2015 and summer 2016 at Bll1

and Bll2 stations. Station Bll3 showed the highest ammonium concentration and reached 9 μmol L^{-1} at 20 m depth in autumn 2016 (**Figures 2A,E,I**). Nitrate concentration showed a marked seasonal variability with higher concentrations in spring 2015 followed by winter 2015. The lowest nitrate concentration was observed in summer 2016 in almost all depths (**Figures 2B,F,J**). Nitrite was higher in winter 2015 at all stations (**Figures 2C,G,K**). The N/P ratio varied seasonally, although maximum values were observed in spring and winter 2015, particularly Bll3 station showed an average ratio of 25 (**Figures 2D,H,L**).

The highest concentrations of Chl-a were observed in summer 2016 in the three stations (**Figure 2**), and the maximum value was observed in surface at Bll3 station ($\sim$ 23 mg m^{-3}; **Figure 2O**). and The lowest concentration was observed in autumn 2016 at Bll1, Bll2, and Bll3, at all depths. The highest bacterioplankton abundance was observed in spring 2015, with the maximum abundance at station Bll3 (3,990 $\times$ 10^3 cell mL^{-1}). Minor changes were observed in winter 2015, summer 2016 and autumn 2016 (**Supplementary Figure 2**).

A seasonal variability was also observed at Caucahue channel stations, lower temperature was observed during winter ($\sim$11°C) compared with summer ($\sim$16°C; **Supplementary Figure 3**). Salinity showed a strong vertical variation in winter, particularly at the station Q6. Ammonium concentration was higher in winter compared to summer in Caucahue Channel (**Figures 3A,F**), specifically at station Q2 (5 μmol L^{-1}) in surface waters, followed by station Q6 with 3 μmol L^{-1} at 20 m depth. The lowest concentration was found at the control station (Qc) with values close to zero throughout the water column (**Figure 3A**). In summer, the concentrations were generally below 0.3 μmol L^{-1} for all stations, with the exception of Q2 station (>1 μmol L^{-1}; **Figure 3F**). As well of summer, in winter, ammonium concentrations at Qc station were nearly zero throughout the water column.

Nitrate concentrations in winter and summer were in general below 3 μmol L^{-1}, except at station Q1 and Q6 (**Figures 3B–G**), with maximum concentration of 11 μmol L^{-1} at 30 m depth and during summer, station Q5 showed maximum concentration of 11.5 μmol L^{-1} at 20. Nitrite concentration were in general higher in winter compared to summer (**Figures 3C–H**). During winter, nitrite concentration tends to increase with the depth, the highest values was found at station Q6 (2 μmol L^{-1}). In summer, the concentration was lower than 0.5 μmol L^{-1}. The N/P ratio varied greatly depending on stations and depths. Station Qc had the lowest ratios, 1.71 $\pm$ 1.17 in winter and 2.84 $\pm$ 1.14 in summer (**Figures 3D–I**). The highest ratio was observed at station Q5 in winter 22.8 at 2 m.

Chl-a concentration was higher in summer at the station Qc and between stations Q3 and Q2, nearly 4 mg m^{-3} (**Figures 3E–J**). Concentration in winter were lower than 1 mg m^{-3} for all stations. Bacterioplankton in Caucahue Channel showed a marked seasonal influence. In winter showed abundances under the 500 $\times$ 10^3 cell mL^{-1} and during summer in general the abundances were over the 500 $\times$ 10^3 cell mL^{-1} (**Supplementary Figures 2E–F**). In winter bacterioplankton was more abundant at station Q9 and lowest at station Q5. In summer, maximum abundances were observed at stations Q9 and the lowest abundances were observed in general at control station (**Supplementary Information**; **Figure 2B**).

In situ Ammonium Uptake Rates at Llico Bay and Caucahue Channel

Ammonium uptake rates were higher in surface waters compared to deeper levels (10 m) at all stations and seasons (**Figure 4**). At station Bll1 assimilation rates observed in spring 2015, were 93 and 95% higher than winter 2015 and autumn 2016 (7.9 and 10.4 μmol $L^{-1}d^{-1}$ at 2 and 4 m depth, respectively; **Figures 4A–C**). Station Bll2 showed the highest ρNH_4^+ values during autumn 2016 reaching 3 μmol $L^{-1}d^{-1}$ at 2 m and the minimum rate was observed in spring at 10 m depth (0.5 μmol $L^{-1}d^{-1}$). The same pattern was observed in Bll3 with higher ammonium uptake during autumn 2016 at 2 m depth (2.5 μmol $L^{-1}d^{-1}$) and a decrease in 81% at 10 m depth. The lowest rate was observed in winter 2015 at 10 m depth (0.9 μmol $L^{-1}d^{-1}$; **Figures 4H–J**).

In treatments where pesticides were added, ammonium uptake showed variable responses compared to the control ($^{15}NH_4$; **Table 2**). The addition of pesticides caused an increase in ammonium assimilation in winter 2015 (**Figures 4A,D,H**) compared to controls, particularly at station Bll3 at 10 m depth, in which rates in all treatments ($^{15}NH_4$ + Az, $^{15}NH_4$ + Dm, and $^{15}NH_4$ + Az + Dm) increased by 42% compared to their controls. At Bll1 and Bll2 the rates increased between 2 and 15% compared to the controls ($^{15}NH_4$), except for the combined treatment $^{15}NH_4$ + Az + Dm at Bll1 station and $^{15}NH_4$ + Az at 10 m at station Bll2.

In general, the addition of pesticides in autumn 2016 resulted in a decrease of ammonium utilization rates compared to the controls. At Bll1 station rates were 20% lower than the control ($^{15}NH_4$) for the treatment $^{15}NH_4$ + Dm (4 m; **Figure 4C**). At Bll2 station the rates decreased between 3 and 18%, in the treatment with deltamethrin and in the combined treatment $^{15}NH_4$ + Az + Dm at 2 m, respectively. However, at this station was also observed an increase in a 55% the ρNH_4^+ values for $^{15}NH_4$ + Az + Dm treatment at 10 m depth. In the station Bll3, an inhibition was only observed in the treatments with a single pesticide ($^{15}NH_4$ + Az and $^{15}NH_4$ + Dm) at 2 m depth. In subsurface layer (10 m) the addition of pesticides caused an increase in the ammonium assimilation rates up to 132% compared to the control for the treatment $^{15}NH_4$ + Az. This increase was also observed for $^{15}NH_4$ + Dm (89%) and $^{15}NH_4$ + Az + Dm (46%; **Figure 4J**). However, all these differences reported were non-significant (t-test > 0.05) for pesticide additions at any station during winter 2015 and autumn 2016. For spring 2015 and summer 2016 no data are available for treatments with pesticides (**Figure 4**).

In Caucahue channel, ammonium uptake varied throughout the stations and also between seasons and depths. The highest ρNH_4^+ values were observed at station Q2 in winter (0.5 μmol L^{-1} d^{-1}) and in summer (0.6 μmol L^{-1} d^{-1}) in surface layer (**Figures 5**, **6**, respectively) inside of the area influenced by the farming centers, and the lowest rates was observed at station Q9 in both season (**Figures 5E**, **6E**). In summer 2015, the chemoautotrophic ammonium utilization (dark treatment)

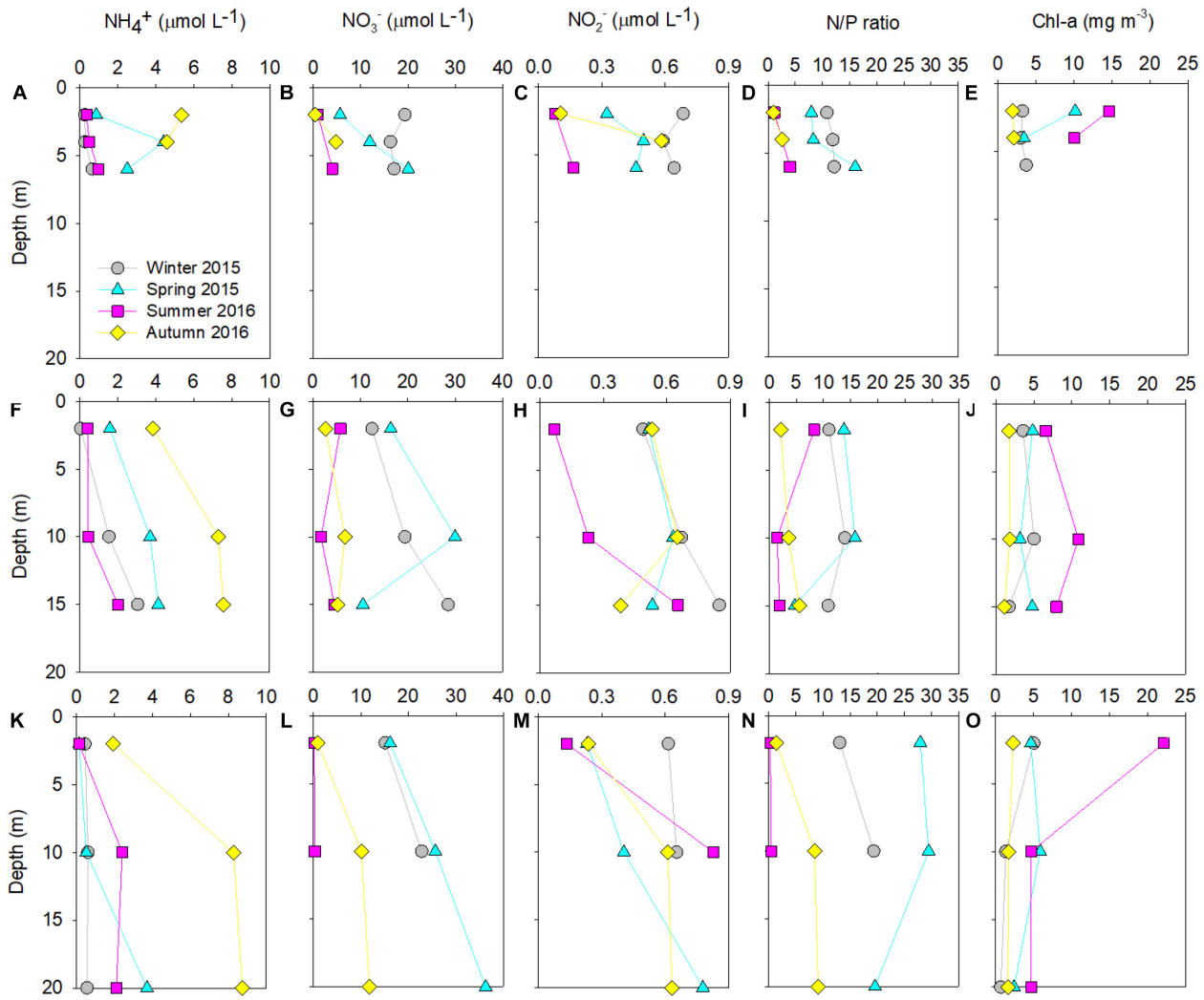

FIGURE 2 | Ammonium (µmol L^{-1}), nitrate (µmol L^{-1}), nitrite (µmol L^{-1}) concentrations, N/P ratio, and Chl-a concentrations (mg m^{-3}) profiles at Llico Bay station in winter and spring 2015, and summer and autumn 2016. **(A–E)** Bll1, **(F–J)** Bll2, and **(K-O)** Bll3.

was 10 times higher than the photoautotrophic nitrogen uptake in surface at Q9, but in general the both photo and chemoautotrophic are in the same range of values.

In winter 2014 (**Figure 5**), pesticide additions resulted in an increase in ammonium uptake in the treatment $^{15}NH_4$ + Az at station Qc between 3% (2 m) and 40% (30 m). In general, deltamethrin addition resulted in a decrease in ammonium assimilation rates, the highest difference found with the control ($^{15}NH_4$) was at station Q2 (**Figure 5B**). At this station which was located close to the farms, ρNH_4^+ decreased by 53% (30 m depth), followed by a reduction of 33% at the station Q5 in surface (**Figure 5C**). However, deltamethrin addition cause an increase in the rates of ammonium assimilation in the first 10 m depth at station Qc, between 7 and 12% higher than the controls (**Figure 5A**).

The combined treatment $^{15}NH_4$ + Az + Dm also resulted in a variable response to the pesticide addition (**Figure 5**). Qc station showed a decrease in the ammonium assimilation rates up to 47% at the surface. This pattern was also observed at station Q9, observed rates up to 29% less than the controls. Higher rates compared to the control was observed at Q2, up to 13% higher at 10 m depth. At the same depth, an increase was observed at stations Q5 (13%) and Q6 (23%). However, these values were not significantly different from the control treatment ($^{15}NH_4$; paired *t*-test, $p < 0.05$).

In summer (**Figure 6**), the *in situ* incubations were made under light (photoautotrophic) and dark conditions (chemoautotrophic). At station Qc, the addition of azamethiphos resulted in a significant decrease in ammonium uptake under light conditions (in average 13%; paired *t*-test > 0.05). However, we also observed an increase in ρNH_4^+ values at 2 and 30 m in the station Q9, being up to 100 times higher the rates obtained after the addition of azamethiphos. However, these increases were not significant, since they were not observed for

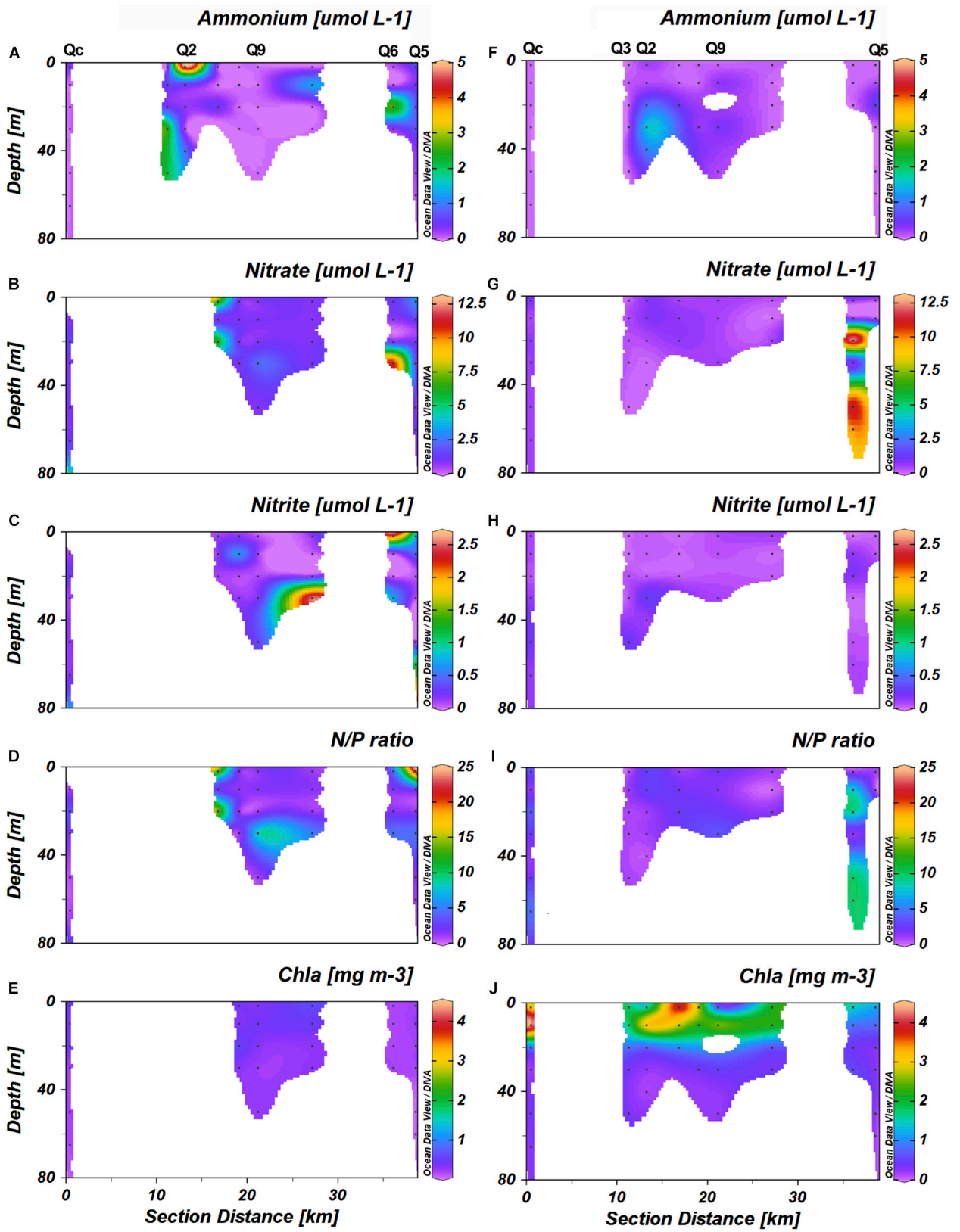

FIGURE 3 | Ammonium (μmol L^{-1}), nitrate (μmol L^{-1}), nitrite (μmol L^{-1}), N/P ratio and Chl-a concentrations transects at Caucahue channel stations in winter 2014 **(A–E)** and summer 2015 **(F–J)**.

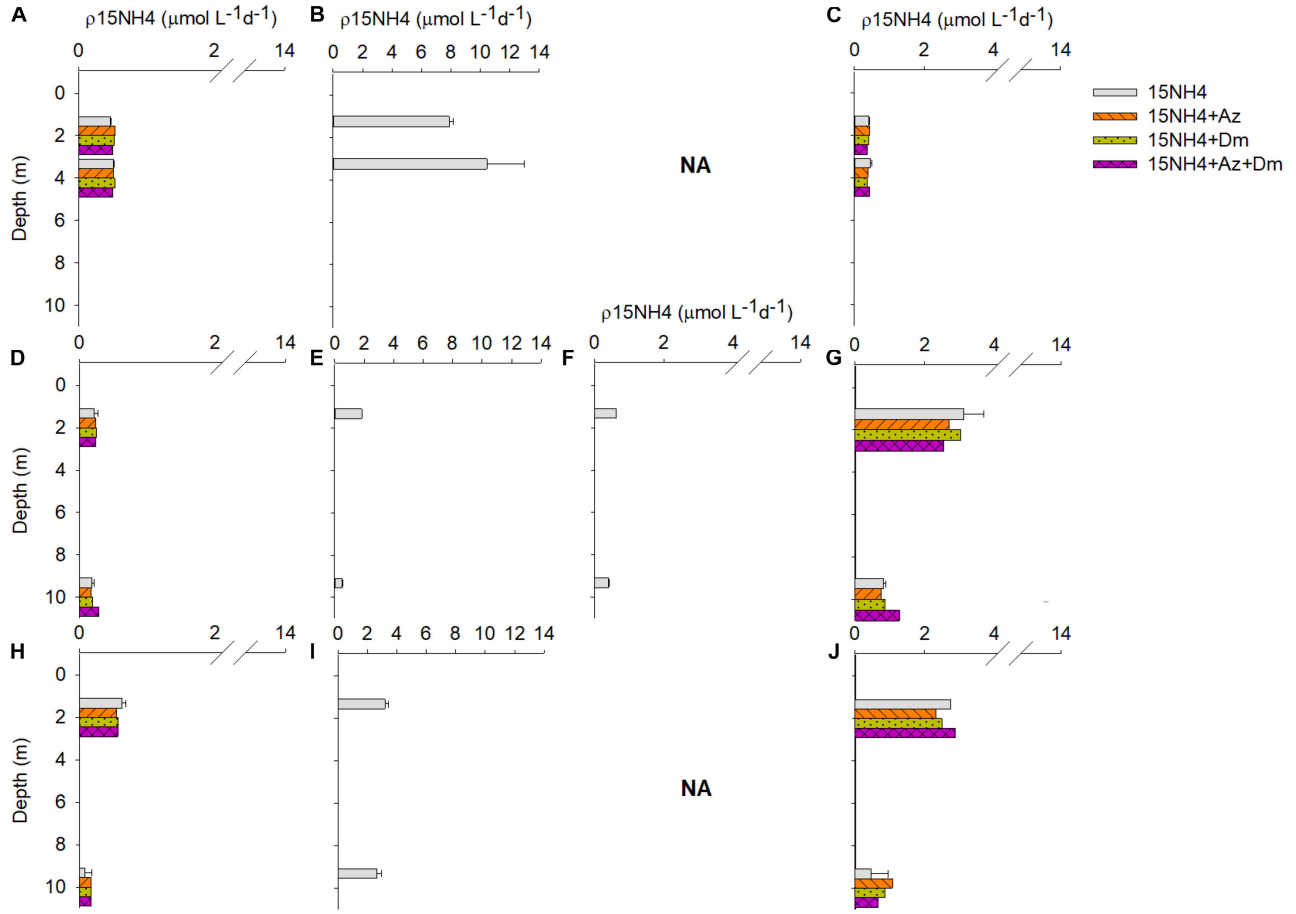

FIGURE 4 | *In situ* ammonium uptake rates (μmol L^{-1} d^{-1}) profiles at Llico Bay. Upper panels for BII1 station, middle panels for BII2 and lower panels for BII3 station. **(A,D,H)** Winter 2015; **(B,E,I)** Spring 2015; **(F)** Summer 2016; **(C,G,J)** Autumn 2016. NA are not available data for BII1 and BII3 station in Summer 2016. Errors bars represent the standard deviations.

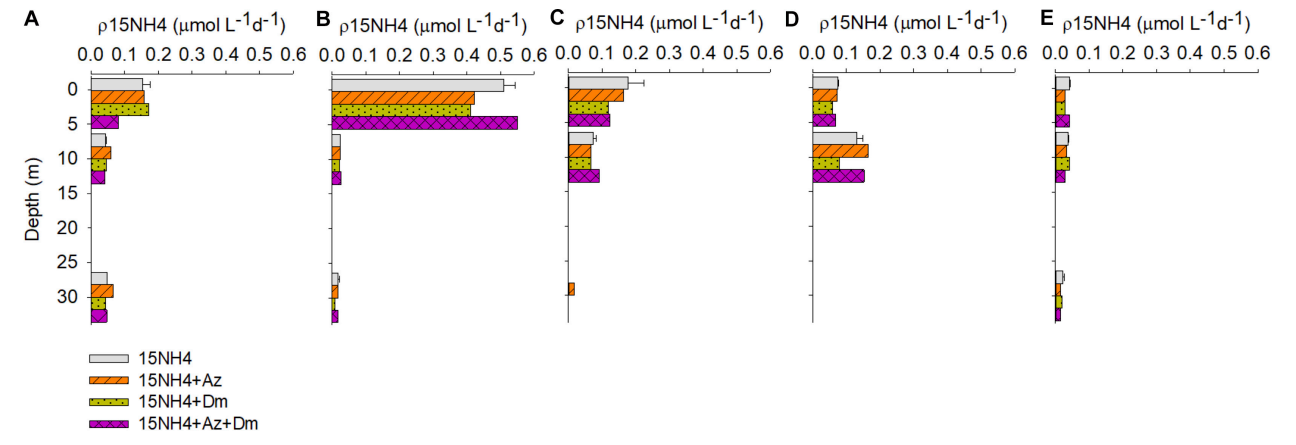

FIGURE 5 | *In situ* ammonium uptake rates (μmol L^{-1} d^{-1}) at Caucahue Channel stations during winter 2014. **(A)** Qc, **(B)** Q2, **(C)** Q5, **(D)** Q6, and **(E)** Q9 station.

all depths (paired *t*-test > 0.05). The chemoautotrophic uptake showed a decrease thought the water column only at station Q3 between 23 and 72% lower than the controls. Slight increase was observed for the chemoautotrophic ammonium utilization (**Figures 6F,G,I,J**) after the addition of azamethiphos, except for station Q9 in which we observed rates 570% higher than the

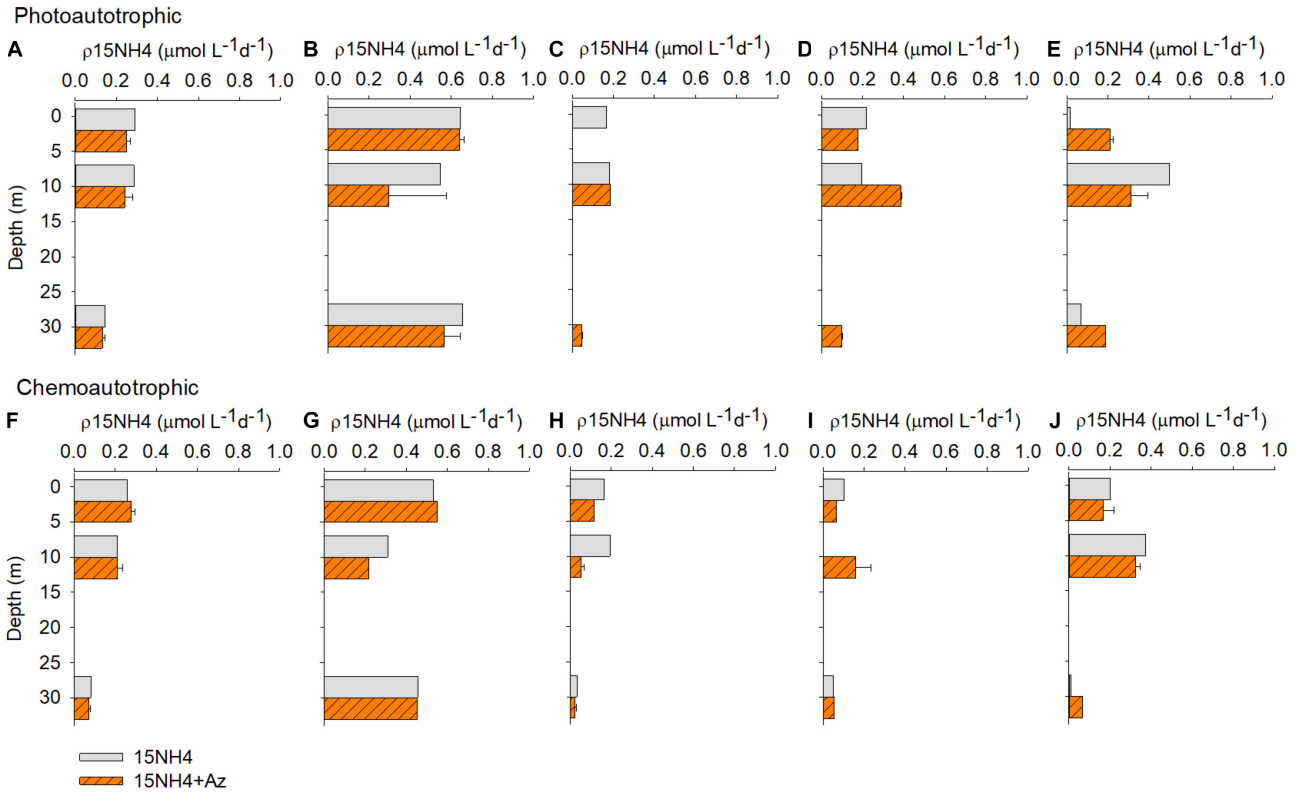

FIGURE 6 | *In situ* photoautotrophic (upper panel) and chemoautotrophic (lower panel) ammonium uptake rates (μmol L^{-1} d^{-1}) during summer 2015. **(A,F)** Qc; **(B,G)** Q2; **(C,H)** Q3; **(D,I)** Q5; **(E,J)** Q9 station.

control (**Figure 6J**). But, these effects were not significant (paired *t*-test > 0.05).

Pesticide Effect on Surface Ammonium Uptake Under Light and Dark Conditions: On-Deck Experiments

On-deck ammonium uptake experiments (**Figure 7**) showed higher photoautotrophic control rates ($^{15}NH_4$) in autumn 2016 (0.14 μmol L^{-1} h^{-1}) after 2 h of incubation followed by spring 2015 (0.1 μmol L^{-1} h^{-1}) at the same incubation time (**Figures 7A,B**). On the other hand, the highest chemoautotrophic ammonium uptake rate was observed in spring 2015 (0.1 μmol L^{-1} h^{-1}). This rate was equivalent to 100% of photoautotrophic ammonium assimilation after 2 h of incubation, and after 6 h of incubation the chemoautotrophic assimilation was 7% higher than photoautotrophic ammonium assimilation (**Figures 7E–H**). This was also observed in summer 2016 when the chemoautotrophic ammonium uptake was equivalent to an 85% of the photoautotrophic at 2 h of incubation.

Results from a two-way ANOVA applied to light condition experiments showed significant differences in all the experiments between the treatments with pesticides and/or the time (**Table 4**). In winter 2015, the treatment $^{15}NH_4$ + Az and $^{15}NH_4$ + Dm were significantly different from the control ($^{15}NH_4$). The $^{15}NH_4$ + Az was 32% lower after 2 h of incubation and dropped by 21% after 6 h of incubation compared to their control values (p = 0.001). The treatment $^{15}NH_4$ + Dm was also a 53 and 64% lower after 2 and 6 h of incubation, respectively (p = 0.001). Photoautotrophic ρNH_4^+ values were significantly lower at the end of the incubation (6 h) compared to the first 2 h of incubation for control and treatments with pesticides ($^{15}NH_4$:30%; $^{15}NH_4$ + Az:16%; $^{15}NH_4$ + Em:47%; $^{15}NH_4$ + Dm: 6% lower at 6 h of incubation; **Table 4**). In spring 2015, the treatment $^{15}NH_4$ + Em and the combined pesticides treatment ($^{15}NH_4$ + Az + Dm + Em) were significantly different from their controls (p = 0.001), showing a decrease in ammonium assimilation rates. The $^{15}NH_4$ + Em treatment rates were 77 and 23% lower than their control after 2 and 6 h of incubation, respectively. The combined treatment ($^{15}NH_4$ + Az + Dm + Em) was 39 and 23% lower compared to their controls at 2 and 6 h, respectively. Photoautotrophic ammonium uptake rates during spring 2015 were significantly lower (p = 0.001) after 6 h of incubation (69% average) in control and in the treatments amended with $^{15}NH_4$ + Az, $^{15}NH_4$ + Bm, $^{15}NH_4$ + Em, $^{15}NH_4$ + Az + Dm, $^{15}NH_4$ + Az + Dm + Em. Light treatments during summer 2016 did not show significant differences between the treatments amended with pesticides and controls (p = 0.469) but values over time were significantly different from each other. After 6 h of incubation the light treatments were in average 58% lower than values obtained during the first 2 h of incubation. The same result was found in autumn 2016 when treatments did

not show significant differences with pesticides compared to the controls but assimilation rates were significantly lower (average 59%) at 6 h compared to the first 2 h of incubation.

A two-way ANOVA for dark incubation (**Table 4**) showed that ammonium uptake in spring 2015 was 36 and 30% lower in the treatments $^{15}NH_4$ + Em and $^{15}NH_4$ + Az + Dm + Em compared to the control ($^{15}NH_4$) at 2 and 6 h of incubation, respectively. The combined treatment $^{15}NH_4$ + Az + Dm + Em was a 42 and 25% lower that the control after 2 and 6 h of incubation ($p = 0.001$). These differences were also found between time ($p = 0.001$) and also the interaction of the pesticides and time ($p = 0.013$). In average, dark ammonium utilization was 56% lower after 6 h of incubation that the first 2 h in spring 2015. In winter 2015, did not found significant differences in the chemoautotrophic ammonium assimilation between control and the treatments amended with pesticides ($p = 0.6$) and between the incubation times ($p = 0.06$). On-deck experiments in summer and autumn 2016 in dark conditions did not show differences between the treatments with pesticides and its controls ($p = 0.97$ and $p = 0.94$, respectively). However, values were significantly higher at 2 compared to 6 h of incubation by 59% in summer and by 69% in autumn 2016.

DISCUSSION

Studies oriented specifically on the impacts of anti-lice pesticides to microbial communities involved in primary production are quite limited (Knapp et al., 2005; Burridge et al., 2010; Rain-Franco et al., 2018). Our results complement a first report of the effects of pesticides on rates of carbon assimilation (Rain-Franco et al., 2018) for the same study area, and as part of the same experiment. Overall the results provide new evidence that anti-lice pesticides can affect fundamental processes of marine ecosystem functioning.

Here we report ammonium uptake rates at Llico Bay and Caucahue Channel. In central-southern Chile, ammonium utilization in spring-summer season is high (0.23 ± 0.4 μmol $L^{-1}d^{-1}$ on average; Fernandez and Farías, 2012). At Llico Bay, ammonium was always present in subsurface waters at relatively high concentrations (**Figures 2A,E,I**), and the rates of ammonium assimilation observed in subsurface waters suggest that the entire surface pool of ammonium cannot be taken within 24 h. This pattern, was also observed in Caucahue Channel, except at control station (Qc), outside of the influence of farms, in which the ammonium concentration was very lower in surface waters, suggesting that the ammonium pool could be used within 24 h. Inside the channel is expected found higher accumulation of organic matter due to the presence of salmon farms and consequently higher remineralization rates that can explain the higher ammonium concentration found in the channel (Olsen et al., 2014; e.g., Q2) and this is contrasted with the Qc station in which concentration was nearly zero.

Ammonium is highly bioavailable and is often the preferred N compound assimilated by bacterioplankton and phytoplankton (Glibert et al., 2016). During dark conditions, ammonium uptake was higher than the photoautotrophic uptake, being up to 10 times higher at station Q9 in Caucahue channel (summer 2015). This was also found during on-deck experiments in Llico, in which the chemoautotrophic ammonium uptake was equivalent to 100% of the photoautotrophic uptake in spring 2015. Dark N uptake has been reported that can be anywhere from 10 to 100% of the uptake rate measured in the light, and this varies with physiological conditions of the populations and the species (Mulholland and Lomas, 2008). Nevertheless, these results suggest a potentially important contribution to regenerated production in these areas, affecting surface N dynamics, modifying the balance between new and regenerated production and consequently the downward flux of N.

The impact of pesticide in ammonium uptake was highly variable between the different pesticides amendments, significant effects were detected for a single pesticide (azamethiphos) during *in situ* incubations and for combined pesticides (azamethiphos-deltamethrin-emamectin benzoate) during on-deck experiments. The response of ammonium utilization to the addition of azamethiphos revealed an inhibition of the photoautotrophic uptake at station control (Qc) in Caucahue Channel in summer 2015. These finding are in contrast to the response obtained in C uptake, in which the addition of azamethiphos trigger an increase in the phototrophic C utilization (Rain-Franco et al., 2018), and also, are in contrast with the findings reported by Burridge et al. (2010) that suggest neutral effects on primary production, since no changes in dissolved oxygen and chlorophyll-a concentrations were observed in field studies in Canada.

Azamethiphos is an organophosphate insecticide highly soluble in water (Canty et al., 2007; Burridge et al., 2010). A very recent study, showed higher microbial degradation capacity of the pesticide azamethiphos nearly to our study area in Caucahue channel, suggesting that microorganism can use organophosphate pesticides as a source of C and phosphorus for their metabolism (Garcés et al., 2020). Periods of N and phosphorus limitation has been reported for the inner Sea of Chiloé (Iriarte et al., 2007; Olsen et al., 2014, 2017), in our results, we observed a higher increase in ammonium assimilation in surface and deeper waters at station Q9 (summer) in Caucahue Channel. This station showed a lower concentration of N and phosphorus (**Figure 3**) and a high bacterioplankton abundance, so the addition of this organic phosphorus compounds should be used as a nutrients source. This also can occur in the limit of the photic zone in which the competition of nutrients increases, and pesticides, such as azamethiphos, can be used by the microbial communities. Such increases in phototrophic and also chemoautotrophic ammonium uptake were seen during winter at stations Q5, and Q2 (**Figure 5**), and at station Bll3 in Llico Bay (**Figure 4**).

On the other hand, emamectin benzoate produces a decrease in photo and chemoautotrophic ammonium utilization between a 22 and 77% as we observed in on-deck experiments at Llico bay. The emamectin benzoate is a semi-synthetic derivative of a chemical produced by the bacterium, *Streptomyces avermitilis* (Bravo et al., 2008). The effects of this pesticide on non-target organism has been reported by a number of authors using, however, a few species (e.g., mussels, fishes, american lobster and copepods; Willis and Ling, 2003; Burridge et al., 2010, 2004).

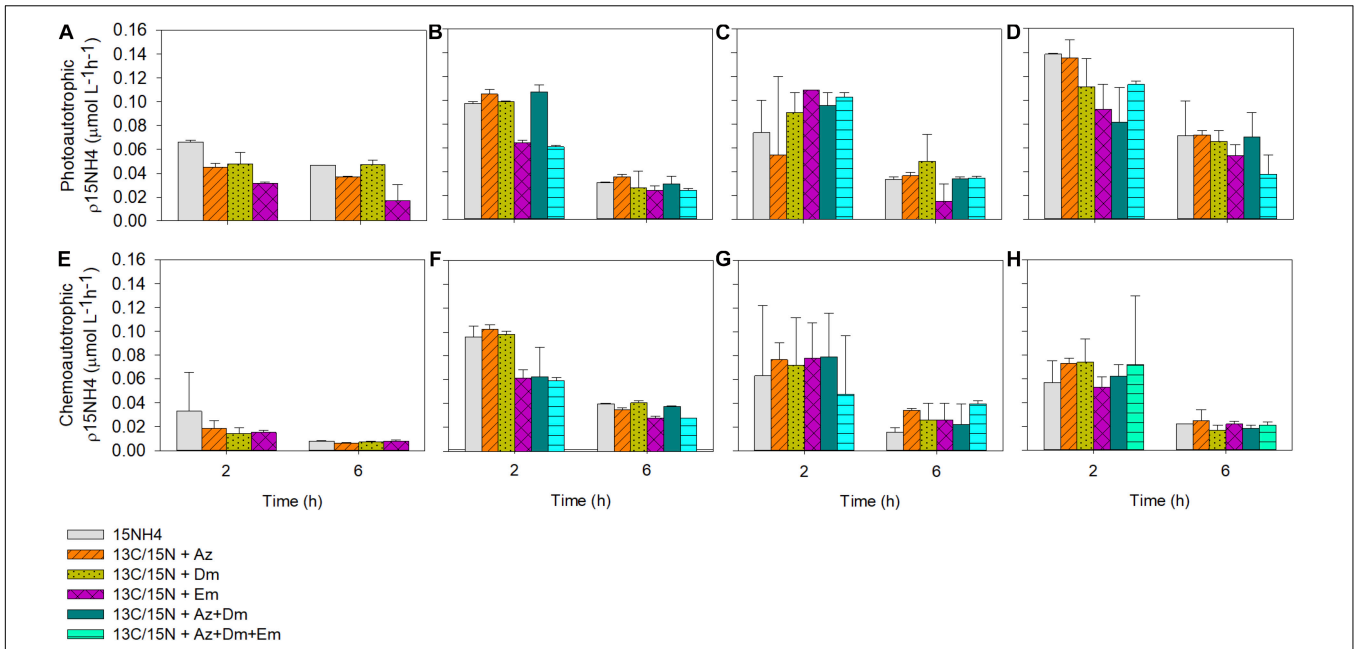

FIGURE 7 | Photoautotrophic and chemoautotrophic ammonium uptake rates (µmol L^{-1} h^{-1}) during on-deck experiments under light and dark conditions. **(A,E)** Winter 2015; **(B,F)** Spring 2015; **(C,G)** Summer 2016; **(D,H)** Autumn 2016.

TABLE 4 | Results from two-way ANOVA examining the effect of pesticides and the incubation time on N uptake rates obtained during on-deck experiments under light and dark conditions at Llico Bay.

Season	Date	Source of variation	d.f	Light		d.f	Dark	
				F	*p*		*F*	*p*
Winter	July 2015	Pesticides	3	19.701	**0.001**	3	0.579	0.644
		Time	1	12.196	**0.008**	1	4.678	0.063
		Pesticides × Time	3	1.815	0.222	3	0.503	0.691
		Residual	8			8		
Spring	October 2015	Pesticides	5	15.363	**0.001**	5	9.711	**0.001**
		Time	1	814.094	**0.001**	1	189.122	**0.001**
		Pesticides × Time	5	9.955	**0.001**	5	4.673	**0.013**
		Residual	12			12		
Summer	January 2016	Pesticides	5	0.985	0.469	5	0.154	0.974
		Time	1	25.101	**0.001**	1	11.881	**0.005**
		Pesticides × Time	5	1.118	0.405	5	0.336	0.881
		Residual	11			12		
Autumn	April 2016	Pesticides	5	2.643	0.078	5	0.232	0.941
		Time	1	49.706	**0.001**	1	32.189	**0.001**
		Pesticides × Time	5	1.734	0.201	5	0.263	0.924
		Residual	12			12		

Significant values are presented in bold.

Our results are in accordance with the results found in C uptake, suggesting that emamectin benzoate can potentially act as a depressor of C fixation (Rain-Franco et al., 2018) and now also for ammonium assimilation. The inhibition in ρNH_4^+ values was also found in the combination of the three pesticides treatment ($^{15}NH_4$ + Az + Dm + Em) in autumn. However, this effect was not detected in the combined treatment with azamethiphos and deltamethrin ($^{15}NH_4$ + Az + Dm), suggesting that the inhibitory effect was related to the addition of emamectin benzoate. Previous studies suggest that toxicity can be increased using a combination of compounds compared to the use of single chemical (Laetz et al., 2009), but in our case the higher inhibitory response was found with a single addition of emamectin benzoate and not after a combined addition.

There are no studies dealing directly with deltamethrin and microorganism. From our data, deltamethrin produce an

inhibitory or toxic effect during winter 2015 reducing up to 64% the ammonium assimilation after 6 h of incubation. The toxic effects have been also observed in in amphibians, crustacean and mollusk (Bhanu et al., 2011; Ernst et al., 2014). However, due to the high variability found in our results further studies are needed.

The interaction between the salmon cages, local hydrodynamics and local hydrographic characteristic are important factors to evaluate the dispersal propagation and the impact on non-target species of pesticides in the aquatic environment. Dispersion and dilution rates of the pesticides depend on the chemical nature (e.g., solubility, adsorption capacity, and chemistry composition) and the hydrographic characteristics of the area. A residual chemical compound concentration can persists in the area which is likely to impact non-target species (Nash, 2003). Uneaten food is point sources of emamectin benzoate to the surrounding ambient, and it is estimated that approximately 5–15% of the administered food is uneaten (Chen et al., 1999). Bloodworth et al. (2019) demonstrated a widespread detection of emamectin benzoate in sediments around Scottish fish farms. As well, Herrera et al. (2018) through a modeling methodology to assess the hydrodynamic effects of a salmon farm in a Patagonia channel, found that a considerable part of the enclosed volume within the cages of a fish farms remains circulating in the area of channels in Patagonia, suggesting an impact in the dispersal of pesticides in the area. The topical bath treatment method applied for azamethiphos will most likely result in rapid dilution of active ingredients. Azamethiphos has been detected up to 1000 m away from the location treatment (Ernst et al., 2014). The dispersion and dilution rates of the different anti-lice treatments utilized in this study can explain the high variability found in our results through the different stations and depths sampled, and this variability was also found in C assimilation (Rain-Franco et al., 2018). These results suggest a strong impact of the choice of pesticide used, the seasonal variability of the study area and the distance of salmon farming on the impact on microbial community and consequently on local primary productivity.

The impact of pesticides can be either positive by enhancing ammonium uptake or could be inhibitory for microorganism but either way it will impact the natural N budget and this impact was not only detected in photoautotrophic ammonium uptake; pesticides can also affect the chemoautotrophic communities, and potentially can modulate the regenerated primary production and therefore the balance between new and regenerated production and organic matter export. Taken together, our findings and those of Rain-Franco et al. (2018) show significant alterations in C and N assimilation.

In conclusion, the use of anti-lice pesticides can produce changes in photo and chemoautotrophic ammonium uptake in central-southern and northern Patagonia in Chile. Azamethiphos act as depressor of ammonium assimilation but also can be used by phyto- and bacterioplankton under nutrient limitation conditions. Emamectin benzoate can act as a strong depressor as well for deltamethrin and these changes were strongest if a single pesticide is applied as opposed to a combination of two or more pesticides. We conclude that pesticides in marine waters have the potential for altering local primary production fluxes and therefore can impact biological ecosystem productivity.

DATA AVAILABILITY STATEMENT

The original contributions presented in the study are included in the article/**Supplementary Material**, further inquiries can be directed to the corresponding author.

AUTHOR CONTRIBUTIONS

CF designed the experiments and lead the research project, carried out the sample collection, and experiments. VV-C analyzed the data and participated in data interpretation. VV-C and CF wrote the manuscript. Both authors contributed to the article and approved the submitted version.

FUNDING

This work was supported by FONDAP grants 15110027 and 1515003, FONDECYT project 1180954, and by COPAS Sur-Austral ANID PIA APOYO CCTE AFB170006. This study was development in the frame of the French-Chilean project LIA-MORFUN and the current LIA-MAST project (CNRS).

ACKNOWLEDGMENTS

The authors are grateful to Claudia Muñoz for assistance during field experiments.

SUPPLEMENTARY MATERIAL

The Supplementary Material for this article can be found online at: https://www.frontiersin.org/articles/10.3389/fmars.2020.602002/full#supplementary-material

REFERENCES

Aminot, A., and Kérouel, R. (2007). *Dossage Automatique Des Nutriments Dans Les Eaux Marins*. France: Editions Quae.

Avendaño-Herrera, R. (2018). Proper antibiotics use in the Chilean salmon industry: policy and technology bottlenecks. *Aquaculture* 495, 803–805. doi: 10.1016/j.aquaculture.2018.06.072

Baskett, M. L., Burgess, S. C., and Waples, R. S. (2013). Assessing strategies to minimize unintended fitness consequences of aquaculture on wild populations. *Evol. Appl.* 6, 1090–1108. doi: 10.1111/eva.12089

Bhanu, S., Archana, S., Ajay, K., Singh, S., and Vandana, B. (2011). Impact of deltamethrin on environment, use as an insecticide and its bacterial degradation – a preliminary study. *Int. J. Environ. Sci.* 1, 977–985.

Bloodworth, J. W., Baptie, M. C., Preedy, K. F., and Best, J. (2019). Negative effects of the sea lice therapeutant emamectin benzoate at low concentrations on benthic communities around Scottish fish farms. *Sci. Total Environ.* 669, 91–102. doi: 10.1016/j.scitotenv.2019.02.430

Bravo, S. (2003). Sea lice in Chilean salmon farms. *Bull. Eur. Assoc. Fish Pathol.* 23, 197–200.

Bravo, S., Sevatdal, S., and Horsberg, T. E. (2008). Sensitivity assessment of *Caligus rogercresseyi* to emamectin benzoate in Chile. *Aquaculture* 282, 7–12. doi: 10.1016/j.aquaculture.2008.06.011

Burridge, L., Weis, J. S., Cabello, F., Pizarro, J., and Bostick, K. (2010). Chemical use in salmon aquaculture: a review of current practices and possible environmental effects. *Aquaculture* 306, 7–23. doi: 10.1016/j.aquaculture.2010.05.020

Burridge, L. E., Hamilton, N., Waddy, S. L., Haya, K., Mercer, S. M., Greenhalgh, R., et al. (2004). Acute toxicity of emamectin benzoate (SLICEtm) in fish feed to American lobster, *Homarus americanus*. *Aquac. Res.* 35, 713–722. doi: 10.1111/j.1365-2109.2004.01093.x

Canty, M. N., Hagger, J. A., Moore, R. T. B., Cooper, L., and Galloway, T. S. (2007). Sublethal impact of short term exposure to the organophosphate pesticide azamethiphos in the marine mollusc *Mytilus edulis*. *Mar. Pollut. Bull.* 54, 396–402. doi: 10.1016/j.marpolbul.2006.11.013

Chen, Y.-S., Beveridge, M. C. M., and Telfer, T. C. (1999). Physical characteristics of commercial pelleted Atlantic salmon feeds and consideration of implications for modeling of waste dispersion through sedimentation. *Aquacult. Int.* 7, 89–100.

Davies, I. (2001). Targeted environmental monitoring for the effects of medicines used to treat sea-lice infestation on farmed fish. *ICES J. Mar. Sci.* 58, 477–485. doi: 10.1006/jmsc.2000.1040

Dresdner, J., Chávez, C., Quiroga, M., Jiménez, D., Artacho, P., and Tello, A. (2019). Impact of *Caligus* treatments on unit costs of heterogeneous salmon farms in Chile. *Aquac. Econ. Manag.* 23, 1–27. doi: 10.1080/13657305.2018.1449271

Ernst, W., Doe, K., Cook, A., Burridge, L., Lalonde, B., Jackman, P., et al. (2014). Dispersion and toxicity to non-target crustaceans of azamethiphos and deltamethrin after sea lice treatments on farmed salmon, *Salmo salar*. *Aquaculture* 424–425, 104–112. doi: 10.1016/j.aquaculture.2013.12.017

Fernandez, C., and Farías, L. (2012). Assimilation and regeneration of inorganic nitrogen in a coastal upwelling system: ammonium and nitrate utilization. *Mar. Ecol. Prog. Ser.* 451, 1–14. doi: 10.3354/meps09683

Fernández, C., Farías, L., and Alcaman, M. E. (2009). Primary production and nitrogen regeneration processes in surface waters of the Peruvian upwelling system. *Prog. Oceanogr.* 83, 159–168. doi: 10.1016/j.pocean.2009.07.010

Garcés, D. V., Fuentes, M. E., and Quiñones, R. A. (2020). Effect of Azamethiphos on enzymatic activity and metabolic fingerprints of marine microbial communities from the water column. *Aquaculture* 529:735650. doi: 10.1016/j.aquaculture.2020.735650

Gebauer, P., Paschke, K., Vera, C., Toro, J. E., Pardo, M., and Urbina, M. (2017). Lethal and sub-lethal effects of commonly used anti-sea lice formulations on non-target crab *Metacarcinus edwardsii* larvae. *Chemosphere* 185, 1019–1029. doi: 10.1016/j.chemosphere.2017.07.108

Glibert, P. M., Wilkerson, F. P., Dugdale, R. C., Raven, J. A., Dupont, C. L., Leavitt, P. R., et al. (2016). Pluses and minuses of ammonium and nitrate uptake and assimilation by phytoplankton and implications for productivity and community composition, with emphasis on nitrogen-enriched conditions: pluses and minuses of NH4+ and NO3-. *Limnol. Oceanogr.* 61, 165–197. doi: 10.1002/lno.10203

González, L., and Carvajal, J. (2003). Life cycle of *Caligus rogercresseyi*, (*Copepoda*: *Caligidae*) parasite of Chilean reared salmonids. *Aquaculture* 220, 101–117. doi: 10.1016/s0044-8486(02)00512-4

González, M. P., Marín, S. L., and Vargas-Chacoff, L. (2015). Effects of *Caligus rogercresseyi* (Boxshall and Bravo, 2000) infestation on physiological response of host *Salmo salar* (Linnaeus 1758): establishing physiological thresholds. *Aquaculture* 438, 47–54. doi: 10.1016/j.aquaculture.2014.12.039

Hargrave, B. (2010). Empirical relationships describing benthic impacts of salmon aquaculture. *Aquac. Environ. Interact.* 1, 33–46. doi: 10.3354/aei00005

Helgesen, K. O., Bravo, S., Sevatdal, S., Mendoza, J., and Horsberg, T. E. (2014). Deltamethrin resistance in the sea louse *Caligus rogercresseyi* (Boxhall and Bravo) in Chile: bioassay results and usage data for antiparasitic agents with references to Norwegian conditions. *J. Fish Dis.* 37, 877–890. doi: 10.1111/jfd.12223

Herrera, J., Cornejo, P., Sepúlveda, H. H., Artal, O., and Quiñones, R. A. (2018). A novel approach to assess the hydrodynamic effects of a salmon farm in a Patagonian channel: coupling between regional ocean modeling and high resolution les simulation. *Aquaculture* 495, 115–129. doi: 10.1016/j.aquaculture.2018.05.003

Holm-Hansen, O., Lorenzen, C. J., Holmes, R. W., and Strickland, J. D. H. (1965). Fluorometric determination of chlorophyll. *ICES J. Mar. Sci.* 30, 3–15. doi: 10.1093/icesjms/30.1.3

Holmes, R., Aminot, A., Kérouel, R., Hooker, B., and Peterson, B. (1999). A simple and precise method for measuring ammonium in marine and freshwater ecosystems. *Can. J. Fish. Aquat. Sci.* 56, 1801–1808. doi: 10.1139/f99-128

Iriarte, J. L., González, H. E., Liu, K. K., Rivas, C., and Valenzuela, C. (2007). Spatial and temporal variability of chlorophyll and primary productivity in surface waters of southern Chile (41.5–43° S). *Estuar. Coast. Shelf Sci.* 74, 471–480. doi: 10.1016/j.ecss.2007.05.015

Johnson, S. C., Treasurer, J. W., Bravo, S., and Nagasawa, K. (2004). A review of the impact of parasitic copepods on marine aquaculture. *Zool. Stud.* 43, 8–19.

Knapp, C. W., Caquet, T., Hanson, M. L., Lagadic, L., and Graham, D. W. (2005). Response of water column microbial communities to sudden exposure to deltamethrin in aquatic mesocosms. *FEMS Microbiol. Ecol.* 54, 157–165. doi: 10.1016/j.femsec.2005.03.004

Laetz, C. A., Baldwin, D. H., Collier, T. K., Hebert, V., Stark, J. D., and Scholz, N. L. (2009). The synergistic toxicity of pesticide mixtures: implications for risk assessment and the conservation of endangered Pacific Salmon. *Environ. Health Perspect.* 117, 348–353. doi: 10.1289/ehp.0800096

Marie, D., Partensky, F., Jacquet, S., and Vaulot, D. (1997). Enumeration and cell cycle analysis of natural populations of marine picoplankton by flow cytometry using the nucleic acid stain SYBR Green I. *Appl. Environ. Microbiol.* 63, 186–193. doi: 10.1128/aem.63.1.186-193.1997

Millanao, B. A., Barrientos, H. M., Gómez, C. C., Tomova, A., Buschmann, A., Dölz, H., et al. (2011). Uso inadecuado y excesivo de antibióticos: salud pública y salmonicultura en Chile. *Rev. Médica Chile* 139, 107–118. doi: 10.4067/s0034-98872011000100015

Mulholland, M. R., and Lomas, M. W. (2008). "Chapter 7 - nitrogen uptake and assimilation," in *Nitrogen in the Marine Environment*, 2nd Edn, eds D. G. Capone, D. A. Bronk, M. R. Mulholland, and E. J. Carpenter (San Diego: Academic Press), 303–384. doi: 10.1016/b978-0-12-372522-6.00007-4

Nash, C. E. (2003). Interactions of Atlantic salmon in the Pacific Northwest. *Fish. Res.* 62, 339–347. doi: 10.1016/s0165-7836(03)00068-7

Núñez-Acuña, G., Gonçalves, A. T., Valenzuela-Muñoz, V., Pino-Marambio, J., Wadsworth, S., and Gallardo-Escárate, C. (2015). Transcriptome immunomodulation of in-feed additives in Atlantic salmon *Salmo salar* infested with sea lice *Caligus rogercresseyi*. *Fish Shellfish Immunol.* 47, 450–460. doi: 10.1016/j.fsi.2015.09.009

Olsen, L., Hernández, K., Van Ardelan, M., Iriarte, J., Can Bizsel, K., and Olsen, Y. (2017). Responses in bacterial community structure to waste nutrients from aquaculture: an in situ microcosm experiment in a Chilean fjord. *Aquac. Environ. Interact.* 9:2017.

Olsen, L., Hernández, K., Van Ardelan, M., Iriarte, J., Sánchez, N., González, H., et al. (2014). Responses in the microbial food web to increased rates of nutrient supply in a southern Chilean fjord: possible implications of cage aquaculture. *Aquac. Environ. Interact.* 6, 11–27. doi: 10.3354/aei00114

Quiñones, R. A., Fuentes, M., Montes, R. M., Soto, D., and León-Muñoz, J. (2019). Environmental issues in Chilean salmon farming: a review. *Rev. Aquac.* 11, 375–402. doi: 10.1111/raq.12337

Rain-Franco, A., Rojas, C., and Fernandez, C. (2018). Potential effect of pesticides currently used in salmon farming on photo and chemoautotrophic carbon uptake in central – southern Chile. *Aquaculture* 486, 271–284. doi: 10.1016/j.aquaculture.2017.12.048

Reyes, X., and Bravo, S. (1983). Nota sobre una copepoidosis en salmones de cultivo. *Invest. Mar.* 11, 55–57.

Rozas, M., and Asencio, G. (2007). Evaluación de la situación epidemiológica de la caligiasis en chile: hacia una estrategia de control efectiva. *Salmociencia* 2, 43–59. doi: 10.1787/9789264284272-4-es

Siwicki, A. K., Terech-Majewska, E., Grudniewska, J., Malaczewska, J., Kazun, K., and Lepa, A. (2010). Influence of deltamethrin on nonspecific cellular and humoral defense mechanisms in rainbow trout (*Oncorhynchus mykiss*). *Environ. Toxicol. Chem.* 29, 489–491. doi: 10.1002/etc.75

Willis, K. J., and Ling, N. (2003). The toxicity of emamectin benzoate, an aquaculture pesticide, to planktonic marine copepods. *Aquaculture* 221, 289–297. doi: 10.1016/s0044-8486(03)00066-8

Conflict of Interest: The authors declare that the research was conducted in the absence of any commercial or financial relationships that could be construed as a potential conflict of interest.

frontiers in Microbiology

ORIGINAL RESEARCH
published: 25 March 2021
doi: 10.3389/fmicb.2021.620458

Thermal Stress Interacts With Surgeonfish Feces to Increase Coral Susceptibility to Dysbiosis and Reduce Tissue Regeneration

Leïla Ezzat[1†], Sarah Merolla[2], Cody S. Clements[3], Katrina S. Munsterman[4], Kaitlyn Landfield[1], Colton Stensrud[5], Emily R. Schmeltzer[5], Deron E. Burkepile[1,6] and Rebecca Vega Thurber[5]*

[1] Department of Ecology, Evolution and Marine Biology, University of California, Santa Barbara, Santa Barbara, CA, United States, [2] Bodega Marine Laboratory, University of California, Davis, Davis, CA, United States, [3] School of Biological Sciences, Georgia Institute of Technology, Atlanta, GA, United States, [4] Department of Ecology and Evolutionary Biology, University of Michigan, Ann Arbor, MI, United States, [5] Department of Microbiology, Oregon State University, Corvallis, OR, United States, [6] Marine Science Institute, University of California, Santa Barbara, Santa Barbara, CA, USA

OPEN ACCESS

Edited by:
Camila Fernandez, UMR 7621 Laboratoire d'océanographie microbienne (LOMIC), France

Reviewed by:
Julie L. Meyer, University of Florida, United States
Diogo Antonio Tschoeke, Federal University of Rio de Janeiro, Brazil

***Correspondence:**
Leïla Ezzat
leila.ezzat@gmail.com

†Present address:
Leïla Ezzat, Stream Biofilm and Ecosystem Research Laboratory, School of Architecture, Civil and Environmental Engineering, École Polytechnique Fédérale de Lausanne, Lausanne, Switzerland

Specialty section:
This article was submitted to Aquatic Microbiology, a section of the journal Frontiers in Microbiology

Received: 22 October 2020
Accepted: 28 February 2021
Published: 25 March 2021

Citation:
Ezzat L, Merolla S, Clements CS, Munsterman KS, Landfield K, Stensrud C, Schmeltzer ER, Burkepile DE and Vega Thurber R (2021) Thermal Stress Interacts With Surgeonfish Feces to Increase Coral Susceptibility to Dysbiosis and Reduce Tissue Regeneration. Front. Microbiol. 12:620458. doi: 10.3389/fmicb.2021.620458

Dysbiosis of coral microbiomes results from various biotic and environmental stressors, including interactions with important reef fishes which may act as vectors of opportunistic microbes via deposition of fecal material. Additionally, elevated sea surface temperatures have direct effects on coral microbiomes by promoting growth and virulence of opportunists and putative pathogens, thereby altering host immunity and health. However, interactions between these biotic and abiotic factors have yet to be evaluated. Here, we used a factorial experiment to investigate the combined effects of fecal pellet deposition by the widely distributed surgeonfish *Ctenochaetus striatus* and elevated sea surface temperatures on microbiomes associated with the reef-building coral *Porites lobata*. Our results showed that regardless of temperature, exposure of *P. lobata* to *C. striatus* feces increased alpha diversity, dispersion, and lead to a shift in microbial community composition – all indicative of microbial dysbiosis. Although elevated temperature did not result in significant changes in alpha and beta diversity, we noted an increasing number of differentially abundant taxa in corals exposed to both feces and thermal stress within the first 48h of the experiment. These included opportunistic microbial lineages and taxa closely related to potential coral pathogens (i.e., *Vibrio vulnificus*, *Photobacterium rosenbergii*). Some of these taxa were absent in controls but present in surgeonfish feces under both temperature regimes, suggesting mechanisms of microbial transmission and/or enrichment from fish feces to corals. Importantly, the impact to coral microbiomes by fish feces under higher temperatures appeared to inhibit wound healing in corals, as percentages of tissue recovery at the site of feces deposition were lower at 30°C compared to 26°C. Lower percentages of tissue recovery were associated with greater relative abundance of several bacterial lineages, with some of them found in surgeonfish feces (i.e., Rhodobacteraceae, Bdellovibrionaceae, Crocinitomicaceae). Our findings suggest that fish feces interact

with elevated sea surface temperatures to favor microbial opportunism and enhance dysbiosis susceptibility in *P. lobata*. As the frequency and duration of thermal stress related events increase, the ability of coral microbiomes to recover from biotic stressors such as deposition of fish feces may be greatly affected, ultimately compromising coral health and resilience.

Keywords: surgeonfish, coral, thermal stress, feces, *Vibrio*, global change, dysbiosis, 16S rRNA

INTRODUCTION

Reef-building corals form associations with a wide array of microorganisms including dinoflagellate algae ("Symbiodinaceae"), bacteria, viruses and archaea, which collectively form the coral holobiont (Rohwer et al., 2002). Interactions between corals and these microbial associates likely play key roles in a number of vital host functions including coral immune response and nutrient cycling (Maynard et al., 2015; McDevitt-Irwin et al., 2017; Robbins et al., 2019; van Oppen and Blackall, 2019). At the same time, coral-associated microbial communities are sensitive to numerous environmental (i.e., temperature, nutrient pollution, and overfishing) and biotic (i.e., corallivory and macroalgal competition) stressors (McDevitt-Irwin et al., 2019). Many of these stressors have been associated with disruptions to coral microbiomes that can lead to microbial dysbiosis (i.e., the loss of beneficial microbes or increase of opportunists) (McDevitt-Irwin et al., 2017; van Oppen and Blackall, 2019), bleaching, and mortality (Hughes et al., 2017) – emphasizing the importance of coral-associated microbial communities to the integrity of reef ecosystems.

Despite the disproportionate role that combinations of stressors are predicted to play as reefs further degrade (Bourne et al., 2016; Hughes et al., 2017; van Oppen and Blackall, 2019), their impacts on coral microbiomes remain poorly understood (Zaneveld et al., 2016; Maher et al., 2019; Rice et al., 2019b). This is especially true for biotic stressors resulting from interactions between corals and reef fishes, such as corallivory (i.e., consumption of living corals) or the deposition of fish fecal material onto corals (Nicolet et al., 2018; Ezzat et al., 2019; Rice et al., 2019a). These interactions are both common and integral to reef ecosystems, but could promote coral dysbiosis and mortality when coupled with anthropogenic stressors (Zaneveld et al., 2016). Identifying and quantifying these microbial interactions will be important for predicting the future dynamics of coral reefs.

Reef fishes play critical and often positive roles in the function and dynamics of coral reef ecosystems (Burkepile and Hay, 2008; Mora, 2015). Herbivores and detritivores remove macroalgae that can harm coral growth, recruitment and survival (Burkepile and Hay, 2008; Rasher et al., 2013), while fish communities more broadly help retain and recycle nutrients within reef ecosystems (Allgeier et al., 2016). Despite these benefits, evidence suggests that a number of species may also harm corals – promoting dysbiosis via transmission or enrichment of opportunistic and/or pathogenic microbial taxa (Chong-Seng et al., 2011; Ezzat et al., 2019). For example, corallivorous butterflyfishes and parrotfishes may spread parasites and bacteria among coral colonies via oral transmission while feeding (Chong-Seng et al., 2011; Ezzat et al., 2020; Noonan and Childress, 2020). Many reef fishes also harbor a diverse gut microbiota that include opportunists and pathogens with the potential to alter coral health (Smriga et al., 2010). A recent study demonstrated that fecal pellets from the surgeonfish *Ctenochaetus striatus* may vector and/or favor the enrichment of opportunistic taxa when they land on coral colonies (Ezzat et al., 2019), possibly leading to tissue mortality when feces sit on corals for prolonged periods.

Negative effects on coral microbiomes due to biotic interactions, such as fecal pellet deposition, may normally be transient (Ezzat et al., 2019; Garren et al., 2009), but such impacts may become more severe as human-induced stressors increase in frequency and intensity (Maynard et al., 2015; McDevitt-Irwin et al., 2019). For instance, rising sea surface temperature is a common abiotic stressor on reefs that can induce shifts in coral bacterial community composition, increase community variability, and promote blooms of opportunistic and pathogenic taxa – all of which are indicative of dysbiosis (Ritchie, 2006; Bourne et al., 2016; McDevitt-Irwin et al., 2017; Maher et al., 2019). Elevated sea surface temperature could therefore interact with fish fecal deposition to enhance the growth and virulence of specific microbes, including potential pathogens (i.e., *Vibrio, Photobacterium*) that could compromise coral immunity, health and resilience.

In light of our previous work (Ezzat et al., 2019), this study investigated how fish feces deposition impacted coral microbiomes and tissue regeneration when corals also experienced thermal stress. Working in Mo'orea, French Polynesia, we focused on the line bristletooth surgeonfish *Ctenochaetus striatus*, a functionally important and widely distributed detritivore known to produce substantial amounts of fecal pellets that frequently land on corals (Krone et al., 2008) and can disrupt coral microbiomes (Ezzat et al., 2019). Coral reefs in Mo'orea have been experiencing periodic bleaching events since the 1990's, with average seawater temperatures fluctuating from 26°C up to 30°C during periods of thermal stress related to bleaching (Pratchett et al., 2013). Therefore, using a factorial designed experiment, we monitored temporal changes in the diversity, stability and compositionality of bacterial communities on massive *Porites lobata* corals exposed to *C. striatus* feces under ambient and elevated sea surface temperatures. In addition, we tracked the recovery of *P. lobata* bacterial communities and rates of tissue regeneration following removal of fish feces from coral tissues when exposed to either thermal condition. We hypothesized that the diversity and variability of *P. lobata*

microbiomes would increase when exposed to either stressor alone and would exceed these individual effects when stressors were combined, thus acting synergistically. Specifically, we hypothesized that the combination of fish feces and temperature would (i) shift bacterial assemblages toward greater abundances of opportunistic bacteria involved in bleaching and coral diseases (e.g., *Vibrio* spp.), and (ii) prolong the persistence of bacterial opportunists following removal of fish fecal pellets from a coral's surface. Finally, we hypothesized that (iii) following fecal pellet removal, feces-induced coral lesions would exhibit lower percentage of tissue recovery when exposed to elevated temperature.

MATERIALS AND METHODS

Sample Collections

The present study was conducted in Mo'orea, French Polynesia (17° 29′ 26.0″ S, 149° 49′ 35.10″W) in August 2018 and based on the previous work by Ezzat et al. (2019). Briefly, thirty-two *Porites lobata* colonies (∼20 cm diameter) were collected at 3 m depth in the back reef area along the north shore of Mo'orea, immediately stored in coolers, and transported back to the Gump South Pacific Research Station. At the station, coral colonies were immediately placed in eight 150 L mesocosms (n = 4 colonies per mesocosm) and exposed to comparable light intensity (800 μmol photons m^{-2} s^{-1}) and temperature (26°C ± 1°C) regimes. Mesocosms received a continuous supply of seawater from the nearby reef at a flow rate of ∼ 30L h^{-1}. Submersible pumps were placed in each mesocosm to ensure proper water mixing.

A total of 15 individuals of *Ctenochaetus striatus* (∼ 20 cm total length) were collected at ∼ 3 m depth within the same back reef area using hand and barrier nets. Fish were then euthanized and dissected to retrieve feces samples from the lowest part of their intestines (last 3–7 cm before the anus). Feces samples were then homogenized in a sterile Whirl-Pak and directly placed on coral fragments as described below. Fish collections, as well as feces sampling, processing, and placement on corals, were completed on the same day.

Experimental Design of Feces and Temperature Interactions

Each *P. lobata* colony was cut into 4 coral fragments using a band saw, to produce a total of 128 fragments that were ∼ 8 cm diameter. Coral fragments were then evenly sorted into 8 mesocosms, so that one fragment of each colony was placed in each treatment (n = 2 mesocosms per treatment, n = 4 treatments, n = 16 coral fragments per mesocosm). Each fragment was then allowed to recover for 24 h prior to any change in temperature regime. Following the recovery period, four mesocosms remained at 26°C ± 1°C while seawater temperatures in the four remaining mesocosms increased from 26°C ± 1°C to 30°C ± 1°C over a 4 day-period (1°C per day). At the end of the fourth day, mesocosms were designated both by treatment (Control vs Feces) and temperature conditions (26°C vs 30°C) (**Figure 1A**): (1) tanks with coral fragments exposed to ambient seawater temperature (Control 26°C), (2) tanks where a fish fecal pellet was deposited on each coral fragment and exposed to ambient seawater temperature (Feces 26°C), (3) tanks with coral fragments exposed to elevated seawater temperature (Control 30°C), and (4) tanks where a fish fecal pellet was deposited on each coral fragment and exposed to elevated seawater temperature (Feces 30°C). The experiment commenced (T0) upon placement of fecal pellets on all designated coral fragments (∼ 300 mg per fragment).

Four coral fragments were randomly sampled from each mesocosm at three different timepoints during our experiment: (1) immediately after placing fecal pellets on all designated coral fragments (T0), at 24h (T24), and 48h (T48) (**Figures 1B,C**). Upon collection, all coral fragments were rinsed with a turkey baster using 0.2 μm filtered seawater to remove residual fecal matter from exposed corals. Then, using a sterilized bone cutter, a 1 × 1 cm portion of coral tissue (mucus, tissue and part of the skeleton) was sampled where the treatment was applied (feces deposition) or at a comparable location on corals lacking feces. All samples were then placed in separate (or individual) Whirl-Pak(s). At T48, all remaining coral fragments (n = 8 per treatment) were rinsed as mentioned above and placed back in their respective mesocosm to assess recovery of the corals' microbiomes (hereafter called "recovery phase") and rate of coral tissue regeneration among corals subjected to fecal pellet deposition (see Ezzat et al., 2019 and the paragraph below). This 48 h timepoint was chosen to reflect the residence time of *C. striatus* fecal pellets on corals previously observed in the field (Ezzat et al., 2019). At the end of the experiment (TF, 1 week), the remaining coral fragments (n = 8 per treatment) were collected (**Figures 1B,C**) and coral tissues sampled as described above. In addition, one 1L sample of seawater was collected from each mesocosm at each timepoint and directly filtered onto a 0.2 μm filter (MilliporeSigma) to compare their microbial communities to the ones of coral samples from the same mesocosm. Finally, three samples of surgeonfish feces were collected following dissection of the same group of fishes and directly disposed in independent Whirl-Pak bags to compare their bacterial communities to those of coral samples and establish potential route of transmission and/or enrichment. Coral tissue, filter and fish feces samples were then transferred into bead tubes (MoBio/Qiagen Power Soil) and stored at -80°C until processing.

Percentage of Coral Tissue Recovery

We previously observed that deposition of surgeonfish fecal pellets onto *P. lobata* coral fragments induced apparent bleaching and subsequent tissue loss (Ezzat et al., 2019). Thus, in the present study, we monitored the percentage of tissue recovery between T48 and TF (1 week) on coral fragments that were initially exposed to fecal pellets (Feces 26°C and Feces 30°C). Photographs of coral fragments previously exposed to fecal pellets were taken at both T48 and TF. In each case, we measured the surface area (SA) of coral bleaching using ImageJ (Schneider et al., 2012). To quantify tissue recovery after

5 days, we calculated the difference between the initial and final lesion size as a percentage of the initial lesion size: $(SA_{T48} - SA_{TF})/(SA_{T48})*100$.

DNA Extraction and 16 rRNA Gene Amplification

DNA extraction was performed on coral tissue, filters and feces samples using DNeasy PowerSoil Kit (Qiagen) following the manufacturer's instructions. High-throughput sequencing of the 16S rRNA gene was performed to compare the diversity, composition and stability metrics of bacterial communities. AccuStart II PCR ToughMix PCR reagent (Quanta BioSciences, Gaithersburg, Maryland, USA) was used in a two-step method to amplify and tag the V4 hypervariable region of the 16S rRNA gene using the primers 515F (5′GTGYCAGCMGCCGCGGTAA-3′) (Parada et al., 2016) and 806R (5′-GGACTACNVGGGTWTCTAAT-3′) (Apprill et al., 2015) targeting bacterial and archaeal communities. The reaction included 6.25 µl AccuStart II ToughMix (2X), 1.25 µl forward primer (10 µM), 1.25 µl reverse primer (10 µM), 0.5 µl sample DNA, and 3.25 µl PCR-grade water. PCR amplification followed a 3 min denaturation at 94°C; 35 cycles of 45 s at 94°C, 60 s at 50°C, and 90 s at 72°C; ending with 10 min at 72°C. To avoid host DNA contamination, amplified samples were run on a 1.5% agarose gel and each visible 16S band was individually poked up to five times with a sterile 10 µl plastic pipette tip. In this way, we ensured that the majority of barcoded product was the 16S V4 region target for the 2nd-step amplification. Tips were then placed into separate PCR tubes already prepared with second-step barcoding master mix solution (12.5 µl ToughMix (2X), 9.5 µl water, and 1 µl of gel-purified sample DNA), swirled in solution to incorporate, and then removed. Following addition of 1 µl each of custom forward and reverse multiplexing barcodes, the 12-cycle barcoding reaction followed a 5 min denaturation at 95°C, 30 s melting at 95°C, 3 min annealing at

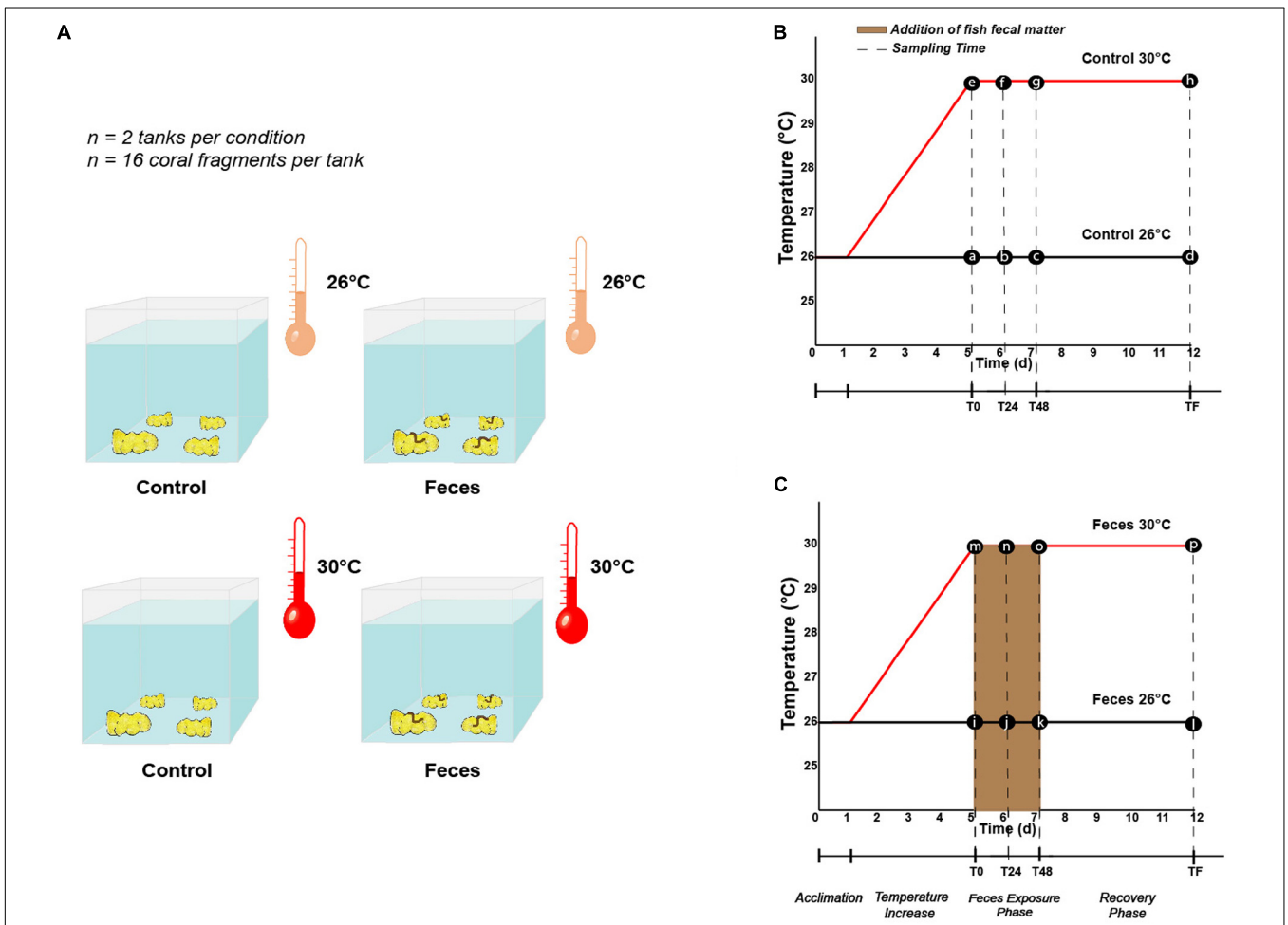

FIGURE 1 | (A) Illustration describing the different treatments (Control vs Feces) and temperature regimes (26°C vs 30°C) in which *Porites lobata* were exposed (Illustration by Nathalie Técher). Experimental design illustrating the temperature regimes (26°C and 30°C), the different phases (exposure and recovery) and specific time points at which **(B)** control corals and **(C)** corals exposed to fish feces were sampled (dashed lines). Letters respectively stand for (a) Control T0 26°C, (b) Control T24 26°C, (c) Control T48 26°C, (d) Control TF 26°C, (e) Control T0 30°C, (f) Control T24 30°C, (g) Control T48 30°C, (h) Control TF 30°C, (i) Feces T0 26°C, (j) Feces T24 26°C, (k) Feces T48 26°C, (l) Feces TF 26°C, (m) Feces T0 30°C, (n) Feces T24 30°C, (o) Feces T48 30°C, (p) Feces TF 30°C.

63°C, 30 s extension at 72°C, and 10 min hold at 72°C. Barcoded amplicons were pooled in equivolume ratios and purified with Agencourt® AMPure XP beads. Relative libraries were submitted to the Center for Genome Research and Biocomputing (CGRB at Oregon State University (OSU) for sequencing on the Illumina MiSeq Platform (2 × 300bp paired-end reads, MiSeq v.3).

Amplicon Sequence Data Processing and Quality Control

A total of 166 amplicon sequence libraries were generated, including those from coral tissue, fish feces, water filters and negative control samples (i.e., no-template-controls from PCR). 16S rRNA gene V4 amplicon sequences were processed using Quantitative Insights into Microbial Ecology 2 (QIIME2[1]; v. 2019.9; Bolyen et al., 2019). Plugin demux was used to visualize interactive quality plots and assess read quality. Paired-end sequencing generated a total of 2,828,626 reads across 166 samples. Raw sequences were first trimmed of primers with plugin cutadapt (Martin, 2011). Using DADA2 (Callahan et al., 2016), sequences were truncated for poor-quality bases (quality score < 35), chimeras were filtered, and paired-end reads were merged. This process resulted in a final dataset of 1,298,170 reads across 162 samples, after four samples were discarded in the workflow including one coral sample exposed to feces and the negative controls. Taxonomy was assigned against the SILVA reference database (v.123) (Quast et al., 2012), using classify-sklearn algorithm in QIIME2 (Bokulich et al., 2018). Mitochondria, chloroplasts and host DNA related reads were filtered out using the taxa plugin, further resulting in a total of 1,196,579 reads across 162 samples. A phylogenetic tree was processed with the plugins alignment and phylogeny for further downstream analyses. The biom table harboring the taxonomic counts, the phylogenetic tree and metadata were imported in R (v.3.6.1) for further statistical analyses. Rarefaction curves (Species richness and Shannon-Wiener indices) were generated (**Supplementary Figure 1**) and rarefaction level was set at 1317 reads per sample, after 20 samples were discarded due to low sampling depth. This included 8 coral samples exposed to control treatment, 11 coral samples exposed to fish fecal treatment and one water sample.

Amplicon Sequence Data Analytics

The following statistical analyses were performed in R (v.3.6.1). Two alpha diversity metrics were computed, including the observed richness and the Shannon-Wiener indices. Using linear mixed effect (LME) models with the package lme4 (v.1.1-21), the effects of the "treatment" (Control vs Feces), "temperature" (26°C vs 30°C), sampling "time" for the exposure (T0, T24, T48) and recovery phases (T48, TF) as well as their interactions on alpha diversity metrics were assessed. Models were fitted using the restricted maximum likelihood, including "treatment," "temperature," and "time" as well as their factorial interactions as fixed factors, while individual "tank" and "colony" were treated as random factors, to take into account the fact that multiple fragments of each treatment were present in each tank. When significant, pairwise comparisons among group levels were processed using the least square means (LSM) present within the package lmerTest (v. 3.1-1). Data residuals were tested for normality and homoscedasticity using Shapiro-Wilk and Levene Tests.

To illustrate the relative abundance of the 25 most abundant amplicon sequence variants (ASVs) as a function of the "treatment," "temperature," and "time" and across the whole dataset, we computed a heatmap and agglomerated the taxa at the family level using the function tax_glom (including the command NArm = F) within the phyloseq package (v.1.30). To assess the effects of "treatment", "time" and "temperature" on the relative abundance of the most abundant family in the coral dataset (i.e., Endozoicomonadaceae), we used a LME as previously described and agglomerated taxa at the family level.

To display shifts in bacterial community composition as a function of the "treatment," "temperature," and "time" within the exposure and recovery phases, two distinct principal coordinate analyses (PCoA) were computed on the Bray-Curtis dissimilarity matrices (999 permutations) using the function plot_ordination within the phyloseq package. Analyses of variance (PERMANOVA) based on the Bray-Curtis dissimilarity matrices were used to test for changes in community composition (beta diversity) as a function of (i) the "treatment," "temperature," "time," "tank," and "colony", (ii) "treatment," "temperature," and "sampletype" (coral vs water samples), "tank" within the exposure and recovery phases, with the function adonis in the package vegan. Pairwise differences were tested using the function pairwise.adonis in the package vegan (v.2.5-6). *P*-values were adjusted according to the Bonferroni method, which accounts for multiple comparisons.

Bacterial composition variability was tested using an analysis of multivariate homogeneity of group dispersions as follows: (i) between treatments (Control vs Feces) within a specific temperature and sampling time (T0, T24, T48 and T48, TF), (ii) between temperatures within a specific treatment and a specific timepoint. For this, we used the function betadisper in the package vegan on the Bray-Curtis dissimilarity matrices. When significant, pairwise tests were performed between groups using Tukey HSD.

The package DESeq2 (v.1.26) was used on the unrarefied ASV table to assess the differential abundance of ASVs as follows: (i) across treatments within a specific time period and temperature, (ii) within a specific treatment, across temperature and within a specific time period. DESeq2 includes a model based on the negative binomial distribution and a Wald's *post hoc* test for significance testing. *P*-values were adjusted according to the Benjamin and Hochberg method (Benjamini and Hochberg, 1995), accounting for multiple comparisons.

We assessed the presence of indicator ASVs for corals in the different treatments, within each time period and temperature at the species level within the indicspecies package (v.1.7.8). The resulting list of indicator ASVs was then screened to highlight bacterial groups previously described as potential coral pathogens.

Furthermore, the effect of temperature on the percentage of coral tissue recovery was tested using an ANOVA with

[1]http://qiime2.org

"temperature" as factor at TF (1 week). Finally, in order to detect associations between specific individual ASVs (from the coral dataset and at the genus level) and the percentage of coral tissue recovery, we deployed a series of linear models in R, linking the percentage of tissue recovery to the relative abundance of each ASV in turn, and allowing for varying intercepts between temperature regimes. Given the relatively low sample size (N = 13), the probability of type II error is high even for moderate to high effect sizes (Cohen, 1998). As a consequence, we chose to focus on model fit as measured by the coefficient of determination (R^2). We ranked ASVs according to the proportion of variance in tissue recovery explained by their relative abundance – i.e., by decreasing R^2. Since there is no objective method for distinguishing "high" from "low" correlation, we looked for discontinuities in the distribution of R^2, expressed as departures from zero in the distribution of empirical second derivatives. We examined the biological relevance of ASVs that correlate more strongly with tissue recovery than expected in a smooth distribution, in other words ASVs whose R^2 values are higher than the discontinuity threshold in the ranked R^2 distribution. Normality and homoscedasticity of the data residuals were tested using Shapiro-Wilk and Bartlett tests. All data presented in the result section are described as mean ± standard error.

RESULTS

Feces Exposure and Time Altered the Relative Abundance of the Dominant Symbiont Endozoicomonadaceae

Coral microbiomes were populated by 254 families across all phyla. Only a few families harbored a relative abundance > 1%, including: Endozoicomonadaceae (71% ± 0.03), Vibrionaceae (4.7% ± 0.01), Arcobacteraceae (2.9% ± 0.006), Fusobacteriaceae (2.01% ± 0.003) and Rhodobacteraceae (1.63% ± 0.001) (**Supplementary Table 1**). Treatment and time significantly affected the average relative abundance of the most abundant family, regardless of temperature (Endozoicomonadaceae; **Figure 2A** and **Supplementary Table 2**; $p_{\text{treatment}*\text{time}} = 0.006$). We observed a significant decrease in the relative abundance of Endozoicomonadaceae in microbiomes of corals exposed to fish feces at T0 compared to T24 (**Figure 2A** and **Supplementary Table 2**; p = 0. 001) and a significant increase between T24 and TF (**Figure 2A** and **Supplementary Table 2**; p = 0.004). Microbiomes of corals exposed to fish feces showed a lower relative abundance of Endozoicomonadaceae at T24 and T48 compared to control corals at all time points (**Supplementary Table 2**; $p < 0.04$ for all tests).

Bacterial Assemblages in *P. lobata* Differed From Tank Water and Fish Feces

Bacterial assemblages in tank water were populated by Proteobacteria, Bacteroidetes and Cyanobacteria. Family-level assignment showed the predominance of, among others, Cryomorphaceae (18.2% ± 0.03), Flavobacteriaceae (11.8% ± 0.01), Cyanobiaceae (6.9% ± 0.006), Rhodobacteraceae (5.8% ± 0.005) across a total of 331 families (**Figure 2B** and **Supplementary Table 3**).

The bacterial assemblages in surgeonfish feces samples were dominated by members from the phylum Proteobacteria, Firmicutes and Fusobacteria. Across all phyla, 60 families were detected and only a few of them were present at a relative abundance > 2%, including Vibrionaceae (31.5% ± 0.15), Lachnospiraceae (20.1% ± 0.04), Rhodobacteraceae (13.2% ± 0.08), Fusobacteriaceae (5.8% ± 0.03), Phormidiaceae (3.6% ± 0.04), Brevinemataceae (3.4% ± 0.02), Pirellulaceae (2.3% ± 0.02) (**Supplementary Table 4**).

We found that the composition of bacterial assemblages in *Porites lobata* significantly differed from assemblages in tank water and in *C. striatus* feces (**Figure 2B** and **Supplementary Table 5**; F = 33.9; p = 0.003 for all tests). In addition, microbial assemblages associated with corals were different from tank waters throughout the exposure and recovery phases, across treatments and regardless of temperature (**Figure 2B** and **Supplementary Table 6**; $F = 4.2$, $p_{\text{sample:treatment}} = 0.02$, $p < 0.01$).

Feces Exposure and Time Increased Bacterial Richness and Diversity

There was a significant interaction between treatment and time on both observed richness (**Supplementary Figure 2A** and **Supplementary Table 7**; F-value = 7.9; $p < 0.001$) and Shannon-Wiener indices (**Supplementary Figure 3A** and **Supplementary Table 8**; F-value = 9.9; $p < 0.001$) throughout the exposure phase (between T0 and T48). This pattern was present regardless of temperature (**Supplementary Tables 7, 8**). Corals exposed to feces had consistently greater values of ASV richness and Shannon-Wiener indices compared to control corals (**Supplementary Table 9**; $p_{\text{richness}} < 0.03$ for all tests; **Supplementary Table 10**; $p_{\text{diversity}} < 0.001$ for all tests). In addition, while control corals showed similar values of richness (**Supplementary Table 9**; $p > 0.47$ for all tests) and diversity (**Supplementary Table 10**; $p > 0.59$ for all tests) throughout the exposure phase, corals exposed to feces exhibited greater values of richness and diversity at T24 and T48 compared to T0 (**Supplementary Table 9**; $p_{\text{richness}} < 0.001$; **Supplementary Table 10**; $p_{\text{diversity}} < 0.001$ for all tests respectively).

During the recovery phase (T48-TF), there was a significant effect of the treatment only on both observed richness (**Supplementary Figure 2B** and **Supplementary Table 11**; F-value = 27.8; p = 0.003) and Shannon-Wiener indices (**Supplementary Figure 3B** and **Supplementary Table 12**; F-value = 42.5; $p < 0.001$), with control corals characterized by lower values of richness and diversity compared to corals exposed to feces.

Exposure to Feces and Time Altered Bacterial Assemblages in *P. lobata*

We observed a significant interaction between treatment and time on bacterial community composition throughout the exposure phase (**Supplementary Figure 4** and **Supplementary**

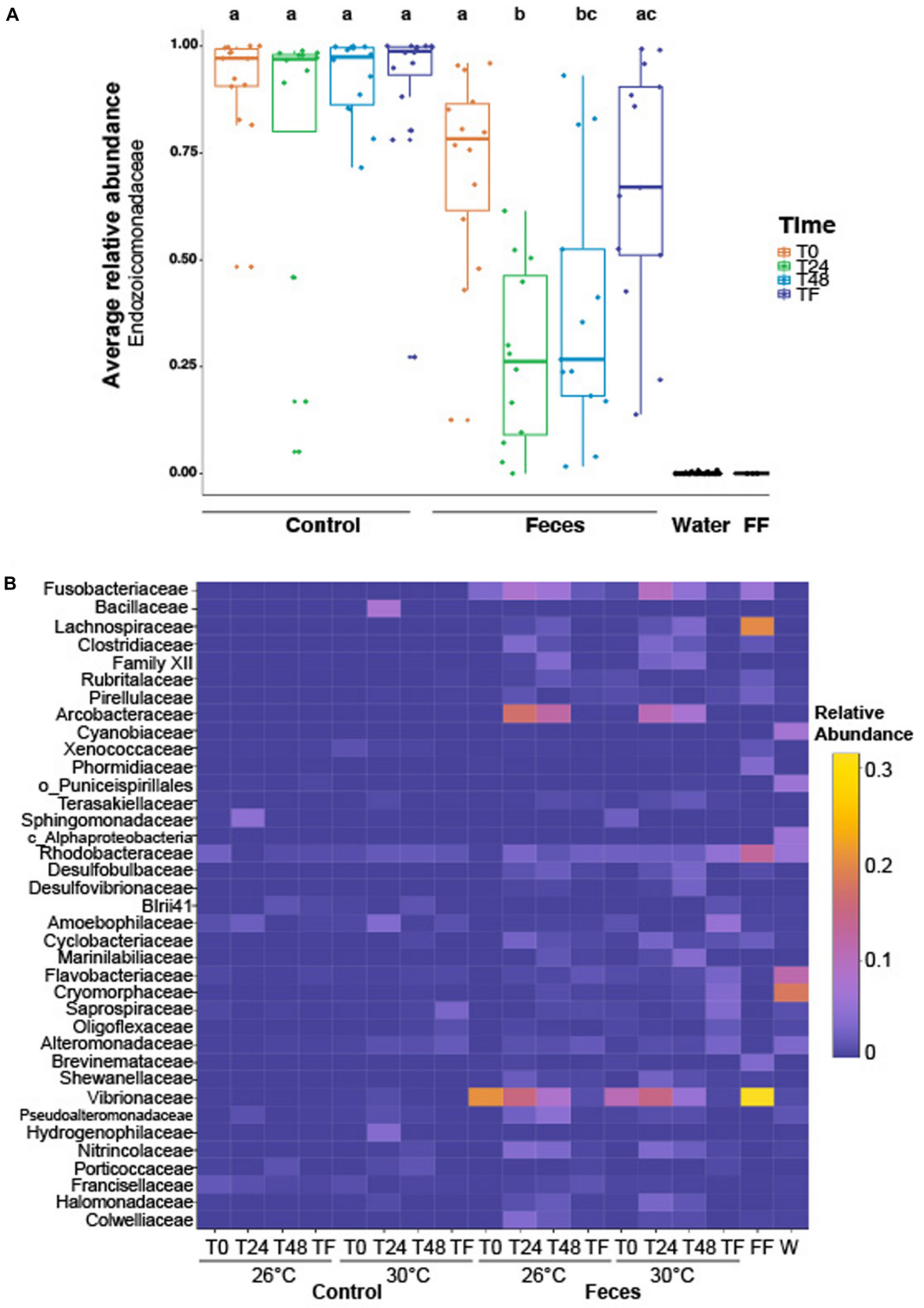

FIGURE 2 | (A) Boxplot illustrating the relative abundance of the most abundant family across the whole dataset (i.e., Endozoicomonadaceae), according to experimental treatments (feces vs control), time periods (T0, T24h, T48h, and TF). Lowercase letters above the plot represent the statistical significances based on pairwise comparisons ($p < 0.05$) computed on the coral dataset. The average relative abundance is based on $n = 12–16$ samples per condition. **(B)** Heatmap representing the relative abundance of the remaining abundant families (not including Endozoicomonadaceae) labeled as family, order or class across the whole dataset, according to experimental treatments, time periods and temperatures. "FF" and "W" stand for fish feces and water samples respectively. The average relative abundance is based on $n = 6–8$ samples per condition.

Table 13; PERMANOVA, F-value = 2.31; R^2 = 0.05; p = 0.015) and recovery phases (**Supplementary Figure 5** and **Supplementary Table 14**; PERMANOVA, F-value = 2.99; R^2 = 0.04; p = 0.009). At the beginning of the experiment (T0), control corals exhibited similar bacterial assemblages compared to corals exposed to feces (**Supplementary Table 16**; p = 0.11). Bacterial communities in control corals and corals exposed to feces were mainly dominated by sequences from the family Endozoicomonadaceae (88.7% and 71.5% respectively; **Supplementary Table 16**). However, bacterial assemblages differed between control corals and corals exposed to feces at T24 (**Supplementary Table 15**; p = 0.015) and T48 (**Supplementary Table 15**; p = 0.015). Specifically, coral microbiomes exposed to feces were mainly populated by members from the families Endozoicomonadaceae, Vibrionaceae, Arcobacteraceae, Rhodobacteraceae, Fusobacteraceae, Flammeovirgaceae, Colwelliaceae, and Nitrincolaceae at T24 and T48 respectively (**Supplementary Table 16**). In contrast control corals were mainly dominated by Endozoicomonadaceae throughout the exposure and recovery phases and few additional microbes were present above the detection level (**Supplementary Table 17**).

At the end of the recovery phase (TF), bacterial assemblages exposed to feces shifted back to their original composition and were similar to assemblages in control corals (**Supplementary Table 18**; p = 0.11), with microbiomes of corals mainly dominated by taxa from the family Endozoicomonadaceae (**Supplementary Table 16**). While control corals showed similar composition in their bacterial assemblages throughout the duration of the exposure and recovery phases (**Supplementary Tables 15, 19**; p = 1 for all tests), corals exposed to feces exhibited distinct composition at T0 compared to T24 (**Supplementary Table 15**; p = 0.015) and T48 (p = 0.015) respectively, as well as T48 compared to TF (**Supplementary Table 18**; p = 0.04).

Feces Exposure Interacted With Temperature to Form Novel Coral Microbiomes

Comparison of the Treatments Within Each Time Period and Temperature

For clarity, all results presented within this section applied to corals exposed to feces and included ASVs with an adjusted $p < 0.05$. Additional results regarding control corals can be found in the **Supplementary Material** (**Supplementary Text 1**). At T0 and under normal temperature (26°C), corals exposed to feces showed a greater abundance of five taxa from the families Vibrionaceae (e.g., ASVs_4496, 4579) (**Figure 3A** and **Supplementary Table 19**; log2 fold change: from 7.6 to 21.9) compared to control corals. At T24, the number of differentially abundant taxa in corals exposed to feces reached 25 ASVs compared to control corals (**Figure 3A**; log2 fold change: from 6.7 to 22.8). This included sequences from the genera *Propionigenium* (ASVs_200, 207-212), *Arcobacter* (e.g., ASVs_1357, 1371) and the family Vibrionaceae (e.g., ASVs_ 4495, 4496). At T48, only four taxa were present in greater abundance in corals exposed to feces compared to control corals (**Supplementary Table 19**; log2 fold change: from 6.7 to 20.7) and included members from the genera *Propionigenium* (ASV_209), *Oceanospirillum* (ASV_5287) and the family Arcobacteraceae (ASVs_1360, 1368). At TF and under

TABLE 1 | Indicator species closely affiliated to potential pathogens across the coral dataset [Closely related taxa are associated with their percent identity (%), appropriate accession number and the experimental conditions (treatment, temperature, and time) in which they were identified].

ASV Number(s)	Closely related species	Percent Identity (%)	Accession number	Conditions(s)	ASV found in Control	ASV found in *C. striatus* 16S fecal sample library (present study)	Taxon found in *C. striatus* fecal metagenome sample (Ezzat et al., 2019)
ASV_4495	*Photobacterium rosenbergii*	99.27	MN339950.1	Feces-26°C-T0	No	Yes	No
ASVs_4496, 4501		99.63	MN339949.1	Feces-30°C-T0 Feces-26°C-T0 Feces-26°C-T24h Feces-30°C-T24h		No	
ASV_4579	*Vibrio harveyi*	99.26	DQ995242.1	Feces-26°C-T0		No	Yes
ASV_4586		99.63	MT071645.1	Feces-26°C-T24h			
ASV_4587		100	MT071638.1	Feces-26°C-T48h Feces-30°C-T0 Feces-26°C-T0 Feces-26°C-T24h Feces-30°C-T24h Feces-26°C-T48h			
ASV_4582	*Vibrio ishigakengsis*	98.9	N339965.1	Feces-26°C-T0		Yes	No
ASV_4623		98.9	MN842811.1	Feces-26°C-T24h Feces-30°C-T24h Feces-26°C-T0 Feces-26°C-T48h		No	
ASV_4589	*Vibrio alginolyticus*	99.63	MN210933.1	Feces-30°C-T24h		No	Yes
ASV_4599, 4607	*Vibrio vulnificus*	99.27	MT052658.1	Feces-26°C-T0 Feces-30°C-T24h		No	Yes

26°C, only two taxa from the genera *Propionigenium* (ASV_210) and *Ruegeria* (ASV_2445) were present in greater abundance in corals exposed to feces compared to control corals (log2 fold change: from 20.5 to 20.7).

At T0 and under 30°C, only two ASVs from the family Vibrionaceae (ASV_4495) and the class Mollicutes (ASV_1646) were present in greater abundance in corals exposed to feces compared to controls (**Figures 3B,C** and **Supplementary Table 20**; log2 fold change: 21.9 to 24.4). However, at T24, this number reached 62 ASVs (**Supplementary Table 20**; log2 fold change: from 7.1 to 23.2) and included, among others, members from the family Clostridiaceae (e.g., ASVs_342, 355) and from the genera *Propionigenium* (ASVs_208-212), *Arcobacter* (e.g., ASVs_1327, 1330), *Photobacterium* (e.g., ASVs_4493, 4501) and *Vibrio* (ASVs_4577, 4579). At T48, the number of differentially abundant taxa in corals exposed to feces decreased to 8 ASVs compared to control corals (**Supplementary Table 20**; log2 fold change: from 19.9 to 21.1), and included members from the families Arcobacteraceae (ASVs_1316, 1318) and Vibrionaceae (ASVs_4532, 4620).

Effect of Temperature on Treatments Within Each Time Period

At T0, control corals showed greater abundance of eight taxa (**Figure 4A** and **Supplementary Table 21**; log2fold change: from −24.1 to −22.2), including members from the family Helicobacteraceae (ASV_1382), and the genera Candidatus Amoebophilus (ASVs_3008, 3009) and *Caedibacter* (ASV_5056-5058) at 26°C compared to 30°C. Only one ASV from the Mollicutes class was present in greater abundance at 30°C compared to 26°C in corals exposed to feces (Table S21; log2-fold change: 25.2), while four taxa from the genus *Vibrio* (e.g., ASVs_4594, 4599) were present in greater abundance at 26°C compared to 30°C (log2-fold change: from −24.4 to −22.7).

At T24, only one ASV from the genus *Ruegeria* (ASV_2441) was present in greater abundance in control corals at 30°C compared to 26°C (Table S22; log2-fold change: 21.5). Importantly, the number of differentially abundant taxa in corals exposed to feces increased to 62 ASVs at 30°C compared to 26°C (**Figure 4A** and **Supplementary Table 22**; log2-fold change: from 8.1 to 24.3). This included members from the families Lentisphaeraceae (ASV_150), Fusobacteriaceae (ASV_208), Clostridiaceae (e.g., ASVs_342, 363), Arcobacteraceae (e.g., ASVs_1330, 1333), Rhodobacteraceae (ASVs_1887, 2452, ASV_2446) and from the genera *Ferrimonas* (e.g., ASVs_4512, 4515), *Thalassotalea* (ASVS_5332, 5349), *Photobacterium* (e.g., ASVs_4497 4445) and *Vibrio* (e.g., ASVs_4563, 4577). Within the Vibrionaceae family, some sequences were closely affiliated to *Photobacterium rosenbergii*, *Vibrio ishigakensis*, *Vibrio harveyi*, *Vibrio alginolyticus* and *Vibrio vulnificus* (**Supplementary Table 22**). In contrast, ten taxa were present in greater abundance at 26°C compared to 30°C (**Supplementary Table 22**; log2-fold change: −23.5 to −8.1) and included taxa from the family Arcobacteraceae (e.g., ASVs_1363, 1369), and Vibrionaceae (ASV_4495) and from the genus *Ruegeria* (ASV_2442).

At T48 and within the feces treatment, 70 taxa were present in greater abundance at 30°C compared to 26°C (**Figures 4A,B** and **Supplementary Table 22**; log2-fold change: from 8.8 to 22.9), including ASVs from the families Lachnospiraceae (e.g., ASVs_323, 324), Clostridiaceae (e.g., ASVs_347, 348), Rhodobacteraceae (e.g., ASVs_1866, 1880), Desulfobacteraceae (ASV_2571), Desulfobulbaceae (ASV_2800), Fusobacteriaceae (ASVs_200), and genera *Halodesulfovibrio* (e.g., ASVs_2816, 2817), *Ferrimonas* (ASV_4512), *Vibrio* (e.g., ASVs_4574, 4581) and *Photobacterium* (ASVs_4498, 4532). Some sequences were closely affiliated to *Photobacterium rosenbergii*, *Vibrio parahaemolyticus*, *Vibrio harveyi*, *Vibrio hangzhouensis*, *Vibrio vulnificus* (Table S18). Conversely, 16 taxa showed greater abundance at 26°C compared to 30°C, such as Arcobacteraceae (ASVs_1330, 1360), Cyclobacteriaceae (ASV_3109), Vibrionaceae (ASVs_4621, 4623; ASV_4503), Pseudoalteromonadaceae (e.g., ASVs_4662, 4663).

At TF, corals exposed to feces showed greater abundance of only three taxa at 30°C compared to 26°C (**Supplementary Table 22**; log2fold change: from 22.4 to 26.2), including a member from the family Amoebophilaceae (ASV_3010). In contrast, 13 taxa were present in greater abundance at 26°C compared to 30°C (log2-fold change: from −23.4 to −21.9) and included, among others, ASVs from the families Fusobacteriaceae (ASVs_202, 204), Desulfobulbaceae (ASV_2806), Vibrionaceae (ASV_4495) and Ferrimonadaceae (ASV_4544).

Exposure to Fish Feces Increases Coral Microbiome Community Variability

Temperature did not affect microbial community variability in control corals or corals exposed to feces throughout the experiment (**Supplementary Tables 23, 24**). However, there was a significant effect of the treatment (Feces vs Control) on community variability through time and within each temperature (**Supplementary Figures 6, 7** and **Supplementary Tables 25, 26**). Under normal temperature (26°C) and at the beginning of the experiment (T0), corals exposed to feces showed similar values of bacterial community variability compared to control corals (**Supplementary Figure 6**; 0.16 ± 0.05; **Supplementary Table 25**; $p = 0.44$). Yet, corals exposed to feces showed greater values of community variability at T24, T48 and TF compared to control corals (**Supplementary Table 25**; $p \leq 0.01$ for all tests). Under elevated temperature (30°C), corals exposed to feces exhibited greater values of community variability at T0, T48 and TF compared to control corals (**Supplementary Figure 7** and **Supplementary Table 26**; $p < 0.03$ for all tests). In addition, time significantly affected bacterial community variability in control corals and corals exposed to feces during the exposure phase (**Supplementary Figures 8, 9** and **Supplementary Tables 27, 28**). In control corals, community variability was greater at T24 compared to T0 (**Supplementary Figure 8A** and **Supplementary Table 27**; $p = 0.02$) and T48 compared to T24 ($p = 0.01$). Corals exposed to feces showed ∼2x greater values of community variability at T24 and T48 compared to T0 (**Supplementary Figure 8B** and **Supplementary Table 28**; $p < 0.001$ for all tests). During the recovery phase, while no change was observed in control corals (**Supplementary Figure 9A** and **Supplementary Table 29**), corals previously exposed to feces exhibited a decrease

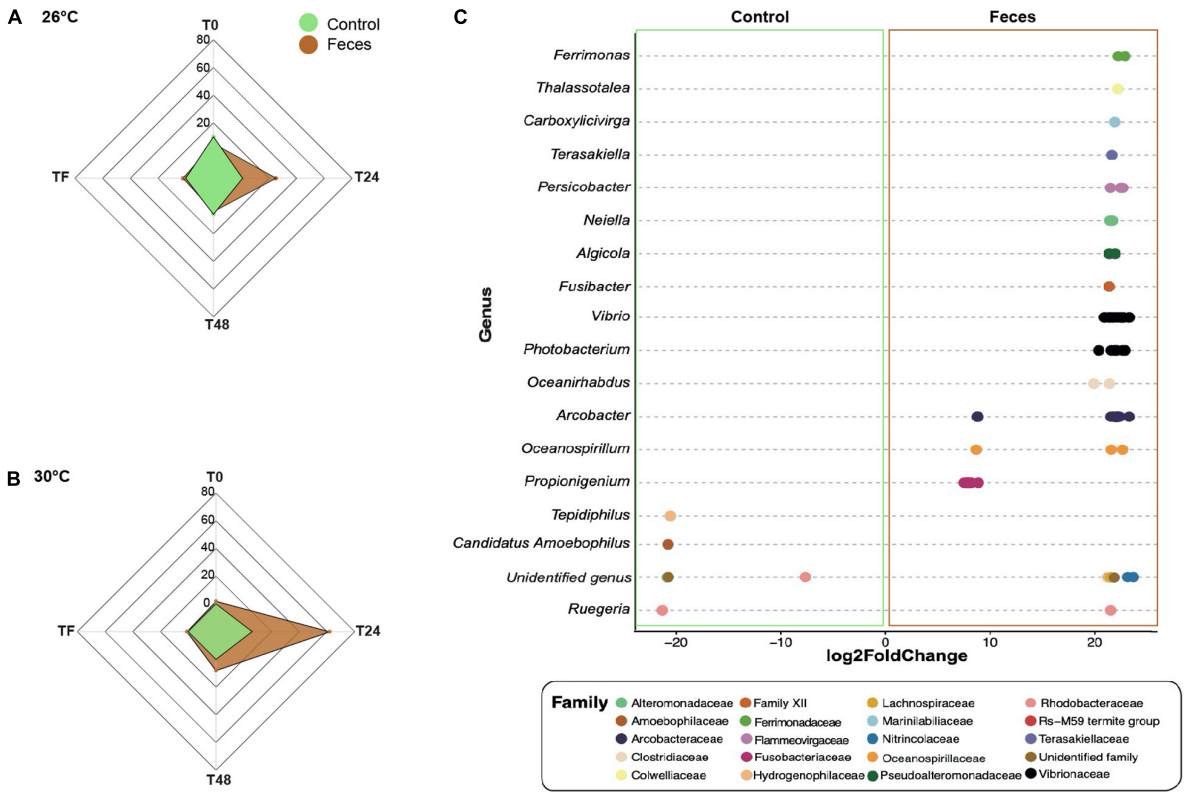

FIGURE 3 | Differential abundance analyses based on DESeq2. Number of differentially abundant ASVs observed in control corals compared to corals exposed to feces within each time point (T0, T24, T48, and TF) at **(A)** 26°C and **(B)** 30°C. **(C)** The ASVs labeled as family and genus that differed significantly between corals exposed to feces and control corals at T24 and under 30°C. Positive values are associated with differentially abundant taxa observed in corals exposed to feces.

in community variability at TF compared to T48 (Figure 8B; **Supplementary Table 30**; $p = 0.006$).

Indicator Species Associated With the Coral Microbiomes Closely Affiliated to Potential Coral Pathogens

BLASTn searches within the indicator species output (indicspecies results; **Supplementary Table 31**; **Table 1**) revealed the occurrence of nine specific ASVs that were closely related to potential coral pathogens. These taxa included *Photobacterium rosenbergii* (ASVs_4495, 4496, 4501; **Table 1**), *Vibrio harveyi* (ASV_4579, 4586, 4587), *Vibrio alginolyticus* (ASV_4589) and *Vibrio vulnificus* (ASV_4599, 4607). They were present in the microbiomes of corals exposed to feces within the first 48h of the experiment and under both temperatures (**Table 1**), but absent from control corals.

Percentage of Tissue Recovery Affected by Elevated Temperature and Correlated With Relative Abundance of Specific Bacterial Taxa

All results presented in this section applied to corals exposed to fish feces only given that there were no areas of tissue bleaching observed on control corals. Elevated temperature significantly decreased the percentages of coral tissue recovery between T48 and TF in *P. lobata* exposed to fish feces (**Figure 5** and **Supplementary Table 32**; F-value = 5.75; $p = 0.031$). Percentage of tissue recovery was 1.5 time lower at 30°C (29.22% ± 5.51%) compared to 26°C (49.23% ± 6.2%).

When examining association patterns between the relative abundance of individual ASVs and the percentage of coral tissue recovery, we found that the distribution of ranked coefficients of determination had a first discontinuity between its 1st and 2nd values, and a second clear discontinuity between its 11th and 12th values, i.e., for values of $R^2 > 0.59$ (**Supplementary Figure 10**). We restricted investigation of biological relevance to 11 ASVs (**Figure 6** and **Supplementary Table 33**), while acknowledging the possibility that associations may be specific to our particular dataset. Therefore, at the end of the experiment (TF), the percentage of tissue recovery was positively correlated with the relative abundance of one indicator taxon from the genus *Endozoicomonas* (**Figure 6**; ASV_5463; $R^2 = 0.77$). In contrast, the percentage of tissue recovery was negatively related with the relative abundance of ten bacterial taxa from the genera *Rubidimonas* (**Figure 6**; ASVs_3754; $R^2 = 0.69$), *Rubritalea* (ASV_ 652; $R^2 = 0.67$), *Lentisphaera* (ASV_175; $R^2 = 0.54$), *Kordiimonas* (ASV_2203; $R^2 = 0.62$), Rubinisphaeraceae (ASV_923; $R^2 = 0.62$), *Bdellovibrio* (ASV_4019; $R^2 = 0.61$), *Crocinitomix* (ASV_3159; $R^2 = 0.6$)

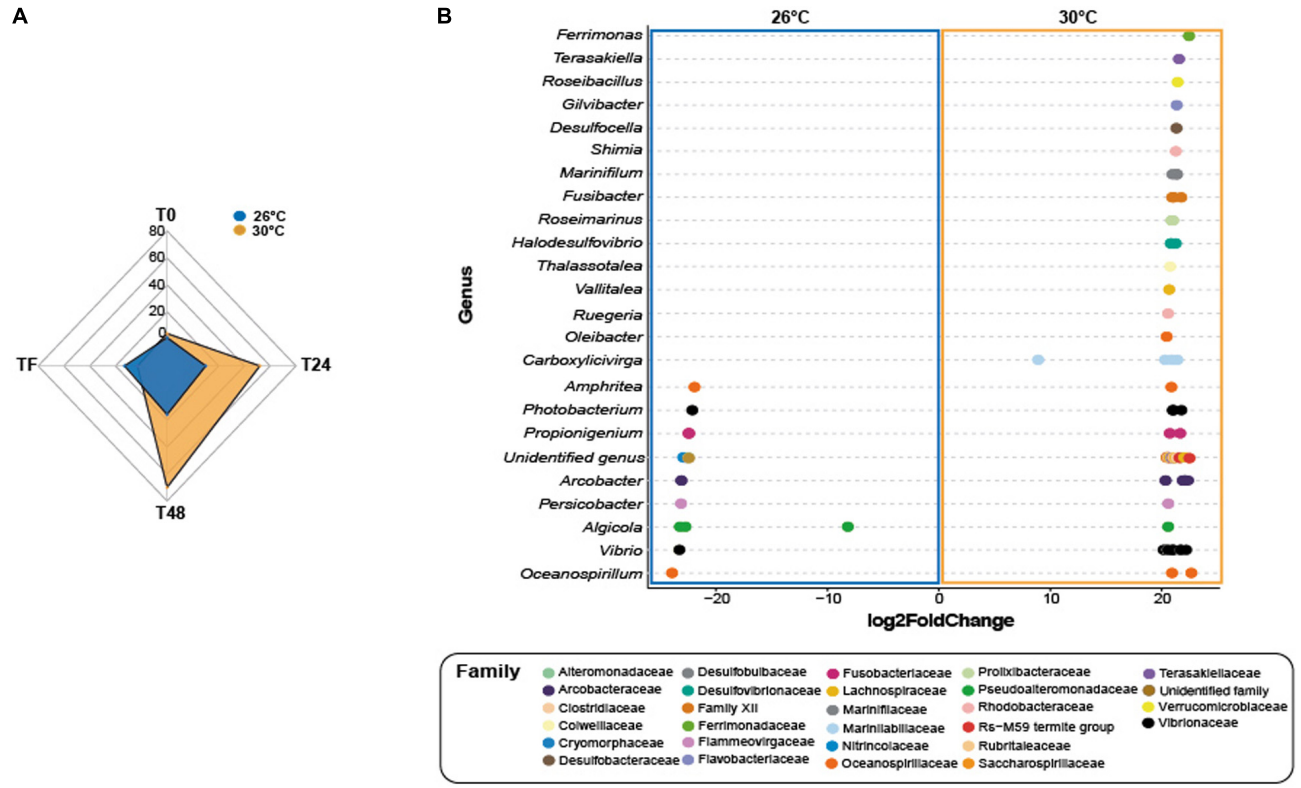

FIGURE 4 | Differential abundance analysis based on DESeq2. **(A)** Number of differentially abundant ASVs observed at 26°C compared 30°C in corals exposed to fish feces exclusively. **(B)** The ASVs labeled as family and genus that differed significantly between 26°C and 30°C in the treatment Feces at time T48. Positive values are associated with differentially abundant taxa observed in corals exposed to the feces treatment at 30°C.

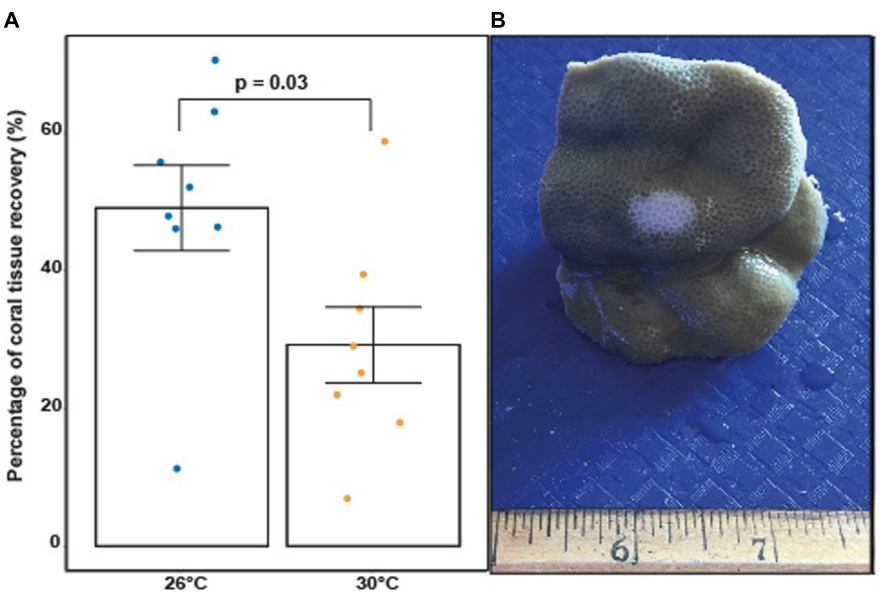

FIGURE 5 | (A) Percentage of coral tissue recovery (%) in coral fragments previously exposed to fish feces at 26°C and 30°C at TF (1 week). *P*-value indicates statistical significance based on an ANOVA. **(B)** *Porites lobata* fragment with apparent sign of tissue loss and bleaching following removal of fecal pellet at T48 under elevated temperature (image: Leïla Ezzat).

and *Peredibacter* (ASV_2658; R^2 = 0.6) as well as members from the families Hyphomonadaceae (ASV_2182; R^2 = 0.63) and Rhodobacteraceae (ASV_1920; R^2 = 0.63) – with some of these families and genera also present in fish fecal libraries (Ezzat et al., 2019 or present study) (**Figure 6**).

DISCUSSION

Coral-associated bacterial communities are sensitive to a variety of biotic and environmental stressors that can lead to microbial dysbiosis. Elevated temperature is among a number of environmental stressors that can favor shifts in bacterial communities and reduce immune function in reef-building corals. Moreover, one recently appreciated factor disrupting coral microbiomes is the deposition of fish feces on coral surfaces (Ezzat et al., 2019). Our findings suggest that the combination of surgeonfish feces and elevated temperatures created unique dynamics in *P. lobata* microbiomes compared to either stressor alone. Regardless of temperature, exposure of *P. lobata* to surgeonfish feces caused a significant shift in bacterial communities and resulted in increased alpha diversity and microbiome variability, all indicative of microbial dysbiosis. Although elevated water temperature did not lead to significant changes in alpha and beta diversity throughout the experiment, we noted a greater number of differentially abundant opportunists and potential pathogens in microbiomes of corals exposed to both feces and thermal stress. Among these taxa, some were associated with surgeonfish feces, suggesting that microbial enrichment and/or transmission from fish feces to corals occurs under, and may be facilitated by, elevated temperature. Furthermore, the impacts of fish feces and higher temperature on coral microbiomes appeared to inhibit wound healing in corals, as coral tissue percentages of coral tissue recovery at the site of feces deposition were significantly lower at 30°C compared to 26°C. Lesion recovery was negatively correlated with relative abundances of various bacterial taxa, including some found specifically in *C. striatus* feces. Our results suggest that increased sea surface temperature may exacerbate the effects of fish feces on coral microbiomes, ultimately altering *P. lobata* resilience.

Fish Feces Increased Dysbiosis Susceptibility in *P. lobata* Regardless of Temperature

Deposition of fish fecal material on coral surfaces is a common biotic event on coral reefs that may result in significant source of nutrients for reef-building corals and other marine organisms (Robertson, 1982; Smriga et al., 2010). Yet, reef fishes harbor a diverse and abundant gut microbiota, including potential coral opportunists and bacterial pathogens (Garren et al., 2009; Smriga et al., 2010; Ezzat et al., 2019). Our findings demonstrate that, regardless of temperature, exposure of *P. lobata* to *C. striatus* feces resulted in an increase in ASV richness and diversity and a significant shift in bacterial community composition within the first 24h of the exposure phase compared to control corals. Patterns of elevated alpha diversity were previously associated with multiple abiotic and biotic stressors (i.e., increased sea surface temperature, ocean acidification, macroalgal competition, mechanical and biological wounding, McDevitt-Irwin et al., 2019), including interactions with fish feces (Ezzat et al., 2019). It should be noted that although statistically significant, the combined effect of fish feces exposure and time explains a relatively small amount of the total variance. That said, changes in bacterial community composition and elevated alpha diversity associated with *C. striatus* feces deposition coincided with increased relative abundance of members from the families Alteromonadaceae, Flammeovirgaceae, Rhodobacteraceae, Pseudoalteromonadaceae, Clostridiaceae, Desulfobulbaceae, Lentisphaeraceae and the genera *Photobacterium, Vibrio, Propionigenium, Thalassotalea and Arcobacter* in coral microbiomes. The presence of specific taxa in surgeonfish feces (i.e., families: Lentisphaeraceae, Lachnospiraceae, Oligoflexaceae, Desulfobulbaceae; genera: *Photobacterium*, *Vibrio*, *Propionigenium, Persicobacter*) and their absence in control corals within the exposure phase suggests potential mechanisms of bacterial enrichment and/or transmission from fish feces to coral surfaces. For instance, microbial lineages from the genera *Propionigenium*, *Photobacterium*, and *Vibrio,* as well as the families Lachnospiraceae and Desulfobulbaceae, are commonly found in the gut of marine fishes (Smriga et al., 2010; Givens, 2012; Miyake et al., 2015; Yamazaki et al., 2016; Smith et al., 2017). Interestingly, some of the aforementioned taxa, such as Vibrionaceae, Colwelliaceae, Clostridiaceae, Arcobacteraceae and Desulfobulbaceae, are often associated with stressed corals, diseased lesions or bleaching (Thompson et al., 2006; Weil et al., 2006; Sunagawa et al., 2009; Arotsker et al., 2015). Additionally, microbiomes of corals exposed to feces showed a significant decrease in the relative abundance of the potential beneficial symbiont Endozoicomonadaceae between T0 and T24 (from 71.65% to 27.3%) - an observation that aligns well with previous results on stressed corals (Morrow et al., 2015; Glasl et al., 2016; Ziegler et al., 2017; Pootakham et al., 2019; Maher et al., 2020).

These findings are in agreement with previous work exploring the effects of fish farm effluents on coral microbiota that documented similar shifts in bacterial communities, mainly explained by the strong prevalence of opportunistic lineages (i.e., *Desulfovibrio*, *Fusobacterium*) in microbiomes of corals exposed to elevated discharges of effluents (Garren et al., 2009). In addition, the present observations reinforce the conclusions of our recent work (Ezzat et al., 2019) and further confirm the potential for surgeonfish feces to act as vectors of microbial opportunists in corals. It is worth noting that corals exposed to *C. striatus* feces showed an overall increase in variability of bacterial communities during the exposure phase compared to control corals, regardless of temperature. These observations are consistent with previous studies demonstrating greater stochasticity and microbiome variability in a wide variety of organisms, including corals, when subjected to environmental and biotic stressors (i.e., Anna Karenina principle Zaneveld et al., 2017), and further support the case that *C. striatus* fecal pellets may enhance dysbiosis susceptibility within reef-building corals.

Despite one week exposure to temperature-induced thermal stress, *P. lobata* corals did not exhibit any significant changes

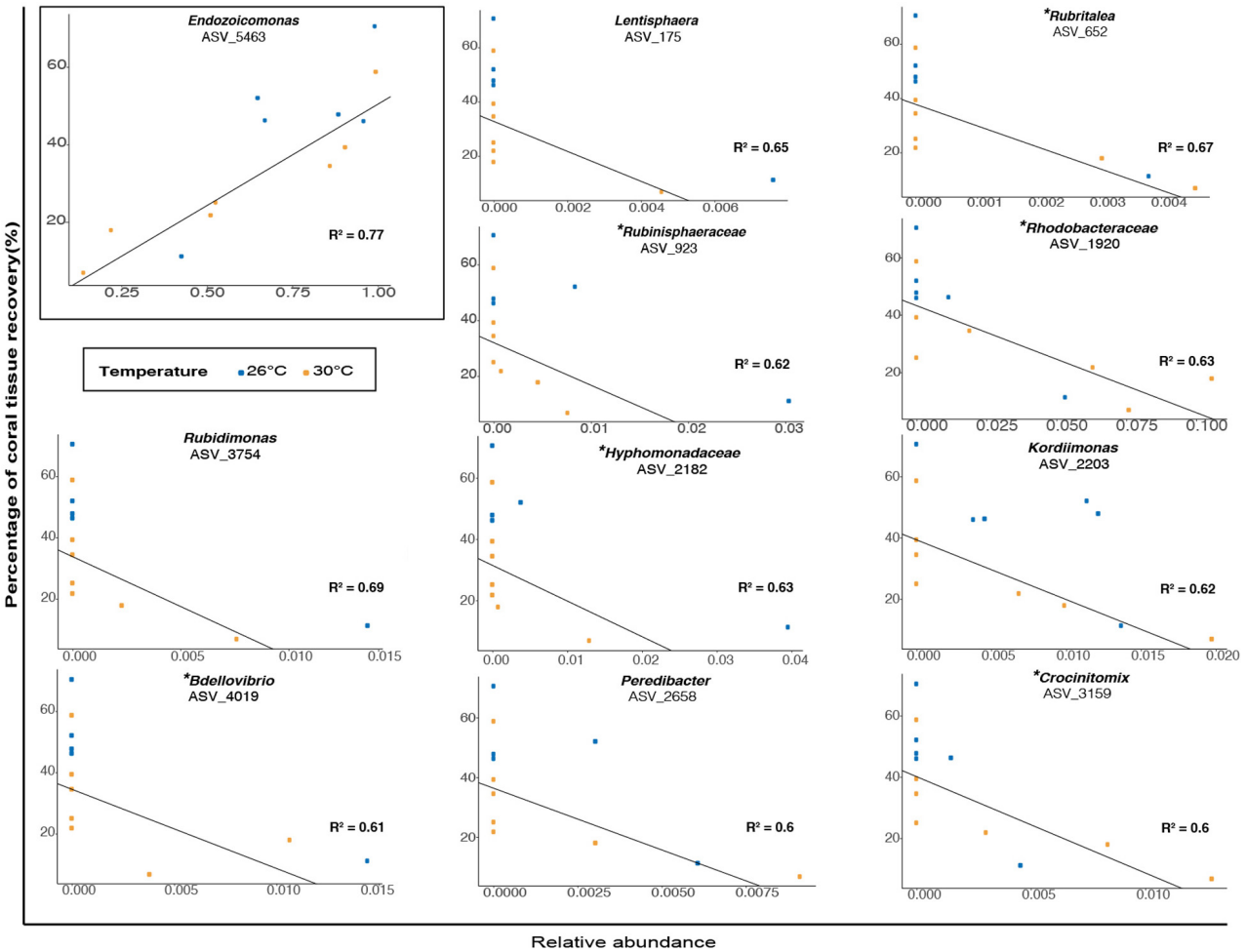

FIGURE 6 | Relationship between the percentage of coral tissue recovery (%) and the relative abundance (proportion) of bacterial taxa (classified as genera or family) in microbiomes of corals previously exposed to fish feces at TF (1 week). Blue and orange dots represent ambient and elevated temperatures respectively. The presence of a specific bacterial taxon in surgeonfish feces is specified by the symbol (*).

in bacterial community composition and alpha diversity. These findings contrast with evidence suggesting that elevated sea surface temperature alone or its combination with other stressors (i.e., contact with macroalgae, nutrient enrichment) drive shifts in bacterial community composition or/and modulate alpha diversity in reef-building corals (Bourne et al., 2008; Mouchka et al., 2010; Zaneveld et al., 2016; Grottoli et al., 2018; Maher et al., 2019). However, other studies demonstrated stability of microbiomes alpha and/or beta diversity following exposure of corals to high temperatures (Salerno et al., 2011; Webster et al., 2016; Ziegler et al., 2017; McDevitt-Irwin et al., 2019; Rice et al., 2019b), including species from the genus *Porites*. These discrepancies among studies indicate a high variability in coral thermal tolerance threshold and microbiome flexibility following changes in environmental conditions. For instance, corals thriving in thermally variable environments that experience frequent episodes of thermal stress, such as the back reef areas in Mo'orea (Putnam and Edmunds, 2011), may exhibit a more stable microbiome throughout the stress events compared to heat-sensitive holobionts from cooler and more stable environments (Ziegler et al., 2017). That said, our results support the general belief that massive colonies from the genus *Porites* exhibit high physiological tolerance and effective immune response to heat stress (Loya et al., 2001; Adjeroud et al., 2009; Palmer et al., 2011; van Woesik et al., 2011; Barshis et al., 2018). More work is required to understand the role of microbial communities in shaping coral responses to thermal stress.

Thermal Stress Exacerbated the Impact of Fish Feces on Coral Microbiomes

Elevated temperature alone did not lead to significant changes in bacterial community composition, but when paired with exposure to surgeonfish feces, we observed increased differential abundance of a variety of microbial taxa in corals – including potential opportunists and coral pathogens – compared to control corals at 30°C. For instance, 24 h exposure of corals to fish feces led to greater numbers of bacterial taxa, such

as members from the genera *Propionigenium*, *Arcobacter*, *Persicobacter*, *Photobacterium* and *Vibrio, Ferrimonas* compared to controls under both temperatures. Importantly, these increases in taxa were considerably greater at 30°C compared to 26°C (i.e., 62 taxa at 30°C vs 25 taxa at 26°C, **Figure 3**). The absence of specific bacterial taxa in microbiomes of control corals (i.e., *Propionigenium*, *Persicobacter*, *Photobacterium*, and *Vibrio*), and their presence in moderate or relatively low abundance in corals exposed to feces and in surgeonfish feces samples suggests patterns of bacterial transmission from fish feces to corals. This was observed at both 26°C and 30°C, but exacerbated when temperatures were higher. Furthermore, we observed significant differences in the abundance of specific taxa when testing the effects of elevated temperature on coral microbiomes within each treatment (control and feces). While elevated temperature did not lead to increased abundance of bacterial taxa in control corals (26°C vs 30°C), we observed blooms of $>$ 60 taxa in corals exposed to fish feces at 30°C compared to 26°C within the first 24 h of the exposure phase (**Figure 4**). This included taxa from the families Clostridiaceae, Arcobacteraceae, Rhodobacteraceae, Flammeorvirgaceae, Marinilabiliaceae, Vibrionaceae, Alteromonodaceae, Pseudoalteromonodaceae, Nitrincolaceae, Oceanospirillaceae, and Colwelliaceae. These observations showed that combination of both fish feces and increased sea surface temperatures resulted in unique microbial dynamics on coral surface when compared to either stressor alone.

Many of the bacterial taxa that bloomed on coral surfaces are known to respond to thermal and fecal stressors. For instance, members from the genera *Ruegeria, Arcobacter*, *Ferrimonas,* and the families Colwelliaceae and Clostridiaceae, often populate the microbiomes of corals and other marine organisms during thermal stress (Kimura et al., 1996; Simister et al., 2012; Gajigan et al., 2017). Evidence also suggests that the abundance of strains from the genera *Vibrio* and *Photobacterium* found in fish gut, corals and other fish food are exacerbated under ocean warming (Kelly, 1982; DePaola et al., 1994; Ben-Haim et al., 2003; Martinez-Urtaza et al., 2010; Vidal-Dupiol et al., 2011; Givens, 2012; Tout et al., 2015; Gajigan et al., 2017). Additionally, the gut of marine fishes includes micro-nutrients which may promote the growth of iron- and sulfate- or sulfur-reducing cells, including strains from the genera *Ferrimonas, Fusibacter* and members from the family Clostridiaceae in microbial communities of corals exposed to feces (Akagi and Campbell, 1962; Ravot et al., 1999; Nolan et al., 2010).

That said, the impact of these bacteria on coral microbiomes may vary, ranging from beneficial to potentially pathogenic. For example, two sequences from the genus *Ruegeria* (observed in microbial communities of corals exposed to feces under both temperatures) were closely related to *Ruegeria arenilitoris*, a bacterial species known to inhibit the growth of the coral pathogen *Vibrio coralliilyticus* (Miura et al., 2019). In contrast, taxa from the genera *Arcobacter*, *Persicobacter* and from the families Colwelliaceae and Clostridiaceae often populate the microbiomes of stressed and diseased corals as well as other marine organisms (Thompson et al., 2006; Kellogg et al., 2013; Sweet and Bythell, 2015; Ramees et al., 2017). Importantly, some sequences from the family Vibrionaceae exhibiting increased abundance at 30°C in corals exposed to feces compared to 26°C during the exposure phase were highlighted as indicator species of the feces treatment (**Table 1**) and closely affiliated to *Vibrio harveyi, Vibrio vulnificus, Vibrio ishigakensis, Vibrio alginolyticus and Photobacterium rosenbergii.* These taxa are often associated with particular diseases in humans, corals or other marine organisms such as fish as well as coral disease lesions and bleaching (DePaola et al., 1994; Thompson et al., 2005; Austin and Zhang, 2006; Luna et al., 2010; Meyer et al., 2019). Interestingly, the aforementioned five taxa, detected in different temperature regimes in our study, were simultaneously absent from control corals but present in either *C. striatus* feces 16S sample or metagenome (Ezzat et al., 2019), suggesting potential mechanisms of microbial transmission between surgeonfish feces and corals. It should be acknowledged that the aforementioned *Vibrio* sequences are equally good matches to several other *Vibrio* strains, confirming the limitations of sequencing the hypervariable V4 region of 16SrRNA gene for the precise identification of *Vibrio* species. Yet, the blooms of potential opportunists and pathogens in corals exposed to feces at elevated temperature are worrisome and raise concerns on potential subsequent impacts on coral health. As the frequency and duration of thermal stress related events may increase in the near future, common biotic interactions with reef fishes, such as release of fish fecal material, could turn harmful for corals. Whether these taxa actively affect *P. lobata* metabolism and resilience to stressors by acting as primary pathogens or simply exploit host resources when its immunity is compromised deserves further investigation.

Differences between microbiomes of control corals and corals exposed to feces were less pronounced by the end of the exposure phase (T48). We noted a drastic decrease in the differential abundance of potentially harmful taxa in microbiomes of corals exposed to feces compared to control at T48 in comparison to T24, regardless of temperature. This indicates a strong resilience of the coral holobiont, especially when both fish feces and elevated temperature interacted. These findings align well with previous studies demonstrating similar patterns in regulation of bacterial communities in corals exposed to stressors, including exposure to fish feces, fish farm effluents and thermal stress (Ritchie, 2006; Garren et al., 2009; Ezzat et al., 2019). The subtle changes observed could have resulted from an acclimative and transitory response of the coral host which lead to an altered state of its microbiome (van Oppen and Blackall, 2019). That said, even at T48, the number of differentially abundant ASVs when stressors were combined (high temperature and fish feces) still exceeded differences between control corals and corals that were exposed to either stressor alone. The persistence of a greater number of opportunistic and potential pathogens (i.e., *Vibrio*, *Photobacterium, Arcobacter*) in microbiomes of *P. lobata* exposed to feces at 30°C compared to 26°C suggests that temperature plays a critical role in exacerbating the effects of surgeonfish feces on coral microbiomes through time. Such taxa may have further contributed to detrimental health effects, such as apparent signs of bleaching and tissue mortality on surfaces of coral fragments previously exposed to fish feces – an observation already noted in the laboratory and in the field (Ezzat et al., 2019).

Coral Tissue Recovery Correlated With the Relative Abundance of Specific Bacterial Taxa

Coral microbiomes largely recovered by the end of the experiment (TF, 1 week), as bacterial communities of corals exposed to feces shifted back toward their original composition and exhibited a significant reduction in community variability when compared to T48, regardless of temperature. The recovery of coral microbiomes was associated with a considerable increase in the relative abundance of Endozoicomonadaceae in microbiomes of corals exposed to feces at the end of the experiment (TF) compared to T48 (from 38.6% to 67.2%). Our findings parallel with a previous study demonstrating the resilience of Endozoicomonadaceae in corals following stressful conditions (Maher et al., 2020).

That said, signs of bleaching and tissue mortality were observed in the area of feces deposition at T48, regardless of temperature. Whether this was caused by opportunistic bacteria, hypoxic mechanisms due to the presence of feces, or combination of these factors deserves further investigation (Weber et al., 2012). Importantly, the percentage of coral tissue recovery between T48 and TF was three times lower at 30°C compared to 26°C. These observations align with previous studies demonstrating a slower rate of coral tissue regeneration following mechanical wounding or natural injury under elevated temperatures (Kramarsky-Winter and Loya, 2000; Lenihan and Edmunds, 2010; Bonesso et al., 2017; Rice et al., 2019b). Thermal stress may have impacted the metabolism and growth of *P. lobata*, thereby reducing the availability in nutritional resources for the holobiont – ultimately altering processes of cellular repair and tissue regeneration (Kramarsky-Winter and Loya, 2000; Bonesso et al., 2017).

Alternatively, one could hypothesize that the presence of potential opportunistic bacterial taxa could impede coral tissue recovery – with particularly negative impacts under elevated temperatures.

For instance, we observed negative relationships between the percentage of coral lesion recovery and the relative abundance of nine bacterial taxa at the end of the experiment and regardless of temperature. This included members from the families Saprospiraceae, Rhodobacteraceae, Bdellovibrionaceae, Kordiimonadaceae, Hyphomonadaceae, Lentisphaeraceae, Rubinisphaeraceae, Crocinitomicaceae, Bacteriovoraceae, Rubritaleaceae. Interestingly, six of these aforementioned bacterial families (i.e., Rhodobacteraceae, Bdellovibrionaceae, Hyphomonadaceae, Crocinitomicaceae, Rubritaleaceae, and Rubinisphaeraceae) were detected in relatively low abundance in *C. striatus* fecal 16S libraries (i.e., present study and Ezzat et al., 2019). Additionally, some of these bacterial lineages have been associated with stressed corals (i.e., Rhodobacteraceae; Pootakham et al., 2019), while other are known to populate coral exudates (i.e., Hyphomonadaceae, Bacteriovoraceae; Nelson et al., 2013; Welsh et al., 2015). Our results indicate that bacterial taxa commonly found in relatively low abundance in fish feces could potentially modulate lesion recovery in corals. It is however important to note that despite being statistically significant, the negative correlations are mostly driven by a small number of samples. Further studies are required to better understand these relationships and establish them with certainty. That said, we noted a strong positive relationship between the percentage of coral tissue recovery and the relative abundance of *Endozoicomonas*. Bacterial taxa from the genus *Endozoicomonas* - often associated with healthy coral colonies (Neave et al., 2016; Shiu and Tang, 2019) - are suggested to play important roles in the holobiont nutrient cycling and in the resilience of coral-associated bacterial communities (Bourne et al., 2016; Neave et al., 2016; Tandon et al., 2020). For instance, sequencing of the first endozoicomonal bacteria (i.e., *E. montiporae* CL-33^T) from corals indicates potentials to prevent host mitochondrial dysfunction and favor gluconeogenesis during periods of stress (Ding et al., 2016). Moreover, evidence suggests that this particular taxon may provide protection to the photosymbionts against bleaching pathogens (Pantos et al., 2015). Although the present work demonstrates a clear relationship between the relative abundance of *Endozoicomonas* and the percentage of coral tissue recovery at the end of our experiment, our findings do not allow to establish whether *Endozoicomonas* has an active role in tissue recovery, or is rather a marker of coral tissue health. Further investigation is warranted to better understand the functional and ecological roles of *Endozoicomonas* and other specific bacterial symbionts in the microbial and physiological responses of reef-building corals to abiotic and biotic stressors.

CONCLUSION

Our findings confirm the potential of surgeonfish to act as a vector of microbes within *P. lobata*, regardless of temperature. Although elevated water temperature alone did not lead to significant changes in microbial alpha and beta diversity, thermal stress exacerbated the impact of fish feces on the coral microbiome as we observed increased number of differentially abundant bacterial taxa in corals exposed to feces compared to controls at 30°C. Among these bacteria, an increasing number of potential pathogenic lineages were detected, including strains from the genera *Vibrio* and *Photobacterium* – previously found in surgeonfish feces. Although the microbiomes of corals exposed to feces began to look increasingly like those of control corals after 48h, the persistence of opportunistic taxa when both stressors interacted indicates that extreme temperatures may exacerbate the effects of fish feces on coral microbiomes. Interestingly, the percentages of lesion recovery related to fish feces deposition on corals were significantly lower at 30°C compared to 26°C at the end of the experiment. Importantly, these lower percentages of tissue recovery were negatively associated with greater relative abundance of specific taxa (i.e., Bdellovibrionaceae, Rhodobacteraceae, and Crocinitomicaceae), with some of them detected in relatively low abundance in surgeonfish feces. Our findings highlight the flexibility of *P. lobata* microbiomes in response to changing environmental and biotic conditions, and suggest the critical role of coral-associated bacterial communities in coral responses to human-induced stressors. However, as the frequency and duration of thermal stress related events may increase in the near future, the ability of coral microbiomes to recover from common biotic stressors such as

deposition of fish feces may be greatly affected, compromising the health and resilience of their host. Our study provides evidence that common biotic interactions between reef fishes and corals, such as deposition of fish fecal material, could turn deadly for corals under anthropogenic stressors – ultimately impacting microbial dynamics in coral reefs. Future work assessing multiple scale response investigations (i.e., physiology, to microbes and genes) of coral species to different combinations of biotic and environmental disturbances will be important for understanding how human-induced stressors impact important biotic interactions in coral reefs.

DATA AVAILABILITY STATEMENT

Raw sequence data have been deposited in the Sequence Read Archive (SUB8734074) with NCBI BioProject accession no. PRJNA690899.

ETHICS STATEMENT

The animal study was reviewed and approved by UC Animal Care and Use Committee (IACUC #196, 2016 – 2019).

AUTHOR CONTRIBUTIONS

LE, RVT, and DB designed the experiment. KM, KL, LE, and CC collected the samples. LE, KM, KL, SM, and CC performed the experiment. ES and CS performed laboratory work. LE analyzed the data. LE, CC, DB, and RVT wrote the paper. All authors contributed to the article and approved the submitted version.

FUNDING

This work represents a contribution of the Mo'orea Coral Reef (MCR) LTER Site (NSF OCE 16-37396) and was performed according to the UC Animal Care and Use Committee (IACUC #196, 2016 – 2019). LE was supported by the Swiss National Science Foundation Postdoc Mobility Fellowship (#P400PB_183867). CC was supported by the Teasley Endowment to the Georgia Institute of Technology. This work was also supported by the National Sciences Foundation (NSF) grants (#2023424) to RVT and (OCE-1547952) to DB.

ACKNOWLEDGMENTS

We are grateful to the staff at the GUMP Research Station in Moorea, French Polynesia. Many thanks to Drs. R. Cristofari, L. Carraro, E. Videvall, D. Beatty, C. Dalhman, and J. van de Water for their help during the data analysis and insightful comments on the manuscript. We thank Nathalie Técher for the illustration of the experimental design. Research was completed under permits issued by la Délégation territoriale à la recherche et à la technologie (DTRT) of the French Polynesian Government and by the Haut-commissariat de la République en Polynésie Francaise (Protocole d'Accueil 2005-2018).

SUPPLEMENTARY MATERIAL

The Supplementary Material for this article can be found online at: https://www.frontiersin.org/articles/10.3389/fmicb.2021.620458/full#supplementary-material

REFERENCES

Adjeroud, M., Michonneau, F., Edmunds, P. J., Chancerelle, Y., De Loma, T. L., Penin, L., et al. (2009). Recurrent disturbances, recovery trajectories, and resilience of coral assemblages on a South Central Pacific reef. *Coral Reefs* 28, 775–780. doi: 10.1007/s00338-009-0515-7

Akagi, J. M., and Campbell, L. L. (1962). Studies on thermophilic sulfate-reducing bacteria III.: adenosine Triphosphate-sulfurylase of *Clostridium nigrificans* and *Desulfovibrio desulfuricans*. *J. Bacteriol.* 84, 1194–1201. doi: 10.1128/jb.84.6.1194-1201.1962

Allgeier, J. E., Valdivia, A., Cox, C., and Layman, C. A. (2016). Fishing down nutrients on coral reefs. *Nat. Commun.* 7:12461.

Apprill, A., McNally, S., Parsons, R., and Weber, L. (2015). Minor revision to V4 region SSU rRNA 806R gene primer greatly increases detection of SAR11 bacterioplankton. *Aquat. Microb. Ecol.* 75, 129–137. doi: 10.3354/ame01753

Arotsker, L., Kramarsky-Winter, E., Ben-Dov, E., Siboni, N., and Kushmaro, A. (2015). Changes in the bacterial community associated with black band disease in a Red Sea coral, *Favia* sp., in relation to disease phases. *Dis. Aquat. Organ.* 116, 47–58. doi: 10.3354/dao02911

Austin, B., and Zhang, X. (2006). Vibrio harveyi: a significant pathogen of marine vertebrates and invertebrates. *Lett. Appl. Microbiol.* 43, 119–124. doi: 10.1111/j.1472-765x.2006.01989.x

Barshis, D. J., Birkeland, C., Toonen, R. J., Gates, R. D., and Stillman, J. H. (2018). High-frequency temperature variability mirrors fixed differences in thermal limits of the massive coral *Porites lobata*. *J. Exp. Biol.* 221:jeb188581. doi: 10.1242/jeb.188581

Ben-Haim, Y., Thompson, F. L., Thompson, C. C., Cnockaert, M. C., Hoste, B., Swings, J., et al. (2003). *Vibrio coralliilyticus* sp. nov., a temperature-dependent pathogen of the coral *Pocillopora damicornis*. *Int. J. Syst. Evol. Microbiol.* 53, 309–315. doi: 10.1099/ijs.0.02402-0

Benjamini, Y., and Hochberg, Y. (1995). Controlling the false discovery rate: a practical and powerful approach to multiple testing. *J. R. Stat. Soc. Ser. B* 57, 289–300. doi: 10.1111/j.2517-6161.1995.tb02031.x

Bokulich, N. A., Kaehler, B. D., Rideout, J. R., Dillon, M., Bolyen, E., Knight, R., et al. (2018). Optimizing taxonomic classification of marker-gene amplicon sequences with QIIME 2's q2-feature-classifier plugin. *Microbiome* 6:90.

Bolyen, E., Rideout, J. R., Dillon, M. R., Bokulich, N. A., Abnet, C. C., Al-Ghalith, G. A., et al. (2019). Reproducible, interactive, scalable and extensible microbiome data science using QIIME 2. *Nat. Biotechnol.* 37, 852–857. doi: 10.1038/s41587-019-0209-9

Bonesso, J. L., Leggat, W., and Ainsworth, T. D. (2017). Exposure to elevated sea-surface temperatures below the bleaching threshold impairs coral recovery and regeneration following injury. *PeerJ* 5:e3719. doi: 10.7717/peerj.3719

Bourne, D., Iida, Y., Uthicke, S., and Smith-Keune, C. (2008). Changes in coral-associated microbial communities during a bleaching event. *ISME J.* 2, 350–363.

Bourne, D. G., Morrow, K. M., and Webster, N. S. (2016). Insights into the coral microbiome: underpinning the health and resilience of reef ecosystems. *Annu. Rev. Microbiol.* 70, 317–340. doi: 10.1146/annurev-micro-102215-095440

Burkepile, D. E., and Hay, M. E. (2008). *Herbivore* species richness and feeding complementarity affect community structure and function on a coral reef. *Proc. Natl. Acad. Sci. U.S.A.* 10, 16201–16206.

Callahan, B. J., McMurdie, P. J., Rosen, M. J., Han, A. W., Johnson, A. J. A., and Holmes, S. P. (2016). DADA2: high-resolution sample inference from Illumina amplicon data. *Nat. Methods* 13:581. doi: 10.1038/nmeth.3869

Chong-Seng, K. M., Cole, A. J., Pratchett, M. S., and Willis, B. L. (2011). Selective feeding by coral reef fishes on coral lesions associated with brown band and black band disease. *Coral Reefs* 30, 473–481. doi: 10.1007/s00338-010-0707-1

Cohen, J. (1998). *Statistical Power Analysis for the Behavioral Sciences*, 2nd Edn, Cambridge, MA: Academic Press.

DePaola, A., Capers, G. M., and Alexander, D. (1994). Densities of *Vibrio vulnificus* in the intestines of fish from the US Gulf Coast. *Appl. Environ. Microbiol.* 60, 984–988. doi: 10.1128/aem.60.3.984-988.1994

Ding, J.-Y., Shiu, J.-H., Chen, W.-M., Chiang, Y.-R., and Tang, S.-L. (2016). Genomic insight into the host-endosymbiont relationship of *Endozoicomonas montiporae* CL-33T with its coral host. *Front. Microbiol.* 7:251. doi: 10.3389/fmicb.2016.00251

Ezzat, L., Lamy, T., Maher, R. L., Munsterman, K. S., Landfield, K., Schmeltzer, E. R., et al. (2019). Surgeonfish feces increase microbial opportunism in reef-building corals. *Mar. Ecol. Prog. Ser.* 631, 81–97. doi: 10.3354/meps13119

Ezzat, L., Lamy, T., Maher, R. L., Munsterman, K. S., Landfield, K. M., Schmeltzer, E. R., et al. (2020). Parrotfish predation drives distinct microbial communities in reef-building corals. *Anim. Microb.* 2:5. doi: 10.1186/s42523-020-0024-0

Gajigan, A. P., Diaz, L. A., and Conaco, C. (2017). Resilience of the prokaryotic microbial community of *Acropora digitifera* to elevated temperature. *Microbiologyopen* 6:e00478. doi: 10.1002/mbo3.478

Garren, M., Raymundo, L., Guest, J., Harvell, C. D., and Azam, F. (2009). Resilience of coral-associated bacterial communities exposed to fish farm effluent. *PLoS One* 4:e7319. doi: 10.1371/journal.pone.0007319

Givens, C. E. (2012). *A Fish Tale: Comparison of the Gut Microbiome of 15 Fish Species and the Influence of Diet and Temperature on its Composition*. Diss. University of Georgia. Available at: https://getd.libs.uga.edu/pdfs/givens_carrie_e_201212_phd.pdf

Glasl, B., Herndl, G. J., and Frade, P. R. (2016). The microbiome of coral surface mucus has a key role in mediating holobiont health and survival upon disturbance. *ISME J.* 10:2280. doi: 10.1038/ismej.2016.9

Grottoli, A. G., Martins, P. D., Wilkins, M. J., Johnston, M. D., Warner, M. E., Cai, W.-J., et al. (2018). Coral physiology and microbiome dynamics under combined warming and ocean acidification. *PLoS One* 13:e0191156. doi: 10.1371/journal.pone.0191156

Hughes, T. P., Barnes, M. L., Bellwood, D. R., Cinner, J. E., Cumming, G. S., Jackson, J. B. C., et al. (2017). Coral reefs in the Anthropocene. *Nature* 546:82.

Kellogg, C. A., Piceno, Y. M., Tom, L. M., DeSantis, T. Z., and Gray, M. A. (2013). Comparing bacterial community composition between healthy and white plague -like disease states in *Orbicella annularis* using PhyloChip^{TM} G3 microarrays. *PLoS One* 8:e79801. doi: 10.1371/journal.pone.0079801

Kelly, M. T. (1982). Effect of temperature and salinity on *Vibrio (Beneckea) vulnificus* occurrence in a gulf coast environment. *Appl. Environ. Microbiol.* 44, 820–824. doi: 10.1128/aem.44.4.820-824.1982

Kimura, B., Kuroda, S., Murakami, M., and Fujii, T. (1996). Growth of *Clostridium perfringens* in fish fillets packaged with a controlled carbon dioxide atmosphere at abuse temperatures. *J. Food Prot.* 59, 704–710. doi: 10.4315/0362-028x-59.7.704

Kramarsky-Winter, E., and Loya, Y. (2000). Tissue regeneration in the coral *Fungia granulosa*: the effect of extrinsic and intrinsic factors. *Mar. Biol.* 137, 867–873. doi: 10.1007/s002270000416

Krone, R., Bshary, R., Paster, M., Eisinger, M., van Treeck, P., and Schuhmacher, H. (2008). Defecation behaviour of the lined bristletooth surgeonfish *Ctenochaetus striatus* (Acanthuridae). *Coral Reefs* 27, 619–622. doi: 10.1007/s00338-008-0365-8

Lenihan, H. S., and Edmunds, P. J. (2010). Response of *Pocillopora verrucosa* to corallivory varies with environmental conditions. *Mar. Ecol. Prog. Ser.* 409, 51–63. doi: 10.3354/meps08595

Loya, Y., Sakai, K., Yamazato, K., Nakano, Y., Sambali, H., and van Woesik, R. (2001). Coral bleaching: the winners and the losers. *Ecol. Lett.* 4, 122–131. doi: 10.1046/j.1461-0248.2001.00203.x

Luna, G. M., Bongiorni, L., Gili, C., Biavasco, F., and Danovaro, R. (2010). Vibrio harveyi as a causative agent of the White Syndrome in tropical stony corals. *Environ. Microbiol. Rep.* 2, 120–127. doi: 10.1111/j.1758-2229.2009.00114.x

Maher, R. L., Rice, M. M., McMinds, R., Burkepile, D. E., and Vega Thurber, R. (2019). Multiple stressors interact primarily through antagonism to drive changes in the coral microbiome. *Sci. Rep.* 9:6834. doi: 10.1038/s41598-019-43274-8

Maher, R. L., Schmeltzer, E. R., Meiling, S., McMinds, R., Ezzat, L., Shantz, A. A., et al. (2020). Coral microbiomes demonstrate flexibility and resilience through a reduction in community diversity following a thermal stress event. *Front. Ecol. Evol.* 8:356. doi: 10.3389/fevo.2020.555698

Martin, M. (2011). Cutadapt removes adapter sequences from high-throughput sequencing reads. *EMBnet J.* 17, 10–12. doi: 10.14806/ej.17.1.200

Martinez-Urtaza, J., Bowers, J. C., Trinanes, J., and DePaola, A. (2010). Climate anomalies and the increasing risk of *Vibrio parahaemolyticus* and *Vibrio vulnificus* illnesses. *Food Res. Int.* 43, 1780–1790. doi: 10.1016/j.foodres.2010.04.001

Maynard, J., Van Hooidonk, R., Eakin, C. M., Puotinen, M., Garren, M., Williams, G., et al. (2015). Projections of climate conditions that increase coral disease susceptibility and pathogen abundance and virulence. *Nat. Clim. Chang.* 5:688. doi: 10.1038/nclimate2625

McDevitt-Irwin, J. M., Baum, J. K., Garren, M., and Vega Thurber, R. L. (2017). Responses of coral-associated bacterial communities to local and global stressors. *Front. Mar. Sci.* 4:262. doi: 10.3389/fmars.2017.00262

McDevitt-Irwin, J. M., Garren, M., McMinds, R., Vega Thurber, R., and Baum, J. K. (2019). Variable interaction outcomes of local disturbance and El Niño-induced heat stress on coral microbiome alpha and beta diversity. *Coral Reefs* 38, 331–345. doi: 10.1007/s00338-019-01779-8

Meyer, J. L., Castellanos-Gell, J., Aeby, G. S., Häse, C. C., Ushijima, B., and Paul, V. J. (2019). Microbial community shifts associated with the ongoing stony coral tissue loss disease outbreak on the Florida Reef Tract. *Front. Microbiol.* 10:2244. doi: 10.3389/fmicb.2019.02244

Miura, N., Motone, K., Takagi, T., Aburaya, S., Watanabe, S., Aoki, W., et al. (2019). Ruegeria sp. strains isolated from the reef-building coral *Galaxea fascicularis* inhibit growth of the temperature-dependent pathogen *Vibrio coralliilyticus*. *Mar. Biotechnol.* 21, 1–8. doi: 10.1007/s10126-018-9853-1

Miyake, S., Ngugi, D. K., and Stingl, U. (2015). Diet strongly influences the gut microbiota of surgeonfishes. *Mol. Ecol.* 24, 656–672. doi: 10.1111/mec.13050

Mora, C. (2015). *Ecology of Fishes on Coral Reefs*. Cambridge: Cambridge University Press.

Morrow, K. M., Bourne, D. G., Humphrey, C., Botté, E. S., Laffy, P., Zaneveld, J., et al. (2015). Natural volcanic CO_2 seeps reveal future trajectories for host-microbial associations in corals and sponges. *ISME J.* 9, 894–908. doi: 10.1038/ismej.2014.188

Mouchka, M. E., Hewson, I., and Harvell, C. D. (2010). Coral-associated bacterial assemblages: current knowledge and the potential for climate-driven impacts. *Integr. Comp. Biol.* 50, 662–674. doi: 10.1093/icb/icq061

Neave, M. J., Apprill, A., Ferrier-Pagès, C., and Voolstra, C. R. (2016). Diversity and function of prevalent symbiotic marine bacteria in the genus *Endozoicomonas*. *Appl. Microbiol. Biotechnol.* 100, 8315–8324. doi: 10.1007/s00253-016-7777-0

Nelson, C. E., Goldberg, S. J., Kelly, L. W., Haas, A. F., Smith, J. E., Rohwer, F., et al. (2013). Coral and macroalgal exudates vary in neutral sugar composition and differentially enrich reef bacterioplankton lineages. *ISME J.* 7:962. doi: 10.1038/ismej.2012.161

Nicolet, K. J., Chong-Seng, K. M., Pratchett, M. S., Willis, B. L., and Hoogenboom, M. O. (2018). Predation scars may influence host susceptibility to pathogens: evaluating the role of corallivores as vectors of coral disease. *Sci. Rep.* 8:5258.

Nolan, M., Sikorski, J., Davenport, K., Lucas, S., Glavina Del Rio, T., Tice, H., et al. (2010). Complete genome sequence of *Ferrimonas balearica* type strain (PATT). *Stand. Genomic Sci.* 3, 174–182. doi: 10.4056/sigs.1161239

Noonan, K. R., and Childress, M. J. (2020). Association of butterflyfishes and stony coral tissue loss disease in the Florida Keys. *Coral Reefs* 39, 1–10.

Palmer, C. V., McGinty, E. S., Cummings, D. J., Smith, S. M., Bartels, E., and Mydlarz, L. D. (2011). Patterns of coral ecological immunology: variation in the responses of Caribbean corals to elevated temperature and a pathogen elicitor. *J. Exp. Biol.* 214, 4240–4249. doi: 10.1242/jeb.061267

Pantos, O., Bongaerts, P., Dennis, P. G., Tyson, G. W., and Hoegh-Guldberg, O. (2015). Habitat-specific environmental conditions primarily control the microbiomes of the coral *Seriatopora hystrix*. *ISME J.* 9:1916. doi: 10.1038/ismej.2015.3

Parada, A. E., Needham, D. M., and Fuhrman, J. A. (2016). Every base matters: assessing small subunit rRNA primers for marine microbiomes with mock communities, time series and global field samples. *Environ. Microbiol.* 18, 1403–1414. doi: 10.1111/1462-2920.13023

Pootakham, W., Mhuantong, W., Yoocha, T., Putchim, L., Jomchai, N., Sonthirod, C., et al. (2019). Heat-induced shift in coral microbiome reveals several members of the Rhodobacteraceae family as indicator species for thermal stress in *Porites lutea*. *Microbiologyopen* 8:e935.

Pratchett, M. S., McCowan, D., Maynard, J. A., and Heron, S. F. (2013). Changes in bleaching susceptibility among corals subject to ocean warming and recurrent bleaching in Moorea, French Polynesia. *PLoS One* 8:e70443. doi: 10.1371/journal.pone.0070443

Putnam, H. M., and Edmunds, P. J. (2011). The physiological response of reef corals to diel fluctuations in seawater temperature. *J. Exp. Mar. Bio. Ecol.* 396, 216–223. doi: 10.1016/j.jembe.2010.10.026

Quast, C., Pruesse, E., Yilmaz, P., Gerken, J., Schweer, T., Yarza, P., et al. (2012). The SILVA ribosomal RNA gene database project: improved data processing and web-based tools. *Nucleic Acids Res.* 41, D590–D596.

Ramees, T. P., Dhama, K., Karthik, K., Rathore, R. S., Kumar, A., Saminathan, M., et al. (2017). *Arcobacter*: an emerging food-borne zoonotic pathogen, its public health concerns and advances in diagnosis and control-a comprehensive review. *Vet. Q.* 37, 136–161. doi: 10.1080/01652176.2017.1323355

Rasher, D. B., Hoey, A. S., and Hay, M. E. (2013). Consumer diversity interacts with prey defenses to drive ecosystem function. *Ecology* 94, 1347–1358. doi: 10.1890/12-0389.1

Ravot, G., Magot, M., Fardeau, M.-L., Patel, B. K. C., Thomas, P., Garcia, J.-L., et al. (1999). *Fusibacter paucivorans* gen. nov., sp. nov., an anaerobic, thiosulfate-reducing bacterium from an oil-producing well. *Int. J. Syst. Evol. Microbiol.* 49, 1141–1147. doi: 10.1099/00207713-49-3-1141

Rice, M. M., Ezzat, L., and Burkepile, D. E. (2019a). Corallivory in the anthropocene: interactive effects of anthropogenic stressors and corallivory on coral reefs. *Front. Mar. Sci.* 5:525. doi: 10.3389/fmars.2018.00525

Rice, M. M., Maher, R. L., Thurber, R. V., and Burkepile, D. E. (2019b). Different nitrogen sources speed recovery from corallivory and uniquely alter the microbiome of a reef-building coral. *PeerJ* 7:e8056. doi: 10.7717/peerj.8056

Ritchie, K. B. (2006). Regulation of microbial populations by coral surface mucus and mucus-associated bacteria. *Mar. Ecol. Prog. Ser.* 322, 1–14. doi: 10.3354/meps322001

Robbins, S. J., Singleton, C. M., Chan, C. X., Messer, L. F., Geers, A. U., Ying, H., et al. (2019). A genomic view of the reef-building coral *Porites lutea* and its microbial symbionts. *Nat. Microbiol.* 4, 2090–2100. doi: 10.1038/s41564-019-0532-4

Robertson, D. R. (1982). Fish feces as fish food on a Pacific coral reef. *Mar. Ecol. Prog. Ser. Oldend.* 7, 253–265. doi: 10.3354/meps007253

Rohwer, F., Seguritan, V., Azam, F., and Knowlton, N. (2002). Diversity and distribution of coral-associated bacteria. *Mar. Ecol. Prog. Ser.* 243, 1–10. doi: 10.3354/meps243001

Salerno, J. L., Reineman, D. R., Gates, R. D., and Rappé, M. S. (2011). The effect of a sublethal temperature elevation on the structure of bacterial communities associated with the coral *Porites compressa*. *J. Mar. Biol.* 2011:969173. doi: 10.1155/2011/969173

Schneider, C. A., Rasband, W. S., and Eliceiri, K. W. (2012), NIH image to ImageJ: 25 years of image analysis. *Nat. methods* 9, 671–675. doi: 10.1038/nmeth.2089

Shiu, J.-H., and Tang, S.-L. (2019). "The bacteria endozoicomonas: community dynamics, diversity, genomes, and potential impacts on corals," in *Symbiotic Microbiomes of Coral Reefs Sponges and Corals*, (Dordrecht: Springer), 55–67. doi: 10.1007/978-94-024-1612-1_5

Simister, R., Taylor, M. W., Tsai, P., Fan, L., Bruxner, T. J., Crowe, M. L., et al. (2012). Thermal stress responses in the bacterial biosphere of the Great Barrier Reef sponge, *Rhopaloeides odorabile*. *Environ. Microbiol.* 14, 3232–3246. doi: 10.1111/1462-2920.12010

Smith, P., Willemsen, D., Popkes, M., Metge, F., Gandiwa, E., Reichard, M., et al. (2017). Regulation of life span by the gut microbiota in the short-lived African turquoise killifish. *eLife* 6:e27014.

Smriga, S., Sandin, S. A., and Azam, F. (2010). Abundance, diversity, and activity of microbial assemblages associated with coral reef fish guts and feces. *FEMS Microbiol. Ecol.* 73, 31–42.

Sunagawa, S., DeSantis, T. Z., Piceno, Y. M., Brodie, E. L., DeSalvo, M. K., Voolstra, C. R., et al. (2009). Bacterial diversity and white plague disease-associated community changes in the caribbean coral *Montastraea faveolata*. *ISME J.* 3:512. doi: 10.1038/ismej.2008.131

Sweet, M., and Bythell, J. (2015). White Syndrome in *Acropora muricata*: nonspecific bacterial infection and ciliate histophagy. *Mol. Ecol.* 24, 1150–1159. doi: 10.1111/mec.13097

Tandon, K., Lu, C.-Y., Chiang, P.-W., Wada, N., Yang, S.-H., Chan, Y.-F., et al. (2020). Comparative genomics: dominant coral-bacterium *Endozoicomonas acroporae* metabolizes dimethylsulfoniopropionate (DMSP). *ISME J.* 14, 1290–1303. doi: 10.1038/s41396-020-0610-x

Thompson, F. L., Barash, Y., Sawabe, T., Sharon, G., Swings, J., and Rosenberg, E. (2006). *Thalassomonas loyana* sp. nov., a causative agent of the white plague-like disease of corals on the Eilat coral reef. *Int. J. Syst. Evol. Microbiol.* 56, 365–368. doi: 10.1099/ijs.0.63800-0

Thompson, F. L., Thompson, C. C., Naser, S., Hoste, B., Vandemeulebroecke, K., Munn, C., et al. (2005). *Photobacterium rosenbergii* sp. nov. and *Enterovibrio coralii* sp. nov., *Vibrios* associated with coral bleaching. *Int. J. Syst. Evol. Microbiol.* 55, 913–917. doi: 10.1099/ijs.0.63370-0

Tout, J., Siboni, N., Messer, L. F., Garren, M., Stocker, R., Webster, N. S., et al. (2015). Increased seawater temperature increases the abundance and alters the structure of natural *Vibrio* populations associated with the coral *Pocillopora damicornis*. *Front. Microbiol.* 6:432. doi: 10.3389/fmicb.2015.00432

van Oppen, M. J. H., and Blackall, L. L. (2019). Coral microbiome dynamics, functions and design in a changing world. *Nat. Rev. Microbiol.* 17, 557–567. doi: 10.1038/s41579-019-0223-4

van Woesik, R., Sakai, K., Ganase, A., and Loya, Y. (2011). Revisiting the winners and the losers a decade after coral bleaching. *Mar. Ecol. Prog. Ser.* 434, 67–76. doi: 10.3354/meps09203

Vidal-Dupiol, J., Ladrière, O., Destoumieux-Garzón, D., Sautière, P.-E., Meistertzheim, A.-L., Tambutté, E., et al. (2011). Innate immune responses of a *Scleractinian* coral to *Vibriosis*. *J. Biol. Chem.* 286, 22688–22698. doi: 10.1074/jbc.m110.216358

Weber, M., de Beer, D., Lott, C., Polerecky, L., Kohls, K., Abed, R. M. M., et al. (2012). Mechanisms of damage to corals exposed to sedimentation. *Proc. Natl. Acad. Sci. U.S.A.* 109, E1558–E1567. doi: 10.1073/pnas.1100715109

Webster, N. S., Negri, A. P., Botté, E. S., Laffy, P. W., Flores, F., Noonan, S., et al. (2016). Host-associated coral reef microbes respond to the cumulative pressures of ocean warming and ocean acidification. *Sci. Rep.* 6:19324.

Weil, E., Smith, G., and Gil-Agudelo, D. L. (2006). Status and progress in coral reef disease research. *Dis. Aquat. Organ.* 69, 1–7. doi: 10.3354/dao069001

Welsh, R. M., Rosales, S. M., Zaneveld, J. R. R., Payet, J. P., McMinds, R., Hubbs, S. L., et al. (2015). Alien vs. predator: pathogens open niche space for opportunists, unless controlled by predators. *PeerJ* 3:e1537v1. doi: 10.7287/peerj.preprints.1537v1

Yamazaki, Y., Meirelles, P. M., Mino, S., Suda, W., Oshima, K., Hattori, M., et al. (2016). Individual *Apostichopus japonicus* fecal microbiome reveals a link with polyhydroxybutyrate producers in host growth gaps. *Sci. Rep.* 6: 21631.

Zaneveld, J. R., Burkepile, D. E., Shantz, A. A., Pritchard, C. E., McMinds, R., Payet, J. P., et al. (2016). Overfishing and nutrient pollution interact with temperature to disrupt coral reefs down to microbial scales. *Nat. Commun.* 7: 11833.

Zaneveld, J. R., McMinds, R., and Thurber, R. V. (2017). Stress and stability: applying the Anna Karenina principle to animal microbiomes. *Nat. Microbiol.* 2:17121.

Ziegler, M., Seneca, F. O., Yum, L. K., Palumbi, S. R., and Voolstra, C. R. (2017). Bacterial community dynamics are linked to patterns of coral heat tolerance. *Nat. Commun.* 8:14213.

Conflict of Interest: The authors declare that the research was conducted in the absence of any commercial or financial relationships that could be construed as a potential conflict of interest.

frontiers in Microbiology

ORIGINAL RESEARCH
published: 02 June 2021
doi: 10.3389/fmicb.2021.617703

Molecular Detection and Distribution of Six Medically Important *Vibrio* spp. in Selected Freshwater and Brackish Water Resources in Eastern Cape Province, South Africa

Oluwatayo E. Abioye[1,2,3]*, *Ayodeji Charles Osunla*[1,2,4] and *Anthony I. Okoh*[1,2,5]

[1]*SAMRC Microbial Water Quality Monitoring Centre, University of Fort Hare, Alice, South Africa,* [2]*Applied and Environmental Microbiology Research Group, Department of Biochemistry and Microbiology, University of Fort Hare, Alice, South Africa,* [3]*Department of Microbiology, Obafemi Awolowo University, Ife, Nigeria,* [4]*Department of Microbiology, Adekunle Ajasin University, Akungba-Akoko, Nigeria,* [5]*Department of Environmental Health Sciences, University of Sharjah, Sharjah, United Arab Emirates*

Water resources contaminated with pathogenic *Vibrio* species are usually a source of devastating infection outbreaks that have been a public health concern in both developed and developing countries over the decades. The present study assessed the prevalence of six medically significant *Vibrio* species in some water resources in Eastern Cape Province, South Africa for 12 months. We detected vibrios in all the 194 water samples analyzed using polymerase chain reaction (PCR). The prevalence of *Vibrio cholerae*, *Vibrio mimicus*, *Vibrio fluvialis*, *Vibrio vulnificus*, *Vibrio alginolyticus*, and *Vibrio parahaemolyticus* in freshwater samples was 34, 19, 9, 2, 3, and 2%, and that in brackish water samples was 44, 28, 10, 7, 46, and 51%, respectively. The population of the presumptive *Vibrio* spp. isolated from freshwater (628) and brackish water (342) samples that were confirmed by PCR was 79% (497/628) and 85% (291/342), respectively. Twenty-two percent of the PCR-confirmed *Vibrio* isolates from freshwater (n = 497) samples and 41% of the PCR-confirmed *Vibrio* isolates from brackish water samples (n = 291) fall among the *Vibrio* species of interest. The incidences of *V. cholerae*, *V. mimicus*, *V. fluvialis*, *V. vulnificus*, *V. alginolyticus*, and *V. parahaemolyticus* amidst these *Vibrio* spp. of interest that were recovered from freshwater samples were 75, 14, 4, 6, 1, and 1%, whereas those from brackish water samples were 24, 7, 3, 3, 47, and 18%, respectively. Our observation during the study suggests pollution as the reason for the unusual isolation of medically important vibrios in winter. Correlation analysis revealed that temperature drives the frequency of isolation, whereas salinity drives the composition of the targeted *Vibrio* species at our sampling sites. The finding of the study is of public health importance going by the usefulness of the water resources investigated. Although controlling and preventing most of the factors that contribute to the prevalence of medically important bacteria, such as *Vibrio* species, at the sampling points might be difficult, regular monitoring for creating health risk awareness will go a long way to prevent possible *Vibrio*-related infection outbreaks at the sampling sites and their immediate environment.

Keywords: pathogenic *Vibrio* spp., temperature, salinity, public-health, brackish-water, freshwater

OPEN ACCESS

Edited by:
Rodrigo Gouvea Taketani, Rothamsted Research, United Kingdom

Reviewed by:
Eiji Arakawa, National Institute of Infectious Diseases (NIID), Japan
Helena D. M. Villela, Federal University of Rio de Janeiro, Brazil

***Correspondence:**
Oluwatayo E. Abioye
abioyethayor@gmail.com

Specialty section:
This article was submitted to Aquatic Microbiology, a section of the journal Frontiers in Microbiology

Received: *15 October 2020*
Accepted: *29 March 2021*
Published: *02 June 2021*

Citation:
Abioye OE, Osunla AC and Okoh AI (2021) Molecular Detection and Distribution of Six Medically Important Vibrio spp. in Selected Freshwater and Brackish Water Resources in Eastern Cape Province, South Africa. Front. Microbiol. 12:617703. doi: 10.3389/fmicb.2021.617703

INTRODUCTION

The *Vibrio* genus is made up of over one hundred species (Romalde et al., 2014; Fernández-delgado et al., 2015) of which about 12 have been associated with human infections. The three major human pathogens in the *Vibrio* genus are *Vibrio cholerae*, *Vibrio vulnificus*, and *Vibrio parahaemolyticus* (Guardiola-avila et al., 2015; Kokashvili et al., 2015; Jones, 2017). Pathogenic members of the *Vibrio* genus are very common in the aquatic environment and can cause water- and food-related infections (Ajin et al., 2016; Kirchberger et al., 2016; Machado and Bordalo, 2016; Shaheen et al., 2016). Infections caused by these human pathogenic *Vibrio* species include cholera and vibriosis, e.g., wound infections, septicemia, and gastroenteritis, which is often self-limiting (Baker-Austin et al., 2018). Human pathogenic *Vibrio* species include *V. carchariae*, *V. mimicus*, *V. cincinnatiensis*, *V. fluvialis*, *V. cholerae*, *V. parahaemolyticus*, *V. vulnificus*, *V. alginolyticus* (now *Grimontia hollisae*), *V. furnissii*, *V. metschnikovii*, *V. hollisae*, and *V. damsela* (*Photobacterium hollisae*; Finkelstein, 1996; Levinson and Jawetz, 1996; Turner, 1997; Morris, 2019). The most notable human *Vibrio* pathogens are *V. cholerae*, *V. parahaemolyticus*, *V. vulnificus*, and *V. fluvialis* (CDC, 1999; Finkelstein et al., 2002; Kothary et al., 2003; Chakraborty et al., 2006). On the other hand, *V. mimicus*, which diverged from a common ancestor as *V. cholerae*, and *V. alginolyticus*, which was formerly classified as *V. parahaemolyticus*, are emerging human pathogens (Mustapha et al., 2013; Guardiola-avila et al., 2015). *V. cholerae* causes cholera, whereas other human pathogenic members of the *Vibrio* genus cause infections generally refer to as vibriosis (Baker-Austin et al., 2018). The vehicles of transmission of the etiological agents of cholera and vibriosis to humans are water and food most especially seafood (Di et al., 2017). Water- and food-related diseases continue to be a huge problem for humanity (Tantillo et al., 2004). To circumvent the scourge of cholera and vibriosis, localized monitoring of the environment for etiological agents of the infections was recommended, and this should be done without prejudice to either *Vibrio*-related outbreak is ongoing or not (CDC, 2015). To better protect human health, monitoring the environment for agents of waterborne and foodborne infections, such as human pathogenic *Vibrio* spp., has been emphasized in the literature (European Commission, 2001; Baffone et al., 2006; Jones and Oliver, 2009). Members of the *Vibrio* genus are halophiles; thus, they are not expected to be found in freshwater resources, and this may explain why studies on the prevalence of human pathogenic *Vibrio* spp. in freshwater are relatively small. However, the ability of *Vibrio* spp. to adapt to varying ecological niches (Ceccarelli and Colwell, 2014; Payne et al., 2016; Osunla and Okoh, 2017) supported the need to investigate the role of freshwater resources in the spread of etiological agents of cholera and vibriosis.

Of the approximately 139 serogroups of *V. cholerae*, only O1 and O139 cause pandemic and epidemic cholera, but the non-O1/non-O139 serogroups also cause sporadic cholera-like infections (Glenn Morris, 1994; Rippey, 1994; Sharma et al., 1998; Deen et al., 2019). On the other hand, *V. parahaemolyticus* causes most of the seafood-related diarrhea infections in Florida (Klontz et al., 1993; Letchumanan et al., 2015), and it causes septicemia occasionally (Rippey, 1994; Letchumanan et al., 2015). *V. vulnificus* biotype 1 is the most deadly of all *Vibrio* species because of its high invasiveness and its fatality rate that is higher than that of any other bacteria (Oliver et al., 1991; Oliver and Bockian, 1995; Bisharat, 2002; Bisharat et al., 2005; Drake et al., 2007). *V. fluvialis* commonly cause food poisoning (Bhattacharjee et al., 2010; Kanungo et al., 2012; Chowdhury et al., 2013), and it is an emerging pathogen that possesses epidemic potentials (Vinothkumar et al., 2013). Cholera and vibriosis outbreaks had been reported from several parts of the globe. The isolation of these pathogens from various aquatic milieu around the globe (Sarkar et al., 1985; Venkateswaran et al., 1989; Barua and Greenough, 1991; Kazi et al., 2005; Binh et al., 2009; Safa et al., 2009; Grim et al., 2010; Reimer et al., 2011; Esteves et al., 2015; Okoh et al., 2015; Di et al., 2017; Abioye and Okoh, 2018) has been reported. The occurrence of cholera in the Eastern Cape Province (ECP) has been well documented over the years (Mudzanani et al., 2003; Mema, 2008). The previous studies carried out in our laboratory (Applied and Environmental Microbiology Research Group, Department of Biochemistry and Microbiology, University of Fort Hare, South Africa) confirmed the occurrence of medically important *Vibrio* species in some wastewater treatment plants (WWTPs) of the ECP and their receiving watershed, especially those that discharge poorly treated final effluent (Igbinosa et al., 2009, 2011a,b; Nongogo and Okoh, 2014; Okoh et al., 2015).

These previous findings support the need for spatial and temporal investigation of the presence and distribution of these bacterial species in freshwater resources in the province since there is interconnectivity between WWTPs receiving watershed and other freshwater resources most especially rivers. Going by the scarcity of freshwater resources in South Africa, this kind of investigation is needful since all available freshwater resources in the country are potential alternatives to regular sources of treated freshwater during freshwater scarcity. Some of the anthropogenic activities that contribute to the occurrence of pathogenic *Vibrio* spp. in the aquatic environment include indiscriminate dumping of refuses into water bodies, discharge of poorly treated wastewater from the treatment plant into receiving watershed, run-off from farms especially farmland treated with manure, and defecating and urinating into water bodies by humans and grazing animals (Nevondo and Cloete, 2001; USEPA, 2001; Rees et al., 2010; Abakpa et al., 2013). Contamination due to the aforementioned factors is evident around some of the freshwater resources in the ECP. This is not a surprise since most of the ECP waterbodies are not well protected (Christine et al., 2013). Diseases outbreak in Eastern Cape as a result of watershed contaminated with poorly treated effluent from WWTPs has occurred in the past (Cottle and Deedat, 2002). Unfortunately, recent studies showed that the problem persists in the ECP (Mema, 2008; Nongogo and Okoh, 2014; Okoh et al., 2015; Edokpayi et al., 2017). Poorly treated WWTP's effluent has been identified as a significant contributor of pathogens to the water milieu of the ECP (Okeyo et al., 2018).

Vibrio spp. of medical importance including four of the six *Vibrio* spp. focused on in this study have been reported from various WWTPs of Eastern Cape and their receiving watershed. A significant amount of *V. cholerae*, *V. parahaemolyticus*, *V. metschnikovii*, *V. fluvialis*, and *V. vulnificus* were reportedly isolated from final effluents in some WWTPs in Nkonkobe rural community, Chris Hani, and Amathole district municipalities (Igbinosa et al., 2009, 2011a,b; Nongogo and Okoh, 2014). A more comprehensive study on final effluents of 14 WWTPs in Amathole and Chris Hani district municipalities reported 66.8% *Vibrio* spp. prevalence of the 1,000 randomly selected isolates recovered from the WWTPs. Of the 300 confirmed *Vibrio* spp., 68.2% belong to one of *V. parahaemolyticus*, *V. fluvialis*, and *V. vulnificus* (Okoh et al., 2015). The aforementioned is of potential health risk to individuals using watershed for recreational, agricultural, and domestic purposes most especially at the downstream of WWTP final effluents discharge points. In some studies from other provinces of South Africa, the isolation of *Vibrio harveyi*, *V. parahaemolyticus*, *V. cholerae*, *V. mimicus*, and *V. vulnificus* from tap, borehole, and dam in North West province (Maje et al., 2020) and *V. cholerae* from four WWTPs located in Gauteng Province (Dungeni et al., 2010) has also been reported. Health risks that an individual using these water resources could be exposed to include gastrointestinal infections caused by *V. parahaemolyticus*, *V. mimicus*, and *V. fluvialis*; wound infections caused by *V. vulnificus* and *V. harveyi*; cholera caused by *V. cholerae*; and cholera-like bloody diarrhea caused by *V. fluvialis* (Ramamurthy et al., 1994; Igbinosa and Okoh, 2010; Jones, 2017; Brehm et al., 2020).

The occurrences of dysfunctional WWTPs that discharge unacceptable final effluent (Herbig and Meissner, 2019) and the lack of adequate protection for surface water in the ECP suggest that pathogenic vibrios could have contaminated some water resources in the province. Although extensive work has been done on the contribution of WWTPs to the abundance of *Vibrio* spp. in the province, however, work on major rivers, their tributaries, and brackish water resources is still limited.

The findings of Momba et al. (2006), which confirmed the presence of toxigenic *V. cholerae* in the surface and groundwater of rural locality of Nkonkobe Local Municipality of Amathole District, Eastern Cape Province, South Africa, showed that surface water is of significant importance to the understanding of the abundance of *Vibrio* spp. in the province water milieu. However, the study by Momba et al. (2006) reported for toxigenic *V. cholerae* alone but not for non-cholera causing *Vibrio* pathogens of public health importance. In addition, the study was carried out more than a decade ago, and it does not cover all the important surface water resources in the province. The only one report found on the occurrence of *V. vulnificus* while developing this manuscript was from the KwaZulu-Natal beach, but the information was found in local news (Comins, 2012) rather than in research articles publishing outlets. The other few reports on occurrences of cholera and non-cholera causing *Vibrio* pathogens in rivers were carried out in KwaZulu-Natal, Mpumalanga, and Limpopo provinces, South Africa (Bessong et al., 2009; Madoroba and Momba, 2010; Ntema et al., 2014; Marie and Lin, 2018). Although studies on occurrences of cholera and non-cholera causing *Vibrio* pathogens have been carried out in the ECP in the past, they were limited to up, final effluents discharge points, and some meters downstream of the receiving watershed for the WWTPs (Igbinosa et al., 2009, 2011a,b; Nongogo and Okoh, 2014; Okoh et al., 2015). Therefore, our understanding of the abundance and distribution of *Vibrio* spp. beyond the targeted points along the receiving watershed of the WWTPs and rivers that do not serve as receiving watershed for WWTPs in the province is still unclear. Based on the aforementioned, information on the occurrence of the etiological agents of cholera and vibriosis in South Africa freshwater and brackish water resources at the moment is limited most especially in the ECP. Going by the advice of the CDC (2017) to monitor the environment for *Vibrio* pathogens as a means of preventing cholera and vibriosis outbreaks, this study assesses the microbial quality of some important freshwater and brackish water sources in the ECP based on the presence or absence of six medically important *Vibrio* pathogens. The six medically important *Vibrio* spp. targeted were *V. cholerae*, *V. parahaemolyticus*, *V. vulnificus*, *V. fluvialis*, *V. mimicus*, and *V. alginolyticus*. The last two have not been reported from this region before now. It is intended that the study will contribute to the information needed for the epidemiology of the etiological agents of cholera and vibriosis in the aquatic milieu of the province most especially rivers and brackish water resources. It was also anticipated that this study will encourage *Vibrio* pathogens monitoring programs in the brackish and freshwater milieu of the ECP most especially those that humans access regularly.

MATERIALS AND METHODS

Study Areas and Sample Collection

Water samples were collected from freshwater and brackish water resources located along Kowie and tributaries, Kubusi, Sunday, Swartkops, and Buffalo Rivers as shown in **Figure 1**. Two freshwater dams in Amathole District Municipality were also included in the study, and their coordinates are S32°46.507^{l}E026°51.604^{l} and S32°47.406^{l}E026°50.821^{l}. The dams are used for fishing by the local anglers. The water sampling method employed is as documented in the previous study carried out in our laboratory (Igbinosa et al., 2011b; Okoh et al., 2015). Briefly, water samples were collected at 3–5 different points at each sampling site into 1-L sterile sterilin bottles by midstream dipping of sample bottles at 25–30 cm down the water column. The sample bottle cap was replaced while the sample bottle was still beneath the water column, transferred into cooler boxes containing ice, and afterwards transferred to the Applied and Environmental Microbiology Research Group (AEMREG) laboratory, University of Fort Hare, Alice. All the samples collected were analyzed within 6 h of collection, and samples were collected once a month for 1 year. The characteristics of each of the sampling sites are given in **Table 1**.

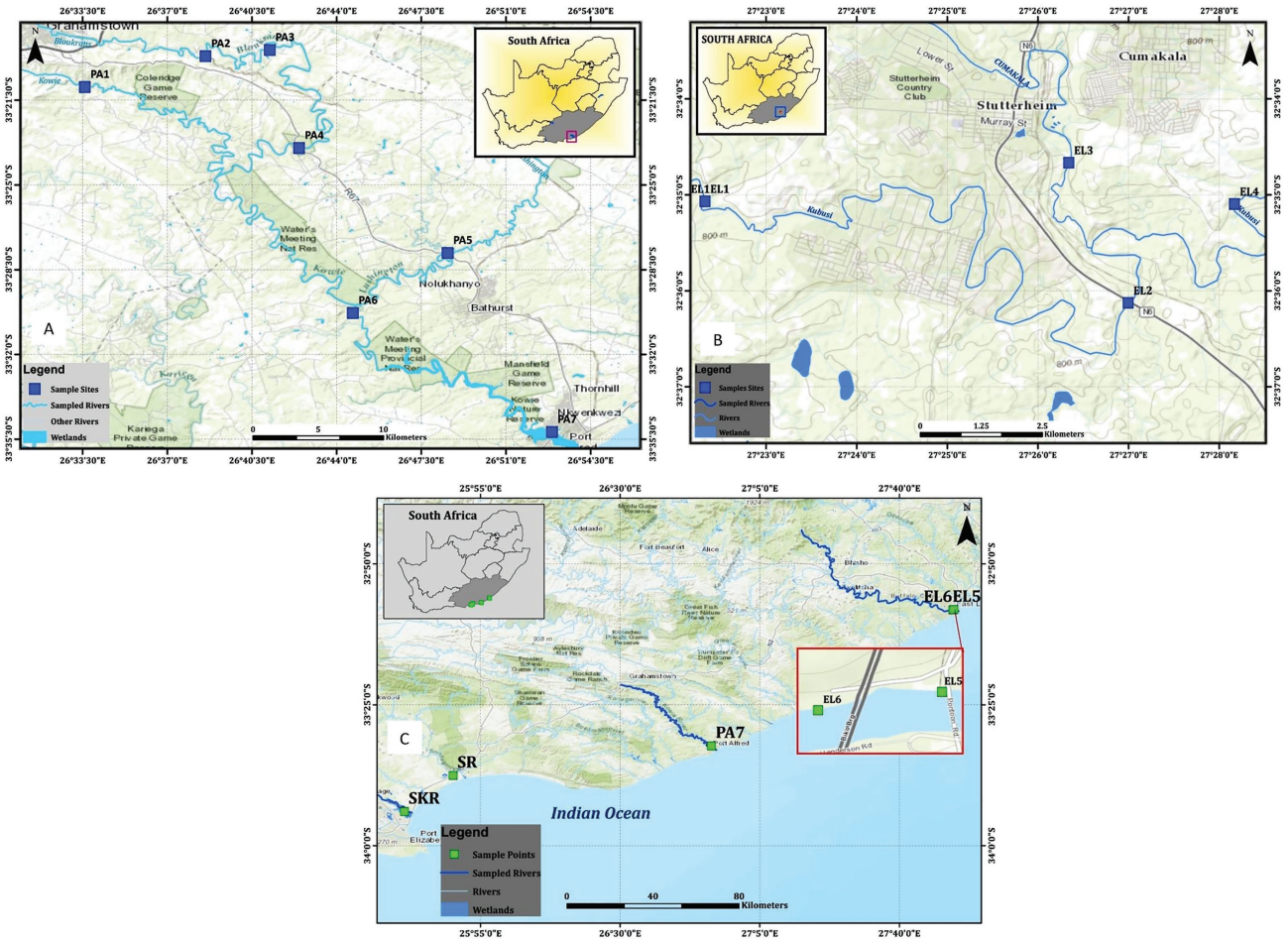

FIGURE 1 | Maps showing locations of the sampling sites, **(A)** sampling sites along the Kowie River, **(B)** sampling sites along the Kubusi River, and **(C)** sampling sites at Buffalo, Sunday, and Swartkops Rivers.

Temperature, Salinity, and Presumptive *Vibrio* Density Determination

The salinity and temperature were determined using a multiparameter ion-specific meter (version HI98195; Hanna Instruments) following the manufacturer's guidelines. The presumptive *Vibrio* density (PVD) was determined following the membrane filtration technique described in the literature (Nongogo and Okoh, 2014). A 100 ml of raw or diluted water samples, as the case may be, was filtered with the aid of a vacuum pump using a 0.45 µm membrane filter. Afterwards, the resulting membrane filters were placed on sterile thiosulfate citrate bile salts sucrose (TCBS) plates and incubated for 24–48 h at 37°C in triplicates. The mean of the yellow and green colonies on the TCBS triplicate plates per sample was recorded as PVD.

Total *Vibrio* spp. Density

The most probable number coupled with polymerase chain reaction (MPN-PCR) method detailed in the literature was adapted for determining the total *Vibrio* spp. density (TVD) in water samples (Ahmad et al., 2011; Copin et al., 2012; Ramos et al., 2014; Abioye and Okoh, 2018). As a statistical-based method, MPN only estimates the viable numbers of bacteria in a sample by the principle of extinction dilution, i.e., inoculating liquid medium in 10-fold dilutions to a dilution factor at which no turbidity is observed after the incubation period. Unfortunately, the turbidity observed could be due to the presence of other bacteria other than the organism of interest. To overcome this shortcoming and make the methods more accurate and precise, MPN turbid tubes were subjected to PCR to ascertain the presence of the organism of interest. In this approach, MPN turbid tubes that tested negative for the organism of interest when subjected to PCR are counted as false positive and are not useful for calculating the density. Thus, this approach corrects for the shortcoming of using only MPN for determining the density of specific bacteria species. This is called the MPN-PCR method. Briefly, a 10-fold serial dilution of water sample was prepared up to the power of five, and afterwards, 1 ml of aliquots from raw and each of the diluted water sample was aseptically introduced into test tubes containing 10 ml of sterile freshly prepared alkaline peptone

TABLE 1 | Sampling site characteristics.

Sample sites/coordinates	Codes	Site peculiarities
Kowie River site 1 (S33°20.953′E026°33.601′)	PA1	Very close to the source of Kowie River and devoid of any notable human activities during the sampling period. Wild animals have unrestricted access to the water resource at this point.
Bloukrans River site 2 (S33°19.658′E026°38.561′)	PA2	It is one of the sites along the Kowie River tributary. It is used for agricultural purposes and serves as receiving watershed for wastewater treatment plant.
Bloukrans River site 3 (S33°21.218′E026°43.561′)	PA3	It is one of the sites along the Kowie River tributary. It is used for agricultural purposes.
Bloukrans River site 4 (S32°23.478′E026°42.456′)	PA4	It is one of the sites along the Kowie River tributary. It is used for agricultural and spiritual purposes.
Lashinton River site 5 (S32°27.783′E026°48.584′)	PA5	It is one of the sites along the Kowie River tributary. It is used for agricultural purposes. An awful smell at this site suggests discharge of improperly treated effluent at the upstream.
Kowie River site 6 (S33°30.265′E026°44.679′)	PA6	Use for fishing activities.
Kowie River Estuary site 7 (S33°35.193′E026°53.009′)	PA7	It is located in Port Alfred. It is used for recreational activities, e.g., leisure fishing and swimming.
Kubusi River site 8 (S32°35.026′E027°22.311′)	EL1	Not many human activities occur here, but the upstream is located within a game reserve. It is located at the outskirt of Stutterheim.
Kubusi River site 9 (S32°35.686′E027°25.417′)	EL2	It is located around one of the local Stutterheim settlements. Free-range cows drink water and defecate at this point. The river is used for agricultural purposes some meters upstream of this site.
Kumukala River 10 (S32°34.675′E027°26.350′)	EL3	It is one of the tributaries of Kubusi River. It serves as a final effluent receiving watershed for treatment plants. We observed eutrophication and algal bloom at this site. It is very close to Kumukala-Kubusi confluence. Kubusi River is used for an agricultural purpose just immediately after this site.
Kubusi River site 11 (S32°35.078′E027°28.168′)	EL4	Eutrophication and algal bloom occurred at this site. Some agricultural activities were going on around this site.
Buffalo River Estuary site 12 (S33°01.357′E027°53.604′)	EL5	An estuarine located along the Buffalo River. It receives industrial effluents, and it is used for fishing activities.
Buffalo River Estuary site 13 (S33°01.385′E027°53.470′)	EL6	An estuarine located along the Buffalo River. It receives industrial effluents, and it is used for fishing activities. A fish slaughterhouse/cutting plant discharges its untreated effluents at the sampling site.
Sunday River Estuary site 14 (S33°41.580′E025°49.563′)	SR	An estuary that is located close to Port Elizabeth. Serious fishing and recreational activates occur at this site.
Swartkops River Estuary site 15 (S33°51.444′E025°35.940′)	SKR	It is an estuary located in Port Elizabeth. Serious fishing and recreational activates occur at this site. Companies and wastewater treatment plants surround the river. The water smells awful, and this suggests that the surrounding companies might be discharging poorly treated effluents into the river.
DAM 1 site 16 (S32°46.507′E026°51.604′)	ALD1	The dam is used by the University of Fort Hare for agricultural purposes. The presence of cow droppings at the edge of the dam suggests that free-range cows visit the site to drink water. Local fishermen also fish from the dam, especially during the summer season. It is close to Alice wastewater treatment plant.
DAM 2 site 17 (S32°47.406′E026°50.821′)	ALD2	The dam is used by the University of Fort Hare for agricultural purposes. The presence of cow droppings at the edge of the dam suggests that free-range cows visit the site to drink water. Local fishermen also fish from the dam, especially during the summer season. Tyume, which is the sources of the dam that serves as receiving watershed for a couple of wastewater treatment plants.

water (APW) in triplicates and incubated at 37°C for 24 h. Turbid tubes were separated, and total genomic DNA was extracted from each turbid tube by the boiling method (Maugeri et al., 2006). For the total genomic DNA extraction, 1 ml of aliquot from the turbid tubes was aseptically transferred into a sterile microcentrifuge tube and centrifuged for 2 min at a speed of 11,000 × *g* using a MiniSpin microcentrifuge. After centrifugation, the supernatant was discarded while 200 µl of sterile distilled water was added to the cell pellet at the bottom of the microcentrifuge tubes and vortexed to form a solution containing evenly distributed cells. The cells in the solution were afterwards lysed with the aid of an AccuBlock (Digital dry bath; Labnet) for 15 min at 100°C, and the solution of the lysed cells was centrifuged at a speed earlier mentioned. The supernatant that was the genomic extraction was subjected to 25 µl PCR reaction to confirm the presence of *Vibrio* spp. using a primer that targets a variable region of *16S rRNA* gene that is specific for members of the *Vibrio* genus. Furthermore, to determine the absolute density of each of the targeted *Vibrio* spp., DNA templates from MPN tubes that were positive for *Vibrio* spp. were subjected to another round of PCR that targeted each of the six *Vibrio* spp. using species-specific primers used for delineation (**Table 2**). The composition of the PCR reaction was 5 µl of DNA template, 12.5 µl of one Taq 2X Master Mix Standard Buffer (BioLabs, UK), 1 µl each of 10 µM of forward and reverse primers, and 5.5 µl of nuclease-free water. The concentration of the DNA in templates ranges between 80 and 195 ng/µl through the experiment. The positive controls used for the PCR assay were *V. parahaemolyticus* (DSM 10027), *V. vulnificus* (DSM 10143), *V. fluvialis* (DSM 19283), *V. mimicus* (DSM 19130), and *V. alginolyticus* (DSM 2171) and one locally isolated *V. cholera*. The TVD was determined by extrapolating the equivalent MPN values for turbid tubes that were positive for members of the *Vibrio* genus and each of the targeted *Vibrio*

TABLE 2 | List of species-specific primers.

Species	Sequence	Size bp	References
V. cholerae	F: 3'-CAC CAA GAA GGT GAC TTT ATT GTG-5'		
	R: 3'-AGG ATA CGG CAC TTG AGT AAG ACTC-5'	304	GOEL et al., 2010; de Menezes et al., 2014
V. parahaemolyticus	F: 3'-GCA GCT GAT CAA AAC GTT GAG T-5'		
	R: 3'-ATT ATC GAT CGT GCC ACT CAC-5'	897	Tarr et al., 2007; Okoh et al., 2015
V. vulnificus	F: 3'-GTC TTA AAG CGG TTG CTG C-5'		
	R: 3'-CGC TTC AAG TGC TGG TAG AAG-5'	410	Wong and Chow, 2002; Okoh et al., 2015
V. fluvialis	F: 3'-GAC CAG GGC TTT GAG GTG GAC GAC-5'		
	R: 3'GGT TTG TCG AAT TAG CTT CAC C-5'	217	Osorio and Klose, 2000; Chakraborty et al., 2006
V. mimicus	F: 3'-GGTAGCCATCAGTCTTATCACG-5'	390	Lei et al., 2000; Shinoda et al., 2004; Sultan et al., 2007; Guardiola-avila et al., 2015
	R: 3'-ATCGTGTCCCAATACTTCACCG-5'		
V. alginolyticus	F: 3'-GAGAACCCGACAGAAGCGAAG-5'		
	R: 3'-CCTAGTGCGGTGATCAGTGTTG-5'	337	Zhou et al., 2007; Wei et al., 2014

spp. using bacteriological analytical manual (BAM) Excel spreadsheet (Blodgett, 2015). The detection limit for the MPN-PCR method is <3 MPN/ml (<0.477 log MPN/ml). The forward sequence for the *Vibrio* genus-specific primer used was 3'CGG TGA AAT GCG TAG AGA T5', whereas that for the reverse sequence was 3'TTA CTA GCG ATT CCG AGT TC5'. The thermal cycler condition for the PCR assay was 15 min at 93°C for initial denaturation, 35 cycles of 92°C for 40 s, 57°C for 1 min, and 72°C for 1.5 min for denaturation, annealing, and elongation, respectively, and 75°C for 7 min for the final extension. The resulting amplicons were electrophoresed on 1.5% agarose, and pictures of amplified DNA bands on agarose gel were viewed and taken using an ultraviolet (UV) transilluminator following the manufacturer's guideline. The expected amplicon size was 663 bp (Kwok et al., 2002; Okoh et al., 2015).

Isolation of Presumptive *Vibrio* spp. From Water Samples

To maximize the isolation of the *Vibrio* species of interest, a water sample (100 ml) was filtered as articulated in the Temperature, Salinity, and Presumptive *Vibrio* Density Determination section, and the resulting membrane filter was introduced into a conical flask containing sterile 100 ml APW. The conical flask with its content was perturbed gently for about 1–2 min before incubating the set-up for 24 h at 37°C (Ntema et al., 2010). The set-up was observed on hourly bases, and as soon as there was the formation of the pellicle at the surface of the incubated APW, a loopful just below the pellicle was carefully streaked on sterile TCBS (Ceccarelli et al., 2015). The newly streaked TCBS plates were incubated for 24 h at 37°C. At the expiration of the incubation period, colonies (5–10 per plate) with typical *Vibrio* yellowish and greenish morphology were carefully picked, re-streaked on fresh sterile TCBS, and incubated for 24 h at 37°C. After the incubation period, a colony from TCBS plates with uniform colonies' morphology were transferred to fresh 1% NaCl nutrient agar plates. Resulting colonies were Gram stained and observed under a microscope to ensure the purity of the isolated presumptive *Vibrio* species to be stocked. Twenty percent glycerol stock of pure isolates were prepared afterwards and stored at −80°C for PCR analysis.

Molecular Identification of Presumptive *Vibrio* Isolates

A total genomic DNA was extracted from the presumptive *Vibrio* isolates using the boiling method as described earlier in the Total *Vibrio* spp. Density section. The DNA was extracted from a colony of an 18-h-old pure culture of presumptive *Vibrio* spp. isolates. A solution of the colony prepared in a microcentrifuge containing 200 µl of sterile distilled water was boiled, and total genomic DNA was afterwards extracted from the cell solutions as earlier described in the Total *Vibrio* spp. Density section. This was followed by the confirmation of all the presumptive isolates as member of the *Vibrio* genus or otherwise following the PCR protocol detailed in the Total *Vibrio* spp. Density section. All PCR-confirmed *Vibrio* isolates were further delineated into the six *Vibrio* spp. targeted in this study.

Delineation of the PCR-Confirmed *Vibrio* Species

A set of species-specific primers were employed in PCR assay for delineating confirmed *Vibrio* spp. into the *Vibrio* species of interest. The respective primers employed for the identification of *V. cholerae*, *V. mimicus*, *V. fluvialis*, *V. vulnificus*, *V. alginolyticus*, and *V. parahaemolyticus* targeted the conserved region on *OmpW*, *vhm*, *ToxR*, *GroEl*, *GyrB*, and *fla E* genes that are specific for the organisms of our interest. *V. cholera* and *V. mimicus* were simultaneously identified using a duplex PCR protocol, whereas *V. vulnificus*, *V. fluvialis*, and *V. alginolyticus* were also simultaneously identified by employing a triplex PCR protocol. *V. parahaemolyticus* isolates were identified using a simplex PCR protocol. The primer sequences, sources, and expected amplicon sizes are given in **Table 2**, and all the PCR protocols were as earlier articulated in our previous study (Abioye and Okoh, 2018). The resulting amplicons were electrophoresed, bands on gels were viewed, and their pictures were taken using a UV transilluminator following the manufacturer's guideline.

Statistical Analysis

Results for freshwater and brackish water samples were distinctively treated on seasonal and annual bases. Density across sites was statistically compared using the Kruskal-Wallis test and the Games-Howell *post hoc* test at $p \leq 0.05$. Spearman correlation analysis was carried out to understand the relationship between PVD, TVD, temperature, and salinity at our sampling sites since salinity and temperature have been reported to modulate the ecology of *Vibrio* spp. differently at different geographical locations. The frequency of isolation (relative density) and absolute density of each of the six targeted *Vibrio* spp. were also correlated with temperature and salinity to establish species-based relationship. Kruskal-Wallis test and Spearman correlation analysis were used because our variables (temperature, density, salinity, and frequency of isolation) were not normally distributed.

Excel version 2013 and SPSS version 2020 were used to organize and analyze our data.

RESULT AND DISCUSSION

Temperature, Salinity, and *Vibrio* spp. Density

The average annual temperature and salinity of water samples at the sampling points were as given in **Table 3**. Salinity ranges between 0.06 ± 0.04 PSU at site EL1 and 2.03 ± 0.47 PSU at site PA5 for freshwater sampling sites, whereas it ranges between 16.14 ± 3.91 PSU at site SR and 31.65 ± 4.19 PSU at site PA7 for brackish water sampling sites. The temperature range was between 15.31 ± 4.25°C at site EL1 and 21.50 ± 3.67°C at site PA6 for freshwater sampling sites, and it was between 18.74 ± 2.12°C at site EL6 and 22.01 ± 4.47°C at site SR for brackish water sampling sites. During the study regime, 194 water samples were collected and analyzed for PVD and TVD. The mean annual PVD and TVD per site (**Figure 2**) differ across the sampling sites. The average annual PVD ranges between 1.23 ± 0.83 log CFU/ml at site ALD2 and 2.92 ± 0.93 log CFU/ml at site EL4 for freshwater samples, whereas that for brackish water samples ranges between 2.36 ± 0.72 log CFU/ml at site PA7 and 2.99 ± 1.0 log CFU/ml at site EL6. On the other hand, the range of annual average TVD was 1.35 ± 0.56 log MPN/ml at site PA1 to 2.63 ± 1.28 log MPN/ml at site EL3 for freshwater samples. The range for brackish water samples was 1.23 ± 0.64 log MPN/ml at site PA7 to 1.83 ± 0.71 log MPN/ml at site SR. The PVD at all sampling sites was more than that at site PA1 except for sites ALD1 and ALD2. This observation was significant at $p \leq 0.05$ for all sampling sites except for sites PA7, EL1, EL2, EL4, ALD1, and SR. A similar scenario was observed for TVD except that TVD at site PA1 was greater than TVD at site PA7. The observation for TVD was only significant for PA2 > PA1. The densities of each of the targeted species are as given in **Supplementary Table SS1B**. A density greater than 0.477 log MPN/ml, which was the maximum detection limit of the three tubes by the five dilutions MPN-PCR density determination method employed, was recorded mainly in summer but scarcely recorded in winter months.

TABLE 3 | Average annual salinity and temperature at the freshwater and brackish water sampling sites.

Sites	Salinity ± SD (PSU)	Temperature ± SD (°C)
Freshwater sampling sites		
PA1	0.18 ± 0.04	18.40 ± 3.14
PA2	0.53 ± 0.17	18.02 ± 3.00
PA3	0.69 ± 0.13	18.30 ± 3.11
PA4	0.71 ± 0.11	19.12 ± 3.17
PA5	2.03 ± 0.47	19.67 ± 3.41
PA6	1.70 ± 0.60	21.50 ± 3.67
EL1	0.06 ± 0.04	15.31 ± 4.24
EL2	0.11 ± 0.09	15.61 ± 4.30
EL3	0.13 ± 0.05	16.45 ± 3.80
EL4	0.14 ± 0.19	16.40 ± 4.18
ALD1	0.12 ± 0.07	18.81 ± 5.47
ALD2	0.13 ± 0.12	19.77 ± 4.68
Brackish water sampling sites		
PA7	31.65 ± 4.19	20.10 ± 2.07
EL5	29.14 ± 8.69	19.37 ± 1.46
EL6	27.94 ± 8.84	18.74 ± 2.12
SR	16.14 ± 3.91	22.10 ± 4.47
SKR	28.45 ± 2.29	21.63 ± 3.56

Key: SD = standard deviation

Of the samples with >0.477 log MPN/ml *V. cholerae*, *V. mimicus*, *V. fluvialis*, *V. vulnificus*, *V. alginolyticus*, and *V. parahaemolyticus* densities, 82, 72, 63, 100, 87, and 58%, respectively, were collected in summer months.

Sites PA1, EL1, ALD1, and ALD2 were anticipated to be pristine and have relatively low microbial load because PA1 and EL1 were around the sources of Kowie and Kubusi Rivers, respectively, whereas sites ALD1 and ALD2 were in a controlled environment. However, in some instance, PVD and TVD at these supposedly said pristine sampling sites were greater than PVD and TVD at other sampling sites, e.g., the mean annual *Vibrio* density at PA1 was greater than that at PA7, which are more exposed to anthropogenic activities. The unanticipated observation could be as a result of the easy access and activities of wild and domesticated animals around the water resources at PA1. South Africa water resources have been adjudged unprotected (Christine et al., 2013; Colvin et al., 2016) while domesticated and wild animals activities around surface water generally cause contamination of water resources with pathogens (Cabral, 2010; McAllister and Topp, 2012; Decol et al., 2017; Topalcengiz et al., 2017; Liu et al., 2018). Furthermore, domestic wastes from informal settlements along the riverbanks, effluents from overloaded and poorly maintained treatment plants, polluted runoff, and solid wastes that are potential contributors of pathogens to surface water (Fatoki et al., 2001; Chigor et al., 2012; Edokpayi et al., 2017; Adams et al., 2019) were evident at our sampling sites. In addition, droppings from free-range and grazing cows were observed at most of our freshwater sampling sites. Animals droppings are major contributors of pathogenic *Vibrio* spp., e.g., toxigenic *V. cholerae* into human environments (Dufour et al., 2013; Momba and Azab El-Liethy, 2017; Penakalapati et al., 2017; Delahoy et al., 2018; Munshi et al., 2019). As anticipated, sites SR, SKR, PA7, EL5, and EL6 located at estuaries where *Vibrio* spp. are commonly isolated

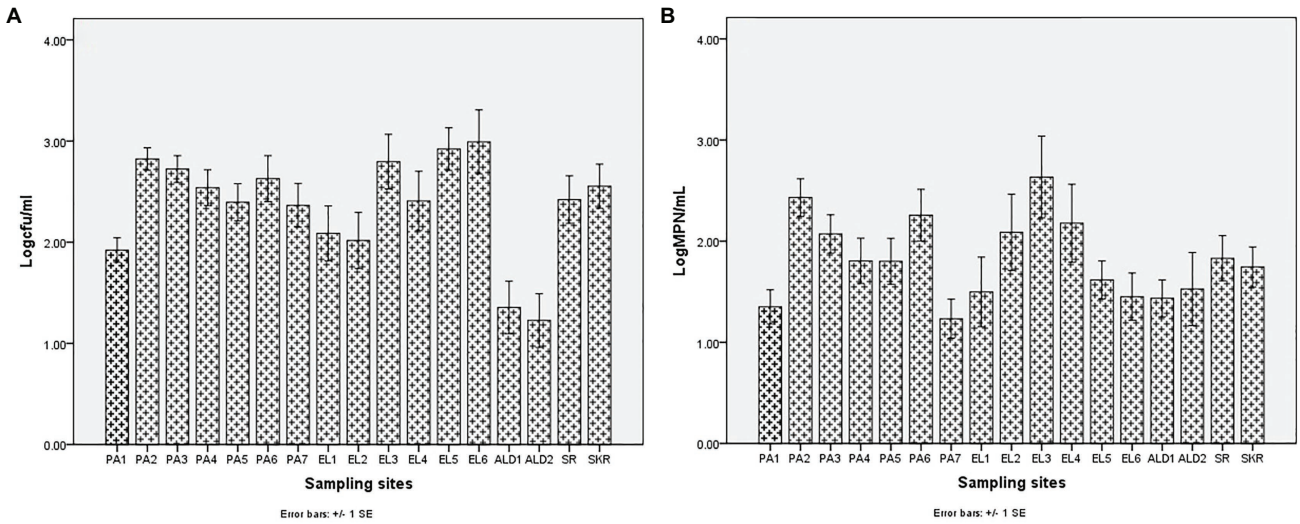

FIGURE 2 | Annual mean density of *Vibrio* spp. **(A)** PVD and **(B)** TVD.

and site EL6 that also serves as receiving watershed for fish slaughterhouse/cutting plant had relatively high *Vibrio* density than some of the freshwater sampling sites. Reports have shown that effluents from fish slaughterhouses contribute significantly to *Vibrio* spp. load in receiving watershed (Novotny et al., 2004; Skall and Olesen, 2011). Surprisingly, the densities of *Vibrio* at some of the freshwater sampling sites were also significantly more than those at some of the brackish water sampling sites (**Figures 2A,B**). This observation could be as a result of the type of industrial effluent and other pollutants that are usually discharged into the water environments around the brackish water sampling sites (Adeniji et al., 2017a,b). Industrial waste has been reported to modulate the microbial biodiversity of the aquatic ecosystem (Li et al., 2017; Jordaan et al., 2019), and this could be on a downward trend for microbial populations when such waste is toxic rather than nutrient-rich. *Vibrio* spp. density (PVD and TVD) also varies across seasons with relatively high density recorded in summer as earlier reported (Igbinosa et al., 2011a,b; Kokashvili et al., 2015); however, few exceptions were observed (**Figures 3, 4**). A relatively high PVD and TVD in winter recorded at sites PA2 and EL3 can be traced to pollution. The two sites serve as receiving watershed for dysfunctional WWTPs (Maclennan, 2019), and dysfunctional WWTPs usually contaminate the water system with pathogens (Edokpayi et al., 2017). The highest density for each of the targeted *Vibrio* spp. (**Supplementary Table SS1B**) was recorded at sites (PA2, PA5, EL3, SR, and SKR) where we observed a high level of pollution.

Statistically speaking, a significantly positive weak correlation ($r = 0.201$, $p = 0.018$) between PVD and salinity was observed for freshwater but a significantly negative weak correlation ($r = -0.327$, $p = 0.014$) for brackish water samples. The correlation between TVD and salinity was not significant for freshwater ($r = 0.058$, $p = 0.503$) and brackish water ($r = -0.163$, $p = 0.203$) samples. The correlation coefficients between PVD vs. temperature ($r = 0.133$, $p = 0.121$ for freshwater; $r = 0.2$, $p = 0.14$ for brackish water) and TVD vs. temperature ($r = 0.018$, $p = 0.252$ for freshwater; $r = -0.068$, $p = 0.619$ for brackish water) were not significant too. The lack of correlation between salinity, temperature, and *Vibrio* density had been reported in the literature (Randa et al., 2004; De Souza Costa Sobrinho et al., 2010; Paranjpye et al., 2015; Nilsson et al., 2019). The finding suggests that the contribution of salinity and temperature to the *Vibrio* genus density at our sampling sites is small, and that some other physicochemical and biological factors could be key to *Vibrio* density dynamics at our sampling sites. Interestingly, the literature has shown that parameters, such as dissolved oxygen and chemical and biological oxygen demands, have a strong relationship with *Vibrio* spp. density and the aforementioned parameters are good indexes for detecting water resources polluted with organic waste that may contain pathogens (Sharma and Chaturvedi, 2007; Prasanthan et al., 2011; Mezgebe et al., 2015; Di et al., 2017; Rabea et al., 2019). Unfortunately, organic waste pollution can occur at any time and cause unexpected offshoot in microbial density and diversity in an ecological niche. This, thus, explain the observation of the highest *Vibrio* density in seasons other than summer at some of our sampling sites because we observed that sources of organic waste pollutants are close to these sampling sites.

Effects of Salinity and Temperature on the Density, Frequency of Isolation, and Seasonality of the Targeted *Vibrio* Species

The frequency of isolation of each of the *Vibrio* species of interest in freshwater and brackish water samples per sampling month and the impact of temperature and salinity on the

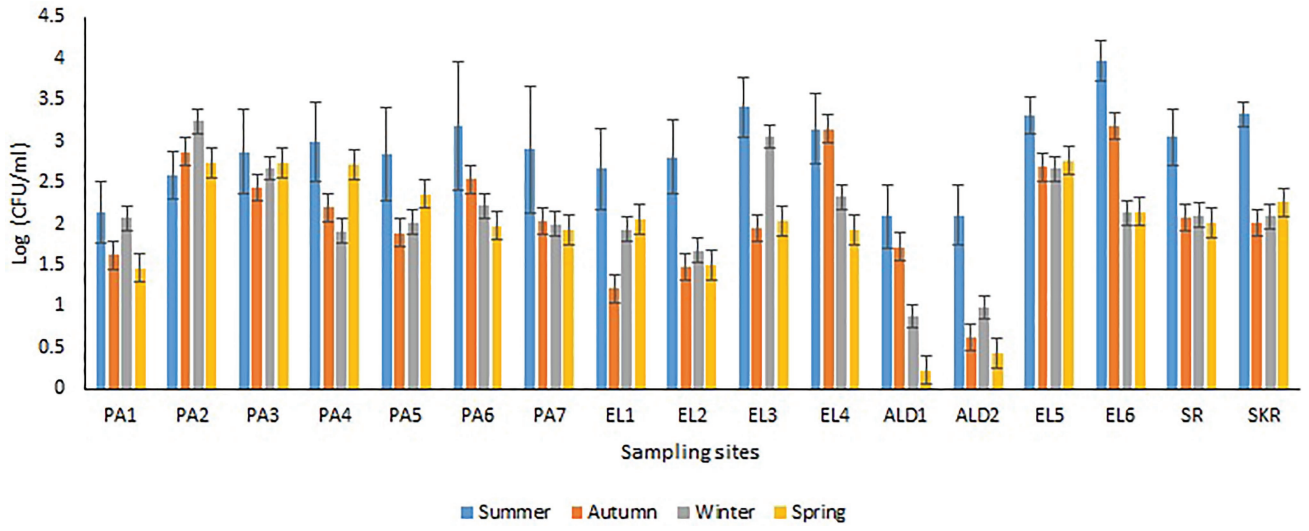

FIGURE 3 | Seasonal variations in PVD.

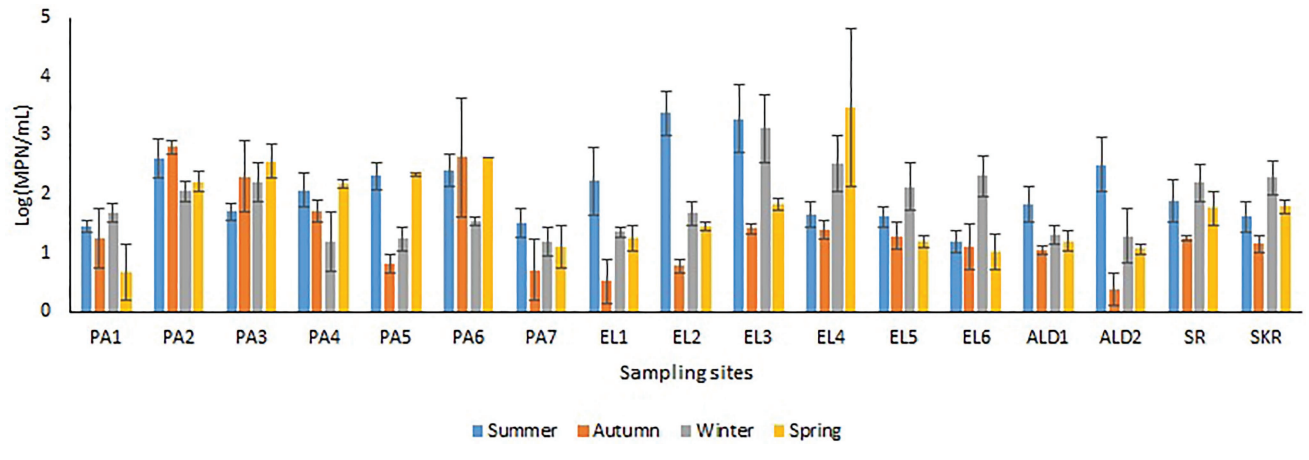

FIGURE 4 | Seasonal variations in TVD.

frequency of detection are given **Figure 5**. The seasonal variation in the frequency of isolation of the *Vibrio* spp. of interest is given in **Figure 6**. The results show that the organism of interest was frequently isolated in summer than other seasons. Surprisingly, while the isolation frequency of organisms of interest in freshwater samples followed a similar pattern as salinity and temperature, only temperature did for brackish water samples. It is an established fact that salinity and temperature are important environmental factors that influence *Vibrio* spp. density, but the literature has also shown that the correlation between these factors and *Vibrio* spp. density differs for different geographical locations and sample types (Kelly, 1982; Kaspar and Tamplin, 1993; Fukushima and Seki, 2004; Randa et al., 2004; Igbinosa et al., 2011a; Takemura et al., 2014; Kokashvili et al., 2015; Colwell, 2016; Urquhart et al., 2016). For example, Kokashvili et al. (2015) observed a linear correlation between the two factors and frequency of isolation of some medically important *Vibrio* species but a negative correlation between temperature and *V. metschnikovii* at the marine and freshwater sampling sites. In addition, Randa et al. (2004) observed a significant moderate negative correlation between salinity and abundance of *V. vulnificus* in estuarine water samples, whereas Colwell (2016) reported a non-significant negative correlation between temperature and the abundances of *V. parahaemolyticus* and *V. vulnificus* in estuary water samples. In this study, the frequency of isolation of at least one of the targeted species from freshwater samples showed a significant positive relationship with salinity and temperature (**Table 4**). However, only temperature had a significant positive relationship with the frequency of isolation of at least one of the targeted *Vibrio* spp. in brackish water samples. Interestingly, correlation coefficients and *p* values for the relationship between frequency of isolation of at least one

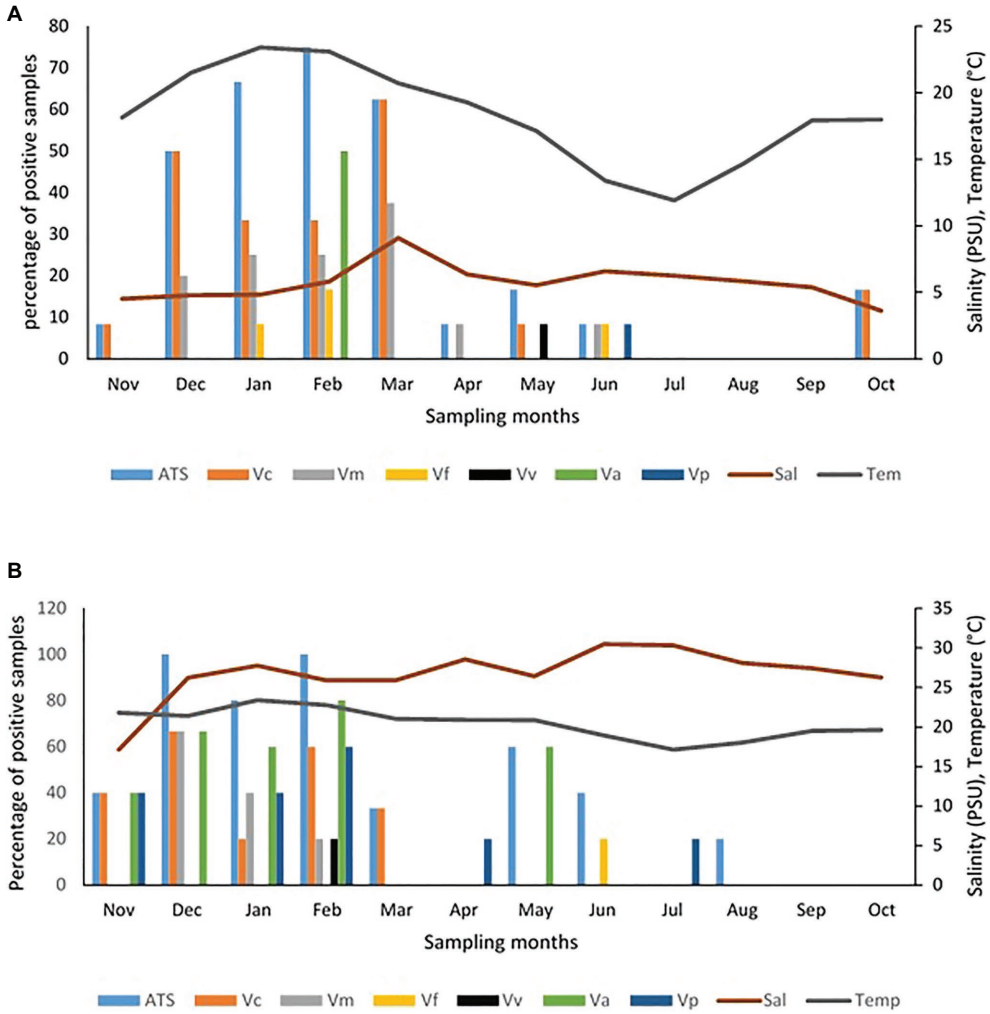

FIGURE 5 | Influence of temperature and salinity on the detection of targeted *Vibrio* spp. in water samples. **(A)** Freshwater samples, **(B)** brackish water samples. Key: Va = *V. alginolyticus*, Vc = *V. cholerae*, Vf = *V. fluvialis*, Vm = *V. mimicus*, Vp = *V. parahaemolyticus*, Vv = *V. vulnificus*, ATS = all targeted *Vibrio* species.

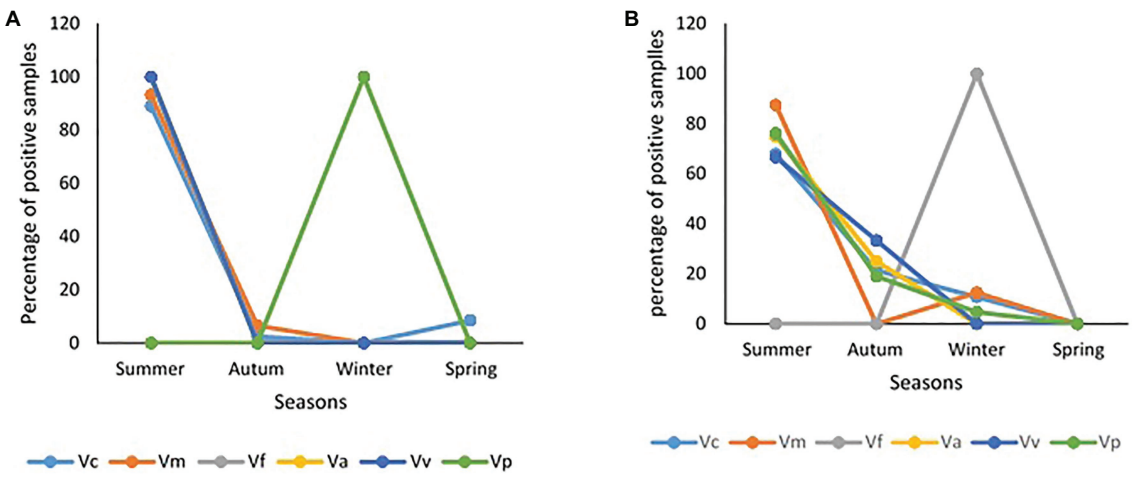

FIGURE 6 | Seasonality of samples positive for targeted *Vibrio* spp. **(A)** freshwater samples, **(B)** brackish water samples.

TABLE 4 | Correlation analysis between the frequency of isolation of targeted *Vibrio* spp. from water samples, temperature, and salinity.

Freshwater				Brackish water			
Organism type	**Parameters**	**R**	***p***	**Organism type**	**Parameters**	**R**	***p***
	Sal	**0.215**	**0.011**		Sal	0.094	0.497
FITV	Temp	**0.462**	**<0.0001**	FITV	Temp	**0.459**	**<0.0001**
	Sal	**0.33**	**<0.0001**		Sal	0.193	0.153
FIVc	Temp	**0.411**	**<0.0001**	FIVc	Temp	0.139	0.308
	Sal	0.028	0.747		Sal	–0.010	0.941
FIVm	Temp	**0.192**	**0.023**	FIVm	Temp	0.072	0.596
	Sal	–0.1	0.244		Sal	0.121	0.374
FIVf	Temp	**0.234**	**0.006**	FIVf	Temp	–0.140	0.305
	Sal	–0.022	0.801		Sal	0.03	0.828
FIVa	Temp	0.153	0.073	FIVa	Temp	**0.51**	**<0.0001**
	Sal	–0.055	0.521		Sal	–0.233	0.084
FIVv	Temp	–0.064	0.453	FIVv	Temp	**0.351**	**0.008**
	Sal	–0.061	0.477		Sal	–0.057	0.679
FIVp	Temp	–0.067	0.435	FIVp	Temp	**0.571**	**<0.0001**

Key: Bolded R and p values show a significant correlation. FIA = frequency of isolation; TV = the targeted Vibrio spp.; Va = V. alginolyticus; Vc = V. cholerae; Vf = V. fluvialis; Vm = V. mimicus; Vp = V. parahaemolyticus; Vv = V. vulnificus; %P = percentage prevalence

of the *Vibrio* spp. and temperature were very similar for the two water types (**Table 4**). This shows that temperature modulates the chances of isolating at least one of the *Vibrio* spp. of interest from the two water types in a similar way. However, at species level, the correlation analysis (**Table 4**) showed that temperature is more effective as guide for the isolation of *V. cholerae*, *V. mimicus*, and *V. fluvialis* (generally called non-halophilic) from freshwater and *V. alginolyticus*, *V. vulnificus*, and *V. parahaemolyticus* (generally called halophilic) from brackish water. In their work, Liu et al. (2016) and Mahoney et al. (2010) reported that temperature is more relevant to the isolation of non-halophilic vibrios from freshwater and halophilic vibrios from brackish water than salinity. Consequently, we adjudged from our data (**Figure 5**) that a temperature range between 20 and 24°C is the optimum temperature for the isolation of *V. cholerae*, *V. mimicus*, and *V. fluvialis* from freshwater sampling sites and *V. alginolyticus*, *V. vulnificus*, and *V. parahaemolyticus* from brackish water sampling sites. It was further inferred that a salinity range between 5 and 9 PSU should be used in adjunct with a temperature range of 20 and 24°C for the isolation of *V. cholerae* at the freshwater sampling sites. Our submission is in concordance with earlier studies that showed that relatively high frequency of isolation of medically important *Vibrio* spp. is usually achieved in summer when the temperature is above 15°C and salinity is between 5 and 25 PSU (Jones and Summer-Brason, 1998; DePaola et al., 2003; Urquhart et al., 2016).

It is good to point out that targeted *Vibrio* spp. from few samples at sites ALD1, ALD2, EL5, and SKR were isolated in winter in this study. This could be attributed to the level of pollution at these sites as earlier discussed and affirm the possibility of isolating medically important *Vibrio* spp. in usual season because of pollution and contamination that is not season dependent. It has been earlier reported by Kopprio et al. (2020) and Watkins and Cabelli (1985) that warmer temperatures and sewage pollution are reasons for the abundance of pathogenic *Vibrio* spp. in the aquatic milieu. In addition, the studies carried out by Jaiani et al. (2013) and Janelidze et al. (2011) suggest that temperature affects *Vibrio* abundance, whereas salinity affects *Vibrio* species composition of any ecological niche. It is important to note here that a similar scenario discussed above was observed when absolute densities of targeted *Vibrio* spp. were statistically analyzed (**Supplementary Tables SS1B,C**; **Supplementary Figures SS1A,B**).

Prevalence of the Six Targeted *Vibrio* Species of Medical Importance

The Kruskal-Wallis test showed that the average annual absolute density of each of the targeted *Vibrio* spp. was significantly different across sites at $p < 0.05$. The Games-Howell *post hoc* test showed the site comparisons with significant differences (**Supplementary Table SS1D**). The comparisons of absolute density of targeted species between freshwater and brackish water sites that showed significant difference revealed that *V. cholerae* and *V. mimicus* are more abundant in freshwater than in brackish water, whereas *V. vulnificus*, *V. alginolyticus*, and *V. parahaemolyticus* are more abundant in brackish water than in freshwater. Furthermore, seasonal comparison of absolute density (**Supplementary Table SS1E**) showed that all the targeted species proliferate in summer significantly than in other seasons of the year. The relative abundance of each of the six targeted *Vibrio* spp. in isolates recovered at the sampling sites is shown in **Figures 7A,B**, whereas the incidence of each of the targeted species among the total *Vibrio* spp. isolates recovered from each of the water sample types is given in **Figures 7C,D**. The prevalence of each of the targeted *Vibrio* spp. per sampling site is given in **Figures 7E,F**. At least one of the targeted *Vibrio* species was detected and isolated from each of the sampling sites. The prevalence of *V. cholerae*, *V. mimicus*, *V. fluvialis*, *V. vulnificus*, *V. alginolyticus*, and *V. parahaemolyticus* in freshwater samples was 34, 19, 9, 2, 3, and 2%, respectively. On the other hand, the prevalence

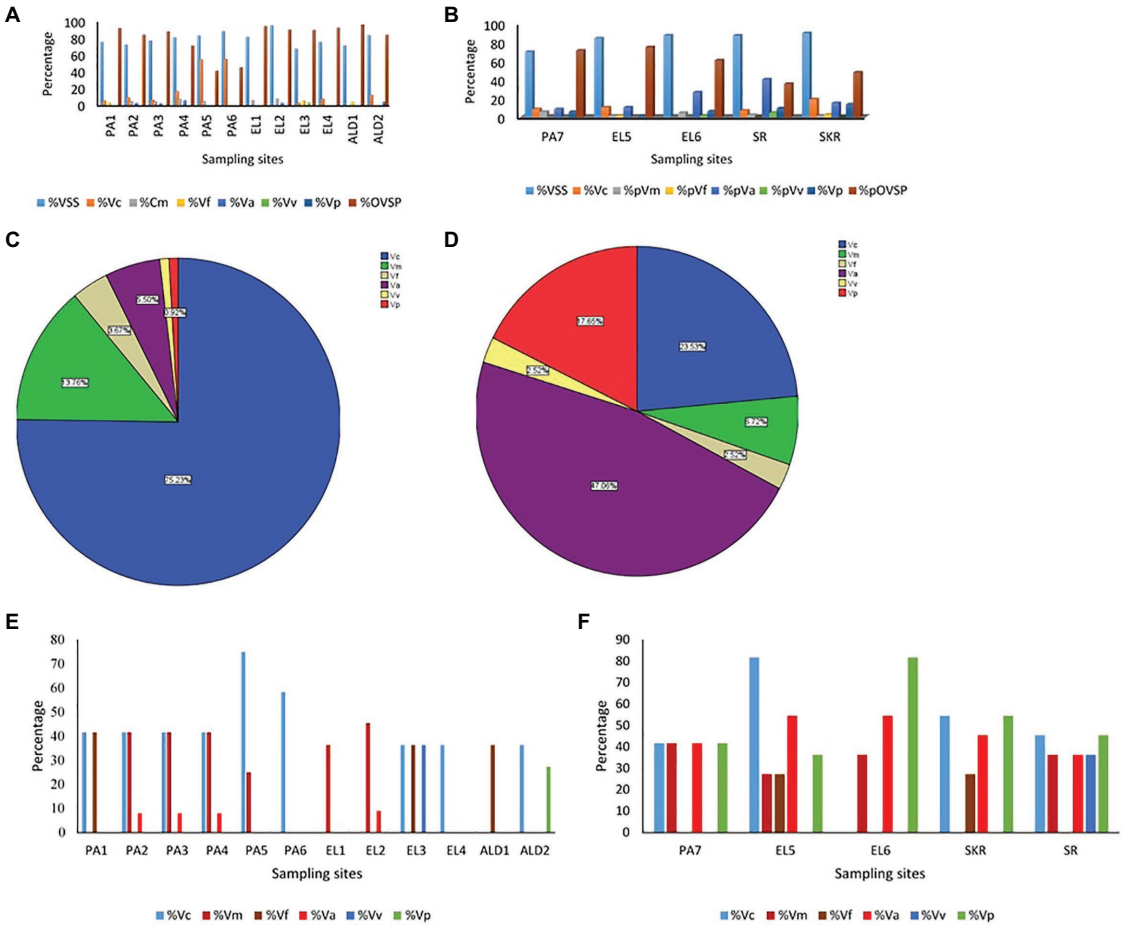

FIGURE 7 | (A,B) Prevalence of targeted *Vibrio* spp. in isolates recovered per sampling sites. **(C,D)** Distribution of targeted *Vibrio* spp. among isolates recovered from samples. **(E,F)** Detection rate of targeted *Vibrio* spp. in samples per sampling site. **(A,E)** Freshwater sampling sites, **(B,F)** brackish water sampling sites, **(C)** isolates from freshwater samples, **(D)** isolates from brackish water samples, % = percentage, VSS = *Vibrio* spp. positive samples, Vc = *Vibrio cholerae*, Vm = *Vibrio mimicus*, Vf = *Vibrio fluvialis*, Va = *Vibrio alginolyticus*, Vp = *V. parahaemolyticus*, OVSP = other *Vibrio* spp.

of *V. cholerae*, *V. mimicus*, *V. fluvialis*, *V. vulnificus*, *V. alginolyticus*, and *V. parahaemolyticus* in brackish water samples was 44, 28, 10, 7, 46, and 51%, respectively. A total of 628 and 342 presumptive isolates from freshwater and brackish water samples, respectively, were analyzed in this study. Of the freshwater presumptive isolates, 79% were confirmed as *Vibrio* spp., whereas 85% of presumptive isolates from brackish water samples were confirmed as *Vibrio* spp. Twenty-two and 41% of the PCR-confirmed isolates from freshwater samples and brackish water samples, respectively, fall among the targeted *Vibrio* species. The samples of gel electrophoresis pictures for the confirmation and speciation of *Vibrio* spp. into the six targeted species are given in **Figure 8**. The incidence of *V. cholerae*, *V. mimicus*, *V. fluvialis*, *V. vulnificus*, *V. alginolyticus*, and *V. parahaemolyticus* of all the six targeted *Vibrio* species recovered from freshwater samples was 75, 14, 4, 6, 1, and 1%, whereas that for brackish water was 24, 7, 3, 47, 3, and 18%, respectively. The predominant species of the freshwater samples were *V. cholerae* and *V. mimicus*, whereas those of the brackish water samples were *V. alginolyticus*, *V. cholerae*, and *V. parahaemolyticus*. The prevalence of the remaining four (*V. fluvialis*, *V. vulnificus*, *V. alginolyticus*, and *V. parahaemolyticus*) of the six targeted *Vibrio* spp. among *Vibrio* isolates from freshwater samples and three (*V. mimicus*, *V. fluvialis*, *V. vulnificus*) of the six targeted *Vibrio* species in brackish water samples were, respectively, low. Our result showed population diversity of targeted *Vibrio* species in freshwater and brackish water samples. Halophilic vibrios were more abundant in brackish water, whereas non-halophilic vibrios were abundant in freshwater samples. The six targeted *Vibrio* spp. were more diverse in brackish water sample than in freshwater sample. These findings corroborate some earlier reports and suggest that salt concentration modulates the diversity of vibrios in water resources (Elhadi, 2013; Mookerjee et al., 2015; de Menezes et al., 2017; Fu et al., 2019). The result (**Figure 7**; **Supplementary Table SS1A**) of the present study showed that the possibility of contracting infections, such as cholera and cholera-like infections, caused by the non-halophilic vibrios is higher at the freshwater sampling sites most especially

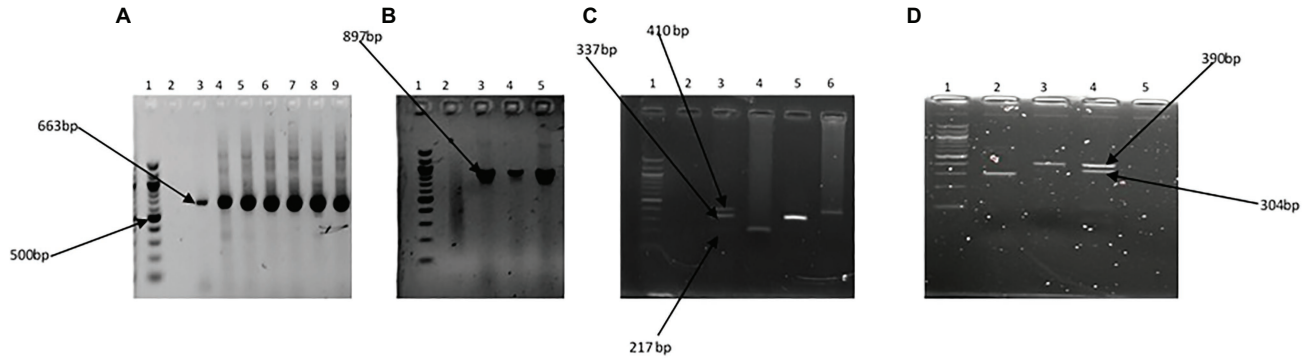

FIGURE 8 | Gel pictures showing PCR amplification products of the specific regions of *16S rRNA* gene for the *Vibrio* genus **(A)**, *fla E* gene for *V. parahaemolyticus* **(B)**, *GroEl*, *ToxR*, and *GyrB* genes in triplex PCR for *V. vulnificus*, *V. fluvialis*, and *V. alginolyticus*, respectively **(C)**, and *OmpW* and *vhm* genes in duplex PCR for *V. cholerae* and *V. mimicus*, respectively. Lane 1 **(A–D)** 100 bp molecular marker, lane 2 **(A–C)** and lane 5 **(D)** negative control, lane 3 **(A–C)** and lane 4 (D) positive controls, and lanes 4–9 **(A)**, lanes 4 and 5 **(B)**, lanes 4–6 **(C)**, and lanes 2 and 3 **(D)** positive isolates.

sites PA4, PA5, PA6, and ALD1 where most of the halophilic vibrios were recovered than at the brackish water sampling sites. Likewise, the chances of contracting gastroenteritis, wound infections, and other vibriosis peculiar to halophilic vibrios are higher at the brackish sampling sites most especially sites EL6, SR, and SKR. Furthermore, the coexistence of medically important non-halophilic and halophilic vibrios at the same ecological niche in most of our sampling sites is of public health concern. As the density and diversity of cholera and vibriosis causing *Vibrio* species increase in a single ecological niche, the chances of acquiring the infections they cause also increase. Furthermore, the possibility of exchanging genetic materials, such as virulence and antibiotics resistance determinants, will be high. The coexistence of medically important *Vibrio* species within the same ecological niche has been reported in an earlier study (Kokashvili et al., 2015). Although the present study focused on freshwater and brackish water that have not been investigated for members of the *Vibrio* genus before, *Vibrio* spp. of medical importance including four of the six *Vibrio* spp. focused on in this study have been reported from various WWTPs of Eastern Cape and their receiving watershed. A significant amount of *V. cholerae*, *V. parahaemolyticus*, *V. metschnikovii*, *V. fluvialis*, and *V. vulnificus* were reportedly isolated from final effluents in some WWTPs in Nkonkobe rural community, Chris Hani, and Amathole district municipalities (Igbinosa et al., 2009, 2011a,b; Nongogo and Okoh, 2014). A more comprehensive study on final effluents of 14 WWTPs in Amathole and Chris Hani district municipalities reported 66.8% *Vibrio* spp. prevalence of the 1,000 randomly selected isolates recovered from the WWTPs. Of the 300 confirmed *Vibrio* spp., 68.2% belong to one of *V. parahaemolyticus*, *V. fluvialis*, and *V. vulnificus* (Okoh et al., 2015). All these studies, including the present one, show that medically important *Vibrio* spp. are present in the aquatic milieu of the ECP. The aforementioned is of potential health risk to individuals using the water resources studied and watershed for recreational, agricultural, and domestic purposes most especially at the downstream of WWTP final effluents discharge points. In some studies from other provinces of South Africa, the isolation of *V. harveyi*, *V. parahaemolyticus*, *V. cholerae*, *V. mimicus*, and *V. vulnificus* from tap, borehole, and dam in North West province (Maje et al., 2020) and *V. cholerae* from four WWTPs located in Gauteng Province (Dungeni et al., 2010) has also been reported. Health risks that an individual using these water resources could be exposed to include gastrointestinal infections caused by *V. parahaemolyticus*, *V. mimicus*, and *V. fluvialis*; wound infections caused by *V. vulnificus* and *V. harveyi*; cholera caused by *V. cholerae*; and cholera-like bloody diarrhea caused by *V. fluvialis* (Ramamurthy et al., 1994; Igbinosa and Okoh, 2010; Jones, 2017; Brehm et al., 2020).

SUMMARY AND CONCLUSION

The present study confirmed the presence of *Vibrio* species of medical importance in both freshwaters (Kowie River, Bloukrans River, Lashinton River, Kubusi River, and two dams in Amathole District Municipality) and brackish water (Buffalo, Sunday, Kowie, and Swartkops estuaries) of the Eastern Cape, Province of South Africa. It is worth mentioning that humans have regular contact with more than 88% of our sampling sites and all the sampling sites had not been investigated for the occurrence of *Vibrio* spp. of medical importance before. The predominant species at the sampling sites showed that the chances of contracting cholera and cholera-like infection are high at the freshwater sampling sites than at the brackish water sampling sites. On the other hand, the chances of contracting other vibriosis are high at the brackish water sampling sites than at the freshwater sampling sites. The findings of the study also suggest pollution as the reason for the isolation of medically important vibrios in the unusual season at some of the sampling sites. It was also observed that temperature drives isolation frequency, whereas salinity drives the composition of the targeted *Vibrio* species at both

freshwater and brackish water sampling sites. Although the virulence status of the isolated medically important *Vibrio* species was not elucidated in this study, the confirmation of their presence in the water resources investigated for the first time is a significant finding. This finding is an eye opener to the potential threat that the water resources investigated pose to public health in terms of cholera and vibriosis. Therefore, our findings are of public health importance going by the usefulness of the water resources investigated. Although controlling and preventing most of the identified factors that could be contributing to the prevalence of medically important *Vibrio* species at the sampling points might be difficult, regular monitoring will go a long way to prevent possible *Vibrio*-related infection outbreaks.

DATA AVAILABILITY STATEMENT

The original contributions presented in the study are included in the article/**Supplementary Material**, further inquiries can be directed to the corresponding author.

AUTHOR CONTRIBUTIONS

OA and AIO initiated the research topic. AIO provided the materials for the study. OA structured the methods and carried out the statistical analysis and wrote the manuscript. OA and ACO carried out the experiment. ACO and AIO proofread and corrected the manuscript. All authors contributed to the article and approved the submitted version.

FUNDING

This work was supported by the Water Research Commission (grant number: K5 2432), South Africa and Medical Research Council, South Africa.

SUPPLEMENTARY MATERIAL

The Supplementary Material for this article can be found online at: https://www.frontiersin.org/articles/10.3389/fmicb.2021.617703/full#supplementary-material

REFERENCES

Abakpa, G. O., Umoh, V. J., Ameh, J. B., and Al, E. T. (2013). Occurrence of Vibrio cholerae in some households engaged in livestock farming in some parts of Zaria, Nigeria. *Adv. Microbiol.* 3, 128–131. doi: 10.4236/aim.2013.31020

Abioye, O. E., and Okoh, A. I. (2018). Limpet (*Scutellastra cochlear*) recovered from some estuaries in the eastern Cape Province, South Africa act as reservoirs of pathogenic *Vibrio* species. *Front. Public Health* 6:237. doi: 10.3389/fpubh.2018.00237

Adams, J., Pretorius, L., and Snow, G. (2019). Deterioration in the water quality of an urbanised estuary with recommendations for improvement. *Water SA* 45, 86–96. doi: 10.4314/wsa.v45i1.10

Adeniji, A., Okoh, O., and Okoh, A. (2017a). Petroleum hydrocarbon fingerprints of water and sediment samples of Buffalo River estuary in the eastern Cape Province, South Africa. *J. Anal. Methods Chem.* 2017:2629365. doi: 10.1155/2017/2629365

Adeniji, A., Okoh, O., and Okoh, A. (2017b). Petroleum hydrocarbon profiles of water and sediment of algoa bay, Eastern Cape, South Africa. *Int. J. Environ. Res. Public Health* 14:1263. doi: 10.3390/ijerph14101263

Ahmad, N., Ghazali, F. M., Cheah, Y. K., and Chilek, T. Z. T. (2011). Prevalence and quantification of Vibrio species and *Vibrio parahaemolyticus* in freshwater fish at hypermarket level. *Int. Food Res. J.* 18, 689–695.

Ajin, A., Silvester, R., Alexander, D., Nashad, M., and Abdulla, M. H. (2016). Characterization of blooming algae and bloom-associated changes in the water quality parameters of traditional pokkali cum prawn fields along the South West coast of India. *Environ. Monit. Assess.* 188, 1–10. doi: 10.1007/s10661-016-5133-6

Baffone, W., Tarsi, R., Pane, L., Campana, R., Repetto, B., Mariottini, G. L., et al. (2006). Detection of free-living and plankton-bound vibrios in coastal waters of the Adriatic Sea (Italy) and study of their pathogenicity-associated properties. *Environ. Microbiol.* 8, 1299–1305. doi: 10.1111/j.1462-2920.2006.01011.x

Baker-Austin, C., Oliver, J. D., Alam, M., Ali, A., Waldor, M. K., Qadri, F., et al. (2018). *Vibrio* spp. infections. *Nat. Rev. Dis. Prim.* 4:8. doi: 10.1038/s41572-018-0005-8

Barua, D., and Greenough, W. B. (1991). *Cholera*. United States: Springer.

Bessong, P. O., Odiyo, J. O., Musekene, J. N., and Tessema, A. (2009). Spatial distribution of diarrhoea and microbial quality of domestic water during an outbreak of diarrhoea in the Tshikuwi Community in Venda, South Africa. *J. Health Popul. Nutr.* 27, 652–659. doi: 10.3329/jhpn.v27i5.3642

Bhattacharjee, S., Bhattacharjee, S., Bal, B., Pal, R., Niyogi, S. K., and Sarkar, K. (2010). Is *Vibrio fluvialis* emerging as a pathogen with epidemic potential in coastal region of eastern India following cyclone Aila? *J. Health Popul. Nutr.* 28, 311–317. doi: 10.3329/jhpn.v28i4.6036

Binh, M. N., Je, H. L., Ngo, T. C., Seon, Y. C., Nguyen, T. H., Dang, D. A., et al. (2009). Cholera outbreaks caused by an altered *Vibrio cholerae* O1 El tor biotype strain producing classical cholera toxin B in Vietnam in 2007 to 2008. *J. Clin. Microbiol.* 47, 1568–1571. doi: 10.1128/JCM.02040-08

Bisharat, N. (2002). Vibrio vulnificus infection can be avoided. *Isr. Med. Assoc. J.* 4, 631–633.

Bisharat, N., Cohen, D. I., Harding, R. M., Falush, D., Crook, D. W., Peto, T., et al. (2005). Hybrid Vibrio vulnificus. *Emerg. Infect. Dis.* 11, 30–35. doi: 10.3201/eid1101.040440

Blodgett, R., (2015). BAM Appendix 2: Most Probable Number from Serial Dilutions | FDA [WWW Document]. Available at: https://www.fda.gov/food/laboratory-methods-food/bam-appendix-2-most-probable-number-serial-dilutions (Accessed June 23, 2020).

Brehm, T. T., Berneking, L., Rohde, H., Chistner, M., Schlickewei, C., Sena Martins, M., et al. (2020). Wound infection with *Vibrio harveyi* following a traumatic leg amputation after a motorboat propeller injury in Mallorca, Spain: a case report and review of literature. *BMC Infect. Dis.* 20:104. doi: 10.1186/s12879-020-4789-2

Cabral, J. P. S. (2010). Water microbiology. Bacterial pathogens and water. *Int. J. Environ. Res. Public Health* 7, 3657–3703. doi: 10.3390/ijerph7103657

CDC (1999). Outbreak of *Vibrio parahaemolyticus* infection associated with eating raw oysters and clams harvested from long Island sound--Connecticut, New Jersey, and New York, 1998. *MMWR Morb. Mortal. Wkly Rep.* 48, 48–51.

CDC (2015). Recommendations for the Use of Antibiotics for the Treatment of Cholera [WWW Document]. Available at: https://www.cdc.gov/cholera/treatment/antibiotic-treatment.html (Accessed December 16, 2019).

CDC (2017). Vibriosis | 2017 Case Definition. Available at: https://wwwn.cdc.gov/nndss/conditions/vibriosis/case-definition/2017/ (Accessed June 21, 2020).

Ceccarelli, D., Chen, A., Hasan, N. A., Rashed, S. M., Huq, A., and Colwell, R. R. (2015). Non-O1/non-O139 *Vibrio cholerae* carrying multiple virulence factors and *V. cholerae* O1 in the Chesapeake Bay, Maryland. *Appl. Environ. Microbiol.* 81, 1909–1918. doi: 10.1128/AEM.03540-14

Ceccarelli, D., and Colwell, R. R. (2014). Vibrio ecology, pathogenesis, and evolution. *Front. Microbiol.* 5:256. doi: 10.3389/fmicb.2014.00256

Chakraborty, R., Sinha, S., Mukhopadhyay, A. K., Asakura, M., Yamasaki, S., Bhattacharya, S. K., et al. (2006). Species-specific identification of *Vibrio*

fluvialis by PCR targeted to the conserved transcriptional activation and variable membrane tether regions of the toxR gene. *J. Med. Microbiol.* 55, 805–808. doi: 10.1099/jmm.0.46395-0

Chigor, V. N., Sibanda, T., and Okoh, A. I. (2012). Studies on the bacteriological qualities of the Buffalo River and three source water dams along its course in the Eastern Cape Province of South Africa. *Environ. Sci. Pollut. Res. Int.* 20, 4125–4136. doi: 10.1007/s11356-012-1348-4

Chowdhury, G., Ghosh, S., Pazhani, G. P., Paul, B. K., Maji, D., Mukhopadhyay, A. K., et al. (2013). Isolation and characterization of pandemic and nonpandemic strains of *Vibrio parahaemolyticus* from an outbreak of diarrhea in north 24 Parganas, West Bengal, India. *Foodborne Pathog. Dis.* 10, 338–342. doi: 10.1089/fpd.2012.1340

Christine, C., Sindiswa, N., and Imelda, H. (2013). An Introduction to South Africa's water sources areas [WWW Document]. Available at: www.journeyofwater.co.za (Accessed January 14, 2020).

Colvin, C., Muruven, D., Lindley, D., and Schachtschneider, K. (2016). Water: Facts and Futures Rethinking South Africa's Water Future [WWW Document]. Available at: http://awsassets.wwf.org.za/downloads/wwf009_waterfactsandfutures_report_web__lowres_.pdf (Accessed January 14, 2020).

Colwell, J. J. (2016). The Effects of Temperature and Salinity on Vibrio Species in Breton Sound Estuary. LSU Master's Theses.

Comins, L. (2012). Deadly bug hits beaches. Available at: https://www.iol.co.za/news/south-africa/kwazulu-natal/deadly-bug-hits-beaches-1227227 (Accessed June 01, 2020).

Copin, S., Robert-Pillot, A., Malle, P., Quilici, M. L., and Gay, M. (2012). Evaluation of most-probable-number-PCR method with internal amplification control for the counting of total and pathogenic *Vibrio parahaemolyticus* in frozen shrimps. *J. Food Prot.* 75, 150–153. doi: 10.4315/0362-028X.JFP-11-165

Cottle, E., and Deedat, H. (2002). The cholera outbreak: a 2000–2002 case study of the source of the outbreak in the Madlebe Tribal Authority areas, uThungulu Region, KwaZulu-Natal. Durban: Health Systems Trust.

de Menezes, F. G. R., da Neves, S. S., Sousa, O. V., Vila-Nova, C. M. V. M., Maggioni, R., Theophilo, G. N. D., et al. (2014). Detecção de genes de virulência em estirpes de *Vibrio cholerae* isolados de estuários no Nordeste do Brasil. *Rev. Inst. Med. Trop. Sao Paulo* 56, 427–432. doi: 10.1590/S0036-46652014000500010

de Menezes, F. G. R., Rodriguez, M. T. T., de Carvalho, F. C. T., Rebouças, R. H., Costa, R. A., de Sousa, O. V., et al. (2017). Pathogenic *Vibrio* species isolated from estuarine environments (Ceará, Brazil) - antimicrobial resistance and virulence potential profiles. *An. Acad. Bras. Cienc.* 89, 1175–1188. doi: 10.1590/0001-3765201720160191

De Souza Costa Sobrinho, P., Destro, M. T., Franco, B. D. G. M., and Landgraf, M. (2010). Correlation between environmental factors and prevalence of *Vibrio parahaemolyticus* in oysters harvested in the southern coastal area of Sao Paulo state, Brazil. *Appl. Environ. Microbiol.* 76, 1290–1293. doi: 10.1128/AEM.00861-09

Decol, L. T., Casarin, L. S., Hessel, C. T., Batista, A. C. F., Allende, A., and Tondo, E. C. (2017). Microbial quality of irrigation water used in leafy green production in Southern Brazil and its relationship with produce safety. *Food Microbiol.* 65, 105–113. doi: 10.1016/j.fm.2017.02.003

Deen, J., Mengel, M. A., and Clemens, J. D. (2019). Epidemiology of cholera. *Vaccine* 38, A31–A40. doi: 10.1016/j.vaccine.2019.07.078

Delahoy, M. J., Wodnik, B., McAliley, L., Penakalapati, G., Swarthout, J., Freeman, M. C., et al. (2018). Pathogens transmitted in animal feces in low- and middle-income countries. *Int. J. Hyg. Environ. Health* 221, 661–676. doi: 10.1016/j.ijheh.2018.03.005

DePaola, A., Nordstrom, J. L., Bowers, J. C., Wells, J. G., and Cook, D. W. (2003). Seasonal abundance of total and pathogenic *Vibrio parahaemolyticus* in Alabama oysters. *Appl. Environ. Microbiol.* 69, 1521–1526. doi: 10.1128/AEM.69.3.1521-1526.2003

Di, D. Y. W., Lee, A., Jang, J., Han, D., and Hur, H. G. (2017). Season-specific occurrence of potentially pathogenic *Vibrio* spp. on the southern coast of South Korea. *Appl. Environ. Microbiol.* 83, e02680–e02616. doi: 10.1128/AEM.02680-16

Drake, S. L., Depaola, A., and Jaykus, L. (2007). An overview of *Vibrio vulnificus* and *Vibrio parahaemolyticus*. *Compr. Rev. Food Sci. Food Saf.* 6, 120–144. doi: 10.1111/j.1541-4337.2007.00022.x

Dufour, A., Bartram, J., Bos, R., and Gannon, V. (2013). Animal waste, water quality and human health. *Water Intell. Online* 12, 1–10. doi: 10.2166/9781780401249

Dungeni, M., van Der Merwe, R. R., and Momba, M. N. B. (2010). Abundance of pathogenic bacteria and viral indicators in chlorinated effluents produced by four wastewater treatment plants in the Gauteng Province, South Africa. *Water SA* 36, 607–614. doi: 10.4314/wsa.v36i5.61994

Edokpayi, J. N., Odiyo, J. O., and Durowoju, O. S. (2017). "Impact of wastewater on surface water quality in developing countries: a case study of South Africa" in *Water quality*. ed. H. Tutu (Rijeka, Croatia: InTech), 401–416.

Elhadi, N. (2013). Occurrence of potentially human pathogenic *Vibrio* species in the coastal water of the Eastern Province of Saudi Arabia. *Res. J. Microbiol.* 8, 1–12. doi: 10.3923/jm.2013.1.12

Esteves, K., Hervio-Heath, D., Mosser, T., Rodier, C., Tournoud, M.-G., Jumas-Bilak, E., et al. (2015). Rapid proliferation of *Vibrio parahaemolyticus*, *Vibrio vulnificus*, and *Vibrio cholerae* during freshwater flash floods in French Mediterranean Coastal Lagoons. *Appl. Environ. Microbiol.* 81, 7600–7609. doi: 10.1128/AEM.01848-15

European Commission (2001). Opinion of the scientific committee on veterinary measures relating to public health on Vibrio vulnificus and *Vibrio parahaemolyticus* (in raw and undercooked seafood).

Fatoki, O. S., Muyima, N. Y. O., and Lujiza, N. (2001). Situation analysis of water quality in the Umtata River catchment. *Water SA* 27, 467–473. doi: 10.4314/wsa.v27i4.4959

Fernández-delgado, A. M., Sanz, V., Giner, S., Contreras, M., and Michelangeli, F. (2015). Prevalence and distribution of *Vibrio* spp. in wild aquatic birds of the Southern Caribbean Sea, Venezuela, 2011–12. *J. Wildl. Dis.* 52, 621–626. doi: 10.7589/2015-06-154

Finkelstein, R., Edelstein, S., and Mahamid, G. (2002). Fulminant wound infections due to *Vibrio vulnificus*. *Isr. Med. Assoc. J.* 4, 654–655.

Finkelstein, R. A. (1996). Cholera, *Vibrio cholerae* O1 and O139, and Other Pathogenic *Vibrios*, Medical Microbiology. University of Texas Medical Branch at Galveston.

Fu, S., Hao, J., Yang, Q., Lan, R., Wang, Y., Ye, S., et al. (2019). Long-distance transmission of pathogenic *Vibrio* species by migratory waterbirds: a potential threat to the public health. *Sci. Rep.* 9:16303. doi: 10.1038/s41598-019-52791-5

Fukushima, H., and Seki, R. (2004). Ecology of *Vibrio vulnificus* and *Vibrio parahaemolyticus* in brackish environments of the Sada River in Shimane Prefecture, Japan. *FEMS Microbiol. Ecol.* 48, 221–229. doi: 10.1016/j.femsec.2004.01.009

Glenn Morris, J. Jr. (1994). "Non-O group 1 *Vibrio cholerae* strains not associated with epidemic disease," in *Vibrio Cholerae and Cholera*. eds. I. K. Wachsmuth, P. A. Blake and O. Olsvik (Wiley: American Society of Microbiology), 103–115.

Goel, A. K., Jain, M., Kumar, P., Kamboj, D. V., and Singh, L. (2010). Virulence profile and clonal relationship among the *Vibrio cholerae* isolates from ground and surface water in a cholera endemic area during rainy season. *Folia Microbiol.* 55, 69–74. doi: 10.1007/s12223-010-0011-z

Grim, C. J., Hasan, N. A., Taviani, E., Haley, B., Chun, J., Brettin, T. S., et al. (2010). Genome sequence of hybrid *Vibrio cholerae* O1 MJ-1236, B-33, and CIRS101 and comparative genomics with *V. cholerae*. *J. Bacteriol.* 192, 3524–3533. doi: 10.1128/JB.00040-10

Guardiola-avila, I., Noriega-orozco, L., and Acedo-félix, E. (2015). Presence of the *Hemolysin* gene of *Vibrio mimicus* in fish and seafood products in Sonora, México. *J. Food Res.* 4, 66–76. doi: 10.5539/jfr.v4n1p66

Herbig, F. J. W., and Meissner, R. (2019). Talking dirty-effluent and sewage irreverence in South Africa: a conservation crime perspective. *Cogent Soc. Sci.* 5:1701359. doi: 10.1080/23311886.2019.1701359

Igbinosa, E. O., Obi, L. C., and Okoh, A. I. (2009). Occurrence of potentially pathogenic vibrios in final effluents of a wastewater treatment facility in a rural community of the Eastern Cape Province of South Africa. *Res. Microbiol.* 160, 531–537. doi: 10.1016/j.resmic.2009.08.007

Igbinosa, E. O., and Okoh, A. I. (2010). *Vibrio fluvialis*: an unusual enteric pathogen of increasing public health concern. *Int. J. Environ. Res. Public Health* 7, 3628–3643. doi: 10.3390/ijerph7103628

Igbinosa, E. O., Obi, L. C., and Okoh, A. I. (2011a). Seasonal abundance and distribution of *Vibrio* species in the treated effluent of wastewater treatment facilities in suburban and urban communities of Eastern Cape Province, South Africa. *J. Microbiol.* 49, 224–232. doi: 10.1007/s12275-011-0227-x

Igbinosa, E. O., Obi, L. C., Tom, M., and Okoh, A. I. (2011b). Detection of potential risk of wastewater effluents for transmission of antibiotic

resistance from Vibrio species as a reservoir in a peri-urban community in South Africa. *Int. J. Environ. Health Res.* 21, 402–414. doi: 10.1080/09603123.2011.572278

Jaiani, E., Kokashvili, T., Mitaishvili, N., Elbakidze, T., Janelidze, N., Lashkhi, N., et al. (2013). Microbial water quality of recreational lakes near Tbilisi, Georgia. *J. Water Health* 11, 333–345. doi: 10.2166/wh.2013.057

Janelidze, N., Jaiani, E., Lashkhi, N., Tskhvediani, A., Kokashvili, T., Gvarishvili, T., et al. (2011). Microbial water quality of the Georgian coastal zone of the Black Sea. *Mar. Pollut. Bull.* 62, 573–580. doi: 10.1016/j.marpolbul.2010.11.027

Jones, J. L. (2017). "Chapter 11 - Vibrio" in *Foodborne Diseases. 3rd Edn*. eds. C. E. R. Dodd, T. Aldsworth, R. A. Stein, D. O. Cliver and H. P. Riemann (Academic Press), 243–252.

Jones, M. K., and Oliver, J. D. (2009). *Vibrio vulnificus*: disease and pathogenesis. *Infect. Immun.* 77, 1723–1733. doi: 10.1128/IAI.01046-08

Jones, S., and Summer-Brason, B. (1998). Incidence and detection of pathogenic "*Vibrio*" sp. in a northern New England estuary, USA. *J. Shellfish Res.* 17, 1665–1669.

Jordaan, K., Comeau, A. M., Khasa, D. P., and Bezuidenhout, C. C. (2019). An integrated insight into the response of bacterial communities to anthropogenic contaminants in a river: a case study of the Wonderfonteinspruit catchment area, South Africa. *PLoS One* 14:e0216758. doi: 10.1371/journal.pone.0216758

Kanungo, S., Sur, D., Ali, M., You, Y. A., Pal, D., Manna, B., et al. (2012). Clinical, epidemiological, and spatial characteristics of *Vibrio parahaemolyticus* diarrhea and cholera in the urban slums of Kolkata, India. *BMC Public Health* 12:830. doi: 10.1186/1471-2458-12-830

Kaspar, C. W., and Tamplin, M. L. (1993). Effects of temperature and salinity on the survival of *Vibrio vulnificus* in seawater and shellfish. *Appl. Environ. Microbiol.* 59, 2425–2429. doi: 10.1128/AEM.59.8.2425-2429.1993

Kazi, A., Mumtaz, A., Nazir, R., Ismail, T., and Akbar, S. (2005). Determination of clobazam by visible spectrophotometry in pure and pharmaceutical preparations. *Proc. Pak. Acad. Sci.* 42:133.

Kelly, M. T. (1982). Effect of temperature and salinity on *Vibrio* (Beneckea) vulnificus occurrence in a Gulf Coast environment. *Appl. Environ. Microbiol.* 44:820. doi: 10.1128/AEM.44.4.820-824.1982

Kirchberger, P. C., Orata, F. D., Barlow, E. J., Kauffman, K. M., Case, R. J., Polz, M. F., et al. (2016). A small number of phylogenetically distinct clonal complexes dominate a coastal *Vibrio cholerae* population. *Appl. Environ. Microbiol.* 82, 5576–5586. doi: 10.1128/AEM.01177-16

Klontz, K. C., Williams, L., Baldy, L. M., and Campos, M. (1993). Raw oyster-associated *Vibrio* infections: linking epidemiologic data with laboratory testing of oysters obtained from a retail outlet. *J. Food Prot.* 56, 977–979. doi: 10.4315/0362-028X-56.11.977

Kokashvili, T., Whitehouse, C. A., Tskhvediani, A., Grim, C. J., Elbakidze, T., Mitaishvili, N., et al. (2015). Occurrence and diversity of clinically important *Vibrio* species in the aquatic environment of Georgia. *Front. Public Health* 3:232. doi: 10.3389/fpubh.2015.00232

Kopprio, G. A., Neogi, S. B., Rashid, H., Alonso, C., Yamasaki, S., Koch, B. P., et al. (2020). *Vibrio* and bacterial communities across a pollution gradient in the bay of Bengal: unraveling their biogeochemical drivers. *Front. Microbiol.* 11:594. doi: 10.3389/fmicb.2020.00594

Kothary, M. H., Lowman, H., McCardell, B. A., and Tall, B. D. (2003). Purification and characterization of enterotoxigenic E1 Tor-like hemolysin produced by *Vibrio fluvialis*. *Infect. Immun.* 71, 3213–3220. doi: 10.1128/IAI.71.6.3213-3220.2003

Kwok, A. Y. C., Wilson, J. T., Coulthart, M., Ng, L. K., Mutharia, L., and Chow, A. W. (2002). Phylogenetic study and identification of human pathogenic Vibrio species based on partial hsp60 gone sequences. *Can. J. Microbiol.* 48, 903–910. doi: 10.1139/w02-089

Lei, S., Miyoshi, S., Kewei, B., Nakamura, M., Hiura, M., Tomochika, K., et al. (2000). Presence of *Hemolysin* genes (vmh, tdh and hlx) in isolates of *Vibrio mimicus* determined by polymerase chain reaction. *J. Health Sci.* 46, 63–65. doi: 10.1248/jhs.46.63

Letchumanan, V., Yin, W., Lee, L., and Chan, K. (2015). Prevalence and antimicrobial susceptibility of *Vibrio parahaemolyticu* s isolated from retail shrimps in Malaysia. *Front. Microbiol.* 6:33. doi: 10.3389/fmicb.2015.00033

Levinson, W., and Jawetz, E. (1996). Medical Microbiology and Immunology 4th Edition by Levinson, Warren E., Jawetz, Ernest (1996) Paperback: Amazon.com: Books [WWW Document]. Availabe at: https://www.amazon.com/Medical-Microbiology-Immunology-Levinson-Paperback/dp/B011DBKQS0 (Accessed June 1, 2020).

Li, D., Jiang, X., Wang, J., Wang, K., and Zheng, B. (2017). Effect of sewage and industrial effluents on bacterial and archaeal communities of creek sediments in the Taihu Basin. *Water* 9:373. doi: 10.3390/w9060373

Liu, B., Liu, H., Pan, Y., Xie, J., and Zhao, Y. (2016). Comparison of the effects of environmental parameters on the growth variability of *Vibrio parahaemolyticus* coupled with strain sources and genotypes analyses. *Front. Microbiol.* 7:994. doi: 10.3389/fmicb.2016.00994

Liu, H., Whitehouse, C. A., and Li, B. (2018). Presence and persistence of *Salmonella* in water: the impact on microbial quality of water and food safety. *Front. Public Health* 6:159. doi: 10.3389/fpubh.2018.00159

Machado, A., and Bordalo, A. A. (2016). Detection and quantification of *Vibrio cholerae*, *Vibrio parahaemolyticus*, and *Vibrio vulnificus* in coastal waters of Guinea-Bissau (West Africa). *EcoHealth* 13, 339–349. doi: 10.1007/s10393-016-1104-1

Maclennan, S. (2019). Fish River sewage and Makhanda: DWS answers questions [WWW Document]. Avilable at: https://www.grocotts.co.za/2019/06/25/dws-takes-muni-to-court-over-sewage/ (Accessed May 22, 2020).

Madoroba, E., and Momba, M. N. (2010). Prevalence of vibrio cholerae in rivers of Mpumalanga province, South Africa as revealed by polyphasic characterization. *Afr. J. Biotechnol.* 9, 7295–7301.

Mahoney, J. C., Gerding, M. J., Jones, S. H., and Whistler, C. A. (2010). Comparison of the pathogenic potentials of environmental and clinical *Vibrio parahaemolyticus* strains indicates a role for temperature regulation in virulence. *Appl. Environ. Microbiol.* 76, 7459–7465. doi: 10.1128/AEM.01450-10

Maje, M. D., Kaptchouang Tchatchouang, C. D., Manganyi, M. C., Fri, J., and Ateba, C. N. (2020). Characterisation of *Vibrio* species from surface and drinking water sources and assessment of biocontrol potentials of their bacteriophages. *Int. J. Microbiol.* 2020:8863370. doi: 10.1155/2020/8863370

Marie, V., and Lin, J. (2018). Microbial indicators and environmental relationships in the Umhlangane River, Durban, South Africa. *Open Life Sci.* 13, 385–395. doi: 10.1515/biol-2018-0047

Maugeri, T. L., Carbone, M., Fera, M. T., and Gugliandolo, C. (2006). Detection and differentiation of *Vibrio vulnificus* in seawater and plankton of a coastal zone of the Mediterranean Sea. *Res. Microbiol.* 157, 194–200. doi: 10.1016/j.resmic.2005.06.007

McAllister, T. A., and Topp, E. (2012). Role of livestock in microbiological contamination of water: commonly the blame, but not always the source. *Anim. Front.* 2, 17–27. doi: 10.2527/af.2012-0039

Mema, V. (2008). Impact of Poorly Maintained Wastewater and Sewage Treatment Plants: Lessons From South Africa.

Mezgebe, K., Gebrekidan, A., Hadera, A., and Weldegebriel, Y. (2015). Assessment of physico-chemical parameters of Tsaeda Agam River in Mekelle City, Tigray, Ethiopia. *Bull. Chem. Soc. Ethiop.* 29, 377–385. doi: 10.4314/bcse.v29i3.5

Momba, M., and Azab El-Liethy, M. (2017). "Vibrio Cholerae And Cholera Biotypes," in *Water and Sanitation for the 21st Century: Health and Microbiological Aspects of Excreta and Wastewater Management (Global Water Pathogen Project*; Part 3: Specific Excreted Pathogens: Environmental and Epidemiology Aspects - Section 2: Bacteria. eds. A. Pruden, N. Ashbolt and J. Miller). eds. J. B. Rose and B. Jiménez-Cisneros. MI, UN: Michigan State University E. Lansing. Available at: http//www.waterpathogens.org/book/Vibrio (Accessed May 22, 2020).

Momba, M. N. B., Malakate, V. K., and Theron, J. (2006). Abundance of pathogenic *Escherichia coli*, *Salmonella typhimurium* and *Vibrio cholerae* in Nkonkobe drinking water sources. *J. Water Health* 4, 289–296. doi: 10.2166/wh.2006.011

Mookerjee, S., Batabyal, P., Sarkar, M. H., and Palit, A. (2015). Seasonal prevalence of Enteropathogenic *Vibrio* and their phages in the riverine estuarine ecosystem of South Bengal. *PLoS One* 10:e0137338. doi: 10.1371/journal.pone.0137338

Morris, J. (2019). Minor Vibrio and Vibrio-like species associated with human disease - UpToDate [WWW Document]. Available at: https://www.uptodate.com/contents/minor-vibrio-and-vibrio-like-species-associated-with-human-disease?search=minor-Vibrio-and-Vibrio-like-species-associated-with-human-disease&source=search_result&selectedTitle=1~150&usage_type=default&display_rank=1 (Accessed June 1, 2020).

Mudzanani, L., Ratsaka-Mathokoa, M., Mahlasela, L., Netshidzivhanii, P., and Mugero, C. (2003). *Cholera*. South African Health Review.

Munshi, S. K., Roy, J., and Noor, R. (2019). Microbiological investigation and determination of the antimicrobial potential of cow dung samples. *S. J. Microbiol.* 8, 34–37. doi: 10.3329/sjm.v8i1.42437

Mustapha, S., Mustapha, E. M., and Nozha, C. (2013). Vibrio alginolyticus: an emerging pathogen of foodborne diseases. *Maejo Int. J. Sci. Technol.* 2, 302–309.

Nevondo, T., and Cloete, T. (2001). The global cholera pandemic. Science in Africa [WWW Document]. Available at: http://www.scienceinafrica.com/global-cholera-pandemic (Accessed June 1, 2020).

Nilsson, W. B., Paranjpye, R. N., Hamel, O. S., Hard, C., and Strom, M. S. (2019). *Vibrio parahaemolyticus* risk assessment in the Pacific Northwest: It's not what's in the water. *FEMS Microbiol. Ecol.* 95:fiz027. doi: 10.1093/femsec/fiz027

Nongogo, V., and Okoh, A. I. (2014). Occurrence of vibrio pathotypes in the final effluents of five wastewater treatment plants in Amathole and Chris Hani District municipalities in South Africa. *Int. J. Environ. Res. Public Health* 11, 7755–7766. doi: 10.3390/ijerph110807755

Novotny, L., Dvorska, L., Lorencova, A., Beran, V., and Pavlik, V. (2004). Fish: a potential source of bacterial pathogens for human beings. *Vet. Med.* 49, 343–358. doi: 10.17221/5715-VETMED

Ntema, V. M., Potgieter, N., and Barnard, T. G. (2010). Detection of *Vibrio cholerae* and *Vibrio parahaemolyticus* by molecular and culture based methods from source water to household container-stored water at the point-of-use in South African rural communities. *Water Sci. Technol.* 61, 3091–3102. doi: 10.2166/wst.2010.222

Ntema, V. M., Potgieter, N., Van Blerk, G. N., and Barnard, T. G. (2014). Investigating the occurrence and survival of *Vibrio cholerae* in selected surface water sources in the KwaZulu-Natal province of South Africa Report to the Water Research Commission.

Okeyo, A. N., Nontongana, N., Fadare, T. O., and Okoh, A. I. (2018). *Vibrio* species in wastewater final effluents and receiving watershed in South Africa: implications for public health. *Int. J. Environ. Res. Public Health*. 1266:15. doi: 10.3390/ijerph15061266

Okoh, A. I., Sibanda, T., Nongogo, V., Adefisoye, M., Olayemi, O. O., and Nontongana, N. (2015). Prevalence and characterisation of non-cholerae *Vibrio* spp. in final effluents of wastewater treatment facilities in two districts of the Eastern Cape Province of South Africa: implications for public health. *Environ. Sci. Pollut. Res.* 22, 2008–2017. doi: 10.1007/s11356-014-3461-z

Oliver, J. D., and Bockian, R. (1995). In vivo resuscitation, and virulence towards mice, of viable but nonculturable cells of Vibrio vulnificus. *Appl. Environ. Microbiol.* 61, 2620–2623. doi: 10.1128/AEM.61.7.2620-2623.1995

Oliver, J. D., Nilsson, L., and Kjelleberg, S. (1991). Formation of nonculturable *Vibrio vulnificus* cells and its relationship to the starvation state. *Appl. Environ. Microbiol.* 57:2640. doi: 10.1128/AEM.57.9.2640-2644.1991

Osorio, C. R., and Klose, K. E. (2000). A region of the transmembrane regulatory protein ToxR that tethers the transcriptional activation domain to the cytoplasmic membrane displays wide divergence among vibrio species. *J. Bacteriol.* 182, 526–528. doi: 10.1128/JB.182.2.526-528.2000

Osunla, C. A., and Okoh, A. I. (2017). *Vibrio* pathogens: a public health concern in rural water resources in sub-Saharan Africa. *Int. J. Environ. Res. Public Health* 14, 1–27. doi: 10.3390/ijerph14101188

Paranjpye, R. N., Nilsson, W. B., Liermann, M., Hilborn, E. D., George, B. J., Li, Q., et al. (2015). Environmental influences on the seasonal distribution of *Vibrio parahaemolyticus* in the Pacific Northwest of the USA. *FEMS Microbiol. Ecol.* 91:fiv121. doi: 10.1093/femsec/fiv121

Payne, S. M., Mey, A. R., and Wyckoff, E. E. (2016). *Vibrio* iron transport: evolutionary adaptation to life in multiple environments. *Microbiol. Mol. Biol. Rev.* 80, 69–90. doi: 10.1128/MMBR.00046-15

Penakalapati, G., Swarthout, J., Delahoy, M. J., Mcaliley, L., Wodnik, B., Levy, K., et al. (2017). Exposure to animal feces and human health: a systematic review and proposed research priorities. *Environ. Sci. Technol.* 51, 11537–11552. doi: 10.1021/acs.est.7b02811

Prasanthan, V., Udayakumar, P., and Ouseph, P. P. (2011). Influence of abiotic environmental factors on the abundance and distribution of *Vibrio* species in coastal waters of Kerala, India. *Indian J. Geo-Mar. Sci.* 40, 587–592.

Rabea, E., Bahia, B., Youssef, M., Ahlam, F., Ghita El, M., Bouchra, O., et al. (2019). Microbiological and physicochemical characterization of hospital effluents before and after treatment with two types of sawdust. *J. Chem.* 2019, 1–10. doi: 10.1155/2019/3275101

Ramamurthy, T., Albert, M. J., Huq, A., Colwell, R. R., Takeda, Y., Takeda, T., et al. (1994). *Vibrio* mimicus with multiple toxin types isolated from human and environmental sources. *J. Med. Microbiol.* 40, 194–196. doi: 10.1099/00222615-40-3-194

Ramos, R. J., Miotto, L. A., Miotto, M., Silveira Junior, N., Cirolini, A., da Silva, H. S., et al. (2014). Occurrence of potentially pathogenic *Vibrio* in oysters (*Crassostrea gigas*) and waters from bivalve mollusk cultivations in the South Bay of Santa Catarina. *Rev. Soc. Bras. Med. Trop.* 47, 327–333. doi: 10.1590/0037-8682-0069-2014

Randa, M. A., Polz, M. F., and Lim, E. (2004). Effects of temperature and salinity on *Vibrio vulnificus* population dynamics as assessed by quantitative PCR. *Appl. Environ. Microbiol.* 70, 5469–5476. doi: 10.1128/AEM.70.9.5469-5476.2004

Rees, G., Pond, K., and Kay, D. (2010). Safe management of shellfish and harvest waters. *Water Intell. Online* 12, 1–10. doi: 10.2166/9781780405797

Reimer, A. R., Domselaar, G. Van Stroika, S., Walker, M., Kent, H., Tarr, C., et al. (2011). Comparative genomics of *Vibrio cholerae* from Haiti, Asia, and Africa. *Emerg. Infect. Dis.* 17, 2113–2121. doi: 10.3201/eid1711.110794

Rippey, S. R. (1994). Infectious diseases associated with molluscan shellfish consumption. *Clin. Microbiol. Rev.* 7, 419–425. doi: 10.1128/CMR.7.4.419

Romalde, J. L., Diéguez, A. L., Lasa, A., and Balboa, S. (2014). New *Vibrio* species associated to molluscan microbiota: a review. *Front. Microbiol.* 4:413. doi: 10.3389/fmicb.2013.00413

Safa, A., Nair, G. B., and Kong, R. Y. C. (2009). Evolution of new variants of *Vibrio cholerae* O1. *Trends Microbiol.* 18, 46–54. doi: 10.1016/j.tim.2009.10.003

Sarkar, B. L., Nair, G. B., Banerjee, A. K., and Pal, S. C. (1985). Seasonal distribution of *Vibrio parahaemolyticus* in freshwater environs and in association with freshwater fishes in Calcutta. *Appl. Environ. Microbiol.* 49, 132–136. doi: 10.1128/AEM.49.1.132-136.1985

Shaheen, A., Saeed Baig, H., Shahana, A., and Kazmi, U. (2016). Microbial flora isolated from polluted and non-polluted coastal waters of Karachi. *Pak. J. Bot.* 48, 1703–1708.

Sharma, A., and Chaturvedi, A. N. (2007). Population dynamics of *Vibrio* species in the river Narmada at Jabalpur. *J. Environ. Biol.* 28, 747–751.

Sharma, C., Thungapathra, M., Ghosh, A., Mukhopadhyay, A. K., Basu, A., Mitra, R., et al. (1998). Molecular analysis of non-O1, non-O139 *Vibrio cholerae* associated with an unusual upsurge in the incidence of cholera-like disease in Calcutta, India. *J. Clin. Microbiol.* 36, 756–763.

Shinoda, S., Nakagawa, T., Shi, L., Bi, K., Kanoh, Y., Tomochika, K., et al. (2004). Distribution of virulence-associated genes in *Vibrio mimicus* isolates from clinical and environmental origins. *Microbiol. Immunol.* 48, 547–551. doi: 10.1111/j.1348-0421.2004.tb03551.x

Skall, H. F., and Olesen, N. J. (2011). Treatment of wastewater from fish slaugtherhouses. Evaluation and recommendations for hyginisation methods, National Veterinary Institute, Technical University of Denmark.

Sultan, Z., Mizuno, T., Sakurai, A., Takata, N., Okamoto, K., and Miyoshi, S.-I. (2007). Growth phase dependant activation of the precursor of *Vibrio mimicus* Hemolysin (Pro-VMH). *J. Health Sci.* 53, 430–434. doi: 10.1248/jhs.53.430

Takemura, A. F., Chien, D. M., and Polz, M. F. (2014). Associations and dynamics of vibrionaceae in the environment, from the genus to the population level. *Front. Microbiol.* 5:38. doi: 10.3389/fmicb.2014.00038

Tantillo, G. M., Fontanarosa, M., Pinto, A. Di, and Musti, M. (2004). Updated perspectives on emerging vibrios associated with human infections. *Lett. Appl. Microbiol.* 39, 117–126. doi: 10.1111/j.1472-765X.2004.01568.x

Tarr, C. L., Patel, J. S., Puhr, N. D., Sowers, E. G., Bopp, C. A., and Strockbine, N. A. (2007). Identification of Vibrio isolates by a multiplex PCR assay and rpoB sequence determination. *J. Clin. Microbiol.* 45, 134–140. doi: 10.1128/JCM.01544-06

Topalcengiz, Z., Strawn, L. K., and Danyluk, M. D. (2017). Microbial quality of agricultural water in Central Florida. *PLoS One* 12:e0174889. doi: 10.1371/journal.pone.0174889

Turner, J. W., (1997). Environmental factors and reservoir shifts contribute to the seasonality of pathogenic.

Urquhart, E. A., Jones, S. H., Yu, J. W., Schuster, B. M., Marcinkiewicz, A. L., Whistler, C. A., et al. (2016). Environmental conditions associated with elevated *Vibrio parahaemolyticus* concentrations in Great Bay Estuary, New Hampshire. *PLoS One* 11:e0155018. doi: 10.1371/journal.pone.0155018

USEPA (2001). Source Water Protection Practices Bulletin Managing Septic Systems to Prevent Contamination of Drinking Water. United States Environ. Prot. Agency i, July.

Venkateswaran, K., Kiiyukia, C., Takaki, M., Nakano, H., Matsuda, H., Kawakami, H., et al. (1989). Characterization of toxigenic vibrios isolated from the freshwater environment of Hiroshima, Japan. *Appl. Environ. Microbiol.* 55, 2613–2618. doi: 10.1128/AEM.55.10.2613-2618.1989

Vinothkumar, K., Kushwaha, A., and Ramamurthy, T. (2013). Triplex PCR assay for the rapid identi fi cation of 3 major *Vibrio species*, *Vibrio cholerae*, *Vibrio parahaemolyticus*, and *Vibrio fluvialis*. *Diagn. Microbiol. Infect. Dis.* 76, 526–528. doi: 10.1016/j.diagmicrobio.2013.04.005

Watkins, W. D., and Cabelli, V. J. (1985). Effect of Fecal pollution on *Vibrio parahaemolyticus* densities in an estuarine environment. *Appl. Environ. Microbiol.* 49, 1307–1313. doi: 10.1128/AEM.49.5.1307-1313.1985

Wei, S., Zhao, H., Xian, Y., Hussain, M. A., and Wu, X. (2014). Multiplex PCR assays for the detection of *Vibrio alginolyticus*, *Vibrio parahaemolyticus*, *Vibrio vulnificus*, and *Vibrio cholerae* with an internal amplification control. *Diagn. Microbiol. Infect. Dis.* 79, 115–118. doi: 10.1016/j.diagmicrobio.2014.03.012

Wong, R. S. Y., and Chow, A. W. (2002). Identification of enteric pathogens by heat shock protein 60 kDa (HSP60) gene sequences. *FEMS Microbiol. Lett.* 206, 107–113. doi: 10.1111/j.1574-6968.2002.tb10994.x

Zhou, S., Hou, Z., Li, N., and Qin, Q. (2007). Development of a SYBR green I real-time PCR for quantitative detection of *Vibrio alginolyticus* in seawater and seafood. *J. Appl. Microbiol.* 103, 1897–1906. doi: 10.1111/j.1365-2672.2007.03420.x

Conflict of Interest: The authors declare that the research was conducted in the absence of any commercial or financial relationships that could be construed as a potential conflict of interest.

frontiers in Microbiology

ORIGINAL RESEARCH
published: 08 June 2021
doi: 10.3389/fmicb.2021.669570

Microbiome Analysis Reveals Microecological Balance in the Emerging Rice–Crayfish Integrated Breeding Mode

*Yi Wang[1], Chen Wang[1,2], Yonglun Chen[1,2], Dongdong Zhang[3], Mingming Zhao[1], Hailan Li[1] and Peng Guo[1,2]**

[1] Institute of Agricultural Products Processing and Nuclear Agriculture Technology Research, Hubei Academy of Agricultural Sciences, Wuhan, China, [2] College of Biology and Pharmacy, Three Gorges University, Yichang, China, [3] Institute of Marine Biology, Ocean College, Zhejiang University, Zhoushan, China

The interaction between the microbial communities in aquatic animals and those in the ambient environment is important for both healthy aquatic animals and the ecological balance of aquatic environment. Crayfish (*Procambarus clarkii*), with their high commercial value, have become the highest-yield freshwater shrimp in China. The traditional cultivation in ponds (i.e., monoculture, MC) and emerging cultivation in rice co-culture fields (i.e., rice–crayfish co-culture, RC) are the two main breeding modes for crayfish, and the integrated RC is considered to be a successful rice-livestock integration practice in eco-agricultural systems. This study explored the ecological interactions between the microbial communities in crayfish intestine and the ambient environment, which have not been fully described to date. The bacterial communities in crayfish intestine, the surrounding water, and sediment in the two main crayfish breeding modes were analyzed with MiSeq sequencing and genetic networks. In total, 53 phyla and 1,206 genera were identified, among which Proteobacteria, Actinobacteria, Tenericutes, Firmicutes, Cyanobacteria, Chloroflexi, Bacteroidetes, Acidobacteria, RsaHF231, and Nitrospirae were the dominant phyla. The microbiota composition significantly differed between the water, sediment, and crayfish intestine, while it did not between the two breeding modes. We also generated a co-occurrence correlation network based on the high-confidence interactions with Spearman correlation $\rho \geq 0.75$. In the genera co-correlation network, 95 nodes and 1,158 edges were identified, indicating significant genera interactions between crayfish intestine and the environment. Furthermore, the genera clustered into three modules, based on the different environments. Additionally, *Candidatus_Bacilloplasma, g_norank_f_Steroidobacteraceae, Dinghuibacter, Hydrogenophaga, Methyloparacoccus*, and *Defluviicoccus* had the highest betweenness centrality and might be important in the interaction between crayfish and the ambient environment. Overall, this study enhances our understanding of the characteristics of the microbiota in crayfish and their surrounding environment. Moreover, our findings provide insights into the microecological balance in crayfish eco-agricultural systems and theoretical reference for the development of such systems.

Keywords: aquaculture environment, eco-agriculture, gut microbiota, microbial interaction, genetic network

OPEN ACCESS

Edited by:
Rodrigo Gouvea Taketani, Rothamsted Research, United Kingdom

Reviewed by:
Valeria D'Argenio, University of Naples Federico II, Italy
Pijush Basak, Jagadis Bose National Science Talent Search, India

***Correspondence:**
Peng Guo
gpeng_2008@cau.edu.cn

Specialty section:
This article was submitted to Aquatic Microbiology, a section of the journal Frontiers in Microbiology

Received: *19 February 2021*
Accepted: *11 May 2021*
Published: *08 June 2021*

Citation:
Wang Y, Wang C, Chen Y, Zhang D, Zhao M, Li H and Guo P (2021) Microbiome Analysis Reveals Microecological Balance in the Emerging Rice–Crayfish Integrated Breeding Mode. Front. Microbiol. 12:669570. doi: 10.3389/fmicb.2021.669570

INTRODUCTION

The crayfish (*Procambarus clarkii*) was originally found in the southeastern United States but was introduced into China in the late 1930s. Crayfishes dig burrows as refugia against environmental stresses such as dehydration, low temperature, lack of food, and predation, and thus exhibit strong environmental adaptability. Notably, damage to agricultural fields, including uprooting, plant fragmentation, seedling consumption, and interference with seed germination and seedling establishment, has made them a pest in many countries (Si et al., 2017). However, in recent years, as crayfish have become a table delicacy, their value has remarkably increased. In China, crayfish aquaculture has increased rapidly, and crayfish has become the highest-yield freshwater shrimp. From 2003 to 2018, the yield of crayfish increased more than 30 times. In 2018, crayfish aquaculture used an area of 1.12 million hectares, its yield was of 1.64 million tons, and its total economic output was of 369 billion yuan (Bureau of Fisheries et al., 2019).

There are two main breeding modes for crayfish, namely the traditional cultivation in pond (i.e., crayfish monoculture, MC) and emerging cultivation in rice co-culture fields (i.e., rice–crayfish co-culture, RC). In the latter, crayfishes are bred in waterlogged rice fields, and this mode takes advantage of the shallow water environment and the idle production period of rice paddies in winter (Si et al., 2017). Furthermore, the combination of agriculture and aquaculture raises the utilization and productivity rates of the fields. Thus, RC is favorable, considering the increasing shortage of farmland resources. In 2018, RC occupied 0.84 million hectares in China, accounting for 75.1% of the total crayfish aquiculture area (National Bureau of Statistics of China [NBSPRC], 2018). RC is one of the most popular rice–livestock integration practices (Yang et al., 2019). Nevertheless, due to the use of fertilizers in rice farming and the return of rice straw to the field in RCs, there is a concern about their influence on both the surrounding environment and crayfish health. For instance, it has been documented that organic compound accumulation negatively affects the ambient microbial equilibrium by enriching potential pathogens and reducing probiotics, thereby causing environmental stresses in aquaculture (Sun et al., 2020).

In contrast to terrestrial animals, aquatic animals are directly exposed to the ambient microbiota in aquaculture ecosystems. Environmental microbes not only directly influence aquatic animals but also influence their gut microbes. Recently, numerous studies found that environmental microbes, such as Proteobacteria (Hou et al., 2018), Chloroflexi (Björnsson et al., 2002; Lv et al., 2018), Acidobacteria (Dedysh and Damsté, 2018), Cyanobacteria (Zehr and Ward, 2002; Hou et al., 2018), and Nitrospirae (Zecchin et al., 2018), play important roles in matter and energy recycling, and some of them contribute to the decomposition of eutrophication pollution (Douterelo et al., 2004). Furthermore, many gut microbes are derived from the aquaculture environment, and the gut microbiota are strongly influenced by ambient microbial communities (Zhao et al., 2020). The internal microbiota plays crucial roles in the nutrition, immunity, and disease resistance of animals (Giatsis et al., 2015; Carbone and Faggio, 2016). A previous study reported that the ratio of Firmicutes to Bacteroidetes in shrimp intestines was positively related to lipid metabolism (Sun et al., 2020). Some Proteobacteria (Shin et al., 2015) and Tenericutes (Huang et al., 2020) were considered to be opportunistic pathogens of aquatic animals, while Actinobacteria might be a good candidate for screening native aquatic probiotics (Mahajan and Balachandran, 2012; Liberton et al., 2019). Therefore, a comprehensive comparison between the microbiota in the ambient environment and that in aquatic animals is critical for our understanding of the complex interactions between animals and their surroundings. In turn, the microbiota characteristics of aquatic animals and the ambient environment may serve as valuable indicators for the assessment of environmental conditions.

In freshwater aquaculture, the potential relationship between the microbial communities in crayfish intestine and those in the surroundings, and the differences between the microbial communities in the two main breeding modes, namely MC and RC, have seldom been studied. Therefore, in this study, we investigated the bacterial communities in water, sediment, and crayfish intestine samples obtained from these two breeding modes. In other words, this study explored the relationship between the microbial communities in crayfish intestine and those in the surrounding environment. In addition, the influence of RC on crayfish and their surroundings was evaluated by comparing the microbial communities in the RC and traditional MC breeding modes.

MATERIALS AND METHODS

Study Area

The experiment was carried out in Jianli County (29.91°N, 112.63°E), Hubei province, China, located in the Middle–Lower Yangtze Valley Plain. This area is low and flat, densely covered with rivers and lakes, and is one of the main production regions for both rice and crayfish. The soil type is waterloggogenic paddy soil, which has developed from river and lake sediments. The average annual temperature is 16.3°C, with a frost-free period of 255 days. The average annual rainfall is 1,226 mm (Liu et al., 2010).

Experimental Design and Plot Maintenance

Traditional crayfish breeding in the pond mode (MC) and rice–crayfish co-culture breeding in the rice paddy mode (RC) were investigated. To ensure consistency in the experimental conditions, the MC and RC were established five kilometers apart, in two stations on the same river. Three fields within the same station were selected for each breeding mode, and all the irrigation and aquaculture water was pumped from the river. Each subplot had a surface area of approximately 1,300 m^2 and was surrounded with 0.3-m-high nylon nets to prevent the crayfish from escaping. The RC field included a center paddy and a surrounding crayfish gutter that was 3.0–4.0 m wide and 1.0–1.5 m deep.

In the MC, routine feeding management was performed. In the RC, the field was irrigated after the harvest of mid-season rice, and the crayfish returned to the paddy along with the irrigation water at the beginning of October. Meanwhile, an additional broodstock was added as appropriate. All the rice straw was left in the paddy without tilling, and the crayfish grew in the paddy until the second season. Mature crayfishes were harvested at the beginning of June, and immature crayfishes migrated to the gutter after drainage of the paddy. Mid-season rice was planted by mechanical rotary tilling and artificial transplantation. A shrimp feed supply of 500 kg was added from March to May of each year, and the rice plants were fertilized with 120.0 kg/hm^2 N, 36.0 kg/hm^2 P_2O_5, and 60.0 kg/hm^2 K_2O each season.

Sample Collection

To evaluate the global effect of the emerging RC on farm ecology, we studied the end of the entire farming cycle. All crayfish, water, and sediment samples were collected from the six subplots when mature crayfishes were harvested at the beginning of June. In the RC, samples were taken from the crayfish gutter to mitigate disturbance of the shallow water environment in the paddy fields. Water samples (0.25 L) were taken from the surface, middle, and bottom of the aquaculture water, mixed together into one sample, and filtered through a 0.22-micrometer millipore filter (Millipore, Merck) for DNA extraction (Sun et al., 2020). Water samples from the MC were labeled as MCw1, MCw2, and MCw3, and those from the RC as RCw1, RCw2, and RCw3. Sediment samples (200 g) were collected with an S-shaped 5-point collection method within 5 cm from the surface mud (Fan et al., 2019). After mixing together into one sample, 50 g of the sediment sample was used for DNA extraction. Sediment samples obtained from the MC were labeled as MCs1, MCs2, and MCs3, and those from the RC as RCs1, RCs2, and RCs3. Twenty samples were taken from healthy crayfishes with similar weights (18.9 $\pm$ 2.6 g), and the scarfskin was sterilized with 75% ethanol (Huang et al., 2018). The intestines of these 20 crayfishes were then collected and pooled into one intestine sample for DNA extraction. Intestine samples from crayfish bred in the MC were labeled as MCc1, MCc2, and MCc3, and those from the fish bred in the RC as RCc1, RCc2, and RCc3. The final samples of water, sediment, and crayfish intestine were flash frozen with liquid nitrogen and stored at $-80°C$ until DNA extraction.

DNA Extraction, PCR Amplification, and MiSeq Sequencing

The total DNA of water, sediment, and crayfish intestine samples was extracted using the E.Z.N.A. Soil DNA kit (Omega, Norcross, GA) according to the manufacturer's instructions. DNA quantity and purity were detected using a NanoDrop 2000 microspectrophotometer (Thermo Fisher, Waltham, MA), and DNA integrity was assessed using 1% agarose gels. The V3-V4 hypervariable region of 16S rRNA was amplified using the 338F (5′-ACT CCT ACG GGG AGG CAG CAG-3′) and 806R (5′-GGA CTA CHV GGG TWT CTA AT-3′) primers to investigate the bacterial communities (Han et al., 2020). High-throughput sequencing was performed in a paired-end model using the Illumina MiSeq PE300 platform (Majorbio, China).

Bioinformatic and Statistical Analyses

Before proceeding with the analyses, raw data from the Illumina MiSeq platform were obtained with Flash (version 1.2.11)[1] and demultiplexed and quality-filtered using Qiime (version 1.9.1)[2]. Operational taxonomic units (OTUs) were clustered with a 97% similarity threshold using the Uparse software (version 7.0.1090)[3]. To correct for uneven sequencing efforts, OTU abundance information was normalized according to the least sequence number (Li et al., 2018). The normalized OTU abundance data were then used to calculate the diversity and distance between samples. The taxonomy of each OTU was classified with the RDP Classifier (version 2.11)[4], against the SILVA rRNA database (SSU132)[5], using a confidence threshold of 70% (Amato et al., 2013; Quast et al., 2013).

Alpha-diversity indices were calculated to illustrate the complexity of each sample, based on the normalization OTUs and using Mothur (version v.1.30.2; Schloss et al., 2011)[6], which included the community richness parameters Ace and Chao1 and diversity parameters, namely the Shannon and Simpson indices. Beta-diversity analyses, namely hierarchical clustering tree, heatmap, and principal coordinates analysis (PCoA) on OTUs levels, were performed based on the Bray-Curtis distance (Jiang et al., 2019). To compare the similarity of the microbial composition in the different samples, a dendrogram based on Bray–Curtis distances was generated using the unweighted pair-group method with arithmetic mean (UPGMA) and displayed at the top of the heatmap. Analysis of similarities (ANOSIM) and Adonis analysis were further performed to check the microbial community similarities between the MC and RC modes, and the significance levels between groups were determined with 999 permutations (Leung et al., 2016). Functional profiling was inferred from the 16S rRNA marker gene sequences using PICRUSt I (Blankenberg et al., 2010). That is, the presumptive functions of the microbial communities in the crayfish intestine and the surrounding environment, namely the water and sediment, were illustrated using PICRUSt. Moreover, the clusters of orthologous groups (COG) functions of the predicted genes were classified in the Eggnog databases.

Various network approaches were used to analyze the data sets. A bipartite co-occurrence network was generated using the treatments as source nodes and the OTUs as target nodes, with edges corresponding to the connection of particular OTUs with specific treatments, to visualize the associations between the genera and the different samples. We divided the 18 samples into six groups (MCs, RCs, MCw, RCw, MCc, and RCc), corresponding to three environments (water, sediment, and crayfish intestine). Species co-correlations were calculated based

[1]https://ccb.jhu.edu/software/FLASH/index.shtml
[2]http://qiime.org/install/index.html
[3]http://drive5.com/uparse
[4]https://sourceforge.net/projects/rdp-classifier/
[5]https://www.arb-silva.de/
[6]https://www.mothur.org/wiki/Download_mothur

on Spearman's rank correlation coefficient. The connections between two species that indicated a strong (i.e., Spearman correlation coefficient $\rho \geq 0.75$) and significant (i.e., $P < 0.05$) correlation were reserved and a co-correlation network was generated in Gephi (version v.0.9.3).

All reported values were the average of triplicate results (i.e., mean ± SD). Differences between populations were analyzed using a one-way ANOVA, and results with $P < 0.05$ were considered significant. Statistical analyses were performed and visualized on the online platform I-Sanger (Majorbio, Shanghai, China)[7], based on various R packages. The raw data of the 16S rDNA gene sequence reads from the 18 samples were deposited into the NCBI Sequence Read archive (SRA) database with the following BioProject accession number: PRJNA663764 (SRR12650255 to SRR12650272).

RESULTS

Characteristics of 16S rRNA Sequencing and Microbial Community Diversity

The bacterial 16S rRNA genes of the 18 samples were sequenced to study the microbial communities of crayfish intestines and the cultured environment, water, and sediment. After quality filtering and assignment, a total of 715,020 high-quality sequences were obtained, and the read depth was between 32,991 and 44,928 reads per sample (39,723 ± 3,026; raw sequence data are presented in **Supplementary Table 1**). Then, uneven sequencing depths were normalized to 32,991 reads in all samples, which generated a total of 6,347 OTUs, ranging from 334 to 3,434.

The average Good's coverage was 0.983342 (values ranged from 0.971 to 0.998) and indicated a saturated sequencing depth. The Ace and Chao1 indices were used to quantify species richness. The Ace index ranged from 371.882 to 4,277.969, and the Chao1 index ranged from 381.273 to 4,226.235 (**Figure 1** and **Supplementary Table 2**). As for the Shannon and Simpson indices, they were used to calculate species diversity. The Shannon index ranged from 2.250 to 7.111, and the Simpson index ranged from 0.002 to 0.255 (**Figure 1** and **Supplementary Table 2**). In general, the alpha diversity of the microbial community was similar between the two tested breeding modes but significantly differed according to the environment. The bacterial richness and diversity were the greatest in sediment, intermediate in water, and the lowest in crayfish intestine samples.

Overall Microbial Communities in Water, Sediment, and Crayfish Intestine

A total of 53 phyla were identified in the bacterial microbial communities in crayfish intestine and the cultured environment, namely the water and sediment. Low-abundance sequences (i.e., with <1% abundance) were combined and specified as "others". The top ten most abundant phyla, which accounted for approximately 93.4% of the total sequences, and their distribution across different categories (i.e., sediment, water, crayfish intestine – respective percentages are hereafter given in the same order) were as follows: Proteobacteria (33.71%; 38.09%; 28.20%), Actinobacteria (15.21%; 79.00%; 5.79%), Tenericutes (0.01%; 0.17%; 99.81%), Firmicutes (12.60%; 15.05%; 72.35%), Cyanobacteria (6.68%; 74.58%; 18.73%), Chloroflexi (92.71%; 3.98%; 3.31%), Bacteroidetes (44.81%; 48.54%; 6.64%), Acidobacteria (95.30%; 1.40%; 3.30%), RsaHF231 (0.00%; 0.13%; 99.87%), and Nitrospirae (95.73%; 1.38%; 2.89%; **Figure 2A**). The community pie charts in **Figure 2** show the overall microbial communities at the phylum level in water (**Figure 2B**), sediment (**Figure 2C**), and crayfish intestine (**Figure 2D**). Proteobacteria was uniformly dispersed in the three habitats. Bacteroidetes was mainly dispersed in water and sediment. Sediment samples contained the highest abundance of Chloroflexi, Acidobacteria, and Nitrospirae, water samples contained the highest abundance of Actinobacteria and Cyanobacteria, and the crayfish intestine samples contained the highest abundance of Tenericutes, Firmicutes, and RsaHF231.

When the OTUs were analyzed at the genus level, a high diversity of microbes was identified. A total of 1,206 genera were detected across all 18 samples. Sixteen had a relative abundance greater than 1% and are shown in **Figure 3A**. Then, the top 40 most abundant genera were selected to generate a heatmap along with the clustering tree to visualize their distribution (**Figure 3B**). We observed that the samples from sediment, water, and crayfish intestine clearly clustered into three main branches in the sample dendrogram, which indicated a distinct difference in microbial community between the water, sediment, and crayfish intestine environments. The three main branches of the genera cluster tree also followed the sample categories, with the sediment branch, water branch, and crayfish intestine branch.

The characteristic dominant genera in the sediment were *norank_f__Steroidobacteraceae*, *norank_o__RBG-13-54-9*, *norank_o__Rokubacteriales*, *norank_o__Subgroup_7*, *norank_ c__Subgroup_17*, *norank_c__KD4-96*, *norank_f__SC-I-84*, *norank_f__Bacteroidetes_vadinHA17*, *norank_c__Latescibacteria*, *Anaeromyxobacter*, *Geobacter*, *norank_f__Gemmatimonadaceae*, *norank_c__4-29-1*, *norank_f__Anaerolineaceae*, *norank_c__Subgroup_6*, *norank_c__Thermodesulfovibrionia*, and *norank_o__SBR1031*.

In the water, the characteristic dominant genera were *CL500-29_marine_group*, *hgcI_clade*, *norank_f__Sporichthyaceae*, *norank_o__Chloroplast*, *Mycobacterium*, *norank_o__PeM15*, *unclassified_k__norank_d__Bacteria*, *C39*, *norank_f__Rhizobiales_Incertae_Sedis*, *Cyanobium_PCC-6307*, *Polynucleobacter*, *Arenimonas*, *unclassified_f__Sphingomonadaceae*, *unclassified_f__ Burkholderiaceae*, and *Sediminibacterium*.

In crayfish intestine, the characteristic dominant genera were *Candidatus_Bacilloplasma*, *unclassified_f__Enterobacteriaceae*, *Citrobacter*, *Aeromonas*, *norank_p__RsaHF231*, *ZOR0006*, *Tyzzerella_3*, and *Shewanella*. Notably, microbial communities appeared to depend more on the sample category than on the breeding mode.

Furthermore, the Kruskal-Wallis H test was performed to check for significant differences in the microbes among habitats

[7]https://www.i-sanger.com/

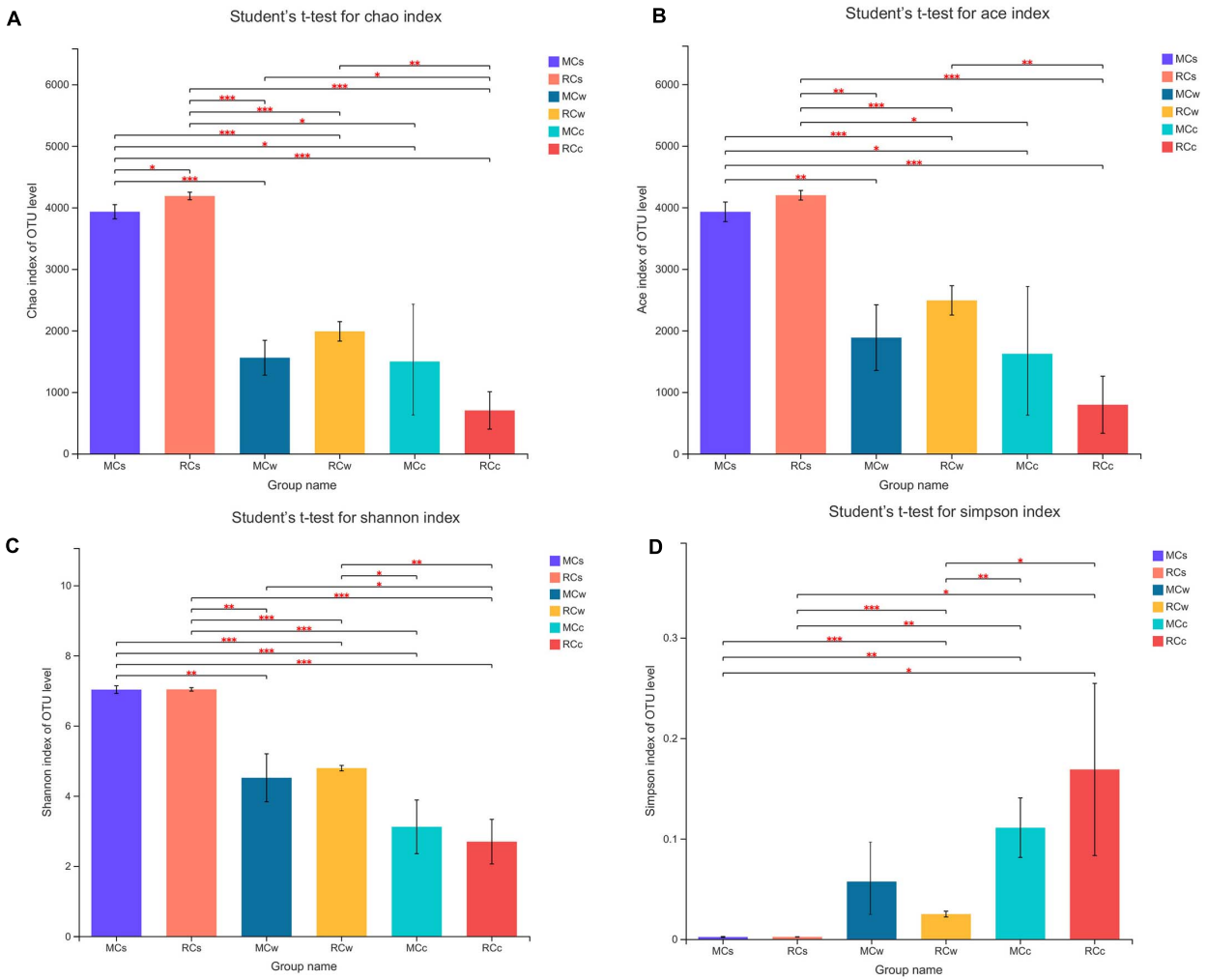

FIGURE 1 | Differences in richness and diversity of bacterial species between sampling groups. **(A)** Chao1 index of OTU level. **(B)** Ace index of OTU level. **(C)** Shannon index of OTU level. **(D)** Simpson index of OTU level. Differences were assessed with Student's *t*-test: * $0.01 < P \leq 0.05$; ** $0.001 < P \leq 0.01$; *** $P \leq 0.001$.

at both phylum and genus levels, and the results are shown in **Supplementary Figure 2**.

ANOSIM/Adonis Analysis of the Differences in Microbial Communities Between Two Breeding Modes

ANOSIM and Adonis analysis revealed significant differences between the clusters of water, sediment, and crayfish intestine (**Table 1** and **Supplementary Figure 1**) at the OTU level. In contrast, ANOSIM and Adonis analysis suggested that the difference between the MC and RC modes in all water, sediment, and crayfish intestine samples at the OTU level was not statistically significant (**Table 1** and **Supplementary Figure 1**). These results indicate that the RC breeding mode had no significant influence on the microbial communities of both crayfish intestines and their cultural surroundings compared with the traditional MC breeding mode.

Relationship Between Microbial Communities in Water, Sediment, and Crayfish Intestines

The microbial communities of each sample clustered with PC1 = 39.33% and PC2 = 34.27% of the total variation (**Figure 4**). Moreover, samples of the same category were clustered together, which was consistent with the UPGMA tree. Additionally, although samples from the different breeding modes were separated to some extent, their 95% confidence ellipses crossed in all water, sediment, and crayfish intestine samples.

A total of 1,207 nodes were identified in the bipartite co-occurrence network; 23.61% (285 genera, clusters 1, 6, and 7) of the sampled genera were most strongly associated with only one environment (**Figure 5**), confirming the basic distinctness of the microbial communities in various systems. Furthermore, 26.26% (317 genera, clusters 2, 4, and 5) of these genera were associated with two environments, and 50.12% (605 genera, cluster 3) were

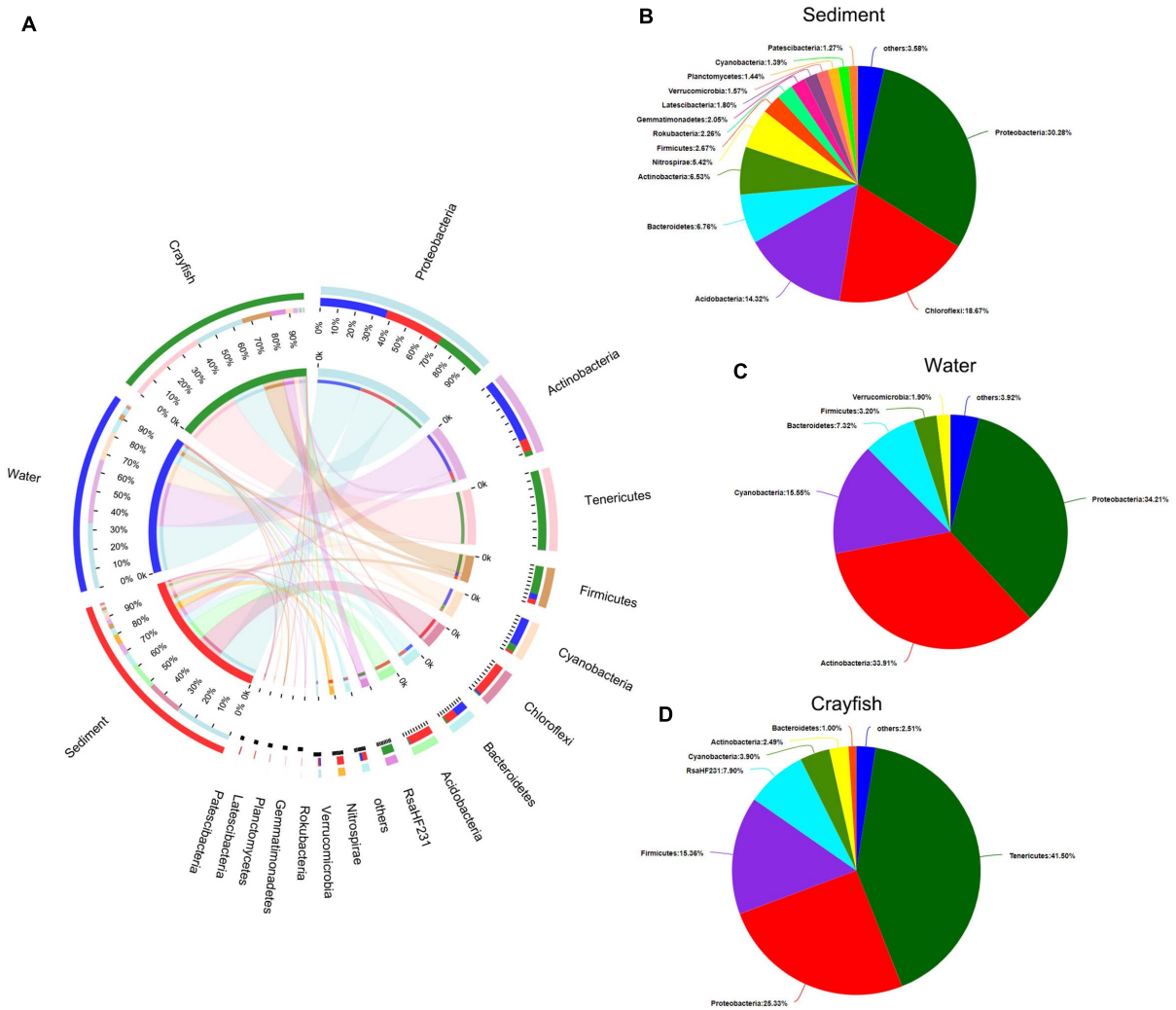

FIGURE 2 | Phylum-level composition of the bacterial community in the sampling groups. **(A)** Distribution of phyla within the microbial community of each sample. The width of the bar of each phylum indicates the relative abundance of that phylum in the sample. **(B)** Composition of the bacterial community in sediment. **(C)** Composition of the bacterial community in water. **(D)** Composition of the bacterial community in crayfish intestine. Low abundance sequences (i.e., <1% abundance) were combined and specified as "others".

associated with all three environments (**Figure 5**), indicating a strong correlation among microbial communities in water, sediment, and crayfish intestines. In particular, the distribution of crayfish intestine microbes (a total of 881 genera) suggested their strong correlation with the aquatic environment. Only 9.19% (81 genera, cluster 1) of crayfish intestine microbiota were unique to crayfish intestines, 82.29% (725 genera, clusters 2 and 3) were shared between crayfish intestines and water, 77.19% (680 genera, clusters 3 and 4) were shared between crayfish intestines and sediment, and 68.67% (605 genera, cluster 3) were shared among the three habitats (**Figure 5**). In addition, the bipartite network also showed that samples from the same environment shared a large number of genera (**Figure 5**), suggesting that the breeding mode had little influence on the microbial communities.

A total of 95 nodes and 1,158 interactions were identified in the genera co-correlation network (**Figure 6**), and the average clustering coefficient was 0.712. The transitivity of the network was 0.777, the network diameter was 6, and the average path length was 2.279. A high level of connectivity indicated significant interactions between the genera in crayfish intestines and the environment. Furthermore, the genera from different environments clustered into three modules in the network, based on their characteristic dominant genera (**Figures 3B**, **6**). The modularity index was 0.409, indicating a valid modular structure in the network (Newman, 2006). Notably, the genera present in the sediment had the tightest cluster, while those found in crayfish intestine displayed frequent connections with the genera encountered in water. To identify the potential key genera connecting different environments, we focused on the hubs with the highest betweenness centrality parameters (Lupatini et al., 2014). *Candidatus_Bacilloplasma* (degree 29, clustering 0.468), which

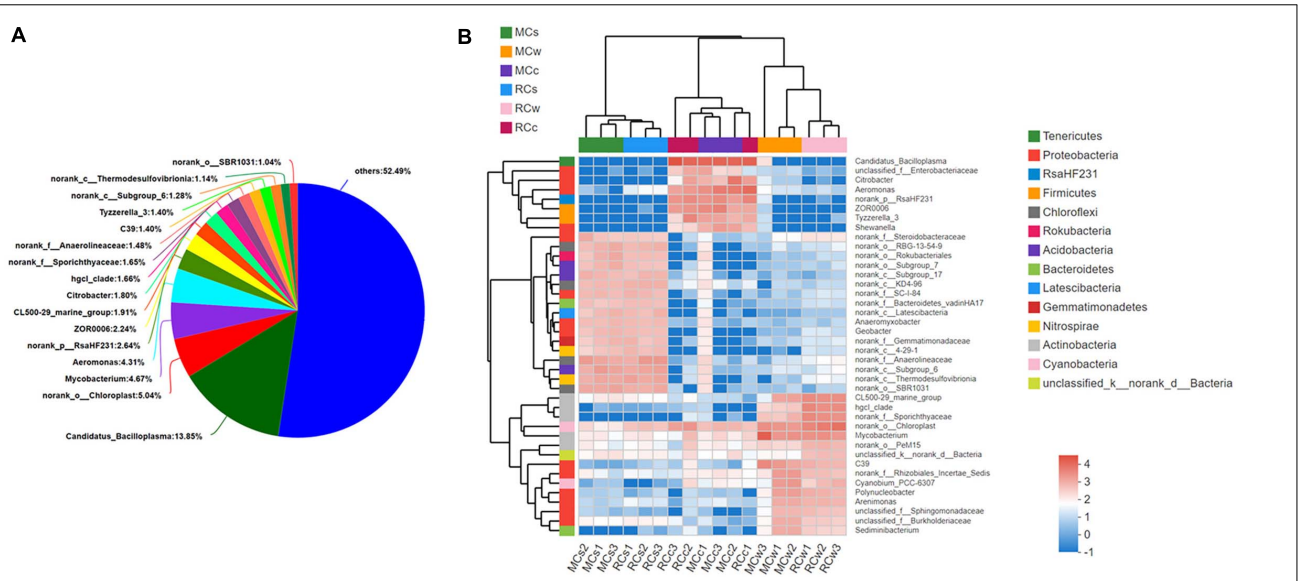

FIGURE 3 | Genus-level composition of the bacterial community in the samples. **(A)** Overall bacterial community composition at the genus level (all samples pooled together). Low abundance sequences (i.e., <1% abundance) were combined and specified as "others." **(B)** Distribution of the 40 most abundant genera across all samples. The log-transformed relative abundance of each genus in sample is depicted by color intensity. Bray–Curtis distances are shown at the top.

TABLE 1 | ANOSIM/Adonis analysis.

Group	ANOSIM[a]			Adonis[b]		
	R[c]	P	Permutation_num	F. model	R^{2d}	Pr (> F)[e]
Sediment vs. Water vs. Crayfish-intestine	1	0.001	999	19.9878	0.7272	0.001
MC-sediment vs. RC-sediment	0.5556	0.098	999	3.1507	0.4406	0.1
MC-water vs. RC-water	0.5556	0.098	999	5.5567	0.5814	0.1
MC-crayfish-intestine vs. RC-crayfish-intestine	0.3333	0.199	999	1.6891	0.2969	0.2

[a] *Analysis of similarities (ANOSIM) was performed based on Bray-Curtis distances.*
[b] *Adonis is a non-parametric statistical method.*
[c] *An R value closer to 1 indicates a greater difference between groups.*
[d] *The R^2 value shows the percentage of variation explained by the supplied mapping file category.*
[e] *Pr (> F) is the p-value representing statistical significance.*
Permuation_num: number of permutations; MC: monoculture mode; RC: rice-crayfish co-culture mode.

belongs to the phylum Tenericutes, had the highest betweenness centrality (i.e., 446.2839). As a genus mainly distributed in crayfish intestine, the presence of *Candidatus_Bacilloplasma* was strongly correlated with both water and sediment clusters. The genus *g_norank_f_Steroidobacteraceae* (degree 43, clustering 0.658), phylum Proteobacteria, was mainly distributed in sediment that exhibited a strong correlation with the crayfish intestine cluster, which had a 253.365 betweenness centrality. The genera *Dinghuibacter* (degree 23, clustering 0.459), belonging to the phylum Bacteroidetes, and *Hydrogenophaga* (degree 25, clustering 0.467), phylum Proteobacteria, were distributed in both water and crayfish intestines and might be the key nodes connecting the water and crayfish intestine clusters, which had 171.590 and 240.221 betweenness centrality, respectively. As for the genera *Methyloparacoccus* (degree 20, clustering 0.421) and *Defluviicoccus* (degree 19, clustering 0.409), both belonging to the phylum Proteobacteria, they were distributed in both water and sediment and might be the key nodes connecting the water and sediment clusters, which had 359.762 and 265.153 betweenness centrality, respectively (**Figure 6** and **Supplementary Table 3**).

PICRUst Functional Prediction of Microbial Communities

PICRUSt is a computational approach to predict the functional composition of a metagenome using marker gene data and a database of reference genomes (Langille et al., 2013). The dominant functions of the microbial communities in the crayfish intestine and the surrounding environment were as follows: energy production and conversion (relative abundance: 6.60–7.60%); amino acid transport and metabolism (7.84–8.25%); nucleotide transport and metabolism (2.34–2.86%); carbohydrate transport and metabolism (5.60–6.12%); coenzyme transport and metabolism (4.07–4.23%); lipid transport and metabolism (3.48–6.06%); translation, ribosomal structure, and biogenesis (5.11–6.68%); transcription (5.38–7.47%);

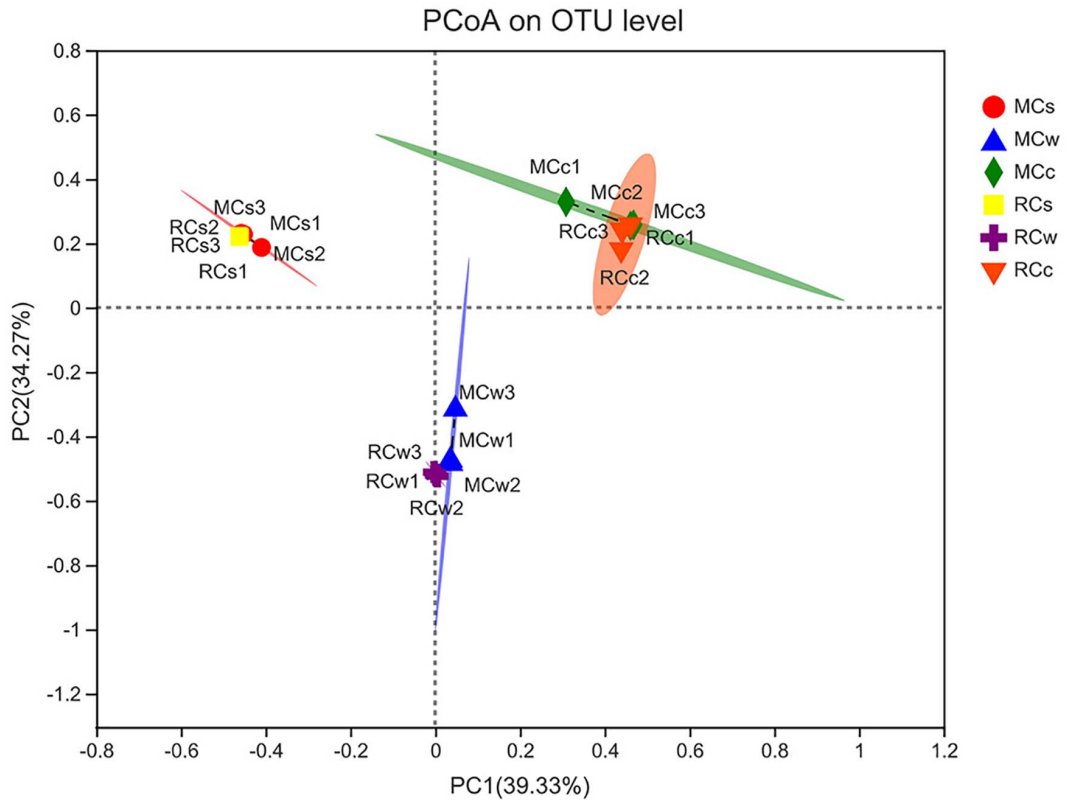

FIGURE 4 | Principal co-ordinates analysis (PCoA) of the bacterial community at the level of operational taxonomic units (OTUs).

replication, recombination, and repair (5.35–6.73%); cell wall, membrane, and envelope biogenesis (6.11–7.46%); inorganic ion transport and metabolism (5.35–6.13%); secondary metabolite biosynthesis, transport, and catabolism (1.78–3.66%); general function prediction only (8.37–8.70%); signal transduction mechanisms (5.65–7.82%); and post-translational modification, protein turnover, and chaperones (3.97–4.44%).

Notably, the RC mode had a higher abundance, compared with that in the MC mode, of functions related to the transport and metabolism of carbohydrates (6.12 vs. 5.38%), amino acids (8.25 vs. 8.07%), and nucleotides (2.37 vs. 2.34%) in water samples (**Figure 7**). In contrast, the RC mode had a lower abundance in functions related to lipid transport and metabolism in water samples than did the MC mode (3.48 vs. 3.79%). These results imply differences in metabolism between the two modes.

DISCUSSION

Food security is becoming a global problem with the rapid increase in the world population. Eco-agricultural systems are considered to be a good strategy to face the challenges of land limitation, water scarcity, and climate change. As one of the most popular rice-livestock integration practices, the rice–crayfish co-culturing system has been developed rapidly in recent years (Yang et al., 2019). Previous studies have shown that eco-agricultural systems contribute to increasing the use of ecological processes and biodiversity, and reduce the rate of chemical fertilizer and pesticide application (Zhang et al., 2015). However, there is concern regarding the influence of the returning rice straw on the surrounding environment because organic compound accumulation might negatively affect the ambient microbial equilibrium by enriching potential pathogens and reducing probiotics, thereby causing environmental stress in aquaculture systems (Sun et al., 2020). In this work, we attempted to apply the microbial community as an indicator for calculating the ecological balance.

Overview of the Dominant Bacterial Taxa

The dominant phyla in our study included Proteobacteria, Actinobacteria, Tenericutes, Firmicutes, Cyanobacteria, Chloroflexi, Bacteroidetes, and Acidobacteria, and their relative abundances varied between crayfish intestine and the surrounding water and sediment, which is consistent with the results of previous studies on shrimp and other aquatic livestock (Hou et al., 2018; Fan et al., 2019). The crucial roles of these phyla in nutrient cycling, water quality control, and the fitness of aquaculture animals have been well established, and thus, discussion on this aspect is not repeated here.

RsaHF231 and Nitrospirae were within the top ten dominant phyla, but as yet, their role in aquaculture had seldom been studied. Nitrospirae had a significantly higher abundance

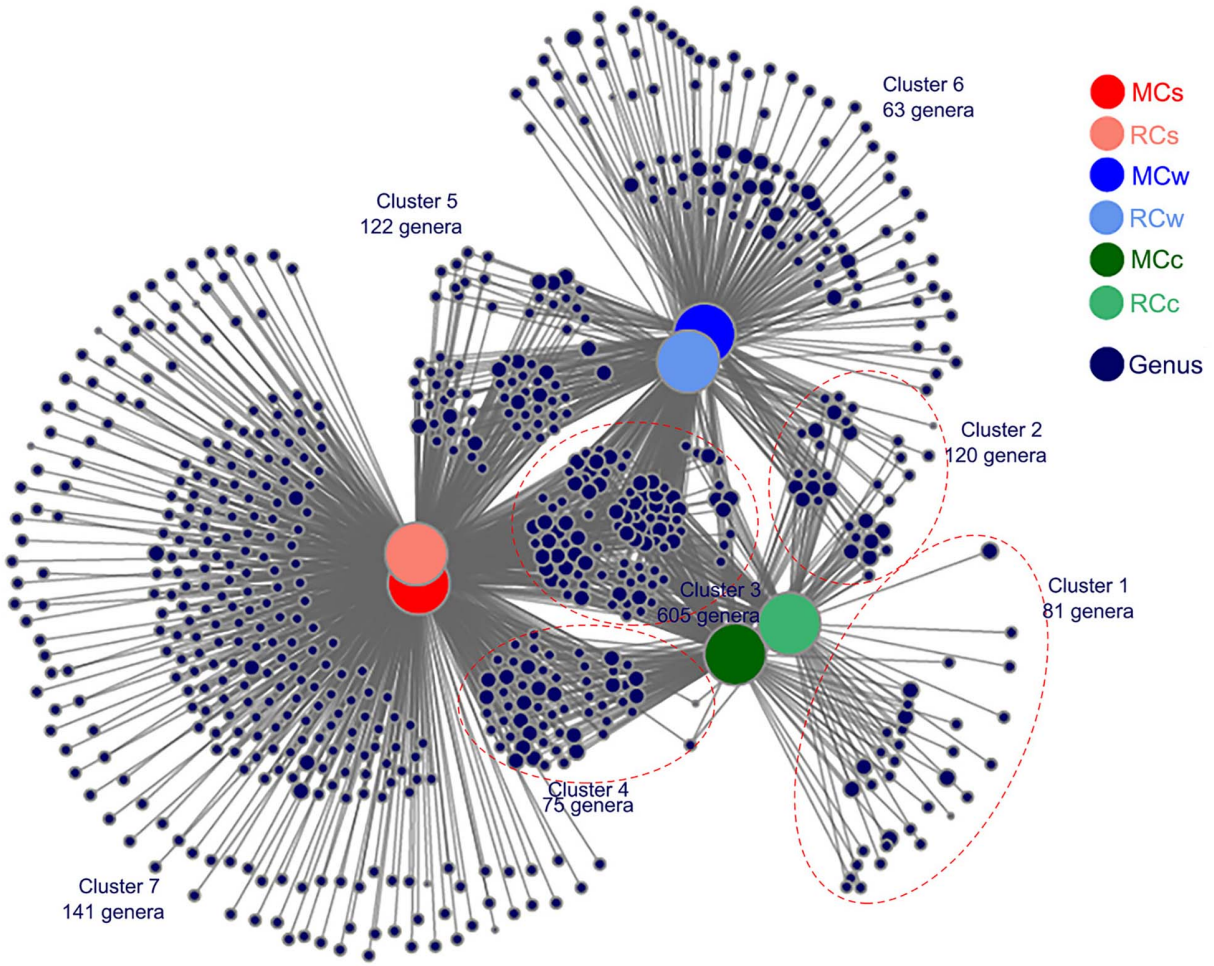

FIGURE 5 | Bipartite co-occurrence network showing the associations between genera and the different samples. Genera with ≥5 sequence numbers were reserved. Node sizes represent the relative abundance of the genera in the data sets, with bigger nodes indicating greater abundances. Edges represent the association patterns of individual genus with the sampling groups.

in sediment samples than in water and crayfish intestines. Nitrospirae have been detected in rice paddies, and they are known to have a versatile metabolism, which includes processed such as the chemolithoautotrophic use of ammonia and nitrite, hydrogen oxidation coupled to oxygen respiration, and formate-driven nitrate respiration to nitrite (Zecchin et al., 2018). RsaHF231 was the most abundant in crayfish intestine. The relative abundance of RsaHF231 in crayfish intestine was of 7.90%, whereas it was of 0.01% in water. RsaHF231 was found in the guts of black soldier fly in a previous study (Jiang et al., 2019), and we speculate that the presence of RsaHF231 in the former might have originated from the black soldier fly larvae meal fed to the crayfish.

Microbial Interactions Between Crayfish and the Surroundings

Co-correlation networks are considered to be a powerful tool for exploring taxa coexistence in complex microbial communities (Jiang et al., 2019). The study of the topological properties of the co-correlation network provided direct and valuable information on the microbial interaction between crayfish and their surroundings. Furthermore, modularity has been suggested to be an important attribute of ecosystem stability and community resilience (Olesen et al., 2007), and modules in a co-correlation network can potentially indicate direct or indirect interactions between microbes. These interactions may also be due to shared niches or a high level of phylogenetic relatedness (Faust and Raes, 2012). It is worth noting that many bacterial taxa with low abundance could also play disproportionately large roles in niches and functions (Sun et al., 2018). Based on these theories, we could find the key microbes that connect various environments.

In this study, *Candidatus_Bacilloplasma* (phylum Tenericutes) was the most central genus in the co-correlation network. Tenericutes is a phylum of bacteria that lack a peptidoglycan cell wall, and the most well-studied clade in this phylum is the class Mollicutes (Wang et al., 2020). Notably,

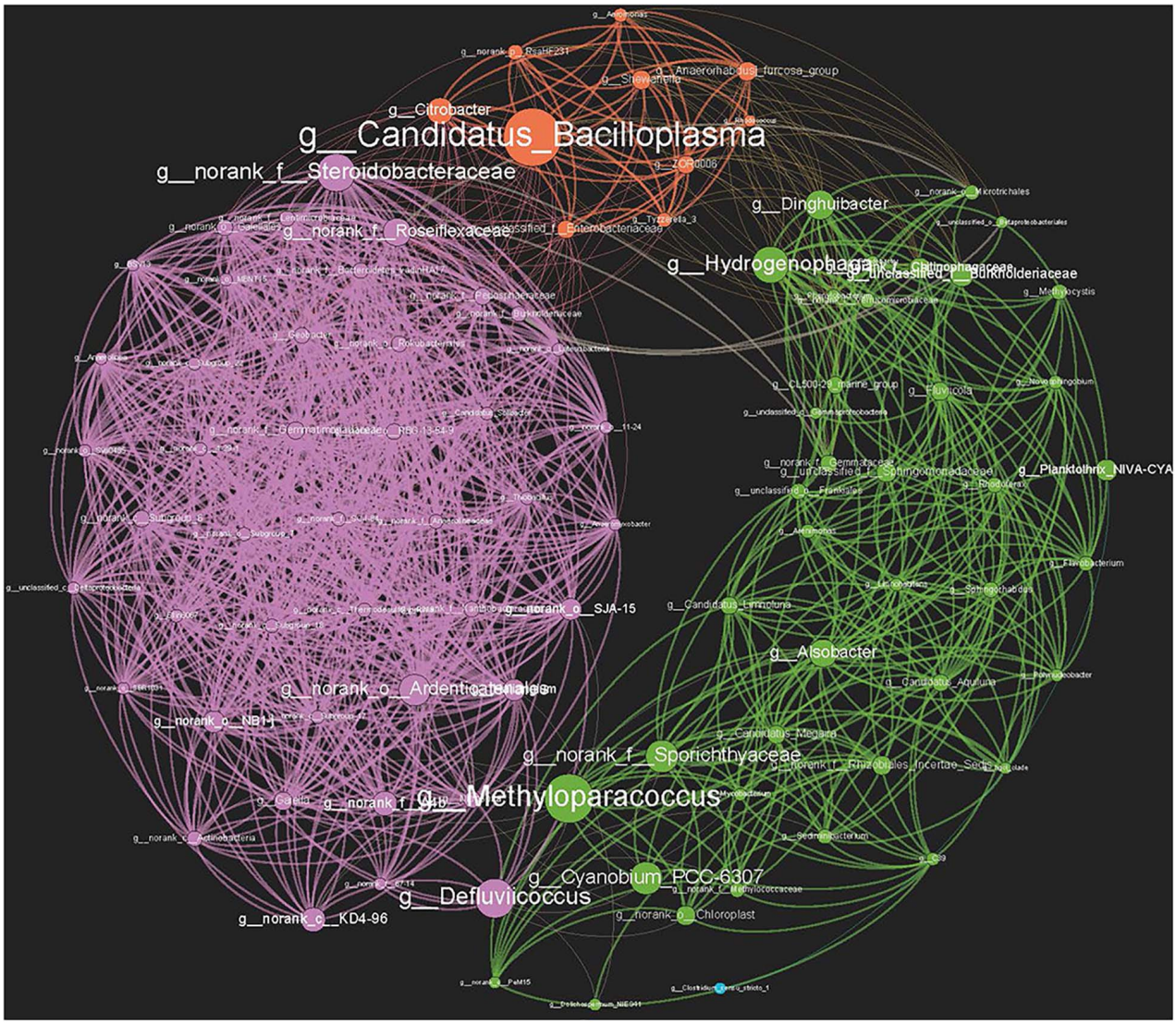

FIGURE 6 | Co-correlation network of bacterial genera based on Spearman correlation. High-confidence interactions with Spearman correlation $\rho \geq 0.75$ were reserved. Three main modules, which correspond to the dominant genera in sediment, water, and crayfish intestine, respectively, were generated with a 0.409 modularity index. All networks are displayed as nodes (genera) and edges (significant interactions among genera nodes). The same node colors represent genera belonging to the same module. Purple: sediment module; green: water module: orange: crayfish intestine module. Node sizes indicate the betweenness centrality of the genera in the data sets.

Tenericutes have been detected in the gut of various aquatic organisms, and some environmental Tenericutes are considered to be pathogens (Huang et al., 2020). Nevertheless, previous research has also shown that Tenericutes can be mutualistic symbionts in the gut of their host species (Wang et al., 2020). For instance, Tenericutes play a role in the degradation of recalcitrant C sources in the stomach and pancreas of isopods (Wang et al., 2004). However, their genomes are linked to an extreme reduction in metabolic capacity resulting from a lack of genes that are related to regulatory elements, biosynthesis of amino acids, and intermediate metabolic compounds, which must be imported from the host. Tenericutes might serve as an important indicator of host homeostasis and health (Wang et al., 2020). A previous study on *Litopenaeus vannamei* reported that *Candidatus_Bacilloplasma* and *Psychromonas* are the only two dominant genera in the shrimp intestine and are correlated with physiological parameters in shrimp (Huang et al., 2018). In addition, a recent study has also linked *Candidatus_Bacilloplasma* enrichment and the disorder of metabolic functions with white feces syndrome in shrimp (Wang et al., 2020). It is obvious that as a mutualistic symbiont, *Candidatus_Bacilloplasma* plays an important role in the microbial interaction of crayfish with the ambient environment, which mainly consists of water and sediment.

Environmental bacteria also strongly connect with the internal microbiota of crayfish. In our study, most of the central hubs

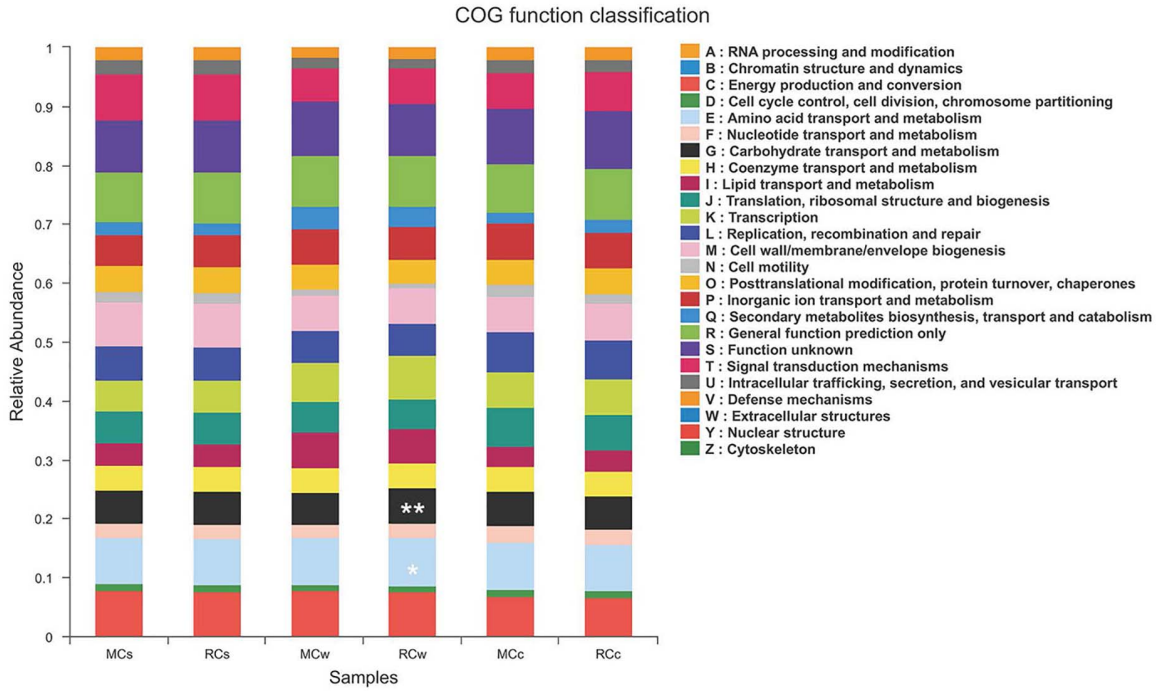

FIGURE 7 | Clusters of orthologous group (COG) function classification of the six sampling groups. * indicate COG functions significant difference between MCw and RCw. * $0.01 < P \leq 0.05$; ** $0.001 < P \leq 0.01$.

belonged to the phylum Proteobacteria. Proteobacteria was the most abundant phylum and was uniformly dispersed in the three environments (sediment, water, and crayfish intestines). The co-correlation network indicated that Proteobacteria, such as those from the genera *Methyloparacoccus*, *Defluviicoccus*, *Hydrogenophaga*, and *g_norank_f_Steroidobacteraceae*, played an important role in the interaction between crayfish and the environment. In addition, the genus *Dinghuibacter*, which belongs to the phylum Bacteroidetes, also corresponded to an important node that connected the water and crayfish intestine samples. As one of the most abundant phyla in aquatic bacteria, Proteobacteria can inhabit various environments and play crucial roles in matter and energy recycling. However, as an abundant generalist colonizer, the abnormal increase in Proteobacteria often generates dysbiosis of the microbial composition in the host and leads to disease (Shin et al., 2015). Thus, Proteobacteria might serve as an important marker of healthy aquaculture.

Furthermore, the PICRUst functional prediction might have provided a microbiological explanation for the microbial connection between crayfish and their surroundings. Functions related to carbohydrate, amino acid, lipid, and inorganic ion transport and metabolism, as well as energy production and conversion, DNA replication and reparation, among others, were found in crayfish and the ambient microbiota. We speculate that diversity functions play an important role in the metabolism of the extra materials brought by the integrated RC breeding mode and maintain a stable microbiota structure in RCs, thus resulting in inconspicuous differences in the microbiota composition between the MC and RC breeding modes. Accordingly, the two testing modes also had little differences in environmental physico-chemical properties. The pH, dissolved oxygen, and ammonia nitrogen were similar between MC and RC modes; nitrate nitrogen and COD were slightly higher in RC mode than MC mode (**Supplementary Table 4**). Therefore, the functional diversity of material and energy metabolism guarantees the microecological balance in crayfish eco-agricultural systems.

Although the difference between the microbial structure in the MC and RC was not statistically significant, we still found traces of the influence of the rice–crayfish co-culturing system on the original crayfish ecosystem from PICRUst functional prediction. This might have been caused by the additional planting of rice and the return of rice straw in the RC mode compared with the MC mode. There was a higher abundance of functions related to the transport and metabolism of carbohydrates, amino acids, and nucleotides in the water samples from the RC than in those from the MC. This may be explained by the fact that an increase in these functions facilitates the degradation of rice straw. In contrast, functions related to lipid transport and metabolism were less abundant in the water samples from the RC than in those from the MC. We speculate that this might be caused by the higher amount of formulated diet, which has a high fat content, that is fed to crayfish in MC.

Overall, the microbial communities of the RC mode had no significant differences with those of the traditional MC mode. Decomposer microbes play a crucial role in maintaining ecological balance in eco-agricultural systems. The shift in PICRUst predicted functions reflected the action of the microbes upon crop materials brought by the plants in the RC

mode. The co-correlation networks showed the diversity and complex interactions of microbial communities among crayfishes and the aquacultural environment, which may guarantee the robustness of the ecological system and also cause the similar microbial structures observed between the MC and RC modes. Evidently, the microbiome constitutes a promising indicator for calculating ecological balance. In particular, the hub microbes in the interaction network between crayfishes and the ambient environment, such as *Candidatus_Bacilloplasma,* Proteobacteria, and Bacteroidetes, are of particular concern in the micro-ecological environment of crayfish farming.

CONCLUSION

The present study analyzed the profiles of microbial communities and highlighted the characteristic bacterial composition in crayfish, water, and sediment, respectively. Furthermore, we established the relationship between the bacterial communities in crayfish intestine and the ambient environment and provided microbial evidence of their interaction. Moreover, this study showed that the rice–crayfish co-culture had little influence on the microecological environment compared with the traditional crayfish monoculture, and provided insight into the microecological balance in crayfish eco-agricultural systems even with the additional ecological load. That is, the additional planting of rice and return of rice straw in the RC mode did not disturb the microbial interactions between crayfishes and the ambient environment. However, it should be noted that this study observed only a snapshot at the end of the entire farming cycle and a limited number of samples, which were limitations of our study. Further studies are still needed on the interaction between rice stalks and shrimp as well as the impact on water quality and the environment during the decomposition process of the returning rice stalk residue. Overall, this study provided a theoretical reference to direct crayfish farming and the development of crayfish eco-agricultural systems.

DATA AVAILABILITY STATEMENT

The raw data of the 16S rDNA gene sequence reads from the 18 samples were deposited into the NCBI Sequence Read archive (SRA) database with the following BioProject accession number: PRJNA663764 (SRR12650255 to SRR12650272).

AUTHOR CONTRIBUTIONS

YW: methodology, conceptualization, writing – original draft, raft, and writing – review. CW: investigation and formal analysis. YC: conceptualization and investigation. DZ and HL: soft-ware and data curation. MZ: visualization and data curation. PG: supervision and project administration. All authors contributed to the article and approved the submitted version.

FUNDING

This work was supported by the Applied Basic Research Frontier Foundation of Wuhan, China (2020020601012265), the Natural Science Foundation of Hubei Province, China (2019CFB588), the Major Technological Innovation Project of Hubei Province, China (2019ABA114), and the Special Funds for Local Science and Technology Development Guided by Central government of China (2019ZYYD030).

ACKNOWLEDGMENTS

We acknowledge Shanghai Majorbio Bio-pharm Technology Co., Ltd., for their technical assistance with sequencing. We would like to thank Editage (www.editage.cn) for English language editing.

SUPPLEMENTARY MATERIAL

The Supplementary Material for this article can be found online at: https://www.frontiersin.org/articles/10.3389/fmicb.2021.669570/full#supplementary-material

Supplementary Figure 1 | ANOSIM analysis of the samples.

Supplementary Figure 2 | Kruskal-Wallis H test bar plot among habitats on both phylum and genus level.

Supplementary Table 1 | OUT reads number raw data of all samples.

Supplementary Table 2 | Alpha-diversity indices of all samples.

Supplementary Table 3 | Attributes of the co-correlation network.

Supplementary Table 4 | The environmental physico-chemical properties in MC and RC breeding modes.

REFERENCES

Amato, K. R., Yeoman, C. J., Kent, A., Righini, N., Carbonero, F., Estrada, A., et al. (2013). Habitat degradation impacts black howler monkey (*Alouatta pigra*) gastrointestinal microbiomes. *ISME J.* 7, 1344–1353. doi: 10.1038/ismej.2013.16

Björnsson, L., Hugenholtz, P., Tyson, G. W., and Blackall, L. L. (2002). Filamentous *Chloroflexi* (green non-sulfur bacteria) are abundant in wastewater treatment processes with biological nutrient removal. *Microbiology* 148, 2309–2318. doi: 10.1099/00221287-148-8-2309

Blankenberg, D., Von Kuster, G., Coraor, N., Ananda, G., Lazarus, R., Mangan, M., et al. (2010). Galaxy: A web-based genome analysis tool for experimentalists. *Curr. Protocols Mole. Biol.* 19, 1–21. doi: 10.1002/0471142727.mb1910s89

Bureau of Fisheries, Ministry of Agriculture and Rural Affairs of the People's Republic of China, National Fisheries Technology Extension Center, and Chinese Society of Fisheries. (2019). *Report on The Development of Crayfish Industry in China. Chinese fisheries economics. 5*. (In Chinese).

Carbone, D., and Faggio, C. (2016). Importance of prebiotics in aquaculture as immunostimulants. Effects on immune system of *Sparus aurata* and *Dicentrarchus labrax*. *Fish Shellfish Immunol.* 54, 172–178. doi: 10.1016/j.fsi.2016.04.011

Dedysh, S. N., and Damsté, J. S. S. (2018). *Acidobacteria. In eLS*. Chichester, UK: John Wiley & Sons, Ltd, doi: 10.1002/9780470015902.a0027685

Douterelo, I., Perona, E., and Mateo, P. (2004). Use of cyanobacteria to assess water quality in running waters. *Environ. Pollut.* 127, 377–384. doi: 10.1016/j.envpol.2003.08.016

Fan, L., Wang, Z., Chen, M., Qu, Y., Li, J., Zhou, A., et al. (2019). Microbiota comparison of Pacific white shrimp intestine and sediment at freshwater and marine cultured environment. *Sci. Total Environ.* 657, 1194–1204. doi: 10.1016/j.scitotenv.2018.12.069

Faust, K., and Raes, J. (2012). Microbial interactions: from networks to models. *Nat. Rev. Microbiol.* 10, 538–550. doi: 10.1038/nrmicro2832

Giatsis, C., Sipkema, D., Smidt, H., Heilig, H., Benvenuti, G., Verreth, J., et al. (2015). The impact of rearing environment on the development of gut microbiota in tilapia larvae. *Sci. Rep.* 5:18206. doi: 10.1038/srep18206

Han, Y., Yang, T., Xu, G., Li, L., and Liu, J. (2020). Characteristics and interactions of bioaerosol microorganisms from wastewater treatment plants. *J. Hazard. Mater.* 391:122256. doi: 10.1016/j.jhazmat.2020.122256

Hou, D., Huang, Z., Zeng, S., Liu, J., Weng, S., and He, J. (2018). Comparative analysis of the bacterial community compositions of the shrimp intestine, surrounding water and sediment. *J. Appl. Microb.* 125, 792–799. doi: 10.1111/jam.13919

Huang, F., Pan, L., Song, M., Tian, C., and Gao, S. (2018). Microbiota assemblages of water, sediment, and intestine and their associations with environmental factors and shrimp physiological health. *Appl. Microbiol. Biotechnol.* 102, 8585–8598. doi: 10.1007/s00253-018-9229-5

Huang, Z., Zeng, S., Xiong, J., Hou, D., Zhou, R., Xing, C., et al. (2020). Microecological Koch's postulates reveal that intestinal microbiota dysbiosis contributes to shrimp white feces syndrome. *Microbiome* 8:32. doi: 10.1186/s40168-020-00802-3

Jiang, C.-L., Jin, W.-Z., Tao, X.-H., Zhang, Q., Zhu, J., Feng, S.-Y., et al. (2019). Black soldier fly larvae (*Hermetia illucens*) strengthen the metabolic function of food waste biodegradation by gut microbiome. *Microb. Biotechnol.* 12, 528–543. doi: 10.1111/1751-7915.13393

Langille, M., Zaneveld, J., Caporaso, J., McDonald, D., Knights, D., Reyes, J. A., et al. (2013). Predictive functional profiling of microbial communities using 16S rRNA marker gene sequences. *Nat. Biotechnol.* 31, 814–821. doi: 10.1038/nbt.2676

Leung, M. H. Y., Chan, K. C. K., and Lee, P. K. H. (2016). Skin fungal community and its correlation with bacterial community of urban Chinese individuals. *Microbiome* 4:46. doi: 10.1186/s40168-016-0192-z

Li, H., Li, T., Li, X., Wang, G., Lin, Q., and Qu, J. (2018). Gut microbiota in Tibetan herdsmen reflects the degree of urbanization. *Front. Microb.* 9:1745. doi: 10.3389/fmicb.2018.01745

Liberton, M., Bandyopadhyay, A., and Himadri, B. P. (2019). Enhanced nitrogen fixation in a *glgX*-deficient strain of *Cyanothece* sp. strain ATCC 51142, a unicellular nitrogen-fixing cyanobacterium. *Appl. Environ. Microbiol.* 85, e2887–e2818. doi: 10.1128/AEM.02887-18

Liu, B., Ai, T., and Tan, L. (2010). Study on soil fertility change in Jianli County. *Hubei Agricult. Sci.* 49, 24–26.

Lupatini, M., Suleiman, A. K. A., Jacques, R. J. S., Antoniolli, Z. I., de Siqueira Ferreira, A., Kuramae, E. E., et al. (2014). Network topology reveals high connectance levels and few key microbial genera within soils. *Front. Environ. Sci.* 2:10. doi: 10.3389/fenvs.2014.00010

Lv, X., Yu, P., Mao, W., and Li, Y. (2018). Vertical variations in bacterial community composition and environmental factors in the culture pond sediment of sea cucumber *Apostichopus japonicus*. *J. Coastal Res.* 84, 69–76. doi: 10.2112/SI84-010.1

Mahajan, G. B., and Balachandran, L. (2012). Antibacterial agents from actinomycetes — a review. *Front. Biosci.* 4:240–253. doi: 10.2741/373

National Bureau of Statistics of China [NBSPRC] (2018). *Statistical Yearbook 2018*. Beijing: China Statistics Press.

Newman, M. E. J. (2006). Modularity and community structure in networks. *Proc. Natl. Acad. Sci. U S A* 103, 8577–8582. doi 10.1073/pnas.0601602103

Olesen, J. M., Bascompte, J., Dupont, Y. L., and Jordano, P. (2007). The modularity of pollination networks. *Proc. Natl. Acad. Sci. U S A* 104, 19891–19896. doi: 10.1073/pnas.0706375104

Quast, C., Pruesse, E., Yilmaz, P., Gerken, J., Schweer, T., Yarza, P., et al. (2013). The SILVA ribosomal RNA gene database project: improved data processing and web-based tools. *Nucleic Acids Res.* 41, D590–D596. doi: 10.1093/nar/gks1219

Schloss, P. D., Gevers, D., and Westcott, S. L. (2011). Reducing the effects of PCR amplification and sequencing artifacts on 16S rRNA-based studies. *PLoS One* 6:e27310. doi: 10.1371/journal.pone.0027310

Shin, N.-R., Whon, T. W., and Bae, J.-W. (2015). *Proteobacteria*: microbial signature of dysbiosis in gut microbiota. *Trends Biotechnol.* 33, 496–503. doi: 10.1016/j.tibtech.2015.06.011

Si, G., Peng, C., Yuan, J., Xu, X., Zhao, S., Xu, D., et al. (2017). Changes in soil microbial community composition and organic carbon fractions in an integrated rice-crayfish farming system in subtropical China. *Sci. Rep.* 7:2856. doi: 10.1038/s41598-017-02984-7

Sun, W., Krumins, V., Dong, Y., Gao, P., Ma, C., Hu, M., et al. (2018). A combination of stable isotope probing, Illumina sequencing, and co-occurrence network to investigate thermophilic acetate- and lactate-utilizing bacteria. *Microb. Ecol.* 75, 113–122. doi: 10.1007/s00248-017-1017-8

Sun, Y., Han, W., Liu, J., Huang, X., Zhou, W., Zhang, J., et al. (2020). Bacterial community compositions of crab intestine, surrounding water, and sediment in two different feeding modes of *Eriocheir sinensis*. *Aquacult. Rep.* 16:100236. doi: 10.1016/j.aqrep.2019.100236

Wang, Y., Huang, J.-M., Zhou, Y.-L., Almeida, A., Finn, R. D., Danchin, A., et al. (2020). Phylogenomics of expanding uncultured environmental Tenericutes provides insights into their pathogenicity and evolutionary relationship with Bacilli. *BMC Genom.* 21:408. doi: 10.1186/s12864-020-06807-4

Wang, Y., Stingl, U., Anton-Erxleben, F., Geisler, S., Brune, A., and Zimmer, M. (2004). "*Candidatus* Hepatoplasma crinochetorum," a new, stalk-forming lineage of Mollicutes colonizing the midgut glands of a terrestrial isopod. *Appl. Environ. Microb.* 70, 6166–6172. doi: 10.1128/AEM.70.10.6166-6172.2004

Yang, B., Ma, Y., Zhang, C., Jia, Y., Li, B., and Zheng, X. (2019). Cleaner production technologies increased economic benefits and greenhouse gas intensity in an eco-rice system in China. *Sustainability* 11:7090. doi: 10.3390/su11247090

Zecchin, S., Mueller, R. C., Seifert, J., Stingl, U., Anantharaman, K., von Bergen, M., et al. (2018). Rice paddy *Nitrospirae* carry and express genes related to sulfate respiration: proposal of the new genus "*Candidatus* Sulfobium". *Appl. Environ. Microbiol.* 84, e2224–e2217. doi: 10.1128/AEM.02224-17

Zehr, J. P., and Ward, B. B. (2002). Nitrogen cycling in the ocean: new perspectives on processes and paradigms. *Appl. Environ. Microbiol.* 68, 1015–1024. doi: 10.1128/AEM.68.3.1015-1024.2002

Zhang, T., Ni, J., and Xie, D. (2015). Severe situation of rural nonpoint source pollution and efficient utilization of agricultural wastes in the Three Gorges Reservoir Area. *Environ. Sci. Pollut. Res.* 22, 16453–16462. doi: 10.1007/s11356-015-5429-z

Zhao, Z., Jiang, J., Pan, Y., Dong, Y., Zhou, Z., et al. (2020). Temporal dynamics of bacterial communities in the water and sediments of sea cucumber (apostichopus japonicus) culture ponds. *Aquaculture* 528:735498. doi: 10.1016/j.aquaculture.2020.735498

Conflict of Interest: The authors declare that the research was conducted in the absence of any commercial or financial relationships that could be construed as a potential conflict of interest.

frontiers in Microbiology

ORIGINAL RESEARCH
published: 23 June 2021
doi: 10.3389/fmicb.2021.673128

Cross-Sectional Variations in Structure and Function of Coral Reef Microbiome With Local Anthropogenic Impacts on the Kenyan Coast of the Indian Ocean

Sammy Wambua[1,2], Hadrien Gourlé[3], Etienne P. de Villiers[4,5], Oskar Karlsson-Lindsjö[3], Nina Wambiji[6], Angus Macdonald[7], Erik Bongcam-Rudloff[3] and Santie de Villiers[1,8]*

[1] Pwani University Bioscience Research Centre (PUBReC), Pwani University, Kilifi, Kenya, [2] Department of Biological Sciences, Pwani University, Kilifi, Kenya, [3] Department of Animal Breeding and Genetics, Swedish University of Agricultural Sciences, Uppsala, Sweden, [4] KEMRI-Wellcome Trust Research Programme, Kilifi, Kenya, [5] Nuffield Department of Medicine, University of Oxford, Oxford, United Kingdom, [6] Kenya Marine and Fisheries Research Institute, Mombasa, Kenya, [7] School of Life Sciences, University of KwaZulu-Natal, Durban, South Africa, [8] Department of Biochemistry and Biotechnology, Pwani University, Kilifi, Kenya

OPEN ACCESS

Edited by:
Rodrigo Gouvea Taketani, Rothamsted Research, United Kingdom

Reviewed by:
Cynthia B. Silveira, University of Miami, United States
Juline Walter, Federal University of Rio de Janeiro, Brazil

***Correspondence:**
Sammy Wambua
sammywambua@gmail.com

Specialty section:
This article was submitted to Aquatic Microbiology, a section of the journal Frontiers in Microbiology

Received: *26 February 2021*
Accepted: *31 May 2021*
Published: *23 June 2021*

Citation:
Wambua S, Gourlé H, de Villiers EP, Karlsson-Lindsjö O, Wambiji N, Macdonald A, Bongcam-Rudloff E and de Villiers S (2021) Cross-Sectional Variations in Structure and Function of Coral Reef Microbiome With Local Anthropogenic Impacts on the Kenyan Coast of the Indian Ocean. Front. Microbiol. 12:673128. doi: 10.3389/fmicb.2021.673128

Coral reefs face an increased number of environmental threats from anthropomorphic climate change and pollution from agriculture, industries and sewage. Because environmental changes lead to their compositional and functional shifts, coral reef microbial communities can serve as indicators of ecosystem impacts through development of rapid and inexpensive molecular monitoring tools. Little is known about coral reef microbial communities of the Western Indian Ocean (WIO). We compared taxonomic and functional diversity of microbial communities inhabiting near-coral seawater and sediments from Kenyan reefs exposed to varying impacts of human activities. Over 19,000 species (bacterial, viral and archaeal combined) and 4,500 clusters of orthologous groups of proteins (COGs) were annotated. The coral reefs showed variations in the relative abundances of ecologically significant taxa, especially copiotrophic bacteria and coliphages, corresponding to the magnitude of the neighboring human impacts in the respective sites. Furthermore, the near-coral seawater and sediment metagenomes had an overrepresentation of COGs for functions related to adaptation to diverse environments. Malindi and Mombasa marine parks, the coral reef sites closest to densely populated settlements were significantly enriched with genes for functions suggestive of mitigation of environment perturbations including the capacity to reduce intracellular levels of environmental contaminants and repair of DNA damage. Our study is the first metagenomic assessment of WIO coral reef microbial diversity which provides a much-needed baseline for the region, and points to a potential area for future research toward establishing indicators of environmental perturbations.

Keywords: coral reef microbiota, microbiome, COGs, human impacts, environmental stressors

INTRODUCTION

Coastal ecosystems are some of the most dynamic and vulnerable environments under various pressures from anthropogenic activities and climate change. Coral reef ecosystems, particularly, are of interest because of their importance for biodiversity, their productivity, and their worrisome decline globally.

The Western Indian Ocean (WIO) is an oceanic region in the warmest ocean (Indian Ocean) that is currently under pressure from global warming and increasing anthropogenic stressors, with unpredictable consequences, yet it is the least studied of all global oceans with respect to the associated microbial ecology (Díez et al., 2016). Indeed, the *Web of Science* records only four papers, published in the last decade (2010 – 2020) on genomic assessment of coral reef microbes in the WIO, compared to 17 in the Caribbean Sea and 114 in the Great Barrier Reef (GBR). Because of the broad variety of biogenic habitats and oceanographic conditions, the region's waters encompass a diverse range of ecologically and nutritionally rich ecosystems (Van Der Elst et al., 2005). With its goods and services supporting over a quarter (more than 60 million people) of the region's population who live within 100 km of the shoreline (Van Der Elst et al., 2005; Obura, 2017), the WIO and its coastal ecosystems are essential to the region's economy. It is feared that with the rapidly increasing development and utilization of coastal zones (Neumann et al., 2015), the WIO's resources are overwhelmed, overexploited and poorly managed, putting its wealth at risk. Indications of distress on the region's ecosystems are noted with increasing frequency characterized by reduced fish catches, diminishing mangrove coverage, and declining coral reef cover (Van Der Elst et al., 2005; Obura, 2017) consequently threatening the livelihoods of dependent coastal communities. Protected areas are the principal tool of marine management in the region – the WIO countries have protected about 2.4 per cent of their marine area (Obura, 2017). Other strategies extensively applied by government institutions, Non-Governmental Organizations (NGO) and communities throughout the WIO to conservation coral reefs are reviewed by Hattam et al. (2020) and include the introduction of alternative livelihoods, coral gardening and payment for ecosystem services (PES) schemes. Monitoring of coral reef status in the WIO is undertaken under the Global Coral Reef Monitoring Network (GCRMN) umbrella, and has mainly involved visual estimations of hard coral cover, fish abundance and coral bleaching (Obura et al., 2019). Technological advancements including autonomous vehicles facilitating underwater, surface, and aerial surveys, and satellites, as well as structure from motion image processing, and acoustic techniques, are set to greatly improve monitoring of coral reef status. Advancements and declining costs of high-throughput sequencing technologies aided by autonomous reef monitoring systems has also improved collection of diversity data on cryptic marine communities for coral reef monitoring (Ransome et al., 2017). Marine microbes are thought to have significant potential as a cryptic community due to their rapid response to environmental change (Glasl et al., 2017).

Shifts in the composition and diversity of microbial communities may be a good indicator for a marine ecosystem's health and for predicting stress responses (Won et al., 2017). Current efforts exploring the potential of microbes as indicators for coral reef ecosystem stressors often correlate taxonomic profiles with biogeographic variation (Glasl et al., 2017, 2018, 2019; Roitman et al., 2018). However, functional profiling may also be informative of environmental disturbance because similar community metabolism may comprise members of phylogenetically variable groups while communities comprised of similar taxa may differ in metabolic capabilities. Indeed, functional diversity has repeatedly been observed to predict ecosystem processes and properties better than taxonomic or phylogenetic diversity (Johnson and Pomati, 2020). Metagenomics provides the opportunity to access microbial community taxonomic and genomic content, as well as their functional potential, which can serve as indicators of the health in an ecosystem (Bellwood et al., 2019). For instance, comparative metagenomics studies have demonstrated that microbial diversity is influenced by the local environment (Behzad et al., 2016) leading to the hypothesis that unique environments harbor unique microbial diversity as well as unique metabolic pathways. Furthermore, Kelly et al. (2014) has shown that, at the ecosystem level, benthos determine core microbial taxa which then adapt to local oceanographic conditions by selecting for advantageous metabolic genes.

Coral reef microbial communities inhabit sediments, overlying water column, and benthic invertebrates such as corals and sponges (Bourne and Webster, 2013). Benthic-pelagic coupling occurs in shallow well-mixed tropical coral reefs where bacterial communities in benthic organisms, the sediments, and the overlaying water column are strongly interlinked (Bourne and Webster, 2013; Vanwonterghem and Webster, 2020). These interactions within the coral ecosphere are known to influence the composition of coral-associated microorganisms (Weber et al., 2019) through the benthos releasing host-specific microbes into the surrounding water, or producing dissolved organic matter which stimulates the activity of specific microbes within the surrounding water layer (Barott and Rohwer, 2012; Silveira et al., 2017; Walsh et al., 2017). Increases in the abundance of microbes in the reef water column has been correlated with an increase in coral disease and reduction in coral cover (Dinsdale et al., 2008; Bruce et al., 2012). Furthermore, since anthropogenic activities most likely impact coral health through the agency of the immediate pelagic and benthic surrounding, the water overlying corals and sediments are often the niches sampled to detect relevant signal in coral ecosphere (McDole et al., 2012; Bourne and Webster, 2013; Kelly et al., 2014; Tout et al., 2014; Walsh et al., 2017; Glasl et al., 2019). To approximate the anthropogenic impact on composition and function of coral reef microbiota, we compared cross-sectional metagenomes of near-coral seawater and sediment samples from three reefs subject to varied suites of environmental perturbations on the Kenyan coast of the WIO. This is the first shotgun metagenomic assessment of coral ecosphere on the WIO – previous studies explored the open water microbiome (Sunagawa et al., 2015) and virome (Williamson et al., 2012).

FIGURE 1 | Map showing the location of the coral reef sites sampled for this study of the Kenyan microbiome. Source: Google Maps.

MATERIALS AND METHODS

Study Sites and Human Activities

Site selection was guided by the Kenya Marine and Fisheries Research Institute (KMFRI) ensuring inclusion of locations in proximity to the range of human activities typical of cosmopolitan urban and rural settlements along the coast of Kenyan. These sites are spread across three of the five counties on the Kenyan coast.

We investigated coral ecosphere within three of the five Kenya marine national parks i.e., Malindi (3°15′35.1″S 40°08′40.0″E), Mombasa (3°59′45.7″S 39°44′50.1″E) and Kisite-Mpunguti (4°42′54.0″S 39°22′23.8″E) (**Figure 1**). Located about 118 km north of Mombasa, Malindi Marine National Park and Reserve is the oldest MPA in Kenya having been gazetted in 1968 (McClanahan et al., 2010). This marine park is popular for glass bottom boat tours and snorkeling among other recreational touristic activities. It also experiences significant year-round discharge of freshwater and sediments with different types of nutrients from the Sabaki River which runs through a catchment area dominated by agricultural settlements (Katwijk et al., 1993; Munyao et al., 2003; Kitheka, 2019; Wanjeri et al., 2021). KWS wardens administering the MPA advised that there is considerable illegal fishing in the park at night spilling over from the "reserve," an area adjoining the park where artisanal fishing is allowed. This represented the "exploited" site. The tidal range at these sites is approximately four meters. Mombasa Marine National Park was established in 1986 (Ngugi, 2002) with restrictions of protection being enforced commencing in 1991 (Tuda and Omar, 2012) and is the most visited of Kenya's marine parks by both local and international tourists (Owens, 1978). It was considered the "polluted" site; owing to its proximity to the urbanized touristic city, the park experiences pollution from hotels, hospitals, domestic and industrial waste disposal (Mwangi et al., 2001; Okuku et al., 2011). Because Mombasa is the primary port serving inland eastern and central African countries, the park is also impacted by marine traffic including oil pollution and dredge-spoil dumping (Mwangi et al., 2001). On the southern coast, 90 km from Mombasa, the Kisite-Mpunguti site served as the "baseline" site. This protected area comprises of Kisite Marine National Park and Mpunguti Reserve created in 1973 and gazetted in 1978. It is bordered by sparsely populated coral islands

and experiences the least human activities because it is 11 km offshore (Emerton and Tessema, 2001). There is no river runoff affecting the site (Okuku et al., 2019) and the most common activity here is snorkeling.

Sampling

Cross-sectional sampling and *in situ* measurements were done in November and December of 2016 in all coral reef sites, 200 – 500 m from the shore at a depth of 1–2 m in low tides and within 15–20 cm of a healthy-looking *Acropora* spp. colony – the dominant species on the Kenyan coral reefs (McClanahan et al., 2007). A total of six samples were collected, three near-coral seawater, and three sediments. From each site, approximately 5L of seawater, and 10 cm column of sediments collected at the base of the same coral colony with a 10 mL syringe barrel. To assess inter-site variations at the time of sampling physicochemical parameters (water temperature, pH, salinity, and dissolved oxygen) were determined *in situ*, using portable multiprobe water quality meters as per the manufacturer's instructions (YSI Inc., Yellow Springs, OH, United States). Finally, seawater samples were collected in triplicate 50-mL, for nutrient analysis. Samples were transported on ice to the laboratory for processing, typically within 3 h of sampling.

DNA Isolation

From each site, 4 L of seawater was vacuum-filtered (VWR, West Chester, PA, United States) through a 0.2-μm pore size membrane (Pall Corporation, Port Washington, WI, United States) to capture microbial cells which were then added to a bead tube with lysis buffer. Microbial DNA from seawater samples was isolated with PowerWater®, and from sediment samples with PowerSoil® DNA isolation kits according to the manufacturer's instructions (Mo Bio, Inc., Carlsbad, CA, United States). Quality and quantity of DNA was checked by NanoDrop spectrophotometry. Suitability for sequencing of DNA samples for metagenomics analysis was confirmed with 1% agarose gel electrophoresis following 16S rRNA PCR amplification (Rohwer et al., 2002).

Library Preparation and DNA Sequencing

Extracted DNA was subjected to whole-genome amplification by multiple displacement amplification (MDA) using the REPLI-g mini Kit according to the manufacturer's instructions (QiaGen, Hilden, Germany), except that incubations were held for 10 h instead of the maximum recommended 16 h. Sequencing libraries were prepared from 1 μg of DNA according to the manufacturers' preparation guide # 15036187 using the TruSeq DNA PCR-free library preparation kit (20015962/3, Illumina Inc.). Briefly, the DNA was fragmented using a Covaris E220 system, aiming at 350 bp fragments. Resulting DNA fragments were end-repaired, and the 3′ end adenylated to generate an overhang. Adapter sequences were ligated to the fragments via the A-overhang and the generated sequencing library was purified using AMPure XP beads (Beckman Coulter). The quality of the library was evaluated using the Fragment Analyzer system and a DNF-910 kit. The adapter-ligated fragments were quantified by qPCR using the Library quantification kit for Illumina (KAPA Biosystems/Roche) on a CFX384Touch instrument (Bio-Rad) before cluster generation and sequencing. A 200 pM solution of the individual sequencing libraries was subjected to cluster generation and paired-end sequencing with 150 bp read length using an S2 flowcell on the NovaSeq system (Illumina Inc.) using the v1 chemistry according to the manufacturer's protocols. Base-calling was done on the instrument by RTA 3.3.3 and the resulting.bcl files were demultiplexed and converted to FASTQ format with tools provided by Illumina Inc., allowing for one mismatch in the index sequence. Sequencing was performed by the NGI SNP&SEQ Technology Platform in Uppsala, Sweden[1].

Bioinformatics Analyses

The raw Illumina reads were trimmed at Q5 threshold (MacManes, 2014), and the adapters were removed using fastp v0.19.5 (Chen et al., 2018). Reads were uploaded into the MGX metagenomics analysis platform v20200508 (Jaenicke et al., 2018) where paired-end reads were merged and quality-filtered at Q35 for subsequent analysis. Trimmed sequences were deposited to the European Nucleotide Archive under the project accession # PRJEB30838.

Taxonomic profiling was performed by applying the Lowest Common Ancestor (LCA) pipeline based on the Kraken tool, against the NCBI non-redundant ("nr") database, enhanced by DIAMOND. Functional annotation was done using the clusters of orthologous groups (COG) of proteins database (Tatusov et al., 2000, 2001) with a BLASTX search of reads vs. the COG database applying MGX pipeline defaults (*E*-value cutoff $1e^{-5}$).

Statistical Analyses

Output files from the MGX metagenomics analysis platform were exported to the R statistical environment (R Core Team, 2020) for analysis and visualization. Taxa and metadata files were merged using *phyloseq* version 1.28.0 (McMurdie and Holmes, 2013) and used in subsequent microbial community analyses. Rarefaction curves were estimated with the *ranacapa* package (Kandlikar et al., 2018) and plotted using *ggplot2* (Wickham, 2016). Estimates of α-diversity were measured within sample categories using *estimate_richness()* function of the *phyloseq* package. Non-metric multidimensional scaling (nMDS) and principal coordinates analysis (PCoA) ordinations of Bray-Curtis dissimilarity were performed using taxonomy relative abundance matrix by the package *vegan* 2.5–6 (Oksanen et al., 2019).

Abundance of each COG was counted as the sum of reads mapping to it (Tatusov et al., 2000), which was then normalized by the size of the dataset. COGs were assigned into functional categories. Functional diversity was estimated by the Shannon index based on COG richness and evenness (Johnson and Pomati, 2020). Bray-Curtis distance based on the relative abundances was calculated to represent functional composition variation among the samples (Bray and Curtis, 1957), and PCoA was used to visualize the relative differences. Normality of distribution of the relative abundances were assessed using the Shapiro-Wilk normality test. Differences in functional relative abundances were tested for statistical significance using Kruskal–Wallis test for

[1] www.sequencing.se

TABLE 1 | Measurements of physicochemical characteristics of the three coral reefs within the marine national parks at the time of sampling for metagenomic sequencing.

Variable	Kisite	Mombasa	Malindi
Temperature (°C)	28.2	28.6	29.8
pH (unit)	8.0	8.1	8.0
Dissolved oxygen (ppm)	8.5	8.3	8.2
Salinity (ppt)	30.1	30.1	27.6

TABLE 2 | Nutrient levels measurements of the three coral reefs within the marine national parks at the time of sampling for microbiome sequencing.

Nutrient	Kisite	Mombasa	Malindi	*p*
NITRATES (NO_3^- -N)				
(mg/L + SD)	0.002 + 0.003	0.046 + 0.029	0.138 + 0.096	0.068
NITRITES (NO_2^- -N)				
(mg/L + SD)	0.063 + 0.019	0.059 + 0.028	0.076 + 0.005	0.552
AMMONIUM (NH_4^+ -N)				
(mg/L + SD)	0.035 + 0.006	0.040 + 0.006	0.040 + 0.07	0.572
PHOSPHATES (PO_4^{3-} -P)				
(mg/L + SD)	0.014 + 0.013	0.025 + 0.008	0.041 + 0.002	0.345

Between-sites comparisons tested by ANOVA.

COG categories, and chi-squared test for COG groups of proteins (p value < 0.05 as significance cut-off). False Discovery Rate (FDR) was corrected for using the Benjamini-Hochberg method (Benjamini and Hochberg, 1995).

Comparison of beta diversity between groups (both taxonomic and functional) was assessed by permutational multivariate analysis of variance (PERMANOVA) (Anderson, 2001) using the *adonis* test based on Bray-Curtis distances with 999 permutations in the package *vegan*.

RESULTS

Inter-Site Variations in Coral Reefs

Physicochemical parameters characteristics are presented in **Table 1**. Measurements were comparable across the sites except for temperature and salinity recorded in Malindi that seemed to vary with the other sites: temperature recordings across the study sites ranged between 28.2°C (Kisite-Mpunguti) and 29.8°C (Malindi), while salinity was estimated as 27.6 ppt at Malindi compared to 30.1 ppt in both Mombasa and Kisite-Mpunguti. Dissolved oxygen and pH varied only slightly between the study sites.

The nutrients assessed, except for nitrites, were highest at Malindi, the "exploited" site, and lowest at Kisite-Mpunguti, the "baseline" site (**Table 2**). Although observed, differences in nutrient concentrations between the study sites were not statistically significant (ANOVA).

Microbial Diversity

A total of 211,966,893 reads from 6 samples were processed, 43% of which were classified taxonomically and functionally. Taxonomic assignment showed that four superkingdoms were represented, the majority (95.8% of the assigned reads) being Bacteria, followed by Eukaryota (1.7%), Archaea (1.3%), and Viruses (1.2%). Eukaryotic taxa included both unicellular (e.g., protists) and multicellular species (including *Acropora* spp. and fish) whose gametes or fragmented cells may have been sampled – associated reads were excluded from analysis.

Rarefaction curves (**Figure 2A**) for most of the sequences from both datasets began to level off suggesting reasonable coverage of the microbial communities characterized with the processed reads. In all, 19,630 species (18,271 bacteria, 801 viruses and 558 archaea) belonging to 74 phyla were identified. Overall, Proteobacteria was the most dominant phylum with over 50% overall relative abundance (**Figure 2B**) followed by Bacteroides (20%) and Cyanobacteria (11%). Except for Kisite-Mpunguti metagenomes, Cyanobacteria was the most dominant phylum in the sediment sequences.

Bacteria

A total of 18,271 bacterial species assigned to 53 phyla were classified from near-coral seawater and sediment samples. Classes belonging to Proteobacteria and Bacteroidetes phyla had the highest relative abundances. Among the Proteobacteria classes, Gammaproteobacteria, Betaproteobacteria and Deltaproteobacteria were the most dominant. Other classes that had a relative abundance higher than 1% belonged to the phyla Actinobacteria (Actinobacteria) and Firmicutes (Bacilli, Clostridia and Planctomycetes). Further inspection was made of the phyla Proteobacteria, Bacteroidetes and Actinobacteria, which are considered copiotrophic i.e., inhabiting nutrient-rich environments. In all, 13,903 copiotrophic species were assigned, the distribution of which did not cluster by site (**Figure 3A**) (PERMANOVA, $p = 0.798$). The "baseline" site had the highest number of unique species and the "polluted" site the lowest (**Figure 3B**).

The first ten most abundant orders of the copiotrophic phyla assigned belonged to Proteobacteria and Bacteroidetes. Sequences assigned to Rhodobacterales (30.5%), Pelagibacterales (22.7%) orders of Proteobacteria, and the order Flavobacteriales (17.2%) of Bacteroidetes, were the most relatively abundant. By comparison, the relative abundance of each copiotrophic order was highest in either the "exploited" or "polluted" site except the orders Pelagibacterales, Cellvibrionales and Xanthomonadales whose relative abundances were highest in the "baseline" site (**Figure 4A**).

The relative abundances for sequences assigned to the common fecal indicator bacteria (FIB) genera (*Escherichia, Salmonella*, and *Campylobacter*) as well the alternative ones employed for microbial source tracking (i.e., *Bacteroides* and *Prevotella*) were less than 1% each (**Figure 4B**). The relative abundance of *Bacteroides* and *Prevotella* sequences from either "exploited" or "polluted" sites was more than three-fold higher than in the sequences from the "baseline" site. Relative abundances for *Campylobacter* and *Salmonella* sequences were comparable across the reef sites while that of *Escherichia* was more than two-fold higher in the sequences from the "baseline" site than in the sequences from either the "exploited" or "polluted" sites.

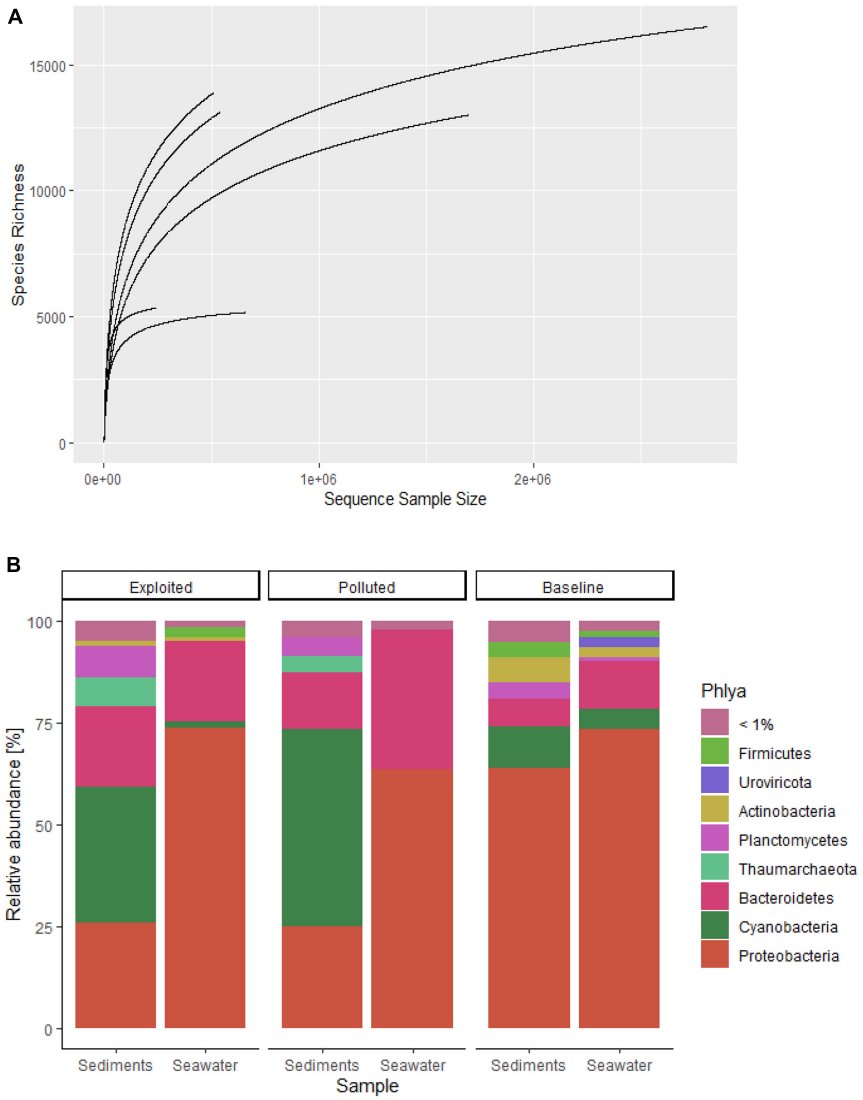

FIGURE 2 | (A) Rarefaction curves for community species richness, and **(B)** stacked charts of the distribution of community phyla with relative abundance >1% sequenced from near-coral seawater and sediment samples from Kenya reefs at Malindi (Exploited), Mombasa (Polluted) and Kisite-Mpunguti (Baseline) Marine National Parks.

Archaea

For the Archaea superkingdom, 558 species were assigned spread in eight phyla. Thaumarchaeota (88.5%) and Euryarchaeota (10.9%) were the most dominant phyla with the other six phyla accounting for only 0.7% of the sequences assigned. The distribution of archaeal orders with relative abundances above 1% is presented in **Figure 5A**. The order Nitrosopumilales recorded the highest relative abundance (>79%) followed by Methanosarcinales (5.1%). Sequences from the "baseline" site showed higher relative abundance for all orders except Nitrosopumilales (31%) for which the "exploited" and "polluted" site sequences were three-fold higher. Non-metric multidimensional scaling did not show any site-specific structuring of the Archaea superkingdom (PERMANOVA, $p = 0.733$).

Viruses

A 801 viral species, harbored in 11 phyla, were assigned to sequences from the near-coral seawater and sediment samples. Uroviricota (88.8%) dominated the sequences assigned. Only three other phyla i.e., Nucleocytoviricota (6.5%), Cressdnaviricota (2.5%), and Phixviricota (1.2%) had relative abundances of >1%.

Coliphages (viruses that infect coliform bacteria) constituted 85% of the sequences assigned at the family level. Myoviridae was the most dominant family (79.8%) (**Figure 5B**) and had higher relative abundance in the "baseline" (82.2%) than in the "exploited" (50.3%) and the "polluted" (69.7%) site metagenomes. The other coliphage families, Podoviridae, Siphoviridae and Microviridae were generally higher in the "polluted" (6.2, 5.9, and 5.5%) and "exploited" (2.4, 2.7, and 16.3%), than in the

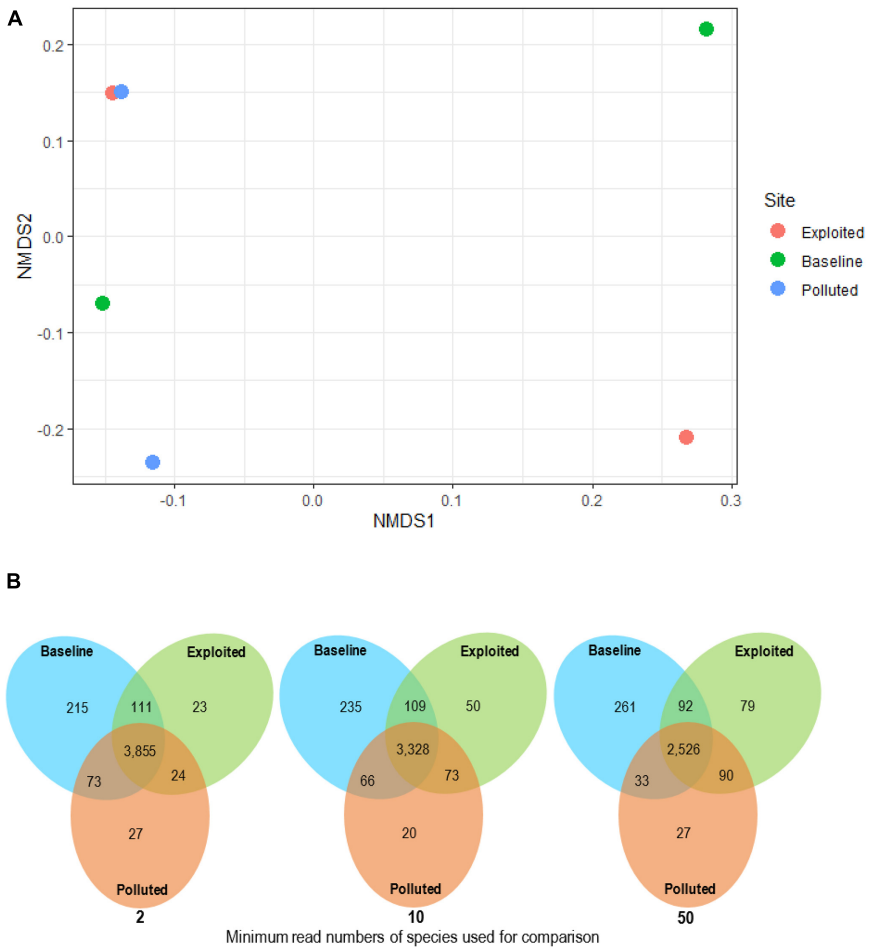

FIGURE 3 | (A) Bacterial community composition analyzed with non-metric multidimensional scaling (nMDS) plots using Bray-Curtis dissimilarity for near-coral seawater and sediment samples from Malindi (peach circle; exploited), Mombasa (aqua circles; polluted) and Kisite-Mpunguti (green circle; baseline) national marine parks. For this nMDS plot, stress = 0.05, r^2 = 0.998, and **(B)** venn diagrams showing the distribution of microbial species across study site metagenomes based on species with more than 2, 10, 50 reads.

"baseline" (2.0, 1.6, and < 0.1%) site sequences. Up to 96% of the relative abundance at the species level comprised of cyanophages particularly viruses for *Prochlorococcus* and *Synechococcus* whose relative abundances were consistently higher (up to five-fold higher) in the "baseline" site sequences than in either the "exploited" or "polluted" site sequences.

Microbiome Function

A total of 4,584 clusters of orthologous groups of proteins (COGs) belonging to 24 COG categories were classified. Overall, the categories of amino acid metabolism and transport (E), general functional prediction only (R), energy production and conversion (C), and translation (J) had the most relative abundance together constituting 41% of all sequences. In contrast, categories of nuclear structure (Y, <0.01%), RNA processing and modification (A, 0.02%), cytoskeleton (Z, 0.05%), and chromatin structure and dynamics (B, 0.08%) had the least relative abundances. Between sequences from the reef sites (**Figure 6**), no statistically significant differences in relative abundances were observed (Kruskal-Wallis, p = 0.997), except for subtle variations in a number of COG categories including amino acid transport and metabolism (E), energy production and conversion (C), translation (J), carbohydrate transport and metabolism (G), and signal transduction (T) where the "baseline" site sequences seemed to have higher relative abundance compared to the "exploited" and "polluted" site sequences. In contrast, the relative abundances for the categories of general functional prediction only (R), replication and repair (L), cell wall membrane biogenesis (M), lipid metabolism (I), coenzyme metabolism (H), and secondary structure (Q) where higher in either "exploited" or "polluted" site sequences than in the "baseline" site sequences.

The rarefaction curves (**Figure 7A**) shows the number of prevalent COGs identified with increasing sample number. The extent of sequencing showed that most COGs were recovered. The average per sample COG richness was estimated to be 4,111 + 205. The most prevalent COGs in all metagenomes corresponded to signal transduction histidine kinase (COG0642,

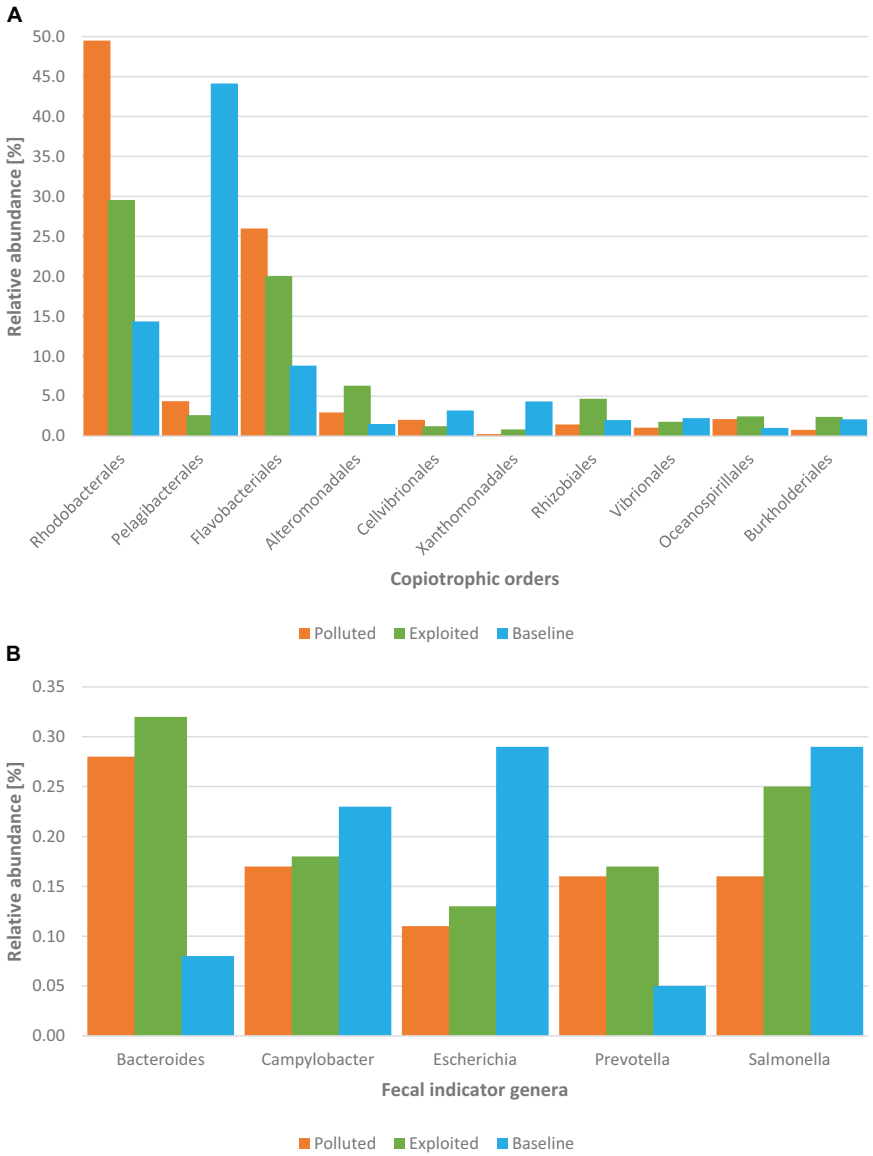

FIGURE 4 | Distribution of **(A)** the top ten most abundant orders of the copiotrophic phyla (Proteobacteria and Bacteroidetes), and **(B)** distribution of common FIB genera from metagenomes of near-coral seawater and sediment samples from Kenyan reefs at the national marine parks classified as "polluted" (Bronze; Mombasa), "exploited" (Olive; Malindi) and "baseline" (Sky; Kisite-Mpunguti).

0.80%), dehydrogenases with different specificities (COG1028, 0.75%), NAD-dependent aldehyde dehydrogenases (COG1012, 0.68%), and RTX toxins and related Ca2 + -binding proteins (COG2931, 0.61%). The "baseline" site sequences recorded 4,324 observed COGs compared to 4,000 ("exploited") and 4,008 ("polluted"), with a Shannon index of 7.12, compared to 7.06 ("exploited") and 7.09 ("polluted") (**Figure 7B**).

The "baseline" sequences had 2,153 COGs that were significantly enriched, the most abundant of which were functions for energy production and conversion including, and transcription regulation COG2414, COG0674, COG1013, COG1145, COG1148, and COG3808. In contrast, 565 COGs were significantly enriched in the "exploited" and "polluted" metagenomes. In these sites, the most abundant COGs were dominated by predicted proteins related to defense mechanisms and removal or sequestration of unwanted compounds (e.g., COG1132, COG0534, COG3491, and COG0488), replication, recombination and repair (e.g., COG0514, COG1193, COG1793, and COG1201), and inorganic ion transport and metabolism (e.g., COG0659, COG4771, and COG4772) (**Figure 8**).

DISCUSSION

Microorganisms play a critical role to reef ecosystem health and resilience through mediating nutrient cycling, interactions

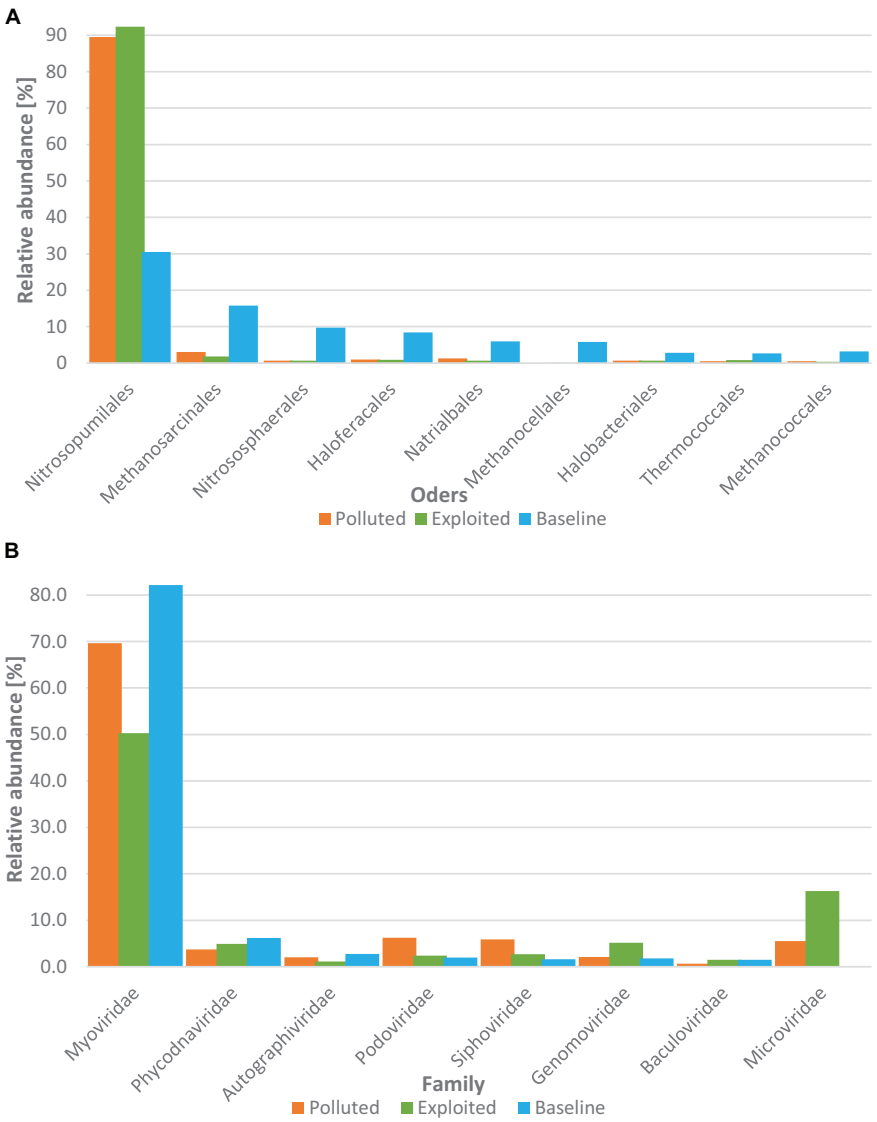

FIGURE 5 | Distribution of **(A)** archaeal orders and **(B)** viral families with overall relative abundance > 1% grouped by study site i.e., "polluted" (bronze), "exploited" (olive) and "baseline" (sky).

with macro-organisms and provision of chemical cues influence the recruitment of diverse reef taxa. These processes may be impacted by environmental changes that cause microbial compositional and functional alterations which may, in turn, have consequences for the functioning of coral ecosystems (Glasl et al., 2018). Therefore, assessing changes in reef microbial communities and functional potential may provide early indicator of ecosystem impacts, and can help with development of diagnostic tools for monitoring shifts in coral reef health under different environmental states (Kisand et al., 2012; Bourlat et al., 2013; Glasl et al., 2017; Goodwin et al., 2017). We annotated near-coral seawater and sediment metagenomes from Kenyan coral reefs and compared microbial taxonomic and functional diversity across a gradient of the human activities the reefs are exposed to. Physicochemical parameters were also estimated to assess inter-site variations at the time of sampling.

Environmental variables at the coral reefs sampled fell mostly within the ranges considered suitable for coral growth in tropical oceans (Kannapiran et al., 2008; Henkel, 2010; Guan et al., 2015; Roik et al., 2016), except for salinity which was low (i.e., 27.6 – 30.1 ppt) compared to previous estimates (32 – 33 ppt) (Obura, 2001). This may have been due to high rainfalls during sampling and, especially for Malindi which had the lowest salinity occasioned by River Sabaki's discharge into the ocean (Kitheka, 2019). During heavy rainfalls, salinity has been known to decrease down to 12 ppt in shallow reef flats (Obura, 2001). Except for nitrites, concentrations for all other nutrients assessed were higher at the "exploited" and "polluted" sites than at the "baseline" site suggesting influence by the surrounding human

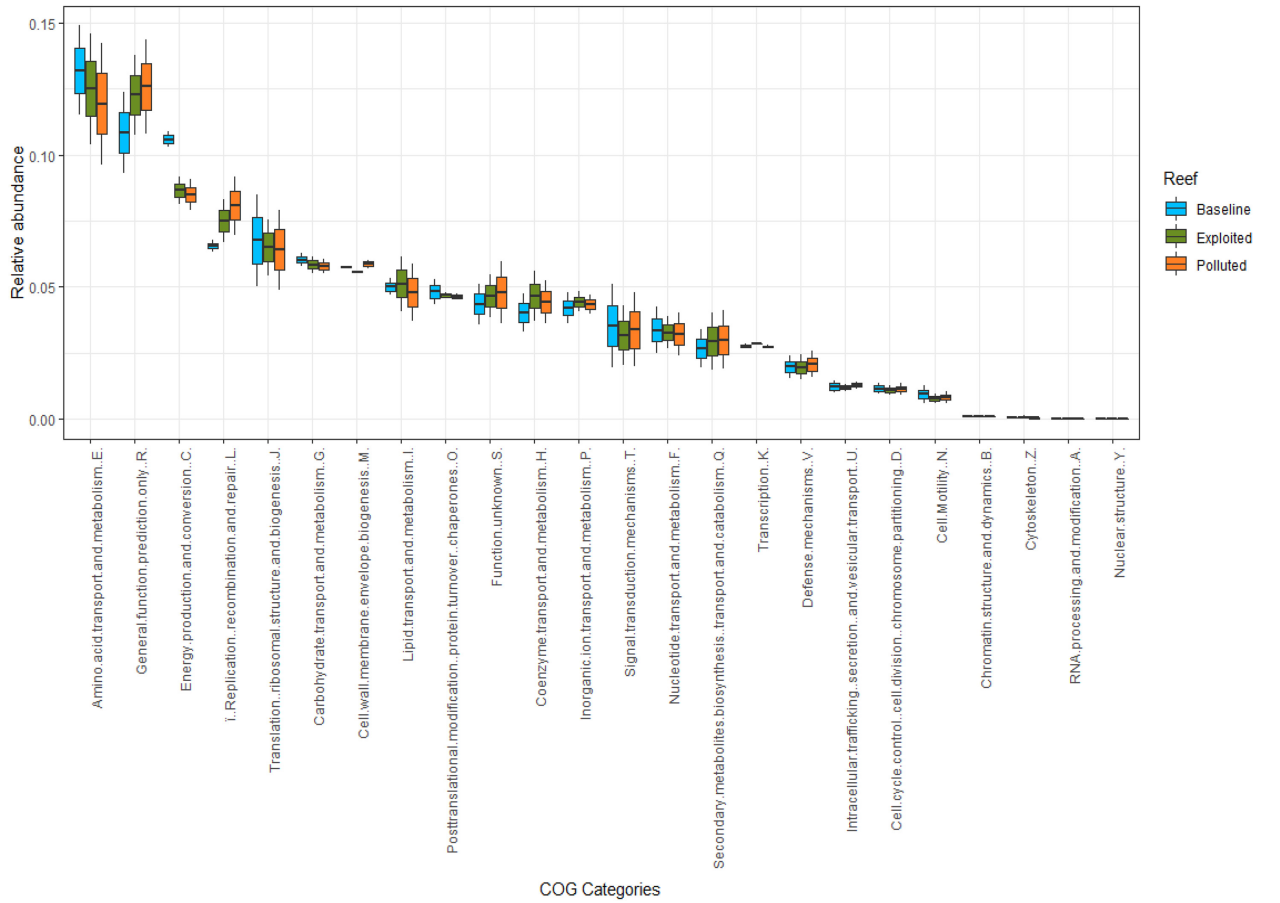

FIGURE 6 | Relative abundances of COG functional categories compared between study sites i.e., "baseline" (sky blue), "exploited" (olive), and "polluted" (bronze).

activities. These differences were, however, not statistically significant. Although temporal variations were not investigated in this study, current estimates in the "no-take" marine protected areas are typical of previous measurements taken about two decades ago (McClanahan, 1988; Obura, 2001). Being a cross-sectional survey, the reported measurements represented the quality of the coral reef water at the time of sampling, and not necessarily the stable state. A recent study modeling the contribution of natural and human factors in predicting water quality identified human influences as the random components of variation associated with site-based differences (Houk et al., 2020). The estimates in this study suggest, therefore, that at the time of sampling human impacts to the coral reefs in the "no-take" marine protected areas were undetectable or indistinguishable by water quality measurements.

Taxonomic composition, especially of the most abundant taxa, was largely consistent with other marine microbiota (Williamson et al., 2012; Sunagawa et al., 2015; Godoy-Vitorino et al., 2017; Santoro et al., 2019). The estimate for species richness was within the same order of magnitude as the previous metagenomic estimate for global oceans (Sunagawa et al., 2015). Although the majority of assignments were shared, there were sequences unique to each site whereby Kisite-Mpunguti ("baseline") had the highest number, reinforcing the hypothesis that rather than every microbe being ubiquitous, taxa are selected or structured by the environment (Flaviani et al., 2018). The seawater and sediment samples collected within coral reefs generally harbored microbial composition consistent with the typical taxa enriched by metabolic products of corals i.e., copiotrophic bacterial groups (including Gammaproteobacteria, Betaproteobacteria, and Bacteroidetes), ammonia oxidizing archaea (AOA) of the order Nitrosopumilales, and phages for the copiotrophic bacteria (coliphages) i.e., Podoviridae, Siphoviridae, and Microviridae (Sunagawa et al., 2010; Kelly et al., 2014; Godoy-Vitorino et al., 2017; Thurber et al., 2017; Weber et al., 2019). Although coral reef seawaters are typically dominated by copiotrophic bacterial community due to increased organic matter from mucus and other nutrients released by corals (Bourne and Webster, 2013), between-sites differences observed in the bacterial relative abundances seemed to correspond to the varying magnitudes of human activities around the coral reef sites compared. Most copiotrophic bacteria, especially the most abundant ones, had higher relative abundances in either the "exploited" or "polluted" than in the "baseline" site sequences. This is significant considering that copiotrophic bacteria thrive in high nutrient environments and include taxa utilized in water microbiology

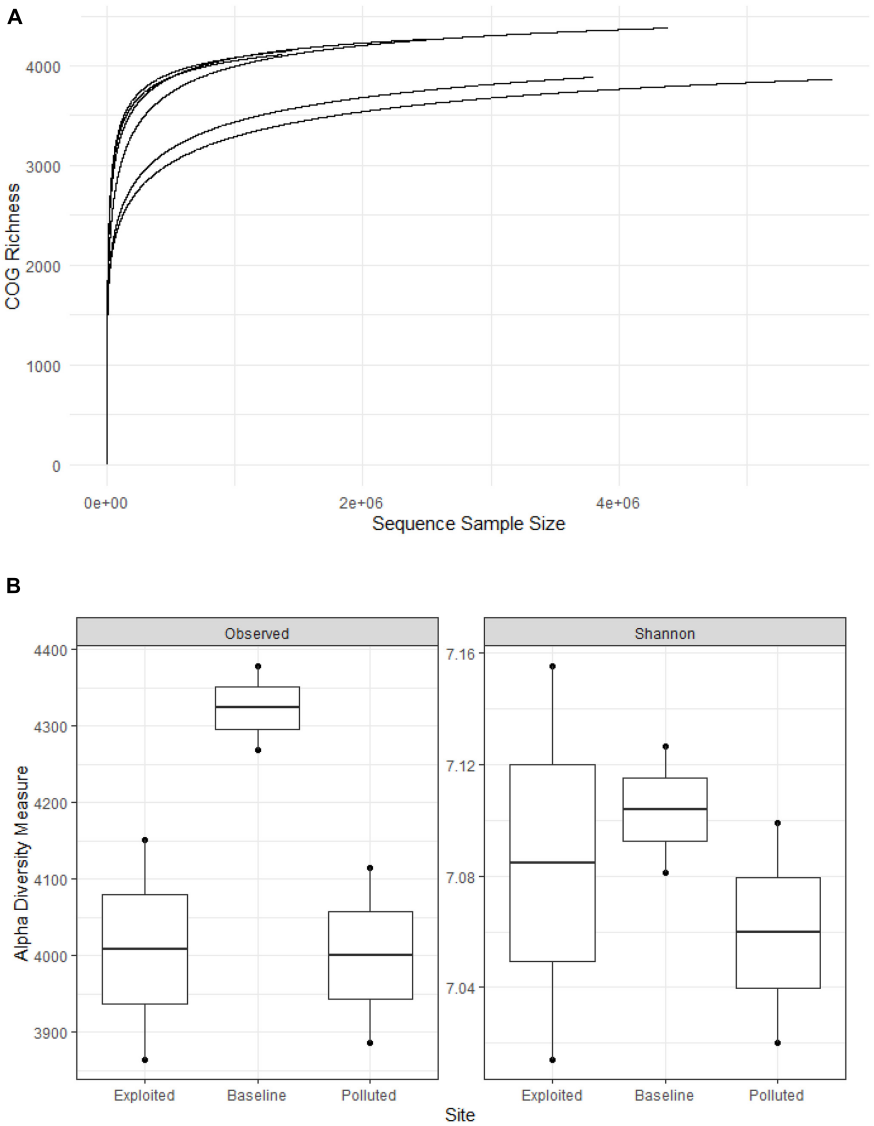

FIGURE 7 | (A) Rarefaction curves and **(B)** plots of alpha diversity metrics for clusters of orthologous groups of proteins (COG) richness on the near-coral seawater and sediment metagenomes from Kenya reefs on the WIO.

as fecal indicators (Buccheri et al., 2019). Also, the genera *Bacteroides* and *Prevotella* exhibited higher relative abundance in both the "exploited" and "polluted" than in the "baseline" site sequences – these genera are increasingly exploited as alternative groups to replace the less reliable traditional FIB. Contrary to expectations, the relative abundance for members of the order Pelagibacterales and the traditional FIB genera *Escherichia, Salmonella*, and *Campylobacter* were higher in the "baseline" than in the "exploited" and "polluted" site sequences (**Figure 4**). Pelagibacterales belongs to the class Alphaproteobacteria whose ubiquitous members, although heterotrophs, are known to thrive at low nutrient concentrations typical of open ocean conditions (Kelly et al., 2014; Zhao et al., 2017). The higher relative abundance of this group in the "baseline" than in the "exploited" and "polluted" site sequences may have been, therefore, indicative of differences in nutrient levels at the sites perhaps due to the surrounding human activities. As for the FIB genera, it is not clear why relative abundances did not correlate with human impact gradients at the coral reef sites. One possible explanation is what has been termed as "connectivity footprint" – the phenomenon that even MPAs thousands of kilometers away can be influenced by human activities due to dispersal by ocean currents (Robinson et al., 2017). The "baseline" site, which recorded highest relative abundances for the traditional FIB genera was sampled in December during the north-east monsoon (NEM) which is characterized by the convergence of the southward flowing Somali current (SC) with the northward flowing East African coastal current (EACC) and upwelling along the Kenyan coast (Heip et al., 1995; Mayorga-Adame et al., 2016). It is conceivable that the fecal bacteria originated elsewhere and

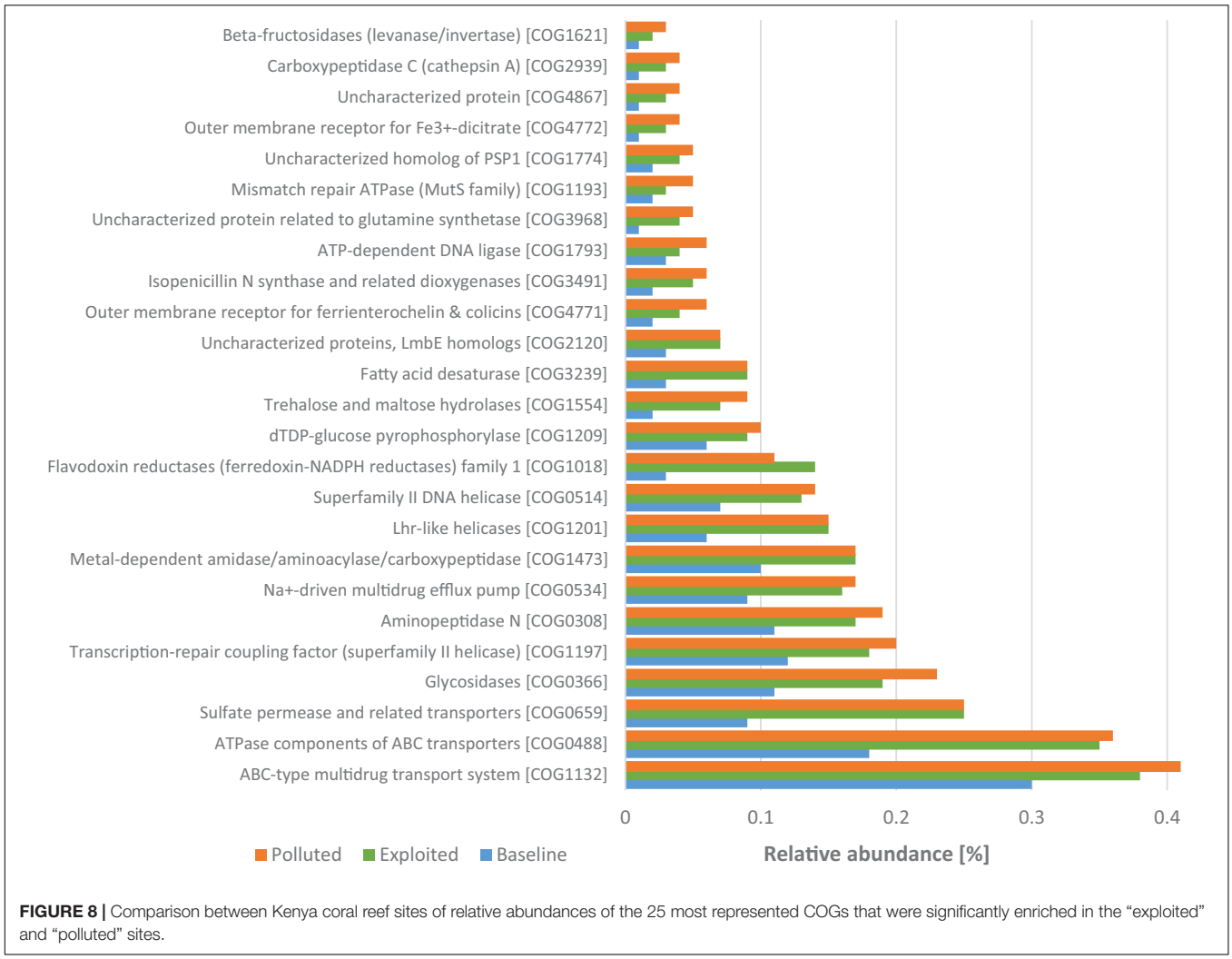

FIGURE 8 | Comparison between Kenya coral reef sites of relative abundances of the 25 most represented COGs that were significantly enriched in the "exploited" and "polluted" sites.

transported to the "baseline" site by the SC as the site is south to the "exploited" and "polluted" sites. However, if this was the case, similar relative abundances would have been observed of the other taxa, for instance copiotrophic bacteria and coliphages. An alternative explanation is that FIB detected at the "baseline" site were of sources not related to human fecal contamination. FIBs are shed in the feces of many different animals (Harwood et al., 2014), and naturalized or environmentally adapted strains of FIB can persist and multiply in a broad range of habitats far removed from their natural reservoir of the animal gut (Devane et al., 2020). It is for these reasons that traditional FIB genera are generally considered unreliable as fecal indicators.

Coliphages i.e., viruses that infect coliform bacteria, are considered better predictor of fecal pollution in seawater than FIBs (Burbano-Rosero et al., 2011) because they outlive their bacterial hosts, they can thrive in marine environments unlike some of their anaerobic hosts, they are more resistant to disinfection and diffuse further distances from pollution sources (Ebdon et al., 2012; Bari and Yeasmin, 2014). In this study, relative abundances of all coliphage families assessed, except one, were higher in the "exploited" and "polluted" site sequences than in the "baseline" site sequences. The coliphage family, Myoviridae, had higher relative abundance in the "baseline" site sequences than in the "exploited" and "polluted" site sequences. The cause for this exception is not clear but it may have been influenced by the relative abundance of *Escherichia* which was higher in the "baseline" site sequences and which members of the Myoviridae family are known to preferentially infect (Tao and Rao, 2019). Cyanophages too recorded relative abundances commensurate to the bacteria they infect, cyanobacteria. Phages for *Prochlorococcus* and *Synechococcus* were up to five-fold higher in the "baseline" site sequences than in either the "exploited" or "polluted" site sequences. *Synechococcus* and *Prochlorococcus* are considered the most important primary producers in the tropical oceans, responsible for a large percentage of the photosynthetic production of oxygen (Waterbury et al., 1979; Biller et al., 2015; Kim et al., 2018) and it is thought that their phages mediate their population sizes and evolutionary trajectories (Sullivan et al., 2005). Being autotrophs, members of these genera are usually found in great abundance in ocean zones low in nutrients (Dinsdale et al., 2008; Kelly et al., 2014). These findings call for further investigations to establish the stability of these

trends over time and space for the potential utilization of these virus groups, especially the coliphages, as surrogates for human impacts in coral reefs.

Among the Archaea groups, the AOA order Nitrosopumilales had the most obvious correlation with human activity gradient; in comparison to the "baseline" site sequences, the order was three times higher in the "exploited" and "polluted" site sequences. Members of this order are key players in nitrification processes (Alvarez-Yela et al., 2019) that have been shown to seek nutrient-rich environments where they utilize urea and ammonia as substrate (Bayer et al., 2016). All the other orders with over 1% relative abundance were higher in the "baseline" than in the "exploited" and "polluted" site sequences.

The COG richness observed in this study was slightly higher but comparable to the others previously reported by studies of global oceans and coral ecosystems (Carlos et al., 2016; Varasteh et al., 2020; Zhang et al., 2020). The predicted proteins for signal transduction histidine kinase which enables microbes to sense, respond, and adapt to a wide range of environments, stressors, and growth conditions (Skerker et al., 2005) were the most abundant. Furthermore, the coral ecosphere sequences had overrepresentation of predicted proteins related to replication, recombination and repair especially transposases that play a role in adaptation to diverse environments (Vigil-Stenman et al., 2017), and predicted proteins for energy production and conversion which is an adaptation for high nutrient uptake and synthesis needed in low nutrient environments (Gudhka et al., 2015). These are likely strategies for optimizing rapid growth in the presence of labile nutrients – an adaptation of copiotrophs e.g., Gammaproteobacteria in environments of high levels of stress factors and nutrients (Kisand et al., 2012). These observations suggest that the three coral reefs had substantial levels of stressors and nutrients. Nonetheless, there were subtle differences across the human impacts' gradient suggesting heterogeneity, possibly anthropogenically influenced.

Kisite-Mpunguti marine park ("baseline") sequences were enriched, more than the "exploited" and "polluted" sequences, with protein groups essential for functions related to uptake and synthesis of nutrients and transcription – a common observation among oligotrophic organisms as an adaptation to low levels of nutrients (Lauro et al., 2009).

Conversely, metagenomes from Malindi ("exploited") and Mombasa ("polluted") marine parks had overrepresentation of COGs suggestive of mitigation of environment stressors. Here the enriched COGs included, for instance, proteins related to defense mechanisms such as transporters that prevent intracellular accumulation of toxic compounds (Wilkens, 2015), which serves as the major defense mechanism against antimicrobial compounds (Lubelski et al., 2007). For instance, a recent study assessing antibiotic resistance genes along a pollution gradient also found the highest abundance of transporters at the most polluted site (Chen et al., 2019). COGs for DNA replication, recombination and repair were also significantly overrepresented suggesting exposure to agents of DNA damage (Buckley et al., 2020; Zhang et al., 2020). Together, these observations reflect hostile environmental conditions. It is potentially significant that the genes that ward off environmental insults are significantly enriched in the metagenomes from Malindi and Mombasa marine parks, the sites with known degradative human activities ashore (Katwijk et al., 1993; Heip et al., 1995; Okuku et al., 2011; Ongore et al., 2013; Wanjeri et al., 2021), and not in Kisite-Mpunguti marine park which is situated farther from human settlements thereby potentially experiencing limited direct human impacts. Similar observations have been made, in a study comparing microbial functions of a highly polluted and protected marine environments (Kisand et al., 2012), and attributed to adaptations to an environment characterized by highly heterogeneous, variable and unfamiliar stimuli from anthropogenic source. These observations provide insights into the functional shifts contributed by human impacts, and potential COGs that may be utilized as indicators of marine health generally, and coral reef specifically. However, being DNA-based observations, these findings need validation by transcriptomics and proteomics approaches to confirm the actual proteins that are overexpressed in the respective sites.

CONCLUSION

Our results reveal subtle taxonomic and functional between-sites heterogeneity suggestive of human influence. The environmental significance of inter-site variations observed in this study needs to be confirmed through robust studies controlling for seasonal variations and spatial stability. Nonetheless our findings underscore the potential of microbial ecology in informing strategies of marine monitoring. We therefore recommend integration of microbial sampling in the management of national marine parks and the respective services they provide by both the national and county government agencies.

DATA AVAILABILITY STATEMENT

The datasets presented in this study can be found in online repositories. Trimmed sequences are deposited to the European Nucleotide Archive under the study accession number PRJEB30838.

AUTHOR CONTRIBUTIONS

SW designed the study, conducted field sampling and laboratory processing, performed the bioinformatics analyses, and drafted and revised the manuscript. HG designed the study, coordinated sequencing, performed the bioinformatics analyses, and drafted the manuscript. EV, OK-L, NW, EB-R, AM, and SV helped design the study and edited the manuscript. All authors contributed to the article and approved the submitted version.

FUNDING

This work was funded by the Swedish University for Agricultural Sciences and by the Swedish Research Council grant 2015-03443.

ACKNOWLEDGMENTS

This work was carried out under research permit from the National Commission for Science, Technology and Innovation (NACOSTI). Kenya Wildlife Service (KWS) provided logistical support and granted permission to work in the marine parks and the National Environment Management Authority (NEMA) provided access permits. The authors would like to acknowledge support from Science for Life Laboratory, the National Genomics Infrastructure, NGI, and Uppmax for providing assistance in massive parallel sequencing and computational infrastructure.

REFERENCES

Alvarez-Yela, A. C., Mosquera-Rendón, J., Noreña-P, A., Cristancho, M., and López-Alvarez, D. (2019). Microbial diversity exploration of marine hosts at serrana bank, a Coral Atoll of the seaflower biosphere reserve. *Front. Mar. Sci.* 6:338. doi: 10.3389/fmars.2019.00338

Anderson, M. J. (2001). A new method for non-parametric multivariate analysis of variance. *Austral. Ecol.* 26, 32–46. doi: 10.1111/j.1442-9993.2001.01070.pp.x

Bari, M. L., and Yeasmin, S. (2014). *Water Quality Assessment: Modern Microbiological Techniques. Encyclopedia of Food Microbiology*, Second Edn. Amsterdam: Elsevier.

Barott, K. L., and Rohwer, F. L. (2012). Unseen players shape benthic competition on coral reefs. *Trends Microbiol.* 20, 621–628. doi: 10.1016/j.tim.2012.08.004

Bayer, B., Vojvoda, J., Offre, P., Alves, R. J. E., Elisabeth, N. H., Garcia, J. A. L., et al. (2016). Physiological and genomic characterization of two novel marine thaumarchaeal strains indicates niche differentiation. *ISME J.* 10, 1051–1063. doi: 10.1038/ismej.2015.200

Behzad, H., Ibarra, M. A., Mineta, K., and Gojobori, T. (2016). Metagenomic studies of the Red Sea. *Gene* 576, 717–723. doi: 10.1016/j.gene.2015.10.034

Bellwood, D. R., Streit, R. P., Brandl, S. J., and Tebbett, S. B. (2019). The meaning of the term 'function' in ecology: A coral reef perspective. *Funct. Ecol.* 33, 948–961. doi: 10.1111/1365-2435.13265

Benjamini, Y., and Hochberg, Y. (1995). Controlling the false discovery rate: A practical and powerful approach to multiple testing. *J. R. Stat. Soc. Ser.B* 57, 289–300. doi: 10.1111/j.2517-6161.1995.tb02031.x

Biller, S. J., Berube, P. M., Lindell, D., and Chisholm, S. W. (2015). Prochlorococcus: the structure and function of collective diversity. *Nat. Rev. Microbiol.* 13, 13–27. doi: 10.1038/nrmicro3378

Bourlat, S. J., Borja, A., Gilbert, J., Taylor, M. I., Davies, N., Weisberg, S. B., et al. (2013). Genomics in marine monitoring: New opportunities for assessing marine health status. *Mar. Pollut. Bull.* 74, 19–31. doi: 10.1016/j.marpolbul.2013.05.042

Bourne, D. G., and Webster, N. S. (2013). "Coral reef bacterial communities," in *The Prokaryotes - Prokaryotic Communities and Ecophysiology*, eds E. Rosenberg, E. DeLong, S. Lory, E. Stackebrandt, and F. L. Thompson (Berlin: Springer), 163–187. doi: 10.1007/978-3-642-30123-0_48

Bray, J. R., and Curtis, J. T. (1957). An ordination of the upland forest communities of southern wisconsin. *Ecol. Monogr.* 27, 325–349. doi: 10.2307/1942268

Bruce, T., Meirelles, P. M., Garcia, G., Paranhos, R., Rezende, C. E., de Moura, R. L., et al. (2012). Abrolhos bank reef health evaluated by means of water quality, microbial diversity, benthic cover, and fish biomass data. *PLoS One* 7:36687. doi: 10.1371/journal.pone.0036687

Buccheri, M. A., Salvo, E., Coci, M., Quero, G. M., Zoccarato, L., Privitera, V., et al. (2019). Investigating microbial indicators of anthropogenic marine pollution by 16S and 18S High-Throughput Sequencing (HTS) library analysis. *FEMS Microbiol. Lett.* 366:fnz179. doi: 10.1093/femsle/fnz179

Buckley, R. J., Kramm, K., Cooper, C. D. O., Grohmann, D., and Bolt, E. L. (2020). Mechanistic insights into Lhr helicase function in DNA repair. *Biochem. J.* 477, 2935–2947. doi: 10.1042/BCJ20200379

Burbano-Rosero, E. M., Ueda-Ito, M., Kisielius, J. J., Nagasse-Sugahara, T. K., Almeida, B. C., Souza, C. P., et al. (2011). Diversity of Somatic coliphages in coastal regions with different levels of anthropogenic activity in São Paulo state, Brazil. *Appl. Environ. Microbiol.* 77, 4208–4216. doi: 10.1128/AEM.02780-10

Carlos, C., Pereira, L. B., and Ottoboni, L. M. M. (2016). Comparative genomics of *Paracoccus sp*. SM22M-07 isolated from coral mucus: insights into bacteria-host interactions. *Curr. Genet.* 63, 509–518. doi: 10.1007/s00294-016-0658-3

Chen, J., McIlroy, S. E., Archana, A., Baker, D. M., and Panagiotou, G. (2019). A pollution gradient contributes to the taxonomic, functional, and resistome diversity of microbial communities in marine sediments. *Microbiome* 7:104. doi: 10.1186/s40168-019-0714-6

Chen, S., Zhou, Y., Chen, Y., and Gu, J. (2018). Fastp: An ultra-fast all-in-one FASTQ preprocessor. *Bioinformatics* 34, i884–i890. doi: 10.1093/bioinformatics/bty560

Devane, M. L., Moriarty, E., Weaver, L., Cookson, A., and Gilpin, B. (2020). Fecal indicator bacteria from environmental sources; strategies for identification to improve water quality monitoring. *Water Res.* 185:116204. doi: 10.1016/j.watres.2020.116204

Díez, B., Nylander, J. A. A., Ininbergs, K., Dupont, C. L., Allen, A. E., Yooseph, S., et al. (2016). Metagenomic analysis of the indian ocean picocyanobacterial community: structure, potential function and evolution. *Plos One* 11:e0155757. doi: 10.1371/journal.pone.0155757

Dinsdale, E. A., Pantos, O., Smriga, S., Edwards, R. A., Angly, F., Wegley, L., et al. (2008). Microbial ecology of four coral atolls in the northern line islands. *PLoS One* 3:e1584. doi: 10.1371/journal.pone.0001584

Ebdon, J. E., Sellwood, J., Shore, J., and Taylor, H. D. (2012). Phages of *bacteroides* (GB-124): A novel tool for viral waterborne disease control? *Environ. Sci. Technol.* 46, 1163–1169. doi: 10.1021/es202874p

Emerton, L., and Tessema, Y. (2001). *Marine Protected Areas: the Case of Kisite Marine National Park and Mpunguti Marine National Reserve, Kenya*. Nairobi, Kenya: IUCN Eastern Africa Regional Office, 32.

Flaviani, F., Schroeder, D. C., Lebret, K., Balestreri, C., Highfield, A. C., Schroeder, J. L., et al. (2018). Distinct oceanic microbiomes from viruses to protists located near the Antarctic Circumpolar current. *Front. Microbiol.* 9:1474. doi: 10.3389/fmicb.2018.01474

Glasl, B., Bourne, D. G., Frade, P. R., Thomas, T., Schaffelke, B., and Webster, N. S. (2019). Microbial indicators of environmental perturbations in coral reef ecosystems. *Microbiome* 7:94. doi: 10.1186/s40168-019-0705-7

Glasl, B., Bourne, D. G., Frade, P. R., and Webster, N. S. (2018). Establishing microbial baselines to identify indicators of coral reef health. *Microbiol. Australia* 39:42. doi: 10.1071/MA18011

Glasl, B., Webster, N. S., and Bourne, D. G. (2017). Microbial indicators as a diagnostic tool for assessing water quality and climate stress in coral reef ecosystems. *Mar. Biol.* 164:91. doi: 10.1007/s00227-017-3097-x

Godoy-Vitorino, F., Ruiz-Diaz, C. P., Rivera-Seda, A., Ramírez-Lugo, J. S., and Toledo-Hernández, C. (2017). The microbial biosphere of the coral acropora cervicornis in Northeastern Puerto Rico. *PeerJ.* 5:e3717. doi: 10.7717/peerj.3717

Goodwin, K. D., Thompson, L. R., Duarte, B., Kahlke, T., Thompson, A. R., Marques, J. C., et al. (2017). DNA sequencing as a tool to monitor marine ecological status. *Front. Mar. Sci.* 4:e1002358–14. doi: 10.3389/fmars.2017.00107

Guan, Y., Hohn, S., and Merico, A. (2015). Suitable environmental ranges for potential coral reef habitats in the tropical ocean. *PLoS One* 10:e0128831. doi: 10.1371/journal.pone.0128831

Gudhka, R. K., Neilan, B. A., and Burns, B. P. (2015). Adaptation, ecology, and evolution of the halophilic stromatolite archaeon halococcus hamelinensis inferred through genome analyses. *Archaea* 2015:241608. doi: 10.1155/2015/241608

Harwood, V. J., Staley, C., Badgley, B. D., Borges, K., and Korajkic, A. (2014). Microbial source tracking markers for detection of fecal contamination in environmental waters: Relationships between pathogens and human health outcomes. *FEMS Microbiol. Rev.* 38, 1–40. doi: 10.1111/1574-6976.12031

Hattam, C., Evans, L., Morrissey, K., Hooper, T., Young, K., Khalid, F., et al. (2020). Building resilience in practice to support coral communities in the Western Indian Ocean. *Environ. Sci. Policy* 106, 182–190. doi: 10.1016/j.envsci.2020.02.006

Heip, C., Hernminga, M., and de Bie, M. (1995). *Moonsoons and Coastal Ecosystems in Kenya*, 5th Edn. Lieden: National Museum of Natural History.

Henkel, T. P. (2010). *Coral Reefs*. Available Online at: https://www.nature.com/scitable/knowledge/library/coral-reefs-15786954/ (accessed November 6, 2019).

Houk, P., Comeros-Raynal, M., Sudek, M., Vaeoso, M., Mcguire, K., and Regis, J. (2020). Nutrient thresholds to protect water quality and coral reefs. *Mar. Pollut. Bull.* 159:111451. doi: 10.1016/j.marpolbul.2020.111451

Jaenicke, S., Albaum, S. P., Blumenkamp, P., Linke, B., Stoye, J., and Goesmann, A. (2018). Flexible metagenome analysis using the MGX framework. *Microbiome* 6:76. doi: 10.1186/s40168-018-0460-1

Johnson, D. R., and Pomati, F. (2020). A brief guide for the measurement and interpretation of microbial functional diversity. *Environ. Microbiol.* 22, 3039–3048. doi: 10.1111/1462-2920.15147

Kandlikar, G. S., Gold, Z. J., Cowen, M. C., Meyer, R. S., Freise, A. C., Kraft, N. J. B., et al. (2018). Ranacapa: An R package and shiny web app to explore environmental DNA data with exploratory statistics and interactive visualizations. *F1000Research* 7:1734. doi: 10.12688/f1000research.16680.1

Kannapiran, E., Kannan, L., Purushothaman, A., and Thangarajdou, T. (2008). Physico-chemical and microbial characteristics of the coral reef environment of the Gulf of Mannar marine biosphere reserve, India. *J. Environ. Biol.* 29, 215–222.

Katwijk, M. M., Van Meier, N. E., Loon, R., Van Hove, E. M., Van Giesen, W. B. J. T., Velde, G., et al. (1993). Sabaki River sediment load and coral stress: correlation between sediments and condition of the Malindi-Watamu reefs in Kenya (Indian Ocean). *Mar. Biol.* 683, 675–676. doi: 10.1007/bf00349780

Kelly, L. W., Williams, G. J., Barott, K. L., Carlson, C. A., Dinsdale, E. A., Edwards, R. A., et al. (2014). Local genomic adaptation of coral reef-associated microbiomes to gradients of natural variability and anthropogenic stressors. *Proc. Natl. Acad. Sci.* 111, 10227–10232. doi: 10.1073/pnas.1403319111

Kim, Y., Jeon, J., Kwak, M. S., Kim, G. H., Koh, I., and Rho, M. (2018). Photosynthetic functions of Synechococcus in the ocean microbiomes of diverse salinity and seasons. *PLoS One* 13:e0190266. doi: 10.1371/journal.pone.0190266

Kisand, V., Valente, A., Lahm, A., Tanet, G., and Lettieri, T. (2012). Phylogenetic and functional metagenomic profiling for assessing microbial biodiversity in environmental monitoring. *PLoS One* 7:43630. doi: 10.1371/journal.pone.0043630

Kitheka, J. U. (2019). Salinity and salt fluxes in a polluted tropical river: The case study of the Athi river in Kenya. *J. Hydrol. Reg. Stud.* 24:100614. doi: 10.1016/j.ejrh.2019.100614

Lauro, F. M., McDougald, D., Thomas, T., Williams, T. J., Egan, S., Rice, S., et al. (2009). The genomic basis of trophic strategy in marine bacteria. *Proc. Natl. Acad. Sci. U S A* 106, 15527–15533. doi: 10.1073/pnas.0903507106

Lubelski, J., Konings, W. N., and Driessen, A. J. M. (2007). Distribution and physiology of ABC-type transporters contributing to multidrug resistance in bacteria. *Microbiol. Mol. Biol. Rev.* 71, 463–476. doi: 10.1128/mmbr.00001-07

MacManes, M. D. (2014). On the optimal trimming of high-throughput mRNA sequence data. *Front. Genet.* 5:13. doi: 10.3389/fgene.2014.00013

Mayorga-Adame, G. C., Ted Strub, P., Batchelder, H. P., and Spitz, Y. H. (2016). Characterizing the circulation off the Kenyan-Tanzanian coast using an ocean model. *J. Geophys. Res. Oceans* 121, 1377–1399. doi: 10.1002/2015JC010860

McClanahan, T. (1988). Seasonality in East Africa's coastal waters. *Mar. Ecol. Prog. Ser.* 44, 191–199. doi: 10.3354/meps044191

McClanahan, T. R., Ateweberhan, M., Graham, N. A. J., Wilson, S. K., Ruiz Sebastián, C., Guillaume, M. M. M., et al. (2007). Western indian ocean coral communities: bleaching responses and susceptibility to extinction. *Mar. Ecol. Prog. Ser.* 337, 1–13. doi: 10.3354/meps337001

McClanahan, T. R., Graham, N. A. J., Calnan, J. M., and Macneil, M. A. (2010). Toward pristine biomass: reef fish recovery in coral reef marine protected areas in Kenya. *Ecol. Appl.* 17, 1055–1067. doi: 10.1890/06-1450

McDole, T., Nulton, J., Barott, K. L., Felts, B., Hand, C., Hatay, M., et al. (2012). Assessing coral reefs on a pacific-wide scale using the microbialization score. *PLoS One* 7:e43233. doi: 10.1371/journal.pone.0043233

McMurdie, P. J., and Holmes, S. (2013). Phyloseq: An R package for reproducible interactive analysis and graphics of microbiome census data. *PLoS One* 8:e61217. doi: 10.1371/journal.pone.0061217

Munyao, T., Tole, M. P., and Jungerius, P. D. (2003). *Sabaki River transport and deposition in the Indian Ocean. Recent Advances in Coastal Ecology, Studies from Kenya*. Netherland: African Studies Centre, 119–132.

Mwangi, S., Dzeha, T., and Kimathi, A. (2001). *State of Marine Pollution in Mombasa Marine ational Park Marine Reserve and Mtwapa Creek*.

Neumann, B., Vafeidis, A. T., Zimmermann, J., and Nicholls, R. J. (2015). Future coastal population growth and exposure to sea-level rise and coastal flooding - A global assessment. *PLoS One* 10:e0118571. doi: 10.1371/journal.pone.0118571

Ngugi, I. (2002). Economic impacts of marine protected areas?: a case study of the mombasa marine park (Kenya). *J. Soc. Sci. Grad. Stud. Assoc.* 1, 1–11.

Obura, D. (2017). *Reviving the Western Indian Ocean Economy: Actions for a Sustainable Future*. Gland, Switzerland: WWF International.

Obura, D. O. (2001). Kenya. *Mar. Pollut. Bull.* 42, 1264–1278. doi: 10.1016/S0025-326X(01)00241-7

Obura, D. O., Aeby, G., Amornthammarong, N., Appeltans, W., Bax, N., Bishop, J., et al. (2019). Coral reef monitoring, reef assessment technologies, and ecosystem-based management. *Front. Mar. Sci.* 6:580. doi: 10.3389/fmars.2019.00580

Okuku, O. E., Linet Imbayi, K., Gilbert Omondi, O., Veronica Ogolla Wayayi, W., Catherine Sezi, M., Mokeira Maureen, K., et al. (2019). "Decadal Pollution Assessment and Monitoring along the Kenya Coast," in *Monitoring of Marine Pollution*, ed. H. B. Fouzia (London: IntechOpen), 1–15.

Oksanen, J., Blanchet, F. G., Friendly, M., Kindt, R., Legendre, P., McGlinn, D., et al. (2019). *vegan: Community Ecology Package. R Package Version 2.5-6*.

Okuku, E. O., Ohowa, B., Mwangi, S. N., Munga, D., Kiteresi, L. I., Wanjeri, V. O., et al. (2011). Sewage pollution in the coastal waters of Mombasa City, Kenya: A norm rather than an exception. *Int. J. Environ. Res.* 5, 865–874.

Ongore, C. O., Okuku, E. O., Mwangi, S. N., Kiteresi, L. I., Ohowa, B. O., Wanjeri, V. O., et al. (2013). Characterization of nutrients enrichment in the estuaries and related systems in Kenya coast. *J. Environ. Sci. Water Res.* 2, 181–190.

Owens, J. D. (1978). Coliform and *escherichia coli* bacteria in seawater around penang island, Malaysia. *Water Res.* 12, 365–370. doi: 10.1016/0043-1354(78)90101-X

Ransome, E., Geller, J. B., Timmers, M., Leray, M., Mahardini, A., Sembiring, A., et al. (2017). The importance of standardization for biodiversity comparisons: A case study using autonomous reef monitoring structures (ARMS) and metabarcoding to measure cryptic diversity on Mo'orea coral reefs, French Polynesia. *PLoS One* 12:e0175066. doi: 10.1371/journal.pone.0175066

Robinson, J., New, A. L., Popova, E. E., Srokosz, M. A., and Yool, A. (2017). Far-field connectivity of the UK's four largest marine protected areas: Four of a kind? *Earth's Future* 5, 475–494. doi: 10.1002/2016EF000516

Rohwer, F., Seguritan, V., Azam, F., and Knowlton, N. (2002). Diversity and distribution of coral-associated bacteria. *Mar. Ecol. Prog. Ser.* 243, 1–10. doi: 10.3354/meps243001

Roik, A., Röthig, T., Roder, C., Ziegler, M., Kremb, S. G., and Voolstra, C. R. (2016). Year-long monitoring of physico-chemical and biological variables provide a comparative baseline of coral reef functioning in the central red sea. *PLoS One* 11:e0163939. doi: 10.1371/journal.pone.0163939

Roitman, S., Joseph Pollock, F., and Medina, M. (2018). *Coral Microbiomes as Bioindicators of Reef Health*. Cham: Springer, 39–57.

Santoro, A. E., Richter, R. A., and Dupont, C. L. (2019). Planktonic marine archaea. *Ann. Rev. Mar. Sci.* 11, 131–158. doi: 10.1146/annurev-marine-121916-063141

Silveira, C. B., Cavalcanti, G. S., Walter, J. M., Silva-Lima, A. W., Dinsdale, E. A., Bourne, D. G., et al. (2017). Microbial processes driving coral reef organic carbon flow. *FEMS Microbiol. Rev.* 41, 575–595. doi: 10.1093/FEMSRE

Skerker, J. M., Prasol, M. S., Perchuk, B. S., Biondi, E. G., and Laub, M. T. (2005). Two-component signal transduction pathways regulating growth and cell cycle progression in a bacterium: A system-level analysis. *PLoS Biol.* 3:e334. doi: 10.1371/journal.pbio.0030334

Sullivan, M. B., Coleman, M. L., Weigele, P., Rohwer, F., and Chisholm, S. W. (2005). Three *Prochlorococcus* cyanophage genomes: signature features and ecological interpretations. *PLoS Biol.* 3:e144. doi: 10.1371/journal.pbio.0030144

Sunagawa, S., Coelho, L. P., Chaffron, S., Kultima, J. R., Labadie, K., Salazar, G., et al. (2015). Structure and function of the global ocean microbiome. *Science* 348, 1261359–1261359. doi: 10.1126/science.1261359

Sunagawa, S., Woodley, C. M., and Medina, M. (2010). Threatened corals provide underexplored microbial habitats. *PLoS One* 5:e9554. doi: 10.1371/journal.pone.0009554

Tao, P., and Rao, V. B. (2019). *Bacteriophage Vaccines. In Reference Module in Life Sciences*. Amsterdam: Elsevier.

Tatusov, R. L., Galperin, M. Y., Natale, D. A., and Koonin, E. V. (2000). The COG database: A tool for genome-scale analysis of protein functions and evolution. *Nucleic Acids Res.* 28, 33–36. doi: 10.1093/nar/28.1.33

Tatusov, R. L., Natale, D. A., Garkavtsev, I. V., Tatusova, T. A., Shankavaram, U. T., Rao, B. S., et al. (2001). The COG database: New developments in phylogenetic classification of proteins from complete genomes. *Nucleic Acids Res.* 29, 22–28. doi: 10.1093/nar/29.1.22

R Core Team. (2020). *R: A Language and Environment for Statistical Computing*. Available Online at: https://www.r-project.org/ (accessed October 12, 2020).

Thurber, R. V., Payet, J. P., Thurber, A. R., and Correa, A. M. (2017). Virus–host interactions and their roles in coral reef health and disease. *Nat. Rev. Microbiol.* 15, 205–216. doi: 10.1038/nrmicro.2016.176

Tout, J., Jeffries, T. C., Webster, N. S., Stocker, R., Ralph, P. J., and Seymour, J. R. (2014). Variability in microbial community composition and function between different niches within a coral reef. *Microbial. Ecol.* 67, 540–552. doi: 10.1007/s00248-013-0362-5

Tuda, A., and Omar, M. (2012). Protection of marine areas in Kenya. *George Wright Forum* 29, 43–50.

Van Der Elst, R., Everett, B., Jiddawi, N., Mwatha, G., Afonso, P. S., and Boulle, D. (2005). Fish, fishers and fisheries of the Western Indian Ocean: Their diversity and status. A preliminary assessment. *Phil. Trans. R. Soc. A Math. Phys. Eng. Sci.* 363, 263–284. doi: 10.1098/rsta.2004.1492

Vanwonterghem, I., and Webster, N. S. (2020). Coral Reef microorganisms in a changing climate. *IScience* 23:100972. doi: 10.1016/j.isci.2020.100972

Varasteh, T., Moreira, A. P. B., Silva Lima, A. W., Leomil, L., Otsuki, K., Tschoeke, D., et al. (2020). Genomic repertoire of Mameliella alba Ep20 associated with Symbiodinium from the endemic coral Mussismilia braziliensis. *Symbiosis* 80, 53–60. doi: 10.1007/s13199-019-00655-x

Vigil-Stenman, T., Ininbergs, K., Bergman, B., and Ekman, M. (2017). High abundance and expression of transposases in bacteria from the Baltic Sea. *ISME J.* 11, 2611–2623. doi: 10.1038/ismej.2017.114

Walsh, K., Haggerty, J. M., Doane, M. P., Hansen, J. J., Morris, M. M., Moreira, A. P. B., et al. (2017). Aura-biomes are present in the water layer above coral reef benthic macro-organisms. *PeerJ.* 5:e3666. doi: 10.7717/peerj.3666

Wanjeri, V. W. O., Okuku, E. O., Barsanti, M., Schirone, A., Delbono, I., Owato, G., et al. (2021). Baseline radionuclide and heavy metal concentrations in sediments of Sabaki River estuary (Kenya, Indian Ocean). *Mar. Pollut. Bull.* 164:112033. doi: 10.1016/j.marpolbul.2021.112033

Waterbury, J. B., Watson, S. W., Guillard, R. R. L., and Brand, L. E. (1979). Widespread occurrence of a unicellular, marine, planktonic, cyanobacterium. *Nature* 277, 293–294. doi: 10.1038/277293a0

Weber, L., Gonzalez-Díaz, P., Armenteros, M., and Apprill, A. (2019). The coral ecosphere: A unique coral reef habitat that fosters coral–microbial interactions. *Limnol. Oceanogr.* 64, 2373–2388. doi: 10.1002/lno.11190

Wickham, H. (2016). *ggplot2-Elegant Graphics for Data Analysis*, 2nd Edn. New York: Springer-Verlag.

Wilkens, S. (2015). Structure and mechanism of ABC transporters. *F1000Prime Rep.* 7, 7–14. doi: 10.12703/P7-14

Williamson, S. J., Allen, L. Z., Lorenzi, H. A., Fadrosh, D. W., Brami, D., Thiagarajan, M., et al. (2012). Metagenomic exploration of viruses throughout the Indian Ocean. *PLoS One* 7:e0042047. doi: 10.1371/journal.pone.0042047

Won, N., Il, Kim, K. H., Kang, J. H., Park, S. R., and Lee, H. J. (2017). Exploring the impacts of anthropogenic disturbance on seawater and sediment microbial communities in Korean coastal waters using metagenomics analysis. *Int. J. Environ. Res. Public Health* 14:130. doi: 10.3390/ijerph14020130

Zhang, W., Cao, S., Ding, W., Wang, M., Fan, S., Yang, B., et al. (2020). Structure and function of the Arctic and Antarctic marine microbiota as revealed by metagenomics. *Microbiome* 8:47. doi: 10.1186/s40168-020-00826-9

Zhao, X., Schwartz, C. L., Pierson, J., Giovannoni, S. J., McIntosh, J. R., and Nicastro, D. (2017). Three-dimensional structure of the ultraoligotrophic marine bacterium "Candidatus Pelagibacter ubique". *Appl. Environ. Microbiol.* 83:e2807–16. doi: 10.1128/AEM.02807-16

Conflict of Interest: The authors declare that the research was conducted in the absence of any commercial or financial relationships that could be construed as a potential conflict of interest.

frontiers in Microbiology

ORIGINAL RESEARCH
published: 01 July 2021
doi: 10.3389/fmicb.2021.669131

Bacterial Community Spacing Is Mainly Shaped by Unique Species in the Subalpine Natural Lakes of China

*Jinxian Liu[1,2,3], Jiahe Su[1,2,3], Meiting Zhang[1,2,3], Zhengming Luo[1,2,3,4], Xiaoqi Li[1,2,3] and Baofeng Chai[1,2,3]**

[1]*Institute of Loess Plateau, Shanxi University, Taiyuan, China,* [2]*Shanxi Key Laboratory of Ecological Restoration on the Loess Plateau, Shanxi University, Taiyuan, China,* [3]*Field Scientific Observation and Research Station of the Ministry of Education of Shanxi Subalpine Grassland Ecosystem, Shanxi University, Taiyuan, China,* [4]*Department of Geography, Xinzhou Teachers University, Xinzhou, China*

Bacterial communities have been described as early indicators of both regional and global climatic change and play a critical role in the global biogeochemical cycle. Exploring the mechanisms that determine the diversity patterns of bacterial communities and how they share different habitats along environmental gradients are, therefore, a central theme in microbial ecology research. We characterized the diversity patterns of bacterial communities in Pipahai Lake (PPH), Mayinghai Lake (MYH), and Gonghai Lake (GH), three subalpine natural lakes in Ningwu County, Shanxi, China, and analyzed the distribution of their shared and unique taxa (indicator species). Results showed that the species composition and structure of bacterial communities were significantly different among the three lakes. Both the structure of the entire bacterial community and the unique taxa were significantly influenced by the carbon content (TOC and IC) and space distance; however, the structure of the shared taxa was affected by conductivity (EC), pH, and salinity. The structure of the entire bacterial community and unique taxa were mainly affected by the same factors, suggesting that unique taxa may be important in maintaining the spatial distribution diversity of bacterial communities in subalpine natural freshwater lakes. Our results provide new insights into the diversity maintenance patterns of the bacterial communities in subalpine lakes, and suggest dispersal limitation on bacterial communities between adjacent lakes, even in a small local area. We revealed the importance of unique taxa in maintaining bacterial community structure, and our results are important in understanding how bacterial communities in subalpine lakes respond to environmental change in local habitats.

Keywords: bacterial community, shared taxa, unique taxa, diversity pattern, subalpine lakes

OPEN ACCESS

Edited by:
Camila Fernandez, UMR7621 Laboratoire d'Océanographie Microbienne (LOMIC), France

Reviewed by:
Yuyi Yang, Wuhan Botanical Garden, Chinese Academy of Sciences (CAS), China
Shuo Jiao, Northwest A&F University, China

****Correspondence:***
Baofeng Chai
bfchai@sxu.edu.cn

Specialty section:
This article was submitted to Aquatic Microbiology, a section of the journal Frontiers in Microbiology

Received: *18 February 2021*
Accepted: *28 May 2021*
Published: *01 July 2021*

Citation:
Liu J, Su J, Zhang M, Luo Z, Li X and Chai B (2021) Bacterial Community Spacing Is Mainly Shaped by Unique Species in the Subalpine Natural Lakes of China. Front. Microbiol. 12:669131. doi: 10.3389/fmicb.2021.669131

INTRODUCTION

Aquatic bacteria are important components of lake ecosystems, having a high level of species diversity and playing essential roles in global biogeochemical cycles. Considerable evidence indicates that bacteria are essential to lake food web (Sanmukh et al., 2012; Cavicchioli, 2015), exert top-down control on other microbial communities and are symbiotic with lake organisms (such as planktonic algae, protozoa, fungi, and metazoa; Liu et al., 2015a, 2019; Xue et al., 2018).

It is clear that bacteria are active and potentially significant players in water biological processes. This means that understanding the diversity of aquatic bacteria and their biogeographical patterns will help to explain the variations in ecosystem functioning, and ultimately to predict ecosystem responses to current and future environmental changes (Hanson et al., 2012). The majority of natural microbial communities is composed of a few abundant taxa and a large number of rare taxa (Liu et al., 2015b). However, abundant taxa are not necessarily the shared taxa of the habitat (Zhang et al., 2018), also the rare taxa are not necessarily the unique taxa of a certain habitat. Biogeographical patterns of shared and unique bacterial taxa in different habitats have been under-researched compared with the abundant and rare bacterial taxa in lakes and reservoirs (Baltar et al., 2015; Wu et al., 2016; Xue et al., 2018). Shared taxa are species that exist in every habitat within a certain boundary, which means that they have a stronger diffusion level and adaptability (Miura et al., 2019). Unique taxa are more restricted in habitat range, and their distribution is strongly affected by habitat conditions and distance between habitats (Mckenzie et al., 2012; Miura et al., 2019). It seems that both rare and unique taxa are mainly affected by environmental factors, but unique taxa have strict habitat specificity. Some studies have shown that abundant and rare bacterial taxa are distinctly different in diversity and biogeographical patterns, and rare bacterial taxa have a much smaller chance of successful diffusion than abundant taxa (Liu et al., 2015b; Jiao et al., 2017; Mo et al., 2018; Xue et al., 2018). However, little is known about the biogeographical basic patterning of shared and unique bacterial taxa, and to what extent lakes share bacterial taxa in a local area.

Most bacterial species are considered to be cosmopolitan because they have been found across biogeographic regions in multiple habitats, such as soil, sediment, lakes, and the sea (Hanson et al., 2012). In fact, bacteria are widely shared at phylum and class level, whereas at species or operational taxonomic unit (OTU) level they have habitat specificity. There is evidence of identical bacterial community composition in global oceans (Gibbons et al., 2013). With respect to community structure, however, regional endemism has been seen in bacteria, with some taxa reportedly being restricted to distinct geographical regions (Oakley et al., 2010; Kumar et al., 2017). Few studies have investigated the details of shared bacterial taxa community distribution in different habitats (Moitinho-Silva et al., 2014), or sought to understand the main drivers of bacterial diversity. Microbes display diverse biogeographical patterns, ranging from cosmopolitanism to provincialism (Hanson et al., 2012), but the underlying mechanisms that generate and maintain those patterns at a distinct range of spatial scales and habitats remain largely under explored (Meyer et al., 2013). Only a few studies have shown significant differences in the bacterial community structure of shared and unique taxa in the phyllosphere of forest, vineyard, and accompanying weed plants in local and regional areas (Samad et al., 2017; Miura et al., 2019). Those studies also showed the important influence of the environment on the structure and composition of a microbial community. Environmental factors, such as temperature (Callieri et al., 2016), dissolved oxygen (Di Cesare et al., 2015), and nutrient status (Liu et al., 2017), have powerful effects on the microbial community structure in alpine and subalpine lakes. Indeed, spatial processes are also important in producing and maintaining microbial diversity (Roguet et al., 2015). Little is known, however, about the mode of action and intensity of these regulatory mechanisms on different taxa.

The Ningwu subalpine natural lakes were formed in the Cenozoic Quaternary glacial period, approximately 3 million years ago (Wang et al., 2014). A group of 15 upland natural freshwater lakes of different sizes appeared on the planation surface; now, there are only three perennial lakes: Mayinghai, Pipahai, and Gonghai. Their water levels are declining yearly as a result of climate change and human disturbance (Liu et al., 2016). A study of Ningwu subalpine lakes (Zhang et al., 2012) found a clear difference in phytoplankton community structure, but the distribution of bacterial communities in Mayinghai, Pipahai, and Gonghai lakes, which were formed at the same time and in the same way is still unclear. The main purpose of our study was to explore bacterial community distribution, and its driving factors, in the three lakes. We characterized the microbiota, paying particular attention to three questions. (i) Are the structures of bacterial communities similar in the three lakes with the same formation conditions and similar climate? (ii) How do shared and unique taxa affect the assemblage of the entire bacterial community structure? and (iii) Can unique OTUs indicate habitat specificity? To achieve our aims, we used community DNA-based amplicon sequencing targeting the bacterial 16S rRNA gene region to conduct analyses.

MATERIALS AND METHODS

Site Description

The study area was in Ningwu County, Shanxi Province, in the northern margin of the Chinese Loess Plateau, and three sampling sites were Pipahai Lake (PPH), Mayinghai Lake (MYH), and Gonghai Lake (GH; **Figure 1**). The size and area of these three lakes vary, and their altitude, maximum depth, and surface area appear in **Table 1**. The lakes are hydrologically closed basins and the main water source is precipitation. The research area has an East Asian monsoon climate with an annual mean temperature of 6.2°C. Annual precipitation is around 490 mm, of which more than 65% rainfalls during the summer (from June to August).

Water Sampling

Water samples were collected every 2 m from top to bottom using a Plexiglass® water sampler (LB-800, Qingdao, China) at the center of the three lakes in July 2017. Due to the different depth of the lake, there are 3, 4, and 5 sampling points in PPH, MYH, and GH, respectively (**Table 1**). Water was sampled three times at each sampling point and each repetition took 1 L water. In total, nine samples were collected

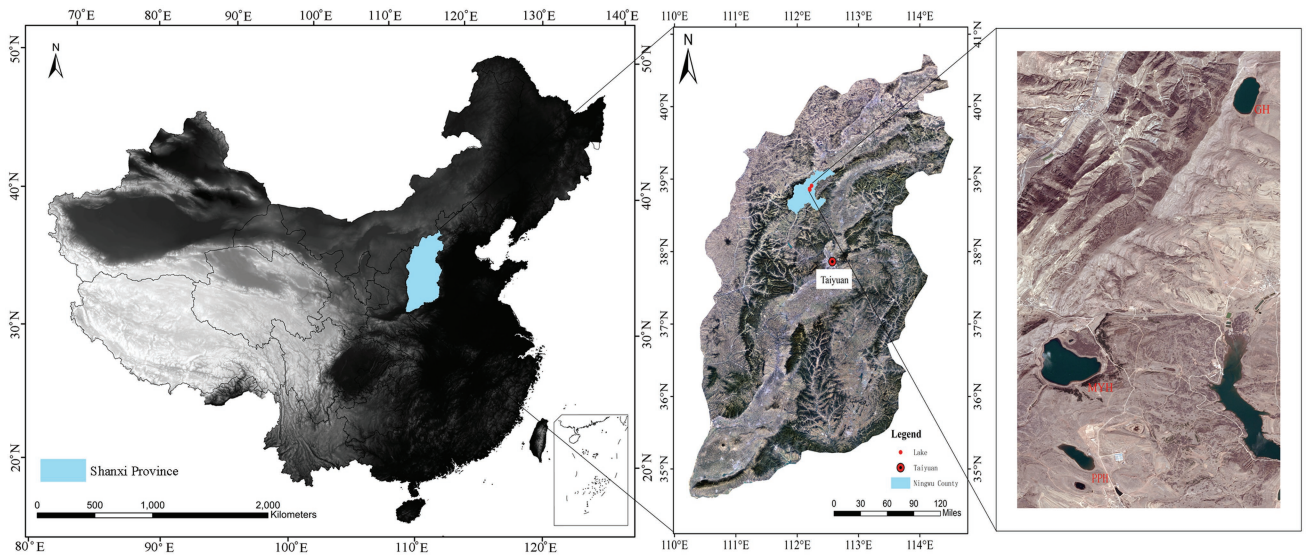

FIGURE 1 | Map showing the location of sampling sites and spatial distribution of Pipahai Lake (PPH), Mayinghai Lake (MYH), and Gonghai Lake (GH) in the Ningwu County of Shanxi, China.

TABLE 1 | Brief description of the sampling sites in the Ningwu subalpine lakes.

Parameter	PPH	MYH	GH
Location	38.85°N, 112.21°E	38.87°N, 112.20°E	38.91°N, 112.23°E
Elevation (m)	1776	1774	1854
Number of sampling points	3	4	5
Surface area (km^2)	~0.21	~0.58	~0.36
Max depth (m)	~4.5	~6.4	~8.5

from PPH, 12 samples from MYH, and 15 samples from GH. Approximately 2.5 L of the water sample from each sampling site was filtered in the laboratory using a sterile 0.2 μm pore size membrane filters (Millipore, Jinteng, Tianjin, China) for DNA extraction. Filters with retaining biomass were sealed and stored at −80°C until analysis. The remaining 0.5 L water was used for analysis of physicochemical properties.

Physicochemical Measurements of Water Samples

For each sample, water physical parameters: temperature (T), pH, dissolved oxygen (DO), electric conductivity (EC), salinity (SAL), nitrate (NO_3^-), and ammonium (NH_4^+) content were measured *in situ* using a portable water multiparameter quality monitor (Aquaread AP-2000, England, United Kingdom). In the laboratory, we measured total nitrogen (TN), nitrite (NO_2^-), sulfate (SO_4^{2-}), and phosphate (PO_4^{3-}) content using an automated discrete analyzer (DeChem-Tech., CleverChem380, Hamburg, Germany); total carbon (TC), total organic carbon (TOC), and inorganic carbon (IC) content were measured using a TOC analyzer (Shimadzu, TOC-VCPH, Shimane, Japan).

DNA Extractions, PCR Amplification, and High-Throughput Sequencing

Filters with retained biomass were cut into pieces and placed into centrifuge tubes for DNA extraction using the Fast soil DNA SPIN extraction kits (OMEGA Bio-tek Inc., Norcross, GA, United States) as described in the manufacturer's protocol. We analyzed 12 samples (mixing the three repeats evenly for a sample from each sampling point) for bacterial communities. The primer pair 338F (5'-ACTCCTACGGGAGGCAGCA-3') and 806R (5'-GGACTACHVGGGTWTCTAAT-3') was used to amplify the V3-V4 hypervariable region of the 16S rDNA gene in bacteria. The PCR reactions were performed in triplicate using a 25 μl mixture containing 2.5 μl 10 × buffer (containing Mg^{2+}), 2 μl of 2.5 mm dNTPs, 0.5 μl of each primer (10 μm), 0.25 μl of 5 U Fast Pfu polymerase, 1 μl of 10 ng template DNA, and 18.25 μl of ultrapure water. Thermal cycling consisted of initial denaturation at 98°C for 2 min followed by 26 cycles of denaturation at 98°C for 15 s, annealing at 55°C for 30 s, and an extension at 72°C for 30 s, with a final extension at 72°C for 5 min. Triplicates of PCR products were pooled and purified by the Agarose Gel DNA purification kit (TIANGEN, Tianjing, China) and quantified with the NanoDrop™ 8000 (Thermo Scientific, Massachusetts, United States) device. After purification and quantification of the PCR product, a genomic DNA library was constructed on an Illumina MiSeq platform in accordance with the manufacturer's instruction manual (Majorbio Bio-Pharm Technology Co. Ltd., Shanghai, China).

Nucleic Acid Sequences

The sequence data of bacterial 16S rDNA genes were submitted to the NCBI GenBank[1] (accession number SRP131941).

[1]https://www.ncbi.nlm.nih.gov/sra/?term=SRP131941

Bioinformatics Data Analysis

Before analysis, raw sequencing reads were demultiplexed and quality filtered using QIIME (version 1.9.1). The low-quality sequences were filtered using the following criteria: sequences that had a length of <150 bp, sequences that had average Phred scores of <20, sequences that contained ambiguous bases, and sequences that contained mononucleotide repeats of >8 bp. Paired-end reads were assembled using FLASH and Trimmomatic (Magoč and Salzberg, 2011). After chimera detection, the remaining high-quality sequences were clustered into OTUs at 97% sequence identity by UCLUST (Edgar, 2010). A representative sequence was selected from each OTU using default parameters. OTU taxonomic classification was conducted by BLAST search of the representative sequences set against the silva132 database using the best hit (Altschul et al., 1997). A OTU table was generated to record the abundance and taxonomy of every OTU in each sample. To minimize the differences in sequencing depth across samples, all were normalized to the number of sequences in the smallest data set for further analysis. Sequence data analyses were mainly performed using QIIME and R packages (version 3.3.1).

Statistical Analysis

The alpha diversity of bacterial communities in each habitat was compared using observed OTU richness and the Shannon diversity index. Shapiro-Wilk tests were used to test the normality of physicochemical factors and alpha diversity data, and no violations of normality were detected. One-way ANOVA was used to assess the differentials in physicochemical factors and alpha diversity in the three habitats (PPH, MYH, and GH), and a least significant difference test was used for multiple comparisons by SPSS 20.0. The correlation between environmental factors and dominant sheared and unique taxa was expressed by a Spearman correlation coefficient. Beta diversity analysis was performed to investigate the structural variation in microbial communities across habitats using weighted UniFrac distance visualized with a hierarchical clustering tree, and Bray-Curtis distance metrics visualized *via* non-metric multidimensional scaling (NMDS). The differences in the three lake communities were examined using the ANOSIM statistics in the vegan package of R-3.3.1 (Oksanen et al., 2013). All environmental factors were selected by stepwise regression and the Monte Carlo permutation test; finally, environmental factors with the variance inflation factor (VIF) of less than 10 were retained for redundancy analysis (RDA; **Supplementary Table S1**). To prove whether appropriate habitat enabled the presence of unique taxa, we then determined which taxa were highly related to their habitat by identifying indicator species using the R package indicspecies (Oksanen et al., 2013). This analysis calculates an indicator value (IndVal) that measures the association between OTUs with each habitat and then identifies the taxa corresponding to the highest association value. We defined indicator OTUs based on an IndVal of >0.80 and a value of $p < 0.05$ assessed after 999 permutation tests (Miura et al., 2019). RDA was used to identify the correlation among the variables (environmental factors and space distance) and bacterial community composition. Firstly, before RDA analysis, six environmental factors with a VIF below 10 were preselected; then, the environmental variables and spatial distance were forward selected and only those with significant impact on community structure were retained for RDA (**Supplementary Table S5**). The contribution of environmental factors and space distance with the variations in the entire bacterial community and unique taxa was measured by variance partitioning analysis (VPA; McArdle and Anderson, 2001) in CANOCO 5.0. The spatial distance was expressed by the principal coordinates of neighboring matrices (PCNM). PCNM eigenfunctions were computed across the lake center locations, and computationally significant variables ($p < 0.05$) were selected in the R vegan package. The confidence interval of all statistical analyses was 95% ($p < 0.05$).

RESULTS

Physicochemical Properties

The concentrations of TN, NO_3^-, NH_4^+, TC, IC, TOC, SO_4^{2-}, pH, and EC were significantly different in the three lakes (**Table 2**). The concentration of TOC was higher in PPH than in GH and MYH; however, the other eight factors were highest in GH ($p < 0.05$). The relatively higher concentration of organic carbon and a lower pH in the PPH water samples indicated that the lake was more polluted and showed a trend of acidification compared with the other two lakes (**Table 2**).

TABLE 2 | Water physicochemical characteristics of studied lakes.

Parameter	PPH	MYH	GH
T (°C)	23.69 ± 0.32a	22.89 ± 0.35ab	21.40 ± 0.50b
pH	7.58 ± 0.02c	7.98 ± 0.14b	8.51 ± 0.04a
DO (mg/L)	7.92 ± 0.57b	10.64 ± 0.79a	9.24 ± 0.23ab
EC (uS/cm)	476.33 ± 1.54b	409.75 ± 2.11c	935.67 ± 3.28a
SAL(ng/L)	6.25 ± 0.39a	7.91 ± 0.64a	7.49 ± 0.37a
TN (mg/L)	1.79 ± 0.12b	1.01 ± 0.04c	2.71 ± 0.09a
NO_3^- (mg/L)	0.23 ± 0.01b	0.17 ± 0.02c	0.28 ± 0.01a
NO_2^- (mg/L)	0.01 ± 0.00b	0.01 ± 0.00b	0.03 ± 0.01a
NH_4^+ (mg/L)	1.44 ± 0.10b	0.73 ± 0.04c	2.09 ± 0.09a
TC (mg/L)	79.72 ± 0.81b	60.42 ± 0.25c	131.31 ± 0.83a
IC (mg/L)	51.87 ± 0.40b	45.79 ± 0.25c	110.39 ± 0.88a
TOC (mg/L)	27.86 ± 0.48a	14.64 ± 0.27c	20.91 ± 0.20b
C/N	46.21 ± 3.46b	59.82 ± 2.45a	49.23 ± 1.88b
SO_4^{2-} (mg/L)	52.68 ± 0.52b	48.82 ± 1.03c	59.48 ± 0.41a
PO_4^{3-} (mg/L)	0.25 ± 0.05a	0.31 ± 0.06a	0.40 ± 0.07a

The data were shown as the means ± standard error. T represents temperature; DO represents dissolved oxygen; EC represents electro conductibility; SAL represents salinity; TN represents total nitrogen; NO_3^- represents nitrate; NO_2^- represents nitrite; NH_4^+ represents ammonium; TC represents total carbon; IC represents inorganic carbon; TOC represents organic carbon; C/N represents ratio of total carbon to total nitrogen; SO_4^{2-} represents sulfate; and PO_4^{3-} represents phosphate. Significant differences between samples were determined using one-way ANOVA at $p < 0.05$ and the different letters indicate significant differences.

Community Composition of Lake Water Bacteria

We obtained 375,171 high-quality bacterial 16S rDNA gene sequences and 850 OTUs by high-throughput sequencing of all water samples. The sample from MYH had higher OTU richness (615 OTUs), based on the number of OTUs, whereas samples from PPH and GH displayed considerably lower richness, with 562 OTUs and 584 OTUs, respectively (**Figure 2A**). The composition of bacterial communities differed in all three lakes, and although the eight dominant phyla were shared, their relative abundance varied among the three lakes (**Figure 2B**). The eight dominant phyla were *Actinobacteria* (relative abundance 24.46–36.18%), *Proteobacteria* (22.78–29.12%), *Cyanobacteria* (8.41–23.85%), *Bacteroidetes* (10.43–13.33%), *Verrucomicrobia* (2.60–8.70%), *Chlorobi* (0.72–11.11%), *Planctomycetes* (0.49–2.88%), and *Chloroflexi* (0.51–2.15%; **Figure 2B**).

The three lakes shared 335 OTUs (**Figure 2A**), including 23 dominant OTUs (with relative abundance greater than 1%; **Figure 3A**). The OTUs shared by the three lakes contained 86.08% of the total bacterial abundance in PPH. In MYH and GH, the shared OTUs accounted for 90.33 and 81.49% of the total OTUs, respectively. The shared dominant OTUs belonged to six different bacterial phyla and their abundance varied with sampling site (**Figure 3B**). Of these 23 OTUs, seven belonged to *Actinobacteria*, five to *Proteobacteria*, four to *Cyanobacteria*, three to *Bacteroidetes*, two to *Verrucomicrobia*, and two to *Chlorobi* (**Figure 3B**). A significant correlation was found between the change in abundance of the dominant shared OTUs and environmental parameters (**Supplementary Table S2**). The changes in EC, carbon (TC and IC), and nitrogen (TN, NO_3^-, and NH_4^+) concentrations in the 15 physicochemical factors tested had significant correlations with the abundance of dominant shared OTUs (**Supplementary Table S2**).

The number of unique bacterial taxa in each lake differed and was 76 (PPH), 105 (MYH), and 93 (GH; **Figure 2**). After screening by IndVal (IndVal > 0.8), we found 54 unique OTUs in PPH, 15 unique OTUs in MYH, and 21 unique OTUs in GH (**Supplementary Table S3**). The most abundantly unique taxa in PPH were OTU1556, belonging to genus *norank_f__0319-6G20* family *LiUU-11-161* order *Sphingobacteriales* class *Sphingobacteriia* phylum *Bacteroidetes*; in MYH was OTU1315, belonging to genus *Methyloparacoccus* family *Methylococcaceae* order *Methylococcales* class *Gammaproteobacteria* phylum *Proteobacteria*; and, in GH was OTU17 belonging to genus *MWH-UniP1_aquatic_group* family *Alcaligenaceae* order *Burkholderiales* class *Betaproteobacteria* phylum *Proteobacteria*. The greatest diversity of unique taxa in all three lakes belonged to *Proteobacteria*, and the numbers of these OTUs in PPH, MYH, and GH were 28, 7, and 7, respectively (**Supplementary Table S3**). A significant correlation was found between the abundance of the top five unique OTUs and EC, as well as between carbon (TC and IC) and nitrogen (TN, NO_3^-, and NH_4^+; **Supplementary Table S4**).

Richness and Diversity of the Bacterial Community

Alpha-diversity characteristics were estimated using the observed OTUs and Shannon's index. One-way ANOVA showed a significant difference in OTU number ($F = 5.55$, $p < 0.05$) and Shannon diversity in the three lakes ($F = 8.46$, $p < 0.01$; **Figure 4**). GH had the lowest mean values of OTUs (366.20 ± 35.20) and Shannon diversity (3.84 ± 0.11) among these three lakes, and multiple comparisons showed that differences in alpha-diversity indexes between GH and the other two lakes were statistically significant (**Figure 4**). A significant correlation was found between environmental factors and alpha diversity of the bacterial community. The trend of bacterial community richness had a significant correlation with pH, DO, SAL, SO_4^{2-}, and PO_4^{3-}, and the change in the Shannon index was significantly correlated with pH, EC, TN, NO_3^-, NH_4^+, IC, and TOC (**Table 3**). The results showed that the environmental gradient among the lakes could lead to a change in the alpha diversity of a bacterial community.

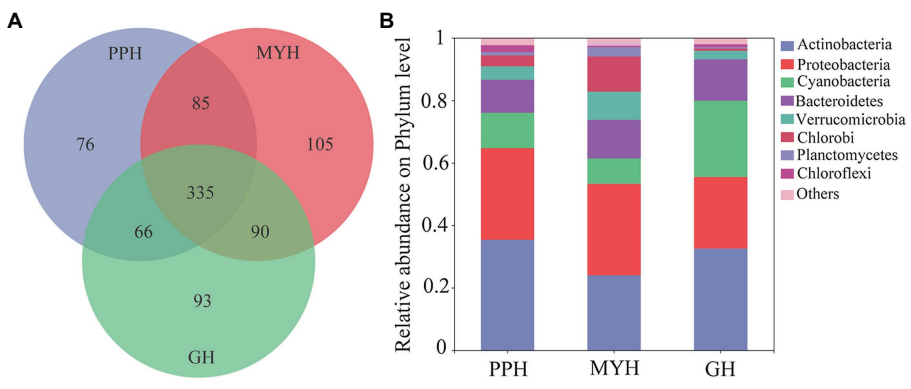

FIGURE 2 | Bacterial community compositions in water samples in PPH, MYH, and GH. **(A)** Venn diagram showing the operational taxonomic units (OTUs) number in the three lakes and **(B)** the composition of the dominant bacterial phyla (with average relative abundance >1%) across the three lakes, where sequences that have a mean relative abundance <1% were assigned to others.

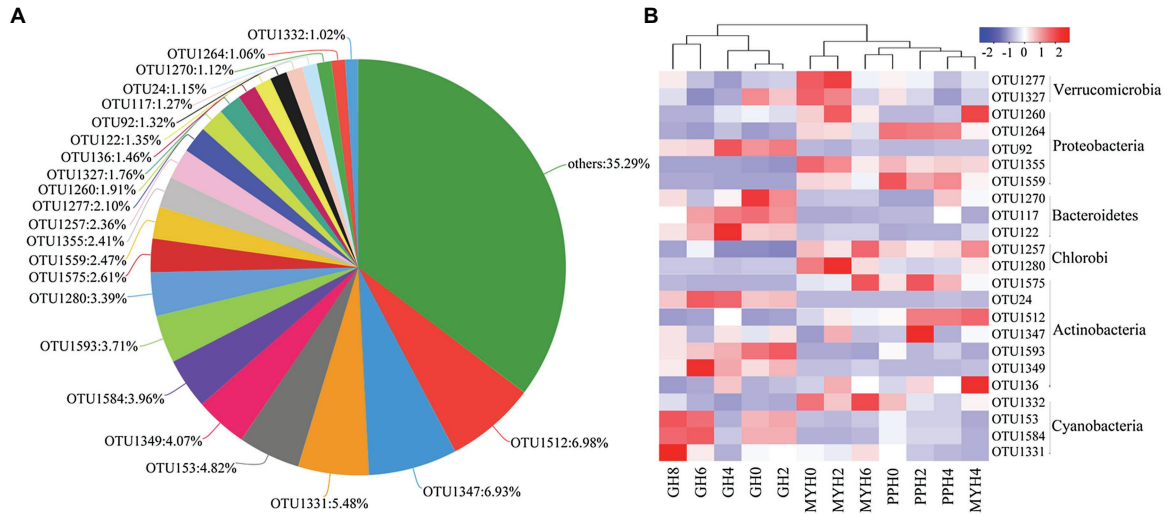

FIGURE 3 | Shared OTUs in the three lakes. **(A)** Pie chart showing the dominant shared OTUs (with average relative abundance >1% and OTUs with relative abundance less than 1% were merged into others). **(B)** Heat map showing the distribution pattern of dominant shared OTUs in 12 water samples.

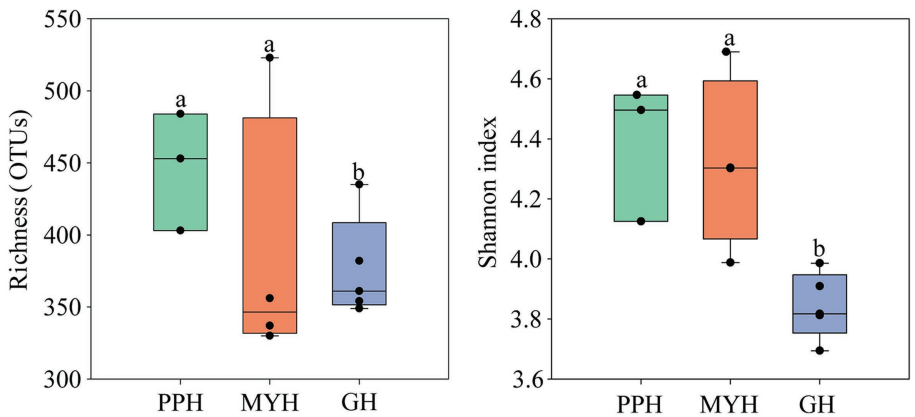

FIGURE 4 | Variation in alpha diversity of bacterial communities on the PPH, MYH, and GH. The error bars represent standard deviations of means. Different letters indicate a significant difference between the three lakes according to LDS multiple comparisons ($p < 0.05$).

Spatial Distribution of Bacterial Community and Driving Factors

A hierarchical clustering tree based on weighted UniFrac distance showed that the spatial distribution of the bacterial community in GH was different from that in MYH and PPH (**Figure 5A**). The NMDS based on Bray–Curtis distance showed that the spatial distribution of the bacterial community differed in the three lakes (**Figure 5B**), and this was further confirmed by PERMANOVA analysis (ANOSIM, $R^2 = 0.73$, $p = 0.002$). The structure of shared taxa (ANOSIM, $R^2 = 0.727$, $p = 0.006$) and unique taxa (ANOSIM, $R^2 = 0.772$, $p = 0.001$) also created significant differences among the three lakes (**Supplementary Figure S1**).

RDA analysis showed that the distribution pattern of the entire bacterial community was mainly affected by TOC, IC, pH, and PCNM1 ($F = 7.8$, $p = 0.002$; **Figure 6A**), and the distribution pattern of shared taxa was mainly affected by EC, pH, and SAL ($F = 9.8$, $p = 0.002$; **Figure 6B**), whereas unique taxa structure was mainly affected by TOC, IC, and PCNM1 ($F = 11.8$, $p = 0.01$; **Figure 6C**).

Variance partitioning analysis revealed that 59% of the variation for the entire community were significantly explained by the selected three environment variables (TOC, IC, and pH) and spatial distance. Among them, environmental variables and spatial distance independently explained 4.2 and 2.9%, respectively (**Figure 7A**). At the same time, the entire community was significantly explained 57.8% of the selected two environment variables (TOC and IC) and spatial variables. Among them, environmental variables and spatial distance independently explained 6.6 and 1.8%, respectively (**Figure 7B**). For unique taxa, the combination of environmental variables and spatial distance explained 78.9%

TABLE 3 | The Spearman correlations between environmental factors and alpha diversity of bacterial communities.

Parameters	OTUs	Shannon
T (°C)	−0.308	0.315
pH	−0.725**	−0.785**
DO (mg/L)	−0.916**	−0.490
EC (uS/cm)	0.266	−0.636*
SAL (ng/L)	−0.909**	−0.371
TN (mg/L)	0.182	−0.720**
NO_3^- (mg/L)	0.147	−0.615*
NO_2^- (mg/L)	0.296	−0.176
NH_4^+ (mg/L)	0.21	−0.692*
TC (mg/L)	−0.497	0.133
IC (mg/L)	−0.077	−0.811**
TOC (mg/L)	0.077	−0.713**
C/N	0.378	−0.168
SO_4^{2-} (mg/L)	0.622*	0.189
PO_4^{3-} (mg/L)	−0.622*	−0.406
Depth	0.383	−0.147
Area	−0.484	0.048

*OTUs represent the number of operational taxonomic units in the bacterial community obtained by high-throughput sequencing, and the values in the table represent the correlation coefficient (r). **$p < 0.01$; *$p < 0.05$.*

of the observed variation (**Figure 7C**), while environmental variables and spatial distance explained 8.4 and 4.9%, respectively. VPA showed that environmental variables and spatial distance explained more than 50% of the composition of the entire community. Notably, pH only explained 1.2% proportion in the composition of the entire community.

DISCUSSION

Environmental Variability of Bacterial Community Composition

To explore the structure and function of an ecosystem, it is necessary to understand the number and kinds of microbial taxa within a community (Shafi et al., 2017). In agreement with the previous studies on freshwater lakes (Llirós et al., 2014), we found typical freshwater bacterial communities in the three lakes, with dominant microbiomes mainly comprising *Actinobacteria*, *Proteobacteria*, *Cyanobacteria*, *Bacteroidetes*, *Verrucomicrobia*, *Chlorobi*, *Chloroflexi*, and *Planctomycetes* groups (**Figure 2B**). The relative abundance of the predominant bacterial phyla differed among the lakes, and *Actinobacteria* and *Cyanobacteria*, in particular, varied significantly (**Figure 2B**). Several ecological factors affected the abundance of *Actinobacteria* and *Cyanobacteria*. Important factors influencing *Actinobacteria* included pH, organic carbon content (Llirós et al., 2014), and water temperature (Tang et al., 2017); *Cyanobacteria* was mainly influenced by water temperature, pH, and trophic status (especially nitrogen and phosphorus content; Liao et al., 2016). It was not difficult to understand why the abundance of *Actinobacteria* and *Cyanobacteria* was the lowest in MYH, because this lake had the lowest nutrition levels (**Table 2**).

Shared OTUs number accounts for more than half of the total number in each lake (**Figure 2**). This phenomenon is common, whether in a soil bacterial community at a regional scale (Pereira et al., 2012) or in a water bacterial community at a local scale (Yu et al., 2018). This kind of pattern formation is mainly because the shared OTUs have a wide range of habitats. Some research has shown that pan-habitat species have a wide habitat tolerance, good exploitation ability, and high functional plasticity (Székely and Silke, 2014), indicating that they have strong adaptability, and that a moderate environmental gradient would not have a significant impact on their diversity. We found that the abundance of the dominant shared OTUs was different among the three lakes (**Figure 3B**), and this was significantly related to EC, carbon (TC and IC), and nitrogen (TN, NO_3^-, and NH_4^+; **Supplementary Table S2**). Water nutritional status (especially carbon and nitrogen) has been shown to significantly impact bacterial composition (Tang et al., 2017). The 23 dominant shared OTUs belonged to six dominant phyla. Of these, most species were from *Actinobacteria*; and OTU1512, which had the highest relative abundance (6.98%), also belonged to *Actinobacteria* (**Figure 3**). This result was similar to the previous observations in a freshwater lake, where the bacterial community from phylum to genus was mainly composed of *Actinobacteria* (Tang et al., 2017). A possible explanation is that *Actinobacteria* have different growth and division patterns, and their habitat niche is broad (Székely and Silke, 2014). This may explain their cosmopolitan behavior.

Most unique taxa were in PPH and the least in MYH (**Supplementary Table S3**). We found that the unique dominant species in the three lakes belonged to different bacterial genera, and the diversity of unique species was the highest in *Proteobacteria* (**Supplementary Table S3**). These results showed that the heterogeneity of habitat determines the functional differences in these groups. However, they also showed that *Proteobacteria* play an important role in the stability of the community structure and the maintenance of functional diversity (Zhou et al., 2020). The most abundant unique taxa in PPH (OTU1556) belonged to genus *norank_f_LiUU-11-161*, which can decompose ammonia nitrogen in water (Sun et al., 2019). The most abundant unique taxa in MYH (OTU1315) belonged to *Methyloparacoccus*. This is a heterotrophic microorganism that obtains energy by decomposing methyl compounds (Li et al., 2020). The most abundant unique taxa in GH (OTU17) belonged to the genus *MWH-UniP1*_aquatic_ group. Members of this genus commonly live in alkaline water with high nutrient concentrations (Krett et al., 2017), obtaining energy through denitrification. Unique taxa exist only in a specific habitat and just like habitat specialists, which were preserved by environmental filtration, and that their existence would largely depend on these specific or combined with environmental factors (Székely and Silke, 2014). Each lake had its own unique bacterial taxa, and there was a certain correlation with carbon, nitrogen, and electrical conductivity (**Supplementary Table S4**). This result can answer our third question, showing that the unique taxa cannot represent the specificity of their habitat.

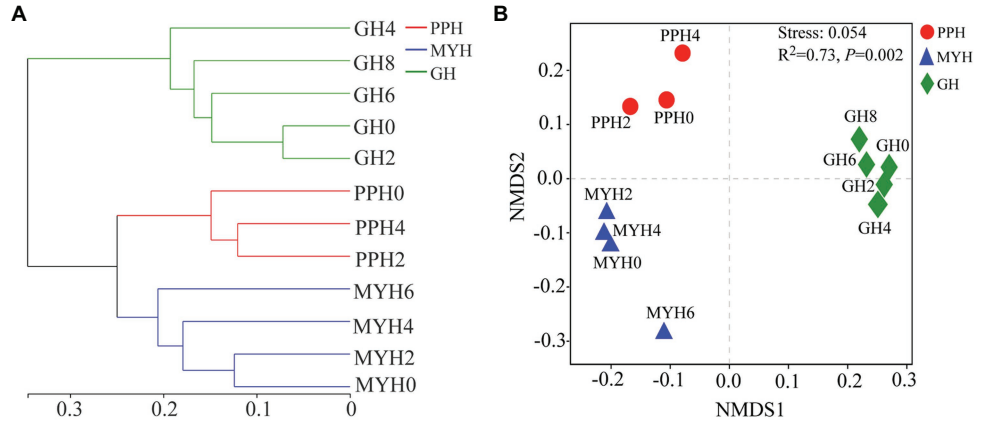

FIGURE 5 | Bacterial community structure analyses shown as hierarchical clustering tree **(A)** and non-metric multidimensional scaling plots **(B)** based on Bray-Curtis distance (in OTU level) for pairwise differences between datasets originating from the PPH, MYH, and GH.

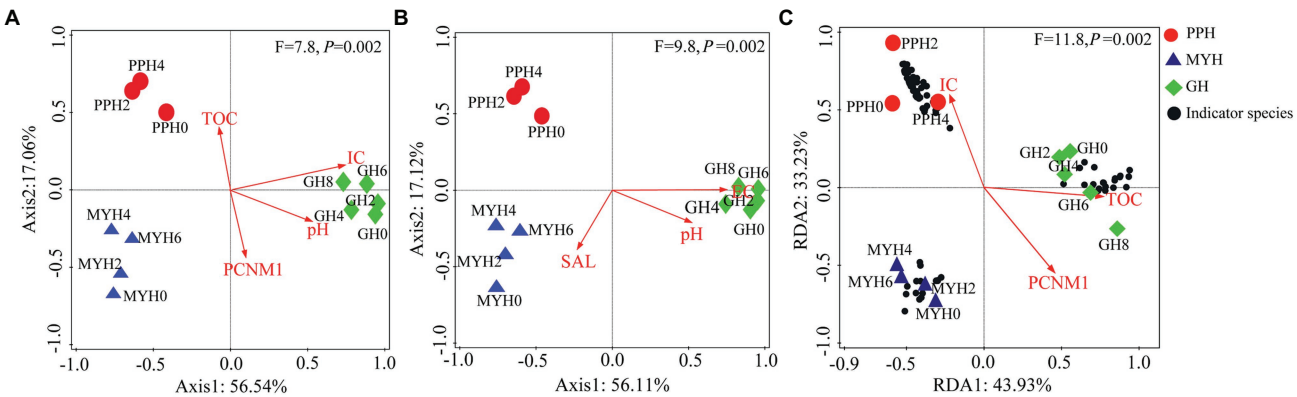

FIGURE 6 | Redundancy analyses of environmental factors and spatial distance on bacterial community structure. **(A)** Entire bacterial community, **(B)** shared taxa, and **(C)** unique taxa.

Factors Shaping Bacterial Community Diversity and Structure in Subalpine Freshwater Lakes

Compared with PPH and MYH, GH exhibited higher nutrient loading (**Table 2**), but we observed a lower alpha diversity in the bacterial community (**Figure 4**). Contrary observations were reported by Zhao (Zhao et al., 2017) who suggested that a higher nutrient state could weaken niche selection by reducing competition for resources and providing more diverse resources to some microbial species, which may contribute to higher diversity. Of course, our results were not difficult to understand, because the GL is the deepest of the three lakes (**Table 1**), and there is an obvious vertical gradient of nutrients (Wang et al., 2019), which leads to the uneven distribution of bacterial community.

Several studies at different spatial scales have shown that ecological factors are responsible for shaping bacterial community structure, such as physicochemical characteristics (Yang et al., 2016), eukaryotic plankton community composition (Yang et al., 2016), and spatial distance (Zinger et al., 2014). Few studies have investigated the effects of these factors on the composition and structure of shared and unique bacterial taxa. Our results show significant differences in the spatial distribution of the entire bacterial community (p = 0.002; **Figure 5**), shared taxa (p = 0.006), and unique taxa (p = 0.001) among the three lakes (**Supplementary Figure S1**; **Figure 6**). VPA analysis revealed that the dissimilarity in the entire bacterial community structure among the three lakes was related to environmental factors and spatial distance. The influence of environmental factors was greater than space distance, and TOC and IC were the main environmental factors (**Figure 7A**). The results also showed that the spatial distribution pattern of the bacterial community in subalpine lakes was affected by dispersal limitation even at a small spatial range (approximately 10 km; **Figure 1**). Although study found that the similarity of bacterial communities is inversely proportional to the geographical distance at small spatial scales in marine waters (Mo et al., 2018), the role of diffusion limitation is higher in

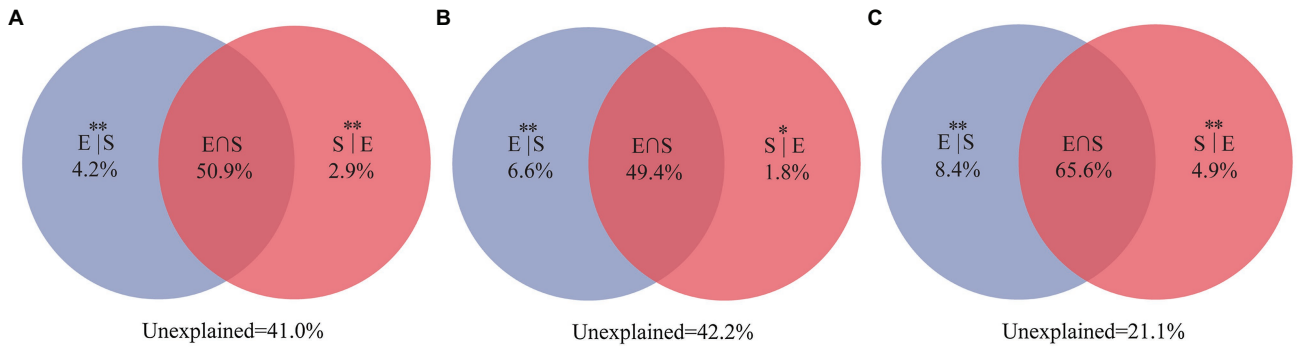

FIGURE 7 | Variation partitioning analyses showing the percentages of variance in water bacterial communities explained by environmental factors and spatial distance. **(A)** For the entire community, including three environmental factors (TOC, IC, and pH) and spatial distance; **(B)** for the entire community, including two selected environmental factors (TOC and IC) and spatial distance; and **(C)** for unique taxa, including two selected environmental factors (TOC and IC) and spatial distance. The variation explained by pure spatial and environmental factors correspond to the bacterial community without the effect of the other by the ANOVA permutation tests. $^{*}p < 0.05$ and $^{**}p < 0.01$. S|E, pure spatial variation; E|S, pure environmental variation; S∩E share explained variation; and 1 − S|E − E|S − S∩E = unexplained variation.

subalpine lakes with clear boundaries than in the indeterminate boundaries water. Nutrient concentrations (especially carbon content) often influence biomass and the taxonomic composition of a heterotrophic microbial community in water (Fujii et al., 2012). The assimilation of organic carbon by heterotrophic microorganisms is a key step in the carbon flow in marine and freshwater ecosystems. Our results also confirmed that the differences in TOC and IC content were key factors controlling bacterial diversity and community composition in freshwater environments (**Figure 6**). Most mountain lakes are characterized by low nutrient concentrations (Fujii et al., 2012), as were our study areas. Our results showed that the area of a lake is inversely proportional to the concentration of organic carbon (**Tables 1** and **2**). Therefore, organic carbon input from terrestrial sources can be considered as an important carbon supply for microbial communities in such lakes. Several studies have confirmed that the pH gradient has a significant effect on the structure of a microbial community (Fujii et al., 2012), but pH had a small rate of explanation (only 1.2%) on the distribution of a bacterial community in this study (**Figures 7A,B**). Compared with another study (Lindstrom et al., 2005), we found a narrow range of pH (7.58–8.51) in our study, and this may have been the main reason for the less significant impact on bacterial community structure. The spatial distribution pattern of the entire bacterial community and unique taxa was mainly affected by the same factors (**Figure 7**), suggesting that unique taxa may play an important role in maintaining the spatial distribution diversity of a bacterial community in subalpine natural freshwater lakes. Species traits of unique taxa, whose successful spread is difficult owing to their small numbers, determined the difference in spatial distribution. Besides, species traits affect the interaction patterns and the organization of microbial dispersal interaction networks (Hanson et al., 2012). In this study, the effect of dispersal limitation on the entire bacterial community was mainly reflected in the effect of dispersal limitation on unique taxa (**Figure 6**). The change of composition and distribution of unique taxa more likely to depend on habitat properties (Pandit et al., 2009), which leads to a high extinction risk of them, and then affects the diversity and function of the entire bacterial community. Unique taxa are known to have a limited niche, but the highest fitness in their optimal habitat. At the same time, these groups occupy an important position in the ecological network, indicating their importance in the food web (Monard et al., 2016). In view of the fact that ecosystem functions may be influenced by the characteristics and relative abundance of unique taxa, an understanding of the local distribution of unique taxa is needed to improve the prediction of ecosystem response to global change.

CONCLUSION

In this study, we found that bacterial community composition, diversity, and structure changed markedly among the three subalpine lakes. Variations in bacterial community composition and alpha diversity strongly correlated with the physical and chemical parameters of lake water. Moreover, although most OTUs were shared by the lakes, there were some unique OTUs in every lake. The composition of the unique OTUs was regulated by the nutritional status (especially carbon sources) of their habitat, suggesting that the type and amount of carbon sources in subalpine oligotrophic lakes determine the number and distribution of unique OTUs. The spatial distribution patterns of bacterial communities were mainly driven by carbon content and spatial distance, highlighting that the differences in bacterial communities structure strongly depended on the fluctuation in nutritional status caused by surrounding land use types around the lakes. At the same time, diffusion restriction also had an important effect on bacterial community structure in the closed small lakes. The spatial distribution pattern of the entire bacterial community and of unique bacterial taxa was mainly affected by the same factors. Finally, our results emphasized the importance of unique bacterial taxa in

maintaining the diversity of entire bacterial communities in subalpine freshwater lakes.

DATA AVAILABILITY STATEMENT

The sequence data of bacterial 16S rDNA genes were submitted to the NCBI GenBank (accession number SRP131941), and the physical and chemical data of environment is not uploaded to the database.

AUTHOR CONTRIBUTIONS

BC and JL designed the study, performed the statistical analyses, and prepared the draft of the manuscript. JL, JS, MZ, ZL, and XL collected the water samples. BC, JL, and XL performed the experiments. JL advised on the figures and tables. All authors revised the manuscript and approved the final version.

FUNDING

This study was supported by the National Science Foundation of China (31801962 and 31772450) and Shanxi Province Science Foundation for Youths (201901D211129 and 201901D211457).

ACKNOWLEDGMENTS

We thank Liwen Bianji, Edanz Group China (www.liwenbianji.cn/ac) for editing the English text of a draft of this manuscript.

SUPPLEMENTARY MATERIAL

The Supplementary Material for this article can be found online at: https://www.frontiersin.org/articles/10.3389/fmicb.2021.669131/full#supplementary-material

REFERENCES

Altschul, S. F., Madden, T. L., Schäffer, A. A., Zhang, J., Zhang, Z., Miller, W., et al. (1997). Gapped BLAST and PSI-BLAST: a new generation of protein database search programs. *Nucleic Acids Res.* 25, 3389–3402. doi: 10.1093/nar/25.17.3389

Baltar, F., Palovaara, J., Vila-Costa, M., Salazar, G., Calvo, E., Pelejero, C., et al. (2015). Response of rare, common and abundant bacterioplankton to anthropogenic perturbations in a Mediterranean coastal site. *FEMS Microbiol. Ecol.* 91:fiv058. doi: 10.1093/femsec/fiv058

Callieri, C., Hernández-Avilés, S., Salcher, M. M., Fontaneto, D., and Bertoni, R. (2016). Distribution patterns and environmental correlates of Thaumarchaeota abundance in six deep subalpine lakes. *Aquat. Sci.* 78, 215–225. doi: 10.1007/s00027-015-0418-3

Cavicchioli, R. (2015). Microbial ecology of Antarctic aquatic systems. *Nat. Rev. Microbiol.* 13, 691–706. doi: 10.1038/nrmicro3549

Di Cesare, A., Eckert, E. M., Teruggi, A., Fontaneto, D., Bertoni, R., Callieri, C., et al. (2015). Constitutive presence of antibiotic resistance genes within the bacterial community of a large subalpine lake. *Mol. Ecol.* 24, 3888–3900. doi: 10.1111/mec.13293

Edgar, R. C. (2010). Search and clustering orders of magnitude faster than BLAST. *Bioinformatics* 26, 2460–2461. doi: 10.1093/bioinformatics/btq461

Fujii, M., Kojima, H., Iwata, T., Urabe, J., and Fukui, M. (2012). Dissolved organic carbon as major environmental factor affecting bacterioplankton communities in Mountain Lakes of eastern Japan. *Microb. Ecol.* 63, 496–508. doi: 10.1007/s00248-011-9983-8

Gibbons, S. M., Caporaso, J. G., Pirrung, M., Field, D., Knight, R., and Gilbert, J. A. (2013). Evidence for a persistent microbial seed bank throughout the global ocean. *Proc. Natl. Acad. Sci.* 110, 4651–4655. doi: 10.1073/pnas.1217767110

Hanson, C. A., Fuhrman, J. A., Horner-Devine, M. C., and Martiny, J. B. (2012). Beyond biogeographic patterns: processes shaping the microbial landscape. *Nat. Rev. Microbiol.* 10, 497–506. doi: 10.1038/nrmicro2795

Jiao, S., Luo, Y., Lu, M., Xiao, X., Lin, Y., Chen, W., et al. (2017). Distinct succession patterns of abundant and rare bacteria in temporal microcosms with pollutants. *Environ. Pollut.* 225, 497–505. doi: 10.1016/j.envpol.2017.03.015

Krett, G., Szabó, A., Felföldi, T., Márialigeti, K., and Borsodi, A. K. (2017). The effect of reconstruction works on planktonic bacterial diversity of a unique thermal lake revealed by cultivation, molecular cloning and next generation sequencing. *Arch. Microbiol.* 199, 1077–1089. doi: 10.1007/s00203-017-1379-9

Kumar, M., Brader, G., Sessitsch, A., Mäki, A., van Elsas, J. D., and Nissinen, R. (2017). Plants assemble species specific bacterial communities from common core taxa in three arcto-alpine climate zones. *Front. Microbiol.* 8:12. doi: 10.3389/fmicb.2017.00012

Li, Y., Li, Y., Li, J., Wu, P., Yang, Z., and Xiang, F. (2020). Construction and mechanism of methanotroph-based ultimate denitrification system for tailwater of urban sewage plants. *Environ. Sci.* 41, 1787–1793. doi: 10.13227/j.hjkx.201910095

Liao, J. Q., Zhao, L., Cao, X. F., Sun, J., Gao, Z., Wang, J., et al. (2016). Cyanobacteria in lakes on Yungui plateau, China are assembled via niche processes driven by water physicochemical property, lake morphology and watershed land-use. *Sci. Rep.* 6, 36357–36368. doi: 10.1038/srep36357

Lindstrom, E. S., Agterveld, M. P. K., and Zwart, G. (2005). Distribution of typical freshwater bacterial groups is associated with pH, temperature, and lake water retention time. *Appl. Environ. Microbiol.* 71, 8201–8206. doi: 10.1128/AEM.71.12.8201-8206.2005

Liu, L., Chen, H., Liu, M., Yang, J. R., Xiao, P., Wilkinson, D. M., et al. (2019). Response of the eukaryotic plankton community to the cyanobacterial biomass cycle over 6 years in two subtropical reservoirs. *ISME J.* 13, 2196–2208. doi: 10.1038/s41396-019-0417-9

Liu, X., Guo, J., and Zhao, P. (2016). Analysis of the attenuation of Tianchi water capacity in Ningwu County of Shanxi Province. *Geotech. Investig. Surv.* 6, 47–50.

Liu, K. S., Liu, Y. Q., Jiao, N. Z., Xu, B. Q., Gu, Z. Q., Xing, T. T., et al. (2017). Bacterial community composition and diversity in Kalakuli, an alpine glacial-fed lake in Muztagh Ata of the westernmost Tibetan plateau. *FEMS Microbiol. Ecol.* 93, 1–9. doi: 10.1093/ femsec/fix085

Liu, L., Yang, J., Lv, H., Yu, X., Wilkinson, D. M., and Yang, J. (2015a). Phytoplankton communities exhibit a stronger response to environmental changes than Bacterioplankton in three subtropical reservoirs. *Environ. Sci. Technol.* 49, 10850–10858. doi: 10.1021/acs.est.5b02637

Liu, L., Yang, J., Yu, Z., and Wilkinson, D. M. (2015b). The biogeography of abundant and rare bacterioplankton in the lakes and reservoirs of China. *ISME J.* 9, 2068–2077. doi: 10.1038/ismej.2015.29

Llirós, M., Inceoğlu, Ö., García-Armisen, T., Anzil, A., Leporcq, B., Pigneur, L., et al. (2014). Bacterial community composition in three freshwater reservoirs of different alkalinity and trophic status. *PLoS One* 9:e116145. doi: 10.1371/journal.pone.0116145

Magoč, T., and Salzberg, S. L. (2011). FLASH: fast length adjustment of short reads to improve genome assemblies. *Bioinformatics* 27, 2957–2963. doi: 10.1093/bioinformatics/btr507

McArdle, B. H., and Anderson, M. J. (2001). Fitting multivariate models to community data: a comment on distance-based redundancy analysis. *Ecology* 82, 290–297. doi: 10.1890/0012-9658(2001)082[0290:FMMTCD]2.0.CO;2

McKenzie, V. J., Bowers, R. M., Noah, F., Rob, K., and Lauber, C. L. (2012). Co-habiting amphibian species harbor unique skin bacterial communities in wild populations. *ISME J.* 6, 588–596. doi: 10.1038/ismej.2011.129

Meyer, S., Wegener, G., Lloyd, K. G., Teske, A., Boetius, A., and Ramette, A. (2013). Microbial habitat connectivity across spatial scales and hydrothermal temperature gradients at Guaymas Basin. *Front. Microbiol.* 4:207. doi: 10.3389/fmicb.2013.00207

Miura, T., Sánchez, R., Castañeda, L. E., Godoy, K., and Barbosa, O. (2019). Shared and unique features of bacterial communities in native forest and vineyard phyllosphere. *Ecol. Evol.* 9, 3295–3305. doi: 10.1002/ece3.4949

Mo, Y., Zhang, W., Yang, J., Lin, Y., Yu, Z., and Lin, S. (2018). Biogeographic patterns of abundant and rare bacterioplankton in three subtropical bays resulting from selective and neutral processes. *ISME J.* 12, 2198–2210. doi: 10.1038/s41396-018-0153-6

Moitinho-Silva, L., Bayer, K., Cannistraci, C. V., Giles, E. C., Ryu, T., Seridi, L., et al. (2014). Specificity and transcriptional activity of microbiota associated with low and high microbial abundance sponges from the Red Sea. *Mol. Ecol.* 23, 1348–1363. doi: 10.1111/mec.12365

Monard, C., Gantner, S., Bertilsson, S., Hallin, S., and Stenlid, J. (2016). Habitat generalists and specialists in microbial communities across a terrestrial-freshwater gradient. *Sci. Rep.* 6:37719. doi: 10.1038/srep37719

Oakley, B. B., Carbonero, F., van der Gast, C. J., Hawkins, R. J., and Purdy, K. J. (2010). Evolutionary divergence and biogeography of sympatric niche-differentiated bacterial populations. *ISME J.* 4, 488–497. doi: 10.1038/ismej.2009.146

Oksanen, J., Blanchet, F., Kindt, R., Legendre, P., Minchin, R., and O'Hara, R. (2013). Vegan: community ecology package. version 2.0-10. Available at: https://cran.r-project.org/web/packages/vegan/vegan.pdf

Pandit, S. N., Kolasa, J., and Cottenie, K. (2009). Contrasts between habitat generalists and specialists: an empirical extension to the basic metacommunity framework. *Ecology* 90, 2253–2262. doi: 10.1890/08-0851.1

Pereira, T. P., Barboza, A. D., Suleiman, A. K. A., and Pereira, A. B. (2012). Pyrosequencing reveals shared bacterial taxa across continents. *Sci. Highlights - Thematic Area* 2, 72–76. doi: 10.4322/apa.2014.098

Roguet, A., Laigle, G. S., Therial, C., Bressy, A., Soulignac, F., Catherine, A., et al. (2015). Neutral community model explains the bacterial community assembly in freshwater lakes. *FEMS Microbiol. Ecol.* 91:fiv125. doi: 10.1093/femsec/fiv125

Samad, A., Trognitz, F., Compant, S., Antonielli, L., and Sessitsch, A. (2017). Shared and host-specific microbiome diversity and functioning of grapevine and accompanying weed plants. *Environ. Microbiol.* 19, 1407–1424. doi: 10.1111/1462-2920.13618

Sanmukh, S. G., Paunikar, W. N., Swaminathan, S., and Lokhande, S. K. (2012). Bacteriophages as a model for studying carbon regulation in aquatic system. *Nat. Preced.* 7, 1–8. doi: 10.1038/NPRE.2012.6770.1

Shafi, S., Kamili, A. N., Shah, M. A., Parray, J. A., and Bandh, S. A. (2017). Aquatic bacterial diversity: magnitude, dynamics, and controlling factors. *Microb. Pathog.* 104, 39–47. doi: 10.1016/j.micpath.2017.01.016

Sun, H., Narihiro, T., Ma, X., Zhang, X., Ren, H., and Ye, L. (2019). Diverse aromatic-degrading bacteria present in a highly enriched autotrophic nitrifying sludge. *Sci. Total Environ.* 666, 245–251. doi: 10.1016/j.scitotenv.2019.02.172

Székely, A. J., and Silke, L. (2014). The importance of species sorting differs between habitat generalists and specialists in bacterial communities. *FEMS Microb. Ecol.* 87, 102–112. doi: 10.1111/1574-6941.12195

Tang, X. M., Chao, J. Y., Gong, Y., Wang, Y. P., Wilhelm, S. W., and Gao, G. (2017). Spatiotemporal dynamics of bacterial community composition in large shallow eutrophic Lake Taihu: high overlap between free-living and particle-attached assemblages. *Limnol. Oceanogr.* 62, 1366–1382. doi: 10.1002/lno.10502

Wang, X., Liu, J. X., Chai, B. F., Luo, Z. M., Zhao, P. Y., and Bao, J. B. (2019). Spatio-temporal patterns of microbial communities and their driving mechanisms in subalpine lake, Ningwu, Shanxi. *Environ. Sci.* 40, 3285–3294. doi: 10.13227/j.hjkx.201901049

Wang, X., Wang, Z., Jian-hui, C., Liu, J., Wang, H., Zhang, S., et al. (2014). Origin of the upland lake group in Ningwu Tianchi region, Shanxi Province. *J. Lanzhou Univ. Nat. Sci.* 50, 208–212. doi: 10.13885/j.issn.0455-2059.2014.02.016

Wu, W., Logares, R., Huang, B., and Hsieh, C. H. (2016). Abundant and rare picoeukaryotic sub-communities present contrasting patterns in the epipelagic waters of marginal seas in the northwestern Pacific Ocean. *Environ. Microbiol.* 19, 287–300. doi: 10.1111/ 1462-2920.13606

Xue, Y., Chen, H., Yang, J. R., Liu, M., Huang, B., and Yang, J. (2018). Distinct patterns and processes of abundant and rare eukaryotic plankton communities following a reservoir cyanobacterial bloom. *ISME J.* 12, 2263–2277. doi: 10.1038/s41396-018-0159-0

Yang, Y., Dai, Y., Wu, Z., Xie, S., and Liu, Y. (2016). Temporal and spatial dynamics of archaeal communities in two freshwater lakes at different trophic status. *Front. Microbiol.* 7:451. doi: 10.3389/fmicb.2016.00451

Yu, S., Pang, Y., Wang, Y., Li, J., and Qin, S. (2018). Distribution of bacterial communities along the spatial and environmental gradients from Bohai Sea to northern Yellow Sea. *PeerJ* 6:e4272. doi: 10.7717/peerj.4272

Zhang, J., Feng, J., Xie, S., and Wang, S. (2012). Characteristics of phytoplankton community structures in Ningwu subalpine lakes, Shanxi Province. *J. Lake. Sci.* 24, 117–122. doi: 10.18307/2012.0116

Zhang, W., Pan, Y., Yang, J., Chen, H., Holohan, B., Vaudrey, J., et al. (2018). The diversity and biogeography of abundant and rare intertidal marine microeukaryotes explained by environment and dispersal limitation. *Environ. Microbiol.* 20, 462–476. doi: 10.1111/1462-2920.13916

Zhao, D. Y., Cao, X. Y., Huang, R., Zeng, J., Shen, F., Xu, H. M., et al. (2017). The heterogeneity of composition and assembly processes of the microbial community between different nutrient loading Lake zones in Taihu Lake. *Appl. Microbiol. Biotechnol.* 101, 5913–5923. doi: 10.1007/s00253-017-8327-0

Zhou, Z., Tran, P. Q., Kieft, K., and Anantharaman, K. (2020). Genome diversification in globally distributed novel marine *Proteobacteria* is linked to environmental adaptation. *ISME J.* 14, 2060–2077. doi: 10.1038/s41396-020-0669-4

Zinger, L., Boetius, A., and Ramette, A. (2014). Bacterial taxa-area and distance-decay relationships in marine environments. *Mol. Ecol.* 23, 954–964. doi: 10.1111/mec.12640

Conflict of Interest: The authors declare that the research was conducted in the absence of any commercial or financial relationships that could be construed as a potential conflict of interest.

frontiers in Microbiology

ORIGINAL RESEARCH
published: 02 August 2021
doi: 10.3389/fmicb.2021.675328

The Interplay of Phototrophic and Heterotrophic Microbes Under Oil Exposure: A Microcosm Study

Manoj Kamalanathan[1], Kathleen A. Schwehr[2], Jessica M. Labonté[1], Christian Taylor[2], Charles Bergen[2], Nicole Patterson[2], Noah Claflin[1], Peter H. Santschi[2,3] and Antonietta Quigg[1,3]*

[1] Department of Marine Biology, Texas A&M University at Galveston, Galveston, TX, United States, [2] Department of Marine and Coastal Environmental Science, Texas A&M University at Galveston, Galveston, TX, United States, [3] Department of Oceanography, Texas A&M University, College Station, TX, United States

Microbial interactions influence nearly one-half of the global biogeochemical flux of major elements of the marine ecosystem. Despite their ecological importance, microbial interactions remain poorly understood and even less is known regarding the effects of anthropogenic perturbations on these microbial interactions. The Deepwater Horizon oil spill exposed the Gulf of Mexico to ∼4.9 million barrels of crude oil over 87 days. We determined the effects of oil exposure on microbial interactions using short- and long-term microcosm experiments with and without Macondo surrogate oil. Microbial activity determined using radiotracers revealed that oil exposure negatively affected substrate uptake by prokaryotes within 8 h and by eukaryotes over 72 h. Eukaryotic uptake of heterotrophic exopolymeric substances (EPS) was more severely affected than prokaryotic uptake of phototrophic EPS. In addition, our long-term exposure study showed severe effects on photosynthetic activity. Lastly, changes in microbial relative abundances and fewer co-occurrences among microbial species were mostly driven by photosynthetic activity, treatment (control vs. oil), and prokaryotic heterotrophic metabolism. Overall, oil exposure affected microbial co-occurrence and/or interactions possibly by direct reduction in abundance of one of the interacting community members and/or indirect by reduction in metabolism (substrate uptake or photosynthesis) of interacting members.

Keywords: phototrophs, heterotrophs, prokaryotes, eukaryotes, oil, photosynthesis, co-occurrence, interactions

OPEN ACCESS

Edited by:
Rodrigo Gouvea Taketani, Rothamsted Research, United Kingdom

Reviewed by:
Lucélia Cabral, São Paulo State University, Brazil
Daniel Lundin, Linnaeus University, Sweden

****Correspondence:***
Manoj Kamalanathan
manojka@tamu.edu

Specialty section:
This article was submitted to Aquatic Microbiology, a section of the journal Frontiers in Microbiology

Received: *02 March 2021*
Accepted: *28 June 2021*
Published: *02 August 2021*

Citation:
Kamalanathan M, Schwehr KA, Labonté JM, Taylor C, Bergen C, Patterson N, Claflin N, Santschi PH and Quigg A (2021) The Interplay of Phototrophic and Heterotrophic Microbes Under Oil Exposure: A Microcosm Study. Front. Microbiol. 12:675328. doi: 10.3389/fmicb.2021.675328

INTRODUCTION

Microbial interactions (viruses, bacteria, archaea, phytoplankton, and fungi) in aquatic systems are considered as one of the most important inter-organism associations that strongly influence carbon, nitrogen, phosphorus, sulfur, and iron cycling (Fuhrman et al., 2015). They are also the very first level of important organic matter transactions in aquatic food webs (Seymour et al., 2017). In the early 1970s, Bell and Mitchell (1972) first proposed the interaction between phytoplankton and bacteria, which could be either symbiotic or antagonistic in nature. These are now known to be integral in shaping aquatic ecosystem functions and global biogeochemistry (Ramanan et al., 2016).

Similarly, phytoplankton are also infected by viruses (Pienaar, 1976) and consumed by protozoa (Caron et al., 1988) and fungi (Paterson, 1960); and often, these interactions tend to be antagonistic/parasitic in nature (Barbeau et al., 1996; Brussaard, 2004; Rasconi et al., 2011). These complex microbial relationships are also considered to be the basis of marine snow formation (Grossart et al., 2006; Azam and Malfatti, 2007), an integral mechanism in the cycling of carbon, nutrients, and trace elements in oceans (Kiørboe, 2001). Despite the significance in the aquatic ecosystems, little is known about the rates of such interactions, the composition of the molecules exchanged, the specificity of the associations, and the effects of human perturbation on these interactions and, therefore, their impact on the marine ecosystem. This knowledge gap can be primarily attributed to methodological limitations, vast spatial–temporal scales, the minute amounts of metabolites exchanged, difficulties in growing most marine microbes in the laboratory, and overall uncharacterized nature of dissolved and particulate organic matter. Although several studies have used modern omics approaches to understand these interactions, very few have focused on direct measurements (Amin et al., 2015; Durham et al., 2015; von Borzyskowski et al., 2019).

Heterotrophs derive nutrients from phytoplankton either *directly* by parasitic consumption or *indirectly* via the phytoplankton-secreted exopolymeric substances (EPSs), which are rich in polysaccharides and are broken down into simple monomers via extracellular enzymatic action (Grossart et al., 2006; Arnosti, 2011; Kamalanathan et al., 2019, 2020). A small number of examples of such interactions have been defined for bacteria and phytoplankton. For example, von Borzyskowski et al. (2019) demonstrated that certain bacteria possess several pathways to assimilate and utilize the glycolate that is widely secreted by phytoplankton. Durham et al. (2015) demonstrated the secretion of 2,3-dihydroxypropane-1-sulfonate by diatoms is assimilated and catabolized by *Roseobacter* in seawater. These interactions can also be synergistic for phytoplankton. For example, bacteria have been shown to assimilate amino acids secreted by phytoplankton and convert them into vitamin B_{12} that is released into the water, which in turn is assimilated by phytoplankton (Amin et al., 2015). Some studies also focused on indirect microbial interactions, for example, Elifantz et al. (2005, 2007) and Taylor et al. (2013), wherein labeled EPS from phytoplankton was added to a natural bacterial community. Although few in number, such detailed studies focusing on phytoplankton–protozoa and phytoplankton–fungi interactions have been virtually non-existent. In addition, the uncharacterized nature of EPS also means the possibility that numerous other pathways may exist. With increasing offshore activities, human perturbations are a great threat to aquatic ecosystems. The single-cell scale of these microbial interactions also means high vulnerability to any anthropogenic perturbations, with abiotic environmental factors previously shown to interfere with these interactions (Wang et al., 2019).

In 2010, the Deepwater Horizon oil spill exposed the Gulf of Mexico to unprecedented amounts of crude oil, resulting in oil surfacing from the wellhead to form slicks that covered a minimum area of 10,000 km^2 of Gulf of Mexico (Hu et al., 2018). This surfacing of oil exposed microbial communities throughout the vertical water column. Several studies revealed that ∼5–31% of the total oil spilled sedimented to the seafloor (Passow et al., 2012; Fu et al., 2014; Brooks et al., 2015; Romero et al., 2015) via marine snow through a process termed Marine Oil Snow Sedimentation and Flocculent Accumulation (MOSSFA) (Daly et al., 2016; Brakstad et al., 2018; Xu et al., 2018b, 2019a). Exposure to oil induces the production of EPS as a microbial community response (e.g., Quigg et al., 2016, 2021) with significant changes to the microbial community structure (Kleindienst et al., 2015; Doyle et al., 2018). As microbial activities are an important driver in the formation of marine snow, exposure to oil is bound to alter their interactions and therefore the marine ecosystem dynamics. In addition, while the Deepwater Horizon oil spill was an extreme event, oil spills are common in the Gulf of Mexico; for example, there were more than 180 oil spills in 2019 alone[1]. Therefore, the aim of our study was to characterize microbial activities and potential microbial interactions and show how these factors are impacted by oil exposure, by combining radiotracer experiments with traditional physiological measurements (photophysiology and EPS composition analysis), microbial community composition (16S and 18S rRNA gene sequencing) and co-occurrence analysis, and a Bayesian hierarchical joint-contaminant modeling approach that combined the data from the above-mentioned analyses to identify potential interactions.

MATERIALS AND METHODS

Two sets of microcosm experiments were conducted in triplicates. The first set of microcosm experiments consisted of a short-term study lasting 8 h with three replicates of control and oil treatments with radiotracers $NaH^{14}CO_3$ and ^{3}H-leucine and an identical set of an experiment without radiotracer additions. The other set of microcosm experiments consisted of a long-term study lasting 72 h similar to the short-term microcosm study with and without radiotracers in triplicates. Microcosm experiments were conducted using seawater collected from the Gulf of Mexico (29°22N, 93°23W), with the short-term experiment (8 h) sampled at hourly intervals of 0, 1, 2, 3, 4, and 8 h on July 18, 2019, and the long-term experiment (72 h) sampled at 0, 24, 48, and 72 h from January 22 to 25, 2019. The salinity, pH, and temperature of the seawater collected on July 18, 2019, were 25 ppt, 7.58, and 29.70°C and on January 22, 2019, were 25.66 ppt, 8.02, and 14.40°C, respectively. No nutrients were supplemented to prevent any additional alterations to the natural microbial community and activity other than those due to oil exposure. In addition, previous mesocosm experiments performed using water collected near this location did not result in nutrient limitation within 72 h (Doyle et al., 2018; Xu et al., 2018a, 2019a; Wozniak et al., 2019). For the oil treatment, Macondo surrogate oil (400 $\mu L \cdot L^{-1}$) was added to the seawater and mixed briefly by

[1]https://incidentnews.noaa.gov/

hand, with the same concentration used for preparation of water-accommodated fraction (WAF) of oil using the more traditional CROSERF method (Singer et al., 2001). Direct exposure to oil was chosen over the CROSERF approach to avoid missing changes to the microbial community that occur under such a procedure, which requires overnight mixing of oil with seawater (Doyle et al., 2020). Overall, each experiment was run in triplicate treatments of seawater (control) and seawater with 4 ppm of oil, containing both radiotracers $NaH^{14}CO_3$ and ^{3}H-leucine. In addition to this microcosm, a parallel microcosm experiment was conducted in triplicates under similar conditions without the addition of radioactive tracers; and measurements including photophysiology, EPS composition, and microbial community composition (16S and 18S rRNA gene sequencing) analysis were performed during the course of these experiments. All the experiments were performed at ∼60 μmol photons·m^{-2}·s^{-1} at 19°C. For both sets of the experiments, microcosm were kept under a 12:12 light:dark cycle.

Experimental Setup With Radiotracers

The experiment was setup in 1-L culture bottles that were first cleaned with Radiac© and acid and then combusted at 450°C for 4 h. The plastic caps were fitted with two holes into which tubing was inserted and sealed into the cap with silicone. Above the cap, each tubing was fitted with a valve that remained closed during the experiment. One tubing extended to the bottom interior of the bottle and was used for withdrawing samples. The other tubing extended only into the headspace of the bottle, above the water or oil–water, and was used to apply positive pressure when withdrawing sample from the long tubing at the bottle bottom. The triplicate treatments with radiotracer additions were (1) a control with incubation of $NaHC^{14}O_3$ and ^{3}H-leucine and (2) incubation of $NaHC^{14}O_3$ and ^{3}H-leucine with oil. The treatments were monitored over time for radioisotope activity in different size fractions to operationally isolate eukaryotes (≥3 μm), free-living prokaryotes (<3 and ≥0.2 μm), and EPS (<0.2 μm and ≥3 kDa). We acknowledge the possibilities of prokaryotes forming aggregates, as a result being captured in 3-μm fraction, and that picoeukaryotes (with an average cellular dimensions of 3 μm or lower) are more likely to pass through this fraction. Also, there is potential for certain prokaryotes to be captured in 3-kDa fraction due to smaller cell volume than 0.2 μm or possessing non-rigid cell walls, allowing them to pass through the utilized 0.2-μm filter. However, we assume that the radiotracer signature resulting from such incidents would be relatively minimal and therefore would not affect our interpretation of results significantly.

The radiolabeled samples were taken at the specified time intervals from the two treatments and gently filtered at <100 mmHg. A 10 ml aliquot was first passed through a 3-μm filter (cellulose acetate, 25-mm diameter; Sterlitech, Kent, WA, United States). Each 3-μm filter was placed in separate 20-ml liquid scintillation vials with 5 ml of liquid scintillation cocktail added to each, and the activities of ^{14}C and ^{3}H retained on the 3-μm filters were counted. The 10 ml of filtrate from the 3-μm filters was then passed through a 0.2-μm filter (cellulose acetate, 25-mm diameter; Sterlitech). Each 0.2-μm filter was placed in separate 20-ml liquid scintillation vials with 5 ml of liquid scintillation cocktail added to each, and the activities of ^{14}C and ^{3}H retained on the 0.2-μm filters were counted. The 10 ml of filtrate from the 0.2-μm filters was then ultrafiltered through a 3-kDa membrane (EMD Amicon-15 centrifugal device; Thermo Fisher Scientific, Waltham, MA, United States), diafiltered against ultrapure 18.2 MΩ·cm water to remove salts, and finally made up to 1-ml volume with the ultrapure water. The 1 ml of colloidal EPS was added to 5 ml of liquid scintillation cocktail to count the activities of ^{14}C and ^{3}H for the 0.3 kDa colloidal EPS retentate.

Permeate (solution passing through the 3-kDa membrane) was also counted. This is the unbound fraction. An aliquot of 0.5 ml with 5 ml of cocktail was counted. The activities for ^{14}C and ^{3}H for each time sample for each fraction (3-μm filter, 0.2-μm filter, colloidal EPS < 0.2 μm and >3 kDa, and the unbound 3-kDa permeate) were counted and corrected to the 10-ml sample volume. The counting was done using 5 ml of Ultima Gold LLT cocktail (PerkinElmer, Waltham, MA, United States) in borosilicate glass liquid scintillation vials. The activities were counted on a Beckman Coulter (Brea, CA, United States) LS-6500 liquid scintillation counter using a dual channel program. Sample activities were corrected for isotope dilution and reagent quenching by counting a known activity spike to the same reagent matrix as the samples.

Photo-Physiological Measurements

Photo-physiological parameters were measured in triplicate samples to monitor the effects of oil exposure on the photosynthetic activity and growth of phytoplankton. Briefly, parameters such as relative electron transport rates, light harvesting efficiency, and maximum quantum yield were measured using a Phyto-PAM fluorometer according to previous studies (Bretherton et al., 2018; Kamalanathan et al., 2019). As Phyto-PAM fluorometer uses multiwavelength excitation, the relative physiological responses of different taxa of phytoplankton were obtained using the fluorescence measurements in the channels 470 and 520 nm (diatoms and dinoflagellates); 470, 645, and 665 nm (chlorophytes); and 645 nm (cyanobacteria). The absorption cross-sectional area, connectivity factor, and Q_A turnover rates were measured using the Satlantic Inc. (Halifax, NS, Canada) FIRe fluorometer (Bretherton et al., 2018; Kamalanathan et al., 2019). Growth of phytoplankton was monitored by chlorophyll *a* fluorescence using Turner Designs (San Jose, CA, United States) fluorometer (Bretherton et al., 2018).

Exopolymeric Substance Protein, Neutral Sugars, and Uronic Acid Determination

Exopolymeric substance concentration and composition were determined in triplicate samples from the parallel microcosm experiment without radiotracers. The methods used to determine protein, neutral sugars, and uronic acid in the EPS fraction are detailed in Schwehr et al. (2018) and Xu et al. (2018a). A modified bicinchoninic acid method (Smith et al., 1985) was used to determine the protein content in EPS. This was performed by

using a Pierce protein assay kit (Thermo Fisher Scientific), with bovine serum albumin (BSA) as the standard. The neutral sugars concentrations were determined using the anthrone method (Morris, 1948), with glucose as the standard. This method was used for determining neutral sugars; it could not detect negatively charged sugars, such as uronic acids. Uronic acid was estimated by adding sodium borate (75 mM) in concentrated sulfuric acid and *m*-hydroxydiphenyl, with glucuronic acid as the standard (Hung et al., 2001).

Microbial Community Composition Analysis

To elucidate the interactions between the microbes in oil and in seawater with no additions, natural seawaters from the Gulf of Mexico with their ambient communities were subsampled in triplicates from the parallel microcosm experiment without radiotracers. Throughout the experiments, the microbial assemblages were revealed using 18S and 16S rRNA sequencing, respectively. PCR amplification, using Platinum Taq DNA Polymerase (Thermo Fisher Scientific), was performed following the 16S/18S rRNA gene Illumina, Inc. (San Diego, CA, United States) amplicon protocol from the Earth Microbiome project[2]. Each sample was amplified in triplicate 25-μl reactions with the following cycling parameters: 95°C for 3 min, 30 cycles of 95°C for 45 s, 50°C for 60 s, and 72°C for 90 s, and a final elongation step at 72°C for 10 min. For prokaryotes, the V4 hypervariable region on the 16S rRNA gene and for eukaryotes the V8–V9 hypervariable region on the 18S rRNA were used for amplification (Caporaso et al., 2011; Bradley et al., 2016). For the prokaryotes, amplifications were performed using the modified 515F-806R primer pair (10 μM each) that reduces bias against the Crenarchaeota and Thaumarchaeota lineages as well as the SAR11 bacterial clade (Apprill et al., 2015; Parada et al., 2016). The primer pair utilized for the eukaryote analysis was V8f–1510r (Bradley et al., 2016). The primer pair was additionally modified to include Golay barcodes and adapters for Illumina MiSeq sequencing. Final primer sequences are detailed in Walters et al. (2016). Following amplification, the triplicate products were combined together and run on a 1.5% agarose gel to assess amplification success and relative band intensity. Triplicate amplicons were then pooled and purified with the Qiagen PCR Clean-up kit (Qiagen, Germantown, MD, United States). Approximately 50 ng of each sample was pooled; and the purified products, along with aliquots of the three sequencing primers, were sent to the Texas A&M Genomics and Bioinformatics Services (College Station, TX, United States) for MiSeq sequencing (v2 Nano chemistry, 2 × 250 bp). Sequence reads for both the 16S rRNA and 18S rRNA were processed separately using *mothur* v.1.39.5 following the MiSeq SOP https://www.mothur.org/wiki/MiSeq_SOP (Schloss et al., 2009; Kozich et al., 2013), which included reducing sequencing and PCR errors, processing the improved sequences, running an alignment using the reference SILVA alignment (v132), removing poorly aligned sequences and undesirables, and clustering utilizing the cluster.split command; and then an amplicon sequence variant (ASV) list was generated using the classify.otu command with the label "asv." Unfortunately, not all samples gave the minimum number of reads necessary for ecological analyses. As such, one replicate from one of the control replicates at 48 h for 16s (CB3 16s), one of the control replicates at 72 h for 18s (CB4 18s), and one of the oil replicates at 0 h for 18s (OC1 18s) samples could not be used, leaving PCR amplicon duplicates for these samples. Graphical analyses were made using ggplot package (Wickham and Wickham, 2007). Diversity and richness indices (observed richness, Simpson, Shannon, and effective diversity) were calculated using the vegan package (Oksanen et al., 2013).

[2]https://earthmicrobiome.org/protocols-and-standards/empo/

Hierarchical Modeling of Species Communities

To determine the contribution of certain parameters measured in the variation of occurrence of each of the microbial species, we utilized a Bayesian hierarchical joint-contaminant modeling [hierarchical modeling of species communities (HMSC)] approach (Ovaskainen et al., 2017). We modeled the abundance of microbial species (as Y-matrix) and certain environmental parameters (treatment, time, Chlorophyll *a*, F_v/F_m, $rETR_{max}$, ^{14}C and ^{3}H labeled >3 kDa, and >0.2- and 3-μm fraction) from the long-term experiment as the X-dataframe, using a Poisson model with a Markov chain Monte Carlo (MCMC) sampling of 10,000 iterations, 1,000 burn-in phase, 10 thinning, and the default priors of the framework.

Co-occurrence Analysis

The co-occurrence networks for microbes from the long-term experiment were created using Spearman's correlation matrix determined using the Hmisc package (Harrell and Harrell, 2019). The *p*-values of the correlations were then adjusted using the Benjamini and Hochberg false discovery rate (FDR)-controlling procedure (Benjamini et al., 2006), available in the Stats package. A cutoff of 0.0005 for FDR-adjusted *p*-values and 0.8 for Spearman's rho values was then applied, and the co-occurrence was visualized using a chord diagram plotted using the package circlize (Gu et al., 2014).

Statistics

Diversity and richness indices, HMSC modeling and co-occurrence network, and visualization were performed in R (version 4.0.2). In addition, statistical analyses of other results presented in this study such as one-way ANOVA with Tukey's honestly significant difference (HSD), *t*-test, and Pearson's correlation were also performed using the Vegan package (Oksanen et al., 2013) in R (R Core Team, 2013).

RESULTS

Two different sets of microcosm experiments with and without radiotracers were conducted in this study, one to understand the short-term (8 h) exposure of oil and the other to understand the long-term (72 h) exposure of oil. These studies were intended to capture the acute and chronic effects of exposure to oil on

microbial interactions, with radiotracer study used to understand the uptake, turnover, and exchange of metabolites between phototrophs and heterotrophs, and the non-radiotracer study used to capture the physiology and community dynamics.

Microbial Activity Signatures Using Radiotracers in the Short-Term Experiment

Monitoring of the ^{14}C signature ($H^{14}CO_3^-$) in the ≥ 3-μm fraction (hereafter referred to as eukaryotic phototrophic organic matter) over a period of 24 h showed no significant difference between the control and oil treatments (p = 0.355) (**Supplementary Figure 1A**). The eukaryotic phototrophic carbon label significantly increased with time in both control and oil treatments ($p = 3.93e^{-11}$) (**Supplementary Figure 1A**). Although measurements of ^3H-leucine in the ≥ 0.2-μm (and < 3-μm) fraction (hereafter prokaryotic organic matter) were not significantly different between the control and oil treatments for every time point (p = 0.311), overall, the values were higher in the control (p = 0.0001) (**Supplementary Figure 1B**). Similar to the eukaryotic phototrophic organic matter, prokaryotic organic matter also significantly increased with time ($p < 2e^{-16}$) (**Supplementary Figure 1B**). The levels of ^{14}C-labeled molecules in the ≥ 3-kDa (and < 0.2-μm) fraction (hereafter phototrophic EPS) over a period of 24 h significantly increased with time for both the treatments ($p = 1.47e^{-08}$) (**Supplementary Figure 1C**); however, there were no significant differences over time between the control and oil treatments (p = 0.255) (**Supplementary Figure 1C**). On the other hand, the levels of ^3H-labeled molecules in the ≥ 3-kDa (hereafter heterotrophic EPS) fraction significantly increased over 4 h but then decreased at the 8-h time point ($p = 2.35e^{-07}$) (**Supplementary Figure 1D**), with no significant differences between the treatments (p = 0.814) (**Supplementary Figure 1D**). The levels of ^{14}C in the ≥ 0.2-μm (and < 3-μm) fraction (hereafter prokaryotic uptake of phototrophic organic matter) significantly increased with time ($p = 9.39e^{-10}$) (**Supplementary Figure 1E**); however, no significant differences were observed between the control and the oil treatments (p = 0.385) (**Supplementary Figure 1E**). Similarly, the levels of ^3H signature in the ≥ 3-μm fraction (hereafter eukaryotic uptake of heterotrophic organic matter) increased significantly with time ($p = 3.04e^{-14}$) (**Supplementary Figure 1F**), showing no significant differences between the treatments (p = 0.121) (**Supplementary Figure 1F**).

Microbial Activity Signatures Using Radiotracers in the Long-Term Experiment

Similar to the short-term experiment, longer-term monitoring of the eukaryotic phototrophic organic matter over a period of 72 h revealed patterns of significantly increasing labeling in both treatments with time ($p = 1.09e^{-05}$) (**Figure 1A**). However, the levels of radiotracer signatures of ^{14}C and ^3H-labeled compounds in the control were significantly higher compared with those of the oil treatment (p = 0.001) (**Figure 1A**). Levels of prokaryotic organic matter labeling showed the opposite patterns to eukaryotic phototrophic organic matter, with decreasing activity with time in both the treatments (p = 0.002) (**Figure 1B**) and significantly higher levels of prokaryotic organic matter in the control treatments compared with those in the oil (p = 0.009) (**Figure 1B**). Labeled phototrophic EPS also increased with time for both the treatments ($p = 9.17e^{-09}$) (**Figure 1C**), with the control treatment showing significantly higher signal than the oil (p = 0.0003) (**Figure 1C**). On the other hand, prokaryotic EPS was variable over time (**Figure 1D**), with a significantly higher signal in the control compared with oil treatment ($p = 2.02e^{-08}$) (**Figure 1D**). The levels of prokaryotic uptake of phototrophic organic matter increased significantly with time for both treatments until 48 h and then decreased at 72 h (p = 0.034), with no differences observed between the control and oil treatments (p = 0.585) (**Figure 1E**). The eukaryotic uptake of heterotrophic organic matter increased in both control and oil treatments with time ($p = 5.62e^{-07}$) (**Figure 1F**). However, the two treatments showed very different patterns, whereby the control had significantly higher levels of eukaryotic uptake of heterotrophic organic matter than the oil treatment ($p = 2.70e^{-08}$) (**Figure 1F**). The levels in the control treatment peaked at 48 h and remained stable until 72 h, while this increased continuously in the oil treatment throughout the 72-h period of the experiment.

Correlation analysis between phototrophic EPS and eukaryotic uptake of heterotrophic organic matter was performed for both the short- and long-term experiments as an additional measure of phototroph–heterotroph interactions. This analysis revealed a significant linear correlation (Pearson's R = 0.637, $p = 4.279e^{-06}$) (**Supplementary Figure 2A**). Further analysis of the distribution of control and oil data points along the correlation plot revealed slightly higher distribution for control over oil; however, this difference was not statistically significant (t-test, p = 0.207) (**Supplementary Figure 2B**).

Photosynthetic Physiology

Photophysiology of the phytoplankton was monitored by measuring the light harvesting ability of phytoplankton (α, μmol photons·μmol electrons^{-1}), relative maximum electron transport rates between photosystem (PS) II and I ($rETR_{max}$, μmol electrons·m^{-2}·s^{-1}), maximum quantum yield of PS II, a proxy of photosynthetic efficiency (F_v/F_m, relative units), connectivity between PS II units (ρ, relative units), and lastly absorption cross-sectional area of PS II, a proxy of the photosynthetic antennae size (σ, Å (quanta)$^{-1}$) (Suggett et al., 2003). α and $rETR_{max}$ were measured for the major taxonomic classes of phytoplankton (chlorophytes, cyanobacteria, diatoms, and dinoflagellates), whereas the other photosynthetic parameters were measured for the whole community. In the short-term experiment, although both α and $rETR_{max}$ were not significantly different between the control and oil treatments for all taxa at every measured time point (p = 0.999), the overall values were higher in the control compared with the oil treatment ($p < 9.74e^{-05}$) (**Supplementary Figures 3A,B**). In the long-term experiment, α was overall significantly higher in the control treatments compared with oil ($p < 2e^{-16}$), although these differences were not significant

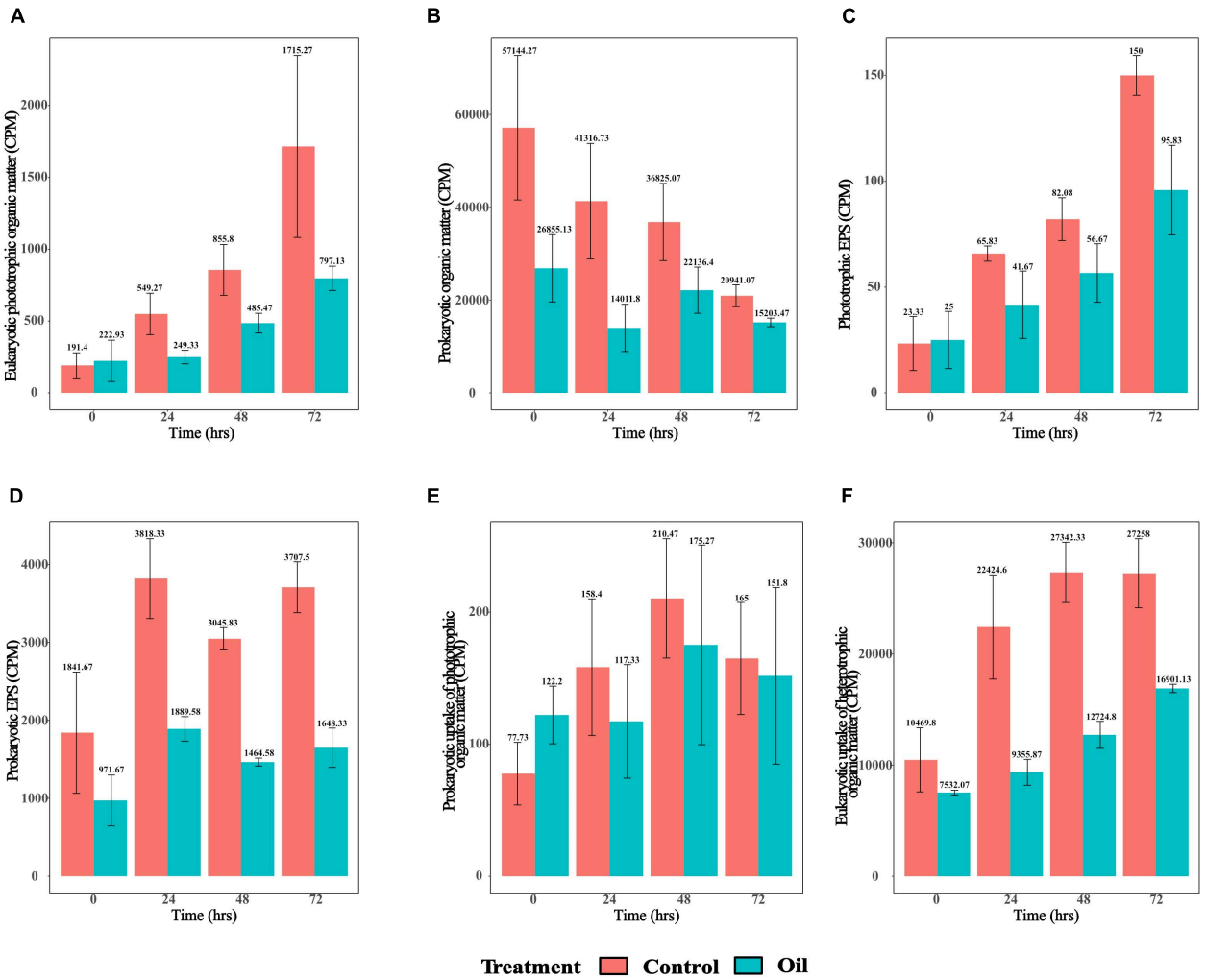

FIGURE 1 | Radiotracer signals from the long-term experiment. **(A)** Eukaryotic phototrophic organic matter as indicated by the ^{14}C signatures in ≥ 3-μm fraction (CPM), **(B)** prokaryotic organic matter as indicated by ^{3}H signatures in ≥ 0.2-μm fraction (CPM), **(C)** phototrophic exopolymeric substance (EPS) as indicated by ^{14}C signatures in ≥ 3-kDa fraction (CPM), **(D)** heterotrophic EPS indicated by ^{3}H signatures in ≥ 3-kDa fraction (CPM), **(E)** prokaryotic uptake of phototrophic organic matter as indicated by ^{14}C signatures in ≥ 0.2-μm fraction (CPM), and **(F)** eukaryotic uptake of heterotrophic organic matter as indicated by ^{3}H signatures in ≥ 3-μm fraction (CPM).

for all time points in all taxa of phytoplankton (p = 0.448) (**Figure 2A**). Similarly, $rETR_{max}$ values also were overall higher in the control compared with oil ($p < 2e^{-16}$), but not in all taxa of phytoplankton across all time points (p = 0.781) (**Figure 2B**). It appears that diatoms and dinoflagellates had lower α and $rETR_{max}$ than cyanobacteria, which were also less than the chlorophytes; but these were not significant (p = 0.192). The effects of oil were more pronounced in the long-term experiment compared with the short-term experiment. F_v/F_m values were similar in the control treatment compared with oil in the short-term experiment for every time point (p = 0.858) (**Supplementary Figure 4A**), but they were only significantly higher in the long-term experiment (p = 0.005) (**Supplementary Figure 4D**). The connectivity between PS II was similar in the control and oil treatments in both the short- (p = 0.164) and long-term (p = 0.107) experiments (**Supplementary Figures 4B,E**). On the contrary, σ values were overall similar in the short-term experiment between the two treatments (p = 1.000), while they were higher in the control compared with oil treatment in the long-term experiment (p = 0.003); however, these were not significantly different for every measured time point (p = 0.238) (**Supplementary Figures 4C,F**).

Exopolymeric Substances

Exopolymeric substance concentrations were monitored in the long-term experiment every 24 h by measuring the carbohydrates, proteins, and uronic acids in the ≥ 3 kDa/colloidal fraction (**Supplementary Figure 5**). Although an increasing trend was observed in the carbohydrate content of EPS with time in both treatments, these trends were similar between oil treatment and control (p = 0.189) (**Supplementary Figure 4A**). In addition, no significant differences were observed

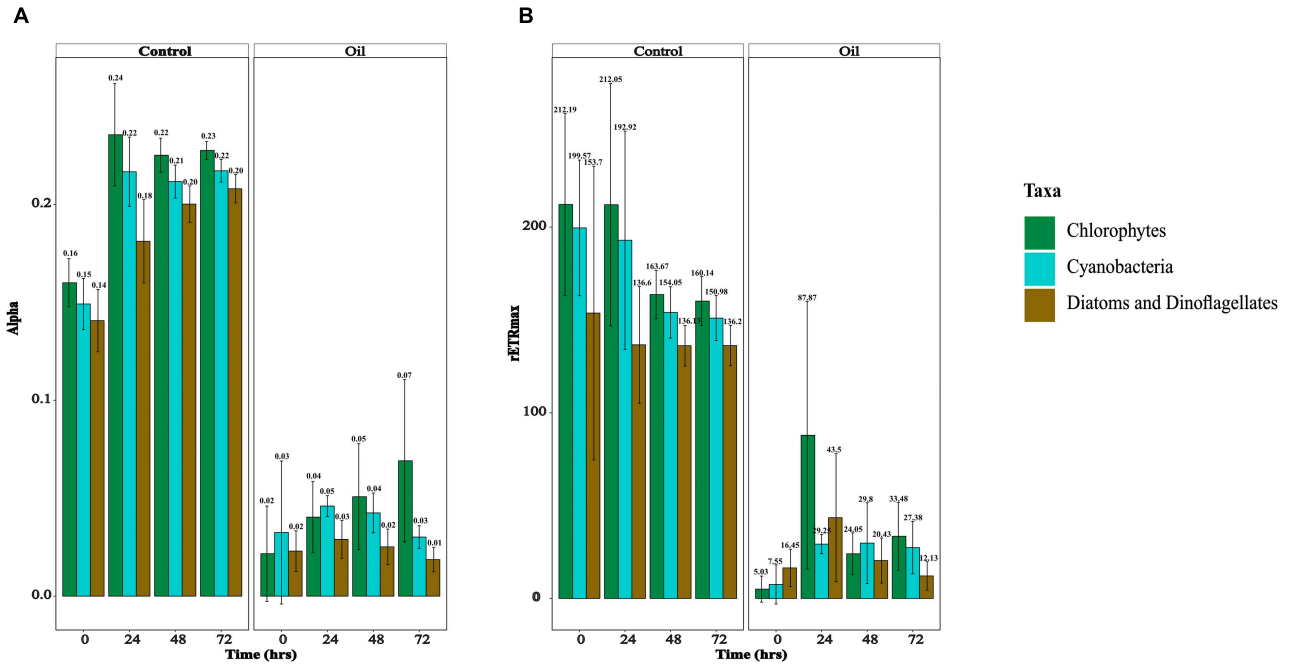

FIGURE 2 | Photosynthetic physiology of different classes of phytoplankton. **(A)** Alpha/light harvesting ability (μmol e^{-}·μmol photons^{-1}) in the long-term experiment and **(B)** relative electron transport rates (μmol e^{-}·m^{-2}·s^{-1}) in the long-term experiment.

between the carbohydrates in the control and oil treatments (p = 0.277) (**Supplementary Figure 5A**). The protein content of EPS showed trends similar to the carbohydrate, with no significant increase in levels over time in both the treatments (p = 0.105) (**Supplementary Figure 5B**). However, protein content in the EPS of oil treatment was overall significantly higher than that in the control except for the 48-h time point (p = 0.003), although these differences were not significant for every measured time point (p = 0.098) (**Supplementary Figure 5B**). Uronic acid content of the EPS showed a very similar pattern to the proteins, with overall higher values in oil (p = 0.005), but no significant increase for every measured time point (p = 0.237) (**Supplementary Figure 5C**). Total EPS content determined by summing the carbohydrates, proteins, and uronic acids also showed trends of increasing levels with time in both the treatments, but this trend was not significant (p = 0.133) (**Supplementary Figure 5D**). However, oil treatments overall had higher levels of EPS than the control treatment (p = 0.039), but not for every measured time point (p = 0.632) (**Supplementary Figure 5D**).

Microbial Community Analysis

Species richness and the Shannon–Weaver, Simpson, and effective diversity indices were similar between control and oil treatments at the starting point of the long-term experiment for both prokaryotes and eukaryotes. However, the effective diversity, Shannon–Weaver, and Simpson values were significantly lower in the oil treatment than the control at the end of the experiment for prokaryotes ($p \leq 0.007$), while the species richness values were similar (**Table 1**). No such significant differences were observed for eukaryotes. While other classes of prokaryotes such as *Actinomarinales, Flavobacteriales*, *Rhodobacterales*, and *Synechococcales* were present along with Gammaproteobacteria in the control, the oil treatment was mostly dominated by Gammaproteobacteria members (**Supplementary Figures 6A,B**). Further analysis showed that the relative abundance of Gammaproteobacteria members *Oceanospirillales, Alteromonadales*, and *Cellvibrionales* was the highest in the oil treatments, with the relative abundance of *Oceanospirillales* increasing with time (**Supplementary Figure 7B**). In the control treatment, the relative abundance of *Cellvibrionales* decreased with time, while that of *Alteromonadales* increased (**Supplementary Figure 7A**). Interestingly, the relative abundance of *Synechococcales* was similar in the control treatment through time, while it was drastically reduced in the oil treatment after 24 h (**Supplementary Figures 6A,B**). Among eukaryotes, *Spirotrichea* decreased in relative abundance in both the control and oil treatments through time (**Supplementary Figures 6C,D**), while the abundance of *Mediophyceae* members increased with time The relative abundance of *Dinophyceae* remained considerably higher in oil, while it decreased in the control treatment through time (**Supplementary Figures 6C,D**). Lastly, the relative abundance of *Diatomea* and *Bacillariophyceae* members increased with time in both control and oil treatments, and the abundances were lower in the oil treatment (**Supplementary Figures 6C,D**).

Positive and negative co-occurrences of species through time in the long-term experiment were determined for control and oil treatments (**Figure 3**). We found 89 significant co-occurrences

TABLE 1 | Spices richness and diversity of the microbial community in control and oil treatments at time 0 and 72 h of the long-term experiment.

	Species richness		Shannon–Weaver		Simpson		Effective diversity	
	0	72	0	72	0	72	0	72
Control								
Prokaryotes	539.75	663	3.58	5.11	0.90	0.98	36.46	168.13
Eukaryotes	756.5	341.33	4.37	3.15	0.96	0.95	79.35	24.33
WAF								
Prokaryotes	515	502	3.62	1.64	0.89	0.77	37.58	23.98
Eukaryotes	730	986	4.04	3.34	0.90	0.88	68.78	28.44

WAF, water-accommodated fraction.

(rho $> \pm$ 0.8, p-adjust < 0.0005) between microbial species in the control treatments, with 37 positive co-occurrences between prokaryotes, 25 positive co-occurrences between eukaryotes, and 27 co-occurrences between prokaryotes and eukaryotes (one negative and 26 positive) (**Figure 3A**). On the other hand, oil treatment showed only 51 significant co-occurrences (rho $> \pm$ 0.8, p-adjust < 0.0005) between microbial species with 42 significant co-occurrences between prokaryotes (6 negative and 36 positive), seven co-occurrences between eukaryotes (all 4 positive), and two co-occurrences between prokaryotes and eukaryotes (one negative and one positive) (**Figure 3B**).

Lastly, we determined the amount of variation in the occurrence of microbial species accounted by the measured parameters in the long-term experiment (treatment, time, chlorophyll *a*, F_v/F_m, $rETR_{max}$, and all the radiolabel measurements) using HMSC (**Figure 4**). Parameters such as treatment and time explain the effects of oil and changes to overall growth and oil concentration that occurred over time. Chlorophyll *a*, F_v/F_m, and $rETR_{max}$ were chosen to test the effect of phytoplankton concentration, photosynthetic efficiency, and rates of photosynthesis, while parameters such as the radiolabel measurements allowed for consideration of the effects of microbial uptake of substrates and exchange of different molecules. Overall, we found that F_v/F_m (photosynthetic efficiency) explained the highest amount (20%) of variation in the occurrence of microbial species, followed by treatment (15%), $rETR_{max}$ (relative rates of photosynthesis) (14), and prokaryotic organic matter (10%) (**Figure 4**). On the other hand, factors such as time alone accounted for 9% of the variation, whereas both prokaryotic uptake of heterotrophic phototrophic matter and eukaryotic uptake of heterotrophic organic matter explained only 9.7 and 4.9%, respectively (**Figure 4**).

The variation in the occurrence of *Flavobacteriales* and *Rhodobacterales*, the two most abundant prokaryotes in the control treatment, was explained mostly by the treatment (25.4 and 30.4%, respectively). Similarly, Gammaproteobacteria members *Oceanospirillales* and *Alteromonadales*, the most abundant prokaryotes in the oil treatment, were also mostly explained by the treatment (33.5 and 34.5%, respectively) and photosynthetic efficiency (12.8 and 14.5%, respectively) (**Figure 4**). The variation in the occurrence of *Mediophyceae*, the most abundant eukaryote in the control as well as oil treatment, was most explained by F_v/F_m (33.6%), $rETR_{max}$ (24.1%), and treatment (15.9%) (**Figure 4**). Similarly, *Dinophyceae* (unclassified), the most abundant eukaryote in the oil treatment, was mostly explained by $rETR_{max}$ (37.8%) and F_v/F_m (21.2%) (**Figure 4**). Among the eukaryotes, the variation in the occurrence of for most phototrophs was explained by F_v/F_m and/or $rETR_{max}$. The variation in occurrence of heterotrophic eukaryote *Maxillopoda* was explained mostly by chlorophyll (33.33%), while that of *Peronosporomycetes* was explained by time (29.67%), followed by F_v/F_m (23.89%). On the other hand, while the variation in the occurrence of most prokaryotes was explained by treatment (8–35%), unlike eukaryotes, the abundance of several species was explained by other factors as well. For example, *Micrococcales* and *Chitinophagales* were also explained by prokaryotic uptake of phototrophic organic matter (20.38 and 16.11%), whereas *Synechococcales* was explained by eukaryotic phototrophic organic matter (21.1%), and *Actinomarinales* and *Rhodospirillales* were also explained by heterotrophic organic matter (23.5 and 18.9%, respectively) (**Figure 4**).

DISCUSSION

Bacteria, viruses, protozoa, and fungi (heterotrophs) act as active filters between phytoplankton (phototrophs) and the rest of the marine environment, by consuming and transforming most of the organic matter, major and minor chemical elements, and energy derived by the growth of phytoplankton in the euphotic zone. These interactions between phototrophs and heterotrophs are crucial for vertical transport of nutrients in the ocean. However, the limited knowledge of these interactions makes understanding of the impacts of anthropogenic perturbations and their consequences on the biogeochemical cycles elusive. Here, we attempt to address this by specifically focusing on oil spill.

As there are uncertainties surrounding the direct estimation of primary productivity from ^{14}C-bicarbonate uptake rates (Milligan et al., 2015) and bacterial productivity from ^{3}H-leucine uptake rates (Franco-Vidal and Morán, 2011), we simply interpret the uptake of these radiotracers as a function of their metabolic activity. Even though there are bacteria with phototrophic and chemolithoautotrophic abilities (hence can uptake ^{14}C-bicarbonate) and phototrophic eukaryotes with heterotrophic abilities (hence can uptake ^{3}H-leucine), due to limitations of our experimental approach, we assume the following two scenarios for the interpretation of data from the labeling experiment: (1) uptake of radiolabeled bicarbonate

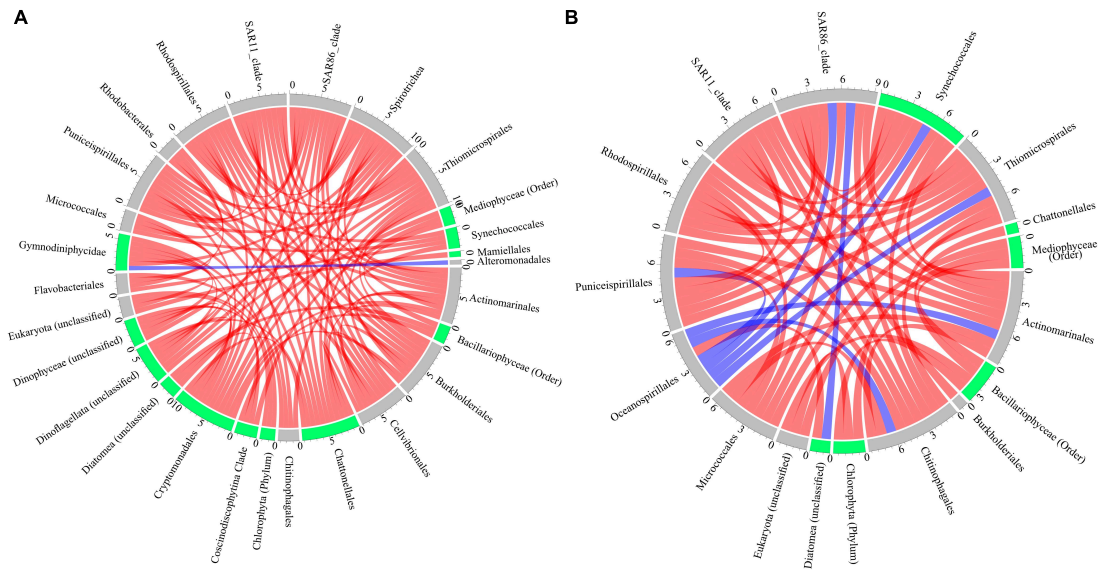

FIGURE 3 | Co-occurrence of prokaryotes and eukaryotes (cutoff of false discovery rate (FDR)-adjusted *p*-values < 0.0005 and Spearman's rho values $= \pm 0.8$) in the **(A)** control and **(B)** oil treatments, with red color indicating positive, blue color indicating negative co-occurrence, and blue- and gray-colored tracks labeling phototrophic and heterotrophic microbes.

was primarily carried out by phototrophs (phytoplankton and cyanobacteria) and (2) uptake of radiolabeled leucine was primarily carried out by heterotrophs and not phototrophs.

The short-term experiment with radiotracers suggested no acute effects of oil exposure on eukaryotic phototrophic uptake of inorganic carbon or secretion of organic carbon, whereas it showed slight negative effects on prokaryotic metabolic activity. Similar effects have been observed by Griffiths et al. (1981), where they observed a decrease in uptake of glucose and glutamic acid. Griffiths et al. (1981) attributed this metabolic inhibition to an event of sudden oil exposure, as an incubation over 9 days showed metabolic adjustments with higher uptake rates in their experiment. Surprisingly, these acute effects of oil on prokaryotic heterotrophic metabolism did not lead to a reduction of organic matter secretion by heterotrophs. The higher ^{14}C signatures in prokaryotic fraction at 1 h and after the start of the experiment under both treatments suggested either rapid uptake of phototrophic EPS by prokaryotes or photosynthesis by smaller cyanobacteria. The earlier scenario is not surprising, as Taylor et al. (2013) previously reported incorporation of labeled EPS into the phospholipids of bacteria within 6 h. Similarly, significant increase in ^{3}H signature in the eukaryotic fraction at 1 h and beyond suggests either rapid uptake of heterotrophic EPS by eukaryotes or uptake of ^{3}H-leucine by prokaryotic heterotrophs residing in the phycosphere and/or *direct* uptake of ^{3}H-leucine by heterotrophic eukaryotes especially protozoans or fungi (Buesing and Gessner, 2003; Matz and Jürgens, 2003). Overall, our results of microbial exchange of organic matter indicate the rapid processing of organic matter that can occur within 1 h. Moreover, the absence of any significant differences in microbial exchange of organic matter as indicated by the radiolabel signatures in the short-term experiment suggests no acute impact of oil exposure.

The long-term experiment showed severe effects of oil exposure on the uptake of radiolabeled substrates by both eukaryotic phototrophs and prokaryotic heterotrophs, with similar effects also seen for phototrophic and heterotrophic EPS secretion. However, these effects were more pronounced for prokaryotic organic matter production and the release of heterotrophic EPS. Taken together, these findings suggest that the observed severe effects on eukaryotic uptake of heterotrophic organic matter could be due to either overall lower heterotrophic radiolabeled EPS or poor performance of eukaryotic phototrophs in the presence of oil, thereby affecting the microenvironment of the phycosphere and resulting in reduced uptake of heterotrophic EPS. Interestingly, prokaryotic uptake of phototrophic organic matter was relatively unaffected in oil. As the cell diameter of *Synechococcales* (which accounted for 96.12% of the cyanobacterial community in our long-term experiment; data not shown) ranges from 0.8 to 1.2 μm (Morel et al., 1993; Garcia et al., 2016), it can occur in either filamentous or unicellular forms (Dvořák et al., 2014). Therefore, the unicellular forms of *Synechococcales* members are likely to account for the phototrophic organic matter signature in the $\geq$ 0.2-μm filter. However, the cyanobacterial relative abundance decreased in the presence of oil, suggesting a higher heterotrophic uptake of EPS produced from eukaryotic phototrophs.

Interestingly, a correlation of the phototrophic EPS versus eukaryotic uptake of heterotrophic organic matter (**Supplementary Figure 2**) showed a linear relationship, which could be interpreted as (a) evidence of metabolic dependence of prokaryotes in the phycosphere on the organic matter released by eukaryotic phototrophs and/or (b) evidence of prokaryotic organic matter uptake by phytoplankton that is

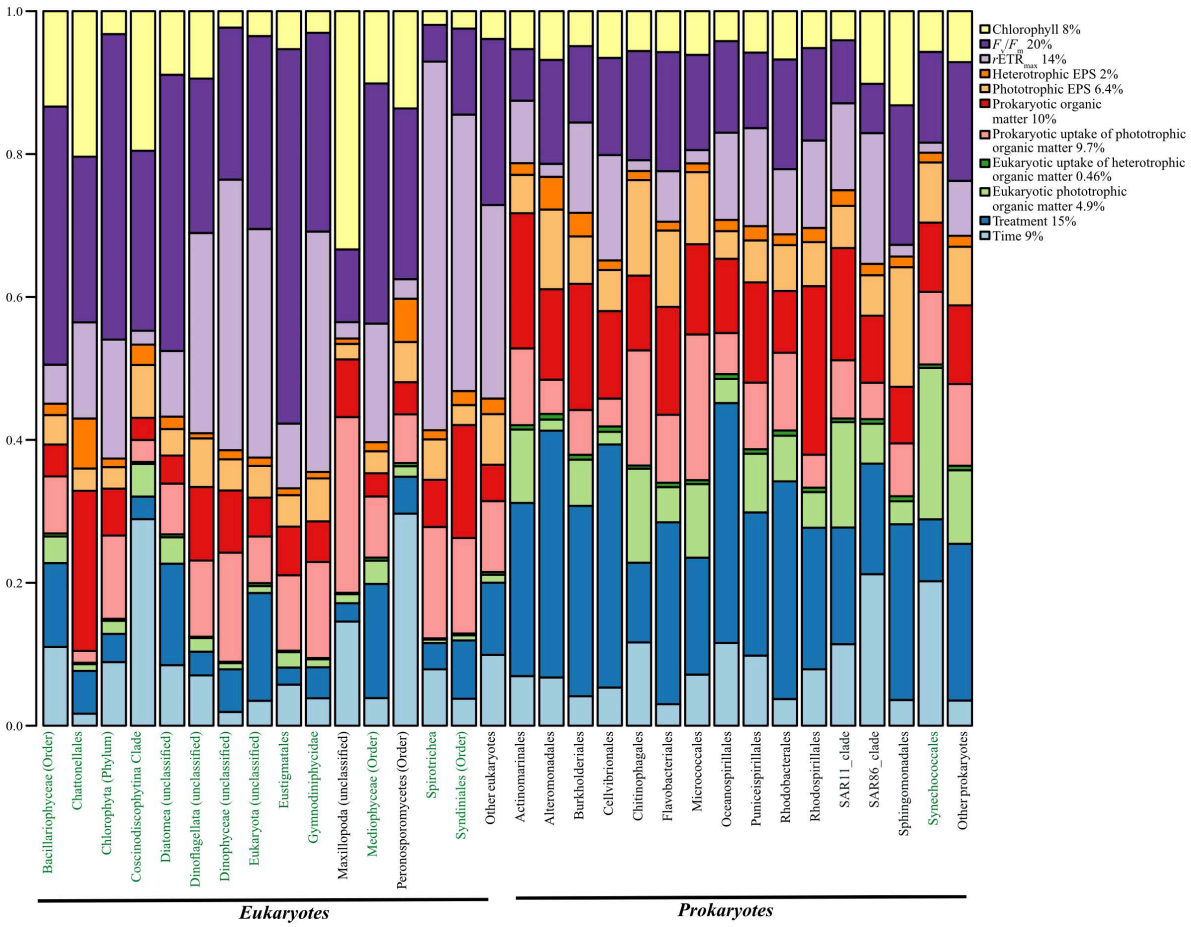

FIGURE 4 | Total proportion of variation in the occurrence of prokaryotic and eukaryotic species (phototrophs marked in green) explained by various environmental parameters tested in the long-term experiment.

linearly correlated with their organic matter secretion and/or (c) eukaryotic heterotrophic activity especially by fungi and protozoans. As it is impossible to differentiate the contribution of phototrophs from heterotrophs in our dataset, more experimentation is needed to gain further insight into this linear relationship. Regardless, the observed linear increase in the relationship with time could be due to an increase in the microbial exchange of organic matter with time, leading to an increase in intracellular accumulation of radiotracer signals, which was lower in the presence of oil. This could simply be attributed to oil toxicity and/or the competition of oil components acting as carbon source as opposed to organic matter secreted by phytoplankton.

Measurement of photosynthetic physiology suggests slight acute and severe chronic effects of oil exposure on photosynthesis of all classes of phytoplankton. This observation was surprising as there were no acute effects of oil on the uptake of ^{14}C-bicarbonate seen in the eukaryotic fraction. We assume that the observed discrepancy between photosynthetic electron transport and uptake of ^{14}C-bicarbonate in the eukaryotic fraction could be due to a carbon-concentrating mechanism (Raven et al., 2011) or due to the higher expenditure in the control treatment of reducing equivalents from the photosynthetic electron transport in reactions other than carbon fixation such as inorganic nitrogen assimilation or Mehler's reaction (Raven et al., 1992; Roberty et al., 2014). Further analysis of photosynthetic physiology revealed higher connectivity of photosystems only during the short-term exposure to oil and a lower antenna size of the photosystems during the long-term exposure. Overall, consistent with previous studies (Bretherton et al., 2019, 2020), exposure to oil had differential effects on the photosynthetic physiology during short and long-term exposure, reflecting the individual- and community-level changes and acclimation induced by sudden exposure to oil.

Excess EPS production by microbes is widely considered to be a physiological response to stressful conditions such as oil exposure (Nichols et al., 2005; Quigg et al., 2016, 2021), and higher levels of EPS have been reported in the laboratory (Bacosa et al., 2018; Shiu et al., 2020), mesocosm experiments (Fu et al., 2014; Xu et al., 2018a, 2019a,b), and field observations in response to oil (Passow, 2016), whereby the protein to carbohydrate (P/C) ratio plays a critical role

on EPS aggregation propensity ("stickiness") (Santschi et al., 2020). In comparison with these observations, we found higher levels of EPS in response to oil exposure in our long-term experiment, with proteins and uronic acids contributing the most. However, the observation of higher EPS levels in the oil treatments contradicts lower levels of radiotracer signals found in the $\geq$ 3 kDa/colloidal fraction, suggesting that the majority of carbon especially in the protein and uronic acids of the EPS may have been derived from oil degradation. This discrepancy in our results of EPS measurements draws attention to the following limitations that cannot be directly answered in this study: (a) the contribution of organic carbon and energy from sources other than phytoplankton, i.e., oil (growth of oil-degrading bacteria and the EPS produced by them) and (b) any interaction between oil-degrading bacteria and phytoplankton.

Microbial community analysis revealed an overall decrease in prokaryotic diversity in oil treatments compared with controls as observed in several mesocosm studies (Kleindienst et al., 2015; Doyle et al., 2018). Furthermore, a higher relative abundance of eukaryotes such as *Dinophyceae, Mediophyceae*, and *Diatomea* members and prokaryotes such as oil-degrading Gammaproteobacteria members (*Oceanospirillales, Cellvibrionales*, and *Alteromonadales*) in the oil treatment are in line with the observations made in the field following the Deepwater Horizon oil spill (Karthikeyan et al., 2019; Hancock et al., 2021; Quigg et al., 2021) and also by several other mesocosm studies (Kimes et al., 2013; Kleindienst et al., 2015; Parsons et al., 2015; Almeda et al., 2018; Doyle et al., 2018; Kamalanathan et al., 2018; Bretherton et al., 2019; Gutierrez, 2019; Barbato and Scoma, 2020; Finkel et al., 2020). Assessment of co-occurrence of microbes to get insights of possible microbial interactions indicated severe effects of oil with ∼43% lower co-occurrences, which can be attributed to the observed slight decrease in microbial diversity. Interestingly, the number of negative co-occurrence was seven-fold higher in the oil treatment compared with the control. However, HMSC analysis (Ovaskainen et al., 2017) revealed factors other than treatment such as time, phototrophic EPS, heterotrophic organic matter, eukaryotic uptake of heterotrophic organic matter, and photosynthetic efficiency played an important role, suggesting a possible interaction between microbes through their activity (photosynthesis, secondary productivity, and EPS release and uptake) through time. Unsurprisingly, most of the variation in the occurrence of phototrophic eukaryotes was explained by photosynthetic parameters such as F_v/F_m and $rETR_{max}$ with an average of 28 and 21%. As F_v/F_m and $rETR_{max}$ decreased in response to oil, the effects of these two factors on microbial abundances and therefore their co-occurrences could be an *indirect* effect of oil exposure. The variation in the abundance of *Bacillariophyceae, Diatomea*, and *Mediophyceae* members were largely explained by phototrophic EPS (>24%), which along with the strong positive co-occurrence between these phototrophic species suggests a possible direct interaction between them.

Co-occurrence between prokaryotes and eukaryotes was 13-fold lower in the oil treatment compared with the control treatment. The variance in the abundance of *Chattonellales* explained by heterotrophic organic matter, together with the several significant co-occurrence with prokaryotic members such as *Cellvibrionales, Actinomarinales, Puniceispirillales*, *Rhodospirillales*, SAR11 clade, and *Thiomicrospirales* in the control treatment suggests the possibility of interaction. However, the absence of such co-occurrence with *Chattonellales* in oil can be explained by decreased abundance of the respective prokaryotic members in this treatment. Interestingly, the number of co-occurrence between the prokaryotes was nearly the same between both the treatments. *Synechococcales*, a prokaryotic phototroph showed co-occurrence with heterotrophic prokaryotes *Chitinophagales* and *Micrococcales* under both oil and control treatments. Moreover, the variation in occurrence of *Chitinophagales* and *Micrococcales* members was explained mostly by heterotrophic uptake of phototrophic organic matter and photosynthetic efficiency, suggesting (1) a possible direct interaction of *Chitinophagales* and *Micrococcales* in the phycosphere with members of *Synechococcales* and (2) that members of *Synechococcales* associated with this interaction were most likely filamentous in nature, as the variation in their occurrence was mostly explained by eukaryotic phototrophic organic matter signal that was obtained in the $\geq$ 3 fraction. However, further research is needed to confirm this interaction. The interaction between heterotrophic prokaryotes is, however, impossible to deduce, as the same radiolabeled substrate used was differentially assimilated by the heterotrophic prokaryotes. Regardless, treatment alone explained an average of ∼23% of the variation in the occurrence among the prokaryotes. This in combination with the reduced diversity and richness indices, which suggest a substantial effect of oil exposure on prokaryotic community and therefore their co-occurrence and/interaction with eukaryotic members. The above examples from our study indicate a reduction among several types of microbial interaction (phototrophic and heterotrophic eukaryotes, phototrophic eukaryotes and heterotrophic prokaryotes, and phototrophic and heterotrophic prokaryotes) and exchange of organic matter through EPS caused by exposure to oil.

Overall, we found that exposure to oil had a significant long-term effect on substrate uptake by phototrophs and heterotrophs, with fewer co-occurrences of microbial species and more negative co-occurrences than control. Factors such as oil exposure, photosynthesis, and prokaryotic organic matter explained a large portion of the variation in the occurrence of a microbial species and therefore how it altered microbial interactions. Lastly, our study indicates that the effect of oil exposure could be either direct by reduction of abundance of interacting members and/or indirect by reduction in metabolism (substrate uptake or photosynthesis) of interacting members.

DATA AVAILABILITY STATEMENT

The datasets presented in this study can be found in online repositories. The names of the repository/repositories and accession number(s) can be found in the article/**Supplementary Material**.

AUTHOR CONTRIBUTIONS

MK designed and performed the research, analyzed the data, and wrote the manuscript. KS designed and performed the research and analyzed the data. JL performed the research and reviewed the manuscript. CT, CB, NP, and NC performed the research. PS designed the research and reviewed the manuscript. AQ helped design the research, wrote and reviewed the manuscript, and obtained the funding. All authors contributed to the article and approved the submitted version.

FUNDING

This research was supported by a grant from the Gulf of Mexico Research Initiative to support consortium research entitled ADDOMEx-2 (Aggregation and Degradation of Dispersants and Oil by Microbial Exopolymers) Consortium. The original data can be found at the Gulf of Mexico Research Initiative Information and Data Cooperative (GRIIDC) at the URLs https://doi.org/10.7266/n7-n5p6-p566, https://doi.org/10.7266/n7-321d-vj38, https://doi.org/10.7266/n7-sj41-vw18, and https://doi.org/10.7266/n7-vtz2-9f39. Sequence data are deposited in National Center for Biotechnology Information (NCBI), and the accession numbers, SRR13287671–SRR13287729, are listed in **Supplementary Table 1**.

SUPPLEMENTARY MATERIAL

The Supplementary Material for this article can be found online at: https://www.frontiersin.org/articles/10.3389/fmicb.2021.675328/full#supplementary-material

Supplementary Figure 1 | Radiotracer signals from the short-term experiment. **(a)** eukaryotic phototrophic organic matter (CPM), **(b)** prokaryotic organic matter (CPM), **(c)** phototrophic EPS (CPM), **(d)** heterotrophic EPS (CPM), **(e)** prokaryotic uptake of phototrophic organic matter (CPM), and **(f)** eukaryotic uptake of heterotrophic organic matter (CPM).

Supplementary Figure 2 | Phytoplankton-bacteria interaction. **(a)** Linear correlation of phototrophic EPS (CPM) vs. eukaryotic uptake of heterotrophic organic matter (CPM) in both short and long-term experiment, and **(b)** Distribution of ratio of phototrophic EPS (CPM) and eukaryotic uptake of heterotrophic organic matter (CPM) in both short and long-term experiment.

Supplementary Figure 3 | Photosynthetic physiology of different classes of phytoplankton in the short-term experiment. **(a)** Alpha/light harvesting ability (μmol e^{-1}. μmol photons^{-1}) in the short-term experiment, **(b)** relative electron transport rates (μmol e^{-}. m^{-2}. s^{-1}) in the short-term experiment.

Supplementary Figure 4 | Photosynthetic performance and characteristics of phytoplankton. **(a)** F_v/F_m, maximum quantum yield (relative units) of phytoplankton in the short-term experiment, **(b)** Photosystem II connectivity (ρ, relative units) in the short-term experiment, **(c)** Sigma, absorption cross-section area of photosystem II (σ, Å (Quanta) $^{-1}$) in the short-term experiment, **(d)** F_v/F_m, maximum quantum yield (relative units) of phytoplankton in the long-term experiment, **(e)** Photosystem II connectivity (ρ) in the long-term experiment, and **(f)** Sigma, absorption cross-section area of photosystem II (σ, Å (Quanta) $^{-1}$) in the long-term experiment.

Supplementary Figure 5 | Exopolymeric substance (EPS) composition in the long-term experiment. **(a)** Carbohydrate concentration of EPS (μg.L^{-1}), **(b)** Protein concentration of EPS (μg.L^{-1}), **(c)** Uronic acids concentration of EPS (μg.L^{-1}), and **(d)** Total EPS concentration of EPS (μg.L^{-1}).

Supplementary Figure 6 | Relative ASV abundance of microbes. **(a)** Relative prokaryotic abundance in the control treatment, **(b)** Relative prokaryotic abundance in the oil treatment, **(c)** Relative eukaryotic abundance in the control treatment and **(d)** Relative eukaryotic abundance in the oil treatment through time in the long-term experiment.

Supplementary Figure 7 | ASV Abundance of members belong to class Gammaproteobacteria in **(a)** the control and **(b)** the oil treatment through time in the long-term experiment.

Supplementary Table 1 | Number of sequenced and processed reads and accession numbers for the 16S and 18S rRNA genes.

REFERENCES

Almeda, R., Cosgrove, S., and Buskey, E. J. (2018). Oil spills and dispersants can cause the initiation of potentially harmful dinoflagellate blooms ("Red Tides"). *Environ. Sci. Technol.* 52, 5718–5724. doi: 10.1021/acs.est.8b00335

Amin, S. A., Hmelo, L. R., Van Tol, H. M., Durham, B. P., Carlson, L. T., Heal, K. R., et al. (2015). Interactions and signalling between a cosmopolitan phytoplankton and associated bacteria. *Nature* 522, 98–101. doi: 10.1038/nature14488

Apprill, A., McNally, S., Parsons, R., and Weber, L. (2015). Minor revision to V4 region SSU rRNA 806R gene primer greatly increases detection of SAR11 bacterioplankton. *Aquat. Microb. Ecol.* 75, 129–137. doi: 10.3354/ame01753

Arnosti, C. (2011). Microbial extracellular enzymes and the marine carbon cycle. *Annu. Rev. Mar. Sci.* 15, 401–425. doi: 10.1146/annurev-marine-120709-142731

Azam, F., and Malfatti, F. (2007). Microbial structuring of marine ecosystems. *Nat. Rev. Microbiol.* 5, 782–791. doi: 10.1038/nrmicro1747

Bacosa, H. P., Kamalanathan, M., Chiu, M. H., Tsai, S. M., Sun, L., Labonté, J. M., et al. (2018). Extracellular polymeric substances (EPS) producing and oil degrading bacteria isolated from the northern Gulf of Mexico. *PLoS One* 13:e0208406. doi: 10.1371/journal.pone.0208406

Barbato, M., and Scoma, A. (2020). Mild hydrostatic-pressure (15 MPa) affects the assembly, but not the growth, of oil-degrading coastal microbial communities tested under limiting conditions (5° C, no added nutrients). *FEMS Microbiol. Ecol.* 96:fiaa160.

Barbeau, K., Moffett, J. W., Caron, D. A., Croot, P. L., and Erdner, D. L. (1996). Role of protozoan grazing in relieving iron limitation of phytoplankton. *Nature* 380, 61–64. doi: 10.1038/380061a0

Bell, W., and Mitchell, R. (1972). Chemotactic and growth responses of marine bacteria to algal extracellular products. *Biol. Bull.* 143, 265–277. doi: 10.2307/1540052

Benjamini, Y., Krieger, A. M., and Yekutieli, D. (2006). Adaptive linear step-up procedures that control the false discovery rate. *Biometrika* 93, 491–507. doi: 10.1093/biomet/93.3.491

Bradley, I. M., Pinto, A. J., and Guest, J. S. (2016). Design and evaluation of Illumina MiSeq-compatible, 18S rRNA gene-specific primers for improved characterization of mixed phototrophic communities. *Appl. Environ. Microbiol.* 82, 5878–5891. doi: 10.1128/aem.01630-16

Brakstad, O. G., Lewis, A., and Beegle-Krause, C. J. (2018). A critical review of marine snow in the context of oil spills and oil spill dispersant treatment with focus on the Deepwater Horizon oil spill. *Mar. Pollut. Bull.* 135, 346–356. doi: 10.1016/j.marpolbul.2018.07.028

Bretherton, L., Hillhouse, J., Kamalanathan, M., Finkel, Z. V., Irwin, A. J., and Quigg, A. (2020). Trait-dependent variability of the response of marine phytoplankton to oil and dispersant exposure. *Mar. Pollut. Bull.* 153:110906. doi: 10.1016/j.marpolbul.2020.110906

Bretherton, L., Kamalanathan, M., Genzer, J., Hillhouse, J., Setta, S., Liang, Y., et al. (2019). Response of natural phytoplankton communities exposed to crude oil and chemical dispersants during a mesocosm experiment. *Aquat. Toxicol.* 206, 43–53. doi: 10.1016/j.aquatox.2018.11.004

Bretherton, L., Williams, A., Genzer, J., Hillhouse, J., Kamalanathan, M., Finkel, Z. V., et al. (2018). Physiological response of 10 phytoplankton species exposed to Macondo oil and the dispersant, Corexit. *J. Phycol.* 54, 317–328. doi: 10.1111/jpy.12625

Brooks, G. R., Larson, R. A., Schwing, P. T., Romero, I., Moore, C., Reichart, G. J., et al. (2015). Sedimentation pulse in the NE Gulf of Mexico following the 2010 DWH blowout. *PLoS One* 10:e0132341. doi: 10.1371/journal.pone.0132341

Brussaard, C. P. (2004). Viral control of phytoplankton populations—a review 1. *J. Eukaryot. Microbiol.* 51, 125–138. doi: 10.1111/j.1550-7408.2004.tb00537.x

Buesing, N., and Gessner, M. O. (2003). Incorporation of radiolabeled leucine into protein to estimate bacterial production in plant litter, sediment, epiphytic biofilms, and water samples. *Microb. Ecol.* 45, 291–301. doi: 10.1007/s00248-002-2036-6

Caporaso, J. G., Lauber, C. L., Walters, W. A., Berg-Lyons, D., Lozupone, C. A., Turnbaugh, P. J., et al. (2011). Global patterns of 16S rRNA diversity at a depth of millions of sequences per sample. *Proc. Natl. Acad. Sci. U. S. A.* 108, 4516–4522. doi: 10.1073/pnas.1000080107

Caron, D. A., Goldman, J. C., and Dennett, M. R. (1988). Experimental demonstration of the roles of bacteria and bacterivorous protozoa in plankton nutrient cycles. *Hydrobiologia* 159, 27–40. doi: 10.1007/bf00007365

Daly, K. L., Passow, U., Chanton, J., and Hollander, D. (2016). Assessing the impacts of oil-associated marine snow formation and sedimentation during and after the Deepwater Horizon oil spill. *Anthropocene* 13, 18–33. doi: 10.1016/j.ancene.2016.01.006

Doyle, S. M., Lin, G., Morales-McDevitt, M., Wade, T. L., Quigg, A., and Sylvan, J. B. (2020). Niche Partitioning Between Coastal and Offshore Shelf Waters Results in Differential Expression of Alkane and PAH Catabolic Pathways. *mSystems* 5, e00668–20.

Doyle, S. M., Whitaker, E. A., de Pascuale, V., Wade, T. L., Knap, A. H., Santschi, P. H., et al. (2018). Rapid formation of microbe-oil aggregates and changes in community composition in coastal surface water following exposure to oil and the dispersant Corexit. *Front. Microbiol.* 11:689. doi: 10.3389/fmicb.2018.00689

Durham, B. P., Sharma, S., Luo, H., Smith, C. B., Amin, S. A., Bender, S. J., et al. (2015). Cryptic carbon and sulfur cycling between surface ocean plankton. *Proc. Natl. Acad. Sci. U. S. A.* 112, 453–457. doi: 10.1073/pnas.1413137112

Dvořák, P., Hindák, F., Hašler, P., Hindakova, A., and Poulíčková, A. (2014). Morphological and molecular studies of Neosynechococcus sphagnicola, gen. et sp. nov.(Cyanobacteria, Synechococcales). *Phytotaxa* 170, 24–34.

Elifantz, H., Dittel, A. I., Cottrell, M. T., and Kirchman, D. L. (2007). Dissolved organic matter assimilation by heterotrophic bacterial groups in the western Arctic Ocean. *Aquat. Microb. Ecol.* 50, 39–49. doi: 10.3354/ame01145

Elifantz, H., Malmstrom, R. R., Cottrell, M. T., and Kirchman, D. L. (2005). Assimilation of polysaccharides and glucose by major bacterial groups in the Delaware Estuary. *Appl. Environ. Microbiol.* 71, 7799–7805. doi: 10.1128/aem.71.12.7799-7805.2005

Finkel, Z. V., Liang, Y., Nanjappa, D., Bretherton, L., Brown, C. M., Quigg, A., et al. (2020). A ribosomal sequence-based oil sensitivity index for phytoplankton groups. *Mar. Pollut. Bull.* 151:110798. doi: 10.1016/j.marpolbul.2019.110798

Franco-Vidal, L., and Morán, X. A. (2011). Relationships between coastal bacterioplankton growth rates and biomass production: comparison of leucine and thymidine uptake with single-cell physiological characteristics. *Microb. Ecol.* 61, 328–341. doi: 10.1007/s00248-010-9778-3

Fu, J., Gong, Y., Zhao, X., O'reilly, S. E., and Zhao, D. (2014). Effects of oil and dispersant on formation of marine oil snow and transport of oil hydrocarbons. *Environ. Sci. Technol.* 48, 14392–14399. doi: 10.1021/es5042157

Fuhrman, J. A., Cram, J. A., and Needham, D. M. (2015). Marine microbial community dynamics and their ecological interpretation. *Nat. Rev. Microbiol.* 13, 133–146. doi: 10.1038/nrmicro3417

Garcia, N. S., Bonachela, J. A., and Martiny, A. C. (2016). Interactions between growth-dependent changes in cell size, nutrient supply and cellular elemental stoichiometry of marine Synechococcus. *ISME J.* 10, 2715–2724. doi: 10.1038/ismej.2016.50

Griffiths, R. P., McNamara, T. M., Caldwell, B. A., and Morita, R. Y. (1981). Field observations on the acute effect of crude oil on glucose and glutamate uptake in samples collected from Arctic and subarctic waters. *Appl. Environ. Microbiol.* 41, 1400–1406. doi: 10.1128/aem.41.6.1400-1406.1981

Grossart, H. P., Czub, G., and Simon, M. (2006). Algae–bacteria interactionss and their effects on aggregation and organic matter flux in the sea. *Environ. Microbiol.* 8, 1074–1084. doi: 10.1111/j.1462-2920.2006.00999.x

Gu, Z., Gu, L., Eils, R., Schlesner, M., and Brors, B. (2014). Circlize implements and enhances circular visualization in R. *Bioinformatics* 30, 2811–2812. doi: 10.1093/bioinformatics/btu393

Gutierrez, T. (2019). "Marine, aerobic hydrocarbon-degrading gamma*proteobacteria*: overview," in *Taxonomy, Genomics and Ecophysiology of Hydrocarbon-Degrading Microbes*, ed. T. J. McGenity (Cham: Springer), 143–152. doi: 10.1007/978-3-030-14796-9_22

Hancock, T. L., Blonder, S. L., Bury, A. A., Smolinski, R. A., Parsons, M. L., Robertson, A., et al. (2021). Succession pattern and phylotype analysis of microphytobenthic communities in a simulated oil spill seagrass mesocosm experiment. *Sci. Total Environ.* 784:147053. doi: 10.1016/j.scitotenv.2021.147053

Harrell, F. E. Jr., and Harrell, M. F. E. Jr. (2019). Package 'hmisc'. *CRAN2018* 2019, 235–236.

Hu, C., Feng, L., Holmes, J., Swayze, G. A., Leifer, I., Melton, C., et al. (2018). Remote sensing estimation of surface oil volume during the 2010 Deepwater Horizon oil blowout in the Gulf of Mexico: scaling up AVIRIS observations with MODIS measurements. *J. Appl. Remote Sens.* 12:026008.

Hung, C. C., Tang, D., Warnken, K. W., and Santschi, P. H. (2001). Distributions of carbohydrates, including uronic acids, in estuarine waters of Galveston Bay. *Mar. Chem.* 73, 305–318. doi: 10.1016/s0304-4203(00)00114-6

Kamalanathan, M., Chiu, M. H., Bacosa, H., Schwehr, K., Tsai, S. M., Doyle, S., et al. (2019). Role of polysaccharides in diatom Thalassiosira pseudonana and its associated bacteria in hydrocarbon presence. *Plant Physiol.* 180, 1898–1911. doi: 10.1104/pp.19.00301

Kamalanathan, M., Doyle, S. M., Xu, C., Achberger, A. M., Wade, T. L., Schwehr, K., et al. (2020). Exoenzymes as a Signature of Microbial Response to Marine Environmental Conditions. *mSystems* 5, e00290–e00220.

Kamalanathan, M., Xu, C., Schwehr, K., Bretherton, L., Beaver, M., Doyle, S. M., et al. (2018). Extracellular enzyme activity profile in a chemically enhanced water accommodated fraction of surrogate oil: toward understanding microbial activities after the Deepwater Horizon oil spill. *Front. Microbiol.* 9:798. doi: 10.3389/fmicb.2018.00798

Karthikeyan, S., Rodriguez-R, L. M., Heritier-Robbins, P., Kim, M., Overholt, W. A., Gaby, J. C., et al. (2019). "Candidatus Macondimonas diazotrophica", a novel gamma*proteobacteria*l genus dominating crude-oil-contaminated coastal sediments. *ISME J.* 13, 2129–2134. doi: 10.1038/s41396-019-0400-5

Kimes, N. E., Callaghan, A. V., Aktas, D. F., Smith, W. L., Sunner, J., Golding, B. T., et al. (2013). Metagenomic analysis and metabolite profiling of deep–sea sediments from the Gulf of Mexico following the Deepwater Horizon oil spill. *Front. Microbiol.* 15:50. doi: 10.3389/fmicb.2013.00050

Kiørboe, T. (2001). Formation and fate of marine snow: small-scale processes with large-scale implications. *Sci. Mar.* 65, 57–71. doi: 10.3989/scimar.2001.65s257

Kleindienst, S., Seidel, M., Ziervogel, K., Grim, S., Loftis, K., Harrison, S., et al. (2015). Chemical dispersants can suppress the activity of natural oil-degrading microorganisms. *Proc. Natl. Acad. Sci. U. S. A.* 112, 14900–14905. doi: 10.1073/pnas.1507380112

Kozich, J. J., Westcott, S. L., Baxter, N. T., Highlander, S. K., and Schloss, P. D. (2013). Development of a dual-index sequencing strategy and curation pipeline for analyzing amplicon sequence data on the MiSeq Illumina sequencing platform. *Appl. Environ. Microbiol.* 79, 5112–5120. doi: 10.1128/aem.01043-13

Matz, C., and Jürgens, K. (2003). Interaction of nutrient limitation and protozoan grazing determines the phenotypic structure of a bacterial community. *Microb. Ecol.* 45, 384–398. doi: 10.1007/s00248-003-2000-0

Milligan, A. J., Halsey, K. H., and Behrenfeld, M. J. (2015). Advancing interpretations of 14C-uptake measurements in the context of phytoplankton physiology and ecology. *J. Plankton Res.* 37, 692–698. doi: 10.1093/plankt/fbv051

Morel, A., Ahn, Y. H., Partensky, F., Vaulot, D., and Claustre, H. (1993). Prochlorococcus and Synechococcus: a comparative study of their optical properties in relation to their size and pigmentation. *J. Mar. Res.* 51, 617–649. doi: 10.1357/0022240933223963

Morris, D. L. (1948). Quantitative determination of carbohydrates with Dreywood's anthrone reagent. *Science* 107, 254–255. doi: 10.1126/science.107.2775.254

Nichols, C. M., Guezennec, J., and Bowman, J. P. (2005). Bacterial exopolysaccharides from extreme marine environments with special consideration of the southern ocean, sea ice, and deep-sea hydrothermal vents: a review. *Mar. Biotechnol.* 7, 253–271. doi: 10.1007/s10126-004-5118-2

Oksanen, J., Blanchet, F. G., Kindt, R., Legendre, P., Minchin, P. R., O'hara, R. B., et al. (2013). Package 'vegan'. *Community Ecology Package Version* 2, 1–295.

Ovaskainen, O., Tikhonov, G., Norberg, A., Guillaume Blanchet, F., Duan, L., Dunson, D., et al. (2017). How to make more out of community data? A conceptual framework and its implementation as models and software. *Ecol. Lett.* 20, 561–576. doi: 10.1111/ele.12757

Parada, A. E., Needham, D. M., and Fuhrman, J. A. (2016). Every base matters: assessing small subunit rRNA primers for marine microbiomes with mock communities, time series and global field samples. *Environ. Microbiol.* 18, 1403–1414. doi: 10.1111/1462-2920.13023

Parsons, M. L., Morrison, W., Rabalais, N. N., Turner, R. E., and Tyre, K. N. (2015). Phytoplankton and the Macondo oil spill: a comparison of the 2010 phytoplankton assemblage to baseline conditions on the Louisiana shelf. *Environ. Pollut.* 207, 152–160. doi: 10.1016/j.envpol.2015.09.019

Passow, U. (2016). Formation of rapidly-sinking, oil-associated marine snow. *Deep Sea Res. 2 Top. Stud. Oceanogr.* 129, 232–240. doi: 10.1016/j.dsr2.2014.10.001

Passow, U., Ziervogel, K., Asper, V., and Diercks, A. (2012). Marine snow formation in the aftermath of the Deepwater Horizon oil spill in the Gulf of Mexico. *Environ. Res. Lett.* 7:035301. doi: 10.1088/1748-9326/7/3/035301

Paterson, R. A. (1960). Infestation of chytridiaceous fungi on phytoplankton in relation to certain environmental factors. *Ecology* 41, 416–424. doi: 10.2307/1933316

Pienaar, R. N. (1976). Virus-like particles in three species of phytoplankton from San Juan Island, Washington. *Phycologia* 15, 185–190. doi: 10.2216/i0031-8884-15-2-185.1

Quigg, A., Parsons, M., Bargu, S., Ozhan, K., Daly, K. L., Chakraborty, S., et al. (2021). Marine phytoplankton responses to oil and dispersant exposures: knowledge gained since the Deepwater Horizon Oil Spill. *Mar. Pollut. Bull.* 164:112074. doi: 10.1016/j.marpolbul.2021.112074

Quigg, A., Passow, U., Chin, W.-C., Xu, C., Doyle, S., Bretherton, L., et al. (2016). The role of microbial exopolymers in determining the fate of oil and chemical dispersants in the ocean. *Limnol. Oceanogr. Lett.* 1, 3–26. doi: 10.1002/lol2.10030

R Core Team (2013). *R: A Language and Environment for Statistical Computing*. Vienna: R Foundation for Statistical Computing.

Ramanan, R., Kim, B. H., Cho, D. H., Oh, H. M., and Kim, H. S. (2016). Algae–bacteria interactionss: evolution, ecology and emerging applications. *Biotechnol. Adv.* 34, 14–29.

Rasconi, S., Jobard, M., and Sime-Ngando, T. (2011). Parasitic fungi of phytoplankton: ecological roles and implications for microbial food webs. *Aquat. Microb. Ecol.* 62, 123–137. doi: 10.3354/ame01448

Raven, J. A., Giordano, M., Beardall, J., and Maberly, S. C. (2011). Algal and aquatic plant carbon concentrating mechanisms in relation to environmental change. *Photosynth. Res.* 109, 281–296. doi: 10.1007/s11120-011-9632-6

Raven, J. A., Wollenweber, B., and Handley, L. L. (1992). A comparison of ammonium and nitrate as nitrogen sources for photolithotrophs. *New Phytol.* 121, 19–32. doi: 10.1111/j.1469-8137.1992.tb01088.x

Roberty, S., Bailleul, B., Berne, N., Franck, F., and Cardol, P. (2014). PSI Mehler reaction is the main alternative photosynthetic electron pathway in Symbiodinium sp., symbiotic dinoflagellates of cnidarians. *New Phytol.* 204, 81–91. doi: 10.1111/nph.12903

Romero, I. C., Schwing, P. T., Brooks, G. R., Larson, R. A., Hastings, D. W., Ellis, G., et al. (2015). Hydrocarbons in deep-sea sediments following the 2010 Deepwater Horizon blowout in the northeast Gulf of Mexico. *PLoS One* 10:e0128371. doi: 10.1371/journal.pone.0128371

Santschi, P. H., Xu, C., Schwehr, K. A., Lin, P., Sun, L., Chin, W. C., et al. (2020). Can the protein/carbohydrate (P/C) ratio of exopolymeric substances (EPS) be used as a proxy for their 'stickiness' and aggregation propensity? *Mar. Chem.* 218:103734. doi: 10.1016/j.marchem.2019.103734

Schloss, P. D., Westcott, S. L., Ryabin, T., Hall, J. R., Hartmann, M., Hollister, E. B., et al. (2009). Introducing mothur: open-source, platform-independent, community-supported software for describing and comparing microbial communities. *Appl. Environ. Microbiol.* 75, 7537–7541. doi: 10.1128/aem.01541-09

Schwehr, K. A., Xu, C., Chiu, M. H., Zhang, S., Sun, L., Lin, P., et al. (2018). Protein: polysaccharide ratio in exopolymeric substances controlling the surface tension of seawater in the presence or absence of surrogate Macondo oil with and without Corexit. *Mar. Chem.* 206, 84–92. doi: 10.1016/j.marchem.2018.09.003

Seymour, J. R., Amin, S. A., Raina, J. B., and Stocker, R. (2017). Zooming in on the phycosphere: the ecological interface for phytoplankton–bacteria relationships. *Nat. Microbiol.* 2:17065.

Shiu, R. F., Chiu, M. H., Vazquez, C. I., Tsai, Y. Y., Le, A., Kagiri, A., et al. (2020). Protein to carbohydrate (P/C) ratio changes in microbial extracellular polymeric substances induced by oil and Corexit. *Mar. Chem.* 26:103789. doi: 10.1016/j.marchem.2020.103789

Singer, M. M., Aurand, D. V., Coelho, G. M., Bragin, G. E., Clark, J. R., Sowby, M., et al. (2001). Making, measuring, and using water-accommodated fractions of petroleum for toxicity testing. *Int. Oil Spill Conference Proc.* 2001, 1269–1274. doi: 10.7901/2169-3358-2001-2-1269

Smith, P. E., Krohn, R. I., Hermanson, G. T., Mallia, A. K., Gartner, F. H., Provenzano, M., et al. (1985). Measurement of protein using bicinchoninic acid. *Anal. Biochem.* 150, 76–85. doi: 10.1016/0003-2697(85)90442-7

Suggett, D. J., Oxborough, K., Baker, N. R., MacIntyre, H. L., Kana, T. M., and Geider, R. J. (2003). Fast repetition rate and pulse amplitude modulation chlorophyll a fluorescence measurements for assessment of photosynthetic electron transport in marine phytoplankton. *Eur. J. Phycol.* 38, 371–384. doi: 10.1080/0967026031000161265 5

Taylor, J. D., McKew, B. A., Kuhl, A., McGenity, T. J., and Underwood, G. J. (2013). Microphytobenthic extracellular polymeric substances (EPS) in intertidal sediments fuel both generalist and specialist EPS−degrading bacteria. *Limnol. Oceanogr.* 58, 1463–1480. doi: 10.4319/lo.2013.58.4.1463

von Borzyskowski, L. S., Severi, F., Krüger, K., Hermann, L., Gilardet, A., Sippel, F., et al. (2019). Marine *Proteobacteria* metabolize glycolate via the β-hydroxyaspartate cycle. *Nature* 575, 500–504. doi: 10.1038/s41586-019-1748-4

Walters, W., Hyde, E. R., Berg-Lyons, D., Ackermann, G., Humphrey, G., Parada, A., et al. (2016). Transcribed Spacer Marker Gene Primers for Microbial Community Surveys. *mSystems* 1, e00009–15.

Wang, H., Zhu, R., Zhang, X., Li, Y., Ni, L., Xie, P., et al. (2019). Abiotic environmental factors override phytoplankton succession in shaping both free-living and attached bacterial communities in a highland lake. *AMB Express* 9:170.

Wickham, H. and Wickham, M. H. (2007). *The ggplot package*.

Wozniak, A. S., Prem, P. M., Obeid, W., Waggoner, D. C., Quigg, A., Xu, C., et al. (2019). Rapid degradation of oil in mesocosm simulations of marine oil snow events. *Environ. Sci. Technol.* 53, 3441–3450. doi: 10.1021/acs.est.8b06532

Xu, C., Chin, W.-C., Lin, P., Chen, H. M., Lin, P., Chiu, M. C., et al. (2019a). Marine Gels, Extracellular Polymeric Substances (EPS) and Transparent Exopolymeric Particles (TEP) in natural seawater and seawater contaminated with a water accommodated fraction of Macondo oil surrogate. *Mar. Chem.* 215, 10–16.

Xu, C., Lin, P., Zhang, S., Sun, L., Xing, W., Schwehr, K. A., et al. (2019b). The interplay of extracellular polymeric substances and oil/Corexit to affect the petroleum incorporation into sinking marine oil snow in four mesocosms. *Sci. Total Environ.* 693:133626. doi: 10.1016/j.scitotenv.2019.133626

Xu, C., Zhang, S., Beaver, M., Lin, P., Sun, L., Doyle, S. M., et al. (2018a). The role of microbially-mediated exopolymeric substances (EPS) in regulating Macondo oil transport in a mesocosm experiment. *Mar. Chem.* 206, 52–61. doi: 10.1016/j.marchem.2018.09.005

Xu, C., Zhang, S., Beaver, M., Wozniak, A., Obeid, W., Lin, Y., et al. (2018b). Decreased sedimentation efficiency of petro-and non-petro-carbon caused by a dispersant for Macondo surrogate oil in a mesocosm simulating a coastal microbial community. *Mar. Chem.* 206, 34–43. doi: 10.1016/j.marchem.2018.09.002

Conflict of Interest: The authors declare that the research was conducted in the absence of any commercial or financial relationships that could be construed as a potential conflict of interest.

Publisher's Note: All claims expressed in this article are solely those of the authors and do not necessarily represent those of their affiliated organizations, or those of the publisher, the editors and the reviewers. Any product that may be evaluated in this article, or claim that may be made by its manufacturer, is not guaranteed or endorsed by the publisher.

frontiers in Microbiology

ORIGINAL RESEARCH
published: 29 September 2021
doi: 10.3389/fmicb.2021.626048

Machine Learning Predicts the Presence of 2,4,6-Trinitrotoluene in Sediments of a Baltic Sea Munitions Dumpsite Using Microbial Community Compositions

René Janßen[1], Aaron J. Beck[2], Johannes Werner[1], Olaf Dellwig[3], Johannes Alneberg[4], Bernd Kreikemeyer[5], Edmund Maser[6], Claus Böttcher[7], Eric P. Achterberg[2], Anders F. Andersson[4] and Matthias Labrenz[1]**

[1] Biological Oceanography, Leibniz Institute for Baltic Sea Research Warnemünde, Rostock, Germany, [2] Marine Biogeochemistry, GEOMAR Helmholtz Centre for Ocean Research Kiel, Kiel, Germany, [3] Marine Geology, Leibniz Institute for Baltic Sea Research Warnemünde, Rostock, Germany, [4] Science for Life Laboratory, Department of Gene Technology, School of Engineering Sciences in Chemistry, Biotechnology and Health, KTH Royal Institute of Technology, Solna, Sweden, [5] Institute of Medical Microbiology, Virology and Hygiene, University of Rostock, Rostock, Germany, [6] Institute of Toxicology and Pharmacology for Natural Scientists, University Medical School Schleswig–Holstein, Kiel, Germany, [7] State Ministry of Energy, Agriculture, The Environment, Nature and Digitization, Kiel, Germany

Bacteria are ubiquitous and live in complex microbial communities. Due to differences in physiological properties and niche preferences among community members, microbial communities respond in specific ways to environmental drivers, potentially resulting in distinct microbial fingerprints for a given environmental state. As proof of the principle, our goal was to assess the opportunities and limitations of machine learning to detect microbial fingerprints indicating the presence of the munition compound 2,4,6-trinitrotoluene (TNT) in southwestern Baltic Sea sediments. Over 40 environmental variables including grain size distribution, elemental composition, and concentration of munition compounds (mostly at pmol·g^{-1} levels) from 150 sediments collected at the near-to-shore munition dumpsite Kolberger Heide by the German city of Kiel were combined with 16S rRNA gene amplicon sequencing libraries. Prediction was achieved using Random Forests (RFs); the robustness of predictions was validated using Artificial Neural Networks (ANN). To facilitate machine learning with microbiome data we developed the R package phyloseq2ML. Using the most classification-relevant 25 bacterial genera exclusively, potentially representing a TNT-indicative fingerprint, TNT was predicted correctly with up to 81.5% balanced accuracy. False positive classifications indicated that this approach also has the potential to identify samples where the original TNT contamination was no longer detectable. The fact that TNT presence was not among the main drivers of the microbial community

OPEN ACCESS

Edited by:
Camila Fernandez, UMR 7621 Laboratoire d'Océanographie Microbienne (LOMIC), France

Reviewed by:
Marco J. L. Coolen, Curtin University, Australia
Ian P. G. Marshall, Aarhus University, Denmark

***Correspondence:**
Matthias Labrenz
matthias.labrenz@io-warnemuende.de
René Janßen
rene.janssen@io-warnemuende.de

Specialty section:
This article was submitted to Aquatic Microbiology, a section of the journal Frontiers in Microbiology

Received: *04 November 2020*
Accepted: *24 August 2021*
Published: *29 September 2021*

Citation:
Janßen R, Beck AJ, Werner J, Dellwig O, Alneberg J, Kreikemeyer B, Maser E, Böttcher C, Achterberg EP, Andersson AF and Labrenz M (2021) Machine Learning Predicts the Presence of 2,4,6-Trinitrotoluene in Sediments of a Baltic Sea Munitions Dumpsite Using Microbial Community Compositions. Front. Microbiol. 12:626048. doi: 10.3389/fmicb.2021.626048

composition demonstrates the sensitivity of the approach. Moreover, environmental variables resulted in poorer prediction rates than using microbial fingerprints. Our results suggest that microbial communities can predict even minor influencing factors in complex environments, demonstrating the potential of this approach for the discovery of contamination events over an integrated period of time. Proven for a distinct environment future studies should assess the ability of this approach for environmental monitoring in general.

Keywords: munition compounds, Kolberger Heide, mercury, random forest, 16S rRNA gene amplicon sequencing, monitoring, fingerprint, TNT

INTRODUCTION

Microbes are the most diverse, abundant, and ubiquitous life forms on Earth. They live in complex microbial communities, which can react rapidly to environmental changes, a result of consistent evolutionary pressures applied by fluctuating conditions (Lindh and Pinhassi, 2018). The developed variety of physiologies enables communities to respond in specific ways to environmental drivers, hence functioning as indicators for surrounding conditions. This principle was demonstrated for very different habitats: it was possible to match individual human skin microbiomes with those on the occupant's household surfaces (Wilkins et al., 2017), to associate subway microbiomes to the major cities they were located in Ryan (2019) or to distinguish microbial communities in the brackish Baltic Sea along the salinity gradient (Herlemann et al., 2011) and its anoxic regions (Thureborn et al., 2016). However, relevant indicative fractions of the communities, conceivably acting as microbial fingerprints, may only emerge by analyzing a sufficiently large number of communities. Next generation sequencing allows for processing such larger amounts of samples to extract this information, but it might be accompanied by a large portion of irrelevant data with regard to the particular indication.

The ensemble classifier Random Forest (RF) is capable of identifying such potential fingerprints—even if they include non-linear relations—in large and complex data sets (Breiman, 2001). RF is among the most popular machine learning methods and has frequently been used in biological sciences (Fernández-Delgado et al., 2014). The features relevant for the model's decisions can be assumed equivalent to an indicative fingerprint and the RF variable importance measure readily identifies them (e.g., Altmann et al., 2010; Janitza et al., 2018). Fingerprints related to community-shaping drivers are revealed by performing unsupervised classification, whereas specific influences can be targeted by the application of supervised machine learning. In microbiological studies, RF has been deployed to predict various geochemical features as well as to detect oil spills (Smith et al., 2015) and to localize the geographic origin of port water across three continents based on dominant bacterial phyla (Ghannam et al., 2020). Moitinho-Silva et al. (2017) used RF among other classifiers to separate between sponges of high and low microbial abundance. Thompson et al. (2019) used RF and artificial neural networks (ANN) to identify important taxa for the prediction of dissolved organic carbon concentrations. In a previous study we demonstrated the identification of glyphosate-impacted free-living community compositions by ANN and RF after a 82.45 nmol mL^{-1} glyphosate pulse in a lab microcosm experiment (Janßen et al., 2019b).

In this study, we are particularly interested in to what extent environmental microbial communities can reliably predict anthropogenic pollutants using the above algorithms. As a proof of principle, we tested this approach for a munitions dumpsite in the southwestern Baltic Sea, where sediments are contaminated with explosive compounds such as 2,4,6-trinitrotoluene (TNT). The munitions dumpsite Kolberger Heide in the Kiel Bight (Germany) is an approximately 1,260 ha large area of 10–15 m water depth. Conventional munition, mostly incomplete or unfused was disposed of at this site after World War II (Kampmeier et al., 2020). About 30,000 tons are estimated to be still on site, containing mainly TNT and 1,3,5-trinitroperhydro-1,3,5-triazine (RDX) as munition compounds (Böttcher et al., 2011). The containments such as mines, shells and torpedo heads display various states of corrosion (Kampmeier et al., 2020), resulting in the leakage of munition compounds (Beck et al., 2019). In addition, bare munition chunks are scattered across the sediment bed, potentially due to low-order, or incomplete detonation during blow-in-place clearance activities (Pfeiffer, 2009; Maser and Strehse, 2020). Dissolved TNT can be rapidly dissipated or metabolized in direct proximity to its source, complicating the quantification of TNT released into the environment (Elovitz and Weber, 1999; Beck et al., 2019). However, the presence of munition compounds including TNT and its transformation products in the Kolberger Heide water column samples (ca. 1–15 $ng{\cdot}L^{-1}$) and biota (1–24,000 $ng{\cdot}g^{-1}$) has been reported (Gledhill et al., 2019). Little is known about the munition compounds' concentrations in accordant sediments.

Sediment in the Kolberger Heide is contaminated by TNT at $pmol{\cdot}g^{-1}$ levels. It was our aim (a) to investigate if machine learning is capable of predicting TNT in these sediments and identifying indicative microbial fingerprints; (b) to assess how robust the predictions are and which factors influenced the model's performance; and (c) to evaluate whether a microbial fingerprint is sufficiently persistent to detect a history of TNT, indicated by TNT transformation products. Finally, we discuss how the described approach could supplement and be integrated into regular monitoring activities.

MATERIALS AND METHODS

Collection of Sediments and Determination of Munition Compounds

One hundred sixty-seven sediment samples were collected within the Kolberger Heide munitions dumpsite and its surroundings during the course of the Umweltmonitoring für die DElaboration von Munition im Meer (UDEMM) (Environmental monitoring for the delaboration of munitions on the seabed, Greinert, 2019) project. Samples were obtained during several cruises and individual sampling events. Additional sampling took place at defined distances from mines and at a site of a controlled detonation. Sediment samples within the dumpsite were collected manually by scientific divers or using an remotely operated underwater vehicle (ROV). Outside the dumpsite's restriction zone, surface sediments were collected using a Van Veen grab. Duplicate sediment cores were collected using a multi-corer at two sites east and west of the dumpsite (map provided in **Supplementary Figure 1**). Sampling was conducted in December 2016 and from June to December 2017. **Supplementary Figure 2** details contextual data such as position of sample collection, cruises, and experiments as well as measured parameters. "Experiments" refer to the goal of a sampling, e.g., investigating a spatial munition compounds gradient in cardinal directions around a mine, analyzing the munition compounds distribution across a mine mound or along a sediment profile. Sediments were stored in sealable plastic bags (Whirl-paks; Nasco, Madison, WI, United States) at −20°C for subsequent munition compounds analysis using an ultra-high performance liquid chromatographic system coupled to a heated electrospray ionization source and a high resolution quadrupole/orbitrap mass analyzer (UHPLC-HESI-MS, Q Exactive, Thermo Fisher Scientific) detection after thawing and extraction using liquid chromatography-mass spectrometry (LCMS)-grade acetonitrile (Fisher). Munition compounds were measured according to Gledhill et al. (2019) including TNT, RDX, 2-amino-4,6-dinitrotoluene (2-ADNT), 4-amino-2,6-dinitrotoluene (4-ADNT), 2,4-dinitrotoluene (2,4-DNT), 2,6-dinitrotoluene (2,6-DNT), 1,3-dinitrobenzene (DNB), 1,3,5-trinitrobenzene (TNB), octahydro-1,3,5,7-tetranitro-1,3,5,7-tetrazocine (HMX), and tetryl (*N*-methyl-*N*-2,4,6-tetranitrolaniline). The TNT transformation products, 2,4-diamino-6-nitrotoluene (2,4-DANT), and 2,6-diamino-4-nitrotoluene (2,6-DANT) are not included in the Gledhill et al. (2019) suite of compounds, but were analyzed using the same method, and quantified after standardization using single-compound standards (AccuStandard, New Haven, CT, United States). For geological and molecular biology analyses sediments were slowly thawed, homogenized under a clean bench, and split into two 15 mL aliquots. The aliquots were stored at −80°C.

Geochemical and Sedimentological Analyses

Sample Preparation

The frozen (−20°C) sediment samples were freeze-dried (Christ LOC-1M Alpha 1-4 and Christ Delta 1-24 LSCplus, Osterode am Harz, Germany) for 60–72 h. Except for the grain size analyses, the dried samples were homogenized in an agate ball mill (Fritsch Pulverisette, Idar-Oberstein, Germany) at 200 rpm for 10 min.

Carbon, Nitrogen, and Sulfur

About 10–17 mg of the sediments were weighted into tin crucibles, a spatula tip of vanadium(V) oxide (Alpha Resources, Stevensville, MI, United States) was added as catalyzer and total C, total N, and total S were determined by an elemental analyzer (EuroEA, HEKAtech, Wegberg, Germany). For total inorganic carbon, 50–70 mg of sediment was treated with 40% orthophosphoric acid and analyzed with an elemental analyzer (multiEA 4000, Analytik Jena, Jena, Germany). Total organic carbon was calculated by subtracting total inorganic carbon from total carbon. Precision and trueness were checked with in-house standards [Mecklenburg Bay Sediment Standard (MBSS), Oder Bay Sediment Standard (OBSS)] and were <3.5% (Häusler et al., 2018).

Mercury

The sedimentary mercury content was determined by a direct mercury analyzer (DMA 80, Milestone Srl, Italy) using 100–120 mg per analysis (50 mg for sample "Udemm1277," which exceeded the calibration range). Precision and trueness were checked with the certified reference material BCR-142R (Community Bureau of Reference) and an in-house standard comprising Baltic Sea sediments (MBSS) and were <3 and <10%, respectively (Häusler et al., 2018). Sediments exceeding 1,000 $\mu g\ Hg \cdot kg^{-1}$ were measured three times and averaged.

Reactive Iron and Trace Element Contents

For determination of reactive element contents, about 200 mg of sediment material was weighed into pre-cleaned 11.5 mL polystyrene tubes and 10 mL of 0.5 M HCl was added. The tubes were shaken for 60 min at 175 rpm, followed by 6 min of centrifugation at 4,000 × *g* and filtration of the solutions with 0.45 µm syringe filters. Three procedural blanks were analyzed together with the samples. The contents of Fe, P, and trace metals in the 0.5 M HCl extracts were determined by Q-ICP-MS (iCAP Q; Thermo Fisher Scientific, Germany) after automated 50-fold dilution with 2 vol% HNO_3 *via* a prepFAST module (Elemental Scientific, Omaha, NE, United States) and external calibration. Helium was used as collision gas (KED mode) to minimize polyatomic interferences and a Rh and Ir containing solution added online by the prepFAST module served as internal standard to compensate for matrix effects and instrument fluctuations. The calibration was checked with the international reference material SGR-1b (USGS), which underwent total acid digestion in closed PTFE vessels using a HNO_3–HF–$HClO_4$ mixture (Dellwig et al., 2019). For stable $^{206/207}Pb$ isotope ratios the NIST SRM-981 was used as reference material (Dellwig et al., 2018). Precision and trueness of the measurements of the reference materials were <4.4 and 8.1%, respectively.

Grain Size Distribution

The grain size of the <2 mm sediment faction was measured using a Hydro EV accessory to the Mastersizer 3000 (Malvern

Panalytical GmbH, Herrenberg, Germany). The samples were stirred at 2,500 rpm and sonicated for 10 s. Eight measurements were performed per sample, followed by purging steps with distilled water. Outliers (values exceeding 1.5 times the interquartile range) were removed and the remaining values per sediment were averaged.

Molecular Biology and Bioinformatics

The methods described in the following were applied to the molecular biology aliquots of each sediment sample.

Extraction of Nucleic Acids

The sediments were collected using the appropriate collection and storage procedures for the determination of munition compounds. To retrieve the best possible results in subsequent molecular biological analyses and due to the long term presence of TNT in the Kolberger Heide, the more robust 16S rRNA gene was preferred over the more sensitive 16S rRNA as sequencing target. DNA was extracted from 250 mg wet sediment using the Qiagen PowerSoil DNA Kits or from 2,000 mg wet sediment using the Mobio PowerSoil RNA kit with the DNA elution kit (Hilden, Germany). For each kit an extraction control without sediment was processed along with regular samples.

Sequencing 16S rRNA Gene Amplicons

The V4 region of the 16S rRNA gene was targeted with the universal prokaryotic primer set 515f-806r (forward 5′ GTGCCAGCMGCCGCGGTAA 3′, reverse 5′ GGACTACHV GGGTWTCTAAT 3′, Caporaso et al., 2011). Indexed amplicon libraries were pooled to a concentration of 4 μM. As usual for low diversity libraries, the PhiX control was spiked into the library pools at a concentration of 40 pM (10%). Each final library pool (4 pM) was subjected to 1 of 3 consecutive individual paired-end sequencing runs using 500 cycle V2 chemistry kits on an Illumina MiSeq (Berlin, Germany). Additional information with regard to the 16S rRNA gene libraries is provided in **Supplementary Figure 3**.

Processing 16S rRNA Gene Amplicon Sequences

Amplicon read processing—including the removal of primer and two-parent chimera sequences, the quality filtering step and the taxonomic annotation—was conducted using the DADA2 pipeline v. 1.10.0 (Callahan et al., 2016) with R v. 3.5.1 (R Core Team, 2017). DADA2 corrected for sequencing errors during the generation of amplicon sequence variants (ASVs). As recommended, such a correction was applied separately for each sequencing run. The individual tables were merged afterward. Only ASVs of length from 231 to 272 bp were kept according to the expected amplicon lengths reported in Ziesemer et al. (2015).

Taxonomic annotation of herein presented data was accomplished using the Silva release 132 (Yilmaz et al., 2014), including the taxonomic changes that were proposed by Parks et al. (2018). The ASV and taxonomy table were imported to and analyzed with phyloseq v. 1.30.0 (McMurdie and Holmes, 2013) accelerated by speedyseq v. 0.1.1 (McLaren, 2020). Plots were generated using ggplot2 v. 3.3.1 (Wickham, 2016).

Amplicon sequence variants which were present in negative PCR or extraction controls and also found abundantly in actual samples were individually checked due to potential cross contamination directed from samples toward the controls. ASVs with more than 35 reads in controls were removed from the dataset. ASV00001 was excluded from this rule because it was much more abundant in actual samples (extraction control: 75 reads, samples: >10,000 reads). ASVs which were present in controls and less abundant in samples were removed. Subsequently, it was checked if any of the as important detected taxa were also present in control samples. ASV00063 belonged to the important genus *Maribacter* (4 reads in positive PCR control) and ASV00074 to *Cobetia* (5 reads in negative PCR control). As no reads were found in the extraction control and they were as abundant as up to 3,000 reads in sediments, these ASVs were left unaltered.

Machine Learning Analyses

Machine learning analyses were conducted to evaluate whether microbial community compositions contain sufficient information about their environment and are sensitive enough to contamination to act as a proxy for in this case sea-dumped munitions. Such approach would allow to detect a variety of substances per community data set, once trained models for those substances are available. It allows for analyzing and understanding the mutual effects of TNT and bacteria on each other and thereby investigating the larger ecological context, leading to a potential application in environmental monitoring. If the goal is solely to measure TNT, traditional instrumental analyses should be conducted.

Analyses were carried out on six virtual machines provided by the German Network for Bioinformatics Infrastructure (de.NBI Cloud). The virtual machines ran Ubuntu 18.04.4 LTS as operating system on 28 Intel Xeon Gold 6140s cores with 256–512 GB memory available. RF analyses were performed utilizing R package ranger v. 0.12.1 (Wright and Ziegler, 2017). ANNs were generated with the R Keras framework v. 2.3.0.0 (Allaire and Chollet, 2020) and the TensorFlow back end v. 2.2.0 (Allaire and Tang, 2020). Our efforts to extract abundance, taxonomical and contextual data from phyloseq objects and subject those to machine learning led to the development of the R package phyloseq2ML v. 0.5.1.[1] It facilitates modification and combining such data sets as needed—using objects of class "phyloseq" as source—and formats the data for the above mentioned machine learning implementations in R.

Challenges of a Small Biological Data Set

The presented data set consists of contextual subsets (e.g., by specific transects or sampled by a given method) which are likely to contain samples more similar to each other than to those of other subsets. To ensure that the model's decision making was based on the presence of TNT rather than to a particular cruise or experiment, we developed guidelines to assess which samples were appropriate for machine-learning (ML) analyses. First, the technical replicates were averaged. Then, if for a given subset of

[1]https://github.com/RJ333/phyloseq2ML

samples all of the following questions could be answered with yes, samples had to be removed from the subset to prevent potential spurious relationships between the presence of TNT and the prediction accuracy:

For all samples from the same cruise (including biological replicates) → do they originate from the same experiment? → and the same area? → and do the sediment sampling positions have horizontal distance of <20 m → and do they only contain one class (TNT present or TNT absent) emphasized "or" (OR) is there a strong imbalance (e.g., 20 × TNT absent, 1 × TNT present)?

Following this guideline led to a removal of 17 of the original 167 sediments (**Supplementary Figure 2**). No samples were removed based on other criteria such as low read counts.

As about half of the sediment samples did not contain TNT and the TNT concentration within the other half of the samples was unevenly distributed (see section "TNT Contamination of Kolberger Heide Sediments") and also given the rather small sample size, it was considered unreasonable to perform regression analyses to predict the concentration of TNT. It was decided to investigate whether TNT has an effect at all on the microbial community composition, thus the samples were categorized as "TNT present" and "TNT absent."

Machine Learning Workflow

The remaining 150 samples were split into a training-validation set (in short: training set) consisting of 112 samples (75%) and a holdout test set of 38 samples (25%). This procedure was repeated to yield six different, pseudo-random splits of training and test sets. Using a random seed, the splits were reproducible.

In supervised learning, training and validation data for a model contain the independent variables and the corresponding continuous or discrete response variable. The measured TNT concentrations were categorized as response classes "absent" for concentrations below the detection limit (0.01 $ng \cdot g^{-1}$ or 0.044 $pmol \cdot g^{-1}$ wet sediment) and "present."

Settings automatically derived from the learning process are called parameters, such as the weights between ANN nodes. Hyperparameters, instead, are model settings chosen before training has started. RFs are controlled *via* two main hyperparameters: the number of trees per forest and the number of variables "mtry" to consider for sample separation at each tree node. The default value for mtry for classification tasks is the square root of the total number of independent variables. As this default value might not be optimal for sparse data such as ASV abundance tables, a factor multiplying this number of variables was used instead and will be referred to as "mtry factor" (Hastie et al., 2009).

Random Forest models were trained on various combinations of hyperparameter values and input data to find the best combination. This process is called a grid search and combinations were compared using the out-of-bag validation error, i.e., only using the training sets and not the holdout sets. A confusion matrix was generated to calculate performance metrics. Balanced accuracy was used as score. It corrects for imbalanced response variables and allowed comparisons across training set splits, which displayed class ratios of 43–48% "TNT present" (Brodersen et al., 2010). The validation results of the six data splits were averaged to select the best performing hyperparameter values and input sets. When predicting the holdout set, the model was trained on the full training-validation set. The holdout predictions for the various input data sets took place after all hyperparameter values were determined. This is required to prevent data leakage.

TNT Presence Prediction Based on Random Forest Grid Search

Data sets designed as model input were threefold: (a) community data: describing data deriving from 16S rRNA gene amplicon sequencing; (b) sediment data: sediment parameters derived from geochemical and sedimentological analyses; and (c) combined, a combination of both aforementioned input sets.

The grid search with community data was performed as follows: All combinations of relative abundance thresholds, the number of trees and the mtry factor were investigated. ASVs had to be more abundant than a given threshold in at least one sample. If so, the ASVs remains without change, otherwise it was filtered out. Thresholds were: 0.02, 0.04, 0.06, 0.08, 0.1, 0.2, 0.4, 0.6, 0.8, and 1%. Each of the resulting input sets was provided to models consisting of 100, 500, 1,000, 5,000, 10,000, and 20,000 trees along with mtry factors ranging from 1 to 13 by 2. For each combination 50 models were trained and validated.

Subsequently, the filtered relative ASV abundances were accumulated by taxonomic ranks genus through phylum to train 200 models with the previously identified hyperparameter values of 10,000 trees, an mtry factor of 5, and a threshold of 0.08%.

The sediment data contained 41 independent variables including reactive element contents, sum parameters such as total nitrogen, and the grain size distribution. Hundred models were trained with 1,000, 5,000, 10,000 trees and mtry factors 1, 3, and 5. For combined input data it was found sufficient to apply the same hyperparameters as were applied to the community data.

Validation and holdout scores were tested separately for significant differences between input data sets. Equal means were tested with unequal variance and one-way analysis of variance. The results of the analysis of variance were further subjected to the Tukey's multiple comparisons of means with 95% family-wise confidence level to identify the pairwise significances.

Selection of Most Important Variables

The most important variables for classification were retrieved from models trained with community, sediment and combined data. Importance for community data (0.08% threshold, genus rank) and combined data was calculated utilizing the corrected Gini impurity (Nembrini et al., 2018), followed by *p*-value estimation after Janitza et al. (2018). A 100 models using 10,000 trees and an mtry factor of 5 were trained and the results averaged. Variable importance and associated *p*-value for sediment data required the permutation-based approach by Altmann et al. (2010). A 1,000 permutations with mtry factor 1 and 10,000 trees were applied. The analysis involved elements Zr, which likely was not soluble by HCl extraction as well as Ca and Sn, where the measurement by ICP-MS was later identified as unreliable. The elements were still included in the training

data, but were not reported as important and removed for other analysis such as the Spearman rank correlation.

The variables were ordered by average importance over all splits. The number of variables for further analyses were selected based on decreasing decline in importance, meaning if the variables became more similarly important to each other, the cutoff was set. Thus, 25 genera were selected with Janitza importance > 0.25, $p < 0.01$ and 9 sediment parameters with Altmann importance > 0.001 and $p < 0.05$. The most important 50 combined variables (equal to Janitza importance > 0.15 and $p < 0.01$) were compared to the 25 community and 9 sediment variables.

Random Forest's Proximity Matrix for PCA Ordination and Correlation

Ordination methods are useful to explore multivariate data sets such as microbial community compositions by displaying their similarities. The proximity matrix generated by RFs is a measure of (dis-) similarity, as well. The proximity between two samples is calculated by measuring the number of times they end up in the same terminal node of the same tree of the RF, divided by the number of trees in the forest.

It can be used with unsupervised classification: a synthetic data set is added to the original data set. This consists of shuffled columns of the actual data, thus breaking all relationships between variables. The model (10,000 trees, mtry factor 1) tries to distinguish between permuted and original data and thereby identifies correlations and clusters in the actual data set. For supervised classification, the actual classes were used and no synthetic data set was required.

Principal component analysis (PCA) was performed based on the proximity matrix for the most important 25 genera. To identify microbial community shaping influences for the unsupervised classification, the sediment parameters were correlated with the PCA ordination. The function *envfit()* from R package vegan v. 2.5-6 (Oksanen et al., 2019) with 9,999 permutations was used to achieve this. Correlating parameters with $p < 0.001$ and $R^2 > 0.3$ were displayed. The PCA ordination was performed for sediment data as described above, except the *envfit()* step. Complementary, Spearman's rank-order correlations between sediment variables were investigated. The results were hierarchically clustered and variables with $p < 0.01$ were marked significant.

Assessing Robustness of Classification With Random Forest and Artificial Neural Nets

The classification consistency was examined to increase the understanding of the predictions. All 150 samples were used as training and validation set for 1,000 models (10,000 trees, mtry factor 1). Mean prediction errors <0.5 or $>99.5\%$ accuracy were rounded to 0 and 100%, respectively.

Artificial neural networks were additionally deployed to measure classification robustness across algorithms. The input data for ANNs required additional steps including the one-hot encoding of categorical variables and scaling of the independent variables: the mean of each variable was subtracted, and it was divided by the standard deviation. This yielded values centered around 0 with a standard deviation of 1. ANN grid searches were performed complementary to what is described for RF above. Results suggested that 50 nodes in the first hidden layer and 40 nodes in the second hidden layer were appropriate values, along a mini-batch training size of 4. No regularization was applied. The optimizer function Adaptive Moment Estimation outperformed Root Mean Square Propagation. Binary cross entropy was set as loss function, with accuracy as metric. Learning took a maximum of 100 epochs, stopped by an early callback if the validation loss did not decrease for two ongoing epochs. The node within the hidden layers were rectified linear unit-activated whereas the output nodes' activation function was sigmoid. Further hyperparameters and settings were default values of the keras R package.

Performance assessment was achieved by splitting the training data into three different, non-overlapping equally proportioned subsets. Two partitions were used for training and the remaining one for validation. These three subsets were composed differently for each of the conducted 333 runs. This 333 times repeated threefold cross validation yielded a total of 999 predictions.

Data Availability

Code, scripts and files are available under GitHub.[2] The R package phyloseq2ML is available at https://github.com/RJ333/phyloseq2ML. Sequences were deposited in the NCBI database under BioProject ID PRJNA632711 and SRA accessions SAMN14917999–SAMN14918370. The count tables, taxonomy tables and sample data as well as the thereby generated phyloseq objects and the machine learning classification result tables were lodged at https://zenodo.org/record/4062263. Geochemical data is included in **Supplementary Figure 2**.

RESULTS

TNT Contamination of Kolberger Heide Sediments

Of those 150 samples selected for ML, 137 contained munition compounds: 2-ADNT (127), 4-ADNT (133), 2,4-DANT (67), 2,6-DANT (52). None of the other munition compounds (2,4-DNT, 2,6-DNT, DNB, TNB, HMX, RDX, Tetryl) were detected in more than eight sediments (**Supplementary Figure 2**).

2,4,6-Trinitrotoluene concentration showed a median of 0 and a mean of 16.29 pmol·g^{-1} wet sediment among the 150 samples. It was detected in 68 samples or 45.3% of the samples; TNT was determined at <25 pmol·g^{-1} in 65 samples. Therefore, a binary classification approach was adopted. Notably, the highest value of 1,587 pmol·g^{-1} was found in sediments retrieved from a detonation site, where exposed munition chunks were spread over the sea floor.

The heavy metals mercury and lead were used as proxies for primary explosive compounds in conventional ammunition, which potentially could be present at the dumpsite; chemical warfare agents can contain arsenic. Mercury contents ranged in Kolberger Heide sediments from 3.7 to 4,503 μg Hg·kg^{-1}

[2]https://github.com/RJ333/Kolberger_Heide_manuscript

dry sediment, with a median of 21 μg Hg·kg^{-1} and 15 samples exceeding 450 μg Hg·kg^{-1}. The maximal content of 4,503 μg Hg·kg^{-1} was found during a line transect, where samples were taken every 20 m. The neighboring samples to the maximal value contained 8 and 12 μg Hg·kg^{-1}, demarcating a precise area of elevated Hg presence. Arsenic appeared on level between 0.4 and 4.8 mg·kg^{-1} with a median of 0.8 mg·kg^{-1} and lead ranged from 1 to 75 mg·kg^{-1} with a median of 2 mg·kg^{-1}.

Community Data Predicts TNT Presence More Accurately Than Sediment Data

The microbial community composition of the sediments was investigated for measurable effects caused by the TNT. A total of 259 16S rRNA gene libraries were selected to be appropriate for ML purposes. The selected libraries had a mean size of 82,219 reads, with the 95% confidence intervals being 78,115 and 86,322 reads (**Supplementary Figure 3**). About 97.02% of the reads were annotated as Bacteria, 2.43% as Archaea, and 0.39% as Eukaryota. Averaging across libraries from the same sediment ultimately yielded 150 community tables comprising 66,230 ASVs, 1,703 genera, and 78 phyla available for machine learning. Optimization of the hyperparameters was performed using the validation set with taxa at ASV rank. The achieved validation and prediction scores were averaged over the six training/test splits for each data set.

Taxonomic ranks were then compared for their potential to predict the presence of TNT. The hierarchical structure of the taxonomic annotation allowed investigating the influence of pooling the relative abundance by taxonomic ranks to identify the best compromise between the number of taxa and the information contained in inter-taxa abundance variability (**Figure 1**). The highest mean balanced accuracy was achieved by ASV (82.9%) and decreased toward the broader order rank (74.9%). Training with relative abundance per class (78.8%) and phylum (76.9%), however, still resulted in acceptable predictions, yielding more accurate classifications than on order rank. The genus rank (80.6%) was chosen for further analyses; a compromise between the best accuracy, reduced number of variables and the possibility to add community compositions from other sources, as ASVs are unique to this data set.

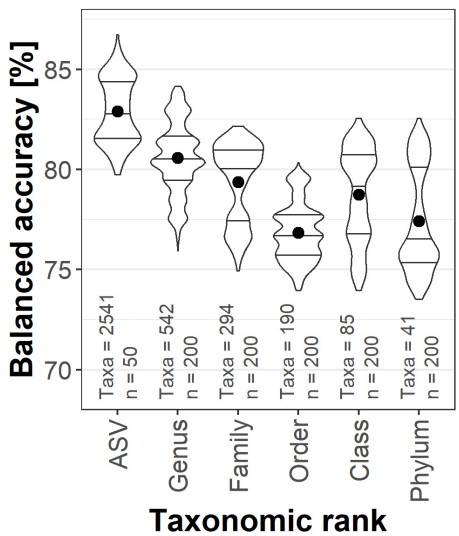

FIGURE 1 | Violin plots with median and interquartile range of correct TNT classifications of the validation set. The relative abundances were agglomerated on the taxonomic ranks. The dot represents the mean balanced accuracy; the classification results of the six different data set splits were averaged. n indicates the number of models calculated, Taxa represents the number of variables for each rank.

A selection of eight input data sets was utilized for TNT prediction (**Figure 2**). "Full sediment" contained 41 independent environmental variables and "Full community" included 542 genera (applying a 0.08% relative abundance threshold). The mtry factor 5 allowed for 115 genera being considered at each node. The 0.08% threshold yielded the second highest mean balanced accuracy among the examined threshold values, and showed a more distinct classification distribution (**Supplementary Figure 4**), therefore it was applied to all community data sets presented here.

With reference to the validation set, selections of either the most important 25 genera or 9 sediment parameters yielded more accurate classifications than using all variables; the lowest scores were achieved by using the remaining non-important variables. In this order, the mean balanced accuracy for sediment data decreased from 78.4 over 77.2 to 71.7% and for the community data from 83.2 over 80.6 to 72.6%. Using the most important variables from both data sets combined also improved the classification from 80.5 to 83.0%. The "Top25 community" represents 4.6% of the genera and increased the balanced accuracy, whereas the other 517 genera significantly reduced it. For each variable selection (Full, Top, and Non-Top), the community data performed better than the corresponding sediment data. The combined input data achieved classifications similar to community data alone.

2,4,6-Trinitrotoluene was present in 44–48% of the samples in the six training data sets. The holdout set contained fewer samples; consequentially one sample's classification represented >2.5% accuracy. This led to more widespread class ratios, from 36 to 52%, and thus a higher standard deviation. Best predictions reached 83.8% with "Full community" and 82.7 and 82.6% with "Full combined" and "Top combined", respectively. Predictions on the holdout set were slightly better than the corresponding validation scores, except for "Top combined" and "Top genus". The largest difference between validation and holdout scores was an increase of 4% for "Non-Top25 community". Validation and holdout scores met the same range from 70 to 85%.

The means of the balanced accuracies in the validation set were significantly different from each other (adjusted $p < 0.005$) except "Full community" to "Full combined" (D) and "Top25 community" to "Top combined" (E) in the validation set. This extended to all groups in the holdout set except for "Full combined" to "Top combined" (J).

The distribution of information among samples was then assessed by comparing the validation scores for the six training data sets. The results showed that "Full community" was more

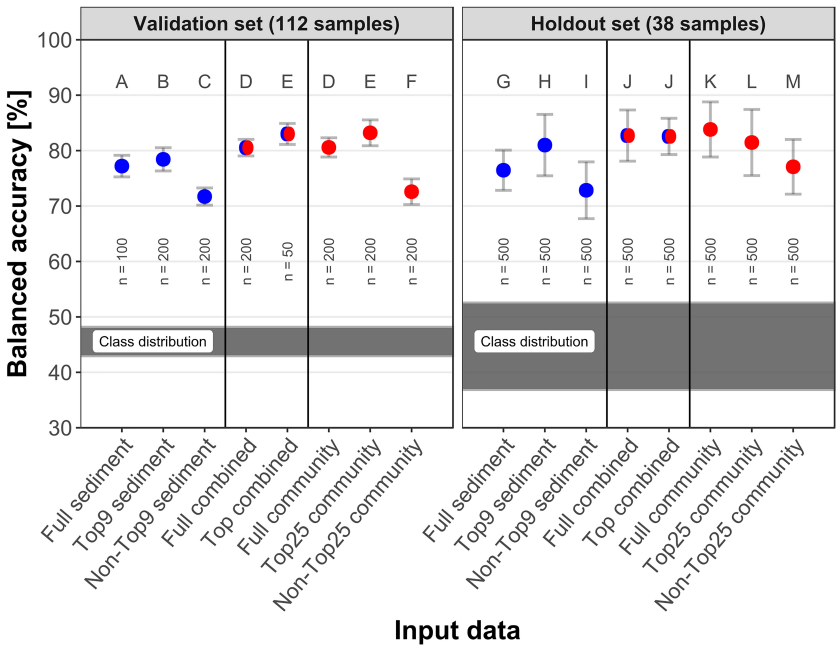

FIGURE 2 | Correct TNT classifications per input data in the validation and holdout test set. Red indicates community data, blue symbolizes sediment data and red-blue combined variables. Of each data type, either all variables were utilized by the model ("Full"), or only the best variables based on variable importance ("Top") or all variables except Top ("Non-Top"). Classification performance is displayed as mean and standard deviation of balanced accuracy, the classification results of the six different data set splits were averaged. The validation values are out-of-bag estimates. The letters indicate which groups were significantly (adjusted $p < 0.005$) different to all other groups within the data set. The shaded area indicates the distribution of samples containing TNT among the six data set splits. n indicates the number of models calculated.

accurate for each set (**Figure 3**). Scores varied by up to 5% between the datasets for "Full sediment" (75.1–80.5% mean balanced accuracy) and "Full community" (77.9–83.2%), but the variation was not well correlated between sediment and community data. For example, comparing data set 1 and 2, the "Full sediment" classification performance dropped whereas the "Full community" balanced accuracy was maintained. These findings signal that the available sediment parameters and taxa abundances did not supply equivalent information.

Grain Size Distribution as the Major Driver of Community Composition

After successful classifications were achieved using community information, TNT was investigated with regard to its potential as important driver of the microbial community composition; as such influence would facilitate the process of prediction. PCA ordination of the Top25 community was performed using the sample proximity obtained by an unsupervised RF classification. PC1 explained 56.1% variation. Along PC1, the grain size fractions <125 μm were separated from those >250 μm (**Figure 4A**). The latter spread along PC2, which explained 18.8% variation. The former fractions co-correlated with further sediment parameters; some of those were important variables for RF when using Full sediment (vanadium, cobalt, and total nitrogen). Significant correlations with munition compounds were not found. The highest accordance among munition compounds with the community composition ordination was shown by 2,6-DNT with R^2 of 0.033 and p of 0.07. TNT (R^2: 0.014, p: 0.38) was detected across all clusters, but predominantly present in mine mound samples. Only a few core samples contained TNT.

The multicorer samples comprised smaller sized particles than most surface sediments. They were sliced at 2 cm, from the sediment-water interface to 22 cm depth (**Figure 4A**, West and East areas, no black outline) and formed a prominent cluster, with communities driven by the grain size distribution and presumably the redox potential declining with depth. The region did not play a role for clustering, as cores were collected kilometers east and west of the mine mound, which itself is centrally located in the restricted area (**Supplementary Figure 1**).

The samples from the mine mound area (a cluster of about 70 mines) were mostly taken within a defined distance of 0–5 m to a mine. Although this is a part within the restricted area, the communities mostly grouped together. Several transects with sampling intervals of 20 m were conducted across the restricted area, surrounding the mine mound (**Figure 4A**, Restricted Area, no black outline). The corresponding communities formed a distinct cluster, too. Three more samples with no detected TNT were collected multiple kilometers away toward northwest. To validate these results using a more traditional approach, the same data was subjected to a non-metric multidimensional scaling (nMDS) using Bray–Curtis dissimilarity, which lead to the same conclusions (**Supplementary Figure 5**).

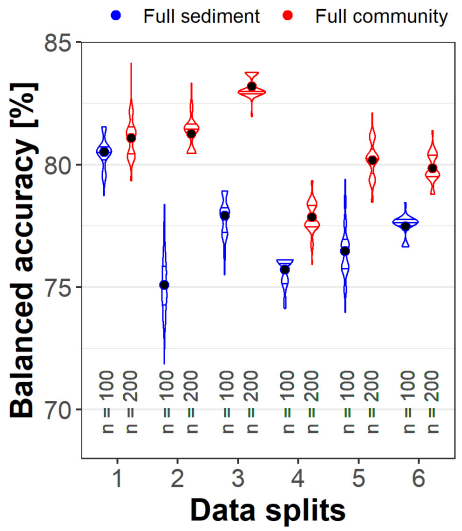

FIGURE 3 | Violin plots with median and interquartile range of correct TNT classifications for six different validation sets. Full community (red) always performed better than Full sediment (blue) and their performances changed independent of each other toward the different validation set compositions. The dot represents the mean balanced accuracy; n indicates the number of models calculated.

An ordination based on only the sediment parameters including the munition compounds was generated to compare with the microbial community ordination. Again, no separation based on TNT presence was observed (**Supplementary Figure 6**). Furthermore, the mine mound and the overall restricted area sediments clustered alongside, with eastern samples placed in proximity. In this ordination the multicorer samples to the east and west were clearly separated, with west and far northwest samples forming a remote cluster.

The seasonal conditions during sampling should be mentioned, as they might have influenced the community composition more strongly than the sediment parameters. The restricted area was sampled mostly manually in June and September 2017 at the sediment surface by divers; three more sediments were obtained using Van Veen grab samplers. The mine mound samplings by divers took place in December 2016 and November and December 2017, which could explain the division between mine mound and restricted area microbial communities. The cores were collected on 1 day in October 2017.

Random Forest was able to predict TNT using only sediment parameters, although no driving influence by munition compounds were detected in the ordinations. Therefore, Spearman rank-order correlation was performed to investigate which variables significantly ($p < 0.01$) correlated with TNT. A cluster of munition compounds consisting of TNT and its metabolites 2-ADNT, 4-ADNT, 2,4-DANT, and 2,6-DANT was identified, which also showed a loose positive correlation with RDX (**Supplementary Figure 7**). Another cluster consisted of DNB, HMX, TNB, 2,4-DNT, and 2,6-DNT. The latter two munition compounds are co-contaminants of TNT. However, the munition compounds were not part of the RF input data set. Furthermore, some weaker correlations with TNT were identified.

The results confirmed that community compositions were primarily controlled by factors other than the presence of TNT; therefore, supervised classification was applied to still extract such a potential impact. Both community and sediment data-based ordination demonstrated as well, that the distribution of TNT containing samples was appropriate to utilize machine learning.

Community Information Important in Combined Data Sets

Foregoing results indicated that a potential impact of TNT was masked by stronger drivers. Therefore, it was essential to investigate the variables that enabled RF predictions. Potential microbial fingerprints (in case of community data) indicative for the presence of TNT were examined. The variable importances, extended by maximal relative abundances and taxonomic lineage of the genera are provided in **Supplementary Figure 8**.

The most supportive genera (**Figure 5**) were *Cocleimonas* (1.65% maximal relative abundance), the unclassified Anaerolineae SBR1031 A4b (0.11%) and an unclassified Gemmatimonadaceae (0.38%). Relative abundances of the Top25 genera ranged from 5.65% for the unclassified Cyanobacterium Sericytochromatia to 0.09% for the unclassified Planctomycete Gimesiaceae. The important sediment variables contained grain size fractions, elemental contents, and total nitrogen as a sum parameter for various nitrogen compounds. Among these, arsenic and the 63–125 μm fraction were most important. This grain size fraction correlated with sum parameters of sulfur and carbon and element contents of e.g., molybdenum and uranium in direction of the multicorer samples.

The 50 most important Full combined variables were then compared against the foregoing top Full community and Full sediment variables. Interestingly, out of 50 variables only 6 were sediment parameters [arsenic (#9), zinc (#21), 63–125 μm fraction (#35), vanadium (#40), mercury (#45), and cobalt (#48)], all of them were part of the Top9 sediment. The achieved classification score of Full combined was as accurate as by Full community input (**Figure 2**). The 44 genera included all of the Top25 community genera. Further genera were related to them on family or order level, for example Flavobacteriaceae, Clostridiales, Sphingomonadaceae, and Desulfobulbaceae. Overall, recovered variables in the combined data set were as important as in individual data sets. Sediment importance ranking concurred, although they were calculated using two different methods for Full community and Full combined.

Processing of All Samples Depends on a Combination of Important Variables

To understand the model's approach to classify the samples and to validate a potential indicative fingerprint, the reasons for the determination of important variables had to be identified. By analyzing their relative abundances, it became clear that 23 of 25 important genera were in average more abundant in surface

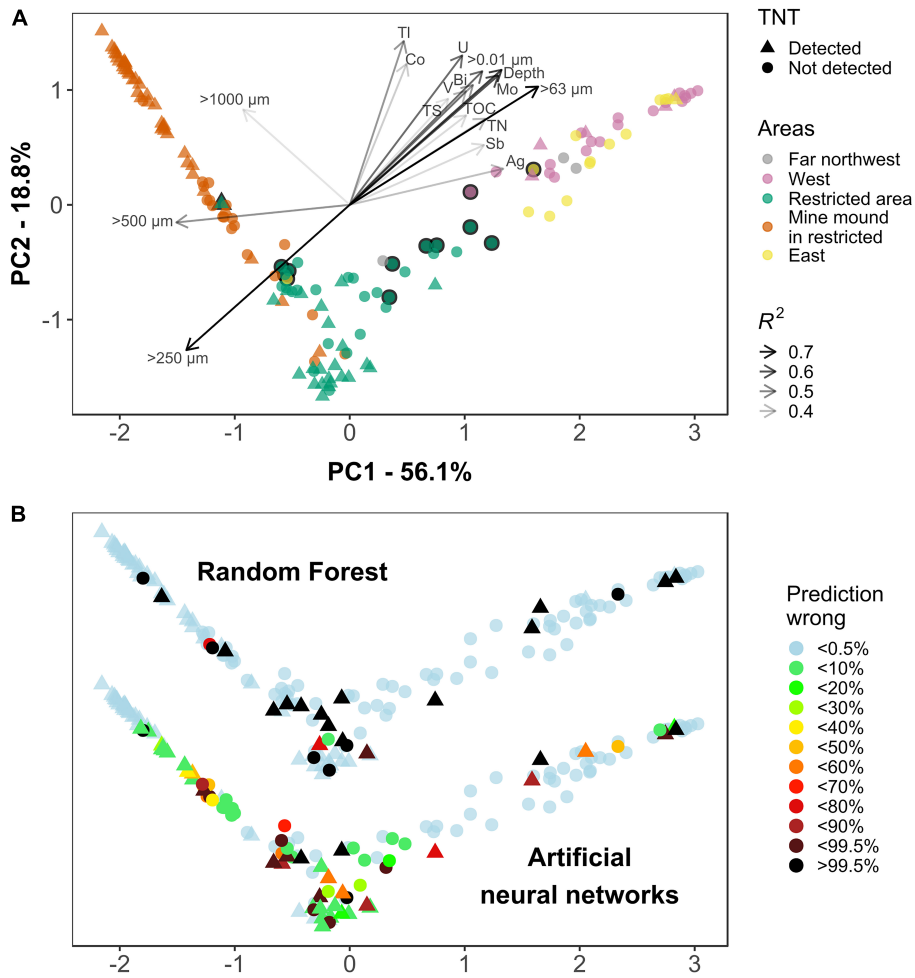

FIGURE 4 | Principal component analysis (PCA) ordination based on the abundance of the most important 25 genera. Dissimilarity between samples was calculated using the proximity matrix of an unsupervised random forest. **(A)** The microbial communities were colored by sample area and shaped to indicate the presence of TNT. The length and shade of correlating sediment parameters ($p < 0.001$, $R^2 > 0.3$) represents the goodness of fit. The black outline marks East (yellow) and West (purple) samples which were not multicorer samples. Similarly, the outline marks Restricted Area samples that were not part of a transect. **(B)** Using the same ordination as in panel **(A)**, the fraction of misclassifications per 1,000 (RF, top) and 999 (ANN, bottom) predictions is displayed for each sample. Light blue colored samples were always correctly predicted, black displays consistently misclassified samples. Please note: the *y*-axis [PC2 in panel **(A)**] was stretched to accommodate the results from both methods.

than core samples, the opposite was true for the clostridium *Anaeromicrobium* and TA06 (**Supplementary Figures 9I,Y**).

Although the abundance of the most important *Cocleimonas* could be very low in samples regardless of class, it mostly occurred in samples with TNT. Second most important *Anaerolineae* SBR1031 A4b proved to be more abundant overall in samples with TNT. Clade TA06, however, was found in as few as 12 samples, and was abundant in very similar sediments of both classes (**Supplementary Figures 9H,P,Y**). The presence of some genera was linked to grain sizes: *Cobetia* was present in medium to finer sediments, *Colwelliaceae* on the contrary in coarser samples (**Supplementary Figures 9C,G**). This goes along with the finding that in a combined data set the grain size information was not as important anymore. But other important genera such as the up to 4.1% abundant *Maribacter*, *Maritimonas* (3.5%), and *Blastopirellula* (4.6%) were present in 131–142 of 150 samples (**Supplementary Figures 9B,D,E**). In a similar fashion, the concentrations of sediment parameters were displayed in **Supplementary Figure 10**.

RF Predictions Were Consistent, With Transect Samples Being Most Challenging

With achieved classification scores for the presence of TNT well above 80% the inner works of the model for the important variables became understandable, but additional information on misclassified samples was required. By recording the mean of 1,000 predictions, it was possible to identify consistently and/or incorrectly classified samples (**Figure 4B**).

Random Forest had cumulatively 24 of 150 samples misclassified (84% accuracy), including 5 of 35 core samples

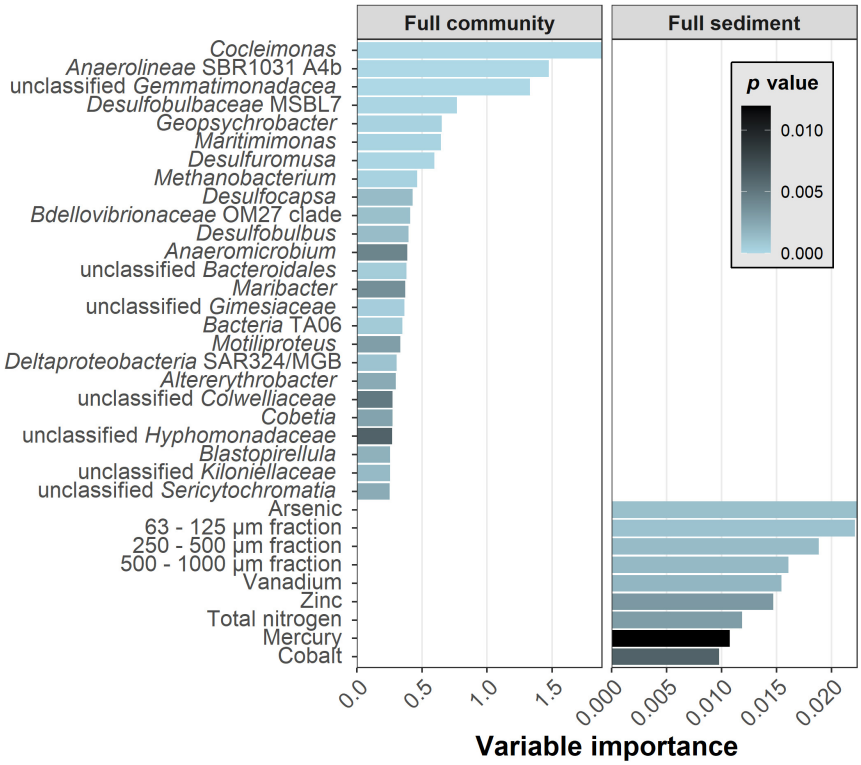

FIGURE 5 | The variable importance and *p*-values for the classification of TNT presence. Twenty-five genera of the Full community and nine sediment parameters of Full sediment were selected. The most detailed taxonomic annotation was provided in case none was available at genus rank. Importance and *p*-values were generated after Altmann (Full sediment) and Janitza (Full community) for six data splits and subsequently averaged.

and 6 of 58 sediments near the mine mound. These predictions were robust; a classification was either wrong or correct, taken 0.5% tolerance into account. Only four samples showed varying classifications, being incorrectly classified 1.3, 71, 79, and 93% of the time.

A PCA ordination based on a TNT classifying model showed the attempt to cluster by class: clusters in top right and bottom center were predominantly TNT-present and in the top left mostly TNT-absent (**Supplementary Figure 11**). The center region displayed communities of both classes intermingled. Samples of all areas were observed there, but those from the restricted area were most present with both classes. The samples in the center region were more often misclassified, mostly predicted as TNT-absent. Finding two separate clusters for TNT-present samples indicated that two distinct groups of important variables contained in the model were required to achieve classifications of those samples.

The restricted area achieved the highest misclassification rate. Within a total of 51 sediments for this region, all 13 misclassifications could be attributed to 41 samples collected by four transects (**Supplementary Figure 11**, Restricted area, no black outline, see also **Figure 4A**). The 200 m long transects, each consisting of 9–11 sampling points, covered different sections of the restricted area.

In general, the less abundant class in a given region is prone to misclassification; however, minority class samples were also predicted correctly. The inconsistently classified samples can be imagined close to the decision boundaries between predominantly "present" and "absent" groups (**Figure 4B**, RF).

The robustness test utilizing an ANN gathered 70 wrongly predicted samples in 999 classifications. Sixty-four of those were not robust. More specifically, 30 samples were misclassified less than 10% of the time and another 11 samples were almost more frequently than 99.5% misclassified. Furthermore, all samples incorrectly classified by RF were misclassified by the ANN, too. Regarding the higher prediction variance of the ANN it should be noted that RF is an ensemble classifier (see section "Discussion").

TNT Metabolites Containing Samples More Likely to Be Classified False Positive

The presence of ADNTs or DANTs in sediments indicates that TNT had been present. It was hypothesized that such former TNT-containing sediments might harbor community compositions which "look like" TNT was still present after its dissipation due to resilience. In consequence such samples should be predicted falsely positive. A "clean" sample on the other hand contains neither TNT nor its metabolites, indicating that it was not contaminated with TNT for a longer time.

The RF models predicted eight false positives; two of them were not consistently misclassified (**Figure 6**). Interestingly,

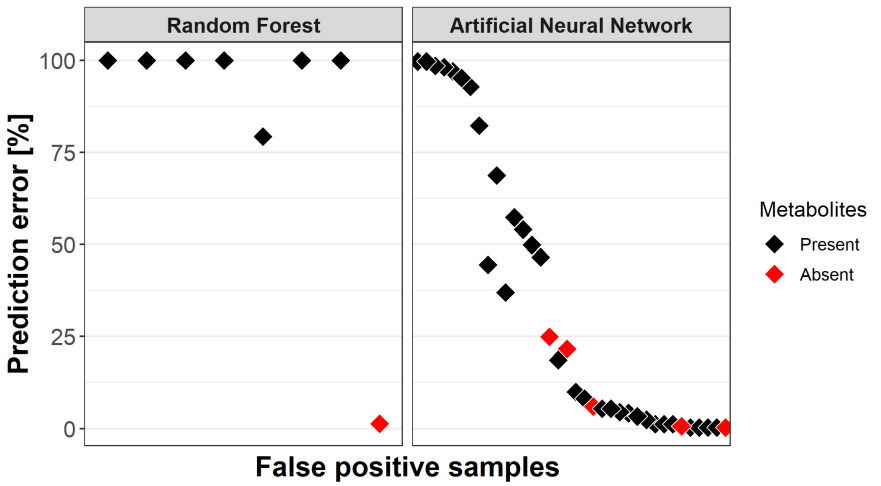

FIGURE 6 | Misclassification rates of samples which were predicted "TNT present" but did not contain the explosive (False positive prediction). Red indicates whether a false positive samples contained TNT metabolites, i.e., ADNTs and DANTs. Samples containing metabolites were more likely to be misclassified as false positives.

seven of the false positives actually contained TNT metabolites and the one "clean" sample was only 1.3% times incorrectly classified. The ANN predicted 36 false positives, 5 of those without metabolites. Their prediction errors ranged from 0.3 to 25% with an average of 10.6%, compared to a mean prediction error of 38.3% for the remaining false positives with metabolites. Furthermore, prediction rates for false positives did not correlate with the individual or summed concentration of TNT metabolites.

It was additionally verified whether a higher TNT concentration goes together with a stronger impact on the community composition, thereby decreasing the probability of a false negative prediction. However, the RF predictions contained only two suitable false negative samples. For ANN a higher TNT concentration did not lead to better prediction rates of the sample.

DISCUSSION

In this study, microbial communities were used to predict the presence of TNT in sediments (at pmol·g^{-1} levels) in and around a munitions dumpsite in the German Baltic Sea with about 84% balanced accuracy. Genera and sediment parameters being most important to reach this value, and the samples that were a challenge to the models, could be identified. Moreover, many TNT false-positive samples had traces of TNT metabolites, indicating that microbial community compositions may conserve information of former TNT presence for a longer period.

Model-Relevant Genera Were Related to TNT-Degrading Taxa

A selection of 9 sediment parameters or 25 bacterial genera predicted TNT as well (holdout set) or even better (validation) compared to using all variables. This is a result similar to the results of Thompson et al. (2019), who conducted a study to predict concentrations of dissolved organic carbon using most effectively a subset of the microbial community compositions of a plant litter decomposition experiment. One reason for such improved performances could be a lower likelihood of overfitting.

The subset was identified by the variable importance metric, which indicates correlation with the response variable. A potential causation between TNT presence and identified important genera is attributable to TNT as a source for biomass generation, energy supply or toxic stress (George et al., 2009; Gallagher et al., 2010). The bacterial enzymatic degradation of TNT is mediated by nitroreductases. Nitroreductases and other common enzyme families have been reported as responsible for the reduction of nitro groups (Esteve-Núñez et al., 2001), which are among the first steps of microbial TNT transformation. Such enzymes are widely distributed among microorganisms, rendering microbial TNT metabolization possible in marine sediments (Roldán et al., 2008). In fact, TNT degradation products as ADNTs and DANTs were present in Kolberger Heide sediments. The ability to degrade TNT was specifically proven for more than 20 different genera, ranging from anaerobic members of the family Clostridiaceae to aerobic members of the family Pseudomonadaceae (Esteve-Núñez et al., 2001). Relatives of these organisms are important for the models of our study; for instance, the Top25 and Top50 members Anaeromicrobium and Clostridiaceae sensu stricto 13, respectively, are phylogenetic members of the Clostridiaceae. Top25 *Altererythrobacter* is also phylogenetically related to TNT-degrading *Sphingomonas sanguinis* (Habineza et al., 2017). However, deriving bacterial activities from phylogenetic relations has to be handled carefully as phylogeny can be an unreliable indicator of bacterial ecology, although tools like PICRUSt2 demonstrated the prediction of the functional potential of a 16S rRNA gene-derived community profile (Douglas et al., 2020). Thus, it is also possible that the obligate anaerobic *Anaeromicrobium* acted as redox indicator for reduced conditions in the investigated sediments or that the abundance of the identified taxa would

also have correlated with the presence of naturally occurring aromatic compounds.

It was furthermore shown that multiple genera were required to separate classes in all samples, because some important taxa, such as clade TA06, were only detected in 12 samples. Consequently, their contribution to classification was limited. However, these genera were likely important, because they allowed classification of otherwise similar samples. In this regard, other variables could not replace this information.

The prediction of TNT was still successful using the available sediment information alone. We assume that, in this case, many samples were separated first and foremost by the grain size distribution, as the finer multicorer samples contained many TNT-free sediments, compared to the coarser mine mound samples, consisting of many TNT-contaminated sediments. The other parameters further on separated within those groups specifically. In order to supplement microbial community variables one might intuitively assume that at least grain size and, where appropriate, redox conditions should be measured as major proxies to inform the model. However, the combined usage of community compositions and sediment parameters did not lead to predictions more accurate than by using the community data on its own. It turned out that the second most important Full sediment variable (63–125 μm grain size fraction) was only the 35th most important Full combined variable and the other grain size fractions were not included in the Top50. These findings show that taxa abundances can replace the grain size information because it is reflected by the community data.

More information would be required to conclusively determine the reason why samples from the mine mound area, which is located in the center of the restricted area, formed a distinct cluster in the unsupervised PCA ordination (**Figure 4A**). This was noticeable, as the transect samples formed another distinct cluster, though the transects geographically encircled the mine mound. We suggest the sampling of the mine mound in a different season than the conduct of the transects as a main reason for varying assemblages (Meyer-Reil, 1983), but the proximity to mines as factor cannot be ruled out. Such an influence, however, was not displayed by the measured sediment variables (**Supplementary Figure 6**), where sediments from the mine mound and the restricted area clustered more similarly.

The Microbial Fingerprint Requires Further Data to Become Indicative

A meaningful indicative microbial fingerprint is equivalent with the abundances of important variables per response class, if they are causally related. Yet the clade TA06 was detected in 12 of 150 samples, which increases the likelihood of being only coincidentally useful; in other words, the sample size is too small to know whether overfitting occurred (Dietterich, 1995). Thus, there is a need to reduce the potential of spurious relationships. To receive a reliable, generalizable and informative fingerprint we propose to: (a) maximize the sample to variable ratio by using a minimum number of taxa while still reaching acceptable predictions, e.g., using backward elimination (Guyon et al., 2002); (b) add samples of further targeted sites and conditions, which cover all response classes; and (c) perform regression instead of classification as long as the concentration of the response variable is appropriately distributed and covered. Regression yields a more informative relation between response and community composition and avoids arbitrary limits between response classes.

In our study, the 150 samples were split into six different training and test sets. The test set is usually the ultimate benchmark for the predictive potential of the model, but it was likely that not all samples in our data set were equally different from each other. Therefore, the hyperparameters as well as the important variables were based on averaged results from the six sample set compositions. This approach can be seen as extra layer of repeated cross validation and helps to maximize the generality of the fingerprint and the chosen settings. It also resulted in more reliable prediction accuracies, as for an individual sample split mean balanced accuracies >90% were achieved. Important is that by this approach a training sample of one split is also a test sample of another split. This results ultimately in information leakage, although in a rather indirect way (Kaufman et al., 2011). We argue that this approach is justifiable for our small data set, where the detection of a generalized TNT-indicative microbial fingerprint as proof of principle was the priority. But in larger data sets, or to compare different prediction methods, regular approaches with a fixed hold out test set should be applied. It should also be remembered that if such a model would be actually deployed, the data to be predicted, e.g., from the next sampling campaign, would not yet exist.

With regard to an indicative fingerprint, we conclude that the presented data set probably contains essential parts of it, but is not yet suited to distinguish accidentally valuable from truly influenced variables. However, we conclude that the first steps were successfully taken to determine a microbial fingerprint indicative of TNT contamination in Kolberger Heide.

An Indicative Microbial Community Fingerprint May Differ Between Habitats

Given the existence of such a fingerprint, part of its value is to use it for other areas of interest. In this regard, the usage of microbial community compositions has both advantages and drawbacks. Advantageous is that the features were assigned at least a partial taxonomy; thus, are interpretable and relatable to literature or cultivation dependent complimentary investigations. Yet, using taxa infers using a proxy, depending on many influences such as nutrients, salinity, redox, pH, temperature (Lindh and Pinhassi, 2018), or as described in this study, grain size.

In order to create meaningful fingerprints, communities likely need to originate from a somewhat similar habitat under specific conditions. But, importantly, our models still could predict using data from various habitats—as from deeper multicorer and surface sediment samples—albeit the variable importance would be a mixture of habitat fingerprints and therefore less interpretable. Additionally, the important taxa might not occur everywhere. To address this issue, higher tax ranks can be used, which are more likely to be found in various areas.

Ghannam et al. (2020), for instance, used phyla to differentiate geographic locations on global scale. In our spatially restricted samples the phylum rank also achieved 76.9% mean balanced accuracy, which is still well above coincidence. But the context of the response variable should be considered, as a higher taxonomic rank is reasonable to cover taxa globally. However, in a previous study we detected distinct reactions to the herbicide glyphosate at OTU-level for *Pseudomonas*, which were not distinguishable anymore on genus level (Janßen et al., 2019a). An alternative is to combine important variables from all taxonomic ranks and train with those. The usage of ASVs in this study would have led to slightly more accurate predictions, but the goal was to utilize a data set which could be amended by additional community compositions targeted with various primer sets or processed by other bioinformatic pipelines. The resulting additional taxa would be incompatible with the already generated ASVs, but could be combined on genus rank.

Furthermore, it is conceivable to target functions (genes or transcripts) directly by shotgun sequencing instead of using taxa as proxy. Alneberg et al. (2020) demonstrated that functional genes from metagenome assembled genomes predicted salinity and depth in Baltic Sea waters. For our study, metatranscriptomes would have been very helpful to identify the used (expressed) degradation pathways among the diverse functional potential of sediment communities. However, this approach would have required that the sediment samples were conserved for high-quality mRNA retrieval which, unfortunately, were non-existent.

Misclassified Samples Define Further Sampling Campaigns

Two mechanistically different ML algorithms were able to predict the presence of TNT in Kolberger Heide sediments using 25 genera. The samples misclassified by RF were also misclassified by the ANN, indicating that the data were insufficient in that case, independent of the algorithm in use. RF worked directly with the relative abundances as input, a form of transformation or normalization could have had a positive effect on the prediction scores (Gloor et al., 2017). However, the performed z-score transformation for the ANN model input at least did not excel the RF predictions (**Supplementary Figure 13**). The more consistent predictions of RF stem in part from it being an ensemble classifier (Breiman, 2001). Thus, all the individual predictions of the tree models are not published, as they are for ANNs, but reduced to a single prediction based on a majority vote. As ANNs do not have this leveling mechanism by default, more variance in cumulated classifications was observed.

It seems reasonable to explore the microbial community composition by proximity matrix-based ordinations, using the same distance metric that is used for the supervised classification. It allows correlating environmental variables, the addition of context data and provides an understanding on the data set dynamics. Combined with the classification robustness it becomes a powerful approach to determine model limitations as well as their overcoming (e.g., more transect samples, **Supplementary Figure 11**). It can be compared to the supervised ordination, which indicates the separation by TNT presence or absence and confirmed that many of the samples consistently misclassified were not well separated. For more insights, decision boundaries can be added [for one model at a time (Hastie et al., 2009)].

Resilience of TNT Presence as a Tool to Detect Historical Contaminations

In addition to investigating whether the composition of microbial communities can indicate TNT-contaminated sediments, it was of interest to us whether these indications could be maintained for a longer period of time, even if the sediment only contained TNT metabolites or was already TNT-free again. In this case, samples would be characterized as being false-positive. Indeed, based on our approach it became apparent that especially samples containing no metabolites at all had a lower chance of a false positive prediction. Unfortunately, the sample size did not allow a meaningful test of significance yet. The possible implications are relevant though, as shown by Smith et al. (2015), who successfully classified microbial communities affected by the Deepwater Horizon oil spill. Their RF models classified samples falsely positive, which were once contaminated, yet subsequently the hydrocarbon concentrations had returned to background levels.

To investigate such a phenomenon based on ecological resilience (Shade et al., 2012) at Kolberger Heide, it should be considered whether TNT and its metabolites result in similar variable importance and fingerprints due to their structural similarity as nitroaromatic compounds. In such a case, a test of true resilience after a TNT contamination—and therefore the time span to detect such—would require to work with once contaminated samples then free of TNT and its metabolites. Another reason for a prolonged taxa detection after TNT has been degraded could be a metabolic shift toward other carbon and energy sources. Such a shift from denitrification to fermentation was described by Orsi et al. (2017). Methodologically, it should also be ensured that the TNT metabolites were not formed e.g., in the water column and subsequently adsorbed to the sediment.

Importance of Microbiological Surveys as a Key Component in Environmental Monitoring

The Kolberger Heide munitions dumpsite is a stressor to blue mussels (*Mytilus edulis*, Strehse et al., 2017; Appel et al., 2018) and dab (*Limanda limanda*, Koske et al., 2020); our study verified the presence of explosives and their transformation products in sediments as well. Furthermore, mines at Kolberger Heide have been proposed as point sources of mercury due to, e.g., mercury(II) fulminate fuses (Bełdowski et al., 2019). However, despite spottily occurring concentrations up to 4,503 $\mu g\ Hg \cdot kg^{-1}$ dry sediment, no correlation with the distance to mines was detected (**Supplementary Figure 12**). Additionally, most mines on-site are registered as discarded munition material (Kampmeier et al., 2020). In comparison to unexploded ordnance, those were not fused and therefore should not contain mercury(II) fulminate.

2,4,6-Trinitrotoluene was found strongly correlated with DANTs and ADNTs, though (**Supplementary Figure 7**). The presence of TNT metabolites proves that Kolberger Heide also represents a disturbance toward the microbial community, as it reacted to the explosives. But it is not clear yet to which extent the community is affected. A potential impact of TNT was surpassed by the main driving grain size distribution and correlating factors, which is expected for such low levels of TNT. Wikström et al. (2000) reported small amounts of degradation and increased microbial growth following the addition of TNT to lake microcosms. However, they did not find a permanent alteration of microbial communities based on random amplified polymorphic DNA analysis. In a study evaluating the toxicity of Harz soil extracts containing TNT, the *Aliivibrio fischeri* luminescence test (EN ISO 11348) reported a long-term EC_{20} of 60–90 $ng \cdot g^{-1}$ or 264–396 $pmol \cdot g^{-1}$ [assuming 1 mL = 1 g (Frische, 2002)]. Such concentrations were met in the Kolberger Heide in exceptional cases, e.g., at the detonation site. A summary of various studies investigating a disturbing or toxic impact on soil microorganisms can be found in the article of Kuperman et al. (2009), although effects were only observed at soil TNT content 10^3–10^6-fold higher than measured in the current study.

The information of a potential munition compounds impact could have been recorded by microbial communities. Such information could be utilized in cases were direct measurements are problematic to realize: it was reported that TNT is hard to detect just in centimeters distance from containments because it slowly dissolves but is rapidly transformed or bound to sediment (Porter et al., 2011; Gledhill et al., 2019). In fact, TNT can be bio-transformed in minutes (Elovitz and Weber, 1999). Therefore, measured TNT concentrations may not fully capture the impact toward the environment and the microbial community specifically. Furthermore, it should be kept in mind that many more sediments contained munition compounds other than TNT; the impact on the environment has to be considered for all munition compounds in terms of combined effects and quantity, especially with the background of continuously corroding of metal housings. There is even an urgent demand to merely identify the actual munition compounds composition of the dumped ammunitions (Beck et al., 2019). The release of munition compounds might also be intermittent ("sudden release"), which emphasizes the advantages of a resilient indicative fingerprint.

We suggest that microbial community data should be included with monitoring strategies and could potentially act as an information repository to complement the snapshot which is generated by standard monitoring methods. In return, monitoring provides a standardized solution to retrieve more and even specifically required samples to overcome the most severe hindrance for ML: limited sample size. With sufficient data, supervised machine learning could identify impacts of contaminants without being main community drivers. Depending on available context information, the sequenced community data can be utilized to train for further variables as Smith et al. (2015) demonstrated, when they predicted 18 highly significant and 8 significant geochemical features such as element concentrations or conductivity of groundwater wells using community data. In this study, the munition compounds showed challenging and partly correlated distributions with strongly imbalanced classes, therefore, the prediction of other compounds than TNT led to overoptimistic results. However, the important consequence is that a single community composition can be utilized as source of information on potentially all relevant shaping environmental factors. This affects the cost/benefit ratio, where the costs for the applied munition compound detection method alone are in the same order of magnitude as those for 16S rRNA amplicon sequencing. An extensive discussion on the opportunities of including sequencing methods into monitoring strategies and a cost comparison for analytical and sequencing methods are presented in Janßen (2020).

It should be reminded, that the herein presented results were achieved using a Kolberger Heide site-specific data set. The models generated based on these data sets do not apply to other geographical areas, yet. However, this limitation is solely due to sample size and distribution and justifiable for a proof of principle. By producing more data from different geographic areas, target compounds and habitats, models can be trained for e.g., the detection of TNT in the Baltic Sea. These models then could be used for monitoring as described above. With regard to munitions, the problem of sea-dumped and leaking munition is not restricted to the Kolberger Heide, yet rather a global problem (Strehse et al., 2021) that already affects humans *via* incorporation into the marine food chain (Maser and Strehse, 2021).

CONCLUSION

This study demonstrated successfully the prediction of TNT presence in Kolberger Heide sediments using microbial community information, and highlighted regions of the munitions dumpsite where further samples should be collected. A possible TNT indicative fingerprint on genus rank was identified as successful proof of principle. Finally, a potential for TNT-dissipation resilient community compositions was observed.

The importance of environmental monitoring including the implementation of the aforementioned approach was laid out, harnessing its predictive potential. In this regard, resilient microbial communities would allow to fill gaps between sporadic samplings; thus, to identify contamination events not measurable at all times. As surplus, each monitoring event would generate more training data for more accurate predictions. This may ultimately lead to a more fundamental monitoring of marine ecosystems; based on highly resolved biological variables and potentially automatable or autonomously operable.

DATA AVAILABILITY STATEMENT

The datasets presented in this study can be found in online repositories. The names of the repository/repositories and accession number(s) can be found in the article/ **Supplementary Material**.

AUTHOR CONTRIBUTIONS

RJ performed the molecular and geological lab work (except munition compounds measuring), acquired funding, planned the data analysis, performed the bioinformatic processing, wrote the analysis scripts, wrote the R package, conducted the machine learning and analyzed the results, and wrote the first draft of the manuscript. AB and EA measured the munition compound concentrations, designed the sampling campaigns at Kolberger Heide, and commented on the manuscript. AB discussed the data and provided a great amount of munition compounds specific knowledge. JW supported the bioinformatics analysis, performed code review, supervised the R package development, provided the IT infrastructure, and commented on the manuscript. JA guided the initial bioinformatic analysis and provided statistical and general coding support, and commented on the manuscript. OD supervised the geochemical analysis and conducted ICP-MS measurements, interpreted the data, and commented on the manuscript. CB connected the various subprojects to make this study possible, provided historical and jurisdictional context, acquired funding, addressed the monitoring requirement, and commented on the manuscript. BK provided the 16S rRNA gene amplicon sequencing device and materials, and commented on the manuscript revision. EM acquired funds and samples and provided a toxicological assessment, and commented on the manuscript revision. AA came up with essential ideas regarding the analysis of microbial communities by machine learning in an ecologically meaningful way, supervised bioinformatics and statistical data analysis discussed the data, and commented on the manuscript. ML conceived the concept, supervised the analyses, discussed the data, acquired and provided funding, rewrote parts of the manuscript, and commented on the manuscript. All authors have read and approved the final version of the manuscript.

FUNDING

RJ was funded partially by the German national BMBF project "Sektorale Verwertung" (01IO1448) and the "German Program on Underwater Munitions", State Ministry of Energy, Agriculture, the Environment, Nature and Digitization. EA and AB's work was funded by the German Federal Ministry of Education and Research (BMBF) through the project UDEMM (Umweltmonitoring für die DElaboration von Munition im Meer, Project number 03F0747, subproject AkViCheMM), and GEOMAR Helmholtz Centre for Ocean Research Kiel. Purchase of the Illumina MiSeq was kindly supported by the EU-EFRE (European Funds for Regional Development) program and funds from the University Medicine Rostock awarded to BK. AA, JA, and ML contributed as part of the BONUS Blueprint project, which was supported by BONUS (Art 185), funded jointly by the EU and the Swedish Research Council FORMAS and the BMBF (03F0775A), respectively.

ACKNOWLEDGMENTS

The Scientific Divers of the University Kiel made this study possible. Jennifer Strehse is thanked for providing additional important sediments. RJ would like to acknowledge the great help of Anne Köhler, Ines Scherff, Sascha Plewe, Mischa Schönke, and Peter Feldens during geochemical/sedimentological analyses and as well as the support of Emilia Friederike Kühn and Christin Laudan with the molecular biology lab work and finally Jana Bull for library preparation and running the MiSeq. RJ and JW personally acknowledge the use of de.NBI cloud and the support by the High Performance and Cloud Computing Group, especially Maximilian Hanussek, at the Zentrum für Datenverarbeitung of the University of Tübingen and the Federal Ministry of Education and Research (BMBF) through Grant No. 031 A535A. We would like to thank the reviewers for their comments which significantly improved the quality of the manuscript.

SUPPLEMENTARY MATERIAL

The Supplementary Material for this article can be found online at: https://www.frontiersin.org/articles/10.3389/fmicb.2021.626048/full#supplementary-material

REFERENCES

Allaire, J. J., and Chollet, F. (2020). *keras: R interface to "Keras*. Available online at: https://cran.r-project.org/package=keras

Allaire, J. J., and Tang, Y. (2020). *tensorflow: R interface to "TensorFlow*. Available online at: https://cran.r-project.org/package=tensorflow

Alneberg, J., Bennke, C., Beier, S., Bunse, C., Quince, C., Ininbergs, K., et al. (2020). Ecosystem-wide metagenomic binning enables prediction of ecological niches from genomes. *Commun. Biol.* 3, 1–10. doi: 10.1038/s42003-020-0856-x

Altmann, A., Toloşi, L., Sander, O., and Lengauer, T. (2010). Permutation importance: a corrected feature importance measure. *Bioinformatics* 26, 1340–1347. doi: 10.1093/bioinformatics/btq134

Appel, D., Strehse, J. S., Martin, H. J., and Maser, E. (2018). Bioaccumulation of 2,4,6-trinitrotoluene (TNT) and its metabolites leaking from corroded munition in transplanted blue mussels (*M. edulis*). *Mar. Pollut. Bull.* 135, 1072–1078. doi: 10.1016/j.marpolbul.2018.08.028

Beck, A. J., van der Lee, E. M., Eggert, A., Stamer, B., Gledhill, M., Schlosser, C., et al. (2019). In situ measurements of explosive compound dissolution fluxes from exposed munition material in the Baltic Sea. *Environ. Sci. Technol.* 53, 5652–5660. doi: 10.1021/acs.est.8b06974

Bełdowski, J., Szubska, M., Siedlewicz, G., Korejwo, E., Grabowski, M., Bełdowska, M., et al. (2019). Sea-dumped ammunition as a possible source of mercury to the Baltic Sea sediments. *Sci. Total Environ.* 674, 363–373. doi: 10.1016/j.scitotenv.2019.04.058

Böttcher, C., Knobloch, T., Rühl, N.-P., Sternheim, J., Wichert, U., and Wöhler, J. (2011). *Munitionsbelastung der Deutschen Meeresgewässer – Bestandsaufnahme und Empfehlungen*. Available online at: www.munition-im-meer.de

Breiman, L. (2001). Random forests. *Mach. Learn.* 45, 5–32. doi: 10.1023/A:1010933404324

Brodersen, K. H., Ong, C. S., Stephan, K. E., and Buhmann, J. M. (2010). "The balanced accuracy and its posterior distribution," in *Proceedings of the 20th International Conference on Pattern Recognition* (Piscataway, NJ: IEEE), 3121–3124. doi: 10.1109/ICPR.2010.764

Callahan, B. J., McMurdie, P. J., Rosen, M. J., Han, A. W., Johnson, A. J. A., and Holmes, S. P. (2016). DADA2: high-resolution sample inference from Illumina amplicon data. *Nat. Methods* 13, 581–583. doi: 10.1038/nmeth.3869

Caporaso, J. G., Lauber, C. L., Walters, W. A., Berg-Lyons, D., Lozupone, C. A., Turnbaugh, P. J., et al. (2011). Global patterns of 16S rRNA diversity at a depth of millions of sequences per sample. *Proc. Natl. Acad. Sci. U.S.A.* 108, 4516–4522. doi: 10.1073/pnas.1000080107

Dellwig, O., Schnetger, B., Meyer, D., Pollehne, F., Häusler, K., and Arz, H. W. (2018). Impact of the major baltic inflow in 2014 on manganese cycling in the Gotland Deep (Baltic Sea). *Front. Mar. Sci.* 5:248. doi: 10.3389/fmars.2018.00248

Dellwig, O., Wegwerth, A., Schnetger, B., Schulz, H., and Arz, H. W. (2019). Dissimilar behaviors of the geochemical twins W and Mo in hypoxic-euxinic marine basins. *Earth Sci. Rev.* 193, 1–23. doi: 10.1016/j.earscirev.2019.03.017

Dietterich, T. (1995). Overfitting and undercomputing in machine learning. *ACM Comput. Surv.* 27, 326–327. doi: 10.1145/212094.212114

Douglas, G. M., Maffei, V. J., Zaneveld, J. R., Yurgel, S. N., Brown, J. R., Taylor, C. M., et al. (2020). PICRUSt2 for prediction of metagenome functions. *Nat. Biotechnol.* 38, 685–688. doi: 10.1038/s41587-020-0548-6

Elovitz, M. S., and Weber, E. J. (1999). Sediment-mediated reduction of 2,4,6-trinitrotoluene and fate of the resulting aromatic (poly)amines. *Environ. Sci. Technol.* 33, 2617–2625. doi: 10.1021/es980980b

Esteve-Núñez, A., Caballero, A., and Ramos, J. L. (2001). Biological degradation of 2,4,6-trinitrotoluene. *Microbiol. Mol. Biol. Rev.* 65, 335–352. doi: 10.1128/MMBR.65.3.335

Fernández-Delgado, M., Cernadas, E., Barro, S., and Amorim, D. (2014). Do we need hundreds of classifiers to solve real world classification problems? *J. Mach. Learn. Res.* 15, 3133–3181. doi: 10.1080/13216597.1999.9751892

Frische, T. (2002). Screening for soil toxicity and mutagenicity using luminescent bacteria—a case study of the explosive 2,4,6-trinitrotoluene (TNT). *Ecotoxicol. Environ. Saf.* 51, 133–144. doi: 10.1006/eesa.2001.2124

Gallagher, E. M., Young, L. Y., McGuinness, L. M., and Kerkhof, L. J. (2010). Detection of 2,4,6-trinitrotoluene-utilizing anaerobic bacteria by 15N and 13C incorporation. *Appl. Environ. Microbiol.* 76, 1695–1698. doi: 10.1128/AEM.02274-09

George, I. F., Liles, M. R., Hartmann, M., Ludwig, W., Goodman, R. M., and Agathos, S. N. (2009). Changes in soil Acidobacteria communities after 2,4,6-trinitrotoluene contamination. *FEMS Microbiol. Lett.* 296, 159–166. doi: 10.1111/j.1574-6968.2009.01632.x

Ghannam, R. B., Schaerer, L. G., Butler, T. M., and Techtmann, S. M. (2020). Biogeographic patterns in members of globally distributed and dominant taxa found in port microbial communities. *mSphere* 5:e00481-19. doi: 10.1128/mSphere.00481-19

Gledhill, M., Beck, A. J., Stamer, B., Schlosser, C., and Achterberg, E. P. (2019). Quantification of munition compounds in the marine environment by solid phase extraction – ultra high performance liquid chromatography with detection by electrospray ionisation – mass spectrometry. *Talanta* 200, 366–372. doi: 10.1016/j.talanta.2019.03.050

Gloor, G. B., Macklaim, J. M., Pawlowsky-Glahn, V., and Egozcue, J. J. (2017). Microbiome datasets are compositional: and this is not optional. *Front. Microbiol.* 8:2224. doi: 10.3389/fmicb.2017.02224

Greinert, J. (2019). *UDEMM - Practical Guide for Environmental Monitoring of Conventional Munitions in the Seas. Berichte aus Dem GEOMAR Helmholtz-Zentrum Für Ozeanforsch. Kiel 54*. Available online at: https://oceanrep.geomar.de/48842/1/geomar_rep_ns_54_2019.pdf

Guyon, I., Weston, J., Barnhill, S., and Vapnik, V. (2002). Gene selection for cancer classification using support vector machines. *Mach. Learn.* 46, 389–422. doi: 10.1023/A:1012487302797

Habineza, A., Zhai, J., Mai, T., Mmereki, D., and Ntakirutimana, T. (2017). Biodegradation of 2,4,6-trinitrotoluene (TNT) in contaminated soil and microbial remediation options for treatment. *Period. Polytech. Chem. Eng.* 61, 171–187. doi: 10.3311/PPch.9251

Hastie, T., Tibshirani, R., and Friedman, J. (2009). *The Elements of Statistical Learning*, 2nd Edn, New York, NY: Springer.

Häusler, K., Dellwig, O., Schnetger, B., Feldens, P., Leipe, T., Moros, M., et al. (2018). Massive Mn carbonate formation in the Landsort Deep (Baltic Sea): hydrographic conditions, temporal succession, and Mn budget calculations. *Mar. Geol.* 395, 260–270. doi: 10.1016/j.margeo.2017.10.010

Herlemann, D. P., Labrenz, M., Jürgens, K., Bertilsson, S., Waniek, J. J., and Andersson, A. F. (2011). Transitions in bacterial communities along the 2000 km salinity gradient of the Baltic Sea. *ISME J.* 5, 1571–1579. doi: 10.1038/ismej.2011.41

Janitza, S., Celik, E., and Boulesteix, A. L. (2018). A computationally fast variable importance test for random forests for high-dimensional data. *Adv. Data Anal. Classif.* 12, 885–915. doi: 10.1007/s11634-016-0276-4

Janßen, R. (2020). *Machine Learning Classification of Microbial Community Compositions to Predict Anthropogenic Pollutants in the Baltic Sea*. Available online at: https://rosdok.uni-rostock.de/resolve/id/rosdok_disshab_0000002432

Janßen, R., Skeff, W., Werner, J., Wirth, M. A., Kreikemeyer, B., Schulz-Bull, D., et al. (2019a). A glyphosate pulse to brackish long-term microcosms has a greater impact on the microbial diversity and abundance of planktonic than of biofilm assemblages. *Front. Mar. Sci.* 6:758. doi: 10.3389/fmars.2019.00758

Janßen, R., Zabel, J., von Lukas, U., and Labrenz, M. (2019b). An artificial neural network and random forest identify glyphosate-impacted brackish communities based on 16S rRNA amplicon MiSeq read counts. *Mar. Pollut. Bull.* 149:110530. doi: 10.1016/j.marpolbul.2019.110530

Kampmeier, M., van der Lee, E. M., Wichert, U., and Greinert, J. (2020). Exploration of the munition dumpsite Kolberger Heide in Kiel Bay, Germany: example for a standardised hydroacoustic and optic monitoring approach. *Cont. Shelf Res.* 198:104108. doi: 10.1016/j.csr.2020.104108

Kaufman, S., Rosset, S., and Perlich, C. (2011). "Leakage in data mining: formulation, detection, and avoidance," in *Proceedings of the 17th ACM SIGKDD International Conference on Knowledge Discovery and Data Mining*, Cambridge, 556–563.

Koske, D., Straumer, K., Goldenstein, N. I., Hanel, R., Lang, T., and Kammann, U. (2020). First evidence of explosives and their degradation products in dab (*Limanda limanda* L.) from a munition dumpsite in the Baltic Sea. *Mar. Pollut. Bull.* 155:111131. doi: 10.1016/j.marpolbul.2020.111131

Kuperman, R. G., Simini, M., Siciliano, S. D., and Gong, P. (2009). "Effects of energetic materials on soil organisms," in *Ecotoxicology of Explosives*, eds G. I. Sunahara, G. Lotufo, R. G. Kuperman, and J. Hawari (Boca Raton, FL: CRC Press), 35–76. doi: 10.1201/9781420004342

Lindh, M. V., and Pinhassi, J. (2018). Sensitivity of bacterioplankton to environmental disturbance: a review of Baltic Sea field studies and experiments. *Front. Mar. Sci.* 5:361. doi: 10.3389/fmars.2018.00361

Maser, E., and Strehse, J. S. (2020). "Don't Blast": blast-in-place (BiP) operations of dumped World War munitions in the oceans significantly increase hazards to the environment and the human seafood consumer. *Arch. Toxicol.* 94, 1941–1953. doi: 10.1007/s00204-020-02743-0

Maser, E., and Strehse, J. S. (2021). Can seafood from marine sites of dumped World War relicts be eaten? *Arch. Toxicol.* 95, 2255–2261. doi: 10.1007/s00204-021-03045-9

McLaren, M. (2020). *speedyseq: Faster Implementations of Common Phyloseq Functions*. Available online at: https://github.com/mikemc/speedyseq

McMurdie, P. J., and Holmes, S. (2013). phyloseq: an R package for reproducible interactive analysis and graphics of microbiome census data. *PLoS One* 8:e61217. doi: 10.1371/journal.pone.0061217

Meyer-Reil, L.-A. (1983). Benthic response to sedimentation events during autumn to spring at a shallow water station in the Western Kiel Bight. *Mar. Biol.* 77, 247–256. doi: 10.1007/BF00395813

Moitinho-Silva, L., Steinert, G., Nielsen, S., Hardoim, C. C. P., Wu, Y. C., McCormack, G. P., et al. (2017). Predicting the HMA-LMA status in marine sponges by machine learning. *Front. Microbiol.* 8:752. doi: 10.3389/fmicb.2017.00752

Nembrini, S., König, I. R., and Wright, M. N. (2018). The revival of the Gini importance? *Bioinformatics* 34, 3711–3718. doi: 10.1093/bioinformatics/bty373

Oksanen, J., Blanchet, F. G., Friendly, M., Kindt, R., Legendre, P., McGlinn, D., et al. (2019). *vegan: Community Ecology Package*. Available online at: https://cran.r-project.org/package=vegan

Orsi, W. D., Coolen, M. J. L., Wuchter, C., He, L., More, K. D., Irigoien, X., et al. (2017). Climate oscillations reflected within the microbiome of Arabian Sea sediments. *Sci. Rep.* 7, 1–12. doi: 10.1038/s41598-017-05590-9

Parks, D. H., Chuvochina, M., Waite, D. W., Rinke, C., Skarshewski, A., Chaumeil, P.-A., et al. (2018). A standardized bacterial taxonomy based on genome

phylogeny substantially revises the tree of life. *Nat. Biotechnol.* 36, 996–1004. doi: 10.1038/nbt.4229

Pfeiffer, F. (2009). *Bericht Über die in-situ-Begleituntersuchungen zur Munitionssprengung in der Ostsee vom 18.2.2009*. Available online at: https://www.schleswig-holstein.de/DE/Fachinhalte/M/meeresschutz/Downloads/Bericht_Begleituntersuchung_2009.pdf

Porter, J. W., Barton, J. V., and Torres, C. (2011). "Ecological, radiological, and toxicological effects of naval bombardment on the coral reefs of Isla de Vieques, Puerto Rico," in *Warfare Ecology: A New Synthesis for Peace and Security*, eds G. E. Machlis, T. Hanson, Z. Špirić, and J. E. McKendry (Berlin: Springer), 65–121. doi: 10.1007/978-94-007-1214-0_8

R Core Team (2017). *R: A Language and Environment for Statistical Computing*. Vienna: R Core Team.

Roldán, M. D., Pérez-Reinado, E., Castillo, F., and Moreno-Vivián, C. (2008). Reduction of polynitroaromatic compounds: the bacterial nitroreductases. *FEMS Microbiol. Rev.* 32, 474–500. doi: 10.1111/j.1574-6976.2008.00107.x

Ryan, F. J. (2019). Application of machine learning techniques for creating urban microbial fingerprints. *Biol. Direct.* 14:13. doi: 10.1186/s13062-019-0245-x

Shade, A., Peter, H., Allison, S. D., Baho, D. L., Berga, M., Bürgmann, H., et al. (2012). Fundamentals of microbial community resistance and resilience. *Front. Microbiol.* 3:417. doi: 10.3389/fmicb.2012.00417

Smith, M. B., Rocha, A. M., Smillie, C. S., Olesen, S. W., Paradis, C., Wu, L., et al. (2015). Natural bacterial communities serve as quantitative geochemical biosensors. *mBio* 6:e0326-15. doi: 10.1128/mBio.00326-15

Strehse, J. S., Appel, D., Geist, C., Martin, H. J., and Maser, E. (2017). Biomonitoring of 2,4,6-trinitrotoluene and degradation products in the marine environment with transplanted blue mussels (*M. edulis*). *Toxicology* 390, 117–123. doi: 10.1016/j.tox.2017.09.004

Strehse, J. S., Bünning, T. H., and Maser, E. (2021). *Ocean Pollution — A Selection of Anthropogenic Implications*. Available online at: https://res.mdpi.com/bookfiles/edition/1405/article/3537/pOcean_PollutionmdashA_Selection_of_Anthropogenic_Implicationsp.pdf?v=1617690575

Thompson, J., Johansen, R., Dunbar, J., and Munsky, B. (2019). Machine learning to predict microbial community functions: an analysis of dissolved organic carbon from litter decomposition. *PLoS One* 14:e0215502. doi: 10.1371/journal.pone.0215502

Thureborn, P., Franzetti, A., Lundin, D., and Sjöling, S. (2016). Reconstructing ecosystem functions of the active microbial community of the Baltic Sea oxygen depleted sediments. *PeerJ* 4:e1593. doi: 10.7717/peerj.1593

Wickham, H. (2016). *ggplot2: Elegant Graphics for Data Analysis*. New York, NY: Springer-Verlag.

Wikström, P., Andersson, A. C., Nygren, Y., Sjöström, J., and Forsman, M. (2000). Influence of TNT transformation on microbial community structure in four different lake microcosms. *J. Appl. Microbiol.* 89, 302–308. doi: 10.1046/j.1365-2672.2000.01111.x

Wilkins, D., Leung, M. H. Y., and Lee, P. K. H. (2017). Microbiota fingerprints lose individually identifying features over time. *Microbiome* 5:1. doi: 10.1186/s40168-016-0209-7

Wright, M. N., and Ziegler, A. (2017). ranger: a fast implementation of random forests for high dimensional data in C++ and R. *J. Stat. Softw.* 77:20426. doi: 10.18637/jss.v077.i01

Yilmaz, P., Parfrey, L. W., Yarza, P., Gerken, J., Pruesse, E., Quast, C., et al. (2014). The SILVA and "All-species Living Tree Project (LTP)" taxonomic frameworks. *Nucleic Acids Res.* 42, D643–D648. doi: 10.1093/nar/gkt1209

Ziesemer, K. A., Mann, A. E., Sankaranarayanan, K., Schroeder, H., Ozga, A. T., Brandt, B. W., et al. (2015). Intrinsic challenges in ancient microbiome reconstruction using 16S rRNA gene amplification. *Sci. Rep.* 5:16498. doi: 10.1038/srep16498

Conflict of Interest: The authors declare that the research was conducted in the absence of any commercial or financial relationships that could be construed as a potential conflict of interest.

Publisher's Note: All claims expressed in this article are solely those of the authors and do not necessarily represent those of their affiliated organizations, or those of the publisher, the editors and the reviewers. Any product that may be evaluated in this article, or claim that may be made by its manufacturer, is not guaranteed or endorsed by the publisher.

frontiers in Marine Science

ORIGINAL RESEARCH
published: 28 October 2021
doi: 10.3389/fmars.2021.632725

Erosion Dynamics of Cultivated Kelp, *Saccharina latissima*, and Implications for Environmental Management and Carbon Sequestration

Reinhold Fieler[1], Michael Greenacre[1,2], Sanna Matsson[1], Luiza Neves[3], Silje Forbord[4] and Kasper Hancke[5]*

[1] Akvaplan-Niva, Tromsø, Norway, [2] Universitat Pompeu Fabra and Barcelona School of Management, Barcelona, Spain, [3] Seaweed Solutions AS, Trondheim, Norway, [4] SINTEF Ocean, Trondheim, Norway, [5] Norwegian Institute for Water Research (NIVA), Oslo, Norway

OPEN ACCESS

Edited by:
Camila Fernandez, UMR 7621 Laboratoire d'Océanographie Microbienne (LOMIC), France

Reviewed by:
Nor Azman Kasan, University of Malaysia Terengganu, Malaysia
Erasmo Macaya, University of Concepción, Chile

***Correspondence:**
Reinhold Fieler
ref@akvaplan.niva.no

Specialty section:
This article was submitted to Marine Fisheries, Aquaculture and Living Resources, a section of the journal Frontiers in Marine Science

Received: *23 November 2020*
Accepted: *04 October 2021*
Published: *28 October 2021*

Citation:
Fieler R, Greenacre M, Matsson S, Neves L, Forbord S and Hancke K (2021) Erosion Dynamics of Cultivated Kelp, Saccharina latissima, and Implications for Environmental Management and Carbon Sequestration. Front. Mar. Sci. 8:632725. doi: 10.3389/fmars.2021.632725

A growing trend of interest for the cultivation of kelp is driven by predictions for high global demands of important commodities, which require the development of alternative supplies of natural resources. In this study the dynamics of loss of biomass from cultivated *Saccharina latissima* were studied from February to August 2018 at two kelp farms in Northern (69°45.26′N/019°02.18′E) and in Mid-Norway (63°42.28′N/08°52.23′E). Kelp fronds at each farm were individually followed throughout the growing season. Sectional regression was applied for conversion of measured frond lengths to estimated dry weights. The study shows that between 40 and 100% of all individuals in the studied kelp population constantly eroded slightly from their distal ends. However, until June the accumulated loss was only 8% of produced dry weight. Due to dislodgement of whole sporophytes this picture changed in July and August to heavy losses in Mid-Norway. Thus, the overall losses of kelp in terms of accumulated dry weight were only 8–13% of the gross growth until harvest in June in Mid-Norway and August in Northern Norway. Losses increased significantly in Mid-Norway during July and reached 49.4% of the annual production in August. The rates of losses were separated into specific erosion and dislodgement rates. Erosion rates over the whole experimental period for the two sites were not significantly different, while differences in dislodgement rates between farm sites proved to be highly significant. The exported annual amount of carbon was estimated on the basis of lost and measured carbon content in the tissue. From these data a scenario was built for a commercial Norwegian kelp farm growing *S. latissima* showing a carbon export of 63–88 g C $m^{-2}y^{-1}$. This is eight times less than has been reported from scenarios for kelp farms in China. This study confirms that optimal timing of harvest is the most important

management tool for avoidance of heavy losses from kelp farms. In conclusion, an industry with early harvest will likely have a low carbon export, while a late-harvested bulk production could export four to six times as much carbon with an increased potential for carbon sequestration.

Keywords: *Saccharina latissima*, macroalgae cultivation, kelp erosion, detritus, carbon sequestration, seaweed aquaculture, sectional regression

INTRODUCTION

Globally, cultivation of seaweed is a fast-growing sector (FAO, 2020). The outlook for Norwegian seaweed farming is expected to be good (Broch et al., 2019) with projected production volumes of 4 million tons per year by 2030 and 20 million tons per year by 2050 (Olafsen et al., 2012). These projections are based on predictions for high global demands of important commodities which require the development of alternative supplies of natural resources. The development of kelp farming in Norway is also fuelled by the potential prospects of integrated multi-trophic aquaculture – IMTA (Soto, 2009; Chopin et al., 2010; Handå et al., 2013; Stévant et al., 2017), and might in the future have several useful applications.

Saccharina latissima (Linnaeus) Lane, Mayes, Druehl, and Saunders (Lane et al., 2006) is currently the most commonly and economically important cultivated species in Norway. *S. latissima* have sporophytes that can be divided into holdfast, stipe and a single lamina. Their blades have a stretched droplet shape with ruffled edges. The morphology of *S. latissima* has substantial phenotypical variation. Growth occurs in the meristematic region which is positioned in the intersection between the stipe and frond. Like in benthic sugar kelp the blade has a branched holdfast which in aquaculture is anchoring them to the rope. After 2 years of growth individual blades can under natural conditions become longer than 400 cm. The blades are usually harvested in Norwegian aquaculture after 4–7 months at a length between 60 and 100 cm.

Saccharina latissima serves as a model species for both IMTA and for processing in the food sector (Stévant et al., 2017). In 2018 a volume of 176 tons wet weight (WW) of cultivated kelp was harvested by Norwegian seaweed farmers, and the production had decreased to 111 tons WW by 2019, while the total value had increased significantly. There are presently 475 permits for macroalgal cultivation distributed over 97 locations along the Norwegian coast. The cultivation potential of *S. latissima* along the Norwegian coast was recently estimated to be 150–200 tons per hectare per year, and industrial kelp cultivation might utilize extensive areas in the marine environment (Broch et al., 2019), and introduce considerable new quantities of kelp detritus into the ecosystem. Until now, we have incomplete knowledge of the ecological footprint of this nascent industry.

Kelp detritus is produced from constantly eroding fronds, from the fragmentation of parts of the fronds or from the dislodgement of entire sporophytes (Pedersen et al., 2020). The rate of erosion and dislodgement of *S. latissima* sporophytes has been described, during some periods of the year, to surpass growth rates and the monthly estimates amount to as much as 40–70% loss of kelp fronds in natural kelp forests (Parke, 1948; Lüning, 1979; Sjøtun, 1993; Krumhansl and Scheibling, 2011). The loss of tissue from the distal part of the frond is a constantly ongoing process in several Laminarian species, which starts when the sporophyte is only few months old (Parke, 1948; Tala and Edding, 2005; Dean and Hurd, 2007; Nielsen et al., 2016a). The annual detrital production from the erosion of kelp forests in Nova Scotia and in Norway has been estimated to range from 150–513 g C m^{-2} $year^{-1}$ and 478 ± 41 g C m^{-2} $year^{-1}$, respectively (Krumhansl and Scheibling, 2011; Pedersen et al., 2020). Globally, in highly productive kelp forests, incremental erosion and fragmentation can amount to 2657 g C m^{-2} $year^{-1}$ with an additional loss of whole fronds of up to 839 g C m^{-2} $year^{-1}$ (Krumhansl and Scheibling, 2012). Dislodgement of large amounts of kelp biomass from aquaculture installations is thus considered likely to occur. The magnitude of rates in loss of biomass from kelp farms has only been documented in a few studies. A 19% loss of total harvested biomass in terms of carbon and 33% loss in terms of nitrogen was documented from mass cultivation of the kelp *Undaria pinnatifida* in Japan, during a normal production cycle (Yoshikawa et al., 2001). In the Japanese aquaculture of *S. japonica*, peak rates of erosion were estimated at 2.4–3.7 g wet weight day^{-1} which surpassed production rates at the end of the growth season (Suzuki et al., 2008). In experiments in Sungo Bay in China cultured *S. japonica* had carbon losses of up to 61% of the total seasonal gross production due to erosion (Zhang et al., 2012). Other studies from Norwegian waters have shown substantial loss of kelp biomass from farms in association with heavy biofouling only late in the season (Matsson et al., 2019; Forbord et al., 2020).

Cultivation of kelp may contribute with significant supplements of organic material to the surrounding marine environment, with possible implications for the ecosystem and carbon turnover (Duarte et al., 2017). If the organic material is deposited in large amounts underneath the farms, it could cause oxygen depletion from upscaled microbial turnover and lead to poor environmental conditions. If more widely distributed and dispersed, kelp organic matter could lead to stimulated benthos activity and change the natural biodiversity. Also, if not broken down or eaten by benthos, kelp organic matter would be buried in the seafloor and thereby stimulate elevated carbon sequestration in the seafloor. Further, big losses of kelp biomass represent a risk regarding profitability of the kelp cultivation business. Despite this potential for loss of kelp biomass, researchers who have studied the seafloor underneath kelp farms, have not found marked negative environmental effects from intensive kelp farming (Zhang et al., 2009, 2020;

Liu et al., 2016). The question that therefore arises is whether the magnitude and fate of kelp detritus that is exported from kelp rigs has been estimated correctly or if the biomass is transported with the water currents away from the rigs, and is dispersed and deposited over large areas, as has been suggested by Wernberg and Filbee-Dexter (2018).

A review of 17 studies conducted on kelp showed that repeated measurements on individually marked sporophytes have not been used, and that erosion is referred to either in terms of loss of length or in weight, usually estimated from an equation using total length and total weight of the whole frond (e.g., Yoshikawa et al., 2001; Krumhansl and Scheibling, 2011; Zhang et al., 2012). In all reviewed growth- and erosion experiments the researchers measure growth by the punch-hole method (Parke, 1948). This assumes that the increment of the distance between a punched hole and the base of the kelp equals growth in length (Mann, 1973), but seaweed fronds can also elongate between punch-holes beyond the meristem (Bartsch et al., 2008; Suzuki et al., 2008). Thus, this common method could lead to both overestimation and underestimation of erosion from kelp rigs. In addition, the estimation of the weight or width of something that is lost and cannot be measured directly, could introduce significant errors into the transport equations for organic matter from kelp rigs to the benthic environment. Hence, employment of data with high resolution is a prerequisite for understanding kelp erosion and dislodgement dynamics and for quantifying loss of cultivated biomass to the surrounding environment.

As kelp cultivation is taking up large amounts of CO_2 during growth, this fact has in recent years been increasingly highlighted as a contributing solution to climate change (Duarte et al., 2017). Climate mitigation through ocean and atmosphere carbon removal requires that the stored CO_2 be permanently sequestered in the seabed or in the deep sea (Duarte and Cebrián, 1996; Trevathan-Tackett et al., 2015). Exported macroalgae biomass that is not consumed or microbially decomposed will sequester. For natural macroalgae ecosystems it has been suggested that 2–3% of the net production, or up to 15% of the exported biomass from kelp forests, is permanently sequestered in this manner (Krause-Jensen and Duarte, 2016). Assuming that this natural process is also relevant to cultivated kelp, it represents a nature-based solution for CO_2 drawdown from the atmosphere, positioning kelp cultivation as a potential means of carbon sequestration instrument.

The aim of this study was to quantify the biomass loss from cultivated *S. latissima* in coastal kelp farming. Export of kelp detritus and its carbon and nitrogen content was quantified through field investigations and application of novel statistical analysis. Potential for ecosystem impacts and kelp carbon sequestration are discussed.

MATERIALS AND METHODS

The Sites

This study was conducted from February to August 2018 at two sites 800 km apart, measured by air distance. Background values for physical and chemical variables were acquired from Forbord's experiments in 2017 (Forbord et al., 2020) or from hydrographical measurements in previous years. The northernmost site (**Figure 1**) was located near Arctic Tromsø (69°45.259′ N/019°02.176′ E) and had a water depth of 15–20 m. It was assigned site number 9–69°N in Forbord's study. The site was sheltered to wave exposure, but tidal forcing lead to well-mixed water masses. Current velocity was measured for 120 days at 12 m depth from March to July 2011 and was moderate with an average of 3.4 cm s^{-1} and a maximum of 22 cm s^{-1}. The main current direction was toward the northwest. Conductivity, temperature, depth (CTD) profiles were taken for 13 months from the surface to the bottom in 2014 and 2015 and showed homogeneous water masses through the year. Salinity ranged from 33.0 to 33.7 psu, and water temperature ranged from 3.1°C in February to 9.5°C in August.

The site in Mid-Norway was off the east coast of the island of Frøya (63° 42.279′ N/08° 52.232′ E) and was identified as site number 6–63°N in Forbord's study (**Figure 1**). It was semi-exposed with depths between 10 and 45 m, and with well mixed water masses. The current velocity was measured through a complete tidal cycle at different depths with an Acoustic Doppler Current Profiler (ADCP) in March 2012. At 6 m depth the average current was 9.4 cm s^{-1}, with a maximum of 47.7 cm s^{-1}. The main current direction was toward the northeast with a strong tidal signal resulting in conciliating currents in opposite direction. Nine series of monthly CTD measurements taken between April and November 2014 showed tendencies for the

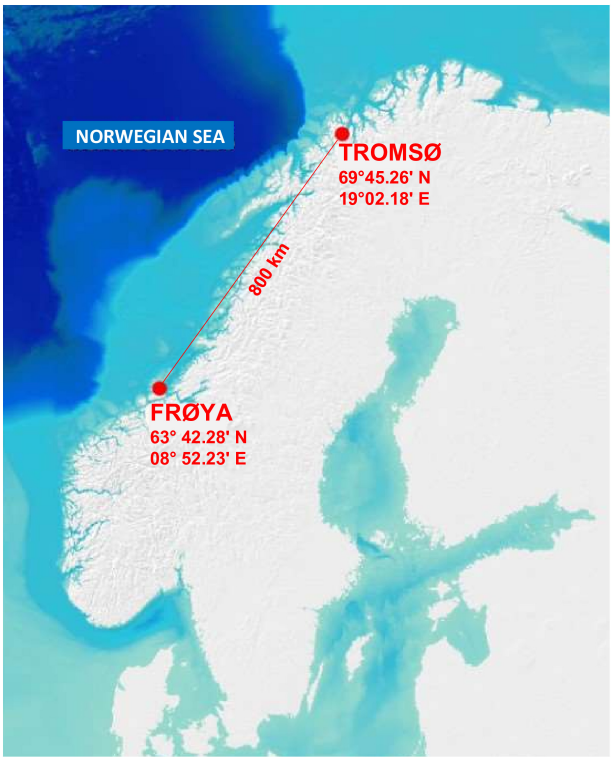

FIGURE 1 | Location of experimental sites in Norway.

development of isoclines from mid-May to mid-August. The rest of the year the water mass was homogeneous. At six meters depth, water temperatures ranged from 7°C in April to 13°C in September 2014 and salinity ranged from 32.7 to 33.7 psu.

Monthly water temperatures at the sites for the year 2017 near Frøya and in Tromsø are shown in **Supplementary Table 1**. Median, minimum, and maximum temperatures were higher in Frøya than in Tromsø. Measurements showed that kelp cultivated at both sites has been well within the temperature tolerance range for *S. latissima* (Fortes and Lüning, 1980; Bolton and Lüning, 1982; Gerard and Du Bois, 1988; Andersen et al., 2013).

Experimental Set-Up

The experiment consisted of two different steps over the same approximate period.

Step 1 was concerned with establishing a relationship between dry weight (DW) and predictor variables length and width measured on the kelp, taking into account the different sections of the fronds. Step 1 was conducted in two experimental groups at the Tromsø and Frøya sites.

Step 2 was concerned with quantifying the gross growth, erosion and dislodgement rates, using the results of Step 1 to predict DW. Step 2 was conducted in two experimental groups at the Tromsø site and one in Frøya.

These steps used different data sets, obtained from the deployments listed in **Table 1** with their corresponding deployment and termination dates, numbers of kelp fronds and numbers of samplings.

Ropes with *S. latissima* seedlings, approximately 5–10 mm long (see Forbord et al., 2020), were hung vertically at the two sites from horizontal long lines on four different deployment dates (see **Table 1**). The seedlings were entwined onto carrier ropes between 1 and 2 m below the surface.

Data Collection

In Step 1 a total of 125 kelp fronds from Tromsø (n = 54) and Frøya (n = 71) were harvested at different sampling dates in 2018 in order to establish and validate a sectional model for predicting dry weight (DW). Between 3 and 13 specimens were harvested each time randomly from the same ropes and, after removal of the stipes, frozen in marked sealed polyethylene bags. Later these sporophytes were thawed, lengths and widths were measured after partitioning each frond into four sections (**Figure 2**). The length and width along each cutting line of each section were recorded. The 125 kelp fronds with four sections each resulted in 500 sections, which were dried at 60°C in a Termaks TS8056 laboratory drying oven on pre-weighed aluminum foils for 48 h until constant weight, and then weighed on a Mettler Toledo MS204TS analytical balance. The DW was calculated for each section.

In Step 2 a total of 131 kelp fronds from the two Tromsø deployments in 2018 (n = 48 and n = 33) and the Frøya site (n = 50) were individually followed every 2–3 weeks throughout the growing season, using the punch-hole technique (Parke, 1948). At each time point, total frond length and width were measured as well as the distances between all punched holes. Due to the small size of the fronds at the start of the experiment the first hole was punched 5 cm from the holdfast for repeated *in situ* measurements on the same individuals over the experimental period. New punch-holes where made at each sampling date and the distance relative to the previous punch-hole, which represents length increment, was measured. Kelp fronds which were lost before the second sampling period were either excluded from further analysis or replaced with new individuals. Growth and erosion in terms of length were calculated as described by Lüning (1979), Tala and Edding (2005), and Dean and Hurd (2007). The distance between older holes from previous sampling dates was compared with the previously measured distance. Where an elongation between older holes of the frond was measured (Suzuki et al., 2008), this additional elongation was included in the length increment for the sampling period and was contrasted with the initial length increment between the two holes closest to the meristem.

All *in situ* measurements of total frond length and width and the changes in the distance between the punch-holes from the stipes and those between the holes following the previous sampling were registered in a database for each marked individual.

Complementary Data From 2017 and 2018

Additional data for whole kelp sporophytes were obtained for 2017 from Forbord et al. (2020), including tissue dry weight content (%DW of WW), tissue nitrogen content (Q_N, mg N g^{-1} DW), tissue carbon content (Q_C, mg C g^{-1} DW), Q_C/Q_N ratio (C/N ratio) and biofouling. For individuals seeded in February 2017 the mean maximum length was approximately 60 cm at Frøya and approximately 100 cm in Tromsø (**Figure 2** in Forbord et al., 2020). At harvest the holdfast had a length of 9 and 17 cm, respectively, in Frøya and in Tromsø. The main fouling organisms were initially filamentous algae and thereafter the bryozoan *Membranipora membranacea* at Frøya, and initially filamentous algae followed by the hydroid *Obelia geniculate* and *M. membranacea* in Tromsø (Figures 8, 9 in Forbord et al., 2020). Additional data were obtained for Tromsø in 2018 from Matsson et al. (2021), for C/N ratios and biofouling. These data were used for interpretation of results and in calculations of carbon export following Step 2 of the analysis.

The relative tissue DW content for whole sporophytes in 2017 ranged from 13.9 to 23.6% of WW in Frøya and from 12.4 to 22.6% of WW in Tromsø (**Supplementary Table 2**). The highest values in Frøya were detected in the months June, July and August and may be caused by heavy biofouling in the late season. Also, these values were based on thawed material and therefore some water could be lost in the process compared to fresh material.

Carbon content ($Q_C \pm$ 95%ME) was 26.6 $\pm$ 0.9% and 23.8 $\pm$ 1.1% of dry matter, respectively, for kelp from Frøya and Tromsø, where 95%ME stands for the margin of error that is

TABLE 1 | Experimental groups, categorized according to date of deployment and sampling program.

Site	Step	Deployment (dd/mm/yy)	Number vertical ropes	Deployed number of kelp	Number of kelp fronds analyzed	Number of samplings	Terminated (dd/mm/yy)
Frøya	1	25/01/18	5	54	54	6	18/08/18
Tromsø	1	18/02/18	5	71	71	10	18/09/18
Frøya	2	25/01/18	5	50	50	5	07/08/18
Tromsø	2	18/02/18	5	50	48	7	13/08/18
Tromsø	2	18/04/18	7	42	33	5	13/08/18

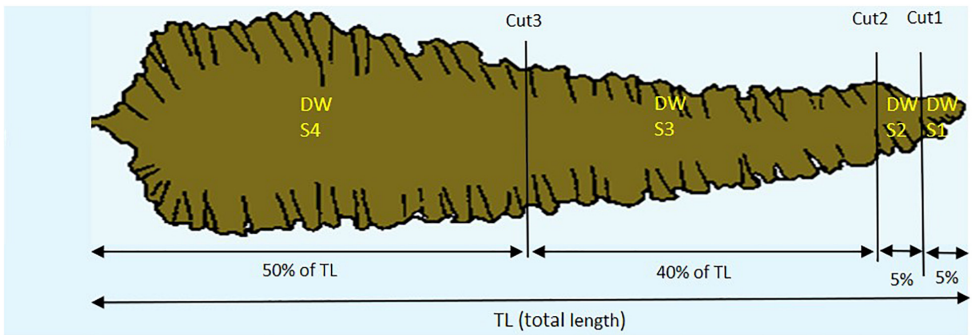

FIGURE 2 | The four sections (S1, S2, S3, and S4) of kelp fronds, e.g., S4 is always 50% of total length (TL), S1 is always 5% of TL.

added and subtracted from the estimated mean to give a 95% confidence interval for the mean. The 95% confidence intervals in **Supplementary Table 3** showed that Q_C did not vary significantly across the months.

The range of nitrogen content ($Q_N \pm$ 95%ME) was from 1.7 ± 0.3% in May to 4.0 ± 1.8% in August for Frøya, and from 1.6 ± 0.4% in August to 3.6 ± 0.3% in April for Tromsø (**Supplementary Table 3**). The highest Q_N value from August from Frøya was most probably the effect from heavy biofouling. The 95% confidence intervals in **Supplementary Table 3** show that Q_N varied significantly between April and early May compared to the remaining months from Frøya, and from April and May compared to the remaining months from Tromsø.

The C/N ratio for Frøya (**Supplementary Figure 1A**) had a steep increase in May 2017 from just below 9 to over 14 by the middle of May, and was constantly that high until a decline in August which coincided with heavy biofouling and loss of sporophytes. In Tromsø the C/N ratio was not above 10 before the middle of June 2017 and June 2018 and increased to a maximum close to 16 in August 2017 and 38 in August 2018. In Tromsø the C/N ratio increased approximately 2 months later than in Frøya (**Supplementary Figures 1C,E**).

Percentage cover from biofouling (**Supplementary Figure 1B**) on kelp fronds increased rapidly in Frøya from below 5% in May to 40% by the end of June. After June, the fronds in Frøya were heavily damaged from biofouling and no further analysis could be conducted. In Tromsø the onset of biofouling in 2017 was one month later than in Frøya, and coverage was below or close to 5% of frond area until the middle of July. Even in August kelp fronds in Tromsø had a coverage just slightly above 20%. In 2018 biofouling is reported as number of epibionts m^{-2}, and the numbers are not directly comparable to 2017. Nevertheless, the data for biofouling (**Supplementary Figures 1D,F**) show the same trend as in 2017 with a notable increase as late as in the middle of August.

Calculating Losses, Expected Increments, and Expected Length

In the case of the data for Step 2, suppose a particular kelp frond is sampled at times t_0, t_1,. . ., t_k. The expected length increment of the frond between samplings at times t_{i-1} and t_i, denoted by ΔL_i, is the increment from the punch-hole closest to the base minus 5 cm, plus the additional elongation between all the older holes in the frond for that period. The observed length at time t_i, denoted by OL_i, is the measured length of the frond. The expected length at time t_i, denoted by EL_i, is calculated by adding the expected length increment to the observed length from the previously measured length:

$$EL_i = OL_{i-1} + \Delta L_i.$$

Length loss at time t_i, denoted by LL_i, is computed by subtracting the observed length from the expected length, both at time t_i:

$$LL_i = EL_i - OL_i$$

The total expected length increment of the frond for the whole experiment is termed grown length and is the sum of all expected length increments:

$$GL = \sum_{i=1}^{k} \Delta L_i$$

Expected length increments, length losses and grown length were calculated for each individual kelp for each sampling period. Since erosion starts from the distal part of the frond it was possible to recalculate what percentage of the frond was eroded compared to the expected length. For each erosion event for all individual fronds during each sampling period, a classification was made of the involved sections S1 through S4 (**Figure 2**). When all four sections were lost, the loss was classified as dislodgement.

Statistical Analysis

The data from Step 1 were used to establish and validate sectional models for predicting DW, using regression analysis on each of the four sections. The aim was to find the best model for predicting erosion and dislodgement expressed as DW on the basis of available biometrical data (length and width) and the number of days since deployment in the sea. An important underlying consideration was that it was not possible to measure precise width data for each eroded part of the frond during each erosion event because sampling in the sea cannot be performed daily. However, based on the 500 dried sections from the complete sporophytes it was possible to simulate erosion and to investigate how much predictive power the regression model would gain or lose with or without width data.

For each of the two sites, four regression models were fitted on the sectional data, thus eight models in total, after log-transforming all the biometric variables DW, length and width, but leaving days untransformed. Furthermore, in each of the eight cases, an additional model was fitted excluding the variable width for the reason described above. The results from the regression analyses were inspected for interaction to check if data from Tromsø and Frøya and from different deployment dates could be pooled.

In order to gauge the additional benefit of including width as a predictor, a simulation exercise was conducted, where sections were randomly deleted, in order to simulate loss of plant sections. More specifically, of the 500 sections, 190 sections were randomly deleted to simulate loss: 30 of Section 1s, 50 of Section 2s (which implies 50 of Section 1s as well) and 20 of Section 3s (which implies 20 of Section 2s and 20 of Section 1s as well). Using the 310 simulated "retained" sections, the regression models were separately fitted again, and their results used to predict the DW of the "lost" sections, thus providing an estimate of "lost" DW which could be compared with the actual known DW of those "lost" sections. An estimate of relative error of prediction was obtained for this simulation by summing the DW predictions and comparing with the sum of the actual DW values, then expressing the relative error as a percentage:

$$\text{relative error} \;=\; 100 \;\times\; (\text{actual DW} \;-\; \text{predicted DW})/\text{actual DW}$$

This exercise was repeated 1000 times, each time deleting a different random subset of 190 sections, thus leading to 1000 estimates of the relative error. Doing this using all the predictors, length, width and days, and doing it again without the predictor width, gave an indication of how much predictive power was being lost by not taking width into account.

An important issue was that the log-transformed estimates for predicted DW needed to be back-transformed including the back-transformation correction for the lognormal distribution (Dambolena et al., 2009; Greenacre, 2016), using the antilog (exponential) of the mean plus half of the regression error variance s^2 for each estimate. That is, if log(DW) was a predicted DW on a logarithmic scale for a particular section, then the estimated DW was back-transformed as:

$$\text{DW} \;=\; \exp[\log(\text{DW}) \;+\; {}^1\!/_2 S^2]$$

In the case of Step 2, the respective models established in Step 1 above, using only length and days as predictors, were used to predict the various DWs of the 131 growing kelp fronds, based on the expected length estimates EL_i and lost lengths LL_i defined in Section "Complementary Data From 2017 and 2018." This provided estimates of production, erosion and dislodgement over time, which also could be used to compute growth and erosion rates. All percentages of losses of DW here are referring to lost DW compared to produced DW.

The average individual rates can give results which might deviate from those estimated from the combined data for the whole stock. Therefore, the specific growth and erosion rates were calculated from the sum of stock data for each experimental group. The growth rate GR_i was estimated as:

$$\text{GR}_i \;=\; \frac{\log(\frac{\text{EW}_i}{\text{OW}_{i-1}})}{(t_i - t_{i-1})}$$

where EW_i is the sum of expected DW for all the kelp at time t_i, and OW_{i-1} is the sum of observed DW for all kelp at the previous time t_{i-1}. The rates on a log-scale were back-transformed to compound rates as percentages to give a specific growth rate (SGR) per day:

$$\text{SGR}_i \;=\; 100\;(e^{\text{GR}_i} - 1)$$

The SGR divided by 100 is the equivalent of the compound rate p in the growth formula:

$$\text{GR}_i \;=\; \text{GR}_{i-1}\left(1+p\right)^{(t_i - t_{i-1})}$$

The specific erosion rate (SER) was calculated in a similar way:

$$\text{ER}_i \;=\; \frac{\log(\frac{\text{OW}_i}{\text{EW}_i})}{(t_i - t_{i-1})}$$

$$\text{SER}_i \;=\; 100\;(e^{\text{ER}_i} - 1)$$

Erosion rates are zero or negative and comprise only kelp fronds that have not dislodged.

The specific dislodgement rate (SDR) is the rate at which kelp biomass is lost due to dislodgement of whole kelp sporophytes. SDR is estimated for the whole stock at each sampling point as

follows, where DW_i is the DW of the dislodged kelp at time t_i:

$$DR_i = \frac{\log(\frac{(EW_i - DW_i)}{EW_i})}{(t_i - t_{i-1})}$$

$$SDR_i = 100\,(e^{DR_i} - 1)$$

Notice that EW_i includes all eroded and dislodged kelp at time t_i.

To obtain a measure of variability in each of the above estimates, the individual data were bootstrapped 1000 times (i.e., sampled with replacement), leading each time to different values of EW_i, OW_i and DW_i, and thus different values of the respective rates defined above. Confidence intervals could thus be established by identifying the 2.5 and 97.5% quantiles of the bootstrapped rates in each case.

Specific growth, erosion and dislodgement rates were also calculated for individual kelp in the same way.

RESULTS

Sectional Regressions

For the 125 fronds that were sectioned and weighed (54 from Frøya and 71 from Tromsø), four regressions were performed separately for the two sampling areas, predicting mean log-DW from log-length and log-width for the four respective sections as well as days since deployment:

$$\text{Mean}[\log(DW_{Sj})] = c + a_L \log(L_{Sj}) + a_W \log(W_{Sj}) + a_D \text{Days}$$

where the subindex Sj indicates section j (j = 1,. . .,4) − see **Figure 2**.

The whole exercise was repeated omitting log-width, using only log-length and Days as predictors.

There were significant differences between the Frøya and Tromsø models to keep them separate. In addition, there were also differences in the regression coefficients between sections, so it was decided to maintain four sectional regressions in each case.

The results of the simulation exercise in Step 1 and the relative errors of the predictions of total loss of DW for the 125 fronds are shown graphically in two different forms in **Figures 3B**, **4B**, with or without log-width included as a predictor, as well as days since deployment in both cases.

In **Figure 3A**, when log-width is included, the scatterplot shows more agreement between predicted and actual DWs at lower values, with the relative percentage errors over the 1000 simulations lying in an interval (of 95% of the errors) from -22.7% (over-predicted) to 20.5% (under-predicted). When log-width is excluded (**Figure 4A**), the scatterplot is more spread out at the lower values, and the corresponding interval is from -23.7 to 28.3%. Even though this represents an 8.8 percentage point worsening of the predictive quality, it is mostly due to the larger inaccuracies in smaller predictions, which give high relative errors. For Step 2 we will, in any case, only be able to take length into account, but the above exercise shows that being unable to use width is not a too serious drawback.

The regression models, including p-values, R^2 (percentages of explained variance) and s^2 (regression error variances, used in the back-transformation from means on log-scale to original scale of DW in g) were estimated as follows, now using the data for all 500 sections of the 125 fronds:

For Frøya:

$$\text{S1}: \log(\text{DW}) = -7.668 + 1.296 \log(\text{Length}) + 0.0207\ \text{Days} \quad R^2 = 58.7\%,\ s^2 = 0.854$$
$$(p = 0.001) \qquad (p < 0.0001)$$

$$\text{S2}: \log(\text{DW}) = -7.260 + 1.347 \log(\text{Length}) + 0.0200\ \text{Days} \quad R^2 = 66.4\%,\ s^2 = 0.720$$
$$(p < 0.0001) \qquad (p < 0.0001)$$

$$\text{S3}: \log(\text{DW}) = -8.848 + 1.713 \log(\text{Length}) + 0.0227\ \text{Days} \quad R^2 = 84.0\%,\ s^2 = 0.520$$
$$(p < 0.0001) \qquad (p < 0.0001)$$

$$\text{S4}: \log(\text{DW}) = -8.608 + 1.979 \log(\text{Length}) + 0.0151\ \text{Days} \quad R^2 = 92.8\%,\ s^2 = 0.282$$
$$(p < 0.0001) \qquad (p < 0.0001)$$

For Tromsø:

$$\text{S1}: \log(\text{DW}) = -6.637 + 1.883 \log(\text{Length}) + 0.0113\ \text{Days} \quad R^2 = 65.4\%,\ s^2 = 0.713$$
$$(p < 0.0001) \qquad (p = 0.0009)$$

$$\text{S2}: \log(\text{DW}) = -5.770 + 1.747 \log(\text{Length}) + 0.0082\ \text{Days} \quad R^2 = 61.1\%,\ s^2 = 0.674$$
$$(p < 0.0001) \qquad (p = 0.009)$$

$$\text{S3}: \log(\text{DW}) = -6.392 + 1.774 \log(\text{Length}) + 0.0057\ \text{Days} \quad R^2 = 68.7\%,\ s^2 = 0.532$$
$$(p < 0.0001) \qquad (p = 0.02)$$

$$\text{S4}: \log(\text{DW}) = -4.904 + 1.458 \log(\text{Length}) + 0.0056\ \text{Days} \quad R^2 = 73.4\%,\ s^2 = 0.404$$
$$(p < 0.0001) \qquad (p < 0.003)$$

The above set of eight equations are used to estimate DW in Step 2 where the evolution of 131 sporophytes at Frøya and Tromsø are followed over time using the punch-hole procedure.

Growth and Loss Measured by Dry Weight

Production, loss and standing biomass of DW increased at all sites during the growing season (**Figure 5**). Lost DW until the middle of June was approximately 8% of production in Frøya (**Figure 5A**) and for the February deployment in Tromsø (**Figure 5B**). Then, losses caused by dislodgement increased to 49.4% of produced kelp in Frøya, and by August the biomass did not increase, indicating that the production rate in July and August was equivalent to the loss rate. Furthermore, in Frøya a substantial fraction of the biomass in August comprised of epibiotic biofouling organisms (see **Supplementary Figure 1B**) and not only kelp tissue (Matsson et al., 2019; Forbord et al., 2020). Dislodgement of whole plants occurred both by holdfast loosening from the ropes and complete break-off close to the stipes.

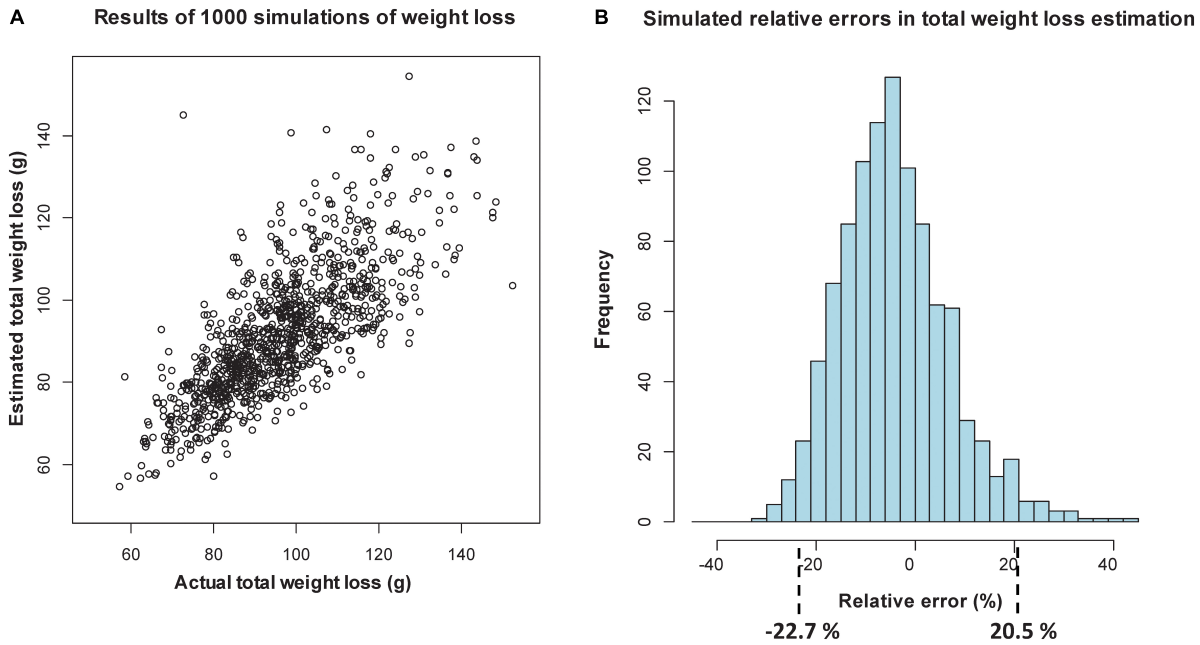

FIGURE 3 | Simulation of relative percentage errors from 1000 simulations of loss, using sectional regression models with length, width data and days from deployment as predictors: scatterplot of estimated versus actual total weight loss **(A)**, and histogram of the relative percentage errors, showing intervals that include 95% of the values **(B)**.

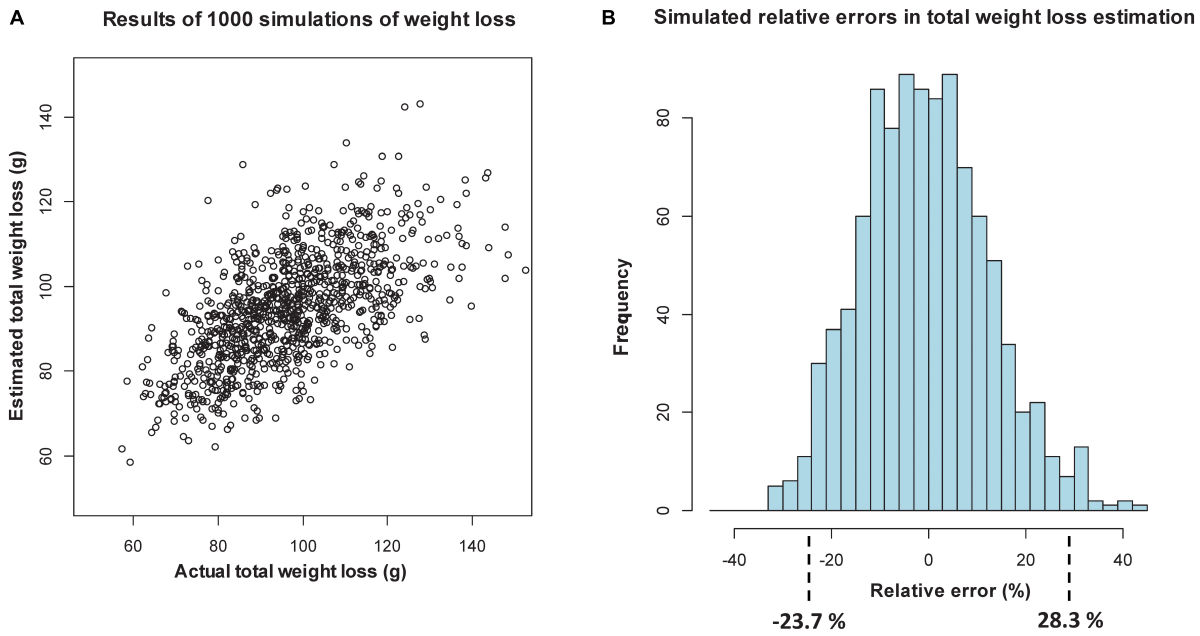

FIGURE 4 | Simulation of relative percentage errors from 1000 simulations of loss, using sectional regression models with only length data and days from deployment as predictors: scatterplot of estimated versus actual total weight loss **(A)**, and histogram of the relative percentage errors, showing intervals that include 95% of the values **(B)**.

From the start of the experiments until the middle of August losses were below 18% in both Tromsø deployments. The data show that the produced DW in the later deployment in April was lower than for the February deployment.

For most months, Specific erosion rates were relatively similar between the deployments in Frøya and Tromsø February (**Table 2**). In August, the SDR increased sharply in Frøya and the data clearly showed that the heavy

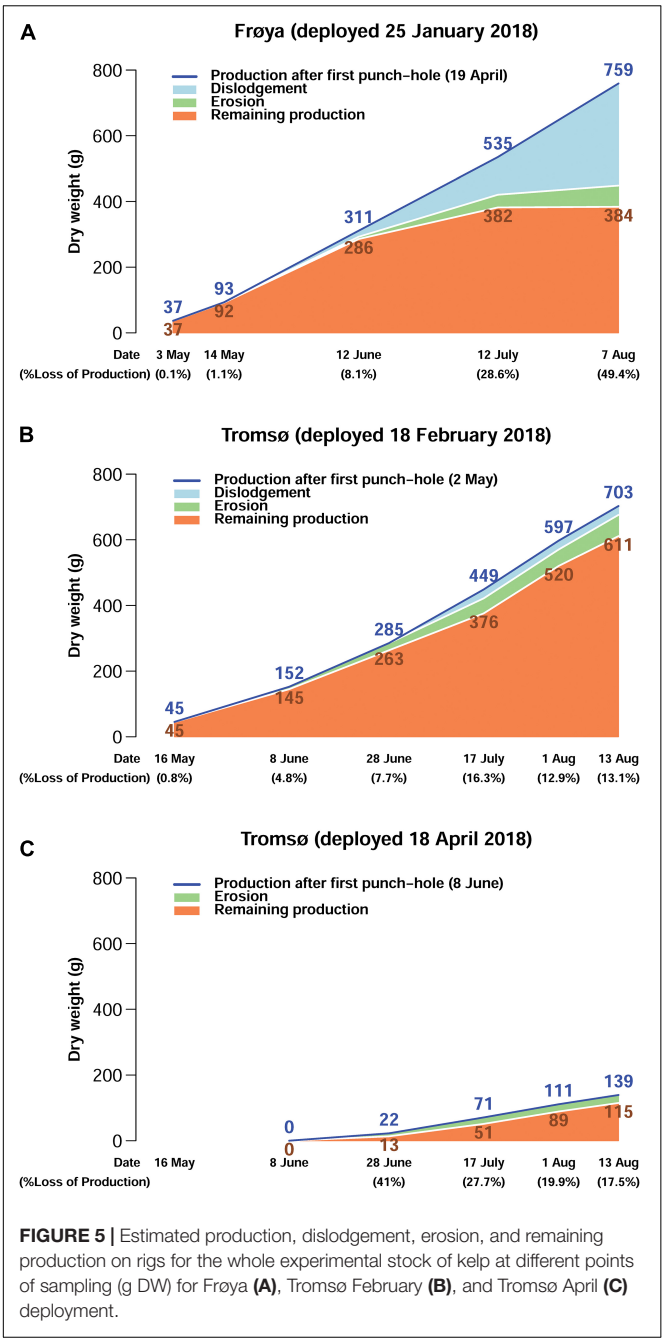

FIGURE 5 | Estimated production, dislodgement, erosion, and remaining production on rigs for the whole experimental stock of kelp at different points of sampling (g DW) for Frøya **(A)**, Tromsø February **(B)**, and Tromsø April **(C)** deployment.

losses in Frøya were related to the dislodgement of whole sporophytes.

The SERs and SDRs for the whole experimental period are also shown in **Table 2**. The overall SERs [mean (95% CI)] were −0.075 [−0.13, −0.04]% day^{-2} and −0.086 [−0.118, −0.05]% day^{-2} for Frøya and for Tromsø February deployment, respectively. The overall SDRs were −0.432 [−0.70, −0.26]% day^{-2} for Frøya, and −0.035 [−0.09,−0.00]% day^{-2} for Tromsø February deployment. By testing the differences between these rates for Frøya and Tromsø with bootstrapping tests it was shown that erosion rates were not significantly different (**Figure 6A**), while dislodgement rates were significantly different ($p < 0.001$) (**Figure 6B**).

To make data from these sites comparable in an aquaculture perspective, erosion, growth, and production at the optimal time for harvest, e.g., June in Frøya and August in Tromsø should be compared. At the time of harvest in Frøya, the accumulated loss of DW was only 8% of total production (**Table 3**).

When comparing the February and April deployments in Tromsø (**Table 4**), results show that the initial erosion rate was high in the April deployment but fell off to low similar levels as the February deployment. Growth rates and losses were of similar magnitude. For the April deployment no dislodgement occurred.

Loss of Frond Sections and Dislodgement

In **Figure 7** it is shown that 40–100% of the distal part of the kelp fronds were partially eroded between every sampling date, except for Frøya (A) in May. On 8 June all the fronds showed erosion in Tromsø's February deployment. Still, the biomass effected here was very small because only 31% of the complete sections S2 (also including sections S1), and 34% of complete sections S1 had been lost. Another 35% of sections S1 were only slightly eroded.

The distal sections S1 and S2 together represent 10% of the length of any sampled frond. Generally, less than 30% of all sections S2 were eroded during each sampling period which gave rise to little erosion.

This pattern of tissue loss was consistent for all sites and sampling periods, except from Frøya. In Frøya, dislodgement rapidly increased to 14% in June, 28% in July and 48% in August (**Figure 7A** – Sections 4). These percentages refer to the standing stock at the beginning of each sampling period. Hence, the accumulated loss for these 2 months in Frøya was 68% of all sporophytes and was caused by dislodgement of complete fronds. In contrast, kelp deployed in Tromsø did not show any loss of the largest frond sections S3 and S4 for either June or August.

Increment of Length Between Punch-Holes

For sporophytes attached on the ropes throughout the whole experimental period, a significant increment of length between older punch-holes beyond the meristem was found in all data sets from 2018. However, these length increments mainly appeared between the newest and the previous punch-hole (**Table 5**). The reason for this could be that the newest hole was punched slightly inside the meristem and that growth occurred on both sides. Almost no additional increment was registered beyond the two holes closest to the meristem.

Growth and Loss Measured by Changes in Length Increment

Analysis of length data revealed that sporophytes at the rigs in Frøya showed heavy losses after June (**Table 6**) while both Tromsø deployments were much less affected. If one uses the ratio of lost length (LL) over produced length (LG_E) (last column in **Table 6**), Frøya showed higher length loss by August than total seasonal length production.

TABLE 2 | Comparison of specific rate of erosion (SER) and dislodgement (SDR) between Frøya and Tromsø February deployment (for selected months), and for the whole experimental period.

Days from deployment			SER [% day^{-1}] [95% CI]		SDR [% day^{-1}] [95% CI]	
Month	**Frøya**	**Tromsø**	**Frøya**	**Tromsø**	**Frøya**	**Tromsø**
May	**109**	**87**	**−0.060** [−0.13, −0.02]	**−0.026** [−0.04, −0.01]	**0**	**0**
June	**138**	**110**	**−0.055** [−0.08, −0.03]	**−0.147** [−0.23, −0.10]	**−0.175** [−0.35, −0.05]	**0**
July	**168**	**149**	**−0.191** [−0.34, −0.09]	**−0.268** [−0.53, −0.09]	**−0.614** [−1.08, −0.26]	**−0.301** [−0.79, 0.00]
Aug	**194**	**164**	**−0.153** [−0.34, −0.05]	**−0.047** [−0.07, −0.03]	**−1.332** [−2.50, −0.66]	**0**
All period	**194**	**176**	**−0.075** [−0.13, −0.04]	**−0.086** [−0.118, −0.05]	**−0.432** [−0.70, −0.26]	**−0.035** [−0.09,−0.00]

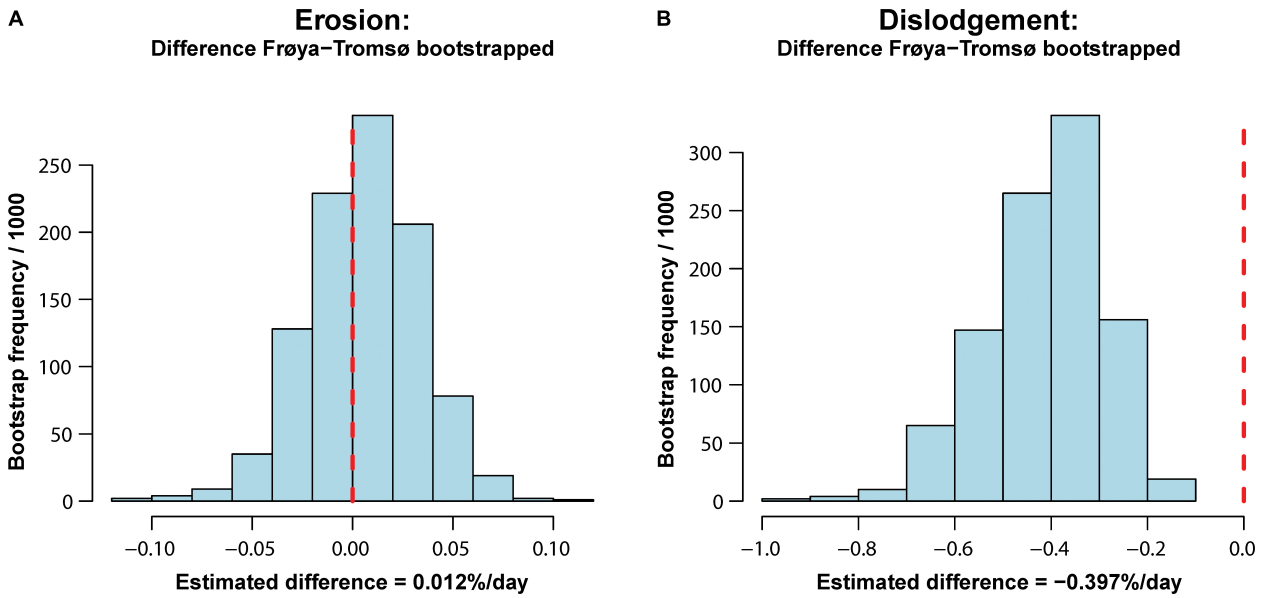

FIGURE 6 | Histograms showing outcome from bootstrap tests of difference in erosion **(A)** and dislodgement **(B)** over the whole experimental period. The vertical dashed line shows the null hypothesis of no difference.

TABLE 3 | Comparison of accumulated loss and SGR between Frøya and Tromsø February deployment for selected months and also showing 95% confidence intervals (CI) for the estimates.

	Accumulated loss (%) [95% CI]		SGR (% day^{-1}) [95% CI]	
Month	**Frøya**	**Tromsø**	**Frøya**	**Tromsø**
May	**1.13** [0.4, 2.5]	**0.80** [0.4, 1.4]	**4.27** [4.08, 4.45]	**4.24** [4.00, 4.47]
June	**8.12** [3.9, 14.1]	**4.81** [3.2, 7.5]	**3.11** [2.82, 3.38]	**3.16** [2.87, 3.41]
July	**28.62** [17.7, 41.8]	**16.24** [8.6, 26.6]	**1.68** [1.34, 2.02]	**2.19** [1.88, 2.48]
Aug	**49.43** [34.4, 70.8]	**12.90** [7.0, 21.2]	**1.59** [1.05, 2.13]	**1.98** [1.87, 2.09]

TABLE 4 | Comparison of specific rates of erosion (SER), dislodgement (SDR), and growth (SGR) between Tromsø February and Tromsø April deployments.

Sample date	SER (% day^{-1}) [95% CI]		SDR (% day^{-1}) [95% CI]		SGR (% day^{-1}) [95% CI]	
(**All tromsø**)	**Deployed feb.**	**Deployed april**	**Deployed feb.**	**Deployed april**	**Deployed feb.**	**Deployed april**
28 June	**−0.221** [−0.41, −0.08]	**−0.634** [−1.08, −0.29]	**0**	**0**	**2.56** [2.28, 2.81]	**1.74** [1.28, 2.20]
17 July	**−0.268** [−0.53, −0.09]	**−0.495** [−0.89, −0.21]	**−0.301** [−0.79, −0.00]	**0**	**2.19** [1.88, 2.48]	**2.87** [2.47, 3.30]
01 Aug	**−0.047** [−0.07, −0.03]	**−0.112** [−0.21, −0.05]	**0**	**0**	**1.98** [1.87, 2.09]	**2.16** [1.73, 2.51]
13 Aug	**−0.181** [−0.32, −0.07]	**−0.107** [−0.16, −0.06]	**0**	**0**	**1.41** [1.16, 1.65]	**1.51** [1.27, 1.76]

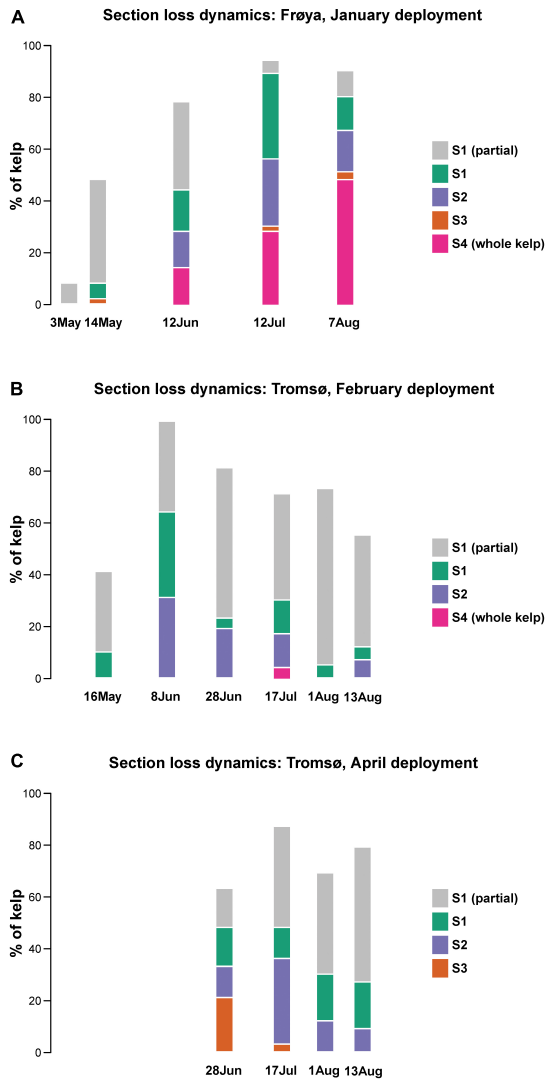

FIGURE 7 | Loss of sections in **(A)** Frøya, **(B)** Tromsø, February deployment, and **(C)** Tromsø, April deployment.

The length loss for kelp fronds in Frøya was 142% of the gross length growth. Hence, some of the initial kelp from before application of the first punch-hole in May was lost. But in terms of DW Frøya lost 49.4 [34.4, 70.8]% of gross growth. Consequently, the interpretation of length data has limitations which the comparison from losses based on DW underlines.

DISCUSSION

Dynamics of Loss and Production

Analyses of length data show that the losses observed in our experiments are mainly of two types, distal erosion, and dislodgement of whole sporophytes. Parts of seaweed fronds may also break off without complete dislodgement (Zhang et al., 2012), but this occurred only to a small extent in the present study. During the main growing season for kelp aquaculture production from February to June, the continuous partial erosion of the distal parts from most sporophytes included less than 10% of the total frond length with low DW. This resulted in low specific erosion rates (SER). The April deployment in Tromsø showed higher SERs in June but these were low again in August to levels around 0.1% day^{-1}. For the kelp that was deployed early in the season, specific growth rates (SGR) largely exceeded the erosion rates during this period. High growth and low erosion rates ensured high production and a steady increase of standing biomass like in natural kelp forests (Dean and Hurd, 2007; Krumhansl and Scheibling, 2011; Nielsen et al., 2016b), and for aquaculture rigs (Yoshikawa et al., 2001; Zhang et al., 2012).

At the Frøya site, which is more than 800 km south of Tromsø, losses were from June on primarily due to the dislodgment of entire kelp fronds resulting in high specific dislodgement rates (SDR), but only a slightly increased specific erosion rate. In Tromsø, the SDR stayed low until the end of the growing season. These results are different from what Zhang et al. (2012) reported where erosion was the main cause for loss of biomass. The currents in Tromsø and Frøya are of moderate strength, and both sites are sheltered from wave exposure. Reported dislodgement velocity and dislodgement wave height for *Saccharina* sp. are higher than generally observed at these sites (Kawamata, 2001; Buck and Buchholz, 2005). Hence, one would not expect that hydrodynamic forces alone would lead to dislodgement of the sporophytes.

Given that the development regarding biofouling, temperature and C/N ratio in 2017 was similar as in 2018, temperature and the intensity of biofouling are expected to be lower in July and August in Tromsø than in Frøya. Also, the C/N ratio would increase 6 weeks later in Tromsø than at the site in Frøya. Biofouling has been recognized as a plausible cause for kelp loss (Scheibling and Gagnon, 2009; Andersen et al., 2011; Krumhansl and Scheibling, 2011). In our experiments the season for onset and increase of biofouling also coincided with the rise in kelp loss. Furthermore, *S. latissima* is a cold-water species, experiencing reduced tissue strength after exposure to 14°C for 3 weeks (Simonson et al., 2015). Temperatures at this level were never reached at the site in Tromsø during the experiment, while in Frøya median temperatures rose above 14°C in August 2017. A possible weakening of tissue in Frøya can act synergistically with biofouling and cause dislodgement. It has been suggested that seaweeds in general are more sensitive to environmental changes, like biofouling, when their intracellular nitrogen reserves are exhausted (Gerard, 1997; Gao et al., 2013). The nutritional history of the sporophytes is of great importance for their ability to take up available nutrients and sustain growth when the ambient nutrient concentration becomes limiting (Forbord et al., 2021), happening earlier in the south compared to the north of Norway due to the phytoplankton blooming in a south to north gradient (Broch et al., 2019). The weakening caused by these factors can increase losses due to mechanical stress from handling in kelp farms.

Increased SDR and SER in Frøya led to a loss of gross produced biomass of 49% by August, while the February deployment in Tromsø accounted for 13% loss of gross production. To avoid

TABLE 5 | Accumulated observed length increment (mean ± 95% ME) for non-dislodged kelp for the whole experimental period, means in bold.

	Growth between newest punch-hole and		
Site, deployment	**Base (cm)**	**Distal end of frond (cm)**	**Previous punch-hole (cm)**
Frøya	**73.1** ± 7.8	**8.9** ± 3.3	**8.9** ± 3.3
Tromsø, February	**85.0** ± 6.5	**20.2** ± 3.9	**18.7** ± 3.5
Tromsø, April	**45.3** ± 3.8	**7.7** ± 2.7	**5.1** ± 2.7

TABLE 6 | Expected length growth (LG_E), length loss (LL), total expected length (LT_E) in cm (mean ± 95% ME), and loss as percent of expected length growth, means in bold.

	To June				To August			
Site, deployment	**LG_E (cm)**	**LL (cm)**	**LT_E (cm)**	**LL/LG_E**	**LG_E (cm)**	**LL (cm)**	**LT_E (cm)**	**LL/LG_E**
Frøya	**45.6** ± 4.9	**−17.9** ± 8.0	**109.4** ± 9.5	**−39%**	**64.0** ± 8.7	**−91.0** ± 14.3	**129.6** ± 11.6	**−142%**
Tromsø, February	**59.3** ± 6.1	**−13.8** ± 6.1	**92.3** ± 8.0	**−23%**	**105.2** ± 9.8	**−33.2** ± 8.8	**137.6** ± 11.1	**−32%**
Tromsø, April	**11.9** ± 2.7	**−10.1** ± 4.8	**47.2** ± 8.5	**−85%**	**52.9** ± 4.1	**−26.1** ± 4.5	**97.2** ± 5.3	**−49%**

Length growth measured from date of first punch-hole.

heavy losses and reduced quality of the kelp, the farmers in Frøya are usually harvesting the kelp before the middle of June. In Tromsø, loss due to erosion and dislodgement was moderate throughout the whole growing season and the farmers could harvest the biomass until August, allowing for an extended growing season which would increase total harvested yield. When comparing growth and production at the appropriate time for harvest which is before the middle of June in Frøya, the accumulated loss of dry weight was only 8% of total production.

Losses between 8 and 13% dry matter of annual production in aquaculture is a much lower figure than losses observed for natural kelp forests that often turn over most of its biomass yearly due to both frond erosion, dislodgement and lamina casts (Tala and Edding, 2005; Krumhansl and Scheibling, 2011; Nielsen et al., 2016b; Pedersen et al., 2020). However, these natural forests consist of kelp of all ages while cultivated kelp are all less than one year old. The relevant loss rates for the cultivated kelp fronds are the losses before harvesting. This can be influenced by the seaweed farmer who can initiate harvest before biofouling has reached destructive levels, and before the structures of sporophytes are weakened by either aging, high temperatures or low nitrogen levels, all of which can lead to lower resistance against mechanical stress during handling. If the kelp biomass is not harvested in due time, extremely high dislodgement rates can be observed. The specific rate of loss in Frøya in August was 1.55% day^{-1}. With such losses one would lose close to 40% of the standing biomass within one month and over 75% within 3 months. In fact, losses of 100% have been observed when inspecting rigs later in the season.

When compared with other studies on cultivated kelp, the losses observed here are substantially lower. Losses of 43 and 58% of WW for June and July, respectively, have been reported before harvest for cultivated *S. japonica* (Zhang et al., 2012). Suzuki et al. (2008) refer to erosion rates (WW) with maximum losses between 2.4 and 3.7 g day^{-1}. For kelp in our experiment, losses would not exceed 0.25 g day^{-1} in Frøya before the month of July and never got this high in Tromsø. For the culture of *U. pinnatifida,* 19% of produced tissue C and 33% of produced tissue N were lost before harvest (Yoshikawa et al., 2001). Both cited studies conclude that kelp aquaculture is releasing a substantial amount of organic matter to the environment.

Export of Dry Matter, Carbon, and Nitrogen From Kelp Rigs and Ecological Implications for Aquaculture

The detrital production from cultivated kelp can be calculated based on growth, erosion, and dislodgement rates, as presented in this study. The calculations presented here are scenarios for two typical cases of normal production for harvest in Frøya and Tromsø, and one worst-case scenario from Frøya where the rigs would be harvested as late as August. These cases are projected to commercial scale kelp farms. Optimal timing of harvest will depend on the market perspective but would biologically be in June in Frøya and in August in Tromsø. It would in the example we have chosen in our scenario, yield approximately 100 tons of harvestable dry matter of kelp per year which is equivalent to 652 tons wet kelp in Frøya and 765 tons wet kelp in Tromsø (**Table 7**). The measured average DW content in 2017 in Tromsø (15%) was lower than in Frøya (19%) and explains why more produced WW is incorporated in the equations for Tromsø. This difference is probably caused by the early onset of biofouling in Frøya. For the worst-case scenario, 98 tons out of 198 produced tons of dry matter could be lost in Frøya (**Table 7**).

A kelp farm covering an area of 4 hectares with rigs could produce the above-mentioned quantities of kelp biomass with a production of roughly 200 tons wet kelp per hectare (Broch et al., 2019). The annual detrital production from our scenarios would be between 63 and 88 g C m^{-2} and 5 and 8 g N m^{-2} of the area covered by the kelp farm. In the worst-case scenario, the losses would contribute with 643 g C m^{-2} and 83 g N m^{-2} of detritus in the production area. During normal production, these export figures are 5 to 8 times lower than detritus production from natural kelp forests of *L. hyperborea* with an estimated

TABLE 7 | Export scenarios from kelp rigs for 100 tons harvestable dry matter per production season.

Site (harvest month)	Harvest DW	Produced WW	Produced DW	Loss of DW	Loss of C	Loss of N
Frøya (June)	100	652	108.8	8.8	2.3	0.2
Tromsø (August)	100	765	114.8	14.8	3.5	0.3
Frøya (August)	100	1058	197.8	97.8	25.7	3.3

All numbers in tons (C = carbon, N = nitrogen).

detrital production of 478 ± 41 g C m^{-2} $year^{-1}$ in a dense forest outside Tromsø (Pedersen et al., 2020). Global estimates of detrital production from natural kelp forests are between 225 and 750 g C m^{-2} $year^{-1}$ (Krumhansl and Scheibling, 2012). Kelp fragments have a low specific weight and can travel over long distances while slowly sinking toward the bottom (Wernberg and Filbee-Dexter, 2018). Hence, it is likely that sedimentation and thus the carbon input per square meter seafloor will be lower than the calculations above are suggesting. The heavy losses in July and August in Frøya, which are mainly due to dislodgement of whole fronds, will lead to detaching particles of larger size with different properties during the sedimentation processes than eroded tips from fronds. Our experiments also show that substantially lower export of carbon and nitrogen is possible from aquaculture to the environment, than previously published. Zhang et al. (2012) have reported an annual export of 500 g C m^{-2} detritus from culture of *S. japonica* in Sungo Bay. In Frøya the annual release of carbon would be 63 g C m^{-2} which is 12.6% of the value in Sungo Bay. One should here keep in mind that physical conditions, latitude, temperature, the nature of the cultured species, mass culture techniques and adjacent ecosystems are different between China and Norway.

In the same way as for salmon farming, our work illustrates that the export of organic matter from kelp aquaculture installations is highly dependent on its operational management (Carroll et al., 2003). Optimal timing of harvest in the context of market perspectives is the key factor for keeping erosion and dislodgement on lowest possible levels. Heavy losses from kelp farms and inferior quality due to biofouling have a negative effect on the economy and on the environment. The kelp farmers have different means for avoiding biofouling. In Asian aquaculture the farmers deploy summer seedlings in autumn, which allows for an early harvest in the grow-out season in the following year before the onset of biofouling (Lüning and Mortensen, 2015). While this method is used in Frøya, it would result in pure growth in Arctic Tromsø because of the lack of sunlight during the Polar Night. As an alternative, the farmers could keep close control on the coverage of organisms associated with biofouling (Matsson et al., 2019, 2021; Forbord et al., 2020). A high coverage with fouling organisms could in some cases be a warning for destructive biofouling and processes which weaken the tissue, and the harvest should be commenced as soon as possible. The percentage of cover would depend on the commercial interest, e.g., for use of kelp for human consumption, one would ideally want close to no fouling at all. The seaweed farmers have everything to win by choosing the optimal time for harvesting by employing methods for monitoring the extent of biofouling and the nutritional state of the kelp. For sites where the summer sporeling method is not available, an early warning system based on the monitored extent of biofouling and high C/N ratios in the kelp tissue could thus become the key to effective environmental management, maximal harvest yields and minimal environmental impact.

Recently, macroalgae cultivation has been suggested as a contributing solution to climate change mitigation and adaptation as it releases and exports carbon that eventually is buried in the seafloor or exported to the deep sea (Duarte et al., 2017). With an 8–13% loss of biomass as found in this study at early harvest (**Figure 5**), and cultivation volumes as of today in Norway and Europe (<2000 tons WW per year, FAO, 2020) the carbon release would be relatively small, and so would be the environmental footprint and the carbon sequestration potential. Nevertheless, the seaweed cultivation industry is rapidly expanding and Olafsen et al. (2012) projected that Norwegian kelp harvest alone can reach 4 mill tons per year by 2030. If harvested late in the season, which could be relevant for high-volume low-cost production of biomass for chemical components extraction (proteins, carbohydrates, metabolites), the carbon export would increase to 30–50% loss by the end of the growth season (**Figure 5**). Assuming a 30% loss of 4 mill tons harvested biomass the carbon export would be 53,000 tons C per year. For the carbon to be sequestered it needs to be permanently buried and made unavailable for turnover by the biosphere. In a global assessment of the fate of carbon from natural macroalgae forests, it appears that approximately 15% (0–36%) of the exported biomass from macroalgae beds is neither consumed nor decomposed and thus is permanently sequestered (Krause-Jensen and Duarte, 2016). Assuming that this applies to cultivated kelp it corresponds to 8,000 tons C sequestered each year, which again is equivalent to a mitigation potential of 29,000 tons CO_2, or the annual emission of 2,900 average Norwegian citizens (SSB, 2018). If kelp is managed as a high-quality food product with harvest early in the growth cycle, the carbon export and sequestration potential is relatively small. But a late-harvested bulk industrial production could export four to six times as much carbon.

Thus, kelp cultivation represents a nature-based solution for CO_2 drawdown from the atmosphere to be permanently sequestered in the ocean seafloor and provides a potential for using algae cultivation for climate mitigation. Depending on the time of harvest, this process will sequester carbon in amounts directly scalable to the harvested biomass and thereby provide an additional ecosystem service to kelp cultivation as mitigating climate warming. Current publications and scientific speculations suggest that seafloor carbon sequestration from macroalgae is increasingly pronounced at low water

temperatures, which implies that the potential for kelp carbon sequestration increases with higher latitudes (Frigstad et al., 2021). This makes Norway in general and the Tromsø and Barents Sea region in Northern Norway especially interesting as an area for kelp cultivation for carbon sequestration. There are, however, still major uncertainties and knowledge gaps about the proportion of kelp carbon actually sequestrated at the seafloor and in the deep sea, including regional dependencies, the effect of species, the chemical composition of biomass, transport ways, and degradation time in the water column while sinking.

Methodological Findings and Recommendations

A significant increment of length between older punch-holes beyond the meristem was detected in our study. But our data showed that this additional increment mainly occurred between the newest and the second newest punch-hole. This additional increment might be caused by the newest hole being punched slightly inside the meristem, and growth could occur on both sides of the hole. By measuring the distance between all punch-holes, a correction for these increments was applied in this study. To correct for length increment beyond the newest punch-hole we recommend that the length increment between several of the older holes on the frond should also be measured.

The morphological plasticity of *S. latissima* is well known. The species show highly variable biometric traits of the frond which are influenced by the physical conditions of their habitat (Parke, 1948; Lüning, 1979; Gerard, 1987; Bartsch et al., 2008). Consequently, even when measuring the width of the frond along a line where erosion might have occurred, the biometry of lost parts of the fronds cannot be inferred and cannot be used reliably in the calculation of the area of lost dry matter. The only reliable measurement for erosion is the eroded length of the frond, calculated by the punch-hole method. The analysis of the DW of the sections of kelp fronds showed a significant difference in the length to DW relationship for different sections, depending on the distance from the stipes. The application of a general length to DW model (Zhang et al., 2012) or an area specific DW coefficient (Nielsen et al., 2016a), derived from the whole frond, could thus bias the conversion for the distal parts of the fronds of measured length data to DW. The conversion of length to DW for distal tissue described by Tala and Edding (2005) and Krumhansl and Scheibling (2011) is more precise but has the disadvantage of being destructive to the fronds and would rule out the possibility to follow the same individually marked frond through the entire experiment. By applying the sectional regression models presented here, it was possible to predict dry weight of the lost fronds with a relative error of −23.7 to +28.3% without being dependent on width data. Using a randomized loss simulation on our data set, where width along a line between sections was reliably measured, revealed that the relative error by excluding width data was increased by only 8.8% points. As width cannot be measured directly from the lost parts in field experiments, the application of this sectional regression method can be a valuable tool in future erosion experiments.

Our results do not support the observation that specific erosion rates depend on sporophyte size (Sjøtun, 1993) or on temperature (Suzuki et al., 2008). Specific daily dislodgement rates were, with one exception, zero until the middle of August, and specific erosion rates were below −0.27% throughout the experiment with kelp deployed in February in Tromsø. In Frøya, specific erosion and dislodgment rates were close to zero until May, increasing to $-0.2\%\ day^{-1}$ for erosion and $-1.3\%\ day^{-1}$ for dislodgement in August. Broch et al. (2013) discuss that their model was overestimating the size of sporophytes during the summer months and suggest that alternative parameters for erosion (Broch and Slagstad, 2012) should be included.

CONCLUSION

When compared with other studies on cultivated kelp, the losses observed in our experiments are substantially lower. Our work illustrates that the export of organic matter from kelp aquaculture installations is highly dependent on its operational management, e.g., timing of harvest. If the kelp industry is managed for a high-quality food commodity, the carbon export and sequestration potential is relatively small. In contrast, a late-harvested bulk industrial production could export four to six times as much carbon. Based on our data we suggest that regional, season-dependent specific erosion and dislodgment rates be implemented in production models, and that biofouling be included as a parameter in model equations.

DATA AVAILABILITY STATEMENT

The raw data supporting the conclusions of this article will be made available by the authors, without undue reservation.

AUTHOR CONTRIBUTIONS

RF contributed to all aspects and was the primary author. MG was responsible for statistical analysis and graphics and contributed to the text. SM was responsible for sampling and laboratory analysis, assisted with the original concept, and contributed to the text. KH assisted with the original concept and contributed to the text and was project leader of the main RCN funded project KelpPro. LN was responsible for sampling in Frøya and contributed to the text. SF contributed data from 2017 and contributed to the text. All authors contributed to the article and approved the submitted version.

FUNDING

This work was funded by the Research Council of Norway, project no. 267536 (KELPPRO, Kelp industrial production: Potential impacts on coastal ecosystems).

ACKNOWLEDGMENTS

We are grateful to Akvaplan-niva in Tromsø and Seaweed Solutions AS in Trondheim for contributing with infrastructure and co-financing.

SUPPLEMENTARY MATERIAL

The Supplementary Material for this article can be found online at: https://www.frontiersin.org/articles/10.3389/fmars.2021.632725/full#supplementary-material

REFERENCES

Andersen, G. S., Pedersen, M. F., and Nielsen, S. L. (2013). Temperature acclimation and heat tolerance of photosynthesis in norwegian saccharina latissima (Laminariales. Phaeophyceae). *J. Phycol.* 49, 689–700. doi: 10.1111/jpy.12077

Andersen, G. S., Steen, H., Christie, H., Fredriksen, S., and Moy, F. E. (2011). Seasonal Patterns of Sporophyte Growth, fertility, fouling, and mortality of saccharina latissima in skagerrak, norway: implications for forest recovery. *J. Mar. Biol.* 2011:375. doi: 10.1155/2011/690375

Bartsch, I., Wiencke, C., Bischof, K., Buchholz, C. M., Buck, B. H., Eggert, A., et al. (2008). The genus *Laminaria sensu* lato: recent insights and developments. *Eur. J. Phycol.* 43, 1–86. doi: 10.1080/09670260701711376

Bolton, J. J., and Lüning, K. (1982). Optimal growth and maximal survival temperatures of Atlantic *Laminaria species* (Phaeophyta) in culture. *Mar. Biol.* 66, 89–94. doi: 10.1007/BF00397259

Broch, O. J., Alver, M. O., Bekkby, T., Gundersen, H., Forbord, S., Handå, A., et al. (2019). The kelp cultivation potential in coastal and offshore regions of norway. *Front. Mar. Sci.* 5:529. doi: 10.3389/fmars.2018.00529

Broch, O. J., and Slagstad, D. (2012). Modelling seasonal growth and composition of the kelp *Saccharina latissima*. *J. Appl. Phycol.* 24, 759–776. doi: 10.1007/s10811-011-9695-y

Broch, O. J., Ellingsen, I. H., Forbord, S., Wang, X., Volent, Z., Alver, M. O., et al. (2013). Modelling the cultivation and bioremediation potential of the kelp *Saccharina latissima* in close proximity to an exposed salmon farm in Norway. *Aquacult. Environ. Interact.* 4, 187–206. doi: 10.3354/aei00080

Buck, B. H., and Buchholz, C. M. (2005). Response of offshore cultivated *Laminaria saccharina* to hydrodynamic forcing in the North Sea. *Aquaculture* 250, 674–691. doi: 10.1016/j.aquaculture.2005.04.062

Carroll, M., Cochrane, S., Fieler, R., Velvin, R., and White, P. (2003). Organic enrichment of sediments from salmon farming in norway: environmental factors, management practices, and monitoring techniques. *Aquaculture* 226, 165–180. doi: 10.1016/S0044-8486(03)00475-7

Chopin, T., Troell, M., Reid, G. K., Knowler, D., Robinson, S. M. C., Neori, A., et al. (2010). *Integrated Multi-Trophic Aquaculture. Part II. Increasing IMTA Adoption. Global Aquaculture Advocate*. Portsmouth: Global Seafood Alliance.

Dambolena, I. G., Eriksen, S. E., and Kopcso, D. P. (2009). Logarithmic transformations in regression: do you transform back correctly? *Primus* 19, 280–295. doi: 10.1080/10511970802234976

Dean, P. R., and Hurd, C. L. (2007). Seasonal growth, erosion rates, and nitrogen and photosynthetic ecophysiology of Undaria pinnatifida (Heterokontophyta) in Southern New Zealand. *J. Phycol.* 43, 1138–1148. doi: 10.1111/j.1529-8817.2007.00416.x

Duarte, C. M., and Cebrián, J. (1996). The fate of marine autotrophic production. *Limnol. Oceanogr.* 41, 1758–1766. doi: 10.4319/lo.1996.41.8.1758

Duarte, C. M., Wu, J., Xiao, X., Bruhn, A., and Krause-Jensen, D. (2017). Can seaweed farming play a role in climate change mitigation and adaptation? *Front. Mar. Sci.* 4:100. doi: 10.3389/fmars.2017.00100

FAO (2020). *The State of World Fisheries and Aquaculture 2020: Sustainability in Action*. Rome: FAO. Available online at: https://doi.org/10.4060/ca9229en

Forbord, S., Etter, S. A., Broch, O. J., Dahlen, V. R., and Olsen, Y. (2021). Initial short-term nitrate uptake in juvenile, cultivated *Saccharina latissima* (Phaeophyceae) of variable nutritional state. *Aquat. Bot.* 168:103306. doi: 10.1016/j.aquabot.2020.103306

Forbord, S., Matsson, S., Brodahl, G. E., Bluhm, B. A., Broch, O. J., Handå, A., et al. (2020). Latitudinal, seasonal and depth-dependent variation in growth, chemical composition and biofouling of cultivated *Saccharina latissima* (Phaeophyceae) along the Norwegian coast. *J. Appl. Phycol.* 32, 2215–2232. doi: 10.1007/s10811-020-02038-y

Fortes, M. D., and Lüning, K. (1980). Growth rates of North Sea macroalgae in relation to temperature, irradiance and photoperiod. *Helgol. Wiss. Meeresunters.* 34, 15–29. doi: 10.1007/BF01983538

Frigstad, H., Gundersen, H., Andersen, G. S., Borgersen, G., Kvile, K. Ø, Krause-Jensen, D., et al. (2021). Blue Carbon – climate adaptation, CO_2 uptake and sequestration of carbon in Nordic blue forests. *Nordic Council Ministers Rep. Ser.* 2020:541.

Gao, X., Endo, H., Taniguchi, K., and Agatsuma, Y. (2013). Combined effects of seawater temperature and nutrient condition on growth and survival of juvenile sporophytes of the kelp *Undaria pinnatifida* (Laminariales; Phaeophyta) cultivated in northern Honshu, Japan. *J. Appl. Phycol.* 25, 269–275. doi: 10.1007/s10811-012-9861-x

Gerard, V. A. (1987). Hydrodynamic streamlining of *Laminaria saccharina* Lamour. in response to mechanical stress. *J. Exp. Mar. Biol. Ecol.* 107, 237–244. doi: 10.1016/0022-0981(87)90040-2

Gerard, V. A. (1997). The role of nitrogen nutrition in high-temperature tolerance of the kelp, *Laminaria saccharina* (Chromophyta). *J. Phycol.* 33, 800–810. doi: 10.1111/j.0022-3646.1997.00800.x

Gerard, V. A., and Du Bois, K. R. (1988). Temperature ecotypes near the southern boundary of the kelp *Laminaria saccharina*. *Mar. Biol.* 97, 575–580. doi: 10.1007/BF00391054

Greenacre, M. (2016). Data reporting and visualization in ecology. *Polar Biol.* 39, 2189–2205. doi: 10.1007/s00300-016-2047-2

Handå, A., Forbord, S., Wang, X., Broch, O. J., Dahle, S. W., Størseth, T. R., et al. (2013). Seasonal- and depth-dependent growth of cultivated kelp (Saccharina latissima) in close proximity to salmon (Salmo salar) aquaculture in Norway. *Aquaculture* 41, 191–201. doi: 10.1016/j.aquaculture.2013.08.006

Kawamata, S. (2001). Adaptive mechanical tolerance and dislodgement velocity of the kelp Laminaria japonica in wave-induced water motion. *Mar. Ecol. Prog. Ser.* 211, 89–104. doi: 10.3354/meps211089

Krause-Jensen, D., and Duarte, C. M. (2016). Substantial role of macroalgae in marine carbon sequestration. *Nat. Geosci.* 9, 737–742.

Krumhansl, K. A., and Scheibling, R. E. (2011). Detrital production in Nova Scotian kelp beds: patterns and processes. *Mar. Ecol. Prog. Ser.* 421, 67–82. doi: 10.3354/meps08905

Krumhansl, K. A., and Scheibling, R. E. (2012). Production and fate of kelp detritus. *Mar. Ecol. Prog. Ser.* 467, 281–302. doi: 10.3354/meps09940

Lane, C. E., Mayes, C., Druehl, I. D., and Saunders, G. W. (2006). A multi–gene molecular investigation of the kelp (Laminariales, Phaeophyceae) supports substantial reorganisation. *J. Phycol.* 42, 493–512. doi: 10.1111/j.1529-8817.2006.00204.x

Liu, Y., Huang, H., Yan, L., Liu, X., and Zhang, Z. (2016). Influence of suspended kelp culture on seabed sediment composition in Heini Bay, China. *Estuar. Coastal Shelf Sci.* 181, 39–50. doi: 10.1016/j.ecss.2016.07.017

Lüning, K. (1979). Growth strategies of three *Laminaria* species (Phaeophyceae) inhabiting different depth zones in the sublittoral region of Helgoland (North Sea). *Mar. Ecol. Prog. Ser.* 1, 195–207. doi: 10.3354/meps001195

Lüning, K., and Mortensen, L. (2015). European aquaculture of sugar kelp (*Saccharina latissima*) for food industries: iodine content and epiphytic animals as major problems. *Bot. Mar.* 58, 449–455. doi: 10.1515/bot-2015-0036

Mann, K. H. (1973). Seaweeds: their productivity and strategy for growth. *Science* 182, 975–981. doi: 10.1126/science.182.4116.975

Matsson, S., Christie, H., and Fieler, R. (2019). Variation in biomass and biofouling of kelp, *Saccharina latissima*, cultivated in the Arctic, Norway. *Aquaculture* 506, 445–452. doi: 10.1016/j.aquaculture.2019.03.068

Matsson, S., Metaxas, A., Forbord, S., Kristiansen, S., Handå, A., and Bluhm, B. A. (2021). Effects of outplanting time on growth, shedding and quality of *Saccharina latissima* (Phaeophyceae) in its northern distribution range. *J. Appl. Phycol.* 33, 2415–2431. doi: 10.1007/s10811-021-02441-z

Nielsen, M. M., Krause-Jensen, D., Olesen, B., Thinggaard, R., Christensen, P. B., and Bruhn, A. (2016a). Growth dynamics of *Saccharina latissima* (Laminariales, Phaeophyceae) in Aarhus Bay, Denmark, and along the species' distribution range. *Mar. Biol.* 161, 2011–2022. doi: 10.1007/s00227-014-2482-y

Nielsen, M. M., Paulino, C., Neiva, J., Krause-Jensen, D., Bruhn, A., and Serrão, E. A. (2016b). Genetic diversity of *Saccharina latissima* (Phaeophyceae) along a salinity gradient in the North Sea-Baltic Sea transition zone. *J. Phycol.* 28, 3071–3074.

Olafsen, T., Winther, U., Olsen, Y., and Skjermo, J. (2012). *Value created from productive oceans in 2050. The Royal Norwegian Society of Sciences and letters and the Norwegian Academy of Technological Sciences*.

Parke, M. (1948). Studies of british laminariaceae. I. growth in *Laminaria saccharina* (L.) Lamour. *J. Mar. Biol. Assoc.* 27, 651–709. doi: 10.1017/S0025315400056071

Pedersen, M. F., Filbee-Dexter, K., Norderhaug, K. M., Fredriksen, S., Frisk, N. L., Fagerli, C. W., et al. (2020). Detrital carbon production and export in high latitude kelp forests. *Oecologia* 192, 227–239. doi: 10.1007/s00442-019-04573-z

Scheibling, R. E., and Gagnon, P. (2009). Temperature-mediated outbreak dynamics of the invasive bryozoan Membranipora membranacea in Nova Scotian kelp beds. *Mar. Ecol. Prog. Ser.* 390, 1–13. doi: 10.3354/meps08207

Simonson, E., Scheibling, R., and Metaxas, A. (2015). Kelp in hot water: I. warming seawater temperature induces weakening and loss of kelp tissue. *Mar. Ecol. Pro. Ser.* 537, 89–104. doi: 10.3354/meps11438

Sjøtun, K. (1993). Seasonal lamina growth in two age groups of *Laminaria saccharina* (L.) Lamour in western Norway. *Bot. Mar.* 36, 433–441. doi: 10.1515/botm.1993.36.5.433

Soto, D. (2009). Integrated mariculture. A global review. *FAO Fish. Aquac.Tech. Paper* 183.

SSB (2018). *Dette er Norge 2018*. Available online at: https://www.ssb.no/befolkning/artikler-og-publikasjoner/dette-er-norge-2018

Stévant, P., Rebours, C., and Chapman, A. (2017). Seaweed aquaculture in Norway: recent industrial developments and future perspectives. *Aquacult. Int.* 25, 1373–1390. doi: 10.1007/s10499-017-0120-7

Suzuki, S., Furuya, K., Kawai, T., and Takeuchi, I. (2008). Effect of seawater temperature on the productivity of Laminaria japonica in the Uwa Sea, southern Japan. *J. Appl. Phycol.* 20, 833–844. doi: 10.1007/s10811-007-9283-3

Tala, F., and Edding, M. (2005). Growth and loss of distal tissue in blades of *Lessonia nigrescens* and *Lessonia trabeculata* (Laminariales). *Aquat. Bot.* 82, 39–54. doi: 10.1016/j.aquabot.2005.02.009

Trevathan-Tackett, S. M., Kelleway, J., Macreadie, P. I., Beardall, J., Ralph, P., and Bellgrove, A. (2015). Comparison of marine macrophytes for their contributions to blue carbon sequestration. *Ecology* 96, 3043–3057. doi: 10.1890/15-0149.1

Wernberg, T., and Filbee-Dexter, K. (2018). Grazers extend blue carbon transfer by slowing sinking speeds of kelp detritus. *Sci. Rep.* 8, 1–7. doi: 10.1038/s41598-018-34721-z

Yoshikawa, T., Takeuchi, I., and Furuya, K. (2001). Active erosion of Undaria pinnatifida suringar (Laminariales, Phaeophyceae) mass-cultured in Otsuchi Bay in northeastern Japan. *J. Exp. Mar. Biol. Ecol.* 266, 51–65. doi: 10.1016/S0022-0981(01)00346-X

Zhang, J., Fang, J., Wang, W., Du, M., Gao, Y., and Zhang, M. (2012). Growth and loss of mariculture kelp Saccharina japonica in Sungo Bay, China. *J. Appl. Phycol.* 24, 1209–1216. doi: 10.1007/s10811-011-9762-4

Zhang, J., Hansen, P. K., Wu, W., Liu, Y., Sun, K., Zhao, Y., et al. (2020). Sediment-focused environmental impact of long-term large- scale marine bivalve and seaweed farming in Sungo Bay, China. *Aquaculture* 528:735561. doi: 10.1016/j.aquaculture.2020.735561

Zhang, J., Kupka Hansen, P., Fang, J., Wang, W., and Jiang, Z. (2009). Assessment of the local environmental impact of intensive marine shellfish and seaweed farmingapplication of the MOM system in the Sungo Bay, China. *Aquaculture* 287, 304–310. doi: 10.1016/j.aquaculture.2008.10.008

Conflict of Interest: The authors declare that the research was conducted in the absence of any commercial or financial relationships that could be construed as a potential conflict of interest.

Publisher's Note: All claims expressed in this article are solely those of the authors and do not necessarily represent those of their affiliated organizations, or those of the publisher, the editors and the reviewers. Any product that may be evaluated in this article, or claim that may be made by its manufacturer, is not guaranteed or endorsed by the publisher.

Advantages of publishing in Frontiers

OPEN ACCESS
Articles are free to read for greatest visibility and readership

FAST PUBLICATION
Around 90 days from submission to decision

HIGH QUALITY PEER-REVIEW
Rigorous, collaborative, and constructive peer-review

TRANSPARENT PEER-REVIEW
Editors and reviewers acknowledged by name on published articles

Frontiers
Avenue du Tribunal-Fédéral 34
1005 Lausanne | Switzerland

Visit us: www.frontiersin.org
Contact us: frontiersin.org/about/contact

REPRODUCIBILITY OF RESEARCH
Support open data and methods to enhance research reproducibility

DIGITAL PUBLISHING
Articles designed for optimal readership across devices

FOLLOW US
@frontiersin

IMPACT METRICS
Advanced article metrics track visibility across digital media

EXTENSIVE PROMOTION
Marketing and promotion of impactful research

LOOP RESEARCH NETWORK
Our network increases your article's readership